Parametric Design of Diesel Engine Inlet Ports

Michael C Bates

A thesis submitted in partial fulfilment of the requirements of the University of Brighton for the degree of Doctor of Philosophy

August 2004

The University of Brighton

Abstract

Inlet port flow characteristics are critical in determining the overall performance of diesel combustion systems. The relationship between inlet port geometry and performance has long been a subject of interest to many researchers, although as yet a comprehensive understanding remains elusive. The ongoing need to provide advanced powertrain design solutions in order to meet increasingly stringent emissions legislation, whilst meeting customer expectations and minimising engineering costs, has driven the development of new approaches to engine design. In particular, the fundamental advantages of multivalve technology, coupled with rapidly improving fuel delivery systems has placed new requirements on inlet port performance characteristics. Statistical methods and knowledge-based design are emerging as potentially powerful tools in this field of research, supported by rapid developments in computing power.

In the present study, a knowledge-based approach for the concept design of diesel engine inlet port geometry has been developed. Parametric modelling and statistical Design-of-Experiments (DoE) techniques have also been used to define a set of design features and a steady-flow test rig has been adapted for use with rapid-prototype port models. The test results have been analysed to identify the most important features and to characterise their influence on in-cylinder flow performance. Alternative modelling approaches have been proposed and the validity of each has been assessed by comparing predicted and experimental results. 3-D CFD calculations were also performed to provide visual representations of the in-cylinder flow topology. The final knowledge-based model has been implemented as a prototype software application and has proven to be useful in generating and assessing real concept design solutions. Furthermore, a selection of design concepts have been optimised, subject to typical constraints within the cylinder head.

Contents

List of Figures

List of Tables

Nomenclature

Roman Symbols

A	Reference area used in flow coefficient (mm^2)
A	Sonic velocity (m/s)
A_l	Valve-lift dependent reference are used for flow coefficient (mm^2)
Ar	Directed/helical port curve angle (°)
As1	Valve skew angle (°)
As2	Valve separation angle (°)
At	Directed/helical port tangential approach angle (°)
Av	Directed port vertical approach angle (°)
Aw	Helical port helix wrap angle (°)
B	Cylinder bore diameter (mm)
Cf	Flow coefficient (-)
D	Valve seat reference diameter (mm)
Db	Cylinder head bolt constraint diameter (mm)
Df	Fuel injector constraint diameter (mm)
Dn	Non-dimensional valve diameter (-)
Do	Valve head outer diameter (mm)
Dp	Port diameter (mm)
Ds	Valve stem diameter (mm)
Dv	Valve seat outer diameter (mm)
E	Eccentricity (valve location) (-)
G	Swirl meter torque (Nm)
Hs	Helical port helix start height (mm)
L, Lv	Valve lift (mm)
MCf	Mean flow coefficient (-)
n	Number of inlet valves, number of parameters in an experiment
Ns	Non-dimensional rig swirl (-)
Q	Volumetric air flow rate (m^3/s)
R	Directed/helical port curve radius (mm)
Rs	Swirl ratio, momentum-based Ricardo methods (-)

S	Piston stroke (mm)
SR	Swirl ratio, paddle wheel-based method (-)
Vo	Velocity head (m/s)
w	Valve seat width (mm)
Wh	Helical port helix width (mm)
Y	Valve location offset (mm)
Z	Inlet Mach Index (Gulp factor) (-)

Greek Symbols

$\alpha 1$	Inlet valve opening timing (radians)
$\alpha 2$	Inlet valve closing timing (radians)
β	Valve seat angle
ω_E	Crankshaft rotational speed (radians/s)

Acronyms

BDC   Bottom Dead Centre (lowest position of piston)

CAD   Computer Aided Design

CC   Central Composite (experimental design)

CFD   Computational Fluid Dynamics

CNC   Computer Numerically Controlled (machining)

DI   Direct injection (diesel engine)

DoE   Design of Experiments

HSDI   High Speed Direct Injection (diesel engine)

HWA   Hot Wire Anemometry

ISM   Impulse Swirl Meter

IVC   Inlet Valve Closes

IVO   Inlet Valve Opens

KBE   Knowledge Based Engineering

LDA   Laser Doppler Anemometry

LFM   Laminar Flow Meter

MIGV   Mean Inlet Gas Velocity

PIV   Particle Image Velocimetry

PTV   Particle Tracking Velocimetry

RSM   Response Surface Methods

SLS   Selective Laser Sintering

STL   Stereo Lithography (solid geometry file format)

TDC   Top Dead Centre (highest piston position)

VBA   Visual Basic for Applications

Acknowledgements

Declaration

I hereby declare that this Thesis is my own work except where otherwise indicated. I have identified my sources of information and in particular have put in quotation marks any passages that have been quoted word for word and identified their origins

Signed   Date

1   Introduction

The importance of in-cylinder charge motion in internal combustion engines has been acknowledged for many years. The effects of turbulence in combustion chambers were enthusiastically debated during the early part of the last century, as documented by articles in *The Autocar* (Fisher 1930) in which Mr (later to become Sir) H. R. Ricardo and Mr. W. A. Whatmough presented alternative views. Ricardo argued that turbulence was required in order to achieve efficient combustion, whereas Whatmough supported the view that streamlined flow of the gases in the combustion chamber was necessary. Around the same time, Alcock (1934) was conducting pioneering research into the effects of bulk motion in diesel engines. As a result of these and numerous other studies, the importance of charge motion is now widely accepted and a great deal of research effort has been directed towards developing a better understanding of in-cylinder flows and their influence on the combustion process. Clearly, there are several factors that contribute to the conditions inside the cylinder at the critical time when combustion begins, but intake-generated flows are perhaps among the most widely studied.

The two terms most commonly used to describe bulk in-cylinder charge motion are *swirl* and *tumble*. Both refer to organised rotational flows that are generated during the intake stroke by means of the inlet port shape, inlet valve location and other detailed features of the combustion chamber. Swirl, shown schematically in Figure 1.1(a) is used to describe a rotational flow in which the axis of rotation is parallel to the cylinder axis. Tumble, occasionally known as barrel swirl (Figure 1.1(b)), refers to a rotational flow in which the axis of rotation is at right angles to the cylinder axis and is usually parallel to the engine crankshaft axis. The aim of intake-generated charge motion is to provide energy that can be stored during the compression stroke for release during the combustion process. In the case of swirl, the charge motion is usually maintained throughout compression and is therefore used to control air-fuel mixing, particularly in a HSDI (high-speed, direct-injection) diesel engine. The high-pressure injection of fuel may also cause the air motion to break down into turbulence, resulting in enhanced combustion rates. Swirl is also employed in conventional PFI (port fuel injection) and direct-injection gasoline engines, although the widespread adoption of 4V (four-valves-per-cylinder; two inlet, two exhaust), pent-roof cylinder head configurations, having a propensity for tumble generation rather than swirl, has lead to the development of tumble-based combustion systems for the majority of applications. In contrast with swirl,

tumble is distorted during compression and high levels of turbulence are generated prior to ignition. This leads to rapid flame propagation during the early stages of combustion, with a more controlled secondary phase that lowers noise and reduces the risk of abnormal combustion events such as knocking. The primary air motion requirement in direct-injection gasoline engines is to control fuel stratification in order to achieve lean overall air-fuel mixtures whilst ensuring that an ignitable mixture reaches the spark plug at the correct time. Appropriate in-cylinder motion has been used successfully to achieve this in so-called air-guided systems, although systems that are intended to be less dependent on air-motion (wall-guided and spray guided) are also being investigated.

(a) Swirl   (b) Tumble
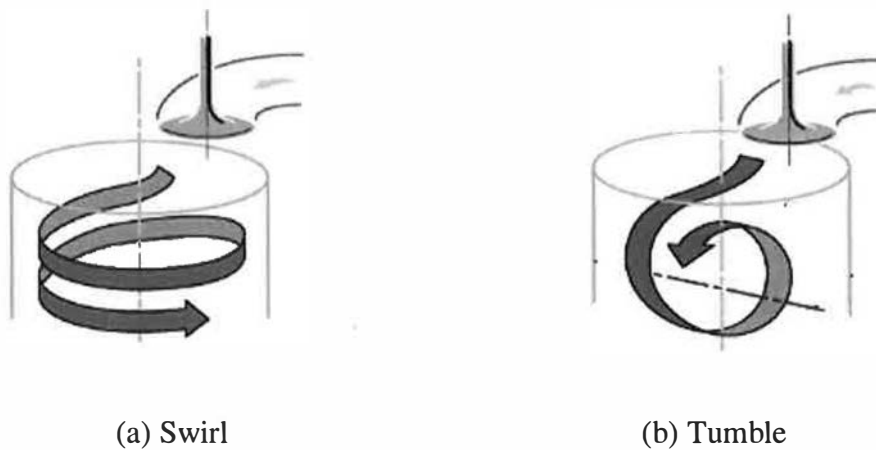
Figure 1.1: Bulk in-cylinder motion

The air capacity of an engine is a fundamental factor that governs power output (Livengood and Stanitz, 1943). In gasoline engines, a stoichiometric air-fuel mixture is required throughout most of the operating range in order to achieve adequate combustion whilst maximising exhaust catalyst efficiency to reduce harmful emissions. Load is controlled by limiting the mass of air entering the cylinder, since this determines the mass of fuel that must be injected. In diesel engines, load is governed by the amount of fuel injected into the cylinder. Air induction is not restricted by a throttle valve, resulting in lean air-fuel ratios throughout the operating range. However, in order to burn this fuel efficiently and reduce smoke emissions at high load, sufficient air is required and in practise maximum load is also determined by the amount of air that can be admitted into the cylinder during the intake stroke. Volumetric efficiency is used almost universally as a measure of engine air capacity. Although it is influenced by a range of factors, including dynamic effects resulting from

pulsations created by the motion of the piston and wave action throughout the inlet and exhaust systems, volumetric efficiency is strongly dependent on quasi-static effects such as flow friction in the inlet system. The design of inlet ports and valves is critical in this respect, as they are usually the most restrictive components of the inlet system, particularly when designed to generate in-cylinder charge motion (Heywood, 1988).

The influence of inlet port design on in-cylinder motion, volumetric efficiency and combustion has been investigated by many researchers, resulting in a plethora of design schemes, guidelines and patents. Numerous experimental methods have been developed to test the effectiveness of these designs, from steady flow rigs to advanced optical techniques capable of taking accurate measurements inside reciprocating engines. The introduction of Computational Fluid Dynamics (CFD) to simulate flows throughout the engine cycle has enabled researchers and engine designers to visualise and understand the process more than ever before. Indeed, much of the experimental work now underway in this field is aimed at validating CFD models with the ultimate goal of a "virtual engine". However, there is still some way to go and CFD is at present used primarily as a screening tool to evaluate concept design solutions before the commitment is made to procure and test real components. A natural extension to this approach is to use a virtual model to evaluate potential design solutions *and* develop an optimum solution, thus minimising the effort required downstream when design changes become increasingly costly. The collective term for a series of techniques that enable this process is Knowledge-Based Engineering (KBE). KBE requires three key components; a parameterised representation of the component or system, a sufficiently accurate, rapid method of evaluating performance and a practical means by which the evaluation results are used to drive development towards an optimum solution. The development of 3-D CAD modelling systems has been an important factor in the growth of KBE. However, parameterisation of the complex organic geometry of inlet ports has been beyond the capabilities of most systems until recently, as demonstrated by the work of Widener (1995). Therefore, the use of KBE in the field of inlet port design is still in its infancy and is not widely reported in the literature. Early investigations into this subject have utilised a range of techniques including iterative CFD optimisation and statistical modelling techniques such as Design of Experiments (DoE) and Response Surface Modelling (RSM).

Although a knowledge-based approach to inlet port design could be beneficial for PFI and direct-injection gasoline engines, HSDI diesel engines have been the subject of rapid

development in recent years. Primarily as a result of developments in electronic control and fuel-systems technology, HSDI diesel engines are able to utilise high-pressure fuel injection over a wide engine speed range. Significant improvements in fuel consumption, engine performance and exhaust emissions are possible as a result, but careful matching of all the factors in the combustion system is necessary. Consequently, previously held views on the requirements of in-cylinder air motion are being revised and inlet port design is clearly influential in this respect. Diesel engine inlet ports are generally more complex than gasoline ports, both in terms of the geometry of the port and the constraints applied due to the presence of other major components in the cylinder head. Successfully packaging inlet and exhaust ports, fuel injectors, coolant passages and structural features provides a significant challenge for engine designers and a knowledge-based system that could be used to assist in this process would represent a significant step forward.

The aim of the present study is to investigate the use of a knowledge-based design methodology for HSDI diesel engine inlet ports. In order to achieve this goal, a literature survey has been conducted to identify appropriate experimental methods, port design features and other critical aspects of the knowledge-based approach. The findings of this survey are reported in Chapter 2. Parametric design schemes, devised to represent common inlet port types, and the experimental designs selected to characterise port performance responses, are presented in Chapter 3. Chapter 4 begins with the presentation and analysis of experimental results; followed by the construction and validation of predictive models. In Chapter 5, the models are developed further to investigate multi-valve design configurations. Finally, conclusions are drawn and recommendations for further work are made in Chapter 6.

2 A Review of Diesel Engine Inlet Port Design, Flow Characterisation and Parametric Modelling

2.1 Introduction

The aim of this review is to investigate the available methods that may be used to develop a virtual model of inlet ports for HSDI diesel engines. The constituent parts of any such method could include in-cylinder flow characterisation techniques, 3-D CAD modelling, CFD simulation, statistical modelling and optimisation. Clearly, these are major areas of study in themselves and it is beyond the scope of this review to cover them completely. However, relevant aspects of each are included and additional material reviewed when necessary. Experimental and computational measurement and characterisation techniques are discussed in sections 2.2 and 2.3 respectively, followed by a review of the relevant aspects of engine design in section 2.4. Knowledge-based design and optimisation is covered in section 2.5 and the chapter concludes with section 2.6; a critical review of parametric port design studies published to date, drawing from the key points raised in the previous sections.

2.2 Experimental Techniques

2.2.1 Steady Flow Test Rigs

Steady flow test rigs have been used extensively to quantify inlet port flow performance and in-cylinder charge motion (Monaghan and Pettifer 1981; Partington 1982; Uzkan, et. al. 1983; Hasegawa and Takahashi 1988). Their use relies on the assumption that steady-state inlet port flow characteristics can adequately represent behaviour in a reciprocating engine. Temperature and pressure measurements taken throughout the system are used to calculate flow parameters. In-cylinder charge motion is measured either by the rotational speed of a paddle wheel located downstream of the valve in the cylinder bore, or more commonly by the torque exerted on a flow straightening element placed in a similar position. A typical steady flow rig is shown schematically in Figure 2.1.
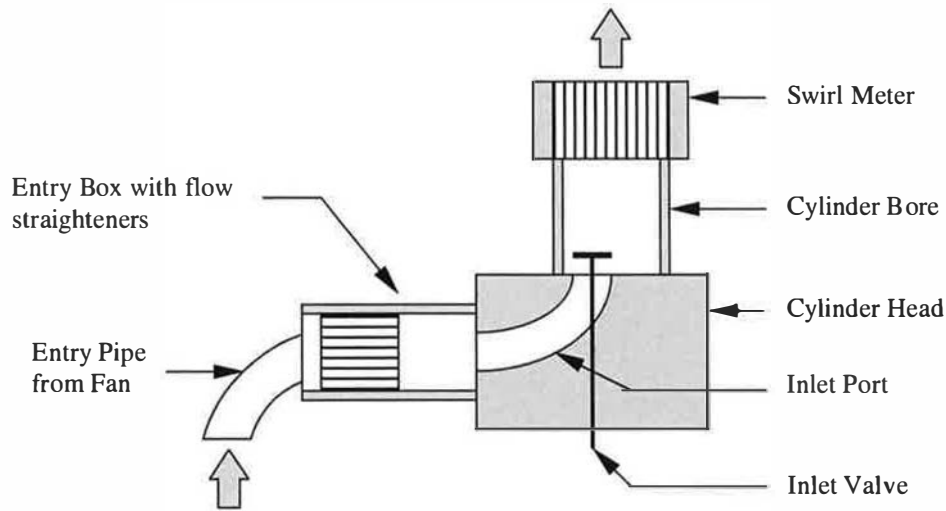
Figure 2.1: Typical steady flow test rig (Monaghan and Pettifer 1981)

2.2.1.1 Port flow performance

Typically, port flow performance is expressed as a range of flow coefficients corresponding to static inlet valve lift positions (discharge coefficient is also used by some authors but the terms are often equivalent in their meaning). Flow coefficient is defined as the ratio of measured flow rate through the inlet valve to the ideal flow rate, based on a reference area such as the valve head area (Taylor 1985) or port area at the valve seat (Woods 1966). The area corresponding to the minimum contact diameter between the valve and valve seat, or inner seat diameter is also used (Monaghan and Pettifer 1981). The valve stem cross-sectional area may also be deducted from the valve seat or port area.

$$C_f = \frac{Q}{AV_o} \tag{2.1}$$

Where Q is the measured volumetric air flow rate (m³/s), V_o is the velocity head dependent on test conditions (m/s) and A is the reference area (m²). Valve lift dependent reference areas may also be used depending on the valve lift range being considered, particularly at low valve lifts when a constant reference area is unlikely to be representative of the ideal flow condition (Kastner, et. al. 1963).

For low valve lifts the reference area is a frustum of a right circular cone; the conical surface being normal to the valve seat faces:

6

$$\frac{w}{\sin \beta \cos \beta} > L_v > 0$$

$$A_1 = \pi L_v \cos \beta \left(D_v - 2w + \frac{L_v}{2} \sin 2\beta \right) \qquad (2.2)$$

For intermediate valve lifts, the reference area is still a frustum of a cone but the conical surface is no longer normal to the seat faces. As lift increases, the surface approximates to a cylinder:

$$\left[\left(\frac{D_p^{\,2} - D_s^{\,2}}{4D_m} \right)^2 - w^2 \right]^{1/2} + w \tan \beta \geq L_v > \frac{w}{\sin \beta \cos \beta}$$

$$A_1 = \pi D_m \left[(L_v - w \tan \beta)^2 + w^2 \right]^{1/2} \qquad (2.3)$$

Where A_1 is the lift-dependent effective valve area, L_v is the valve lift, D_v is the valve seat outer diameter, D_p is the port diameter, D_s is the valve stem diameter, w is the seat width, D_m is the mean seat diameter ($D_v - w$) and β is the valve seat angle. All dimensions are in SI units. The reference areas corresponding to equations 2.2 and 2.3 are shown diagrammatically in Figure 2.2. Note that the orientation of the area changes with respect to the valve seat angle, as valve lift increases.
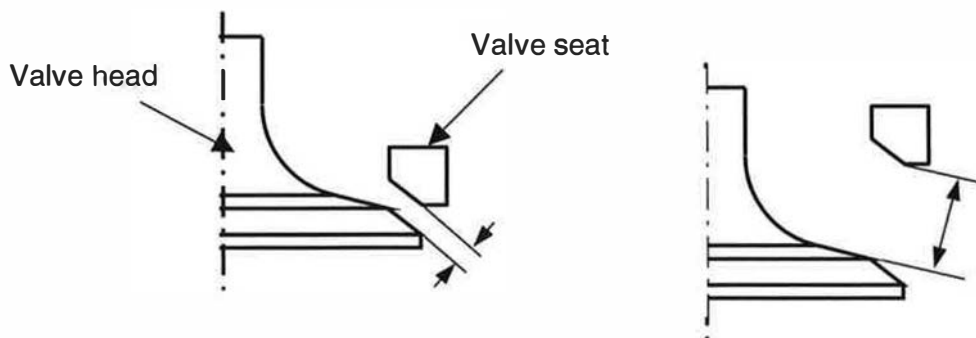
Figure 2.2: Flow coefficient reference areas (Kastener, et. al. 1963)

Lift dependent reference areas provides flow coefficients close to unity at low valve lifts, providing a quick check of flow performance and indicating transitions in the flow regime. Flow coefficients based on a constant such as the valve head area increase with valve lift before levelling off as the maximum flow capacity of the port is reached. Therefore flow coefficients of this type are usually used to indicate performance at high valve lifts. The choice of reference area frequently depends on how easily the corresponding dimension can be measured. Valve head diameter and port throat can usually be measured with the use of simple devices and are therefore commonly used. Valve inner seat diameter is often more difficult to determine, but does represent a common reference to that used to determine the minimum flow area at low valve lift (Equation 2.2). Therefore, the ideal flow coefficient (based on inner seat diameter) can be calculated for the relevant valve lift range and used for comparison with the actual flow coefficient. This relationship is only approximate when alternative reference areas are used to describe valve size.

2.2.1.2 In-cylinder motion

In diesel engines, in-cylinder motion is usually characterised as swirl. Although several definitions of swirl exist (Monaghan and Pettifer 1981; Uzkan, et. al. 1983), it is fundamentally a measure of the organised rotation of the charge about the cylinder axis. Swirl is usually measured on a steady flow rig by a flow straightening element mounted concentrically with the cylinder. The element is fixed to a central shaft and is free to float in the cylinder but is restricted from rotation by a load cell. As the swirling airflow exits the cylinder through the meter, the angular momentum flux on the element is registered as a torque on the shaft. Assuming that all the rotational motion of the air flowing through the cylinder is captured and that friction in the shaft bearings is negligible, the torque is used to calculate non-dimensional swirl at each valve lift condition.

$$Ns = \frac{8G}{mBV_o} \qquad (2.4)$$

Where G is the measured torque on the element (Nm), m is the mass flow rate through the port (kg/s), B is the cylinder bore diameter (m) and V_o is the velocity head (m/s)

A typical meter of this type, a Cussons Impulse Swirl Meter (ISM) is shown in Figure 2.3. The design of the ISM closely follows that proposed by Tippelmann (1977). In comparison

with earlier paddle wheel devices in which the rotational speed of the spindle was taken as an indicator of the rotational speed of the charge, Monaghan and Pettifer (1981) showed that swirl measured using an ISM is less sensitive to errors caused by differences in the size and location of the main swirling structure within the cylinder. Paddle wheel meters underestimate swirl when high flow velocities are present close to the cylinder periphery due to leakage past the clearance gap between the paddles and the cylinder bore. They also overestimate the effect of small concentrated structures in the centre of the cylinder. By definition, the ISM characterises swirl throughout the entire cylinder and such errors do not occur. Leakage past the element is also eliminated by an oil trap; this is only possible because of the lack of relative motion between the element and the cylinder.
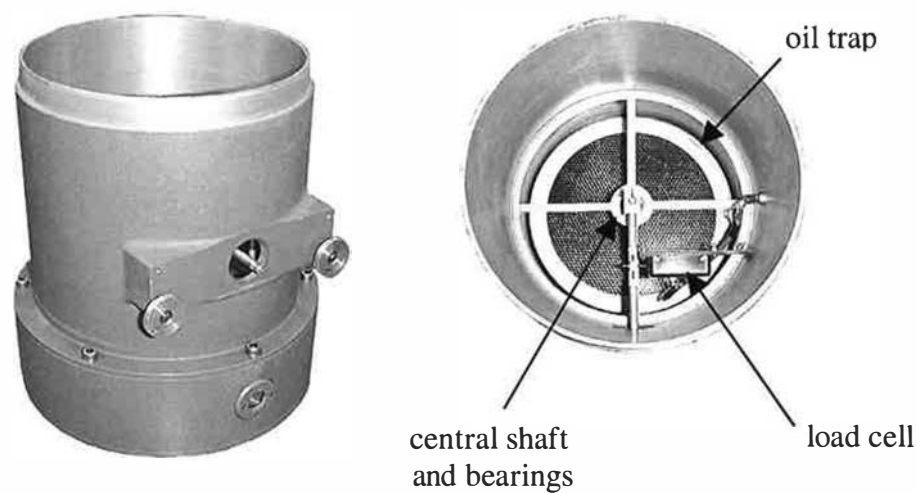
Figure 2.3: Impulse swirl meter
(Source: Ricardo Consulting Engineers Ltd)

It is common practice to combine the results of individual tests, to provide integral parameters that indicate flow characteristics over the complete intake event. The effects of engine operating parameters such as rated speed and valve lift profile may then be simulated. Taylor (1985) defined Inlet Mach index (Z) to indicate the breathing potential of 4-stroke engines based on simple flow coefficients. Inlet Mach Index, also known as "Gulp Factor", has a strong relationship with the measured volumetric efficiency of a range of engines as shown in Figure 2.4.

$$Z = \left(\frac{B}{D}\right)^2 \frac{2S\omega_E}{na\,MC_f} \qquad\qquad (2.5)$$

Where B is the cylinder bore diameter, D is the inlet valve reference diameter, S is the piston stroke, ω_E is the rotational speed of the crankshaft, n is the number of inlet valves per cylinder, a is sonic velocity at standard temperature and pressure and MC_f is the mean flow coefficient. MC_f is determined by integrating the measured C_f values over the intake valve lift profile, $\alpha1$ and $\alpha2$ represent inlet valve opening and closing timings in radians.

$$MC_f = \frac{\int_{\alpha1}^{\alpha2} C_f \, d\alpha}{\alpha2 - \alpha1} \qquad\qquad (2.5a)$$
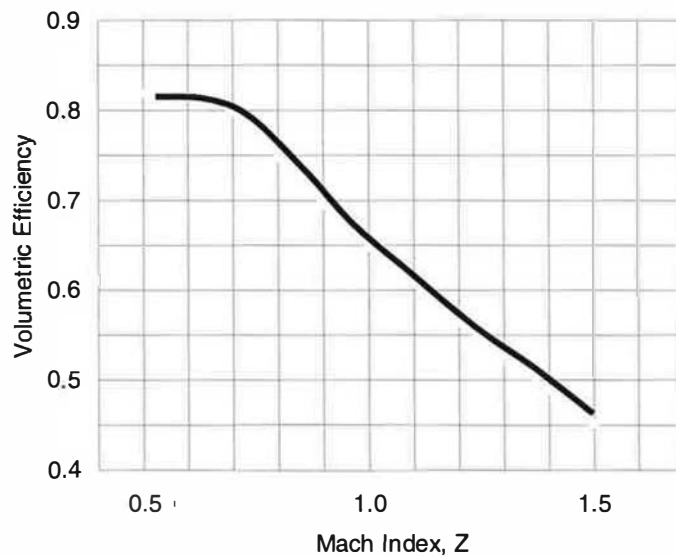
Figure 2.4: Correlation between Z and volumetric efficiency (simplified)
(Taylor 1985)

In a similar manner, swirl ratio (Rs) is calculated by integrating individual swirl measurements over the complete intake event. Swirl ratio is defined by Monaghan and Pettifer (1981) as the angular velocity of a rotating solid body, having the same angular momentum as the inlet charge at the end of the intake event. Although swirl ratio is a non-dimensional measure of in-cylinder motion, it is influenced by cylinder bore, piston stroke and inlet valve size, as can be seen from Equation 2.6. Therefore, in order to compare the swirl generating potential of inlet ports when using steady flow techniques, swirl ratio may

be normalised by the engine shape factor, Ld (Equation 2.6a). It is assumed that the mass flow through the port is dependent only on the flow coefficient and that the intake process takes place between inlet valve opening (IVO) and inlet valve closing (IVC). Volumetric efficiency is also assumed to be unity, therefore the mass of the air in the cylinder at IVC is equal to the mass of air that would occupy the total volume of the cylinder at bottom dead centre (BDC) at a given ambient temperature and pressure.

$$Rs = \frac{L_d \int_{\alpha 1}^{\alpha 2} C_f N_s \, d\alpha}{\left[\int_{\alpha 1}^{\alpha 2} C_f \, d\alpha \right]^2} \qquad (2.6)$$

$$L_d = \frac{BS}{nD^2} \qquad (2.6a)$$

Care must be taken in using steady flow parameters in a quantitative manner and it is usual to use comparative data when baseline engine performance has been established. However, they continue to be used successfully in the design and development of engines. In the absence of an alternative rapid method, port development based on steady flow testing remains as a key tool that continues to have a valuable role.

2.2.2 Dynamic Flow Visualisation

Although the use of steady flow rigs is still widespread in both research and industry, the development of techniques that allow visualisation and measurement of dynamic flows inside engines has provided researchers with a range of tools to characterise in-cylinder processes in a more realistic manner. The majority of techniques rely on optical measurements of in-cylinder charge motion using high-speed photography and laser illumination. The use of water analogue rigs to simulate the intake stroke has been used successfully by several research teams (Kent, et. al. 1989, 1994; Jackson, et. al. 1995; Faure, et. al. 1998). Particle Tracking Velocimetry (PTV) or Particle Image Velocimetry (PIV) techniques were used to measure the velocity of seeding particles in a model of an engine with water acting as the working fluid. Dynamic similarity between the model and an engine was achieved by reducing the operating speed of the rigs, with the added advantage that data capture and processing tasks were simplified. Jackson, et. al. (1997) showed that parameters based on the vorticity and rotational kinetic energy of the in-cylinder flows at BDC correlated with ignition delay and combustion duration in a spark-ignition gasoline engine.

In contrast with the simple approach necessitated by steady state tests, Choi, et. al. (1996) demonstrated that these dynamic methods could be used to study the effect of real-time variation of parameters such as valve timing and lift. Cheung, et. al. (1990) validated the assumption that incompressible flow may be assumed during intake and therefore that the Reynolds analogy is sufficient to achieve dynamic similarity has been validated. Steady flow measurements through a helical port using liquid and air were compared and it was concluded that flow patterns were independent of flow rate.

The effects of engine geometry on charge motion during intake and compression have been studied with the use of motored engines having optical access to the cylinder. Single point velocity measurements using Laser Doppler Anemometry (LDA) have been made by many researchers. Arcoumanis, et. al. (1983, 1991) concluded that the flow patterns at TDC were partially dependent on BDC conditions. Hadded, et. al. (1991) found that steady flow results remained a good indicator of in-cylinder turbulence and a correlation between tumble ratios and combustion stability was developed. Kang, et. al. (1995, 1997) discovered that strong tumble motion was preserved during compression, but weak tumble decayed rapidly, again suggesting a relationship with tumble measurements made using steady state or intake-only measurements. In most cases, researchers have concluded that steady flow techniques provide a good indication of the overall in-cylinder flow characteristics. Full-field PIV measurements in motored engines have been reported (Reeves, et. al. 1994, 1996; Tabata, et. al. 1995). The increased flow velocities compared to those in water rigs has proved to be a problem for image capture and processing. However, developments in hardware and software will provide the opportunity to develop this technique further.

Optical techniques are not limited to the characterisation of in-cylinder charge motion. A range of methods has been developed to determine fuel droplet size and velocity data, fuel vapour concentration and emissions measurements inside the cylinder during engine operation. Although a review of these techniques is beyond the scope of this study, they are clearly important tools that aid in the understanding of all the physical processes that contribute to combustion. Therefore, studies of fuel sprays and air motion are closely linked and must be investigated with this fact in mind.

2.3 Computational Techniques

Computational techniques used for characterising engine performance generally fall into two categories; one dimensional (1-D) computational fluid dynamics (CFD) methods are used for basic engine performance predictions whereas multi-dimensional and in particular three-dimensional (3-D) CFD methods are now preferred for detailed simulation of in-cylinder flows and combustion. 1-D CFD methods are usually used to develop intake and exhaust systems and to investigate the effects of valve timing, turbocharger matching and exhaust gas recirculation. The results can also be processed to provide noise data for engine refinement purposes. The approach taken to characterise inlet flows applies equally to computational and experimental methods. For reasons of cost and time, steady state conditions have often been assumed in defining boundary conditions for simulations (Dhaubhadel,1996). Also, the need to validate computer predictions with experimental results means that the availability of test apparatus may be the limiting factor. Furthermore, the ability of computer simulations to accurately model steady flow conditions may not follow in the case of dynamic, unsteady operation. However, a number of relevant studies investigating the use of CFD simulation to predict in-cylinder flows have been reported.

Steady state CFD investigations of inlet port flows have been widely reported as the use of this technique has grown. Mahmood, et. al. (1996) investigated dual intake port flows with steady state CFD simulations and LDA measurements. In order to compare the two methods, simulations were performed using liquid and air, while experiments were performed with liquid only. The CFD model contained 68,000 cells for a cylinder bore of 80mm; the grid size was based on previous findings (Chen 1995), indicating that grid-independent results could be obtained. Results were calculated for valve lifts of 5mm and 10mm. Calculated and measured axial and transverse velocity components correlated for a range of flow rates, although the velocity magnitudes predicted by CFD were generally lower. Due to the point-wise nature of the LDA measurements, flow characterisation parameters were not presented. Bensler and Opperman (1996) performed CFD simulations of an automotive five-valve inlet port. The similarity between the flow patterns at high valve lift in dynamic and steady state cases was noted, but low lift results were different due to the influence of the moving piston. In contrast with Mahmood, et. al. (1996), the CFD mesh contained over 400,000 cells, suggesting a difference of opinion regarding the requirements of grid-independent solutions. Flow coefficients within 6% of measured results were obtained. Taylor, et. al. (1998) also

13

found that a finer grid was required to achieve acceptable results. In a study of a diesel engine, a CFD model containing approximately 700,000 cells was used to predict discharge coefficients for three valve lift cases. Calculated results were within 6% of those measured using a steady state air flow rig. A significant improvement was claimed over previous studies (Godrie and Zellat 1994; Dent and Chen 1994; Gosman and Ahmed 1987). Taylor also went on to suggest design improvements based on the CFD results, demonstrating that CFD could be used to identify the effects of significant design features. O'Conner and McKinley (1998) used a CFD model with automatic meshing to study steady flow patterns generated in 4-valve diesel engines. The limitations associated with steady state models were identified, but it was claimed that unsteady dynamic simulation was not practical at the time. Results using meshes of approximately 400,000 cells and 200,000 cells were compared and it was concluded that although the main flow patterns were similar, the finer model was necessary to capture detailed flow features. Swirl ratios were calculated, these being within 5% of measured values for low and medium valve lifts, but significantly higher error was recorded at high lift. Further comparison of the results with LDA data showed that the predictions were most accurate in areas of low velocity and where less interaction occurred between the inlet valve flows.

Studies using unsteady, dynamic in-cylinder CFD simulations are limited, although Faure, et. al. (1998) demonstrated that CFD could be used successfully to predict flow patterns throughout the intake and compression process. Flow patterns in a direct injection gasoline engine were measured using the water analogue rig. These were compared with CFD predictions using water and air, and Laser Doppler Anemometry (LDA) measurements of a motored engine. The CFD model predictions were validated by the water rig results during the intake stroke and by the LDA results during compression. This study supported earlier findings with regard to the validity of the Reynolds analogy methods. It also provided confidence in the use of CFD models for complex, dynamic in-cylinder flow predictions.

2.4   Engine Design

For many years, design guidelines based on experience have provided the basis for concept engine design. These guidelines can be thought of as parametric models in that many design features are scaled according to a smaller number of controlling features. In a study of cylinder head design features, Barnes-Moss (1973) proposed that the size and number of

inlet valves was determined primarily by engine performance requirements such as torque and power at rated speed, subject to the available area provided by the cylinder bore. The dimensions of most of the port features were then based directly on inlet valve size. Design guidelines are also knowledge-based in that they are developed using the expertise of experienced designers and the research findings, but they lack the flexibility and optimisation potential of a structured knowledge-based model.

The influence of the fundamental engine design parameters on engine performance are comprehensively covered in the literature and reference books provide excellent summaries. In particular, Taylor (1985) discusses in some detail the effects of bore to stroke ratio, inlet valve size and valve timing on volumetric efficiency. The significance of Mach index (Z), it's dependence on mean inlet gas velocity and relationship with mean piston speed at rated engine speed and inlet valve diameter to cylinder bore diameter ratio are supported by numerous experimental observations. Heywood (1988) discusses the relative contributions of quasi-static effects such as flow friction through the port and inlet valve. Dynamic effects such as valve timing and induction ram are also discussed.

2.4.1 Cylinder Head Design

The cylinder head performs several functions in a diesel engine. It must enclose the cylinders to provide a sealed combustion chamber, provide inlet and exhaust ports and house the valvetrain system to provide fresh charge and expel exhaust gases, house the injector and maintain all the components in a satisfactory condition by ensuring that they are cooled and lubricated. Many of these requirements are conflicting and optimisation of any one aspect in isolation may result in an unacceptable trade-off in another. According to Gilbert, et. al. (1992), the principal design parameters in a DI diesel cylinder head are:

Cylinder head bolting pattern

Valve and port layout

Valve size and position

Valve actuation

Injector and heater plug installation

Cylinder head construction

15

The number of cylinder head bolts and the bolting pattern is usually dependent on cylinder bore size and engine rating. For small bore sizes and moderate cylinder pressures, four bolts are often sufficient. As bore size increases and peak cylinder pressures rise (for heavy duty applications) a six bolt pattern is often necessary to distribute the clamping load more evenly and reduce cylinder bore distortion. This has a significant effect on the valve layout and available space for ports. A multivalve layout is often specified to provide increased valve area compared to a conventional 2-valve design. In addition, the injector can be located centrally in the cylinder to provide improved fuel-air mixing and reduced swirl requirement. The overall effect on inner seat area (relative to the seat area of a typical 2-valve design) is shown in Figure 2.5, clearly indicating the advantage of multivalve designs:
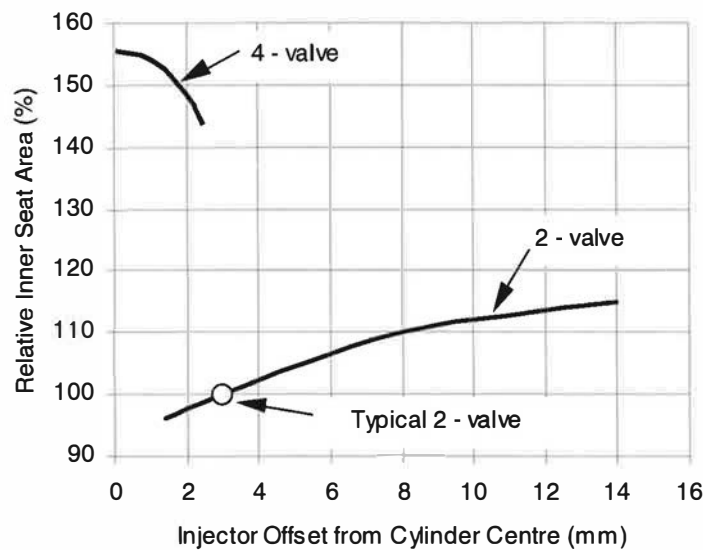
Figure 2.5: Variation of valve area with injector offset

(Gilbert, et. al. 1992)

The inlet port configuration may depend on whether variable air motion is required to match the combustion system over a wide speed range. A siamesed port in which a common entry is divided into two separate ducts for each valve would be easier to package but is not suitable for variable swirl strategies. The swirl requirement of the engine will also influence the port design and valve layout within the constraints imposed by bolting pattern and valve actuation method. Gilbert proposes several options, as shown in Figure 2.6, and recommends the use of a combined helical and directed port configuration with a conventional square crossflow

16

valve layout for applications requiring variable swirl (Figure 2.6(a)). The advantages of this concept include short ports to minimise charge cooling on the inlet side and heat rejection to coolant on the exhaust side. However, twin camshafts are required if long rockers are to be avoided and care must be taken to ensure sufficient cylinder head strength in order to overcome the natural weakness of this design between the inlet and exhaust valves. The configurations shown in Figure 2.6(d) and (e) are recommended for cylinder heads with no variable swirl requirement. Skewing the valves allows the use of a single camshaft and relatively short rockers in both cases.
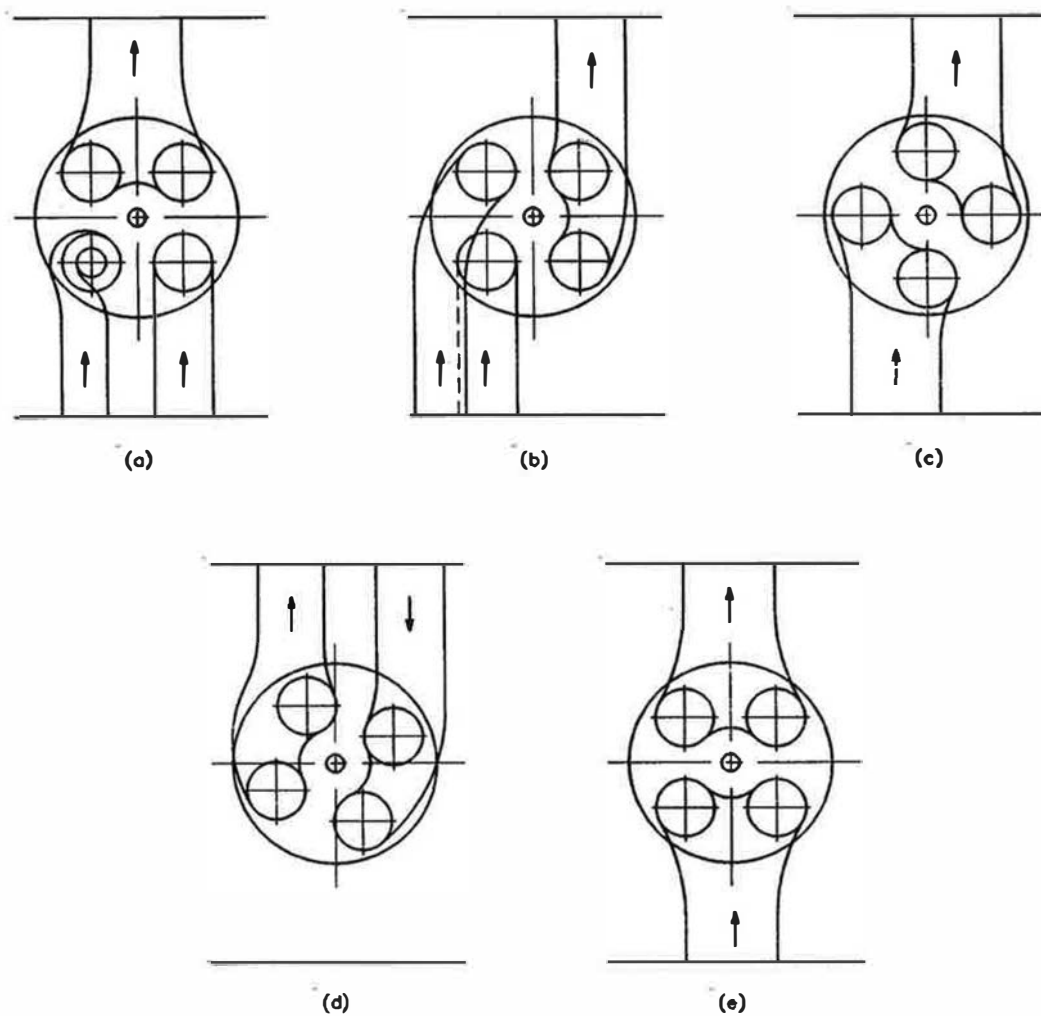
Figure 2.6: Multivalve cylinder head configurations
(Gilbert, et. al. 1992)

An alternative configuration is suggested by Gale (1990) in which the valves are skewed through an angle of approximately 45 degrees to form a diamond pattern, as shown in Figure 2.7(b) . Although the port lengths are slightly longer in this case, they are shorter than the tandem layout shown in Figure 2.6(b). The use of a skewed valve pattern provides well directed inlet ports. In this case the camshaft is mounted in the cylinder block and the inlet ports are constrained by pushrod tubes to the extent that inlet ports from neighbouring cylinders share a single entry. However, this configuration could be used with an overhead camshaft, in which case the inlet port design would be free from these constraints.

(a)   (b)   (c)
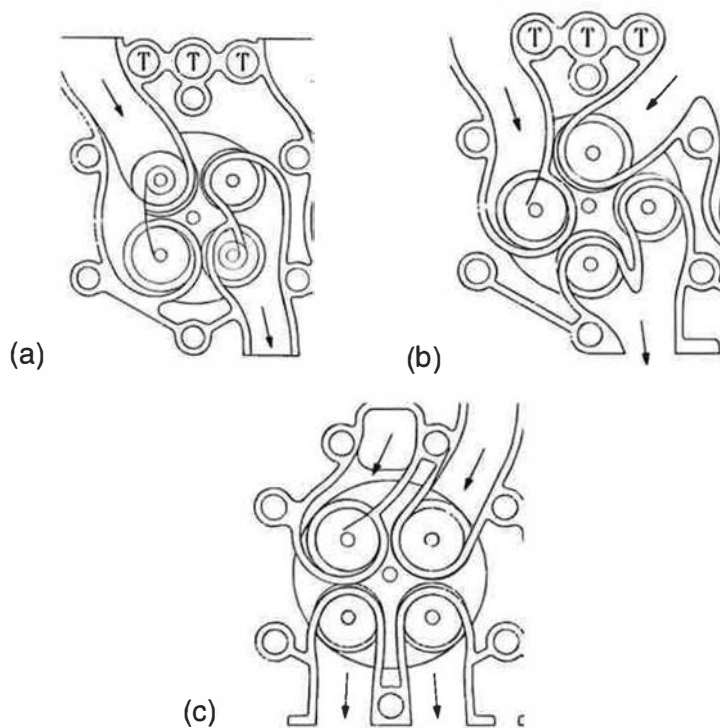
Figure 2.7: Multivalve cylinder head configuration (Gale 1990)

Valve size is dependent on the conflicting requirements of ensuring sufficient valve area whilst retaining adequate valve bridge thickness between valve seat inserts for thermal durability reasons. Also, the injector must be housed in a suitable cast boss or sleeve and be adequately cooled; this effectively pushes the valves towards the edge of the cylinder bore. The shrouding effect of the cylinder walls can be detrimental to port flow performance and a minimum clearance of 1mm is recommended by Gilbert, et. al. (1992). If a machined chamfer on the outer edge of the seat insert is specified, it must not interfere with the sealing bead of the cylinder head gasket. The need for access to the injector for servicing also

influences valvetrain design, which may also have a knock-on effect with regard to valve layout and port configuration.

Cylinder head construction, including material selection and manufacturing processes will influence the cylinder head design. Aluminium alloys are now commonly used for light to medium duty DI diesel engines and a minimum wall thickness of 4mm is specified. It is essential that sufficient cooling of the gas face and other critical zones is achieved. Lubrication of the valvetrain and effective oil draining must also be considered. The design of these features will inevitably constrain the port design. In summary, every one of the design features discussed will have an impact on port design and must be taken into account in developing an optimum solution.

2.4.2 Inlet Port Design

The object of port design is to provide the optimum flow performance for a given air motion requirement. As discussed above, the air motion in HSDI diesel engines is commonly referred to as swirl, due to the rotation of the charge about the cylinder axis. Generally speaking, there are two mechanisms for generating swirl during the intake stroke. The first uses the orientation of the inlet port and location of the inlet valve(s) to direct the incoming charge tangentially into the cylinder. The air is guided by the cylinder walls to form a swirling motion. In order to direct flow in this manner, the port must be designed to encourage a non-uniform velocity profile around the circumference of the inlet valve. Ports of this type are termed "directed". Other methods of generating a non-uniform flow include the use of a masked valve or a deflector wall in the port. Masked valves are seldom used in production, due to the need to prevent valve rotation, which increases valve seat wear. In addition, the offset mass of the valve increases stress on the valvetrain components and valve guide. The second swirl mechanism relies on a helical duct in the port to create a rotational flow about the valve axis upstream of the valve seat. This motion is then transferred into the cylinder during the intake stroke. Under these circumstances, all the available flow area of the valve may be used. A purely "helical" port would be insensitive to valve position in the cylinder, but in practice the swirl response of most helical ports varies to a certain extent with valve location indicating a directed swirl component.

Various port design schemes were discussed in a study by Watts (1964). An investigation into the effect of valve position on the swirl response of directed ports indicated that as the valve was moved from the centre of the cylinder to the outside, the swirl speed measured using a paddle wheel approximately doubled. The port was able to generate swirl even in the central position due to curvature in the inlet duct. The use of offset valve seat machining to create a crescent-shaped recess was also investigated, resulting in the conclusion that this approach could be used to increase swirl at low valve lifts. At this time, masked valves were still in use and it was suggested that the advantage in using this method was that the swirl level could be tuned by adjusting the angular position of the valve. However, the disadvantages outlined above were also noted.

In comparing a range of directed and helical port designs, Monaghan and Pettifer (1981) identified the optimum swirl ratio range for each type. Directed ports were suited to moderate swirl between 1.7Rs and 2.0Rs, whereas helical ports were more efficient over a range from 2.0Rs to 2.3Rs. Differences in the swirl characteristics throughout the valve lift range were also noted; directed ports did not generate significant swirl until high valve lift but helical ports produced a more uniform response throughout the lift range. No conclusions were drawn from this observation, but it would seem logical that the maximum achievable valve lift might be a factor in selecting a particular port type. In comparing the two port types in terms of their suitability for use in production, the insensitivity of helical ports to core shift and other production variations lead the authors to recommend them for use in truck engine applications.

Several researchers have studied the characteristics of helical ports with a significant directed swirl component. Gale (1990) proposed a method using a steady flow rig to quantify the relative contribution of each mode. By testing ports at a fixed valve lift and rotating them through 360 degrees, the swirl response was plotted and typically exhibited a sinusoidal form. The directed swirl component was associated with the varying portion of the plot and the helical component was characterised by a constant offset. The helical/directed swirl balance was ascertained when the directed component was at a maximum and a swirl model was used to determine the optimum balance. The author claimed a good agreement between the model predictions, in which the optimum configuration was when the directed swirl component contributed 30% of the total, and experience with real ports tested over a period

of time. Some of the key parameters in helical port design were identified, as shown in Figure 2.8.
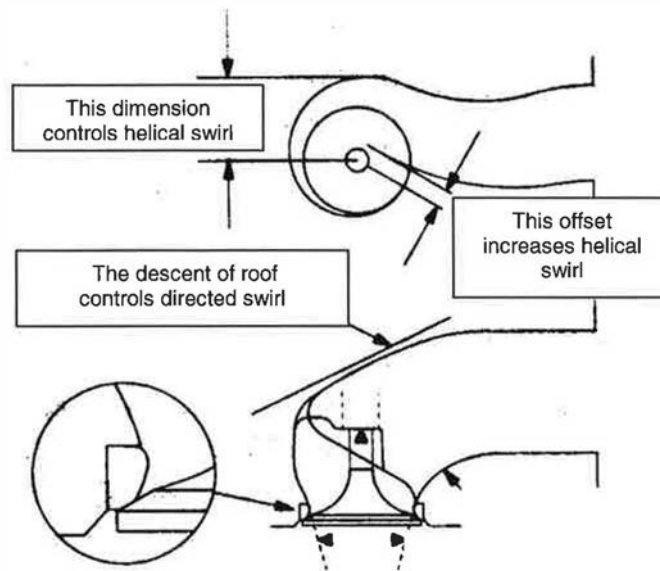
Figure 2.8: Pertinent features of intake port design (Gale 1990)

Li, et. al. (2000) studied the location and orientation of helical and directed inlet ports in a multivalve layout . The authors used the method proposed by Monaghan and Pettifer (1981) to calculate mean flow coefficient (MC_f) and swirl ratio (Rs) from steady flow data. Port orientation in plan view was varied through 360 degrees and combinations of helical and directed ports were interchanged to simulate several layout options. The response in Rs and MC_f for both port types was assessed independently; the results indicated that swirl in directed ports was strongly influenced by orientation but that helical ports were also dependent to a lesser extent. For directed ports, maximum swirl was achieved when the port was orientated tangentially to the cylinder bore. For helical ports, maximum swirl was achieved when the helix entry runner was tangential to the cylinder bore, thus maximising any directed swirl component. Flow coefficient in both cases remained relatively constant. Several multivalve layouts were then assessed, typically by holding the orientation of one port constant whilst varying the other. For layouts of two directed ports, the maximum swirl was achieved when both were arranged tangentially; approximately 1.4Rs was possible. For two helical ports, approximately 2.0Rs was achieved when both were arranged favourably. When both types of ports were used together, approximately 1.7Rs was achievable. The authors then investigated the interference between port flows by defining a simple predictive model of multivalve flow performance (Equation 2.7).

$$C_{f0} = \frac{Q}{nA_v V_o} = \frac{Q_1 + Q_2}{2A_v V_o} = \frac{1}{2}(C_{f1} + C_{f2}) \qquad (2.7)$$

Where C_{f1} and C_{f2} are flow coefficients determined from individual port tests, Q is the total volumetric flow rate from both valves, Q_1 and Q_2 are volumetric flow rates from valves 1 and 2 respectively, A_v is the reference area (inner seat area) and V_o is the velocity head derived from the pressure drop across the inlet port and valve. Implicit in this model is the assumption that the two port flows do not interfere and that individually measured flow rates can be summed to provide the total flow rate. By applying the same method to equation 2.5a, an expression for the mean flow coefficient for a multivalve layout was derived.

$$MC_{f0} = \frac{1}{2}(MC_{f1} + MC_{f2}) \qquad (2.8)$$

A similar approach was employed to indicate the effect of flow interference on swirl, using mean angular momentum, G_m.

$$G_m = \frac{1}{\alpha_2 - \alpha_1} \int_{\alpha_1}^{\alpha_2} G d\alpha \qquad (2.9)$$

Where α_1 is the inlet valve opening time (IVO), α_2 is the inlet valve closing time (IVC) and G is the angular momentum flux (torque) measured using a flow straightening element swirl meter. Therefore, the combined mean angular momentum was also defined assuming a simple summation model.

$$G_{m0} = G_{m1} + G_{m2} \qquad (2.10)$$

The percentage difference between the calculated parameters using this method and the actual measured values were used as indicators of flow interference.

$$\Delta MC_f = \frac{(MC_{f0(meas)} - MC_{f0(calc)})}{MC_{f0(meas)}} \times 100\% \qquad (2.11)$$

22

$$\Delta G_m = \frac{\left(G_{m(meas)} - G_{m(calc)}\right)}{G_{m(meas)}} \times 100\% \qquad (2.12)$$

Typically, ΔMC_f value of 5% were observed, indicating that the model predicted flow performance adequately. However, ΔG_m values of up to 80% indicated that significant swirl interference was taking place. The configurations in which a helical port was located on the upstream valve position exhibited the lowest ΔG_m values and this effect was more prevalent when a tangentially orientated directed port was located on the downstream valve position. By using hot wire anemometry (HWA), the authors investigated these effects and concluded that a strong jet issued from a directed port whereas a more uniform flow pattern issued from the helical port. Therefore, they concluded that the flows from a helical port located on the upstream and a directed port located on the downstream valve would exhibit the lowest amount of interference and was deemed optimal. All other combinations resulted in a greater amount of flow interference and therefore loss in swirl generating potential.

Kawashima, et. al. (1998) investigated several aspects of diesel port design, including helical port design features and combinations of ports in a multivalve layout with port deactivation. In doing so, steady flow measurement and analysis techniques were evaluated and compared. A helical port was defined using nine parameters and an experimental study was conducted to determine their influence on flow characteristics, as shown in Figure 2.9.
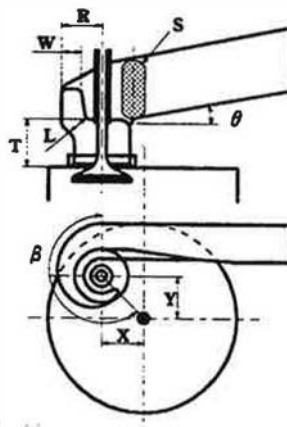
Figure 2.9: Geometric parameters of helical port

(Kawashima, et. al. 1998)

The location of the valve was found to be a significant factor, although due to the geometry of the layout, valve location could be interpreted as port orientation in the configuration suggested previously by Li, et. al. (2000). The authors concluded that it was necessary to position the valve in such a way as to direct the swirling air issuing from the valve along the cylinder wall rather than directly into the cylinder, thereby maximising the effect of any directed flow component. The effect of throat ceiling height (parameter T in Figure 2.9) was also significant in directing air effectively from the helix such that it entered the cylinder tangentially to the cylinder wall. The effect of other parameters was not discussed, although computational meshes for geometry cases with varying scroll angle (parameter β in Figure 2.9) were presented. In estimating multivalve performance, a similar method to that used by Li, et. al. (2000) was adopted; although a combined swirl ratio was defined in preference to mean angular momentum. The former has a more intuitive meaning, since swirl ratio is more widely understood in relation to engine performance. Flow coefficient was defined as in equation 2.1.

$$SR_0 = \frac{SR_1 C_{f1}^{\ 2} + SR_2 C_{f2}^{\ 2}}{(C_{f1} + C_{f2})^2} \qquad (2.13)$$

Where SR is swirl ratio and Cf is the flow coefficient at a given valve lift. The subscripts 0, 1 and 2 denote both ports and each individual port respectively. Note however, that alternative definitions of mean swirl ratio and mean flow coefficient were used in this study; it was assumed that flow rate at each valve lift during induction was proportional to the rate of change of the cylinder volume rather than the calculated flow coefficient at that valve lift. Consequently, flow into the cylinder only occurred between TDC and BDC, not IVO and IVC as assumed in Equation 2.4. Also, since the method was developed originally for paddle wheel swirl meters, torque measurements from an impulse swirl meter were converted to equivalent paddle wheel speeds at each valve lift. Notwithstanding these differences, the overall trends in the study are comparable to those using alternative flow parameter definitions. A good correlation between the predicted performance of twin port systems and test results was claimed. Differences in flow coefficients of the order of +-3% were observed, although larger errors of up to 17% in swirl ratio were in evidence. Some of this error was explained by the effects of cumulative error, since the combined swirl ratios were calculated using flow coefficients. Also, the swirl ratio calculation would be sensitive to measurement

errors associated with the impulse swirl meter torque and mass flow rate. It was found that torque prediction errors were within +-5%. In order to achieve sufficient swirl when one port was deactivated using a throttle valve, a tandem valve arrangement was selected. A helical port was positioned on the downstream valve (furthest from the inlet manifold face) with a directed port on the upstream valve. CFD analysis was used to visualise the in-cylinder flow patterns and the selected configuration exhibited an organised rotational flow around the cylinder periphery. Other port layouts similar to those suggested by Gilbert, et. al. (1992) and later by Li, et. al. (2000) show a greater amount of flow interference. In particular, standard square crossflow valve arrangements with helical and directed ports did not appear to generate any discernible swirl motion.

Until recently, the conventional design guideline approach to port design has received little attention other than to modify the guidelines for use with new applications. Inlet port design and, perhaps more significantly, the development of concept designs through to production solutions, remains a complex iterative process relying on the skill and experience of individuals. Although this in itself does not preclude the application of 3-D parametric design, it is perhaps the combination of this with the clear difficulties in defining a complex, free-form shape such as an inlet port, that has prevented significant improvements in the core process. It is worth noting that this has not prevented innovation in the designs themselves, as shown by the introduction of a number of novel concepts including tumble-generating and top-entry inlet ports for gasoline engines (Hundleby 1989; De Boer 1990). Also, process developments have been achieved through the introduction of supporting activities such as Rapid Prototyping (Raynor 1995; Bertrandt 1999) and Reverse Engineering (Bidanda 1994). The use of 3-D CAD has been influential in bringing about many of these improvements, but the full possibilities have not yet been exploited.

Recent developments in 3-D CAD systems have enabled designers to revisit the possibility of defining parametric inlet ports. This brings about other potential benefits such as design optimisation and improved integration with other parametrically defined components or systems; a clear benefit over the design guidelines approach. The benefits of solid-based parametric modelling were demonstrated by Widener (1995), who proposed a method for defining a helical inlet port. The model was defined using 151 parameters, compared to over 600 in the case of a wireframe model. Furthermore, changes to a single parameter could be made to produce major design variations. This still represented a large number of parameters

with potentially significant effects on port performance. Further rationalisation of such design schemes would be necessary to provide a manageable number of design parameters for use in a knowledge-based model.

2.4.3 Valve Design

The influence of valve geometry on port flow characteristics and in-cylinder motion has been the subject of many investigations (Tanaka 1931; Kastner, et. al. 1963; Bicen and Whitelaw 1984), leading to the identification of several flow regimes at various valve lifts. Variation of the valve seat angle and the introduction of additional angles or radii improved discharge coefficient by preventing flow separation from the seat faces.

Maier, et. al. (2000) conducted a parametric study of inlet valve geometry and investigated the effect of three parameters on the discharge coefficient in an axisymmetric port assembly, using a steady flow test rig. The parameters included in the study are shown in Figure 2.10.
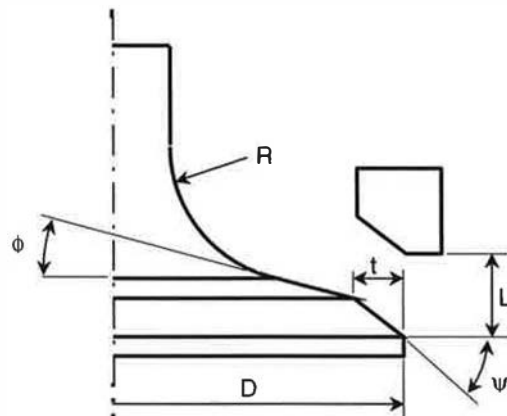
Figure 2.10: Valve geometry (Maier, et. al. 2000)

The discharge coefficient was defined using valve curtain area as the reference for an ideal flow calculation, corresponding to the limiting case in Equation 2.3 when the reference area is cylindrical. The authors claimed that this was the most appropriate reference area since it varied linearly with valve lift and was easier to determine than minimum flow areas at low lift. A preliminary study showed that the discharge coefficients were dependent on the pressure drop applied across the system for low pressure drops, but that this dependency became insignificant at high test pressures (Maier, et. al. 2000a). It was postulated that the

dependency at low pressures was due to the proportional relationship between effective flow area and discharge coefficient. As test pressure and therefore flow velocity increased, flow separation from the seat faces increased, thereby reducing effective flow area. Under turbulent conditions such as those at increased test pressures and higher valve lifts, these effects would be less significant and discharge coefficient would become independent of flow rate and hence test pressure.

Maier then continued to investigate the effects of the three chosen parameters and the results showed that each influenced the discharge coefficient in different ways. Valve cone angle (ϕ) influenced flow separation from the valve seat faces over the entire lift range. Large cone angles improved low-lift flow due to suppression of flow separation from the valve seat face. However, at high valve lifts, smaller cone angles encouraged radial flow and therefore suppressed flow separation from the cylinder head seat face. Fillet radius (R) had little effect for small seat angles, but a larger fillet radius clearly improved low-lift flow in combination with a 45° seat. Again, this was explained by suppressed flow separation at low lifts, due to the combination of a larger seat angle and larger fillet radius. At high lifts and small seat angles, fillet radius did not influence the transition from one flow regime to the next. The influence of seat angle (ψ) was greater than for the other parameters, but was also complex. Generally speaking, 30° seat angles performed well at low valve lifts and 45° seats were superior at high valve lifts. The results supported the earlier findings of Tanaka (1931) in which 30° seats were recommended for engines with low maximum valve lift, although the lift range over which the shallower seat angle was superior was highly dependent on the cone angle. A particular phenomenon was observed for a 40° seat and 0° cone angle in which the discharge coefficient over a mid lift range was extremely high; low and high lift performance was also acceptable. The authors concluded that this was again due to the suppression of flow separation during the transition between flow regimes and could be exploited in high performance engines.

2.5 Knowledge-Based Engineering, Design and Optimisation

Knowledge-Based Engineering (KBE) can be thought of as the integration of parametric design, performance characterisation and (sometimes) optimisation techniques to provide a "virtual prototype" of a product or process (Calkins 1998). Therefore, defining the

relationships between design parameters and performance is a key stage in implementing a virtual prototype. KBE does not necessarily encompass optimisation techniques, in which case a virtual prototype could still be used as a design tool in which the designer interactively modifies model parameters. The performance of the model would be indicated immediately rather than after prototype testing (either experimentally or by a more complex simulation method such as CFD), allowing the designer to make more informed decisions. However, KBE is often used in conjunction with optimisation in order to maximise the benefit.

2.5.1 Statistical Design of Experiments

Statistical design of experiments (DoE) is a technique that can be applied to identify and characterise the significant input parameters in a system. DoE techniques are frequently used to provide structure to an experimental investigation and they can significantly reduce the number of experiments required compared to a more conventional study. Statistical experimental methods such as those suggested by Fisher in the 1930's and subsequently developed by Taguchi (1986) and Box (1990) are now commonly used in a range of engineering activities from product design to process control. Among the large number of books on the subject, Grove and Davis (1992) provide a comprehensive review with an engineering approach. Several relevant case studies are provided. A more conventional approach is taken by Montgomery (1997), who also discusses more general issues in experimental design and statistics. Edwards, et. al. (1997) presented a number of case studies where statistical experimental plans were used for engine development.

The simplest DoE plans are suitable for screening large numbers of parameters in order to determine those that are significant. The responses are usually assumed to be linear and interactions between parameters can be characterised depending on the plan used. However, the construction of the test matrix used to set the parameter values for each experiment often causes unwanted interactions. This situation is known as "confounding" and it may mask the true effects, leading to potentially misleading results. In addition, higher order relationships between inputs and responses cannot be modelled and these may be important. A range of more sophisticated experimental plans have also been developed using DoE; one of the most widely used is the central composite design (CC). This plan provides a second-order model for all the parameters involved in the experiment, plus linear interactions between pairs of parameters. It is necessary to set the test parameters at one of three values (maximum,

28

nominal and minimum) in order to determine second-order effects. However, combinations of parameter settings are used to estimate the overall effect and therefore reduced the number of tests required. A system of three parameters is easy to visualise and is represented in Figure 2.11. If all three parameters were to be varied in all possible combinations, 3^3 tests would be required. However, by limiting the number of tests in a systematic manner, the CC plan reduces the requirement to 15. The arrangement of the test points is balanced around the "centrepoint" (i.e. the centre of the cube representing the design space, where all test parameters are held at their nominal values) and this is an important feature of experimental design. In practical terms, this balance (orthogonality) is desirable in order to accurately represent the contribution of each parameter to the overall response. Orthogonality is required to prevent confounding. In CC plans, centrepoint tests are repeated to maintain orthogonality and to estimate test variability. Randomisation of the order in which tests are performed is also used to prevent systematic errors being interpreted as real parameter effects.

An alternative to the CC plan is the Box-Behnken plan. The two are similar in construction but CC plans tend to be more accurate toward the extremes of the solution space (Box and Draper, 1987). This is because tests are conducted with more parameters simultaneously set at their minimum or maximum values. Second-order models are frequently used in combination with response surface methods (see below) to enable data visualisation and optimisation. A comparison of full-factorial experimental plans in which all parameters are tested in all possible combinations, central composite and Box-Behnken plans is shown in Table 2.1. The number of repeat centrepoints is assumed to be n-1, where n is the number of parameters. Although Box-Behnken plans do not exist in every case, they generally require fewer test runs than the equivalent CC plans for large numbers of parameters.

(a) Full Factorial   (b) Central Composite   (c) Box-Behnken
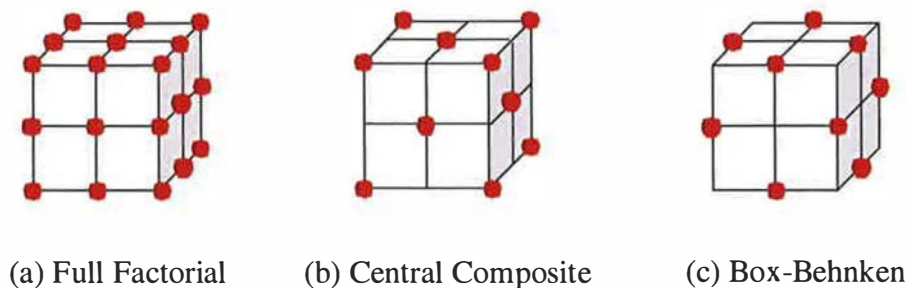
Figure 2.11: Three-parameter quadratic experimental designs

29

Number of parameters, n	Number of tests required (second-order model)		
	Full factorial	Central composite	Box-Behnken
4	$3^4 = 81$	27	27
5	$3^5 = 243$	30	44
6	$3^6 = 729$	49	53
7	$3^7 = 2187$	84	62
8	$3^8 = 6561$	87	-
9	$3^9 = 19683$	154	128

Table 2.1: Comparison of Classical Second-Order DoE Plans

When the most significant input parameters in a system have been identified, possibly by applying a DoE method as described, a common approach is to apply response surface methods (RSM) to visualise and optimise the response of the system. A response surface is usually a graphical representation of the relationship between two input parameters and an output parameter (the response). Therefore, for systems with multiple inputs, several response surfaces may exist. Although the true response of a system may be extremely complex, it is often necessary to limit the response surface to a second-order model (Grove and Davis, 1992). This is deemed to be sufficiently accurate to understand the dominant features of many engineering systems. Dvorak and Hoeskstra (1996) successfully used Taguchi methods and RSM to develop a virtual gasoline engine. Simulation software was used to estimate engine performance and it was concluded that RSM could be used as a robust tool for engine development. Lygoe (1998) applied RSM to develop engine control systems, resulting in a set of look-up tables that could be used to optimise ignition timing whilst avoiding knock. Box & Draper (1987) and Myers & Montgomery (1995) present thorough reviews of RSM.

2.5.2 Neural Networks

Neural networks are an alternative to DoE techniques when a large amount of data is available, or can be produced quickly. As the name suggests, a neural network simulates the brain by "learning" the relationships between input parameters and output responses. By "teaching" the neural network with known inputs and outputs, a model of the system is developed; allowing outputs from untested combinations of inputs to be estimated. The disadvantage is that the results are reliable only after a relatively large data set is used during

the learning process. In addition, the interaction between inputs and the relationships between inputs and outputs are not easily defined. Consequently, the neural network tends to be used as a "black box" and provides little understanding of the underlying system. However, neural networks are superior to other techniques when the system is too complex to define using a limited number of parameters.

Neural networks have been applied to several areas of engine development, most notably in the field of electronic engine control. Beaumont and Frith (1994) applied the technique to control air-fuel ratio in gasoline engines. The advantage of neural networks as compared to RSM in this case was their adaptive learning ability, enabling the engine control system to be re-optimised as engine conditions changed throughout the life of the vehicle. Linear models were considered too simplistic and therefore unable to represent the complex relationships experienced in engine control. The technique has also been applied to engine modelling. Faure (1996) used a simple linear model to predict engine performance and emissions, based on a number of input parameters including in-cylinder motion. However, a small data set was used and the predictions were inaccurate. The use of a neural network was therefore suggested. Brace (1998) and Gamo, et. al. (1999) developed diesel engine performance models based on neural networks, both claiming successful prediction of combustion characteristics and emissions.

2.5.3 Optimisation Methods

In a general sense, the entire design process can be considered as an optimisation process, in which the most suitable solution is selected from a number of alternatives. However, it is more usual to consider optimisation as the systematic improvement of the chosen design. The best solution will depend on a number of parameters that may be varied in order to reach a design goal, subject to constraints (Lee, 1999). From this, it follows that parametric models are therefore particularly suited to optimisation. The simplest methods randomly search the data set and calculate the response in order to find maximum (or minimum) value. These are only suited to very small problems and are seldom used in isolation. The second group of methods, known as guided search methods, evaluate the response at each candidate solution but also the derivatives with respect to each input variable. Therefore, non-optimum results are still useful in indicating the direction in which an optimum may be found. The calculations may be performed classically using calculus but a numerical alternative is

frequently used. Techniques of this type include Newton's method and various modifications. These methods only succeed in finding local optima and care must be taken in using them to avoid misleading results. A combination of a random search and a guided search may be used. The initial conditions for the guided search are selected randomly, then a local optimum is found. If successive searches reach the same solution, it is likely to be a strong local optimum or a true global optimum.

An alternative group of techniques, known as guided random search methods have been developed, examples of which are genetic algorithms and simulated annealing. Genetic algorithms, the principles of which were developed by Holland (1975), produce random mutations from a given design and rely on a type of "natural selection" to determine the optimum. Simulated annealing, developed by Kirkpatrick, et. al. (1983) and Cerny (1985), relies on an analogy between the optimisation of a response to the slow cooling of a solid. Both methods allow the potential solution to "jump out" of false optima and therefore stand a better chance of converging to the global optimum. They are, however, difficult to set up and often require tuning to provide acceptable results in terms of accuracy and time. An overview of design optimisation, including genetic algorithms and simulated annealing techniques is provided by Lee (1999).

2.6   Knowledge-Based Parametric Port Design

Although the use of knowledge-based design techniques has been demonstrated in a range of applications, its use in port design is not widely reported. This is not surprising given the complex and often contradictory performance requirements, coupled with the inherent difficulty in defining realistic port geometry parametrically. However, the lack of consensus on the optimum solution for even the most basic requirements suggests that this is a subject that would benefit greatly from a knowledge-based approach. A range of appropriate evaluation and optimisation techniques are available as discussed in previous sections. In the following section, parametric port design studies published to date are critically reviewed in light of these issues with a view to developing a feasible programme of further work.

There have been three major contributions to this area; all of which take into account the main benefit of parametric design; the ability to rapidly change designs to assess the effect on performance characteristics. In a study of gasoline ports, Blaxill, et. al. (1999) defined a 4-valve inlet port using six design parameters, each varying over three levels. The parametric design scheme is shown in Figure 2.12. The influence of each parameter and interactions between parameters were assessed using DoE techniques and steady-state CFD simulations. A test matrix of 45 test runs was used to identify main effects and interactions between parameters. For each run, the geometry was meshed using approximately 60,000 cells and calculations performed at a single valve lift of 9mm (close to maximum valve lift for a typical automotive 4-valve gasoline engine). The most significant parameters were identified as the port diameter, valve-port angle, distance between the valve seat and the point at which the port curves away towards the entry point, and the angle between each port leg. These were used to define a response surface and it was claimed that the results could be used to aid concept design generation. The simplicity of the model, coarse CFD mesh and single valve lift performance characterisation suggests that the model may be of limited use in practice. The overall influence of the significant parameters is as one might expect but the ability to quantify the effect of each is beneficial and shows that the approach was sound.
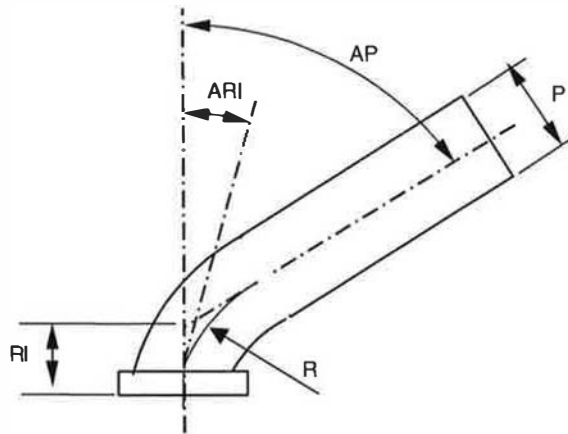
P	Port diameter in the upstream part of the port.
AP	Angle between the valve centre line and the centre line of the upstream part of the port.
ARI	Angle between the valve centre line and the tangent to radius R (see below) at the intersection of the two lines.
RI	Distance between the gas face and the intersection of the valve centre line and the centre line of the upstream part of the port.
RS	Half the angle between the centre lines of each port leg (not shown).
R	Radius of the centre line of the curve joining the upstream part of the port to the valve centre line.

Figure 2.12: Parametric gasoline inlet port DoE parameters (Blaxill, et. al. 1999)

A similar study to investigate the design of a helical diesel port was reported by Brignal and Jin (1999). In this study, eight parameters were defined; three were varied over three levels and the remaining five over two levels. The design scheme is shown in Figure 2.13. DoE techniques were used to provide a test matrix, requiring 16 tests. This was significantly less than the matrix used by Blaxill, et. al. (1999) and was not intended to provide information on interactions between parameters. A single valve lift point was also chosen, this being the valve lift that provided the best signal to noise ratio (defined as the mean swirl speed from 16 tests divided by the standard deviation of the swirl). CFD simulation was then employed to calculate swirl speeds and discharge coefficients for each test run. The CFD models contained 926,000 elements. Of the parameters investigated, only the inner wall lip geometry was found to have a significant influence on flow performance and swirl generation.

34

However, this study was based on an existing port design and most parameters were varied over a small range to investigate design robustness. Other key parameters such as helix features may have been constrained and were therefore not considered as design variables. Larger variations in some of the parameters studied may have resulted in measurable effects.
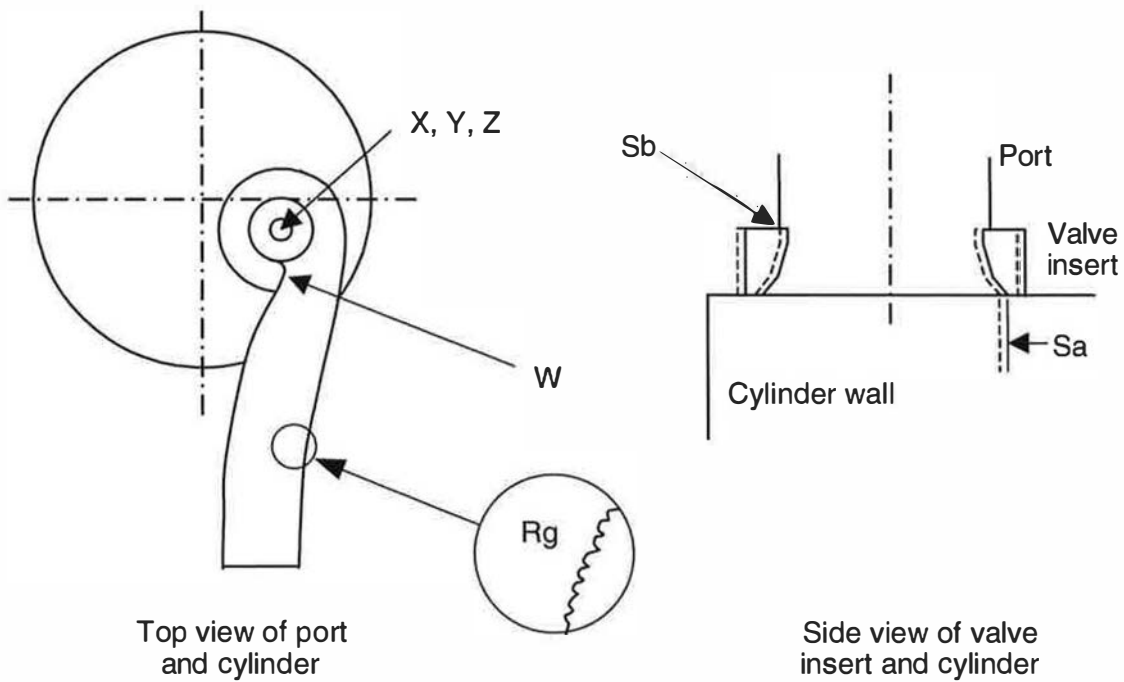
X,Y,Z	Port position in x,y,z directions (relative to cylinder centre)
W	Position and radius of inner wall lip
Sb	Valve seat blend (port throat dia relative to valve insert throat dia)
Rg	Port surface finish
Sa	Valve seat alignment (concentricity of valve seat and port throat)

Figure 2.13: Helical port DoE parameters (Brignal and Jin, 1999)

Page and Blundell (2000) defined a parametric helical inlet port in which the approach angles into the helix were varied in a DoE study. In a similar approach to that of Blaxill, et. al. (1999), steady flow CFD simulations were used to calculate flow and swirl performance. Two discrete valve lift cases were considered. The use of summary parameters integrated over the intake event would have been preferred but the study was limited to individual valve

lift results for expedience. In total, 35 parameters were used to define the design and location of the port and valve, although only four were varied in the DoE study, as shown in Figure 2.14. In an effort to model realistic port geometry, the design parameters were organised into groups representing major features, these being the helix, valve seat, valve, central core and inlet runner. Although the design was representative of modern helical ports, the area around the helix entry was idealised. It is likely that the performance response of a realistic, production-feasible design would be different, although trends in the results would be informative. Rapid model construction was attributed to the use of a common software package for geometry construction and CFD meshing. A quadratic DoE plan consisting of 25 experiments was conducted and the results were used to optimised port geometry for a particular swirl response. The DoE model was validated by comparing predicted swirl speed and flow coefficient with CFD calculations. Generally, the model performed well, with errors typically less than 3%. However, larger errors were observed at low valve lift when the flow pattern was not well established, resulting in unstable swirl. This study represented a significant step forward in the use of parametric modelling and DoE techniques. The logical grouping of design features is a particularly useful concept that helps to structure the design scheme. However, the use of two discrete valve-lift cases remains an issue and the practical application of the results would be limited.
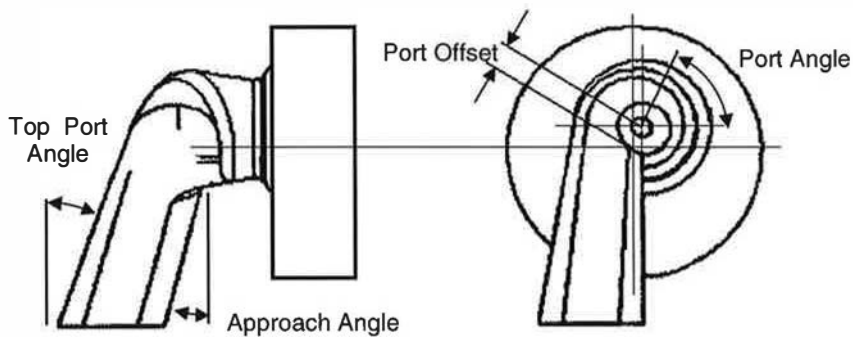
Figure 2.14: Helical port DoE parameters (Page and Blundell, 2000)

An alternative approach was suggested by Affes, et. al. (1998). In this case the inlet port of a 2-valve gasoline engine was defined using only four design parameters (Figure 2.15). In contrast to the indirect method used by other researchers to define the relationships between port geometry and performance, an iterative procedure was used to calculate and then optimise port performance. This was achieved by coupling an optimisation routine with CFD

simulation. The first concept model was automatically meshed and performance characteristics obtained from CFD. Based on these results, the optimisation routine then suggested new values for the parameters and the process was repeated until an optimum point was reached. In this study, the amount of air motion required was set as a performance target and the flow performance was chosen as the optimised parameter. Three levels of air motion were investigated; in each case, an optimum was reached in five design iterations.
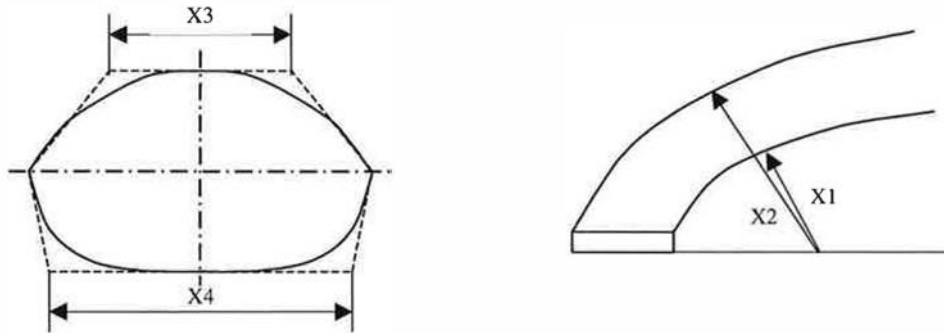
Figure 2.15: Directed inlet port parameters (Affes, et. al. 1998)

In common with the studies discussed previously, the CFD simulations were limited to steady-state and single valve lift. A further simplification involved removing the valve stem and guide from the model to improve the robustness of the automatic meshing routine. Typically, the CFD models contained 37,000 cells. Although this approach differed from those using DoE methods, the use of a parametric port model was a main feature of the study. The use of CFD was also employed to reduce the cost and time associated with procuring test hardware. The repeatability of results was assured, although the accuracy of the results and therefore the effects of each parameter cannot be stated with certainty. In this final study, the use of CFD interactively with parametric design and optimisation is a novel approach, although major compromises have been made to account for limitations in computing power.

3 Development of Generic Inlet Port Models

3.1 Overview

In developing parametric models for use in a knowledge-based system, it was necessary to investigate different engine types and to identify generalised port configurations. Detailed, generic port models were defined using a range of tools and processes. Design features identified in the literature were considered along with alternatives suggested during a "brainstorming" session. Key parameters were chosen to represent the major features within the overall design scheme and each was selected based on its potential influence on port flow capacity and in-cylinder flow characteristics. The number of parameters used to define port geometry was a trade-off between the ability of the model to represent a large number of design features and the number of experiments required to determine the effects of all those features. Statistical Design-of-Experiments (DoE) techniques were used to systematically and efficiently explore the entire design space and an upper limit on the number of parameters that could be investigated was determined by the number of tests required for each experimental plan. The most important parameters were then used to define port geometry using a solid-modelling CAD system. A suitable range of values for each parameter was selected to provide different configurations based on a common generic model. In the following sections, the progression from basic feature identification and selection, through to final parameter definition is presented as a linear process. However, in practice, an iterative approach was necessary in which candidate design schemes were assessed on their suitability for CAD implementation and impact on the size of the experimental plan. In effect, the design scheme, CAD models and experimental plan emerged simultaneously. The reader is asked to bear this in mind throughout sections 3.3, 3.4 and 3.5.

3.2 Selection of Engine Type

Different engine types were investigated in order to determine which, if any, would be more suited to a parametric, knowledge-based design approach. Three types were defined; HSDI diesel, PFI gasoline and direct-injection gasoline. In all cases, multi-valve configurations were assumed, thus representing current design trends. The three primary reasons for this classification are as follows: Firstly, the operational mode of the engine (compression-

ignition or spark-ignition) is synonymous with the fuel type. Secondly, the legislative requirements for engines are also defined according to fuel type and the resulting need to develop new technologies follows the current and future emissions and fuel consumption regulations of each. Finally, in terms of inlet port design and in-cylinder motion, the first two engine types represent a loose division between swirling systems (compression-ignition, diesel) and tumbling systems (spark-ignition, gasoline). In most cases, direct-injection gasoline engines may be grouped with conventional PFI gasoline engines, although the air motion requirements are more complex and therefore this engine type was treated as a separate group. A fourth group of engines potentially complicates matters further; HCCI (homogeneous charge, compression ignition) may be classified separately from the three groups identified above, as HCCI is not fuel-specific. However, HCCI engines currently undergoing development are based on existing gasoline or diesel engines. As such, the structure of the engine (and therefore the port design and basic air motion requirement) is similar to the parent engine. Consequently, these engines could, for the purposes of this study, be categorised according to the engine from which they were derived. From a legislative point of view, it is not yet clear which side of the divide HCCI engines will fall.

Each engine group was assessed according to four criteria; geometry complexity, design constraints, rate of technology change and market share trends (Table 3.1). In terms of geometry, it is more difficult to define a complex port design parametrically. However, it is also potentially more beneficial to do so. Simple port designs are more easily understood and unknown interactions between design features are less likely. It may be possible to successfully optimise a complex port design using current methods, but it may not be feasible given realistic time and cost constraints. HSDI engines usually rely on complex port designs to achieve the required air motion. In comparison to gasoline engines, there is often more scope for different design options but there are also tighter constraints. Packaging inlet ports whilst meeting constraints imposed by the valvetrain, fuel injection system and coolant passages is significantly more challenging in a multi-valve diesel engine. The structure of the cylinder head must also be more rigid due to increased loading, resulting in the need for strengthening ribs, larger diameter cylinder head bolt bosses and/or increased number of head bolts, compared to a similar capacity gasoline engine.

The extent to which engine types are subject to changes in technology, driven by legislation and/or customer demands, also determines the need for improved processes such as

knowledge-based design. In the case of HSDI, the recent development of multi-valve technology and high-pressure fuel injection systems has lead to a rapid change in in-cylinder air motion requirements. In particular, improved control of fuel delivery using common rail (CR) or electronic unit injector (EUI) systems has reduced the need for high levels of swirl. Nevertheless, an appropriate level of air motion is required and engine volumetric efficiency should be maximised to improve fuel economy. Gasoline engines benefited from the shift to multi-valve technology and electronic fuel injection during the early part of the 1990s. Consequently, air-motion requirements are relatively static at present and successful designs for given tumble levels can usually be achieved with a limited amount of development effort. That is not to say that gasoline engines are not undergoing significant development; direct-injection engines have unique air-motion requirements, including high levels of tumble and/or swirl at different operating conditions.

Finally, the extent to which innovative approaches in the design process are likely to be adopted is dependent on how market trends are developing. At present, the popularity of diesel engines in passenger cars is increasing rapidly, particularly in Europe as shown in Figure 3.1. Of course, these trends are closely linked to technological advances that have allowed diesel engines to compete with gasoline in terms of engine performance and refinement, whilst maintaining fuel economy benefits (due to increased compression ratio and therefore thermal efficiency) as has been discussed. Therefore, although it may be the case that the market is driven by a combination of technological developments, marketing effort, legislation and taxation, from a commercial standpoint it is understandable that engine manufacturers concentrate efforts on the engine types that are gaining market share. In this respect, direct-injection gasoline engines are not considered to be particularly attractive; it is thought unlikely that they will represent more than 10% of European passenger vehicle sales in the next decade (Owen, 2001). Although the advantages of direct-injection for gasoline engines are significant, ongoing issues related to fuel effects, exhaust after-treatment and adequate control of the transition between operating modes has limited the adoption of this technology for production vehicles. It is likely that the use of new design processes would be beneficial for direct-injection gasoline engines, especially when considering the unique air motion requirements. However, the greatest benefit would be achieved when more of the fundamental issues have been resolved. HCCI engine development is still in the fundamental research phase, and although opinion varies regarding when HCCI-powered vehicles will reach the market, it is unlikely to be before 2010 (Owen 2001).

	Engine Type		
	DI Diesel (4V HSDI)	PFI Gasoline (4V)	Direct-injection Gasoline
Air motion requirement	Swirl	Tumble	Tumble/Swirl
Port Complexity	High	Low	Variable
Design Constraints	Severe	Moderate	Moderate
Technology Change	Rapid	Slow	Rapid
Market Share (Europe)	32%, rising	68%, falling	<1%, rising

Table 3.1: Engine type comparison
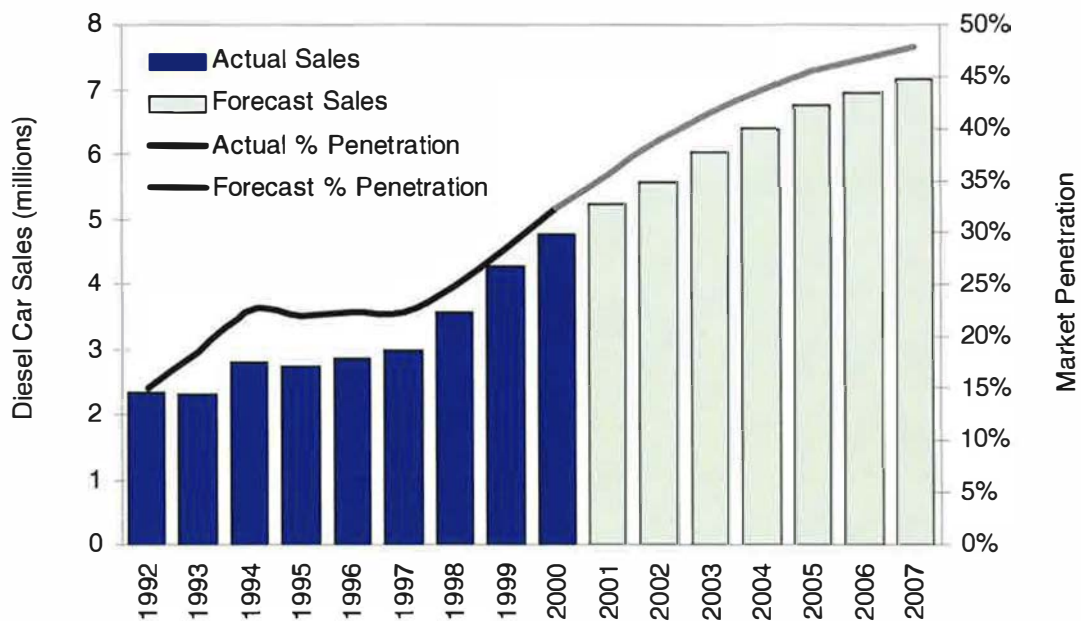
Figure 3.1: Diesel passenger car market trends (Source: AID, 2002)

3.3 Selection of Main Port Types and Geometry Parameters

3.3.1 Selection of Main Port Types

In order to understand the performance characteristics of individual ports before developing a multi-valve model, main port types were defined separately. A comparison could then be made between a performance prediction of a multi-valve configuration, using an additive

41

model similar to those used by other researchers (Li 2000; Kawashima, et al 1998) and the actual performance of a real multi-valve configuration. Directed, or tangential, and helical port types were defined, corresponding to those commonly referred to in the literature. Because of the different swirl generation mechanisms present in each type, it was considered likely that the governing geometry parameters would be different and therefore it was more appropriate to define separate port types in preference to a single, highly complex model. However, some common parameters were considered to be likely and these were incorporated in both port types.

3.3.2 Selection of Port Geometry Parameters

A range of candidate design features were developed by referring to the literature and by conducting a "brainstorming" session. A panel of experienced engine designers and inlet port development experts were consulted during this stage of the study. The raw results from the brainstorming session are shown in Table A1 in Appendix A. Duplicate ideas were removed and notes have been added to clarify the intended meaning of each and to provide a brief explanation of possible airflow effects. These general feature *descriptions* were arranged into main feature *groups,* listed below:

Global Design Features	(e.g. rated speed, bore, stroke)
Operational Features	(e.g. valve profile, port deactivation)
Port Design Features	(e.g. port type, port shape)
Valve Design Features	(e.g. valve size, valve pattern)
Design Constraints	(e.g. injector boss, coolant jacket)

The general feature descriptions were also expanded, if possible, to capture specific design *parameters*. Alternatively, the descriptions were divided into feature *details* to capture individual aspects of the general feature description. Therefore, a three-tiered structure was developed, as shown in figure 3.2. A complete listing of all main feature groups, general feature descriptions and individual parameters or details is provided in Table 3.2. Note that individual parameters tend to have a discrete or continuous quantitative value, whereas the feature details are usually qualitative. For example, cylinder bore diameter is continuously variable parameter between upper and lower bounds, the number of cylinder head bolts is a discrete parameter (usually either 4, 6 or 8) and the valvetrain type can be described in

general terms such as direct/indirect attack and single/twin camshaft. However, even though feature details are qualitative, they are potentially significant in terms of their influence on dependent parameters, either directly or indirectly. The significance of parameter values are generally more obvious. Cylinder bore diameter clearly influences the maximum available inlet valve size and the number of cylinder head bolts constrains the packaging envelope for the inlet ports, thereby influencing the orientation or cross-sectional area of the ports and/or the location of the inlet valves. Valvetrain type, despite being a qualitative feature detail, influences quantitative parameters such as maximum valve lift, lift rate and may also influence inlet valve location if rockers are required.

Feature Groups

A	B
↓	↓

Feature Descriptions

A1	A2	B1	B2
↓	↓	↓	↓

Feature Parameters

A1i	A1ii	A1iii	A2i	A2ii	A2iii	B1i	B1ii	B1iii	B2i	B2ii	B2iii
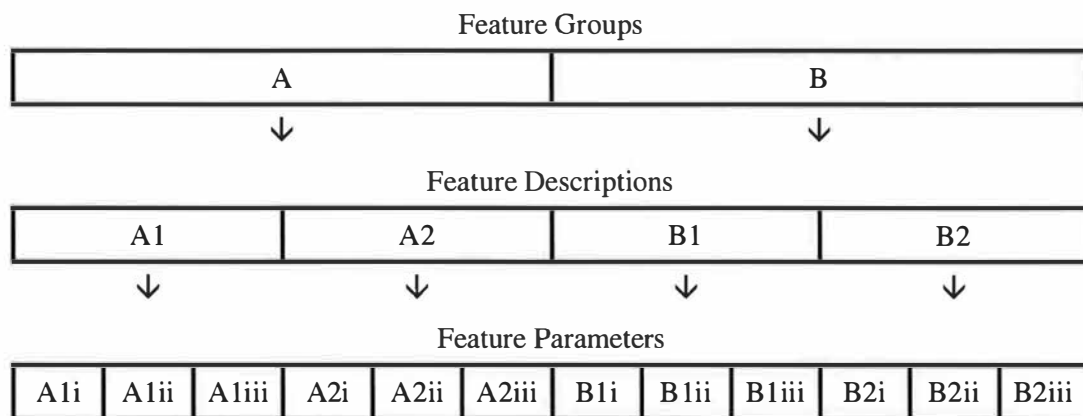
Figure 3.2: Parametric design structure

Each parameter or feature detail was sorted and ranked according to two criteria; firstly, the potential effect of each on port performance characteristics; secondly, the influence that each has on others in order to identify relationships and dependencies between parameters. The second criterion was necessary in order to limit the number of parameters used in the experimental study, whilst capturing the effect of essential features. The parameters identified as being potentially the most important were then compared with published data from related studies.

Feature Group	Feature Description	Feature Detail or Parameter
Global Design Parameters	Cylinder capacity	cylinder bore (mm)
		piston stroke (mm)
	Compression ratio	compression ratio
	Rated speed	rated speed (rev/min)
	Valvetrain type	twin/single cam, direct/indirect
Operational Parameters	Valve lift profile	maximum lift (mm)
		lift rate (acceleration)
		duration (deg crank)
	Valve timing	IVO (deg BTDC), IVC (deg ABDC)
	Port/valve deactivation	fixed/variable swirl (on/off or fully variable)
Valve Design Parameters	Valve stem	diameter (mm)
		unsupported length (mm)
	Valve guide	diameter (mm)
		distance from valve seat (mm)
	Valve size	inner seat diameter (mm)
	Valve pattern	angular location (skew, deg)
		distance from cylinder centre (mm)
		valve bridge widths (mm)
	Valve axis angle	valve axis angle (deg)
	Valve seat	main angle (deg, 30 or 45)
		additional angles (number, deg)
		width (mm)
		recess (mm)
	Valve head	diameter (mm)
		backing profile (radius, mm)
		head thickness (mm)

Table 3.2: Candidate design parameters

Feature Group	Feature Description	Feature Detail (Parameter)
Port Design Parameters	Port configuration	twin/tandem
	Throat cutter	diameter (mm)
		depth (mm)
		profile (angled, curved)
	Valve guide boss	diameter (mm)
		distance from valve seat (mm)
	Port cross-section	area (throat, mm^2)
		area (entry, mm^2)
		shape (entry, mm^2)
	Port entry location	manifold face plane location (y, mm)
		port entry height (z, mm)
		port entry lateral offset (x, mm)
	Port angle	horizontal (deg)
		vertical (deg)
	Port curvature	curve angle (deg)
		radius of curvature (mm)
	Helix geometry	helix width (mm)
		ramp height (mm)
		wrap angle (mm)
External Constraints	Injector/injector boss	location (x-y, mm)
		diameter (mm)
		injector protrusion (mm)
	Heater plug	location (x-y, mm)
		diameter (mm)
		orientation (angle in z, deg)
		protrusion (mm)
	Cylinder head bolt bosses	number (4,6,8)
		pattern (PCD or x-y locations, mm)
		diameter (mm)
	Spring pack	spring seat diameter (mm)
		distance from gas face (mm)
	Coolant jacket features	valve bridge
		injector tip
		gas face under port floor

Table 3.2 (cont.): Candidate Design Parameters

3.3.3 Parameter assessment - Performance Criteria

Following the brainstorming activity, the panel held a further assessment exercise to estimate the likely effect of the selected design parameters on performance characteristics. A description of the possible effects on performance for each parameter are provided in Table 1 in Appendix A. For the purposes of the initial assessment, performance characteristics were described using the terms "flow performance" and "swirl generation". Parameters were assessed according to their combined effect on flow and swirl. Each was scored on a scale of 0 (no effect) to 3 (dominant effect). This method captured both intentional and unintentional relationships between geometry and performance. At this stage, specific performance measures were not used to quantify the results, as this investigation was intended as a screening study. In general, parameters were judged according to their likely effect in a running engine. This interpretation is significant when considering some of the operational parameters. For example, the effect of engine speed on flow performance is significant if inlet mach index (Z, equation 1.5) is used, but has no effect on mean flow coefficient (MCf, equation 1.5a). Similarly, valve size does not have an obvious effect on flow coefficient (Cf, equation 1.1), but is likely to have a major influence on the breathing capacity of a real engine. Consequently, extreme scores tend to be moderated with no obvious dominant parameters. The alternative approach, to judge all parameters according to strict performance criteria, would probably provide a more distinct indication of specific effects on performance, but the risk of a false high or low rating would be greater. It is important to note that the parameter ratings discussed below related to a direct effect on performance and no account was taken of possible indirect effects. These were determined by analysing the relationships between parameters (section 3.3.2). Table 3.3 shows the results for all parameters.

Generally speaking, global design features and constraints did not influence port performance characteristics to a great extent. However, the following were identified as potentially important:

- Cylinder bore
- Piston stroke
- Rated engine speed

All three are fundamental engine design parameters, directly influencing mean inlet gas velocity (MIGV) and therefore volumetric efficiency (Taylor, et. al. 1985). Swirl ratio, derived from steady flow tests, is independent of engine speed but dynamic flow simulations are often performed over a range of speeds due to the influence of time-dependent inlet boundary conditions. Consequently, both parameters must be considered during concept design, even if they are fixed and therefore provide hard constraints that cannot be violated.

Of the operational parameters, those found to be potentially the most important were:

- Maximum valve lift
- Intake duration
- Port or valve deactivation

Inlet valve lift profile is also an important aspect of basic engine design and also has a significant influence on volumetric efficiency. It is required as an input parameter for all but the most simple port flow characterisation techniques and influences both steady flow and dynamic measures of port flow and in-cylinder air motion. In the steady-flow case, the key features are the duration and maximum lift values, since they influence the total flow area throughout the intake event. Valve timings are also important in the dynamic case, due to their variable effects on pressure pulsations in the inlet and exhaust systems over the engine speed range. However, they are not critical at a concept stage, as they can be modified relatively easily during engine development, or indeed optimised with the use of 1-D engine simulation techniques (Gilbert, et. al. 1992). Port or valve deactivation may be used to provide a variable swirl response throughout the engine speed-load range. Although developments in fuel injection systems have lessened the need for swirl enhancement at low engine speeds, variable swirl concepts may be necessary to achieve an increased engine speed range and power output in the future.

It is generally accepted that the features used to describe valve size and location are among the most important in terms of direct influence on performance:

- Valve size (inner seat diameter)

- Valve location (skew angle)
- Valve-to-cylinder centre offset

Valve size, particularly in relation to cylinder bore, directly influences MIGV, as has already been discussed. The location of the inlet valves in the cylinder influences swirl generation due to the effect on any tangential flow component, in both directed and helical ports (Gale 1990; Kawashima 1998; Li 2000). Detail design features such as valve seat geometry also influence flow performance. However, although port design and valve geometry must be compatible and therefore should be considered as a complete system, previous studies have successfully identified the key valve design features (Tanaka 1931; Kastner, et. al. 1963; Maier, et. al. 2000). In addition, it is a relatively straightforward task to design a variety of valve and seat options that may be assessed during port development and interchanged without significantly influencing the design of other components. In comparison, changes in port geometry have an equally large effect on flow characteristics and are influenced to a greater extent by external constraints.

A large number of port design parameters were found to be potentially important. Of those identified, the following were selected to represent the key features:

- Port orientation in plan view
- Port orientation in elevation
- Port curve angle in plan view
- Port curve radius
- Port cross-sectional area
- Helix width
- Helix ramp height
- Helix wrap angle

The orientation of the port in plan view is partially dependent on the valve location. It determines the tangential flow component of inlet ports and therefore governs swirl potential. The port orientation in elevation, described using a characteristic angular measurement, is also influential in determining the direction of the inlet charge as it enters the cylinder. Curvature in the port is likely to be necessary in order to avoid constraints whilst achieving

the required horizontal and vertical approach angles close to the valve. However, the angle through which the port bends and the associated radius of curvature contributes to the overall pressure losses along the length of the port and may also alter the velocity profile through the cross-section. Port cross-sectional area was considered to be of secondary importance when compared to valve size. It is common practice to maintain a constant relationship between valve inner seat diameter, port throat area and port entry area in order to achieve a smooth velocity profile along the port. A constant area equal to the throat is often assumed for concept designs, or a 10% increase in area compared to the throat at the entry may be employed to achieve a small amount of acceleration into the valve area. However, constraints may necessitate localised restrictions in the port and the effect of these is potentially important. In a helical port, the wrap angle would influence the amount of rotational motion generated in the helix section of the port. The ramp height and helix width are likely to be important factors in terms of swirl generation due to their effect on the velocity profile of the air as it enters and flows through the helix section. It is also likely that flow performance will be influenced due to the effect on the cross-sectional area of the port. If a helical port were to be divided into an entry section, comprising of a curved duct similar in shape to that of a directed port, and a helix section, the interactions between helix features and entry section features are likely to be of interest; if a purely helical port form is defined, the overall performance of the port might be less sensitive to those features associated with the entry section (i.e. port orientation and curvature). However, the entry conditions to the helix are governed by these parameters. Alternatively, the overall performance of a port with a "weak" helix might be strongly influenced by entry section parameters because these govern the directed swirl component.

3.3.4 Parameter Assessment - Influence Criteria

Parameters were also compared to determine the relationship between those parameters that were identified as being significant in terms of port performance characteristics, and other parameters, particularly global design features and constraints. Parameters were rated according to the number of parameters they influenced (positive rating) and by the number of parameters that influenced them (negative rating). Parameters within the global design features group were deemed to be independent of all other parameters, consequently the ratings for this group are positive only. Constraints were assumed to be independent of port and valve design features, but could be dependent on global design features (and each other).

The results of the analysis for global design features and constraints are shown in Table 3.4. The total rating for each is shown at the bottom of the table. All other parameters were compared by assuming that each parameter could have a controlling influence on another (Table 3.5). The assumed controlling parameter (arranged along the top row) was compared with all others (left-hand column) and rated accordingly. The total column rating for each parameter, indicating its influencing effect, is shown at the bottom of the table. By summing the row ratings from both tables, the extent to which each parameter is influenced by others is determined. Note that some pairs of parameters influenced each other, indicating co-dependence. In this case, a weighting factor of 0.5 was applied to both to prevent double counting.

Table 3.4 indicates that the global design feature group contains some important influencing parameters. In general, global design features influence all other groups, although valvetrain type primarily influences parameters within the operational and valve design groups. In particular, cylinder bore size dominates, also influencing some of the constraints such as the cylinder head bolt layout. The precise relationship between the global design parameters and the key design parameters that actually determine performance is often complex and there is often a series of intermediate relationships with other parameters. Constraints appear to influence the port design parameters mostly, although parameters within the valve pattern feature are also dependent. The cylinder head bolt pattern has a major impact on port design due to its influence on the available space in the cylinder head. A simple four-bolt pattern is likely to provide several options for routing the ports, whereas six or more bolts may severely restrict space (Gilbert, et. al. 1992). Centrally located injectors are almost universally used, although small offsets may be necessary in order to package other components. Injector location and boss diameter influences the location of the valves in the cylinder bore and may also constrain the port design close to the valve seat. Coolant passages in the cylinder head may also constrain the port design, particularly around the valve bridges and around the injector tip. Some constraints are also influenced by global parameters to a certain extent, as shown by the negative ratings of some constraints.

A general overview of Table 3.5 indicates the major areas of interaction between parameters in the valve and port design feature groups. Interaction between the two groups are relatively few; parameters tend to be co-dependent with others in the same group. Both groups are driven by global design parameters and constraints, as described in the previous section, but

this should not be interpreted as a relationship between parameters in the two groups. Furthermore, the very nature of valve and valve seat geometry dictates that the parameters representing detail design features are co-dependent and are relatively unaffected by the shape and curvature of the port, for example. Note that the *performance response* of a particular design configuration may well be dependent on interactions between port and valve design features. Interactions between valve pattern and various port design parameters are identified, indicating that port geometry is dependent on the location of valves in the cylinder bore, but not necessarily on detailed aspects of the valve design. The general layout of the ports is clearly dependent on the location of the valves in the cylinder bore, in particular parameters such as horizontal port angle, port curve angle and port curve radius. Port cross-sectional area and shape are dependent on a number of constraints, although the primary influence is valve size.

In the valve design group, the dominant parameters are valve skew angle and valve-to-cylinder bore distance. These are also closely related to the co-dependent valve head diameter, seat width, seat angle, inner seat diameter and port throat area parameters. Note that inner seat diameter has been identified as a key parameter in terms of its potential effect on performance. The basic geometrical relationships between these co-dependent valve parameters do suggest that variations in one could capture changes to others, although certain assumptions are necessary. In particular, the effect of valve seat width and angle on the valve head diameter, for a given inner seat diameter, must be simplified. A typical design scheme is shown in Figure 3.4, in which all valve dimensions are related to the valve inner seat diameter.
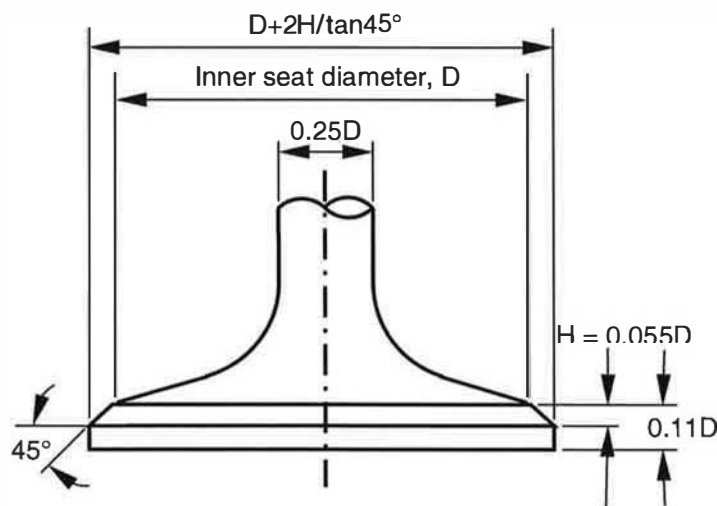
Figure 3.4: Typical inlet valve proportions

In the port design parameters group, a significant degree of co-dependence is evident between parameters describing the overall port layout, as has already been discussed. The relationships between the dimensions of the valve guide boss, valve guide and valve stem are relatively simple, as the diameters of each must be compatible. Essentially, the diameter and unsupported length of the valve stem are the driving parameters, although both are dependent to a large extent on the valve size as shown in Figure 3.4. The operational parameters are also mostly co-dependent, although there are some noteworthy interactions such as that between valve-lift profile and timing, and valve seat dimensions. These relationships govern the clearance between valve head and piston crown around TDC. In order to reduce combustion chamber volume outside the piston bowl and to maintain an acceptable compression ratio, typical clearances of approximately 0.75% of stroke are usually specified, resulting in a limit on the earliest possible IVO and maximum valve lift rate during the early stages of valve lift. A valve seat recess may be used to allow earlier valve opening, but at the expense of flow performance.

The influence of each significant global design parameter on the key valve and port design parameters identified in section 3.3.1, both in terms of direct effects and indirect effects through constraints, is presented in Figures 3.5 to 3.8. In Figure 3.5, the effect of valvetrain type is shown. The influence on valve lift profile is of major importance due to the limitations of certain valvetrain arrangements with regard to the rigidity of the system. Maximum valve lift and valve acceleration may therefore be constrained. A second important relationship, with valve pattern, is also identified. In order to reduce rocker length and therefore increase rigidity, "skewed" valve patterns are required if both the inlet and exhaust valves are actuated from a single camshaft. Alternatively, twin camshaft arrangements may be used, with an associated increase in cost and complexity (Gilbert, et. al. 1992). The influence of piston stroke is shown in Figure 3.6. The primary dependencies are related to valve and port sizing, since piston stroke influences mean inlet gas velocity (MIGV). Clearly, rated engine speed and cylinder bore are also important factors with regard to MIGV, as indicated in Figures 3.7 and 3.8 respectively. Rated engine speed may also influence valve size due to the need for sufficient control of valve motion, although at the relatively low speeds encountered in a HSDI engine (maximum typically 4500 rev/min), high-speed valve motion is unlikely to be the limiting factor. Cylinder bore size influences valve size and location directly, and indirectly influences port geometry parameters due to relationships involving the heater plug and cylinder head bolt constraints. The foregoing

discussion illustrates that although detailed design parameters are likely to influence performance characteristics directly, the global design features that constrain them must also be considered and their effects should be represented in a knowledge-based design system.

| | | | Performance Rating | | |
			Flow	Swirl	Total
Global Design Parameters	cylinder bore			1	1
	piston stroke		2		2
	compression ratio				0
	cylinder head bolt pattern				0
	rated engine speed		2		2
Operational Parameters	valve lift profile	max lift	2	1	3
		lift rate	1	0	1
	valve timing	IVO	1		1
		EVC	1		1
		duration (IVC-IVO)	2		2
	port deact		2	2	4
Valve Design Parameters	valve stem	dia	1		1
		unsupported length			0
	valve guide	dia	1		1
		distance from valve seat	1		1
	valve size	ISD	3	1	4
	valve pattern	skew angle	1	3	4
		location	2	2	4
	no of valves		3		3
	valve angle		2		2
	valve seat	main angle	2		2
		additional angles	1		1
		width			0
		position	1	1	2
	valve head	dia	1		1
		backing profile	2		2
		face profile			0
Port Design Parameters	type	single			0
		tandem			0
		twin			0
	injector pocket	position	1		1
		depth	1		1
	throat cutter	dia	3		3
		depth	2	2	4
		profile	1	2	3
	valve guide boss	dia	1		1
		height from valve seat	1		1
	port cross section	area	2	2	4
		shape	1	2	3
	port entry	position in x,y,z	1	1	2
	port angle (vertical and horizontal)		2	3	5
	port curvature		2	2	4
	helix	ramp angle	1	3	4
		wrap angle	1	3	4
		inner wall position	1	3	4
		ramp width	2	3	5
	bifurcation	position	1		1
		profile			0
		radius	1		1

Table 3.3: Parameter assessment – performance criteria

		Global Design Parameters					External constraints													
		Cylinder Capacity		Compression Ratio	Rated Speed	Valvetrain Type, Indirect/direct	Injector/ injector boss			Heater plug				Cylinder head bolt bosses			Spring pack		Coolant jacket features		
		Bore (mm)	Stroke (mm)	Compression Ratio	Rated Speed (rev/min)	Twin/single cam, Indirect/direct	location (xy, mm)	diameter (mm)	injector protrusion (mm)	location (xy, mm)	diameter (mm)	orientation (angle in z, deg)	protrusion (mm)	number (4,6,8)	pattern (PCD or x/y locations, mm)	diameter (mm)	spring seat diameter (mm)	distance from gas face (mm)	valve bridge	injector tip	gas face under port floor
Valve Lift Profile	max lift (mm)	·	·	·	·	●	·	·	·	·	·	·	·	·	·	·	·	·	·	·	·
	lift rate (acceleration)	·	·	·	●	●	·	·	·	·	·	·	·	·	·	·	·	·	·	·	·
	duration (deg crank)	·	·	·	·	·	·	·	·	·	·	·	·	·	·	·	·	·	·	·	·
Valve timing	IVO (deg BTDC), IVC (deg ABDC)	·	·	·	·	·	·	·	·	·	·	·	·	·	·	·	·	·	·	·	·
Port/valve deactivation	fixed/variable swirl	·	·	·	·	●	·	·	·	·	·	·	·	·	·	·	·	·	·	·	·
Valve stem	diameter (mm)	·	·	·	·	·	·	·	·	·	·	·	·	·	·	·	·	·	·	·	·
	unsupported length (mm)	·	·	·	·	·	·	·	·	·	·	·	·	·	·	·	·	·	·	·	·
Valve guide	diameter (mm)	·	·	·	·	·	·	·	·	·	·	·	·	·	·	·	·	·	·	·	·
	distance from valve seat (mm)	·	·	·	·	·	·	·	·	·	·	·	·	·	·	·	·	·	·	·	·
Valve size	inner seat diameter (mm)	●	●	·	●	·	●	●	·	·	·	·	·	·	·	·	·	·	·	·	·
Valve pattern	angular location (skew, deg)	·	·	·	·	●	●	·	·	●	●	·	·	●	●	·	·	·	·	·	·
	distance from cylinder centre (mm)	●	·	·	·	·	●	●	·	·	·	·	·	·	·	·	·	·	·	●	·
	valve bridges (mm)	●	·	·	·	·	·	·	·	●	●	·	·	·	·	·	·	·	●	·	·
Valve axis angle	valve axis angle (deg)	·	·	●	·	●	·	·	·	·	·	·	·	·	·	·	·	·	·	·	·
Valve seat	main angle (deg, 30 or 45)	·	·	·	·	·	·	·	·	·	·	·	·	·	·	·	·	·	·	·	·
	additional angles (number, deg)	·	·	·	·	·	·	·	·	·	·	·	·	·	·	·	·	·	·	·	·
	width (mm)	·	·	·	·	·	·	·	·	·	·	·	·	·	·	·	·	·	·	·	·
	recess (mm)	·	·	●	·	·	·	·	·	·	·	·	·	·	·	·	·	·	·	·	·
Valve head	diameter (mm)	●	·	·	·	·	·	·	·	·	·	·	·	·	·	·	·	·	·	·	·
	backing profile (radius, mm)	·	·	·	·	·	·	·	·	·	·	·	·	·	·	·	·	·	·	·	·
	head thickness (mm)	·	·	●	·	·	·	·	·	·	·	·	·	·	·	·	·	·	·	·	·

Table 3.4: Parameter assessment – influence of global design parameters and external constraints (part 1)

Table 3.4: Parameter assessment – influence of global design parameters and external constraints (part 2)

Component	Parameter	Bore (mm)	Stroke (mm)	Compression Ratio	Rated Speed (rev/min)	Twin/single cam, Indirect/direct	Injector location (xy, mm)	Injector diameter (mm)	injector protrusion (mm)	Heater location (xy, mm)	Heater diameter (mm)	orientation (angle in z, deg)	protrusion (mm)	number (4,6,8)	pattern (PCD or x/y locations, mm)	diameter (mm)	spring seat diameter (mm)	distance from gas face (mm)	valve bridge	injector tip	gas face under port floor
		Global Design Parameters					External constraints														
		Cylinder Capacity					Injector/injector boss			Heater plug				Cylinder head bolt bosses			Spring pack		Coolant jacket features		
Port configuration	twin/tandem	·	·	·	·	·	·	·	·	·	·	·	·	●	●	●	·	·	·	·	·
Throat cutter	diameter (mm)	·	·	·	·	·	·	·	·	·	·	·	·	·	·	·	·	·	·	·	·
	depth (mm)	·	·	·	·	·	·	·	·	·	·	·	·	·	·	·	·	·	·	·	·
	profile (angled, curved)	·	·	·	·	·	·	·	·	·	·	·	·	·	·	·	·	·	·	·	·
Valve guide boss	diameter (mm)	·	·	·	·	·	·	·	·	·	·	·	·	·	·	·	·	·	·	·	·
	distance from valve seat (mm)	·	·	·	·	·	·	·	·	·	·	·	·	·	·	·	·	·	·	·	·
Port cross-section	area (throat, mm^2)	●	●	·	●	·	·	·	·	·	·	·	·	·	·	·	·	·	·	·	·
	area (entry, mm^2)	●	●	·	●	·	·	·	·	·	·	·	·	·	·	·	·	·	·	·	·
	shape (entry, mm^2)	·	·	·	·	·	·	·	·	·	·	●	·	·	●	·	·	·	·	·	●
Port entry location	manifold face plane location (y, mm)	·	·	·	·	·	·	·	·	·	·	·	·	·	·	·	·	·	·	·	·
	port entry height (z, mm)	·	·	·	·	·	·	·	·	●	●	●	·	·	·	·	·	·	·	·	·
	port entry lateral offset (x, mm)	·	·	·	·	·	·	·	·	●	●	●	·	●	●	·	·	·	·	·	·
Port angle	horizontal (deg)	·	·	·	·	·	·	·	·	·	·	·	·	●	●	·	·	·	·	·	·
	vertical (deg)	·	·	·	·	·	·	·	·	●	●	●	·	·	·	·	·	●	·	·	●
Port curvature	curve angle (deg)	·	·	·	·	·	·	·	·	·	·	·	·	●	●	●	●	·	·	·	·
	radius of curvature (mm)	·	·	·	·	·	·	·	·	·	·	·	·	●	●	●	●	·	·	·	·
Helix geometry	helix width (mm)	·	·	·	·	·	·	·	·	●	●	·	·	·	·	·	·	·	●	●	·
	ramp height (mm)	·	·	·	·	·	·	·	·	·	·	●	·	·	·	·	·	●	·	·	·
	wrap angle (mm)	·	·	·	·	·	·	·	·	·	·	·	·	·	·	·	·	·	·	·	·
Injector/injector boss	location (xy, mm)	·	·	·	·	·		·	·	·	·	·	·	·	·	·	·	·	·	●	·
	diameter (mm)	·	·	·	·	·	·		·	·	·	·	·	·	·	·	·	·	·	·	·
	injector protrusion (mm)	·	·	●	·	·	·	·		·	·	·	·	·	·	·	·	·	·	·	·
Heater plug	location (xy, mm)	●	·	·	·	·	·	·	·		·	·	·	·	●	·	·	·	·	·	·
	diameter (mm)	·	·	·	·	·	·	·	·	·		·	·	·	·	·	·	·	·	·	·
	orientation (angle in z, deg)	·	·	·	·	·	·	·	·	·	·		·	·	·	·	·	·	·	·	·
	protrusion (mm)	·	·	●	·	·	·	·	·	·	·	·		·	·	·	·	·	·	·	·
Cylinder head bolt bosses	number (4,6,8)	·	·	·	·	·	·	·	·	·	·	·	·		·	·	·	·	·	·	·
	pattern (PCD or x/y locations, mm)	●	·	·	·	·	●	·	·	·	·	·	·	·		·	·	·	·	·	·
	diameter (mm)	●	·	·	·	·	·	·	·	·	·	·	·	·	·		·	·	·	·	·
Spring pack	spring seat diameter (mm)	·	·	·	·	·	·	·	·	·	·	·	·	·	·	·		·	·	·	·
	distance from gas face (mm)	·	·	·	·	·	·	·	·	·	·	·	·	·	·	·	·		·	·	·
Coolant jacket features	valve bridge	·	·	·	·	·	·	·	·	·	·	·	·	·	·	·	·	·		·	·
	injector tip	●	·	·	·	·	·	·	·	·	·	·	·	·	·	·	·	·	·		·
	gas face under port floor	·	·	·	·	·	·	·	·	·	·	·	·	·	·	·	·	·	·	·	
Parameter Rating ("influencing")		9	3	5	4	5	4	2	0	7	6	5	0	6	8	3	2	2	2	3	2

Table 3.5: Parameter assessment – interaction of valve and port design parameters (part 1)

Design Parameter Rating ("influenced")	5	4	3	3	0	2	3	1	1	5	6	6	7	3	3	2	6	1	6	0	1

Port Design Parameters

		max lift (mm)	lift rate (acceleration)	duration (deg crank)	IVO (deg BTDC), IVC (deg ABDC)	fixed/variable swirl	diameter (mm)	unsupported length (mm)	diameter (mm)	distance from valve seat (mm)	inner seat diameter (mm)	angular location (skew, deg)	distance from cylinder centre (mm)	valve bridges (mm)	valve axis angle (deg)	main angle (deg, 30 or 45)	additional angles (number, deg)	width (mm)	recess (mm)	diameter (mm)	backing profile (radius, mm)	head thickness (mm)

Row labels (Port Design Parameters):
- Helix geometry: wrap angle (mm); ramp height (mm); helix width (mm)
- Port curvature: radius of curvature (mm); curve angle (deg)
- Port angle: vertical (deg); horizontal (deg)
- Port entry location: port entry lateral offset (x, mm); port entry height (z, mm); manifold face location (y, mm)
- Port cross-section: shape (entry, mm²); area (entry, mm²); area (throat, mm²)
- Valve guide boss: distance from valve seat (mm); diameter (mm)
- Throat cutter: profile (angled, curved); depth (mm); diameter (mm)
- Port configuration: twin/tandem

Row labels (Valve Design Parameters):
- Valve head: head thickness (mm); backing profile (radius, mm); diameter (mm)
- Valve seat: recess (mm); width (mm); additional angles (number, deg); main angle (deg, 30 or 45)
- Valve axis angle: valve axis angle (deg)
- Valve pattern: valve bridge (mm); distance from cylinder centre (mm); angular location (skew, deg)
- Valve size: inner seat diameter (mm)
- Valve guide: distance from valve seat (mm); diameter (mm)
- Valve stem: unsupported length (mm); diameter (mm)

Row labels (Operational Parameters):
- Port/valve deactivation: fixed/variable swirl
- Valve timing: IVO (deg BTDC), IVC (deg ABDC)
- Valve Lift Profile: duration (deg crank); lift rate (acceleration); max lift (mm)

56

Table 3.5: Parameter assessment – interaction of valve and port design parameters (part 2)

Interaction matrix. Influencing parameters (columns) are numbered below; the small dot (·) marks a cell with no/minimal interaction, a filled circle (●) marks a significant interaction, and a shaded cell (▒) marks the self/diagonal cell.

Column legend (influencing parameters):

1 = Port configuration: twin/tandem
2 = Throat cutter: diameter (mm)
3 = Throat cutter: depth (mm)
4 = Throat cutter: profile (angled, curved)
5 = Valve guide boss: diameter (mm)
6 = Valve guide boss: distance from valve seat (mm)
7 = Port cross-section: area (throat, mm²)
8 = Port cross-section: area (entry, mm²)
9 = Port cross-section: shape (entry, mm²)
10 = Port entry location: manifold face plane location (y, mm)
11 = Port entry location: port entry height (z, mm)
12 = Port entry location: port entry lateral offset (x, mm)
13 = Port angle: horizontal (deg)
14 = Port angle: vertical (deg)
15 = Port curvature: curve angle (deg)
16 = Port curvature: radius of curvature (mm)
17 = Helix geometry: helix width (mm)
18 = Helix geometry: ramp height (mm)
19 = Helix geometry: wrap angle (mm)

Design Parameter Rating ("influenced") – top header (columns 1–19):
5 · 0 · 1 · 1 · 1 · 1 · 1 · 5 · 7 · 1 · 5 · 8 · 10 · 9 · 12 · 12 · 9 · 5 · 2

Port Design Parameters

Group	Parameter	1	2	3	4	5	6	7	8	9	10	11	12	13	14	15	16	17	18	19	Rating ("influencing")
Helix geometry	wrap angle (mm)	·	·	·	·	·	·	·	·	·	·	·	·	·	·	·	·	·	·	▒	2
Helix geometry	ramp height (mm)	·	·	·	·	·	·	·	·	·	·	●	·	·	·	·	·	·	▒	·	1
Helix geometry	helix width (mm)	·	·	·	·	·	·	·	·	·	·	·	·	·	·	·	·	▒	·	·	1
Port curvature	radius of curvature (mm)	·	·	·	·	·	·	·	·	·	·	·	·	●	·	●	▒	·	·	·	2
Port curvature	curve angle (deg)	·	·	·	·	·	·	·	·	·	·	·	·	●	●	▒	●	·	·	·	2
Port angle	vertical (deg)	·	·	·	·	·	·	·	·	·	·	·	·	●	▒	·	·	·	·	·	1
Port angle	horizontal (deg)	·	·	·	·	·	·	·	·	·	·	·	·	▒	·	●	●	·	·	·	2
Port entry location	port entry lateral offset (x, mm)	·	·	·	·	·	·	·	·	·	·	·	▒	·	·	●	●	·	·	·	3
Port entry location	port entry height (z, mm)	·	·	·	·	·	·	·	·	·	·	▒	·	·	·	·	●	●	·	·	3
Port entry location	manifold face plane location (y, mm)	·	·	·	·	·	·	·	·	·	▒	·	·	●	·	●	●	·	·	·	3
Port cross-section	shape (entry, mm²)	·	·	·	·	·	·	●	·	▒	·	·	·	·	·	·	·	·	·	·	1
Port cross-section	area (entry, mm²)	·	·	·	·	·	·	●	▒	●	·	·	·	·	·	·	·	·	·	·	3
Port cross-section	area (throat, mm²)	·	·	·	·	·	·	▒	·	·	·	·	·	·	·	·	●	●	·	·	3
Valve guide boss	distance from valve seat (mm)	·	·	·	·	·	▒	·	·	·	·	●	·	·	·	·	●	·	·	·	2
Valve guide boss	diameter (mm)	·	·	·	·	▒	·	●	·	·	·	·	·	●	·	·	·	·	·	·	2
Throat cutter	profile (angled, curved)	·	·	●	▒	·	·	·	·	·	·	·	·	●	·	·	·	·	·	·	2
Throat cutter	depth (mm)	·	·	▒	●	·	·	·	·	·	·	·	·	●	·	·	·	·	·	·	2
Throat cutter	diameter (mm)	·	▒	·	·	·	·	·	·	·	·	·	·	·	·	·	·	·	·	·	0
Port configuration	twin/tandem	▒	·	·	·	·	·	·	●	●	·	●	●	●	·	●	●	·	·	·	8

Valve Design Parameters

Group	Parameter	1	2	3	4	5	6	7	8	9	10	11	12	13	14	15	16	17	18	19	Rating ("influencing")
Valve head	head thickness (mm)	·	·	·	·	·	·	·	·	·	·	·	·	·	·	·	·	·	·	·	4
Valve head	backing profile (radius, mm)	·	·	·	·	·	·	·	·	·	·	·	·	·	·	·	·	·	·	·	0
Valve head	diameter (mm)	·	·	·	·	·	·	·	·	·	·	·	·	·	·	·	·	·	·	·	6
Valve seat	recess (mm)	·	·	·	·	·	·	·	·	·	·	·	·	·	·	·	·	·	·	·	2
Valve seat	width (mm)	·	·	·	·	·	·	·	·	·	·	·	·	·	·	·	·	·	·	·	1
Valve seat	additional angles (number, deg)	·	·	·	·	·	·	·	·	·	·	·	·	·	·	·	·	·	·	·	4
Valve seat	main angle (deg. 30 or 45)	·	·	·	·	·	·	·	·	·	·	·	·	·	·	·	·	·	·	·	3
Valve axis angle	valve axis angle (deg)	·	·	·	·	·	·	·	·	·	·	·	·	·	·	·	·	·	·	·	11
Valve pattern	valve bridge (mm)	·	·	·	·	·	·	·	·	·	·	·	·	●	·	●	●	●	·	●	11
Valve pattern	distance from cylinder centre (mm)	·	·	·	·	·	·	·	·	·	·	·	·	●	·	●	●	●	·	·	7
Valve pattern	angular location (skew, deg)	●	·	·	·	·	·	·	·	●	·	·	·	●	·	●	●	●	·	·	3
Valve size	inner seat diameter (mm)	·	·	·	·	·	·	·	●	·	·	·	·	·	·	·	·	·	·	·	1
Valve guide	distance from valve seat (mm)	·	·	·	·	·	●	·	·	·	·	·	·	·	·	·	·	·	·	·	2
Valve guide	diameter (mm)	·	·	·	·	●	·	·	·	·	·	·	·	·	·	·	·	·	·	·	2
Valve stem	unsupported length (mm)	·	·	·	·	·	·	·	·	·	·	·	·	·	·	·	·	·	·	·	2
Valve stem	diameter (mm)	·	·	·	·	·	·	·	·	·	·	·	·	·	·	·	·	·	·	·	2

Operational Parameters

Group	Parameter	1	2	3	4	5	6	7	8	9	10	11	12	13	14	15	16	17	18	19	Rating ("influencing")
Port/valve deactivation	fixed/variable swirl	●	·	·	·	·	·	·	●	●	·	·	●	·	·	·	·	·	·	·	4
Valve timing	IVO (deg BTDC), IVC (deg ABDC)	·	·	·	·	·	·	·	·	·	·	·	·	·	·	·	·	·	·	·	2
Valve Lift Profile	duration (deg crank)	·	·	·	·	·	·	·	·	·	·	·	·	·	·	·	·	·	·	·	2
Valve Lift Profile	lift rate (acceleration)	·	·	·	·	·	·	·	·	·	·	·	·	·	·	·	·	·	·	·	5
Valve Lift Profile	max lift (mm)	·	·	·	·	·	·	·	·	·	·	·	·	·	·	·	·	·	·	·	2

57

Figure 3.5: Influence of valvetrain type
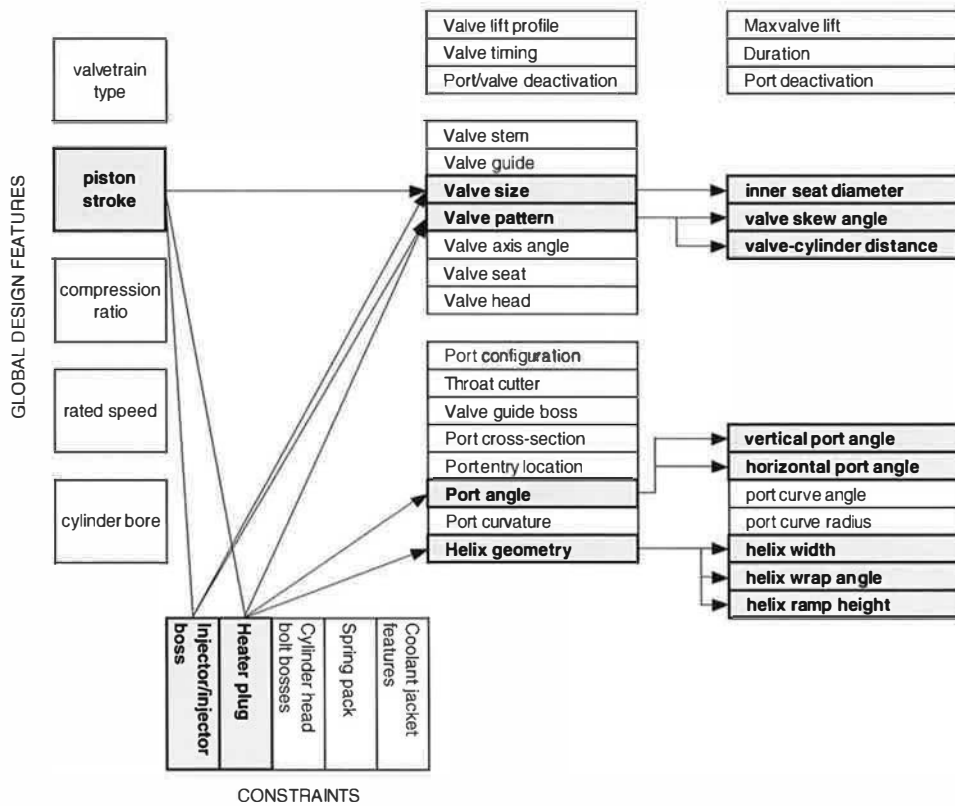
Figure 3.6: Influence of piston stroke

58
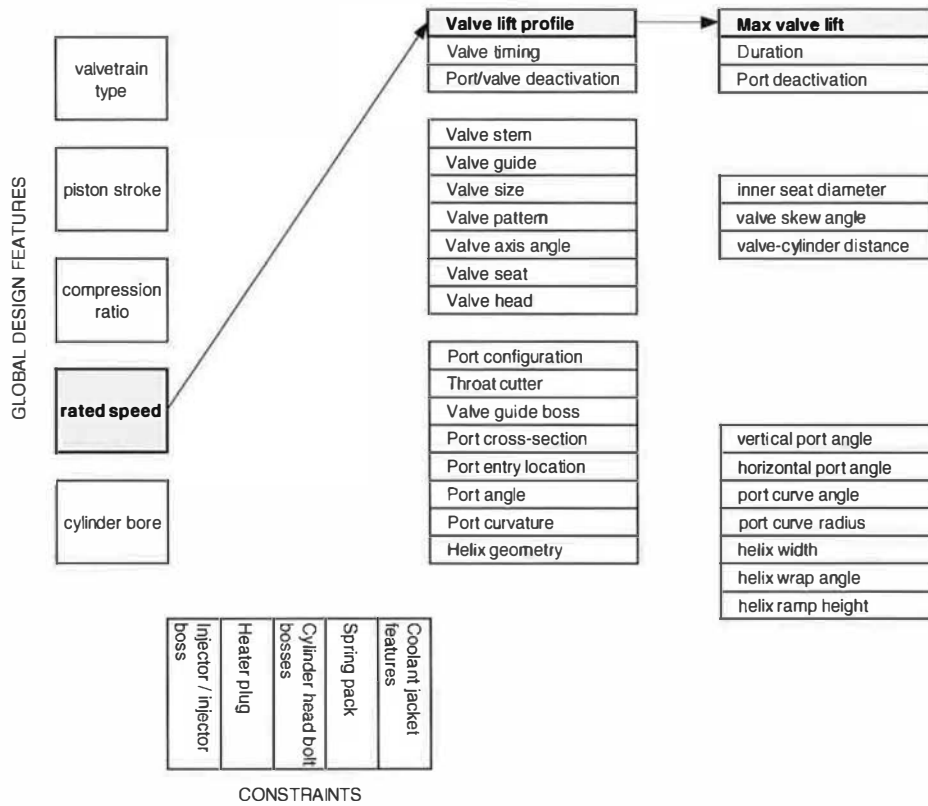
Figure 3.7: Influence of rated speed
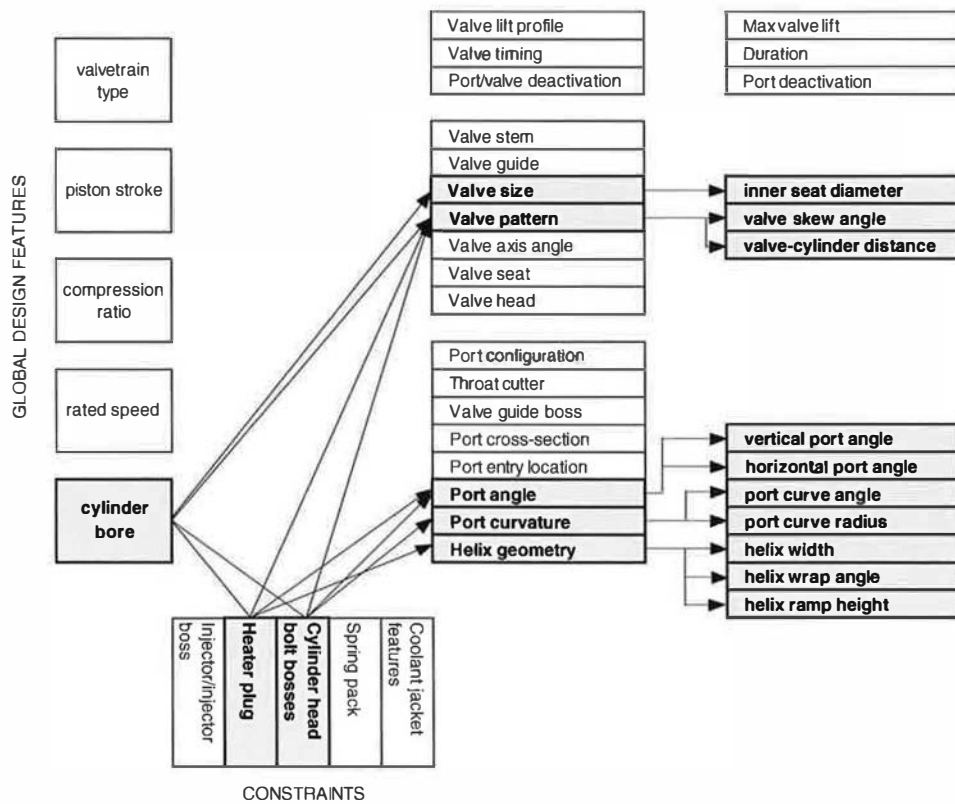
Figure 3.8: Influence of cylinder bore

59

3.3.5 Comparison with Published Data

The parameters identified in section 3.3 may be compared with the findings of four recent studies. Blaxill, et. al. (1999) defined a simple 4V gasoline inlet port and studied the effect of six design parameters on flow performance and tumble generation. The most significant parameters were port diameter, vertical approach angle (relative to the valve axis) and the angle between each port leg (i.e. the horizontal approach angle). Although Blaxill was concerned with tumble generation rather than swirl, the identification of key features representing the orientation and shape of the port are consistent with the initial analysis presented here. The exception to this is the lack of parameters that may be significant in a running engine (such as maximum valve lift). This is because performance was characterised at a single valve lift, with steady flow conditions assumed. In a study of a single helical port, Brignal and Jin (1999) proposed several design parameters, including valve location relative to the cylinder, port surface finish and inlet valve concentricity. The geometry of the port in the helix region was the only parameter found to have a significant influence on flow performance and swirl generation. However, this study was based on an existing port design and most parameters were varied over a small range to investigate design robustness rather than a large range of possible design configurations. Other key parameters may have been constrained and were therefore not considered as design variables. Larger variations in some of the parameters studied may have resulted in measurable effects. Affes, et. al. (1998) used parameters to define the vertical orientation of the port. Variations in these parameters resulted in significant effects on both flow performance and swirl generation. Finally, Page and Blundell (2000), investigated the effect of four design parameters on helical port performance. The location of the inlet valve and the orientation of the inlet port (in horizontal and vertical planes) were varied in a parametric design scheme. In summary, the proposed parameters are consistent with those studied previously and the apparently low significance of some can be attributed to the details of the particular study.

3.4 Detailed Parameter Definition

3.4.1 Valve Layout

The development of design schemes used to define the layout of the inlet valves in the cylinder bore is shown in Figure 3.9. These represent the important design parameters identified in the previous section, including valve size and location. Both these terms were defined using non-dimensional parameters in order to produce a generalised scheme.

$$\text{Non-dimensional inlet valve size, } Dn = \frac{D}{B} \qquad\qquad (3.1)$$

$$\text{Non-dimensional valve offset (eccentricity), } E = \frac{Y}{B - D_O} \qquad\qquad (3.2)$$

Y is the offset distance between the cylinder centre and inlet valve centre, B is the cylinder bore diameter, D_o is the outer diameter of the inlet valve head and D is the inlet valve inner seat diameter. Therefore, E=0 indicates a valve concentric with the cylinder and E=0.5 indicates an inlet valve located on the outer edge of the cylinder bore. Note that the simplified scheme represented in Figure 3.9(a) illustrates the single valve layout used to investigate the performance of each individual port type; the modified scheme shown in Figure 3.9(b) was then developed to define the generalised multi-valve layout. Three angular measurements are used to define the location of the valves in the cylinder bore. In the single valve case, the angular location of the valve is arbitrary unless the port orientation is known. In the multi-valve case, two angles are required to define the angular position of each valve centre relative to a common datum. The angle *As1* defines the skew angle of the valve layout and is the angle between a line parallel to the crankshaft (horizontal in Figure 3.9(b)) and a line through both valve centres. The second angle, *As2*, defines the angular spacing between each valve and is therefore the angle between two lines, each passing though a valve centre and the cylinder centre. Design constraints are represented within the generalised scheme (Figure 3.9(c) and (d)). The fuel injector boss is represented by a circular constraint of diameter *Df*, with a variable offset from the cylinder centre (*Xf* and *Yf*) A simple cylinder head bolt pattern is defined by adding a variable number (*Nc*) of circular constraints around the cylinder bore, respectively. The spacing of each cylinder head bolt was defined using an

61

equispaced pattern on a variable pitch-circle-diameter (Dc). The diameter of each boss is described by the parameter Db.
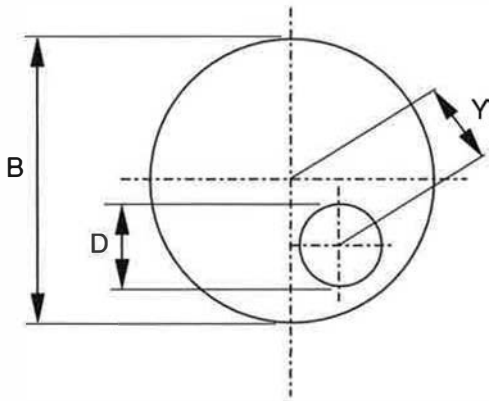
(a) Single valve layout
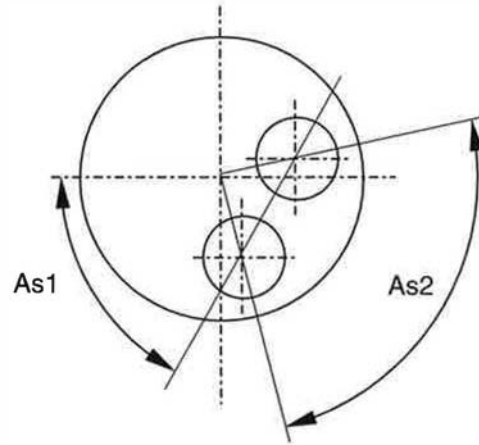
(a) Multi-valve layout
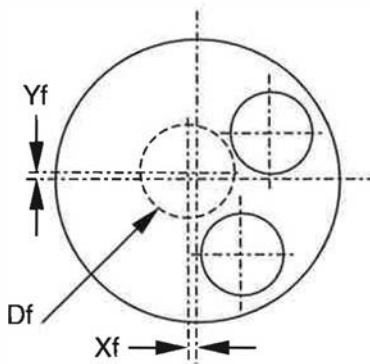
(c) Fuel injector constraint
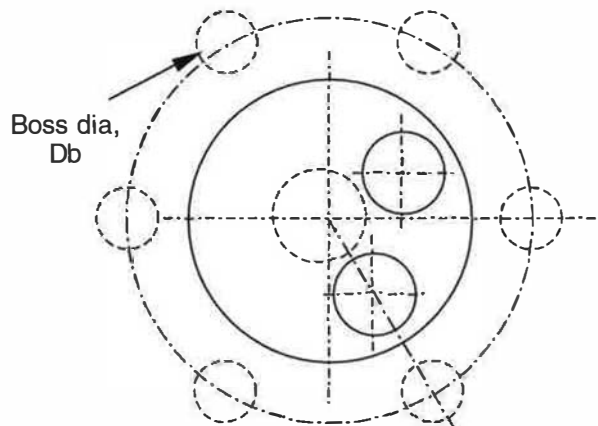
(d) Cylinder head bolt constraints

Figure 3.9: Valve layout and constraints

3.4.2 Directed Port

Following initial selection of the port design parameters most likely to influence performance, a detailed parameter scheme was devised to define the port geometry. The three parameters included in the directed port scheme were:

- Port approach angle in plan view, relative to a tangent to the cylinder bore (At)
- Port curve angle in plan view (Ar)
- Port curve radius in plan view (R)
- Port approach angle in elevation, relative to the horizontal gas face (Av)

The parameter scheme is shown diagrammatically in Figure 3.10. Note that the parameter At is interpreted as the tangential angle of the port in relation to the cylinder bore, and may be varied by a combination of rotation of the port about the valve axis and rotation of the valve centre about the cylinder centre. As multi-valve configurations are defined using skew angle ($As1$) and valve separation angle ($As2$), the effective At value for each port is also dependent on these values. The vertical approach of the port is primarily defined using the vertical approach angle Av. In order to define Av, the port design is divided into an entry section and a throat section. The central axis of the port in the entry section is characterised by a large radius of curvature when the port is viewed in elevation. The section may also be straight and/or inclined relative to the gas face plane in order to provide a suitable inlet manifold location. The throat section acts as a transition between the valve seat and the entry section and must curve from a vertical direction at the valve seat to an inclined angle at the interface with the entry section. In order to provide a suitable port roof line and to prevent an excessively long valve guide boss, the radius of curvature of the throat section is small and does not vary significantly in proportion to the valve size. Av is defined as the angle of the interface between the two port sections, relative to the gas face. In the case of a high Av value, the entry section represents a greater proportion of the total length of the port and will be inclined at a greater angle with respect to the gas face. As Av is decreased, the port inclination is also decreased and a greater proportion of the port is contained within the throat section.

| (a) Plan | (b) Elevation |
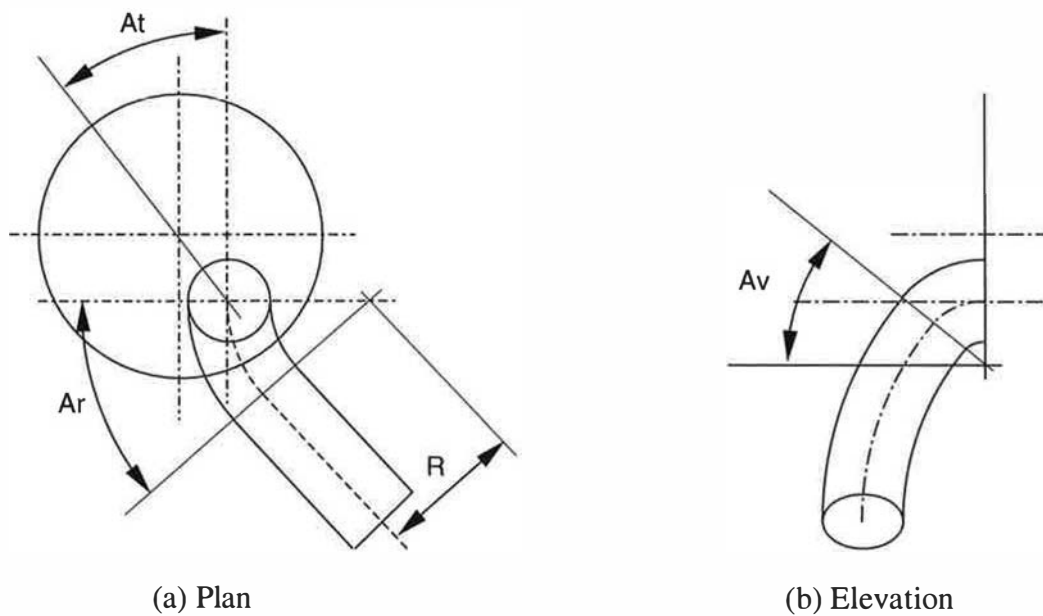
Figure 3.10: Directed port design parameters

3.4.3 Helical Port

In addition to the general parameters used in the directed port, six parameters were defined in the helical port scheme.

- Helix Wrap Angle (Aw)
- Helix Start Height (Hs)
- Helix Width (Wh)
- Inlet runner approach angle in plan view, relative to the tangential flow direction (At)
- Inlet runner curve angle in plan view (Ar)
- Inlet runner curve radius in plan view (R)

The helical port scheme is shown diagrammatically in Figure 3.11. The At, Ar and R parameters have a similar meaning to those in the directed port scheme, although they apply to the inlet runner section of the port, upstream of the helix. Due to the complex design of the helical port, the Av parameter was not sufficient to characterise the vertical approach relative to the gas face. Therefore, Hs was used to define the height of the helix above the gas face at

64

the interface between inlet runner and helix sections. Upstream of this interface, the port axis is assumed to be parallel with the gas face, in accordance with a conventional side-entry configuration in which the inlet manifold face on the cylinder head is perpendicular to the gas face.

(a) Plan   (b) Elevation
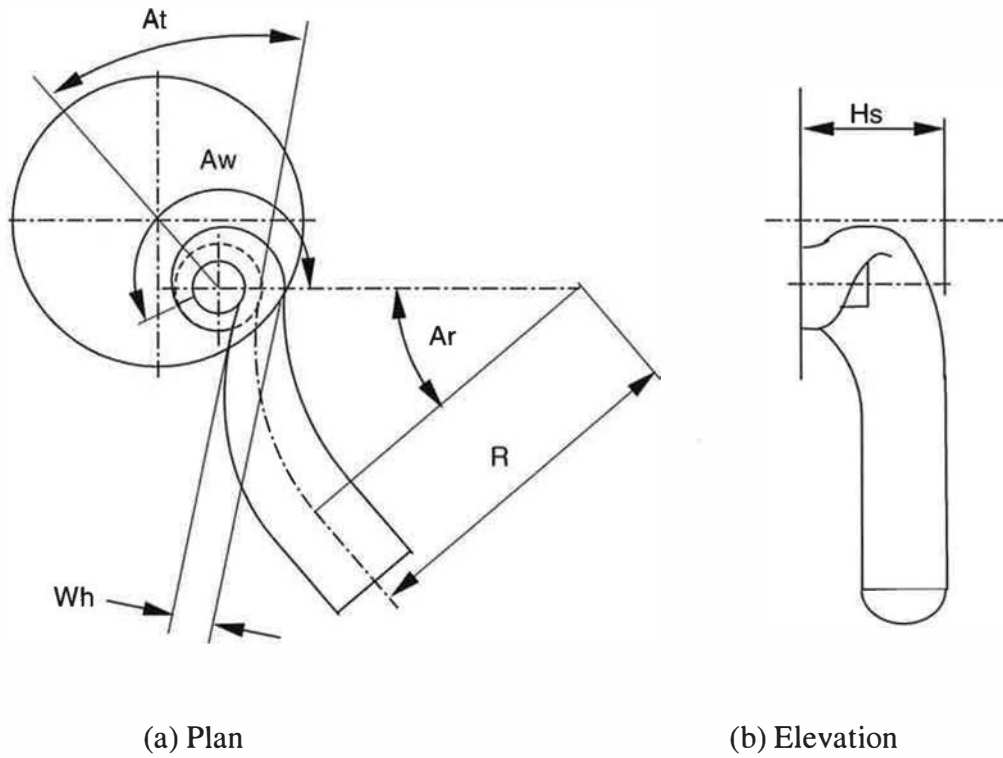
Figure 3.11: Helical port parameter scheme

3.4.4 CAD Model Construction

The generic port designs were defined using Pro/Engineer®, a commercial 3-D CAD package. A common methodology was adopted for the design of both directed and helical port types and consisted of a basic definition using datum features (planes, axes, points and curves) to describe the overall scheme; a set of surfaces built using the datum features and finally a set of solid features to allow manufacture of the test hardware, as illustrated in Figure 3.12. Where possible, dimensions were driven either directly by the chosen parameters or indirectly by mathematical relationships. In particular, relationships were used in the helical port design to define the helix geometry, given the basic *Hs, Aw* and *Wh* parameters. The inlet runner section of the helical port also contained relationships to provide

65

a smooth transition in shape and area from the port entry (fixed area) to the helix (variable area, depending on *Hs* and *Wh* parameter settings).

| Datum curves | Surface model | Solid model |
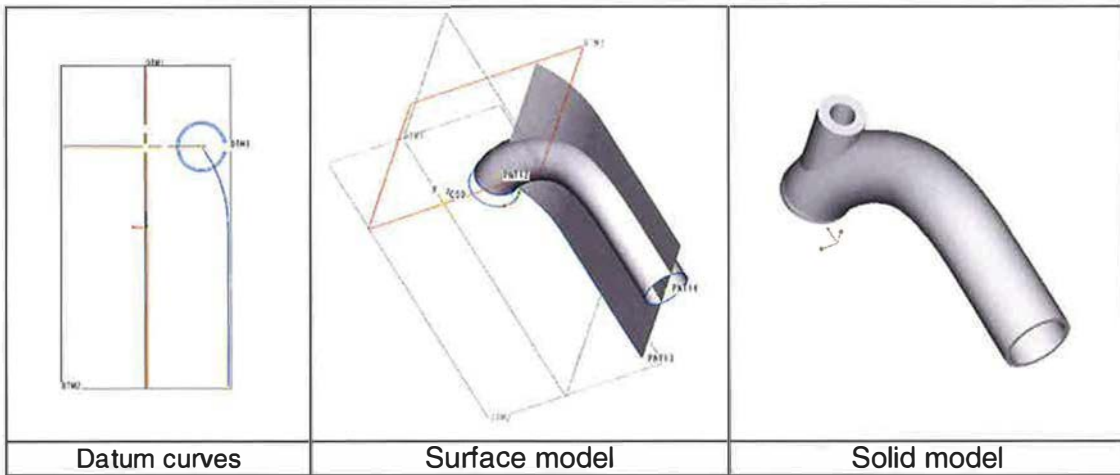
Figure 3.12: CAD model development

3.4.5 Production Features

Additional geometry modifications were added during the CAD modelling process to represent production features. Both port types incorporated a typical machined feature to blend the cast port form into the throat. In a real cylinder head, this operation is necessary to eliminate small geometry variations resulting from misalignment of the sand cores during casting. To ensure consistent geometry, sufficient material must be removed, therefore the diameter of the cast port shape is reduced locally to approximately 1mm less than the throat. The CAD geometry was developed to reproduce this process; the basic port shape was cut away by a rotated feature, thereby ensuring a realistic throat blend. Both port designs also included a valve guide feature that was held at a constant distance of 1.1D from the gas face, irrespective of the *Av* or *Hs* settings. This resulted in a varying amount of valve guide protrusion or recession. The helical ports also included typical minimum casting radii (2mm general, 1.5mm local) around the helix in order to prevent unrealistic effects such as flow separation from artificial sharp corners. Examples of the generic CAD surface models are shown in Figure 3.13.

66
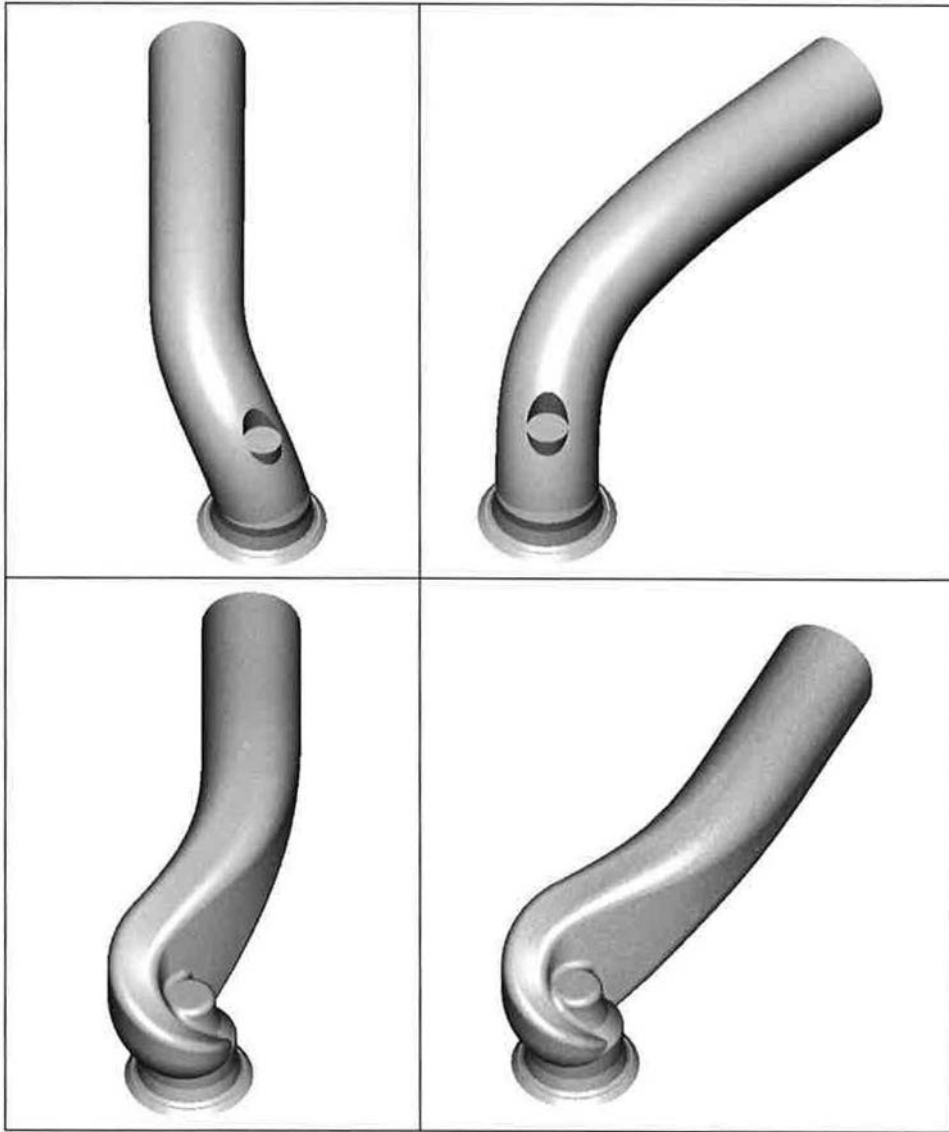
Figure 3.13: Generic CAD models

3.5 Parameter Operating Ranges

3.5.1 Summary

The operating ranges for all design parameters are shown in Tables 3.6 to 3.8. The methods employed to select appropriate values for each parameter are described in the remainder of Section 3.5.

Cylinder capacity	0.39 - 0.64ℓ
Cylinder bore diameter	79.5 - 90mm
Piston stroke	80 - 100mm
Rated engine speed	3500 - 4500 rev/min
Non-dimensional inlet valve inner seat diameter	0.30 - 0.34
MIGV	50 - 80 m/s
Valve lift duration	215 – 245 ° crank
Maximum valve lift	0.27 – 0.35 *D

Table 3.6: General engine design parameters

Range	Parameter				
	Av (°)	At (°)	Ar (°)	R (mm)	E (-)
Low	15	0	0	30	0.35
High	45	90	90	70	0.45

Figure 3.7: Parameter ranges (directed port)

Range	Parameter						
	Aw (°)	Hs (mm)	Wh (mm)	At (°)	Ar (°)	R (mm)	E (-)
Low	190	25	10	0	0	30	0.35
High	270	35	20	90	90	70	0.45

Table 3.8: Parameter ranges (helical port)

3.5.2 Port Design Database

A database of diesel engine inlet port design features and performance data was developed to determine suitable ranges for some design parameters and to investigate typical design trends. The database was collated from existing inlet and exhaust port performance data and engine geometry of thirty multi-valve HSDI engines either in production or undergoing development at Ricardo Consulting Engineers Ltd, plus additional data on larger DI engines. Twelve engine manufacturers were represented. Although details of several of the design parameters selected in the previous section were not available, the following data was captured for all engines in the database:

- Bore/stroke ratio / cylinder capacity
- Rated engine speed
- Valve size
- Mean inlet gas velocity (MIGV)
- Maximum valve lift
- Inlet valve lift duration
- Swirl ratio (Rs)
- Flow coefficient at 0.3L/D ($Cf_{0.3}$)

Much of the port performance data obtained is confidential and individual examples cannot be shown. However, for the purposes of the present study, the overall trends are sufficient. A summary of the database results is shown in Table 3.9 and histograms illustrating the distribution of values for each parameter are shown in Figure 3.14

	B/S	Dn	Lmax/D	MIGV	Rs	$Cf_{0.3}$	Duration
max	1.07	0.34	0.37	83.5	2.6	0.54	244
min	0.82	0.27	0.27	59.2	0.5	0.39	211
mean	0.96	0.31	0.32	68.1	1.7	0.47	228

Table 3.9: HSDI database summary
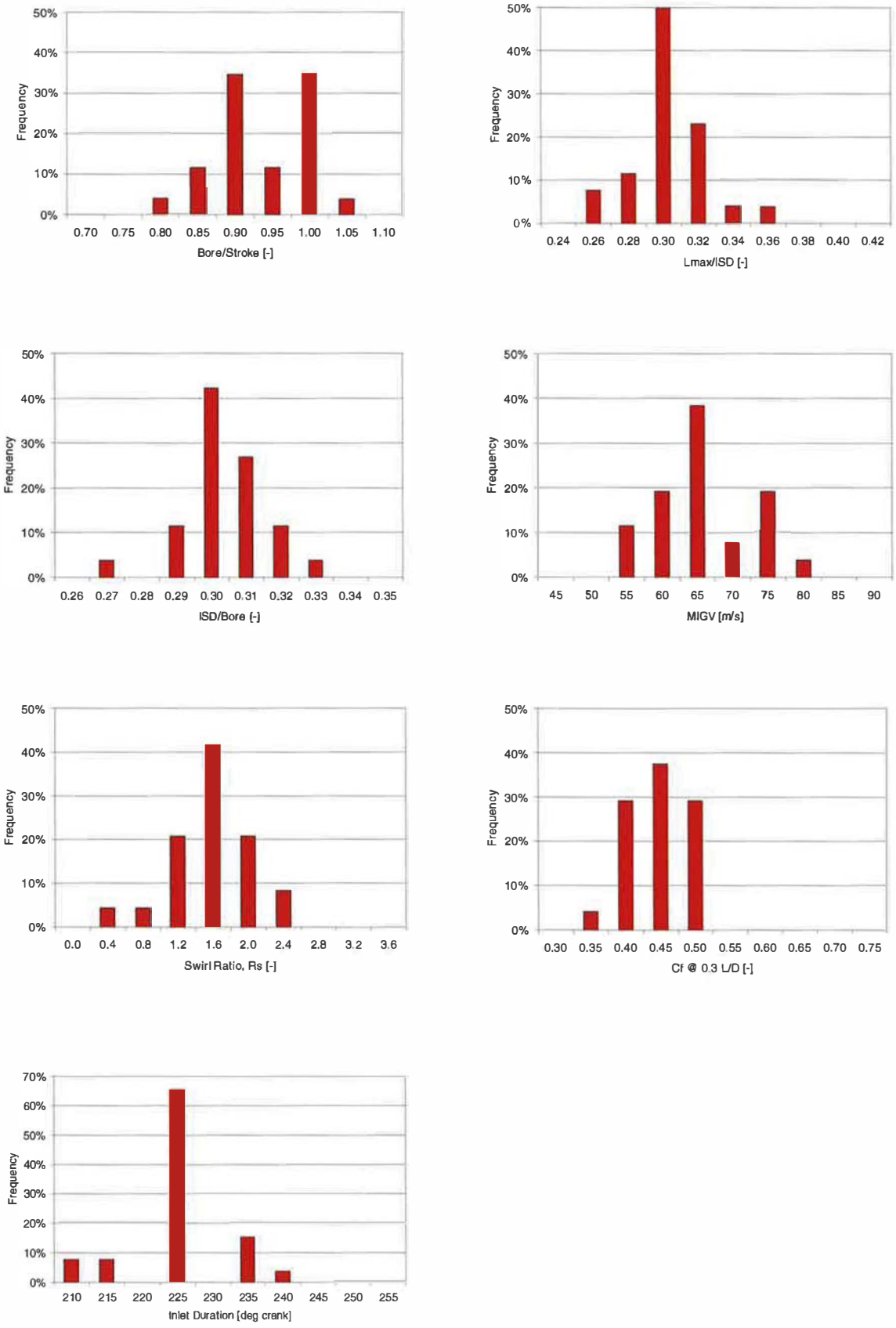
Figure 3.14: Database histograms

70

3.5.2.1 Cylinder capacity and rated speed

Although there is no universally accepted classification system to distinguish HSDI engines from other DI diesel engines, they are generally regarded as light-duty engines for use in passenger and light commercial vehicles. The database indicated a distinct boundary between small capacity, high speed engines and larger, heavier duty engines. The difference is clearly evident when rated engine speed is considered; the majority of HSDI engines have a rated speed of 4000 rev/min or more, whereas the maximum for heavy duty engines is typically 2500 rev/min. In terms of cylinder bore diameter, the transition occurs at approximately 100mm, representing a cylinder capacity of approximately 0.75ℓ for HSDI. The capacity of heavy duty engines with similar bore diameters was typically 1.0ℓ, due to a longer piston stroke.

3.5.2.2 B/S ratio

The database indicated a range of B/S ratios between 0.82 and 1.07. The majority of engines were undersquare; a significant factor in terms of the potential flow performance of the valves and ports. As mean piston speed is proportional to piston stroke, and the maximum available valve diameter is related to bore diameter, decreasing B/S ratio for a given cylinder capacity and rated engine speed has a significant effect on MIGV (and therefore the breathing potential of the engine).

3.5.2.3 Inlet valve size

The mean inlet valve inner seat diameter (D) in the database was 27.0mm. Although non-dimensional valve size (Dn) varied between 0.27 and 0.34, the smaller end of the range is likely to represent offset-injector designs, resulting in a constrained maximum valve size. Dn was in the range 0.30 to 0.34 for 85% of the engines surveyed and it was considered that this was a fairer representation of modern HSDI engine trends. Inlet valve size is limited by fuel injector boss/sleeve diameter, minimum valve bridge thickness (inlet-inlet and inlet-exhaust) and minimum valve head to cylinder bore clearance. A pressed-in injector sleeve is often preferred to a cast boss, due to the reduced outer diameter of the former. The effective diameter of the injector constraint also varies depending on the size of coolant passages around the injector tip.

The effect of injector boss diameter and B/S ratio on the maximum possible inlet valve size and MIGV, for a rated engine speed of 4500 rev/min, 0.5ℓ cylinder capacity, is shown in Figure 3.14. A central injector location is assumed. The range of maximum valve diameters shown is comparable to the database results; increasing the B/S ratio and/or decreasing injector boss diameter allows a larger valve to be packaged, with a corresponding decrease in MIGV. Figure 3.15 is used to indicate the likely effect of B/S, valve size and injector boss size on potential port flow performance. It is also used to select appropriate ranges for Dn and Df. For a typical inner seat diameter of 27mm, cylinder bore diameters between 79.5mm and 90mm, with injector constraint diameters of 18mm to 22mm, are required to provide a Dn range of 0.3 to 0.34, resulting in a MIGV range of 50m/s to 80m/s. In order to compare inlet mach index (Z) for a range of different ports with varying engine geometry, MIGV should be held constant (Taylor, 1985). However, the overall effect of inlet port flow characteristics and engine geometry must be considered when predicting engine performance.

3.5.2.4   Valve lift and duration

The database shows that maximum valve lift, normalised by the inner seat diameter (L/D), falls into the range $0.27 < L/D < 0.37$. In practical terms, flow performance for the majority of port designs does not improve significantly above L/D values of 0.3, when the effective valve curtain area exceeds the effective port throat area. However, swirl generation may continue to develop and therefore the upper end of the database range is certainly of interest. Inlet duration ranged from 211 to 244, with an average of 228. A large number occupied the 225 to 230 range. Interestingly, there was an uneven distribution with two relatively large groups around 215 and 240 values. This is likely to be due either to the use of standard camshaft specifications, or common valve timing and duration settings.

3.5.2.5   Swirl ratio and flow coefficient

The database contained measured swirl ratio (Rs) values between 0.5Rs and 2.6Rs, indicating different approaches to combustion system design. Note that the measured Rs values do not necessarily represent combustion system requirements, as the database contained both production engines and engines under development. Flow coefficient at 0.3L/D ($Cf_{0.3}$) ranged from 0.39 to 0.54, indicating a significant variation in performance.

Ideally, the knowledge-based system should be capable of simulating design configurations capable of a similar range of performance characteristics.
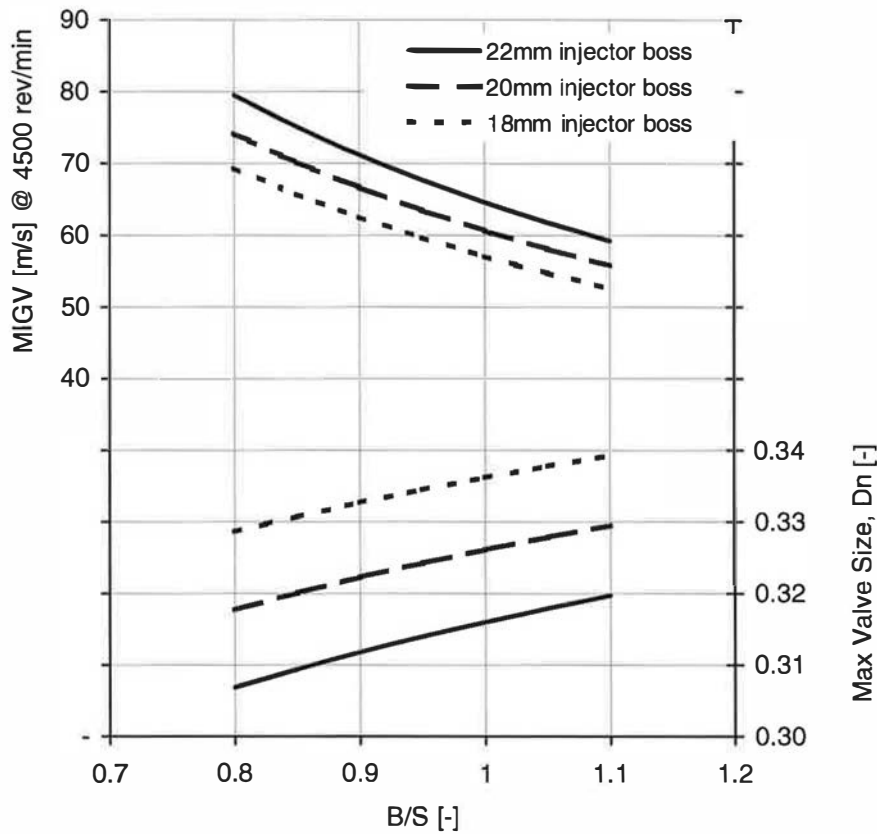
Figure 3.15: Effect of B/S and injector diameter on Dn and MIGV

3.5.3 Determination of Remaining Parameter Ranges

3.5.3.1 Inlet valve eccentricity (E)

A suitable range of inlet valve locations, defined by the eccentricity parameter (E), was determined by referring to the database and design guidelines. Recommendations for the maximum value for E vary; typically, a value of 0.45 is specified in order to prevent shrouding of the valve by the cylinder bore. Alternatively, a minimum valve head to cylinder bore clearance of 1mm is specified, resulting in a value of approximately 0.48 for cylinder bore diameters between 80mm and 90mm. The lower limit for E is influenced by fuel injector offset and valve packaging. As E is decreased, the injector must be offset towards the exhaust side of the cylinder, resulting in a reduction in the maximum possible exhaust valve size. The database indicated a range of exhaust valve inner seat diameters between

73

27% and 31% of the cylinder bore diameter. The critical lower value for E is 0.35, when a small injector and minimum sized exhaust valve can be fitted, albeit with a significant injector offset and minimum valve bridge widths.

3.5.3.2   At, Ar and R

In many cases, parameter range information was unavailable and therefore suitable limits were defined by considering the relevant geometry. The range for *At* is determined by varying the port orientation relative to the cylinder from purely radial to purely tangential, corresponding to *At* values of 0° and 90° respectively. This approach has been adopted by several researchers (Tipplemann 1977, Gale 1990, Li *et al* 2000). In all cases, a sinusoidal swirl response has been reported. The combined effects of *Ar* and At on directed port geometry are shown in Figure 3.16. An *Ar* range of 0° to 90° is logical given that greater angles are both undesirable due to flow losses and unfeasible due to packaging requirements. However, the direction of curvature is significant if *At* is variable only between 0° and 90°. Therefore the effective range of *Ar* is from −90° to +90°. The effect of curve radius R is likely to vary in relation to the port diameter. It may be appropriate to define R in non-dimensional terms (*Rn* = *R/D*), although it cannot be assumed that the effect of *Rn* is the same for all values of *D*. For fixed *D* of 27mm, absolute values for *R* may be used. The use of *Rn* could only be investigated using different valve sizes. To provide a sufficient compromise between packaging space and design flexibility, a range of 30mm<*R*<70mm was specified. In practical terms, the lower limit for *R* was determined by the combined effect of curvature in the vertical and horizontal directions. 30mm was the minimum value that was achievable without causing self-intersection of the port surface. Large *R* values are limited by the space available within each cylinder bay. Configurations in which the port entry lies outside the cylinder bore are unusual, but are occasionally employed when packaging space is particularly tight. The overall effect of *Ar* and *R* on directed and helical ports is shown in Figures 3.17 and 3.18 respectively. Clearly, the influence of *R* becomes increasingly significant as *Ar* increases.

Ar = -90°	Ar = -45°	Ar = 0°	Ar = +45°	Ar = +90°
At = 0°	At = 0°	At = 0°	At = 0°	At = 0°

Ar = -90°	Ar = -45°	Ar = 0°	Ar = +45°	Ar = +90°
At = 45°	At = 45°	At = 45°	At = 45°	At = 45°

Ar = -90°	Ar = -45°	Ar = 0°	Ar = +45°	Ar = +90°
At = 90°	At = 90°	At = 90°	At = 90°	At = 90°
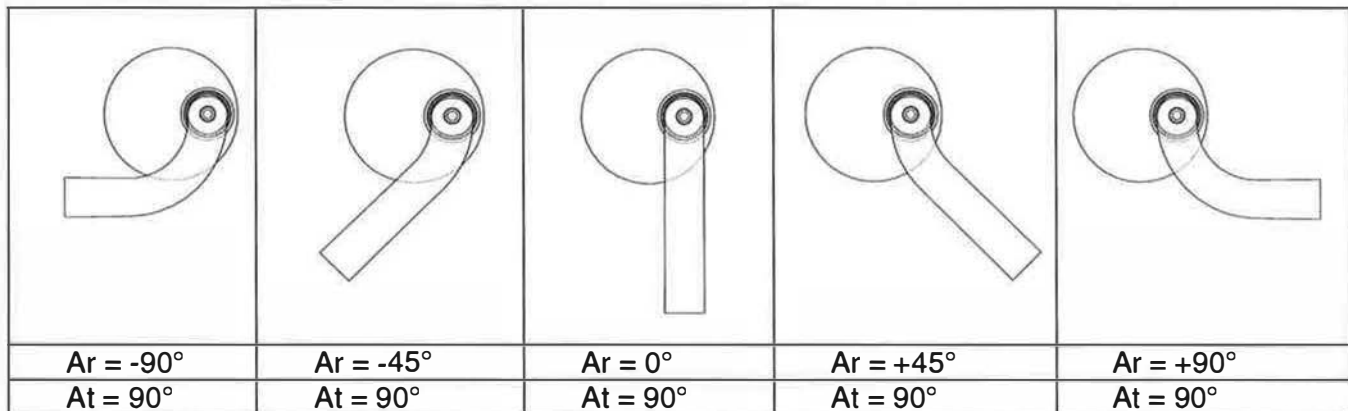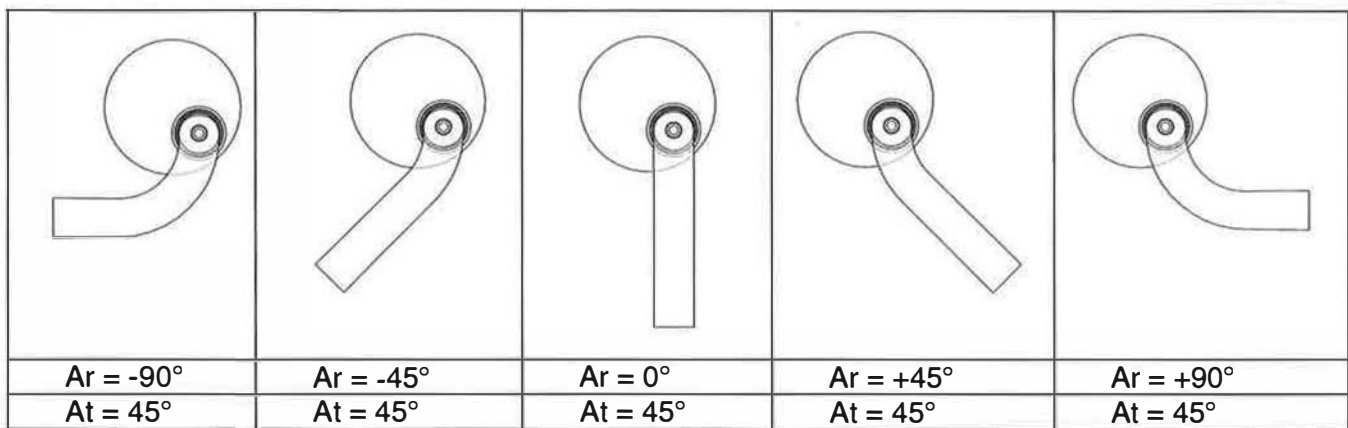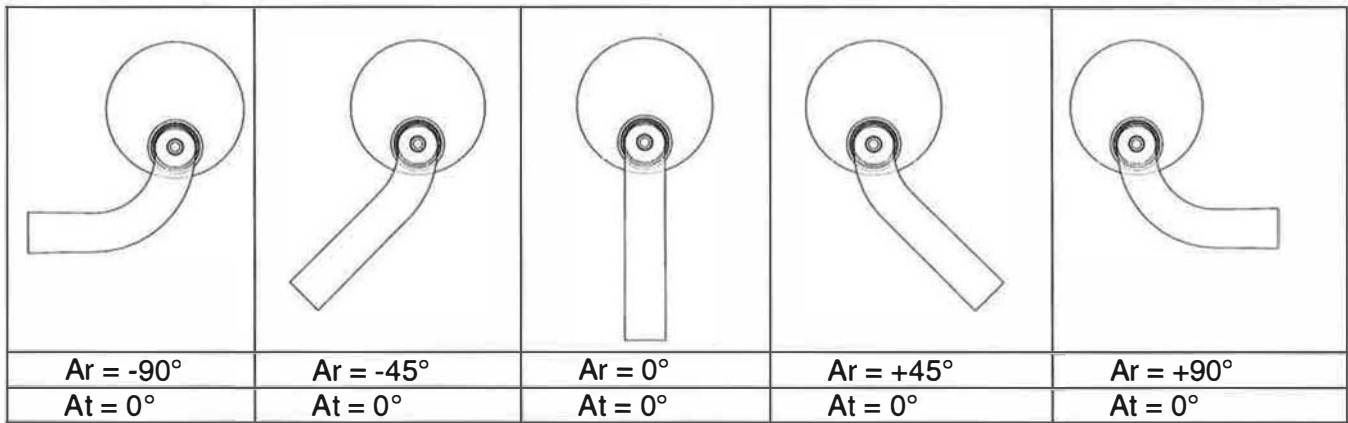
Figure 3.16: At and Ar geomtry (directed port)

75

| Ar = 0° | Ar = 45° | Ar = 90° |
| R = N/A | R = 30mm | R=30mm |

| Ar = 0° | Ar = 45° | Ar = 90° |
| R = N/A | R = 50mm | R=50mm |

| Ar = 0° | Ar = 45° | Ar = 90° |
| R = N/A | R = 70mm | R=70mm |
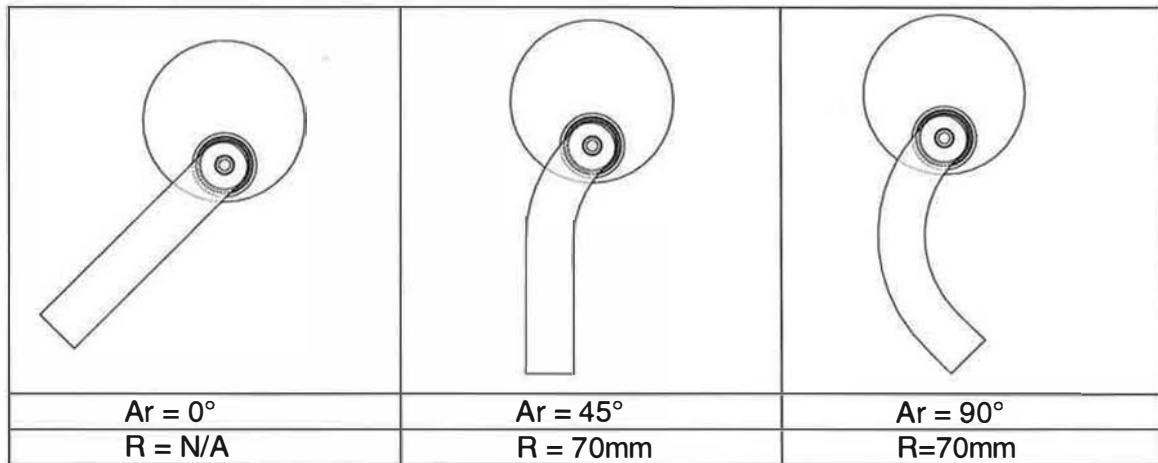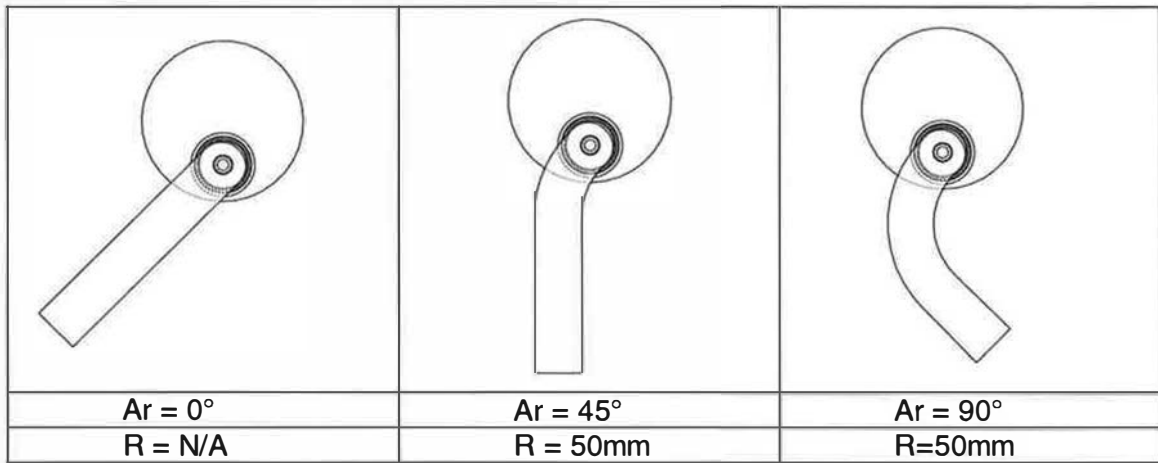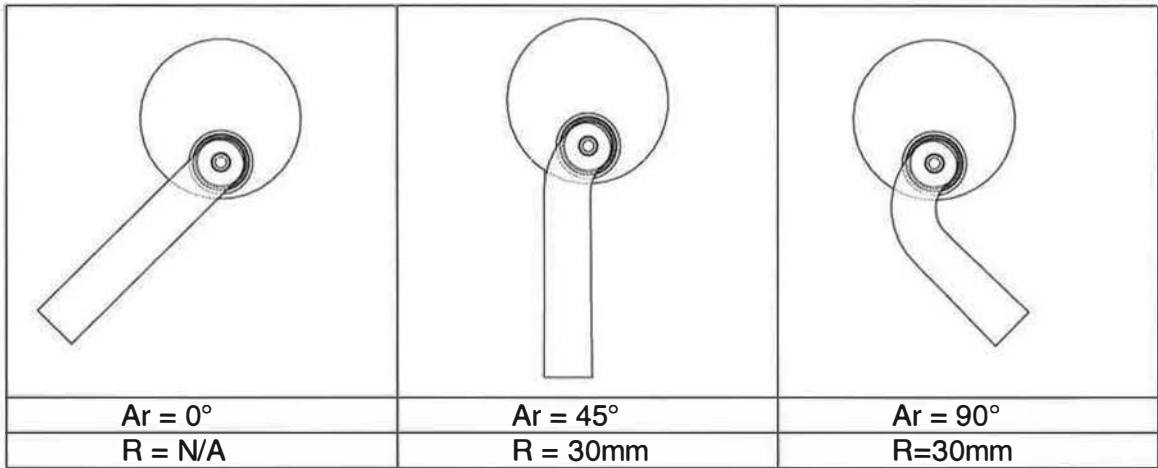
Figure 3.17: Ar and R geometry (directed port)

Ar = 0°	Ar = 45°	Ar = 90°
R = N/A	R = 30mm	R=30mm

Ar = 0°	Ar = 45°	Ar = 90°
R = N/A	R = 50mm	R=50mm

Ar = 0°	Ar = 45°	Ar = 90°
R = N/A	R = 70mm	R=70mm
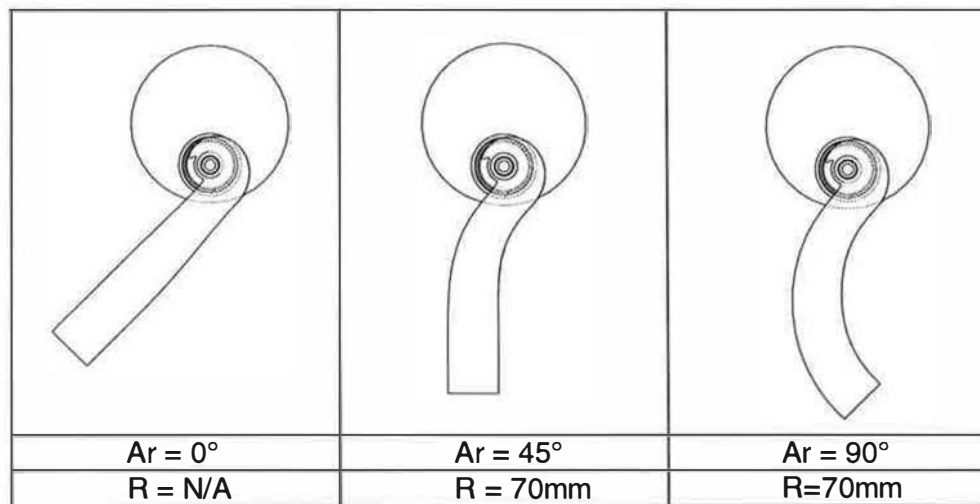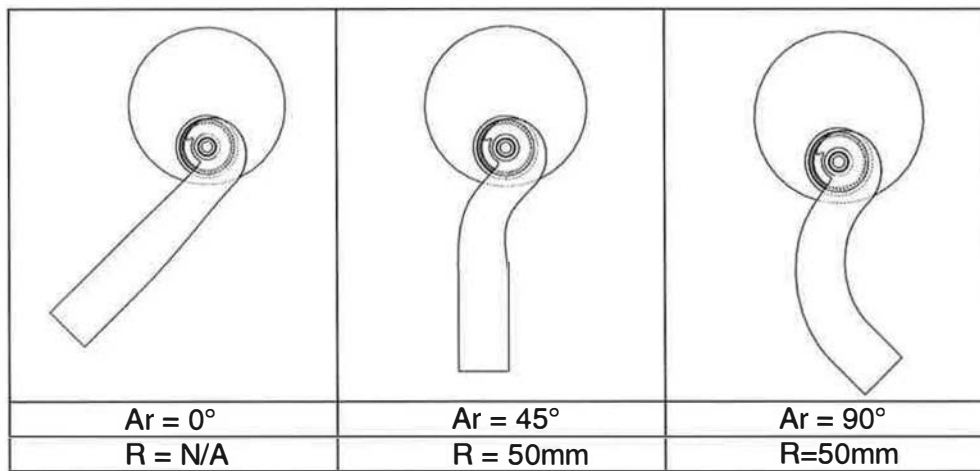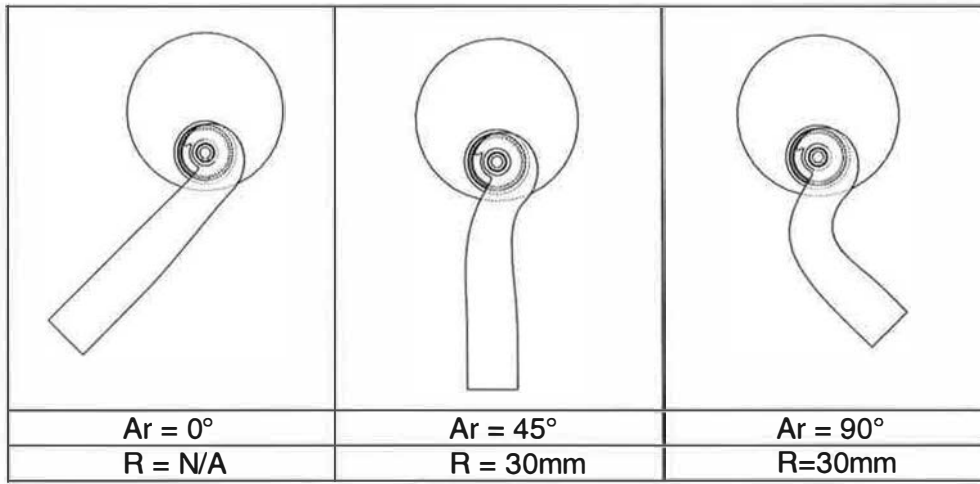
Figure 3.18: Ar and R geometry (helical port)

3.5.3.3 Av

The range for *Av* was determined by considering the impact on cylinder head height and the limitations imposed by any coolant passages under the port floor. In order to achieve a realistic overall cylinder head height, the vertical location of the port on the inlet manifold face must be limited. The vertical location of the valve spring seat may also influence the vertical approach angle of the port, to a lesser extent. Coolant passages under the port floor are usually specified to provide adequate cooling of the gas face. Therefore, the minimum port angle is also limited. Geometry variations based on the range $15<Av<45$ are shown in Figure 3.19; typical coolant passage locations and cylinder head height limits are also indicated.

3.5.3.4 Aw, Hs and Wh,

The range for helix wrap angle (Aw) was defined by considering the geometry range that could be modelled effectively. An upper limit of $270°$ was applied to prevent the helix wrapping completely around the central core of the port and therefore interrupting the form of the inner port wall at the helix entry section. It has been reported that port flow characteristics are extremely sensitive to the geometry in this region (Brignal and Jin, 1999). A lower limit of $190°$ was applied to ensure that the helix was properly formed.

In a similar manner to *Av*, the range for Hs was defined by considering the impact on port entry height and packaging requirements for coolant passages. The resulting range of $25mm<Hs<35mm$ was therefore equivalent, although *Hs* was defined as a linear measurement and as a result was limited in application to a single valve size. As with *R,* a non-dimensional alternative could be proposed, although any assessment of performance would require tests to be performed with a range of valve sizes.

Finally, the range for Wh was defined to provide a realistic variation in helix entry width and, in combination with Hs, cross-sectional area. The minimum value of 10mm corresponded to a helix with zero overhang relative to the valve seat insert outer diameter. The upper limit of 20mm was considered to be the maximum width that could be packaged assuming minimum constraints.

min. port wall 4.5mm

min. deck 10mm

Av = 15°

Av = 30°

min. manifold seal 6mm

80mm

Av = 45°
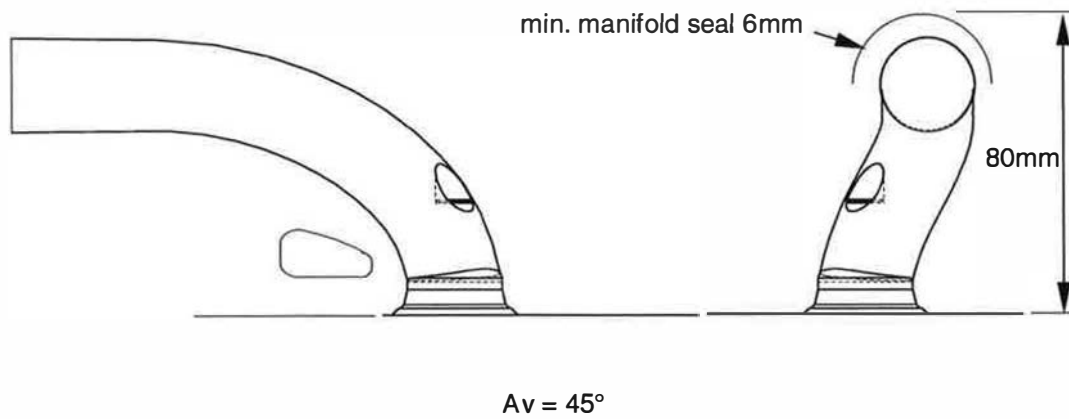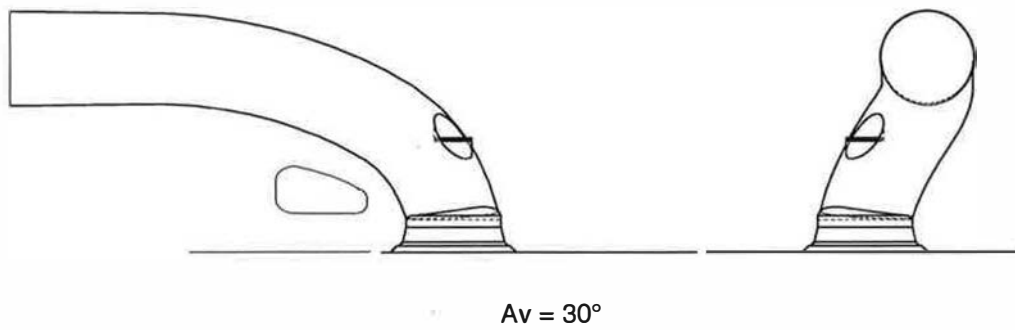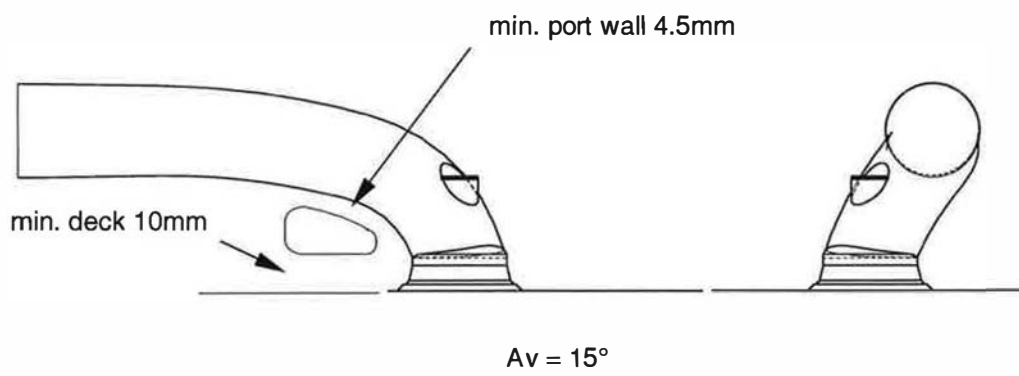
Figure 3.19: Av geometry (directed port)

Aw = 190°	Aw = 230°	Aw = 270°
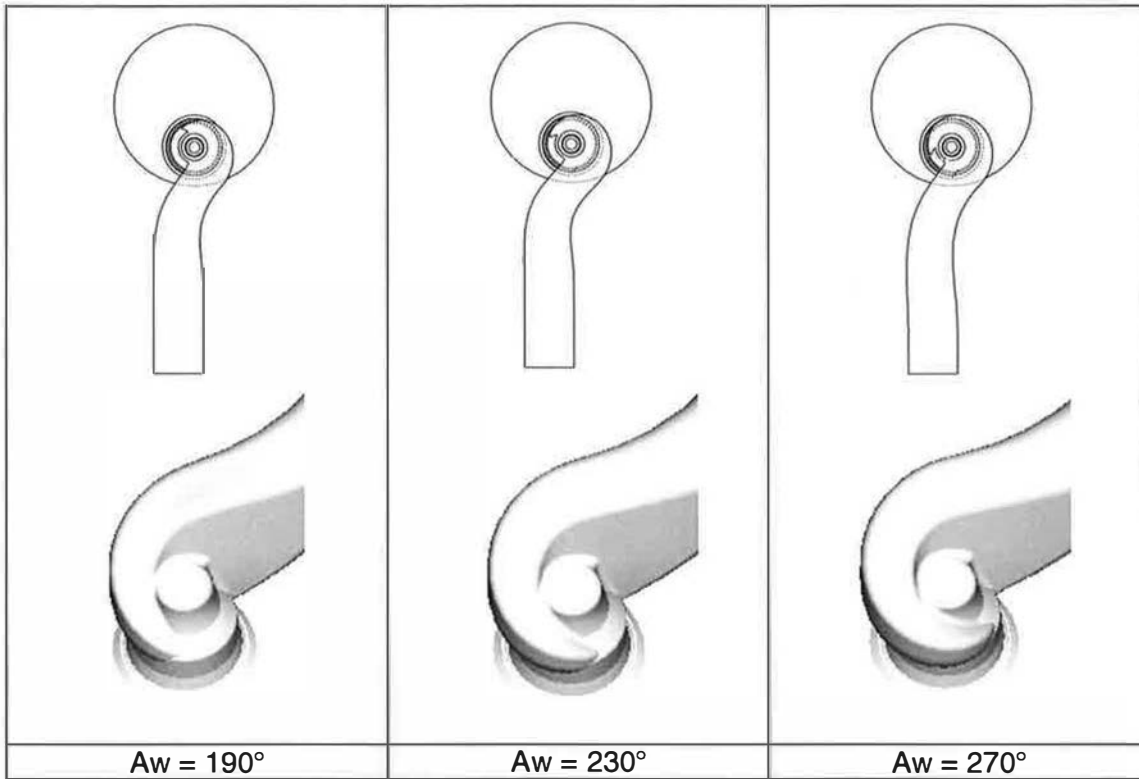
Figure 3.20: Aw geometry (helical port)

Hs = 25mm	
Hs = 30mm	
Hs = 35mm	
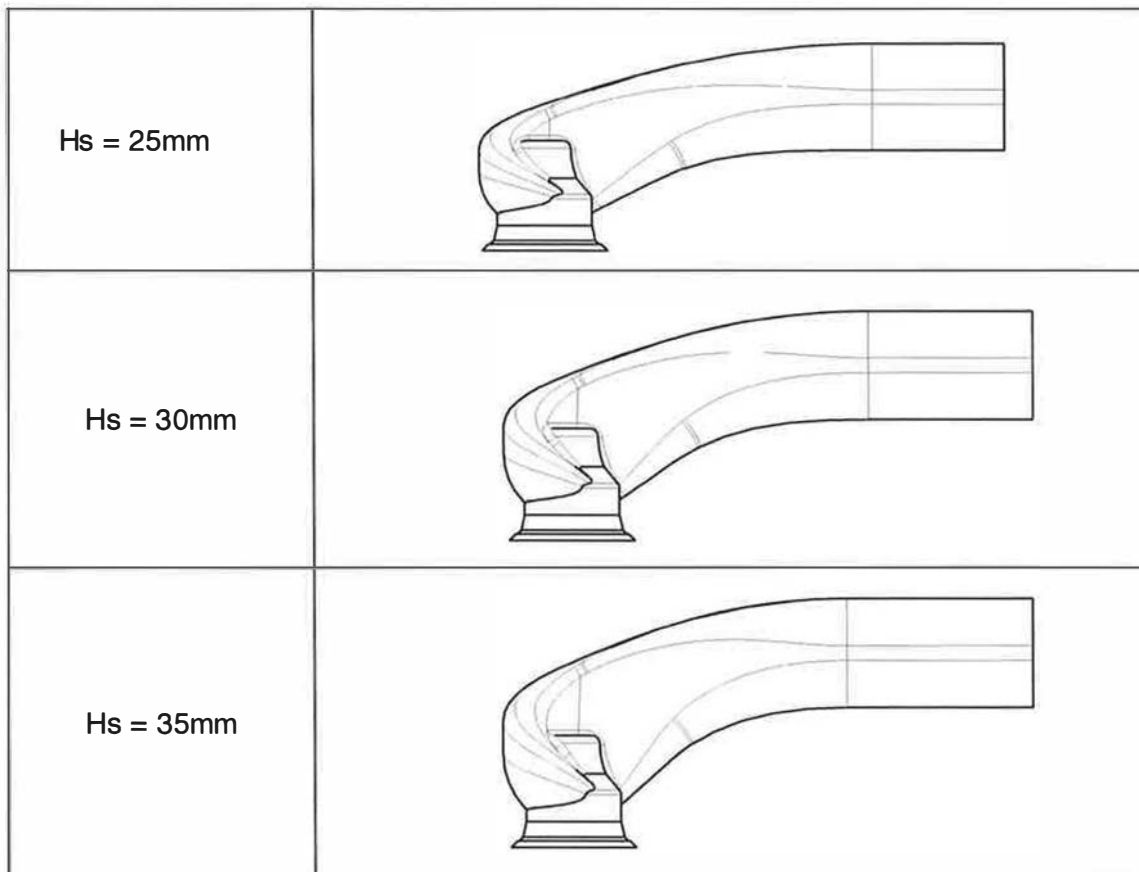
Figure 3.21: Hs geometry (helical port)

| Wh = 10mm | Wh = 15mm | Wh = 20mm |
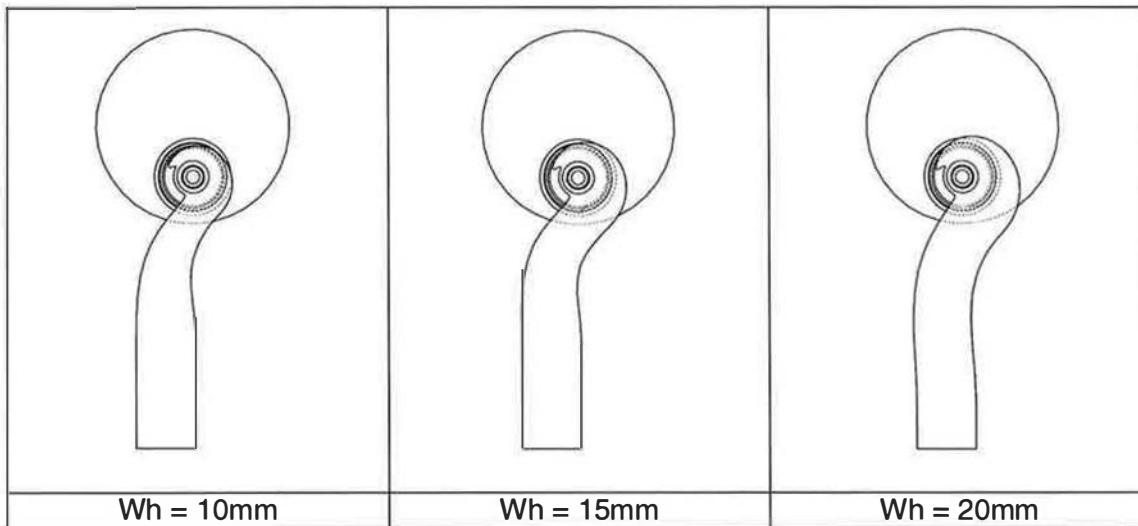
Figure 3.22: Wh geometry (helical port)

3.6   Experimental Design

3.6.1 Overview

The experimental designs for each generic port type were selected from a range of statistical design-of-experiments (DoE) plans. Although the primary concern was to manage the testing resources required to achieve a realistic model of the system, the suitability of a particular approach for visual interpretation of the results was also considered. Therefore, classical experimental plans were chosen in conjunction with conventional response-surface-methods (RSM) for visualisation of the parameter effects. The expected shape of each performance response was considered in order to determine the level of complexity required for each model. Quadratic models were selected for both generic port types in order to capture second order effects, whilst limiting the number of tests required. Maximum, minimum and nominal states were defined for each parameter. The extreme states corresponded to the limits of the parameter range and the nominal value was fixed at the halfway point in the range. A test matrix was then constructed by combining different parameter settings, according to the DoE plan. Each test configuration was modelled in CAD by defining a particular variant of the generic design scheme.

81

3.6.2 Experimental Design for the Directed Port

A classical second-order central composite plan for six factors was selected in preference to a simple screening experiment, due to the possibility of interactions and non-linear main effects. In order to reduce the number of hardware variations required during the test programme, three parameters were varied by modifying the experimental set-up; At and E were both varied by adjusting the location of the cylinder relative to the port and valve. Dn was changed by using a range of cylinder bore diameters with a constant inlet valve size, as indicated in Table 3.6. This approach enabled the use of a single valve, valve guide and valve seat assembly throughout. Vertical port angle (Av), port curve angle (Ar) and port curve radius (R) could only be changed by using different hardware configurations.

The directed port design scheme was divided into two regions of interest for the purposes of the DoE study. Although the generic scheme could be used to describe the geometry and location of a port anywhere in the cylinder, it was considered likely that a single second-order model would not be suitable for the range of Ar. Therefore, two DoE test plans were defined, each providing information on half of the total parameter range. Test plan "A" was used to characterise the response for ports with positive Ar values (type A ports) and test plan "B" was used for ports with negative Ar values (type B ports). In practice, negative Ar values were achieved by mirroring the valve location about the cylinder centre line, as shown in Figure 3.23, thereby eliminating the need for additional physical port models. The swirl response from test plan B was reversed to show the true effect of Ar. Each test matrix consisted of 53 configurations, including 9 repeats of the "centre" test, for which all parameters were set to their nominal values. The centre repeats were used to establish test repeatability. The final experimental design for the directed port is shown in Table, in Appendix B. Parameter values for the 13 unique physical port models are summarised in Table 3.10. Note that R cannot be defined when Ar=0 (model numbers 1,2 and 8). Such conditions should generally be avoided, as it is impossible to determine the effect of ill-defined parameter combinations. However, in this case, port geometry can be said to be independent of R when Ar=0 and therefore will not have an influence on the performance response.

Model number	Av	R	Ar ("A")	Ar ("B")
1	15	-	0	0
2	45	-	0	0
3	15	50	+45	-45
4	45	50	+45	-45
5	30	30	+45	-45
6	30	70	+45	-45
7	30	50	+45	-45
8	30	-	0	0
9	30	50	+90	-90
10	15	30	+90	-90
11	15	70	+90	-90
12	45	30	+90	-90
13	45	70	+90	-90

Table 3.10: Hardware configurations (directed ports)

(a): Positive Ar

(b)　　Negative Ar
(as tested / reversed)
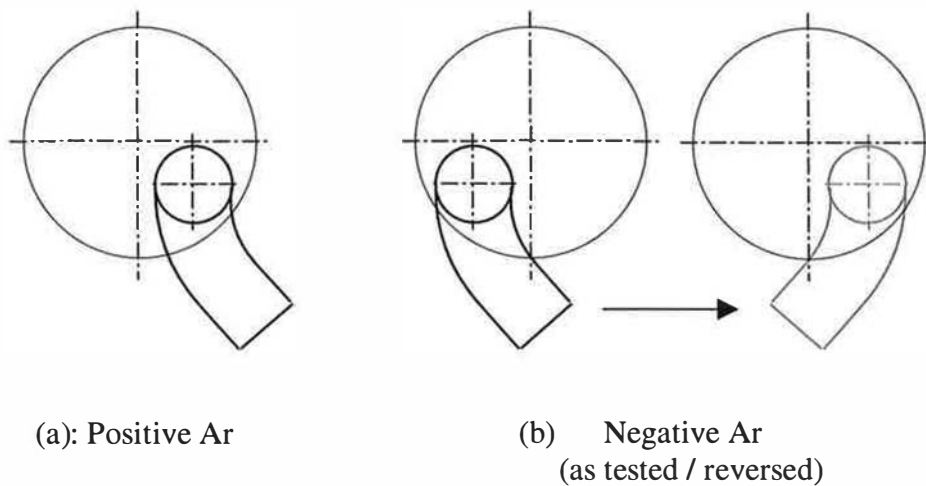
Figure 3.23: Negative Ar mirror transformation

3.6.3 Experimental Design for the Helical Port

For the helical port study, a quadratic model was also required. Due to the increased complexity of the geometry, compared to the directed port, a larger experimental plan for seven parameters was selected. A Box-Behnken plan with 62 test runs was selected in

preference to a central-composite design with 84 test runs. Within the complete set of 62 test runs, 33 unique port geometry cases were identified, the remaining parameter variations being achieved by adjusting the location of the cylinder liner. The complete experimental design is shown in Table B4, in Appendix B.

3.7 Realisation of Generic Port Designs

3.7.1 Geometry Definition – Testing Requirements

Additional features not included in the original generic design schemes were applied to provide suitable overall dimensions for testing purposes, whilst avoiding significant changes to port geometry. In order to provide common entry planes for port models with the same port curve angle (Ar), whilst maintaining similar overall port path lengths, an "entry plane offset" was applied to control the distance between the valve centre and the entry plane. The entry plane offset was reduced for ports with high port curve angles to compensate for the increased path length compared to straight ports and therefore prevent misinterpretation of the effect of Ar. The resulting geometry is shown in Figure 3.24 and the total path lengths for all directed ports is shown in Table 3.11. Port models with a 90-degree curve angle exhibit the greatest variability in total path length because the length of the curved section of these ports is more sensitive to a change in R and Av. An entry plane offset of 90mm provided the best compromise in this case. All other port lengths fall within a range between 134mm and 144mm. Note that the entry plane offset was not intended to represent the inlet manifold face in a real engine. Although it is logical that flow losses would increase with port length, it is not necessarily the case that a longer port would imply a longer overall intake duct from inlet plenum to valve. In practice, this length is often developed to maximise tuning effects and therefore improve volumetric efficiency. Therefore, any local increase in the inlet port length is likely to be offset by a matching decrease in the inlet manifold runner length.
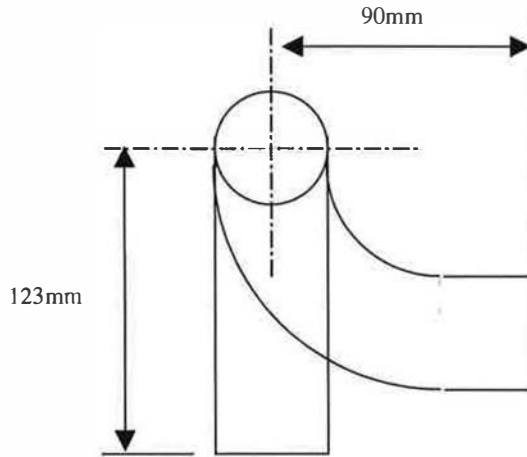
Figure 3.24: Entry plane offset geometry

Model No.	Entry Plane Offset (mm)	Total Path Length (mm)
1	123	134.9
2	123	144.2
3	118	134.7
4	118	144.0
5	118	137.1
6	118	140.3
7	118	138.7
8	123	138.9
9	90	137.4
10	90	122.0
11	90	144.8
12	90	131.3
13	90	154.2

Table 3.11: Directed port path lengths

3.7.2 Data Conversion

The CAD models were converted to neutral geometry files (STL) for manufacture. Knowledge of the rapid-prototyping manufacturing process was important in setting the accuracy of the STL files. A compromise must be struck between adequate accuracy (governs final model accuracy) and file size (governs manufacturing time and cost). The effect of model accuracy, expressed as chord height, is shown in Figure 3.25. Chord height is

a measure of the distance between the chord used to approximate an arc and the arc itself. Therefore, a small chord height results in a larger number of surface patches that lie close to the original surface. As chord height is increased, the number of surface patches is reduced at the expense of accuracy. An increase in chord height from 0.025mm to 0.100mm reduced the number of triangular surface patches (and hence file size) by 77% but the model surface became visibly faceted. As a result, small detail features such as the throat machining area (highlighted) were not represented in a satisfactory manner.
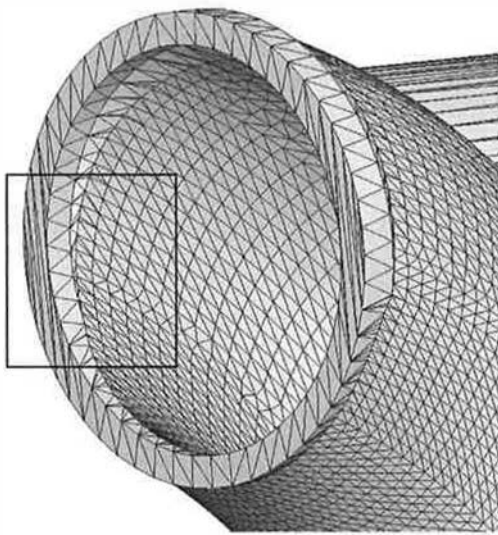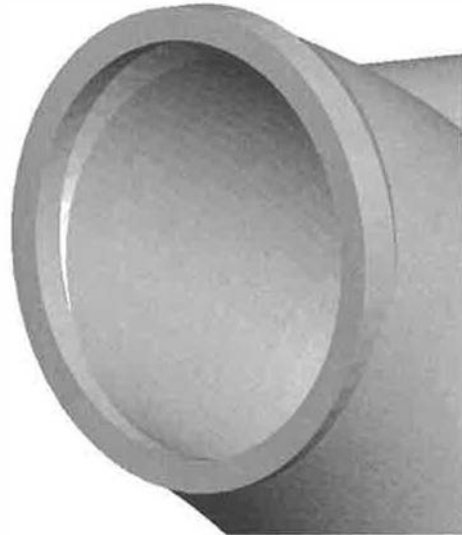
0.025 Chord height, faces & edges shown   0.025 Chord height, faces only
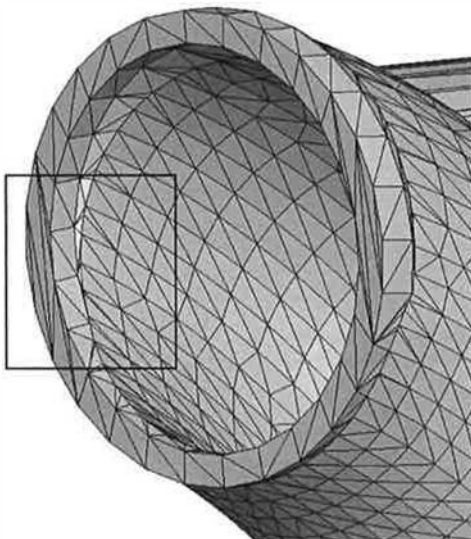
0.100 Chord height, faces & edges shown   0.100 Chord height, faces only

Figure 3.25: STL file accuracy

3.7.3 Manufacturing Process

Conventional and rapid-prototye (RP) processes were compared in order to determine the most suitable for manufacture of physical port models for steady flow testing. Assessments were made on the basis of cost (absolute cost per model), accuracy (error between the surfaces of the original CAD model and the physical model) and durability (results of a simple drop-test onto a hard surface from 1.5m to simulate the model being knocked off the test rig by accident), as indicated in Table 3.12. A conventional resin model produced by CNC machining was also assessed as a baseline for the comparisons.

	Cost (per model)	Accuracy (surface error)	Durability (drop-test result)
CNC Machining (resin)	£3000	<0.5mm	Pass
SLS (Duraform)	£200	<1mm	Pass
Thermojet (wax)	£150	>2mm	Fail

Table 3.12: Assessment of manufacturing processes

Manufacturing tests were performed using the two RP processes: Thermal wax printing and selective laser sintering (SLS). The trial wax model, made using a 3D Systems ThermoJet™ solid object printer, is shown in Figure 3.26. During construction, a temporary support structure was created automatically, resulting in an impaired surface finish on surfaces that faced downwards in the machine (indicated in Figure 3.8(b)). The model was therefore made in two parts with inner surface uppermost. Distortion during the manufacturing and curing processes prevented the two halves from joining correctly. The trial model was destroyed when dropped from 1.5m onto a hard floor, indicating that it would also be unsuitable for air flow testing. An example of one the SLS models, made in Duraform® nylon using a DTM Corporation Sinterstation 2000, is shown in Figure 3.27. The process does not require a support structure so the part was made in one piece with a good surface finish. The physical properties of the SLS model were found to be acceptable and an accuracy check was performed by comparing the original CAD surface with a set of curves constructed from a 3-D scan of the physical SLS model. The process is illustrated in Figure 3.28. The maximum deviation of the scanned SLS model surface from the original CAD surface was

approximately 0.25mm and the overall form of the port was maintained along the full length. As with most rapid-prototyping processes, the physical SLS model was built by dividing the STL model into 0.1mm slices. The resulting model surface should therefore be produced to within 0.125mm of the CAD surface. The maximum error of approximately twice this value suggests that distortion of the model occurred during the curing process, although this was considered to be acceptable given that intended geometry variations resulting from changes to parameter values were significantly greater . Small "steps" in the surface of the model, also created by the manufacturing process, were left unfinished to represent a cast surface finish

| (a) Upper surface | (b) Lower surface |

Figure 3.26: Thermal wax model

Figure 3.27: SLS models

Splines representing scanned SLS model

CAD surface

Measurement of deviation between splines and surface
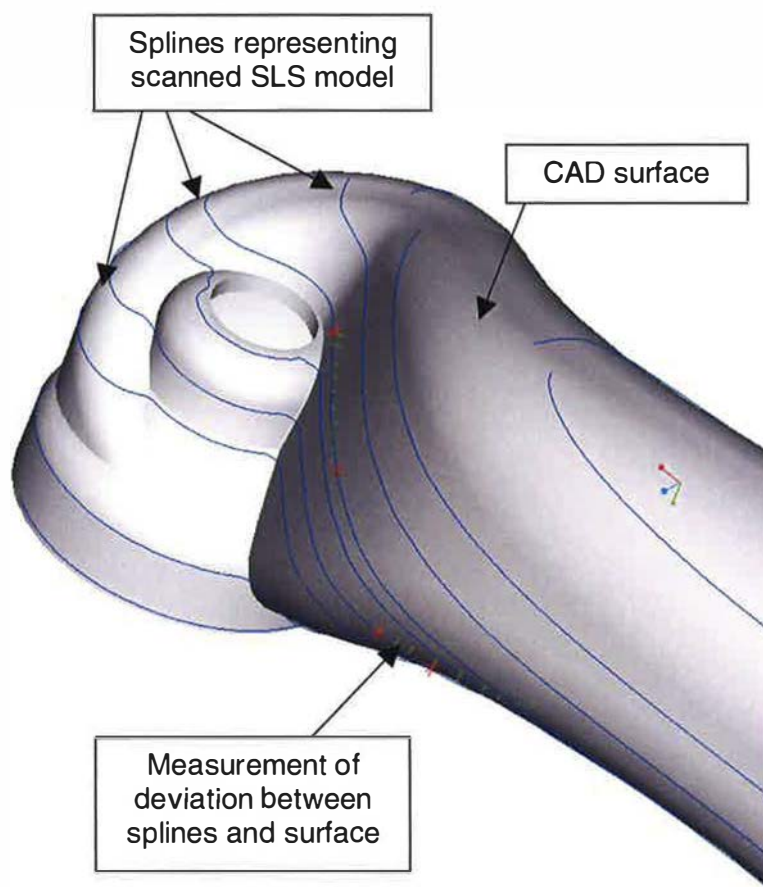
Figure 3.28: Comparison of CAD and SLS model surfaces

3.8 Steady Flow Assessment of Port Models

3.8.1 Test Apparatus

To facilitate steady flow testing of the chosen inlet port configurations, the SLS models were housed in a skeletal frame consisting of the essential mating surfaces and location points. The throat and entry ends of each model were fitted into recesses machined into the frame to provide positive location. A poppet valve, valve seat insert and valve guide were designed using typical geometry for a modern HSDI diesel engine. The valve guide was inserted through a hole in the port model and was also mounted concentrically to the valve seat. A fixture was also made for manually lifting the inlet valve to a known height above the valve seat using a 1mm pitch screw thread. A photograph of the assembled model is shown in Figure 3.29. In order to reduce overall testing time by reducing the number of rebuilds, all test configurations for a particular port model were performed sequentially, including any

Dn, At and/or E variations, before the model was replaced. This procedure resulted in a partial loss of randomness in the test sequence, although the possibility of unwanted hidden effects being mistaken for real parameter effects was reduced by repeated random testing of the centre model. The directed ports were tested first and the results analysed before the commencement of the helical port testing programme. This ensured that any problems were resolved and the test plan could be revised if necessary.
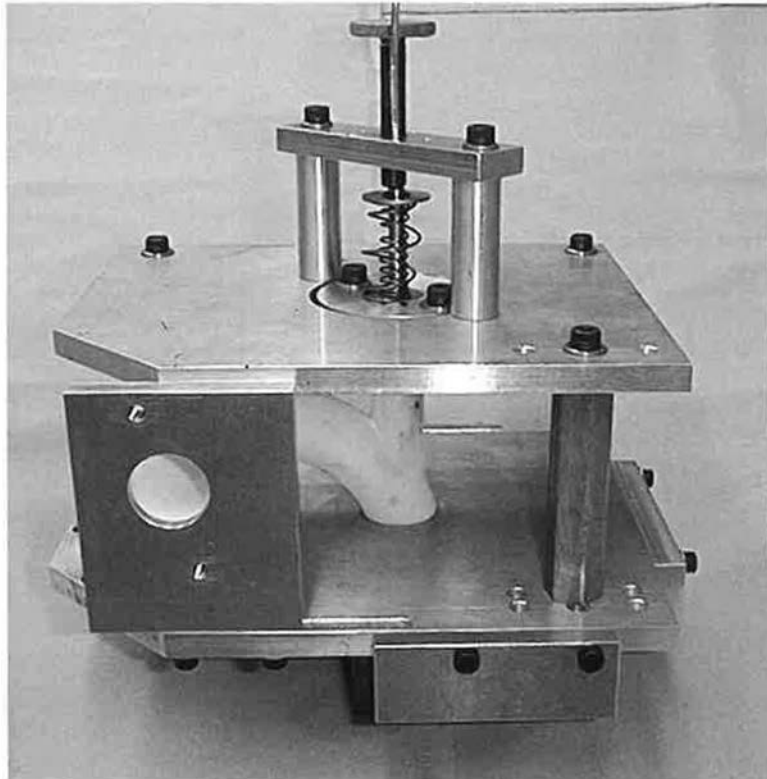
Figure 3.29: Housing of port model in the skeletal frame

The experimental apparatus was a conventional steady flow test rig, similar to that used in previous studies (Monaghan and Pettifer, 1981), as shown in Figure 3.30. The inlet port assembly was mounted with the gas face uppermost and a cylinder liner placed on top. The cylinder location was controlled using gauge blocks inserted between the outer wall of the cylinder and two raised stops mounted at right angles along the edges of the frame. A Cussons impulse swirl meter (ISM) was placed coaxially on top of the cylinder. The port entry was attached to a pressure box by means of an adaptor plate with a smooth entry radius. The pressure box was then connected to a centrifugal fan using a flexible pipe. A Cussons laminar flow meter (LFM), calibrated to traceable standards, was used to measure the

volumetric flow rate downstream of the fan. Additional pressure and temperature measurement apparatus were mounted at several points throughout the system to enable calculation of mass flow rates and performance parameters. Details of the measurement equipment is provided in Table 3.13; measurement uncertainty is based on actual calibration results, not published specification.
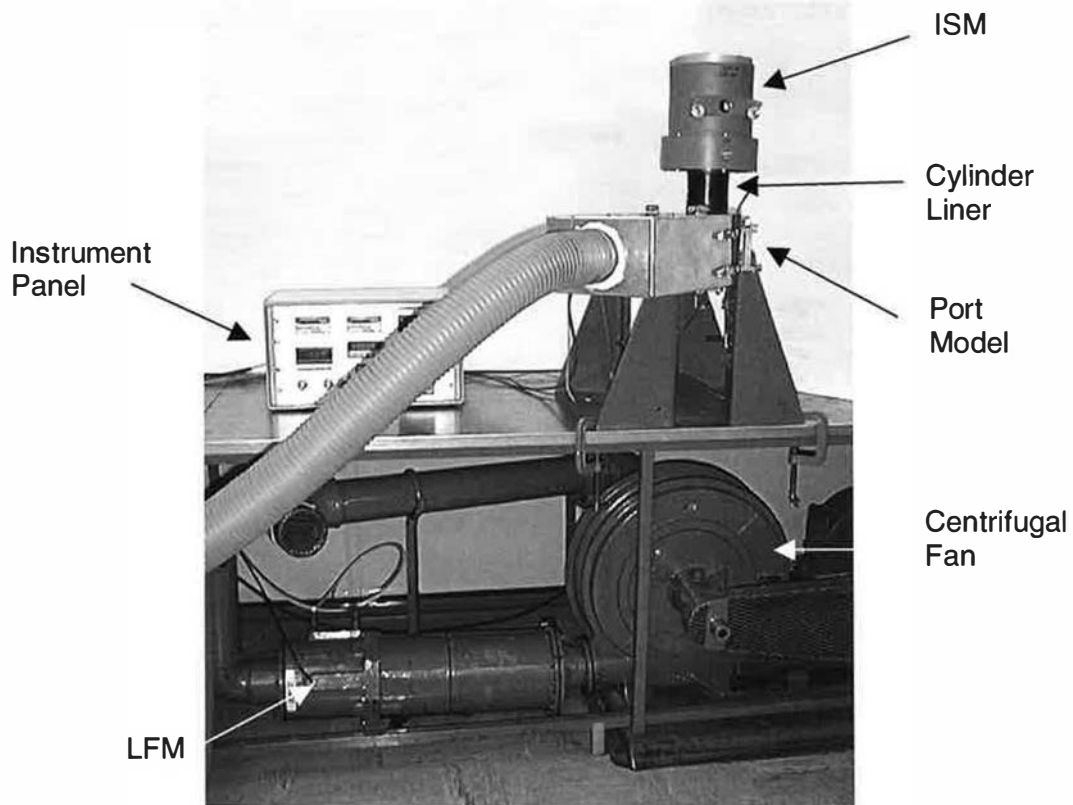
Figure 3.30: Steady flow rig and port model

Quantity Measured	Manufacturer & Model	Type	Range	Resolution	Measurement Uncertainty
Volumetric Air Flow	Cussons 7.5H	LFM	14 – 197 l/s	N/A	<1%FSD
Pressure	Druck DPI260	Silicon diaphragm transducer and digital readout	0-1500 mmH$_2$O gauge	0.1mm H$_2$O	<0.02% FSD
Temperature	Digitron Temperature Indicator	k-type thermocouple and digital readout	0-60°C	0.1°C	<0.2%FSD
ISM Torque	Cussons ISM	Impulse Swirl Meter	0-100E-3 Nm	0.1E-3 Nm	<0.1%FSD

Table 3.13: Steady flow rig sensor data

91

3.8.2 Operating Procedure

Prior to operation, all instruments were visually checked to ensure they were within a valid calibration period. Pressure transducer displays were zeroed and the ISM torque display was calibrated using a known test mass. A test pressure was selected based on the inlet valve area, in order to ensure turbulent flow through the port throughout the valve lift range. The model assembly was visually checked, then tested for air leaks by closing the valve and running the fan to a pressure above the required test pressure. A measured flow through the LFM would signify a system leak. Any small leaks were sealed before commencing the first test. The inlet valve was opened 1mm above the valve seat using the lifting screw, with the fan running. Gauge pressure at the port entry was then set by adjustment of the fan speed. Following a short period to allow the instruments to settle, the test results were recorded. A series of test points were recorded with the inlet valve lift increased incrementally by 1mm to a maximum beyond that expected in an operating engine. A maximum lift of 10mm, corresponding to L/D=0.37, was deemed sufficient in this study. At each test condition the fan speed was adjusted to maintain a constant gauge pressure at the port entry.

3.8.3 Data Processing

The raw test data was processed using a standard software routine to calculate a range of flow parameters according to the Equations described in the preceding chapter. Flow coefficient (Cf) based on constant inner-seat area (Equation 1.1) and non-dimensional rig swirl (Ns, equation 1.4) were calculated at each valve lift point. Mean flow coefficient (MCf, equation 1.5a), inlet Mach index (Z, equation 1.5) and swirl ratio (Rs, equation 1.6) were calculated using all test points plus additional engine data. Raw and processed data for all models were then recorded in a database for further analysis.

The processed test data was then analysed using MODDE, a commercial software package by Umetrics AB, to identify significant design parameters and construct polynomial response surface models. A statistical check using the regression coefficient R^2 was also made to ensure that the models were sound. The response surface models were used to interpret the results, identify the most significant parameters and visualise the relationships between the parameters and responses.

4 Predictive Performance Modelling of Single Inlet Ports

4.1 Overview

Three response surface models were generated. In each case, the raw data was processed to provide alternative flow characteristics. The models characteristics are summarised in Table 4.1. A standard model was constructed to provide simple predictions based on summary flow characterisation parameters. This model was enhanced by including the effects of valve lift profile. Finally, a detailed model was developed to provide port flow and swirl characteristics throughout the valve lift event.

Model Description	Responses	Valve lift profile modelling
Standard Model	Rs/Ld, MCf	Fixed valve lift profile Port design & valve layout effect only
Enhanced Standard Model	Rs/Ld, MCf	Variable lift and duration, generic shape
Detailed Model	Cf_1 to Cf_{10} Ns_1 to Ns_{10}	Fully flexible valve profile, Rs/Ld and MCf calculated

Table 4.1: Model summary

4.2 Standard Model with Fixed Valve Lift Profile

4.2.1 Summary of Test Results

In order to isolate and assess the performance effect of port geometry parameters, excluding operational parameters, raw test data was processed using a fixed inlet valve lift profile of 230 degrees duration; 8.37mm maximum lift. Mean flow coefficient (MCf) was calculated as a summary of inlet port flow performance, independent of engine geometry. In-cylinder air motion was characterised by calculating normalised swirl ratio Rs/Ld, thereby eliminating scaling effects resulting from changes to cylinder bore diameter and piston stroke. The results for directed ports, test plans A and B are shown in Figure 4.1 and 4.2 respectively, A frequency analysis of the directed port results is presented in Figure 4.4. MCf values of between approximately 0.43 and 0.46 were observed for both directed port datasets, indicating a broadly similar distribution in flow performance. However, swirl characteristics

93

varied considerably. The test plan A results contained a range of positive and negative swirl results between -0.13 and +0.22 Rs/L$_d$, indicating a change in swirl direction depending on the test configuration. In comparison, all but one of the test plan B swirl results were positive, in a range between -0.01 and 0.26 Rs/L$_d$. The frequency analysis clearly indicates the difference, indicating a positive shift in the distribution of test plan B results. Although further analysis is required to investigate subtle trends, some remarks based on the summary results can be made. Swirl generating potential, resulting from the tangential orientation of the port, will clearly be enhanced or weakened depending on the direction of curvature of the port. In the case of test plan A, negative swirl is generated when swirl potential due to port orientation is outweighed by swirl potential due to port curvature. Port flow performance, whilst being clearly independent of the direction of curvature, may be influenced by the orientation of the port with respect to the cylinder bore. Therefore, the direction of curvature may be significant when such location effects are considered. However, these effects are not immediately apparent from the results, suggesting that port location effects may be of secondary importance in terms of flow performance.

Rs/Ld and MCf data for helical ports is presented in Figure 4.3, indicating a general increase in swirl compared with the directed port data. In particular, several Rs/L$_d$ results in excess of 0.25 were observed, compared to one in the directed port data. One negative swirl result was observed. There is a corresponding reduction in MCf values, suggesting that the flow capacity of helical ports is compromised. Frequency analysis confirms these observations, as shown in Figure 4.5. The distribution of results for the directed ports is also shown for comparison. Although the maximum swirl generated by helical ports is not substantially greater than for directed ports, fewer helical design configurations produce low levels of swirl, or indeed negative swirl. The flow performance difference between helical and directed port types is clearly shown in the distribution of MCf values.

A flow/swirl trade-off plot for all results is shown in Figure 4.6, indicating a range of swirl-generating capability. When swirl is generated in the most effective manner, flow performance is maximised, but increased swirl is also associated with a loss in flow performance. At zero swirl, the highest mean flow coefficient achieved was 0.461; at a high swirl condition of 0.38 Rs/Ld, the best mean flow coefficient was 0.325. Note also that negative swirl (generated only by some directed port configurations in test plan A) is not generated as effectively as positive swirl, as indicated by the swirl magnitude at equivalent

MCf values. A small number of helical ports were capable of generating swirl as efficiently as directed ports at moderate swirl levels. Helical ports did not generate low swirl as well as the best directed ports. Conversely, a larger number of helical ports generated high levels of swirl but with a considerable penalty in flow performance.
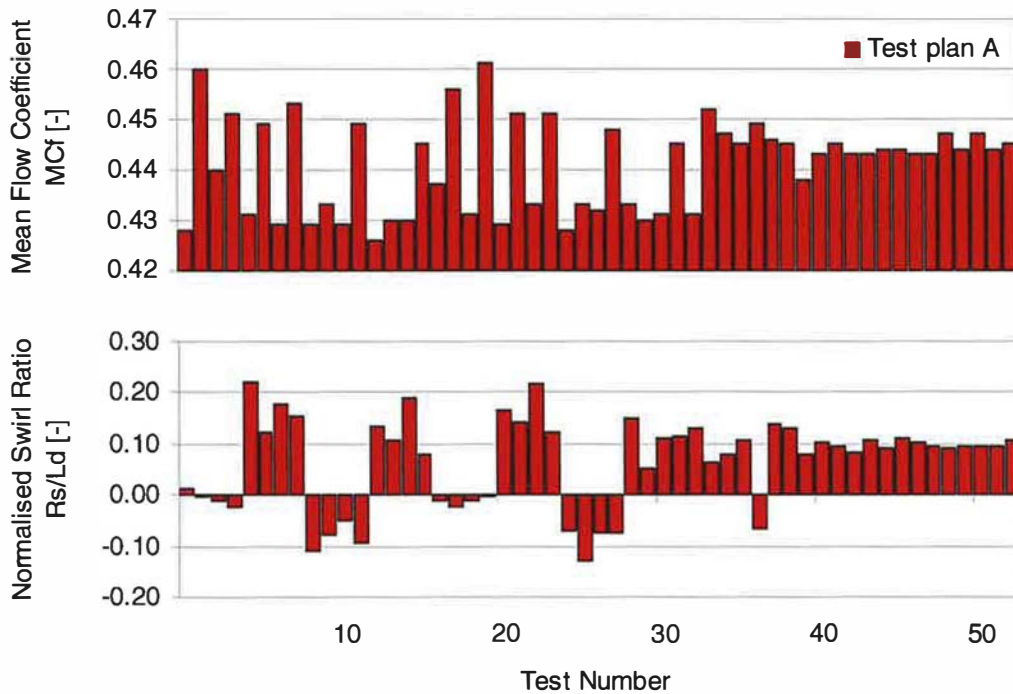
Figure 4.1: Directed port summary results (test plan A)
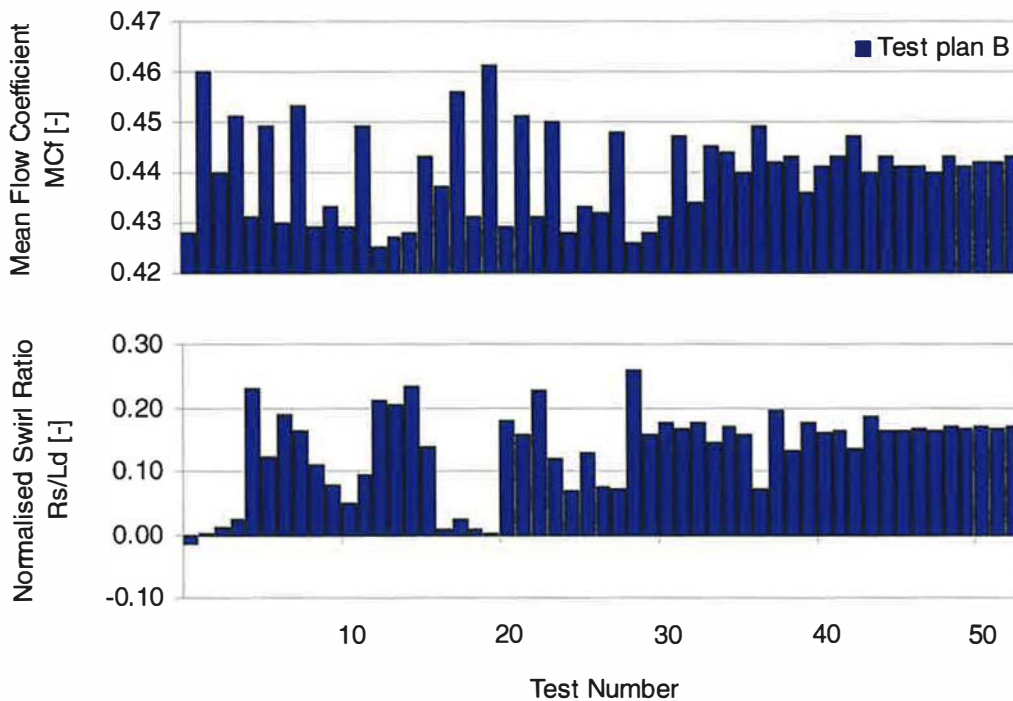
Figure 4.2: Directed port summary results (test plan B)

95
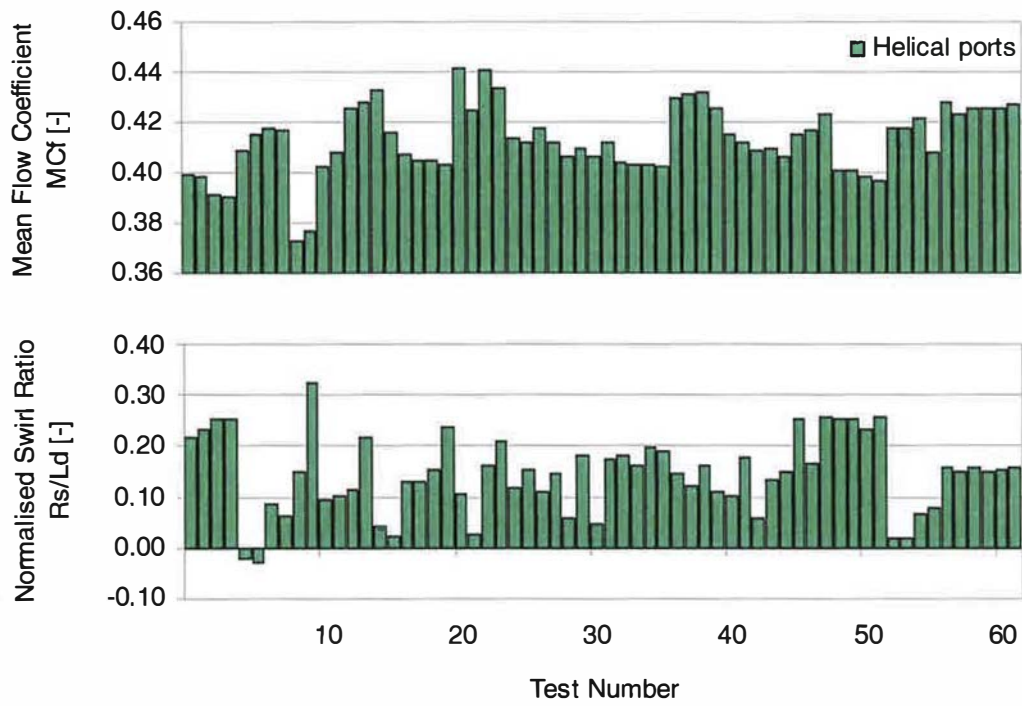
Figure 4.3: Helical port summary results
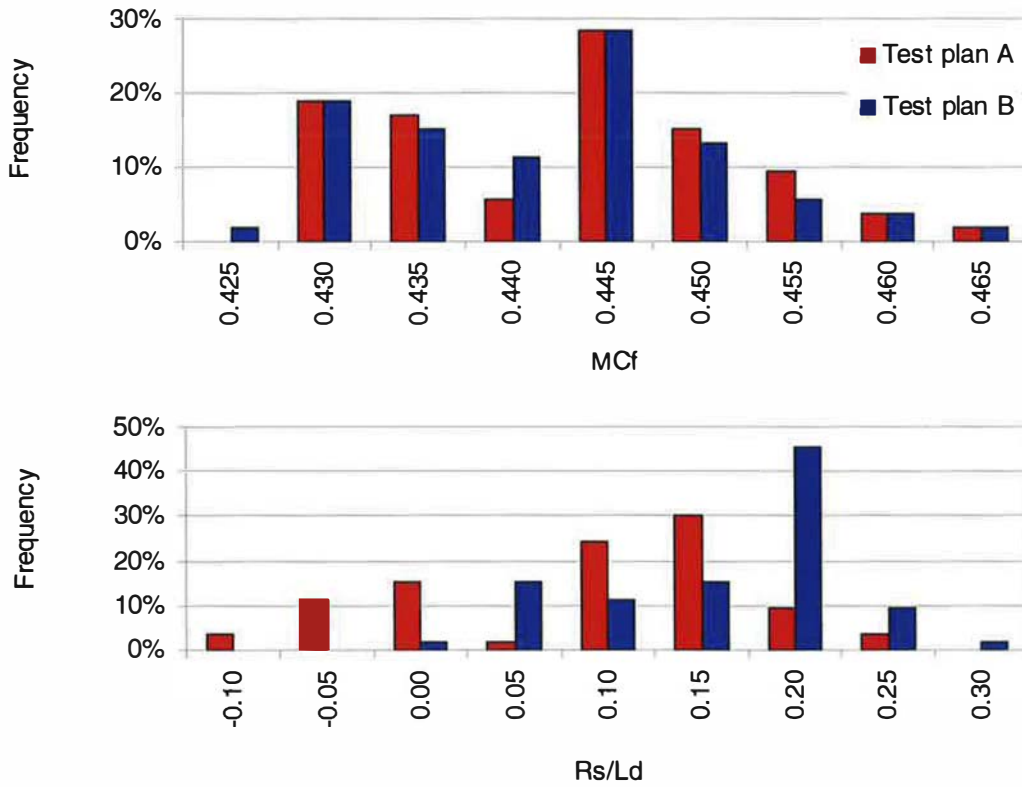
Figure 4.4: Frequency analysis – directed port results
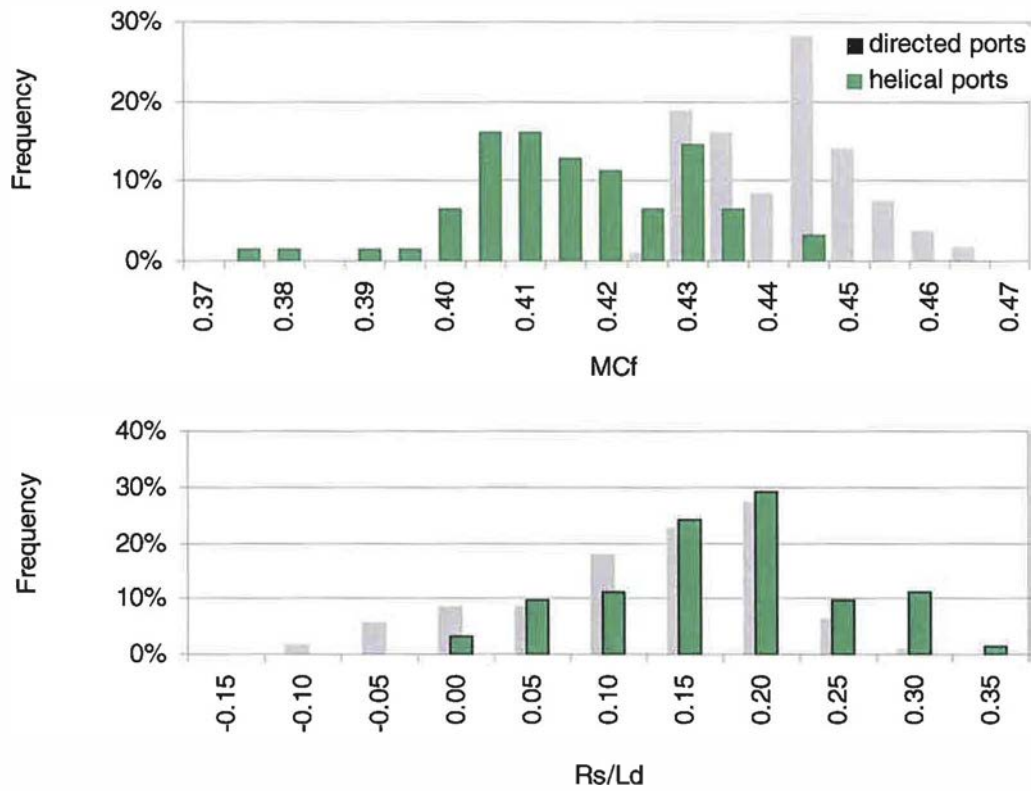
Figure 4.5: Frequency analysis (helical ports)
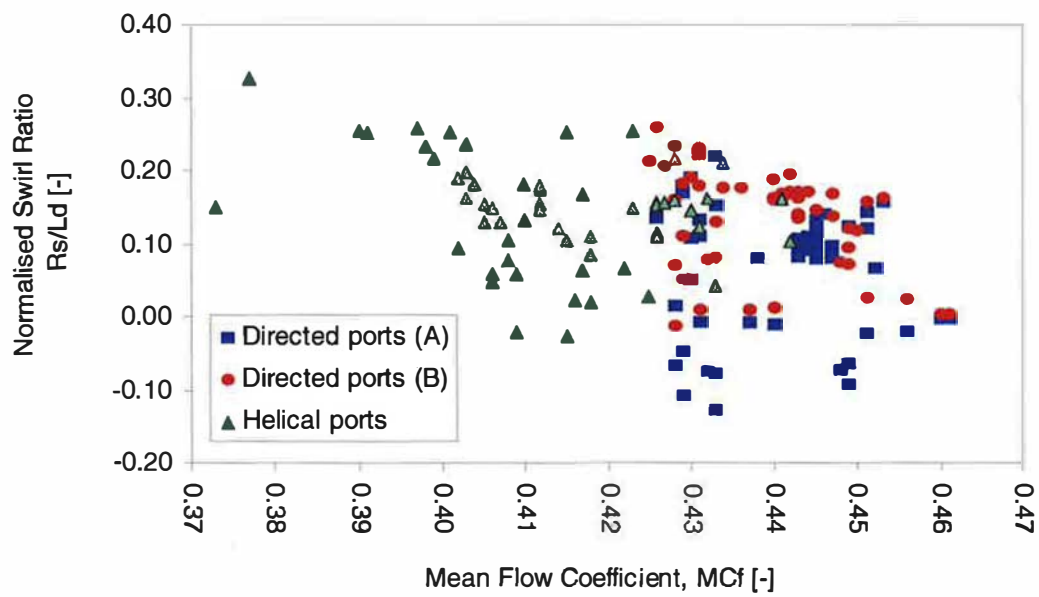
Figure 4.6: Swirl/flow trade-off (all single port types)

4.2.2 Test repeatability

The repeated centre test results in each DoE plan were used to assess test repeatability. Centre tests were performed throughout the test programme in order to identify systematic errors such as drift in instrumentation calibration or progressive wear in any of the test apparatus. Summary results are shown in Table 4.2 and individual Cf and Ns curves are shown in Figure 4.7. In comparing the directed port results, repeatability was clearly superior for test plan B, as indicated by the reduced spread in the swirl results. The Ns curves for test plan A are characterised by low levels of swirl at low valve lift, followed by a rapid increase before stabilising again as lift is increased. Closer inspection of the individual curves clearly shows that the results fall into two distinct groups, characterised by an unstable flow condition at the 6mm valve lift point. An increase in swirl was observed at 6mm lift in three of the tests (shown in red), with a corresponding dip in the Cf curve. The swirl increase occurred in the remaining tests at 7mm lift, causing the results to converge. In comparison, there are no such differences in the test plan B results and although a higher level of swirl is generated, the increase in Ns with valve lift is more linear. The overall contribution of the unstable flow condition to the total range in Rs/Ld values is therefore significant. Variable levels of swirl are also apparent at 1mm lift in the results of both test plans, this is not due to differences in flow rate, as the Cf values remain consistent throughout the low lift region. It is more likely to be caused by unstable swirl conditions when the in-cylinder flow is not well established. The helical port test results indicate good repeatability. In particular, the Ns curves at low valve lift are more consistent than in the directed port study.

	MCf			Rs/Ld		
	Directed A	Directed B	Helical	Directed A	Directed B	Helical
mean	0.445	0.442	0.427	0.098	0.167	0.155
maximum	0.447	0.443	0.428	0.110	0.171	0.158
minimum	0.443	0.440	0.426	0.091	0.163	0.151
range/mean	0.9%	0.7%	0.5%	19.5%	4.6%	5.0%

Table 4.2: Repeatability data (directed ports)
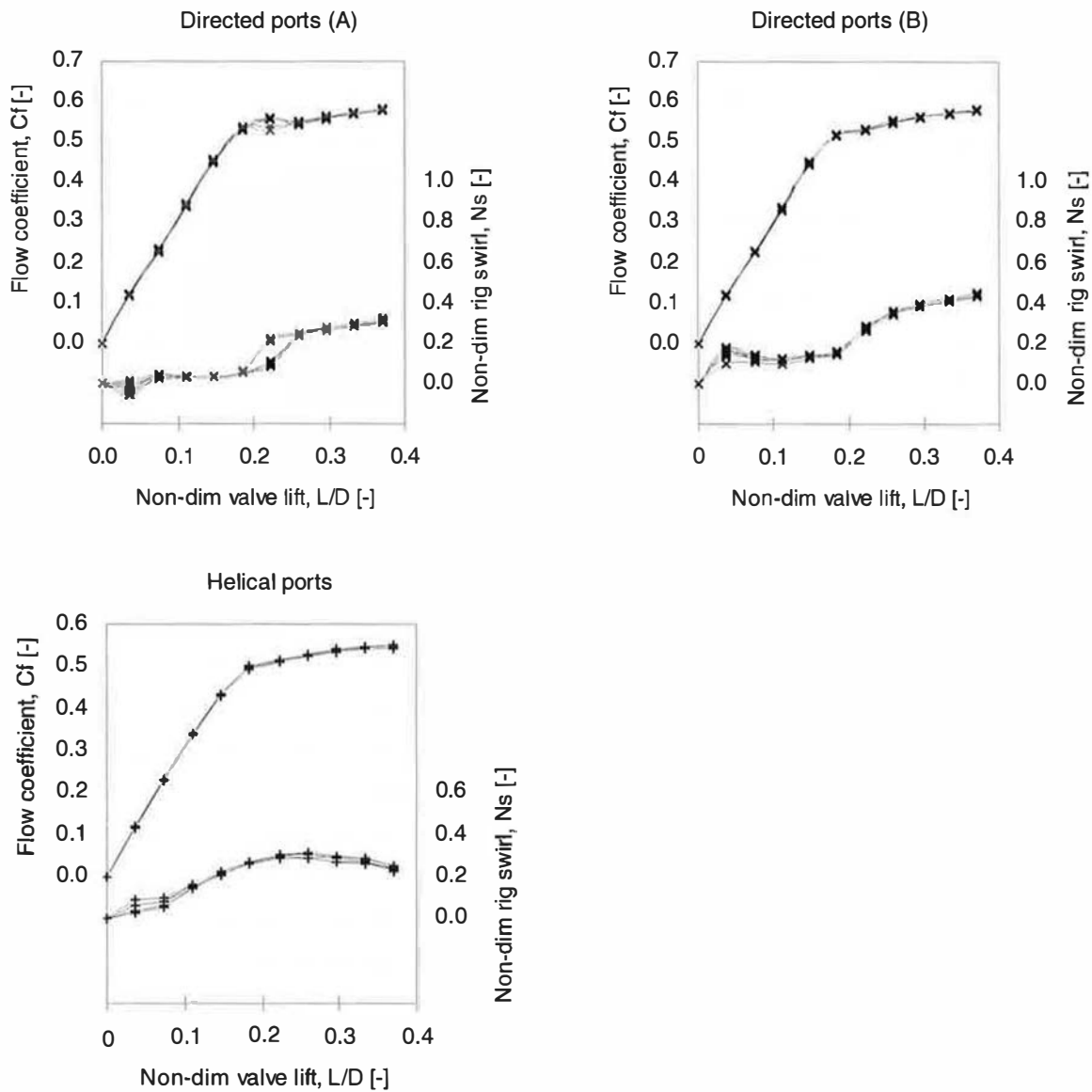
Figure 4.7: Test repeatability (all single port types)

4.2.3 Regression Analysis

The DoE test results were analysed using multiple linear regression, in order to determine the most significant parameter effects and interactions. A polynomial quadratic model of the relationships between the input parameters and performance responses was defined using the results of the regression analysis. The quality of the model was also determined by calculating the squared regression coefficient (R^2) and by checking for outliers in the data that might excessively influence the performance of the model. Separate models were

generated for the MCf and Rs/Ld responses. Model coefficients are presented in Figures 4.8 to 4.11 and model quality is shown in Figures 4.12 to 4.15.

Rs/Ld model coefficients and error bars representing the 95% confidence level are shown for directed and helical ports, in Figures 4.8 and 4.9 respectively. At, Ar and Av were identified as important directed port design parameters. In particular, the second order response of At was evident. The linear E and R parameter terms were more significant in test plan B, in both cases the quadratic terms were insignificant at the 95% confidence level. When comparing each test plan, the most striking difference is in the direction of the Ar and R parameter coefficients (and interactions involving Ar), reflecting the trends observed in the summary results. The Dn parameter was not significant at the 95% confidence interval. Av*At and At*Ar, were the most important interactions in both test plans. R*Ar, At*E and Ar*E were less important, but significant at the 95% confidence interval. In test plan A, At*E, was more significant, indicating a stronger influence on the swirl response. Model coefficients for the helical port Rs/Ld model indicate a strong influence from the helix width (Wh) parameter. Other significant main effects are associated with the helix wrap angle (Aw) and helix start height (Hs) parameters. The tangential approach angle (At) is also important, indicating some similarities with the directed port models. However, the other parameters associated with the geometry of the inlet runner section of the helical ports (port curve angle Ar and port curve radius R) do not appear to be as influential. E is also not significant, alhthough the At*E interaction is. The most important interaction is At*Wh and R*Aw is also present.

MCf model coefficients are shown in Figures 4.10 and 4.11 In general, linear coefficients and interactions were similar for both types of directed port. Linear terms for all parameters were significant, except for Dn. The three most important interactions were Av*Ar, R*Ar and Av*R. There was a significant increase in uncertainty associated with the second order terms, such that even though the Av^2, Ar^2 and At^2 terms were relatively large, they were not significant at the 95% confidence level. The Hs and Wh parameters, and the interaction between them, dominate the helical port responses. Small coefficients for the quadratic terms of E, At, Ar and Aw, but no evidence of linear terms, indicated a practically flat response. A series of minor interactions including Ar*Aw, Aw*Wh and At*Hs are significant at the 95% confidence level, but are unlikely to play a major role in the overall MCf response. It is apparent that the two controlling parameters are directly related to the cross-sectional area of

the port in the helix entry plane. It is therefore likely that this area represents the most important restriction in the port and will govern flow peformance to a large extent.

Rs/Ld model quality was analysed by comparing observed and predicted values for the complete data set. The comparison is shown in Figure 4.12, indicating a strong correlation for both sets of directed port results. The visual comparison was supported by high R^2 values of 0.993 and 0.995 for test plans A and B, respectively. Although the quality of the helical models is lower than the equivalent directed port models, regression coefficients of 0.959 and 0.961 for the Rs/Ld and MCf models respectively, indicate robust correlations. A further data quality check was made by calculating absolute residuals to identify patterns that could signify systematic errors. The comparisons are shown in Figure 4.13. Residuals were randomly distributed and independent of the order in which tests were performed and the observed Rs/Ld value.

The MCf model quality is shown in Figures 4.14 and 4.15. There is a greater amount of scatter when compared to the swirl models, resulting in R^2 values of 0.948 and 0.942 for directed ports, test plans A and B respectively. The quality of the helical port MCf model is higher; R^2 is 0.961. Absolute residuals were greater than the swirl models, in relation to the response changes caused by intentional parameter changes. However, there were no systematic errors associated with run order or measured value.
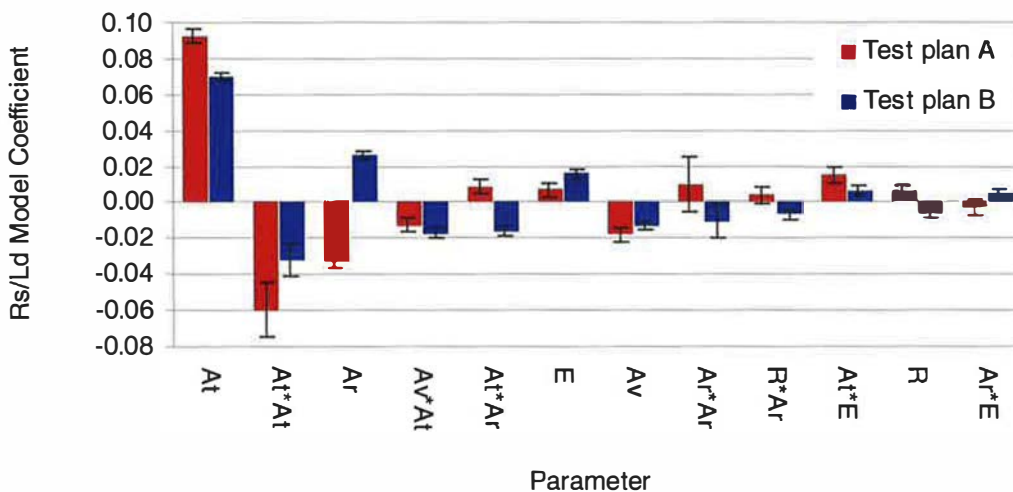
Figure 4.8: Rs/Ld model coefficients (directed ports)
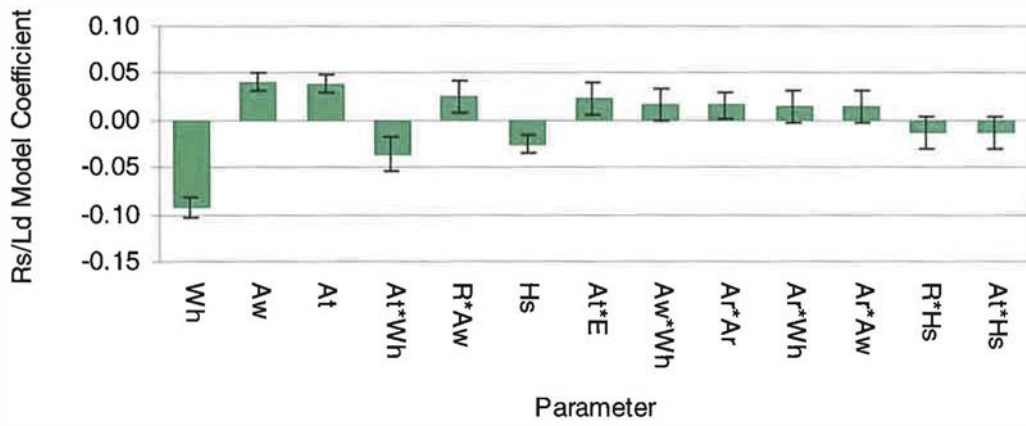
Figure 4.9: Rs/Ld model coefficients (helical ports)
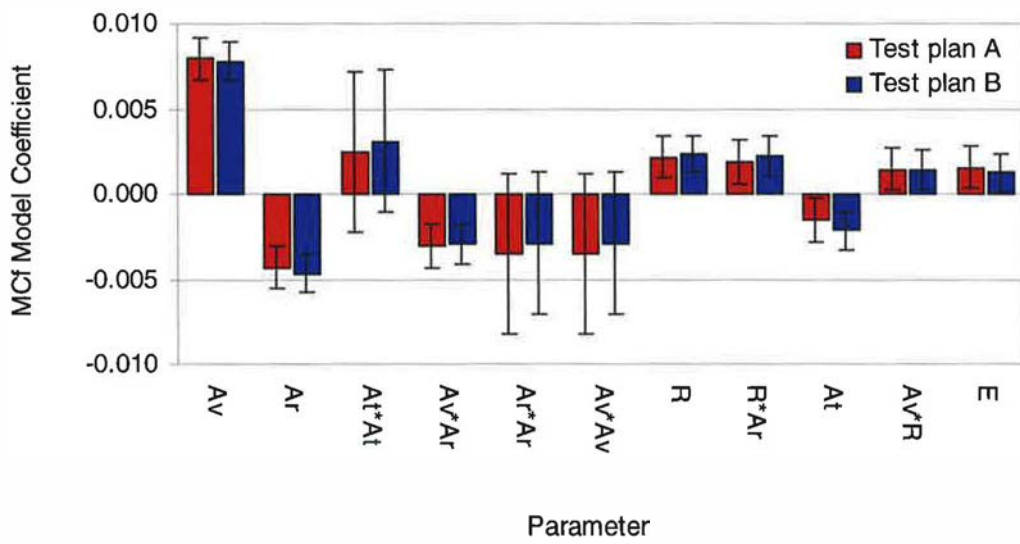
Figure 4.10: MCf model coefficients (directed ports)
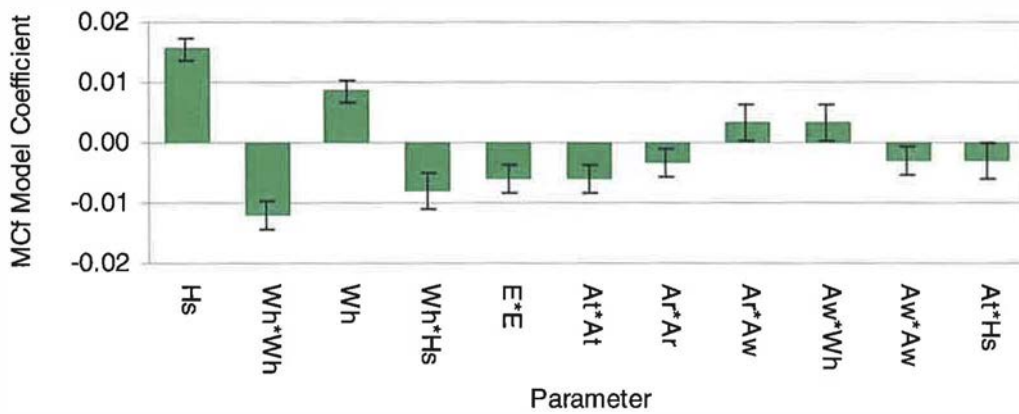
Figure 4.11: MCf model coefficients (helical ports)
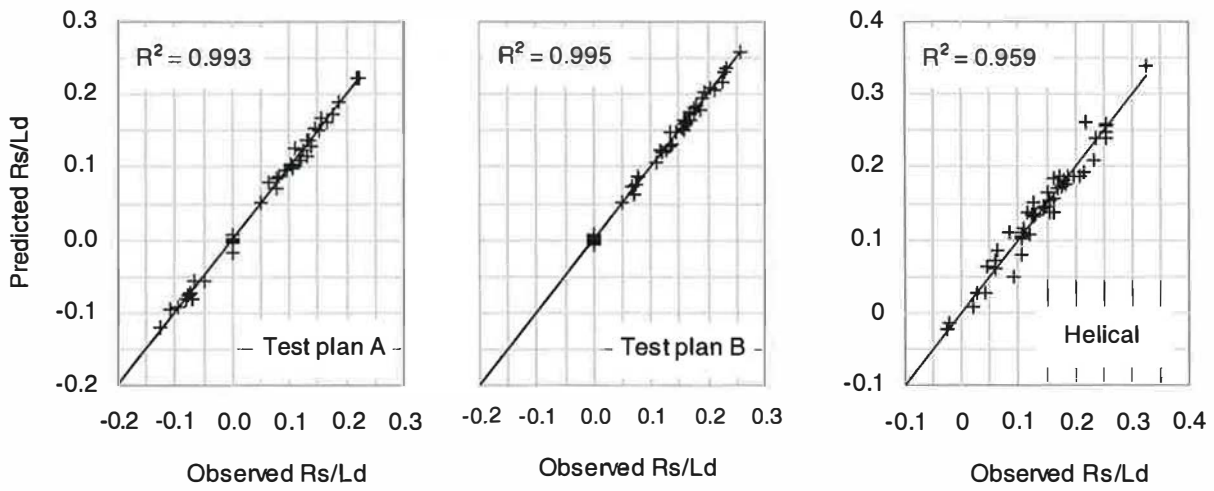
Figure 4.12: Comparison of predicted and observed Rs/Ld responses
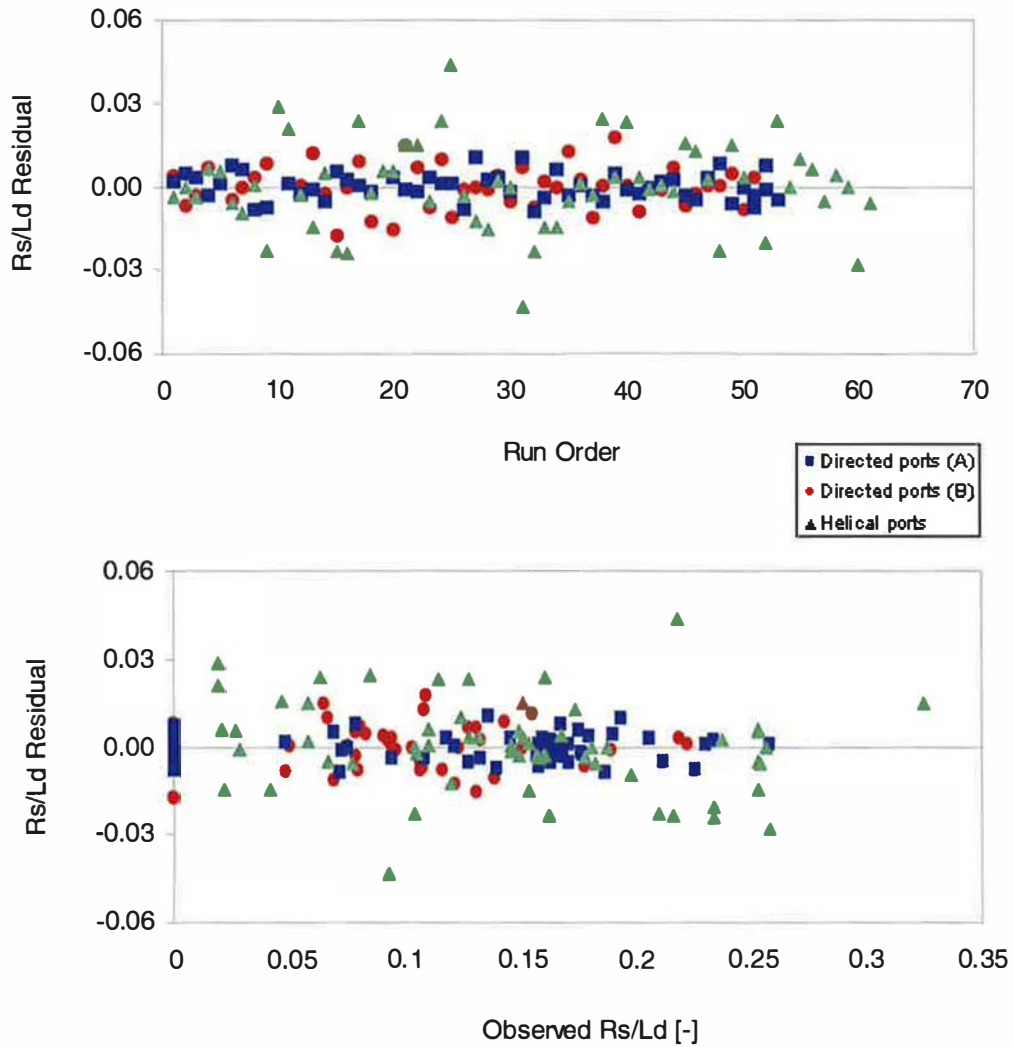
Figure 4.13: Rs/Ld residuals
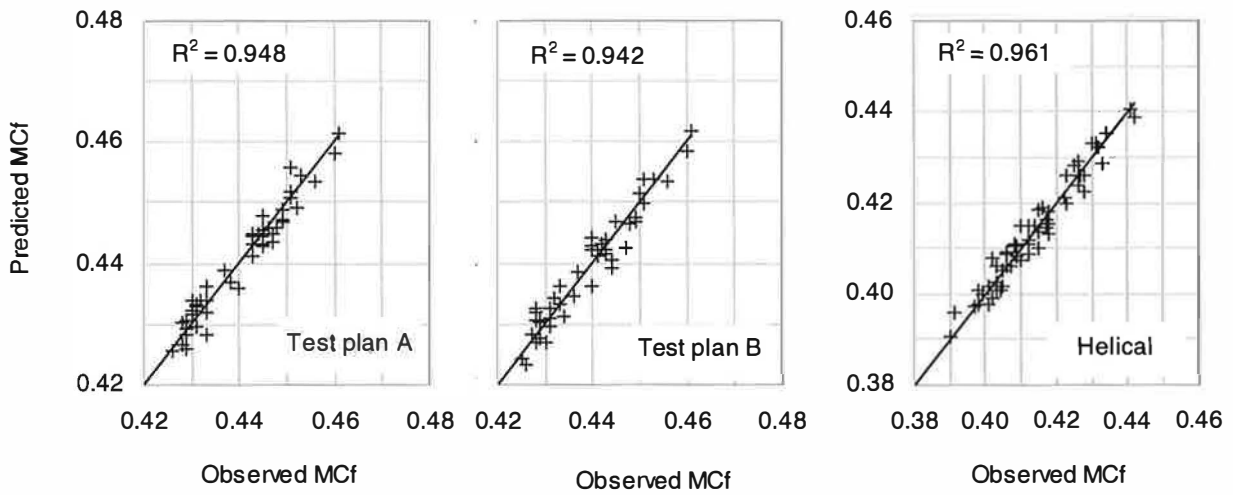
Figure 4.14: Comparison of predicted and observed MCf responses
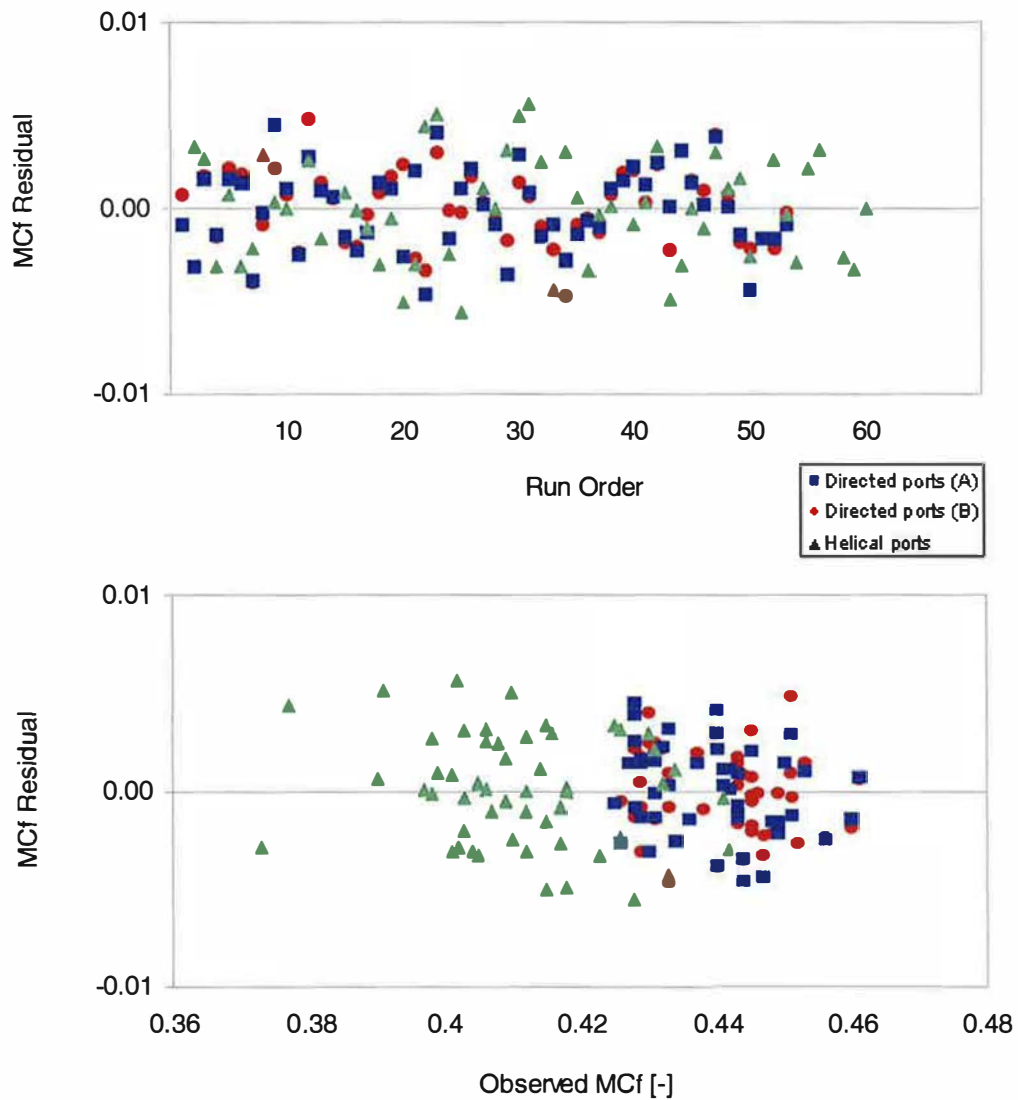
Figure 4.15: MCf residuals

104

4.2.4 Main Effects

The Rs/Ld main effects are shown in detail in Figures 4.16 to 4.18. The shape of the curves is determined by the model coefficients shown in Figures 4.8 and 4.9. Curves showing the 95% confidence interval are included to indicate the robustness of the models. The distance between the curves representing the upper and lower confidence levels show that the Rs/Ld models are more robust than the MCf models, as would be expected given the R^2 values. The contrast between the two directed port types is evident; the response curves show an increased level of swirl for test plan B. The importance of At in terms of swirl generation is clearly shown and the significant second-order response results in a maximum swirl condition at approximately 90 degrees for both test plans. The change in direction of the swirl response to Ar can also be seen, once again illustrating how the response is dependent on the magnitude and direction of port curvature. The minor effects of Av and E can be seen from the shallow slope of the curves. The main effect plots suggest that these parameters contribute a relatively small amount to the overall swirl response, although their presence through interactions with more significant parameters must also be considered. Dn has an almost flat response, as indicated by the insignificant linear and quadratic model coefficients. Helical port swirl responses are mostly linear, the most significant being the Wh parameter response. Increasing helix width drastically reduces swirl generation. At is less significant than for directed ports, suggesting that helical ports are more insensitive to port orientation. Hs and Aw also have secondary effects, but all are significant at the 95% confidence level. Decreasing helix height and increasing helix wrap angle result in increased swirl.

The main parameter effects with respect to the MCf response are shown in Figures 4.19 to 4.21, reflecting the model coefficients shown in Figures 4.10 and 4.11. The curves for both directed port types are similar, and the most important effects are associated with port geometry rather than orientation in the cylinder. In both cases, Av is clearly the most important parameter, indicating an increase in flow performance as the port angle is increased. Of all the other parameter effects, Ar is the most significant, indicating a loss in flow performance as the port curve angle is increased. The R effect is masked by the uncertainty associated with the quadratic term, although the trend is logical; a reduction in curve radius is detrimental to flow performance, resulting in a decrease in MCf. The At curves suggest that there may be a negative influence on MCf from increasing At, possibly as a result of mild

cylinder bore shrouding on one side of the valve. The flat E response supports the recommendation that a maximum value of 0.45 for E should not result in excessive cylinder bore shrouding. The MCf response to Dn is also flat, in common with the swirl response. The helical port MCf responses indicate that helix cross sectional area is important. Increasing helix height Hs (for a constant helix width) improves flow performance. The Wh response indicates a general flow improvement as Wh is increased. Although the main effect response curve has a second order shape, the significance of this is not clear due to the relatively large uncertainty. At and E responses are generally flat within the 95% confidence band.

4.2.5 Response Surfaces

The most important parameter interactions in the Rs/Ld models are shown in Figures 4.22 to 4.24. The Av*At interaction (Figure 4.22(a)) indicates a change in the directed port Rs/Ld response to Av, depending on the At value. At low At settings, the swirl response is flat but at higher At settings swirl is more sensitive to changes in Av. This interaction shows that the swirl response is independent of the vertical orientation of a radial port (At=0), but is increasingly dependent on vertical orientation as the tangential flow component becomes more significant (At=90). The interaction is similar for both types of directed ports, although there is a positive swirl shift in test plan B, due to the effect of the nominal 45 degree port curvature. The At*E interaction, shown for test plan A in Figure 4.19(b), indicates that E becomes significant only at an At value towards the upper end of the total range. This is also expected since the influence of distance between the valve and the cylinder centre becomes stronger as the tangential flow component increases. The At*Ar interaction for both test plans are shown in Figure 4.23(a). The horizontal Ar scale for test plan B has been reversed, so that the effect of the direction of port curvature (Ar) can be seen more clearly. When the directed port is straight (Ar=0), the two surfaces representing each test plan are aligned, as shown by the similarity between colours representing swirl magnitude and the direction of contour lines indicating the slope of each surface. Both surfaces indicate zero swirl when Ar and At values are zero. The R*Ar interaction is shown in Figure 4.23(b). Although the response is not large, the combined effect of port curve angle and curve radius can be seen. Once again, the Ar scale on the surface representing test plan B is reversed in order to show the overall response throughout the complete Ar range. A relatively continuous surface representing both responses can be seen. Three interactions are significant in terms of their influence on the Rs/Ld response in helical ports (Figure 4.24). The most important is the At*Wh interaction.

For high Wh values, the response is independent of At. Furthermore, the level of swirl generated is low, suggesting a loss in swirl-generating potential irrespective of the orientation of the port with respect to the cylinder. As Wh is decreased, the At effect becomes more apparent. High At values are associated with increased Rs/Ld, indicating that a tangential flow component is contributing to the in-cylinder air motion. The At*E surface indicates that the response to At becomes more apparent as E is increased and any tangential flow component is maximised. The Aw*R interaction, although small, has an interesting effect. At high values of R, Aw has a positive influence on the swirl response. However, as R is decreased, swirl becomes less dependent on Aw, possibly due to changes in the flow conditions in the port at the helix entry section.

As with main effects, the MCf response to directed port parameter interactions is similar for both port types. Therefore, the test plan A interaction plots are presented in Figures 4.25. The Av*Ar interaction (Figure 4.25(a)) is the most significant and indicates that the response changes primarily with Av. A steep vertical approach angle (high Av) results in an unrestrictive port. Therefore, curvature in the port controls flow performance. As Av is decreased, it becomes the controlling parameter and flow performance becomes relatively insensitive to Ar. The Ar*R interaction, shown in Figure 4.25(b), illustrates a simple relationship; the flow performance of curved ports is clearly dependent on the angle and radius of curvature. As curve angle is reduced, the radius becomes less important. In the extreme case of straight ports, the radius is undefined and the response is flat. The final MCf interaction, between R and Av, is shown in Figure 4.25(c). The contours indicate a similar response to the Ar*Av interaction, flow performance is influenced by R only when Av is high. The effect of the Wh*Hs interaction on the MCf response indicates the importance of helix cross-sectional area. A rapid decrease in MCf occurs when when both parameters are set to low values. The response flattens as the value of either response is increased.
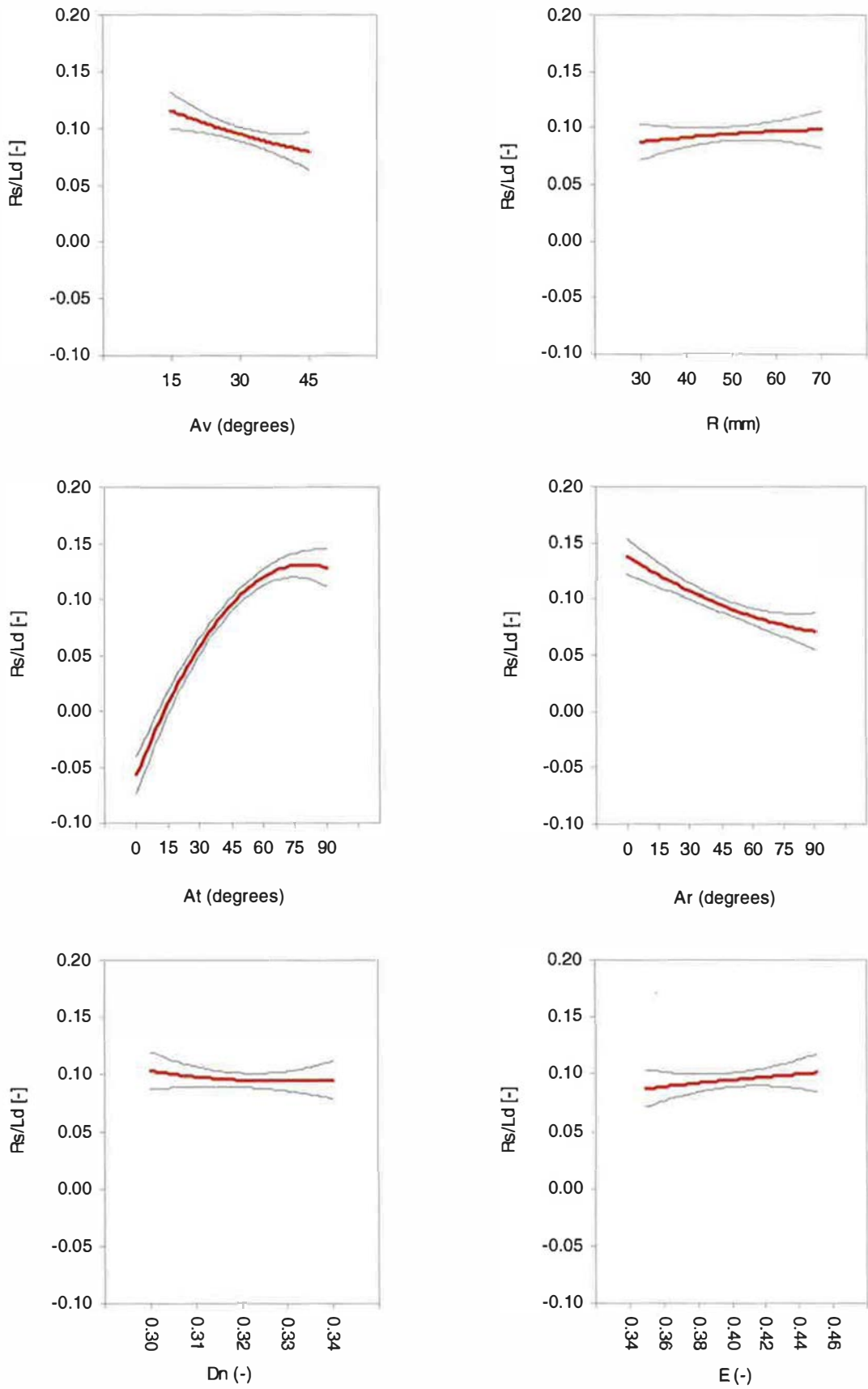
Figure 4.16: Main parameter effects, Rs/Ld response (directed ports, test plan A)
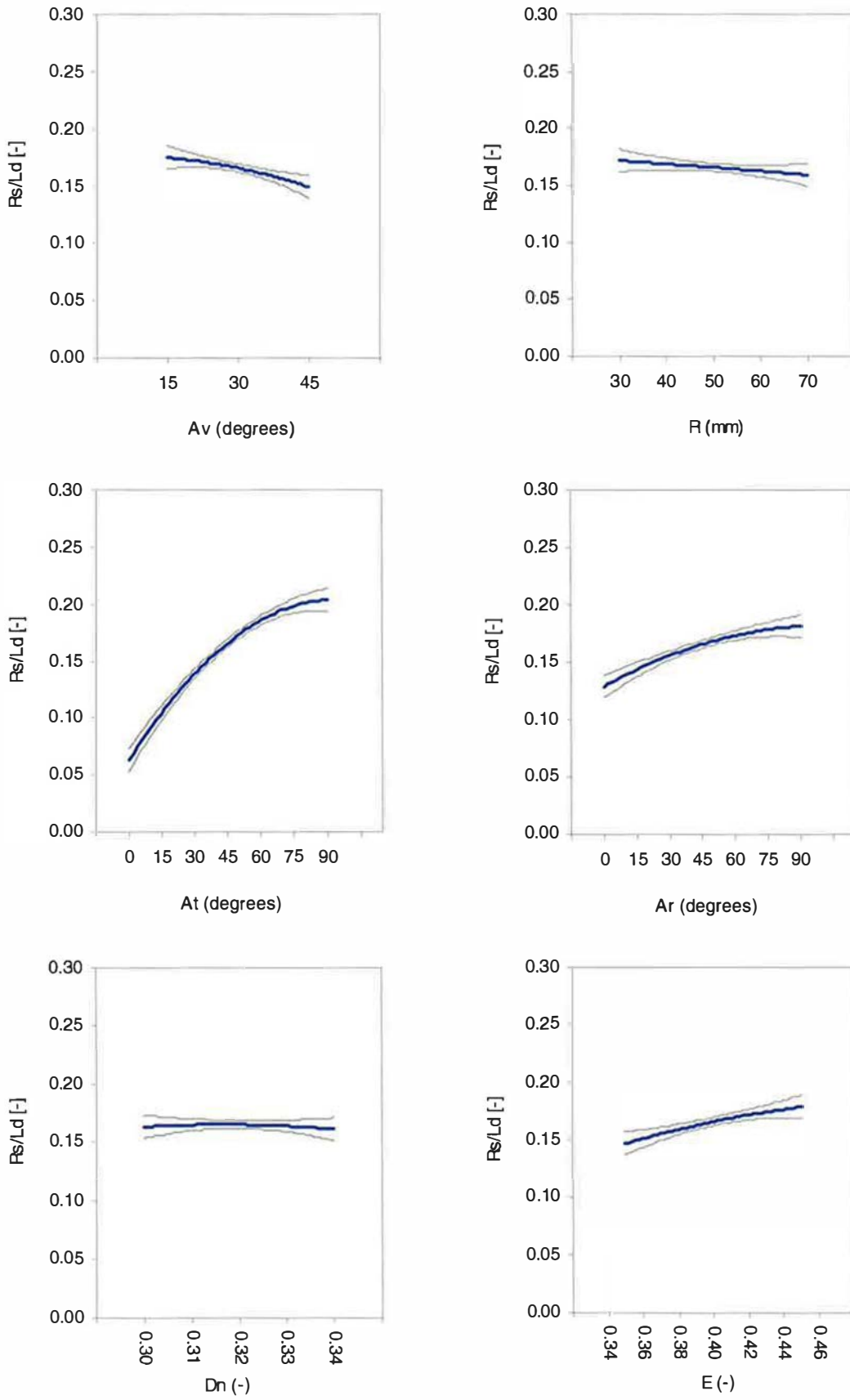
Figure 4.17: Main parameter effects, Rs/Ld response (directed ports, test plan B)
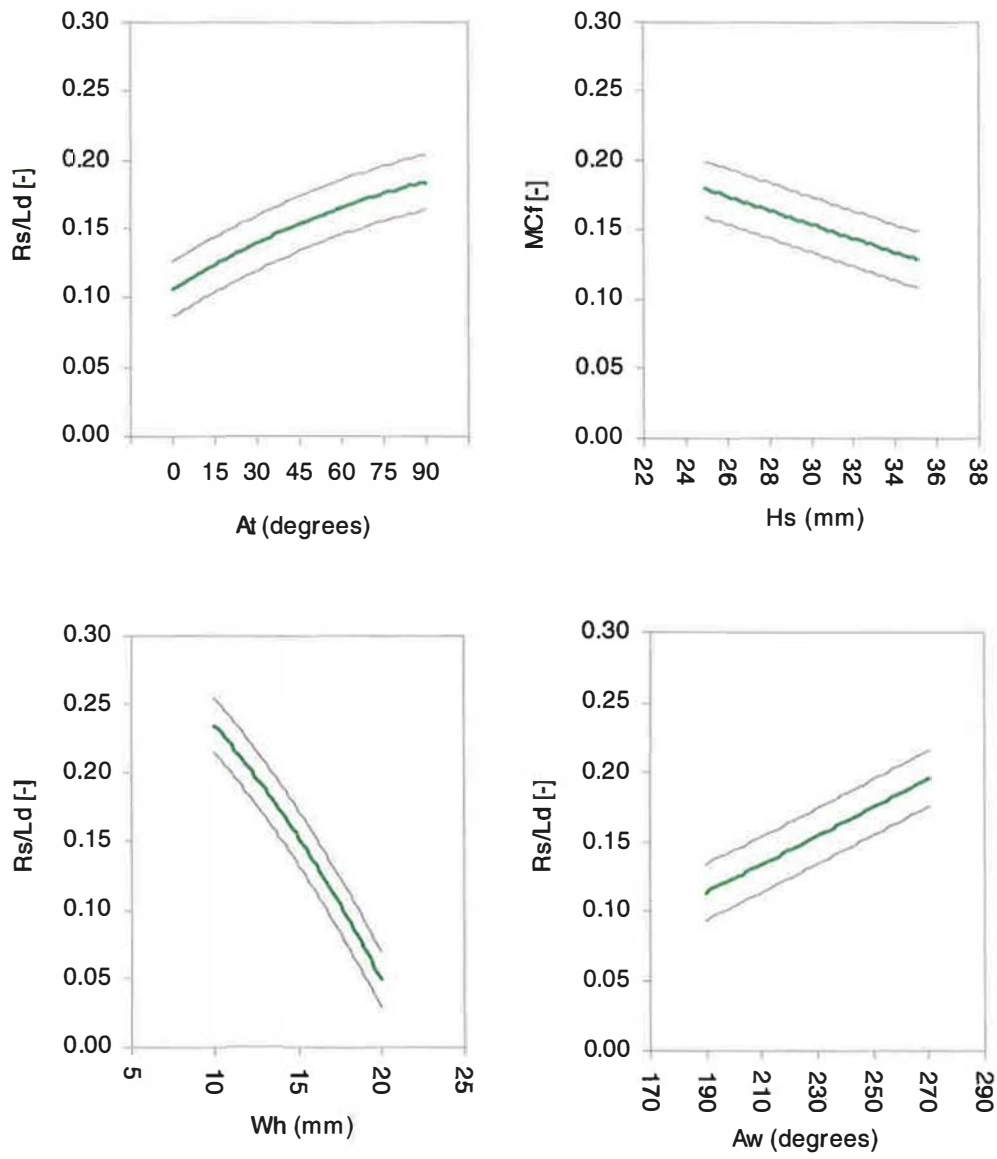
Figure 4.18 : Main parameter effects, Rs/Ld response (helical ports)
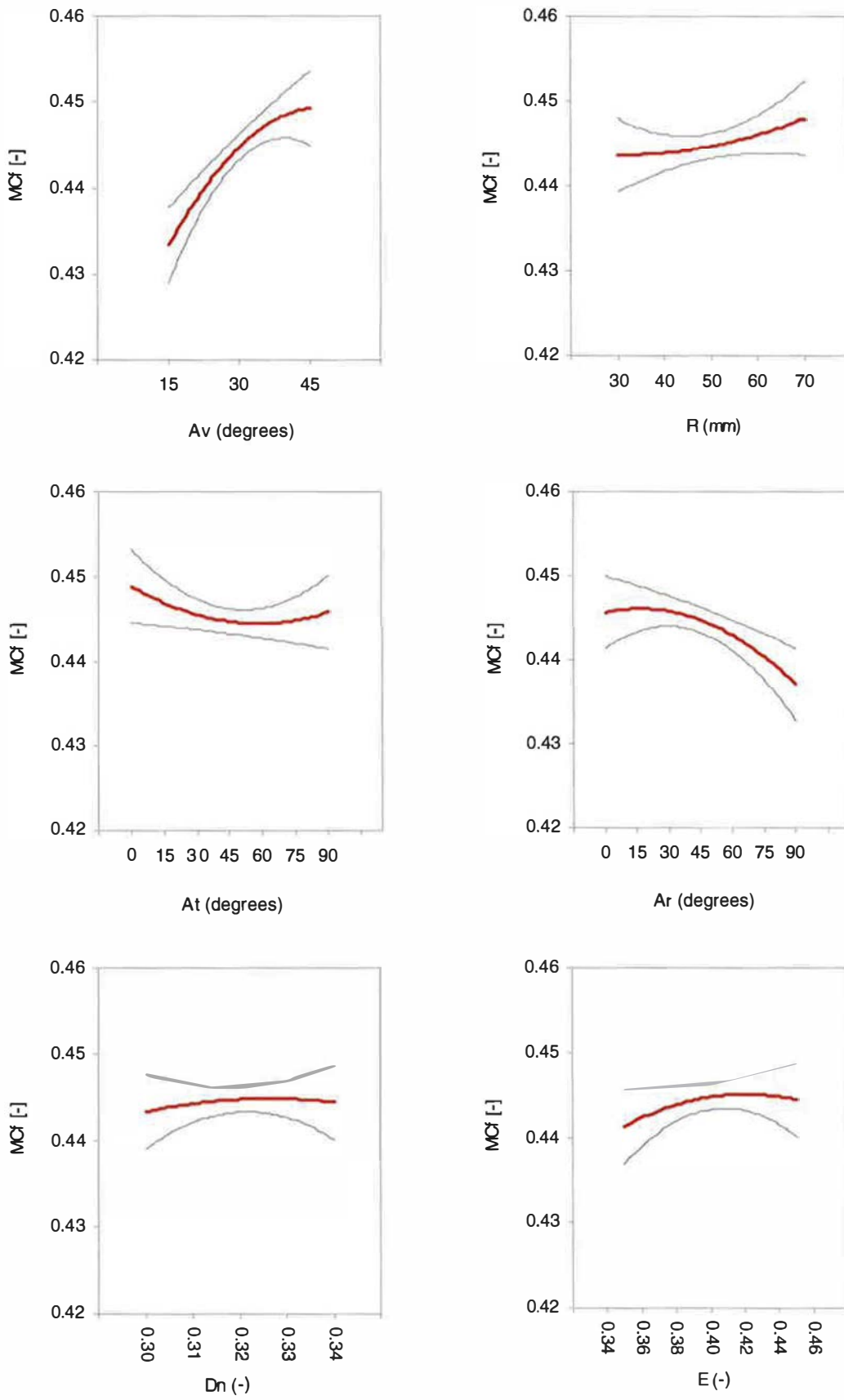
Figure 4.19: Main parameter effects, MCf response (directed ports, test plan A)
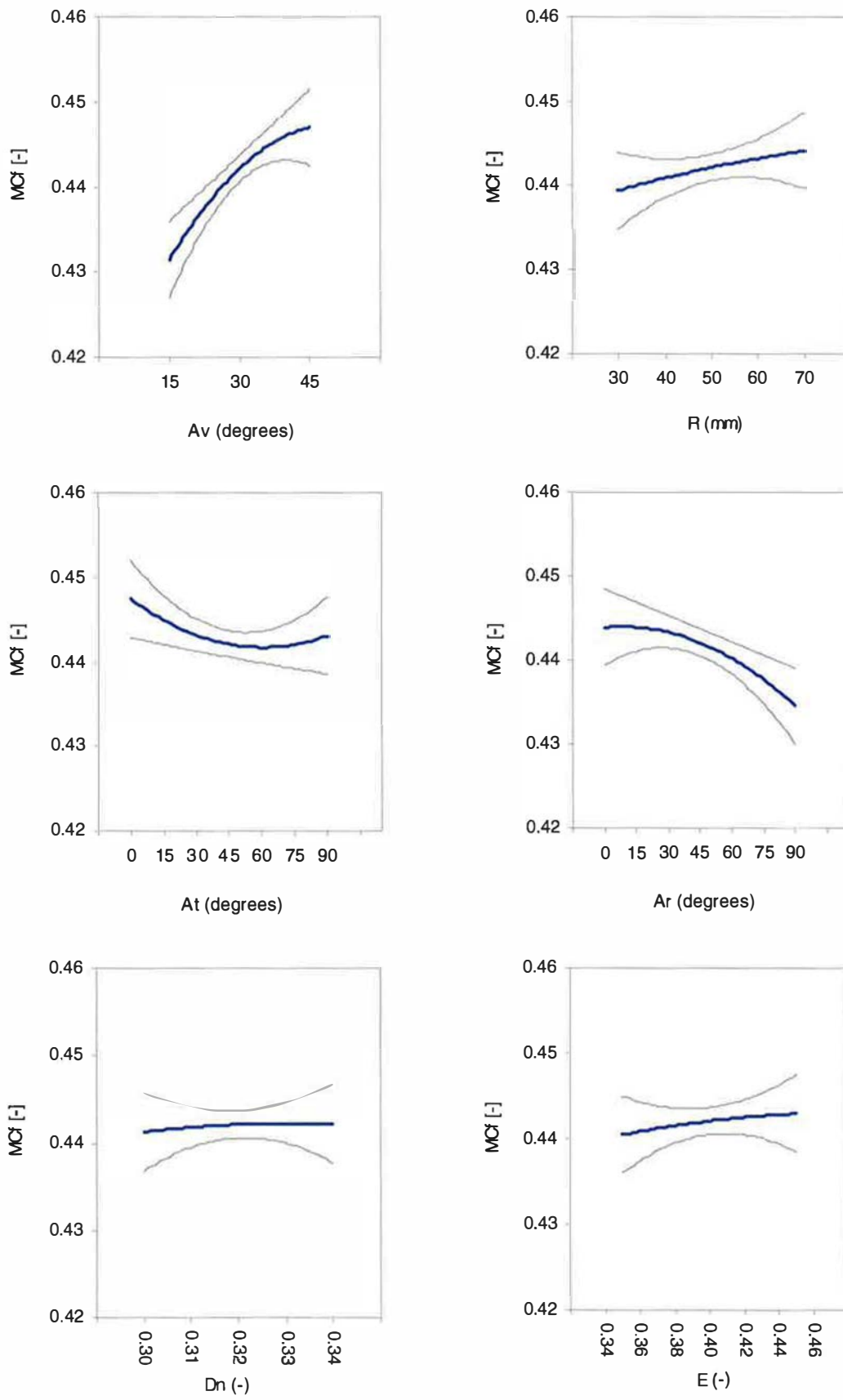
Figure 4.20: Main parameter effects, Rs/Ld response (directed ports, test plan B)
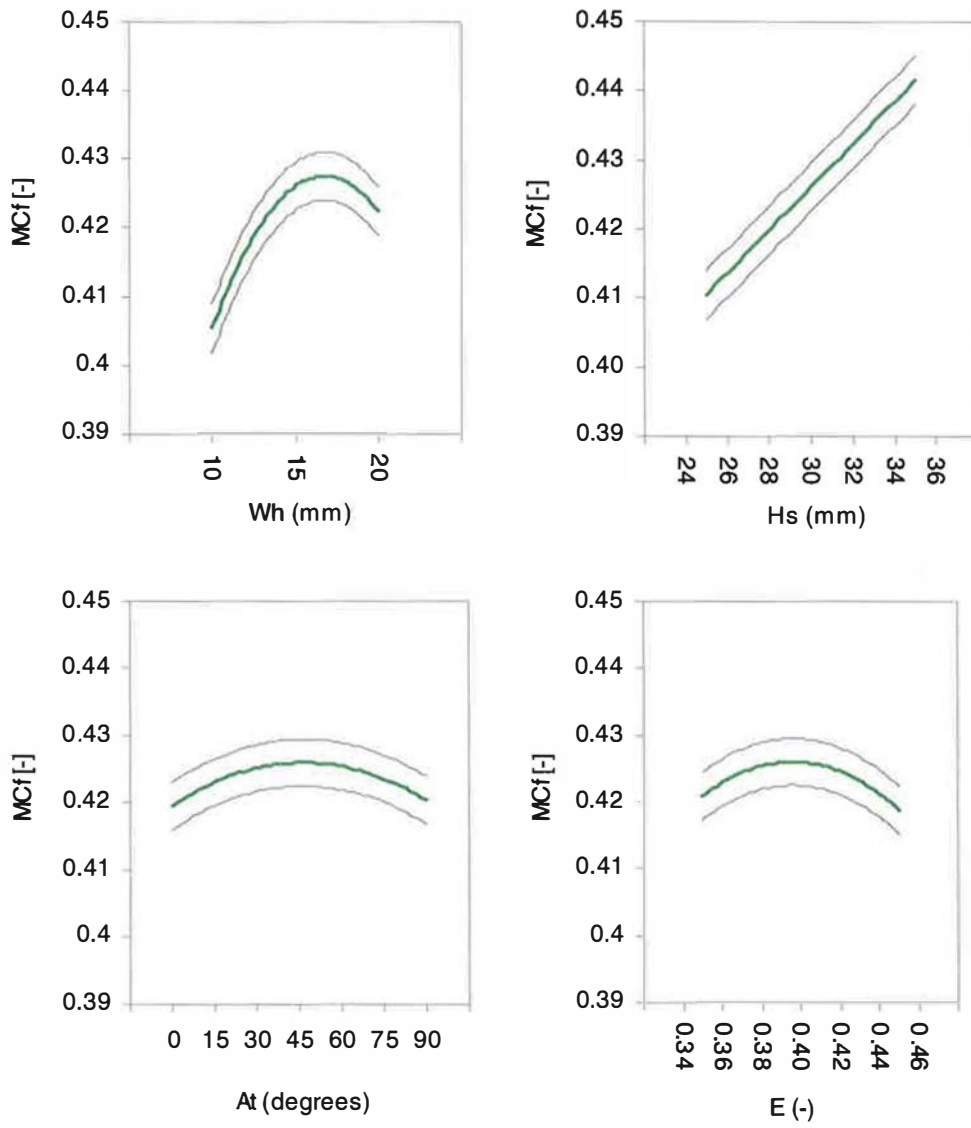
Figure 4.21: Main parameter effects, MCf response (helical ports)
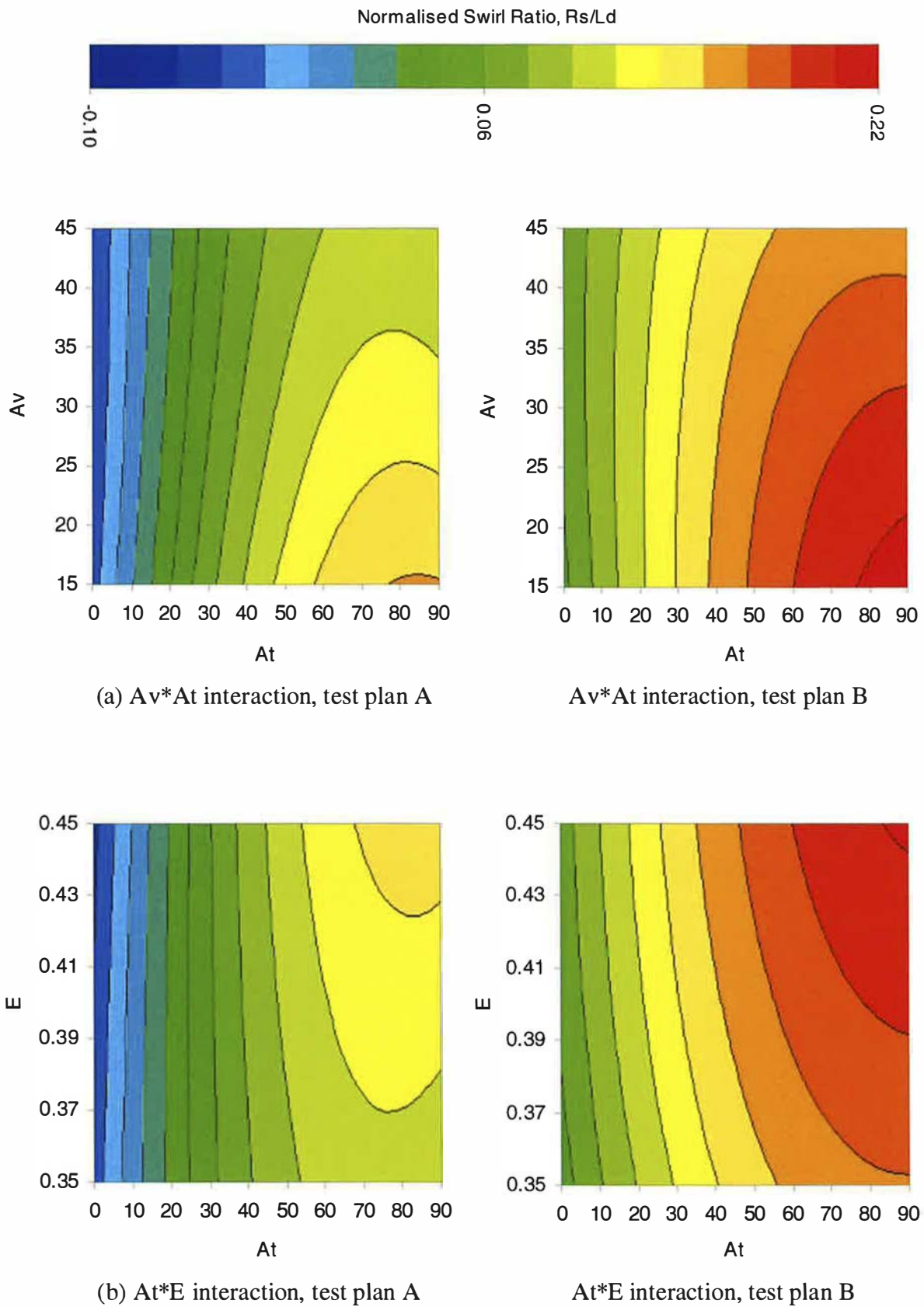
Figure 4.22: Rs/Ld response surfaces (directed ports)

Normalised Swirl Ratio, Rs/Ld
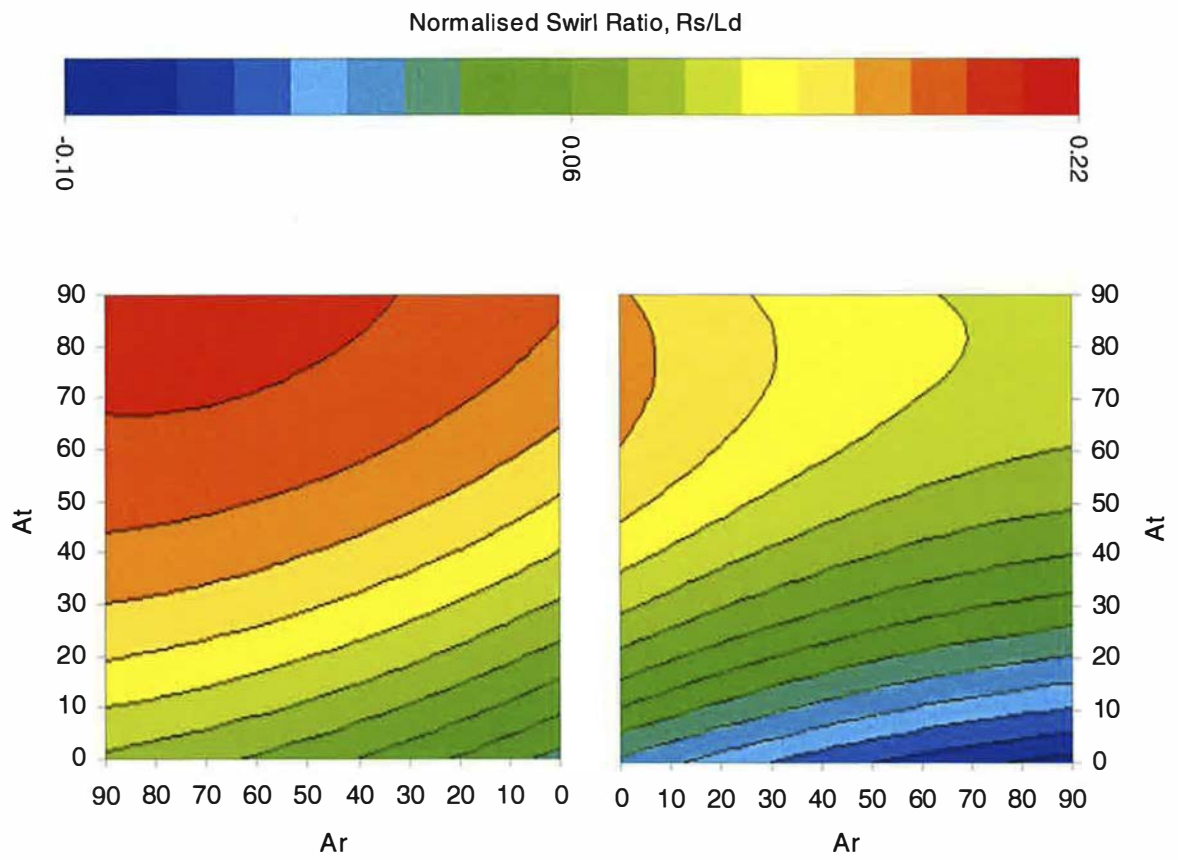
(a) Ar*At interaction, test plan B   Ar*At interaction, test plan A
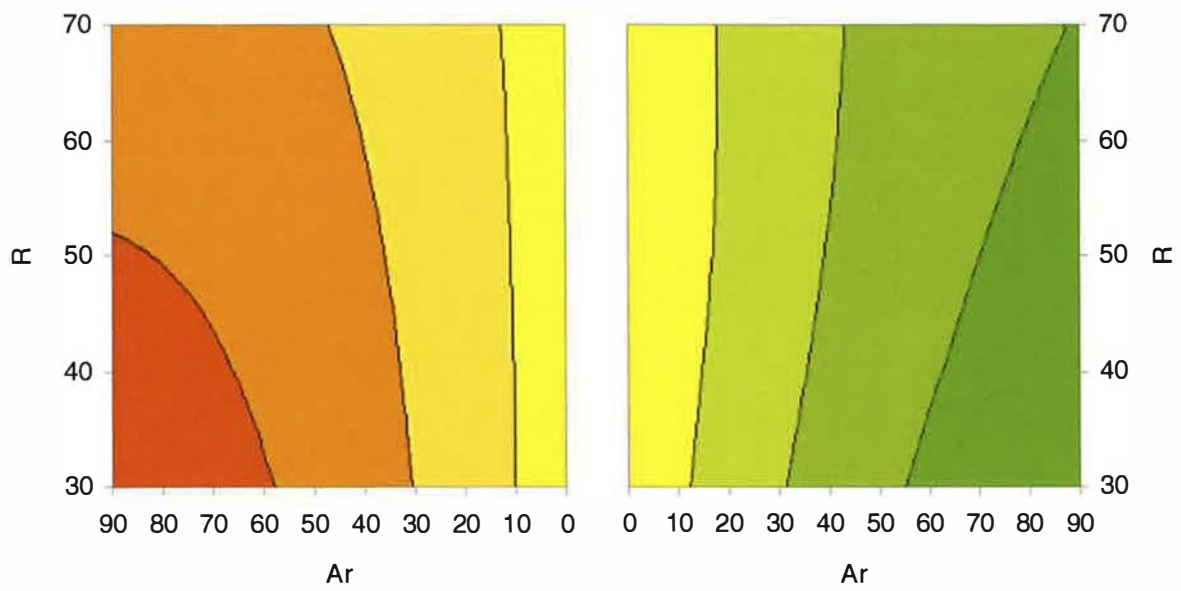
(a) Ar*R interaction, test plan B   Ar*R interaction, test plan A

Figures 4.23: Rs/Ld response surfaces (directed ports)
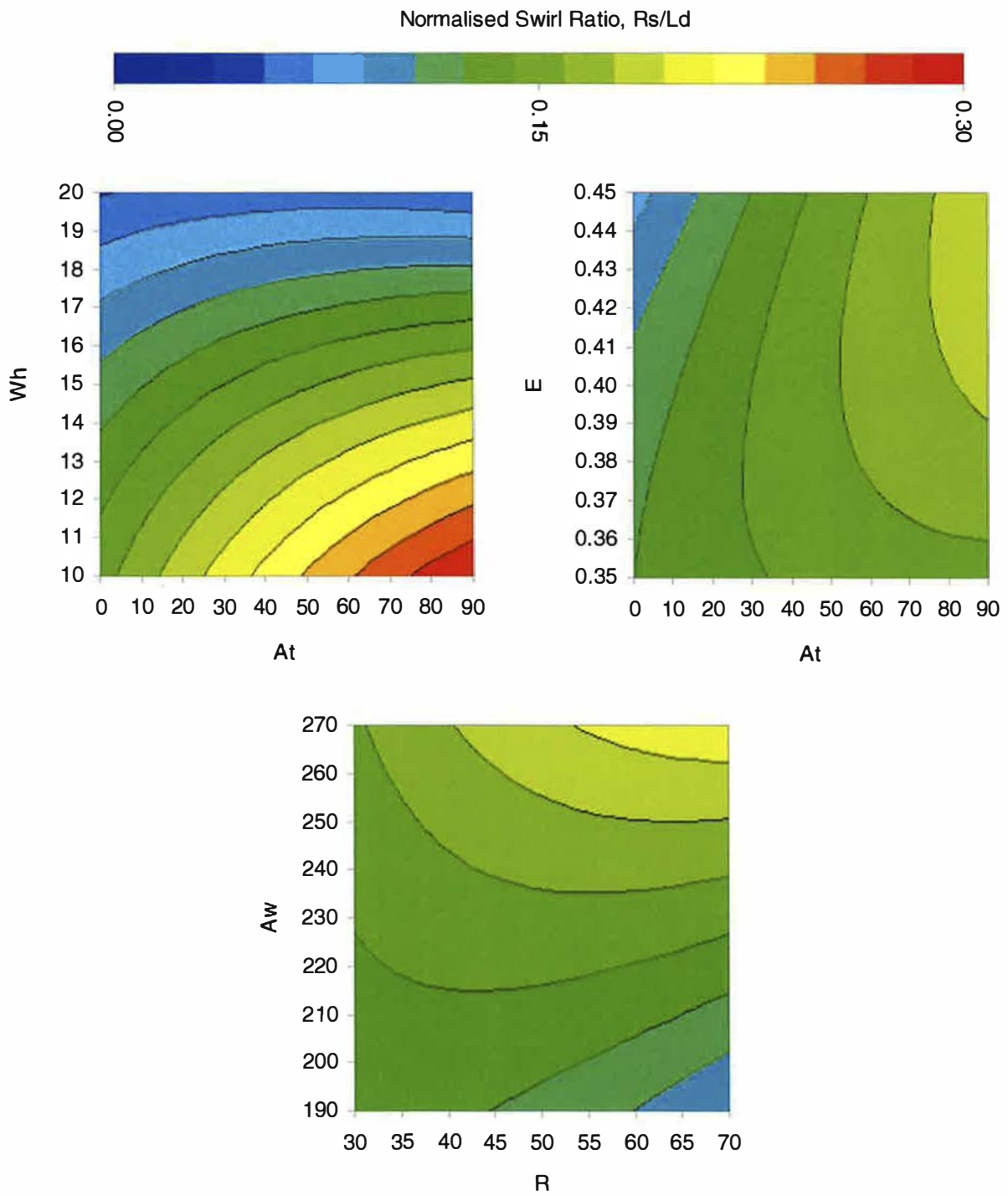
Figure 4.24: Rs/Ld response surfaces (helical ports)

Mean Flow Coefficient, MCf [-]

0.429   0.442   0.455
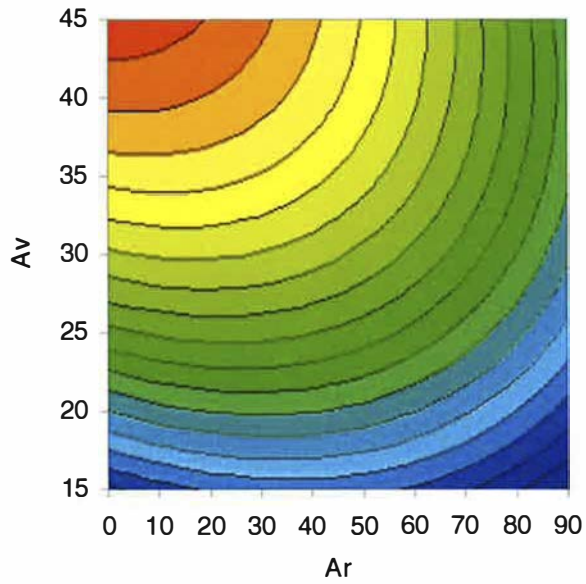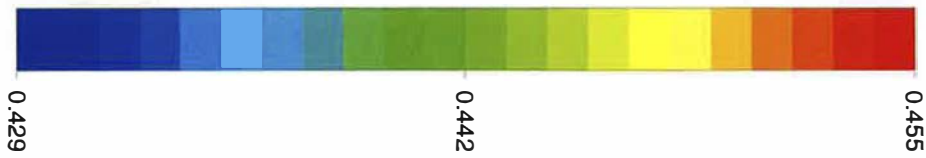
(a) Ar*Av interaction, test plan A
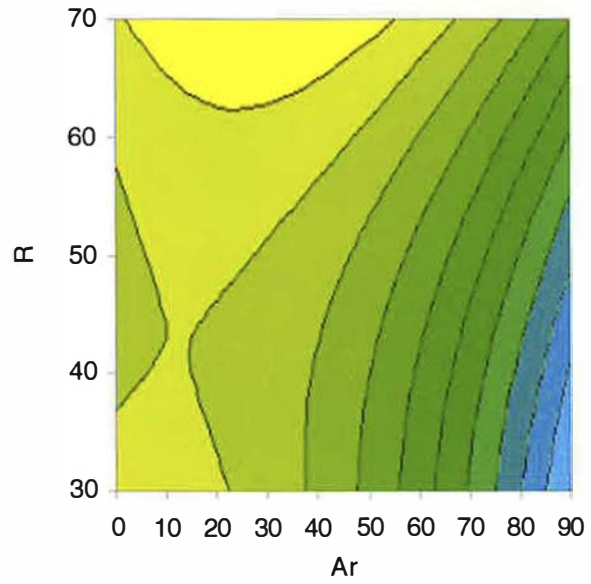
(b) Ar*R interaction, test plan A
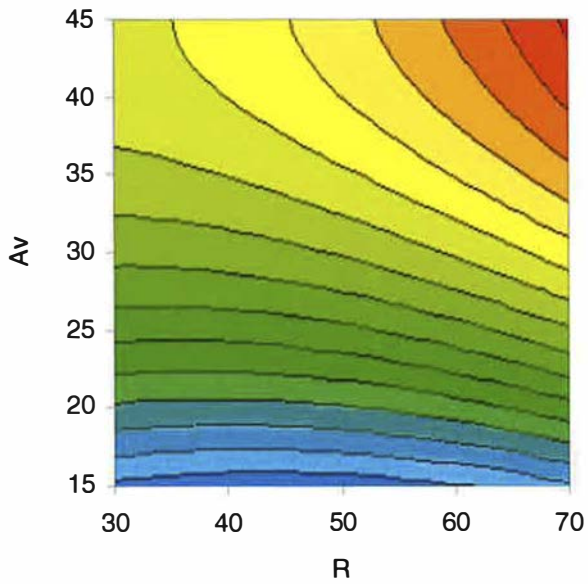
(c) R*Av interaction, test plan A

Figure 4.25: MCf response surfaces (directed ports)

117
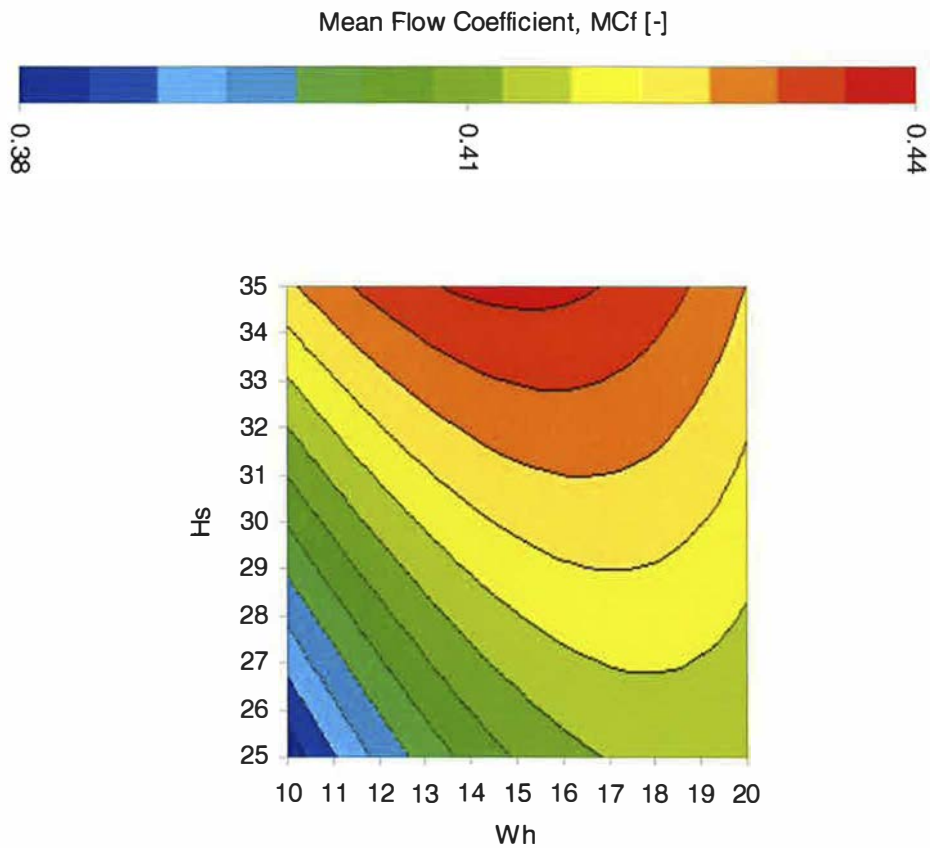
Figure 4.26: MCf response surfaces (helical ports)

4.3   Enhanced Standard Model with Variable Valve Lift Profile

4.3.1 Modelling Technique

The inlet valve lift profile has a considerable effect on flow performance and in-cylinder motion. In a steady state model, although the port flow characteristics at each individual valve lift condition are independent of the lift profile, the effects of maximum valve lift and duration are captured in the parameters that are used to summarise performance over the entire intake event. Therefore, the standard model was enhanced by describing the valve lift profile parametrically and performing two-stage regression on the MCf and Rs/Ld data. The two-stage model was developed by producing a simple DoE test matrix of the valve lift profile parameters (maximum valve lift and duration), as shown in Table 4.3

Parameter	Nominal value	Minimum value	Maximum value
Maximum valve lift, L (mm)	8.37	7.29	9.45
Lift duration, P (degrees crank)	215	230	245

Test Run	P1 (L)	P2 (P)	Note
1	7.29	215	
2	9.45	215	
3	7.29	245	
4	9.45	245	
5	8.37	230	CENTREPOINT

Table 4.3: Valve lift profile parameters and experimental plan

A full-factorial experiment was defined to provide a test matrix of maximum valve lift and duration combinations. Rs/Ld and MCf responses were calculated from the raw test data using these cam profile settings, resulting in 53 responses for each test point of the DoE plan. This model was then analysed using multiple linear regression to provide model coefficients for duration, lift and duration*lift interaction, plus a constant term. These model coefficients were then fed back as responses into the main central composite DoE test matrix. A second stage of multiple regression therefore resulted in each cam profile coefficient being expressed as a function of the port design parameters:

$$Rs/Ld = C_1 + C_2*P + C_3*L + C_4*P*L \qquad (4.1)$$

Where $\quad C_1 = w_1At + w_2Ar + w_3R + \dots \qquad C_2 = x_1At + x_2Ar + x_3R + \dots$

$\qquad\quad C_3 = y_1At + y_2Ar + y_3R + \dots \qquad C_4 = z_1At + z_2Ar + z_3R + \dots$

The technique is based on the assumption that the two groups in the two-stage scheme (i.e. the cam profile parameter group and the port design parameter group) are independent of each other and therefore interactions between parameters from different groups are insignificant. In considering the effect of maximum valve lift and duration on the summary flow characteristics, it is clear that MCf is dependent only on maximum lift, as duration is the denominator in the expression for MCf in Equation 1.5a. In contrast, Rs/Ld is dependent on the maximum lift and duration, due to the influence of the integral terms in equation 1.6. In

order to simplify this expression and therefore simplify the relationship between the swirl response and cam profile, the summary swirl parameter was re-defined as Rs_0, the integral of $Cf*Ns$ throughout the valve lift event. Rs/Ld may then be calculated using the Rs_0 model, combined with the MCf model and duration (P):

$$Rs_0 = \int_{\alpha 1}^{\alpha 2} CfNs \, d\alpha \qquad (4.2)$$

$$Rs/Ld = \frac{Rs_0}{(MCf \cdot P)^2} \qquad (4.3)$$

4.3.2 Regression Analysis

The stage-one regression results indicated that, as expected, the MCf response was linearly dependent on maximum valve lift for each of the main DoE test points. The duration and interaction terms were insignificant. The stage-two regression coefficients for the constant sub-models are shown in Figures 4.27 and 4.28. The port design parameter terms in the constant sub-model are comparable to those of the standard model for directed and helical port types, indicating that the basic MCf predictions are robust with regard to the addition of cam profile parameters and the two-stage regression process.

The maximum valve lift sub-model results for directed ports, shown in Figure 4.29, indicates that the Av parameter is the most important (in common with the constant sub-model), followed by the At and Ar parameters. The At parameter is more influential than in the constant sub-model, indicating that increased maximum valve lift amplifies the negative effect of At on flow performance. Cylinder bore shrouding may account for these differences and is likely to be more prevalent at high valve lifts. The At*E interaction makes a contribution to the maximum lift sub-model but does not appear as a significant term in the constant model. Flow performance is likely to be more sensitive to the combined effects of At and E as maximum valve lift is increased. The Av*Ar and R*Ar interactions are similar for the constant and maximum valve lift sub-models. The coefficients for Dn^2, R^2 and At^2 in the maximum lift sub-model differ from one test plan to another, although the 95% confidence interval for these quadratic effects is large and it is therefore difficult to interpret these results.

120

The regression results for the MCf response in helical ports, shown in Figure 4.30, indicates that most important parameter in the maximum lift sub-model was At, followed by Wh and Hs. The difference when compared to the constant sub-model indicates that a change in maximum lift alters the response, particularly to At and Wh. At is not significant in the constant sub-model, but the positive coefficient in the maximum lift sub-model indicates that increasing At improves flow performance at high valve lift conditions. In comparison with directed ports, this suggests that cylinder bore shrouding is not detrimental to flow in helical ports. This could be due to different velocity profiles around the inlet valve. The negative effect of increased helix width as maximum valve lift is increased suggests that a larger helix cross-sectional area is not necessarily beneficial in all circumstances.

The stage-one regression results for the Rs_0 model indicated that the swirl response was dependent on maximum lift and, to a lesser extent, duration. In general, the interaction terms were not significant at the 95% confidence level. The results are normalised by dividing each model coefficient by the sum of all model coefficients to allow a comparison of the different models to be made. A comparison of the standard and enhanced model regression results for directed ports, shown in Figures 4.31 and 4.32, indicate that the constant sub-model is similar in form to the basic Rs/Ld model. The effect of Ar and R differs between test plans A and B, closely resembling the trends observed in the standard model. The swirl model coefficients for helical ports, shown in Figure 4.33, indicate that the standard model and constant sub-model behave similarly. However, the difference between the Hs coeffcients is worthy of mention. In the standard modelling approach, the Rs/Ld response is used and therefore represents swirl momentum in the cylinder. In the enhanced approach, the swirl response is simplified by the use of Rs_0. The Hs coefficient is smaller in the enhanced model, but Hs is also important in the MCf response and the combined effect of Rs_0 and MCf is taken into account in the calculated Rs/Ld value (equation 4.2). The overall effect on swirl is therefore greater than is immediately apparent than from the Hs coeffcient in the Rs_0 model.

The total Rs_0 response for directed ports, consisting of constant, maximum lift and duration sub-models, is shown in Figures 4.34 and 4.35. The maximum lift sub-model coefficients exhibit some differences when compared to the constant and duration sub-models. In particular, the normalised At coefficients for both test plans are greater in the maximum lift sub-model. This is likely to be due to the flow characteristics of the directed ports; a large fraction of the total swirl momentum is developed at high valve lift, increasing the sensitivity

of the response to At. The total Rs_0 response for helical ports was influenced by both maximum lift and duration. The results of the stage-two regression analysis are shown in Figure 4.36, indicating similar trends between the constant and duration sub-models. The Aw, At and Hs coefficients differ in the maximum lift sub-model. In particular, the Aw coefficient is small, suggesting that Aw primarily influences swirl generation at low to intermdiate valve lifts. The At coefficient is greater, possibly due to an increase in the tangential flow component at high valve lifts. Interactions involving these parameters also exhibit similar characteristics.
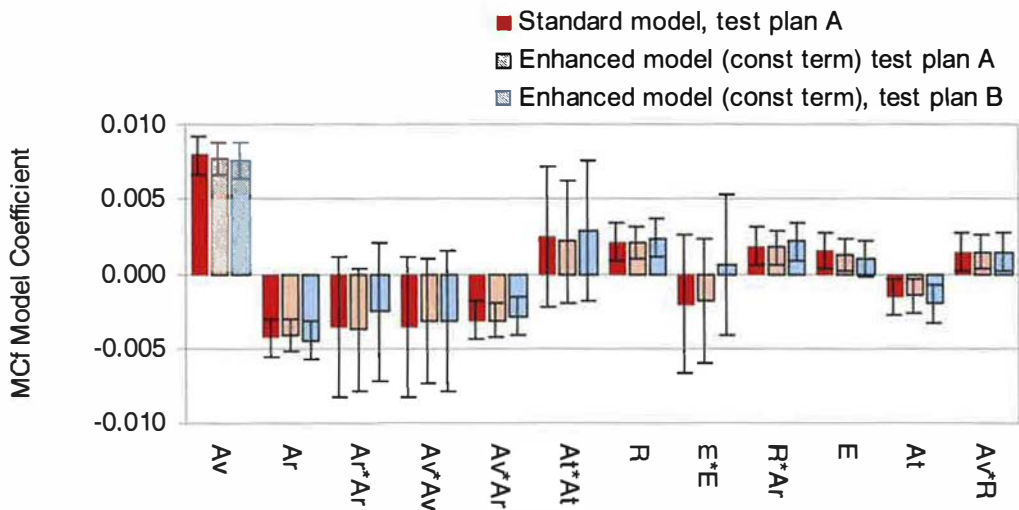
Figure 4.27: Comparison of simple and enhanced model coeffcients,
MCf response (directed ports)
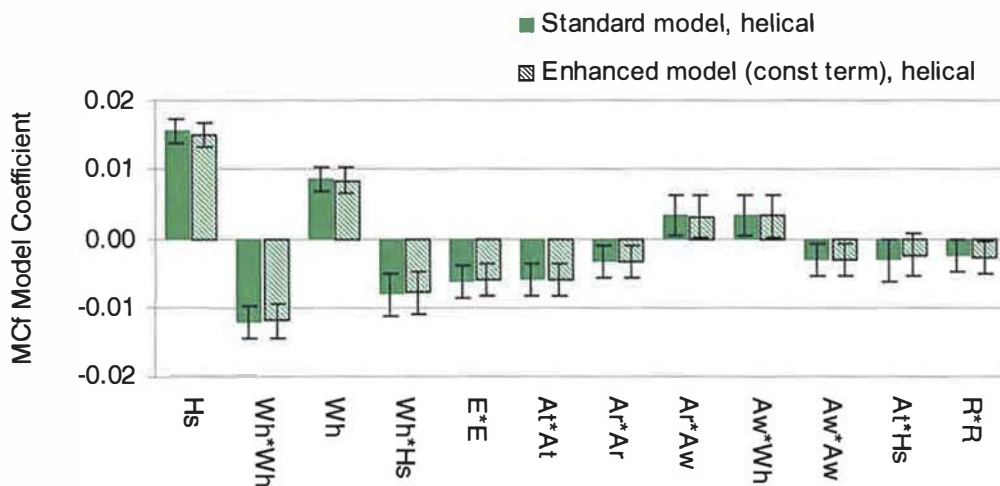
Figure 4.28: Comparison of simple and enhanced model coeffcients,
MCf response (helical ports)
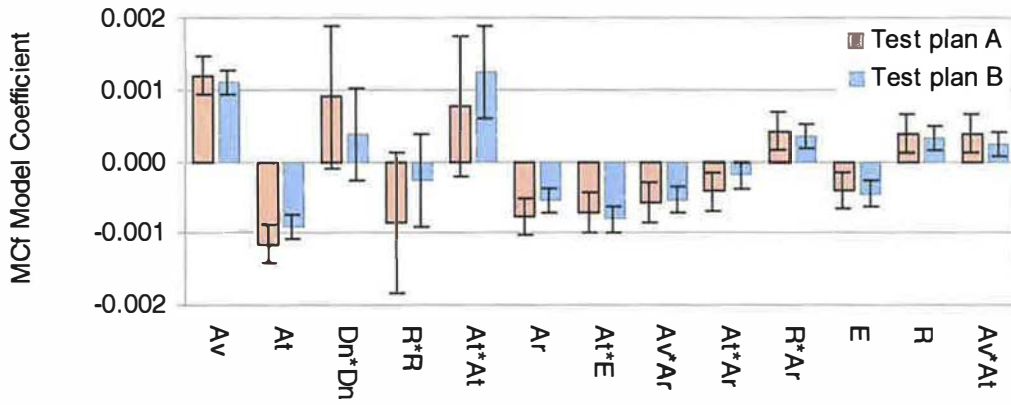
Figure 4.29: Maximum valve lift sub-model coefficients, MCf response (directed ports)
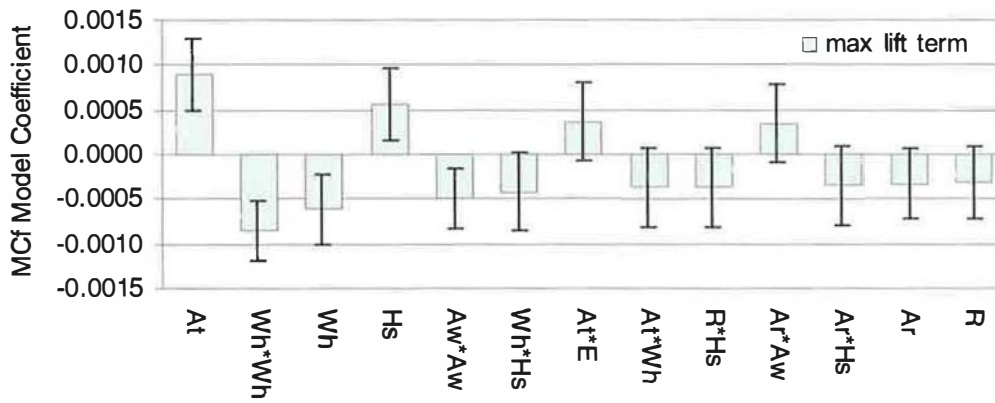
Figure 4.30: Maximum valve lift sub-model coefficients, MCf response (helical ports)
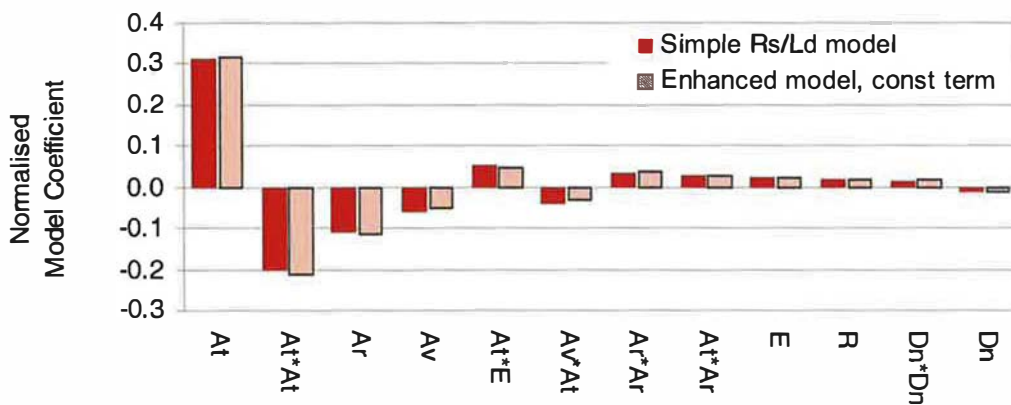
Figure 4.31: Comparison of simple and enhanced model coeffcients,

swirl response (test plan A, directed ports)

Figure 4.32: Comparison of simple and enhanced model coeffcients, swirl response (test plan B, directed ports)

Figure 4.33: Comparison of simple and enhanced models coefficients, swirl response (helical ports)
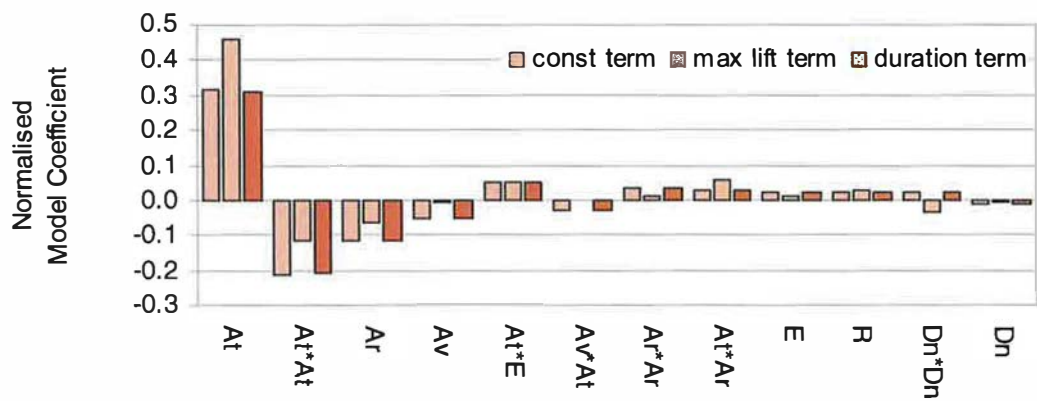
Figure 4.34: Comparison of sub-models, Rs_0 response (test plan A, directed ports)
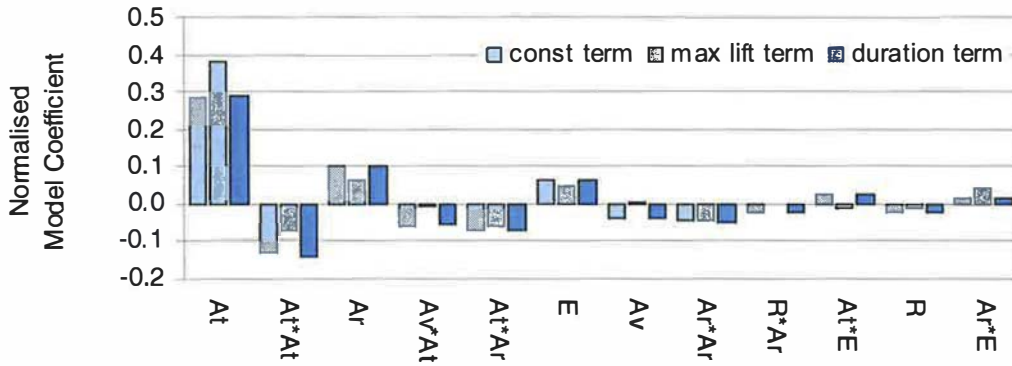
Figure 4.35: Comparison of sub-models, Rs_0 response (test plan B, directed ports)
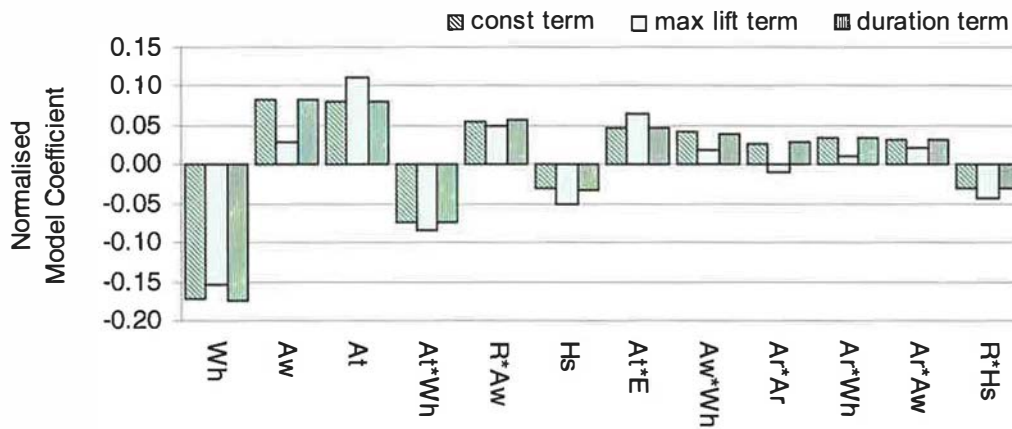
Figure 4.36: Comparison of sub-models, Rs_0 response (helical ports)

4.3.3 Model Predictions

The influence of maximum valve lift on the directed port model predictions is shown in Figure 4.37. The combined effect on Rs/Ld and MCf are shown as two-dimensional performance maps, indicating the importance of maximum valve lift in relation to each of the major port design parameters. Increasing maximum valve lift from 7.29mm to 9.45mm resulted in an average increase in mean flow coefficient of 8.5%. The effect of changes to maximum valve lift on the swirl response varied, depending on the design parameter settings. In particular, increasing maximum lift had a positive effect on Rs/Ld and MCf when At was increased. However, as At was decreased to the minimum setting, swirl becomes independent of maximum lift. The magnitude of the maximum valve lift effect was comparable to that of the most important port design parameters. The effect of maximum

125

valve lift dominated that of the minor port design parameters, such as port curve radius R, resulting in a narrowing of the performance map.

The helical port performance maps, shown in Figure 4.38, indicate that increasing maximum lift from 7.29mm to 9.45mm has a positive effect on MCf. However, the effect on swirl generation is dependent on the port design configuration. For low Wh values, increased maximum valve lift does not influence swirl. As Wh is increased, a trade-off is evident in which improved flow performance is associated with a reduction in swirl generation. The effect of maximum valve lift in relation to changes in At is somewhat different in that increased maximum lift is associated with a reduction in swirl when At is low. This is due to the orientation of the port with respect to the cylinder; any tangential flow component that is enhanced by increased maximum lift will tend to counteract swirl generated in the helix. In contrast, when At is high, increased maximum lift enhances swirl in the same direction and the result is an improvement in flow peformance and an increase in swirl ratio. The peformance map for Hs and maximum lift indicates a similar trend to At, although the reasons for this are not clear. It is possible that a high Hs value, representing a high port roof line and steep helix angle, may induce less tangential swirl into the cylinder than a port with a low roof line. Therefore, increased maximum lift will not induce swirl and the overall effect on swirl ratio may be negative. Finally, the effect of Aw does not appear to be influenced by maximum lift. If Aw governs swirl generation at low to intermdiate lift, as could be interpreted from the regression results, changes to maximum lift will not significantly alter swirl ratio.
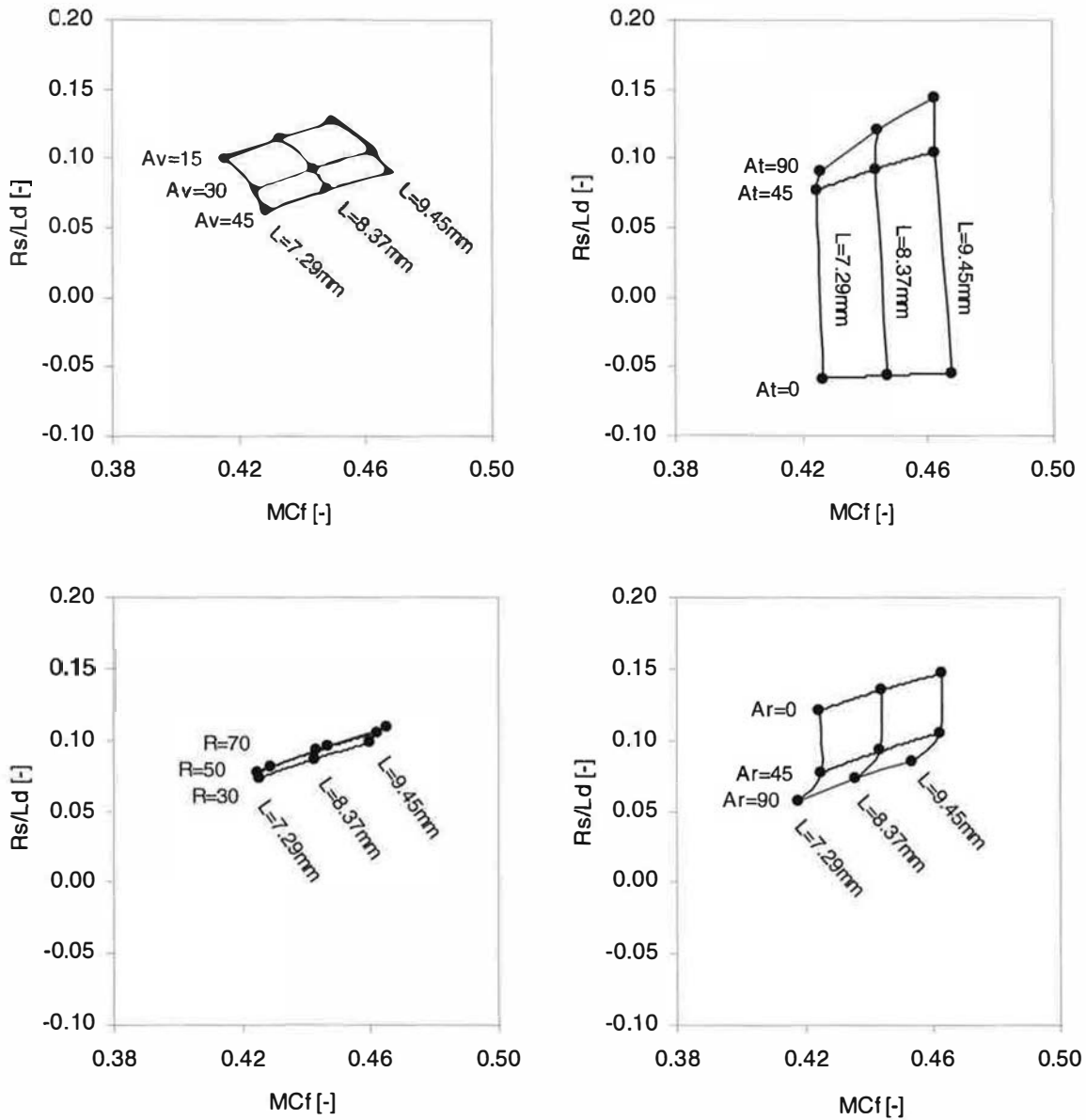
Figure 4.37: Rs/Ld and MCf performance maps, combined effect of maximum valve lift and port design parameters (directed ports)
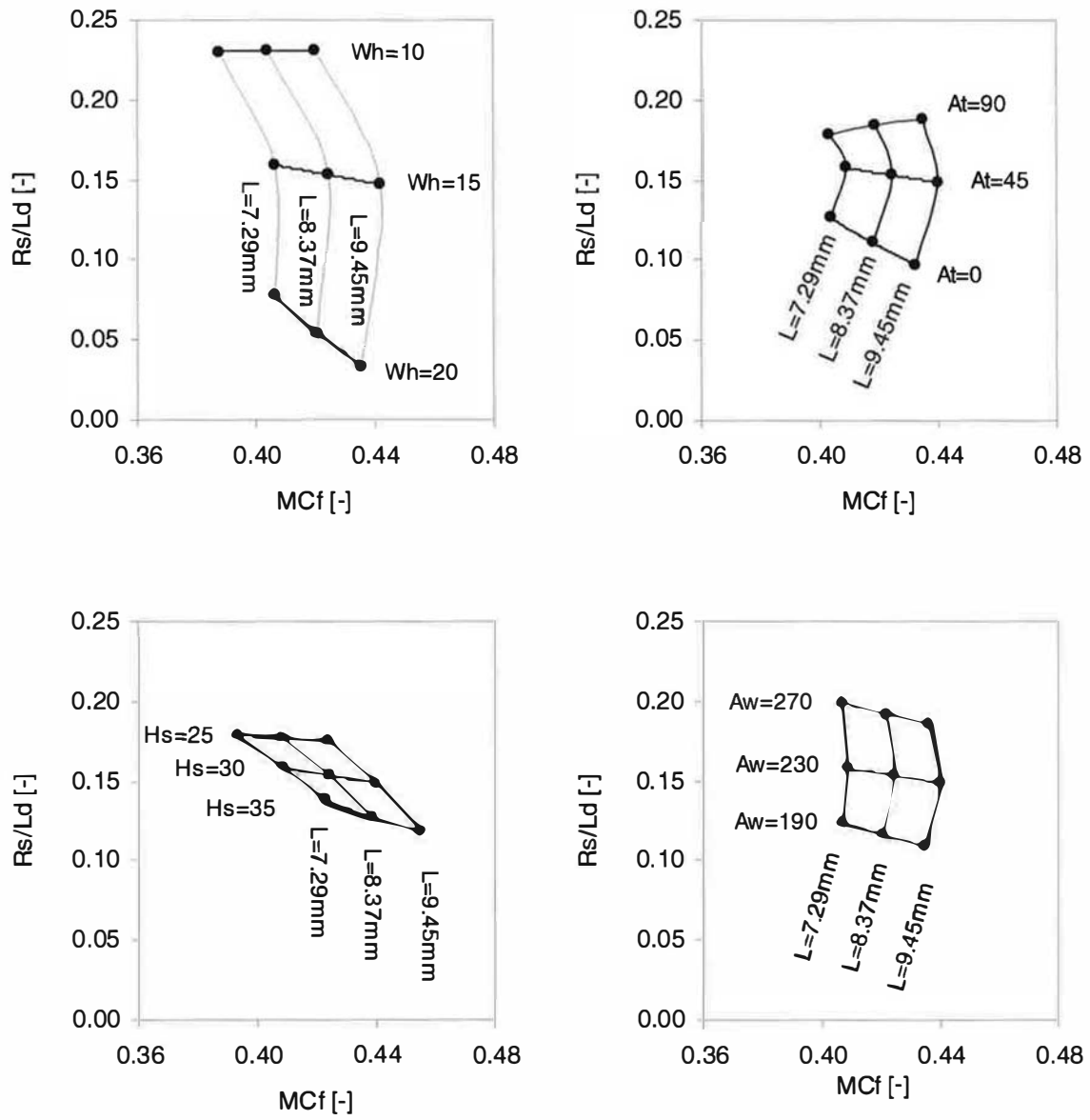
Figure 4.38: Rs/Ld and MCf peformance maps (helical ports)

4.4   Detailed Model

4.4.1   Modelling Technique

In order to fully understand the influence of the chosen design parameters over the entire valve lift range, and to eliminate possible errors resulting from the assumptions present in the previous model, individual DoE models for each valve lift condition were constructed. Flow coefficient (Cf) based on inlet valve inner seat area and non-dimensional swirl (Ns) were chosen to characterise flow performance and swirl responses, respectively. A further potential advantage of this approach was the simplification of complex calculated responses. Cf and Ns represent the most basic performance characteristics and are directly related to the primary measurements of volumetric flow rate and ISM torque. Therefore, each individual model may be considered as a response "element". The overall performance responses, such as Rs and Z, may be calculated as before, although each Cf and Ns value is of course a separate model prediction. The effect of valve lift profile may be calculated more accurately, including complex profiles that do not correspond to a common generic shape and therefore cannot be characterised using the maximum lift and duration parameters. The approach does have some potential disadvantages. Firstly, any measurement errors or unstable flow conditions are likely to influence the response of individual models more than the summary models, as the latter depend on measurements made at approximately ten valve lift conditions and therefore the total response is likely to be smoothed. Secondly, in anticipation of the need to use the models for geometry optimisation, the simultaneous optimisation of up to ten individual models is of course more difficult than a single model.

A major feature of a detailed port performance model is the potential ability to determine not only the effect of design parameters on overall flow performance characteristics, but also their influence throughout the valve lift range. Real mass flows in engines are unsteady; maximum instantaneous flow rates may occur at various times during the valve lift event, depending on engine speed and load. In practice, a detailed port performance model could be used to provide input data for an engine performance simulation tool. The instantaneous mass flows into the engine are calculated according to the relevant port flow coefficient, resulting in a prediction of volumetric efficiency throughout the engine speed and load range. It is therefore clear that such predictions are likely to provide more accurate and illustrative predictions than a simple correlation between volumetric efficiency and inlet

mach index. Notwithstanding these considerations, the latter approach has value during concept design when there is insufficient data to perform complex simulations.

4.4.2 Overview of results

The range of measured Cf and Ns values are shown in Figure 4.29. The range of Cf values recorded for directed ports is narrow (within 6% of the mean value) up to approximately 5mm lift, followed by an increase in the range at high lift as the influence of each design parameter becomes apparent. Flow performance at low valve lift is governed by valve seat geometry, as demonstrated in several previous studies (Maier *et al*, 2000; Tanaka, 1931). In the present study, a common valve seat was used and therefore no significant effects were expected at low valve lift conditions. A straight line through the first four valve lift points indicates that flow performance was consistently close to the ideal case in which the minimum flow area corresponds to the slant surface of a frustum of a cone, the geometry of which is governed by the valve seat angle. However, port design features clearly influence performance as valve lift and flow rate increase. The valve curtain area exceeds the minimum cross-sectional area of the port at 6.75mm valve lift, therefore flow performance above this lift is governed by the cross-sectional area. However, all the directed port designs had a constant cross-sectional area profile and so it is logical that the differences in performance at valve lifts above 5mm are due to intended port geometry variations resulting from design parameter changes.

The directed port results indicate a wide spread of Ns values throughout the valve lift range, reflecting the trends in the standard Rs model test results. At low valve lift conditions, low levels of swirl are generated. The maximum swirl generated by ports in both test plans increases with valve lift, although the maximum swirl generated by configurations in test plan B is consistently higher than in test plan A. Furthermore, the only significant negative results are associated with test plan A and these occur at high valve lift.

Helical port Cf values at valve lifts of 3mm and below are within a narrow range and are comparable to those observed for directed ports. This suggests that none of the port design features investigated in the present study influence flow performance at low valve lift. However, the Cf values reach a maximum more quickly than the directed port results, indicating that the helical ports are generally more restrictive. The trend is also captured in the

MCf results, as previously discussed. The range of Cf values begins to increase at 4mm lift in the helical port data, suggesting that design parameters begin to influence peformance at a lower lift than in directed ports. This corresponds to an increase in swirl momentum, as indicated by the higher Ns values at intermediate valve lifts. The highest Ns values increase linearly from zero to 7mm lift and remain constant. In comparison, the directed ports exhibited a more rapid increase in Ns at high valve lift, following little or no swirl generation up to 5mm lift. However, both port types produced a similar range of Ns values at high valve lifts, suggesting that parameter effects are important in this region.

(a) Directed ports   (b) Helical ports
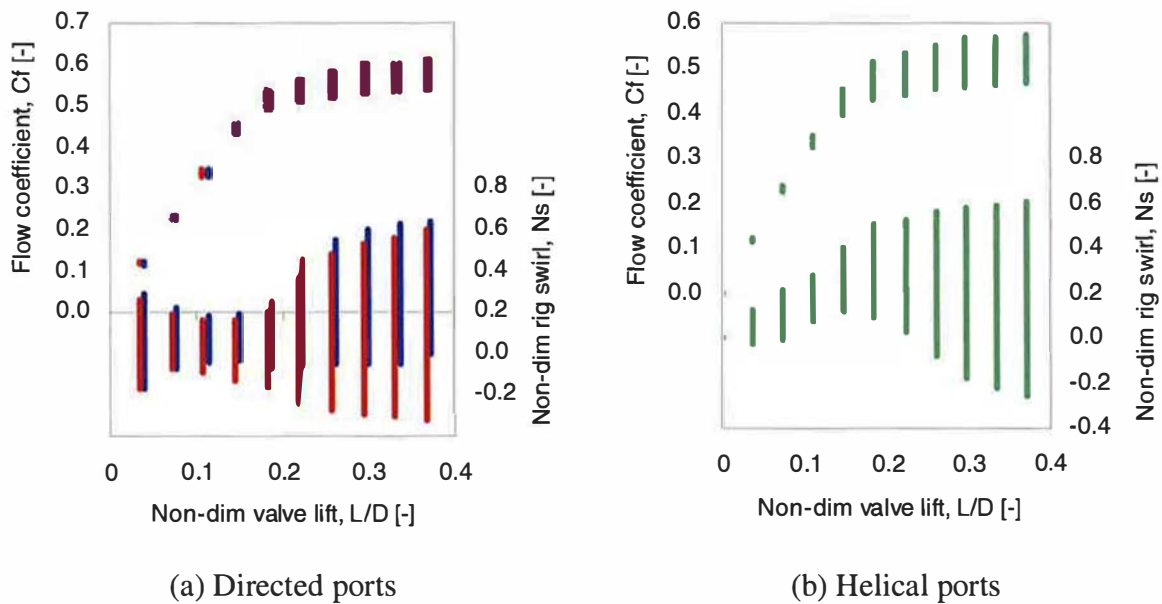
Figure 4.39: Overview of Cf and Ns data (all port types)

4.4.3   Model Regression

Multiple linear regression was used to analyse the data and identify significant design parameters. The overall trends were similar for test plans A and B, consequently the discussion is concerned with the results for test plan A. The directed port Cf model coefficients are presented in Figures 4.40 and 4.41, illustrating the importance of Av, Ar and the Av*Ar interaction at 5mm lift and above. Both these parameters were identified as being among the most important in the simple MCf models. The coefficients for At, R and R*Ar are significant at 7mm lift and above, once again reflecting their secondary importance in the simple model. Av*R and At*E are only significant above 8mm lift. Model coefficients

for each test plan are comparable, indicating similar responses throughout the valve lift range for both port types. The ranges associated with 95% confidence intervals were large in some cases, indicating a significant amount of noise in the data. However, as valve lift increases, model robustness improved and the most important parameter coefficients are associated with less uncertainty.

The helical port Cf results from 4mm to 10mm lift are shown in Figure 4.42. The most important parameters are Hs and Wh, as expected given the MCf results. The characteristics of each parameter vary with valve lift; the model coefficients for Hs increase with valve lift but the Wh coefficients decrease. In addition, the nature of the Wh effect changes as valve lift is increased; the Cf response is linear at 4mm lift, but the quadratic term becomes significant at high valve lifts. The Wh*Hs interaction is also important at all valve lift conditions. The quadratic terms for the less important parameters, such as E, Aw and Ar appear to be significant but also may indicate a substantially flat response given the small linear terms and large confidence intervals (not shown). The linear coefficient of At increases considerably with valve lift, suggesting a small benefit in flow performance at high valve lift as At is increased. There is litle evidence of any trends in the minor interactions and these do not appear to be important at any particular valve lift. The detailed model is potentially capable of illustrating effects that cannot be identified with the latter, although the two approaches are comparable qualitatively.

Regression results for the directed port Ns models are shown in Figures 4.43 and 4.44; model coefficients indicate that the parameters At and Ar are the most important. The magnitude of the At coefficients increase with valve lift; this again suggests that the effect of At is greatest at high valve lifts. The influence of Ar also increases with valve lift, although the effect is not as clear. In general, the minor parameters and interactions followed the trends observed in the simple model. At*Ar was the most important interaction, Av*At, R*Ar and At*E were also significant. The Ar and R model coefficients in test plan A were opposite in sign to those in test plan B and the At*E interaction was more important in test plan A.

The detailed Ns model coefficients for helical ports, shown in Figure 4.45, indicate that the effects of Wh, Hs and At become increasingly important as valve lift increases. Aw influences swirl across the valve lift range, but its effect begins to diminish after 8mm lift.

The relatively small Aw coefficient in the maximum-lift sub-model of the enhanced standard model is therefore logical. The interactions identified in the standard model are also present in the detailed Ns results.

The R^2 correlation coefficients for each valve lift sub-model are shown in Figure 4.46. Directed port Cf model quality improves with valve lift, resulting in R^2 values in excess of 0.95 at 8mm valve lift and above. This represents similar overall quality compared to the simple model, as the overall MCf prediction is influenced predominantly by flow performance at high valve lift. Directed port Ns model quality was superior to the Cf model at all valve lift conditions, although the highest R^2 values were also found at high valve lift conditions when stable swirl conditions were established. The quality of the detailed helical models is also shown in Figure 4.46. R^2 exceeds 0.9 at 4mm lift and remains high until 9mm lift for the Cf model. The quality of the Ns model is high from 2mm and is generally above 0.95. Both models are therefore of similar quality to the detailed directed port models.
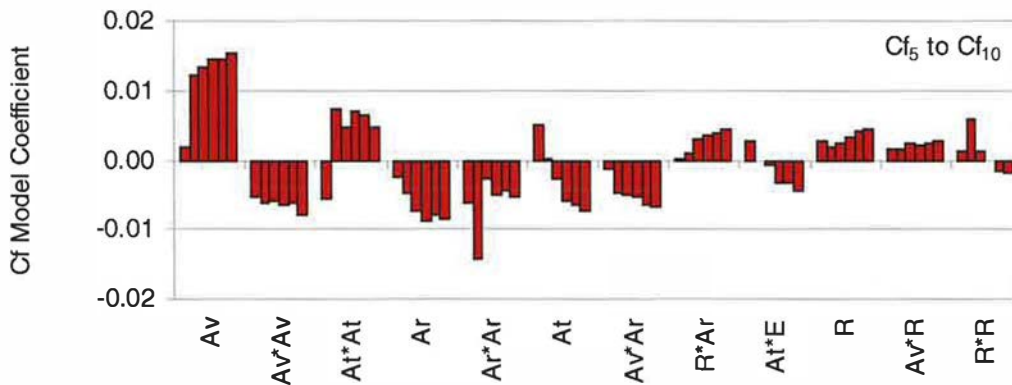
Figure 4.40: Detailed model coefficients, Cf response (directed ports, test plan A)
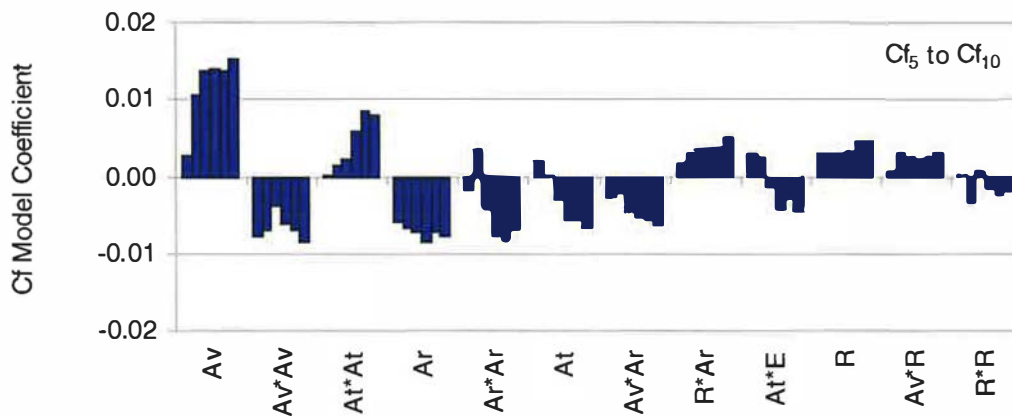
Figure 4.41: Detailed model coefficients, Cf response (directed ports, test plan B)
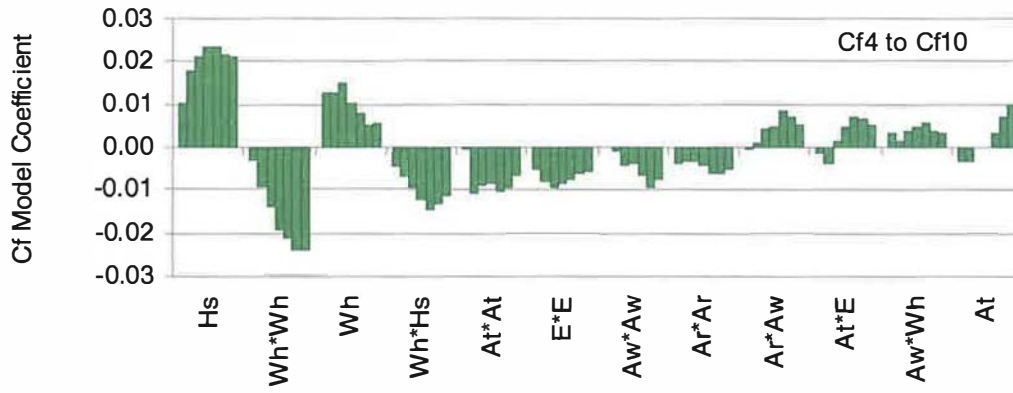
Figure 4.42: Detailed model coefficients, Cf response (helical ports)
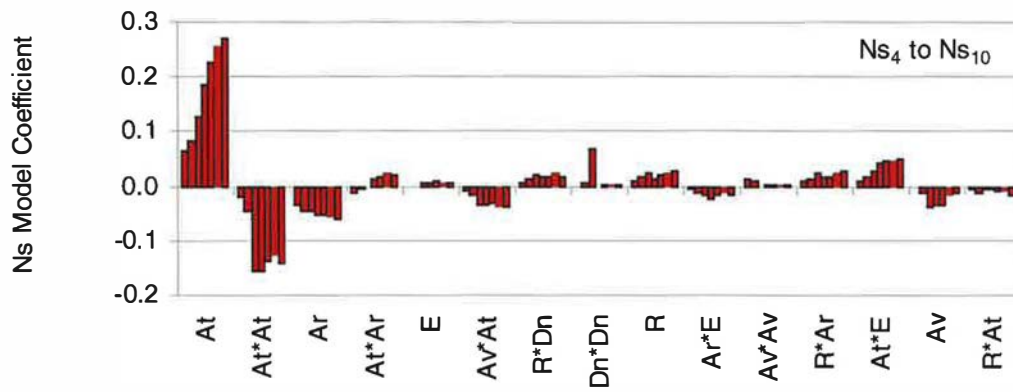
Figure 4.43: Detailed model coefficients, Ns response (directed ports, test plan A)
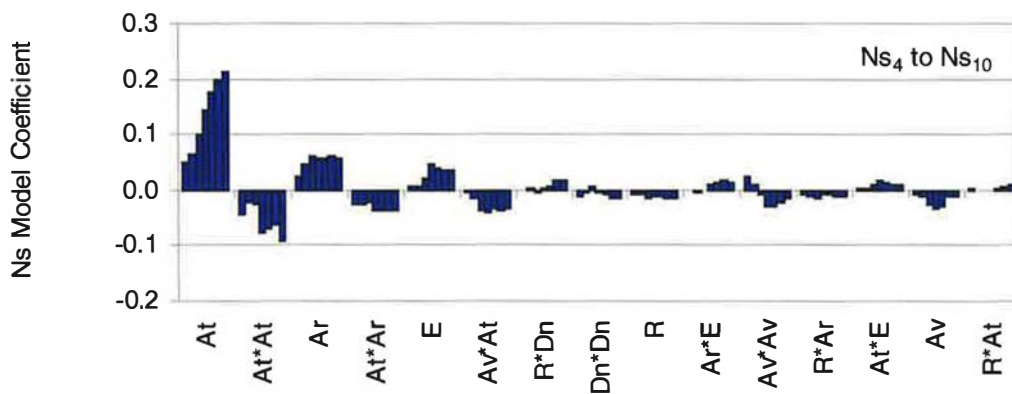
Figure 4.44: Detailed model coefficients, Ns response (directed ports, test plan B)
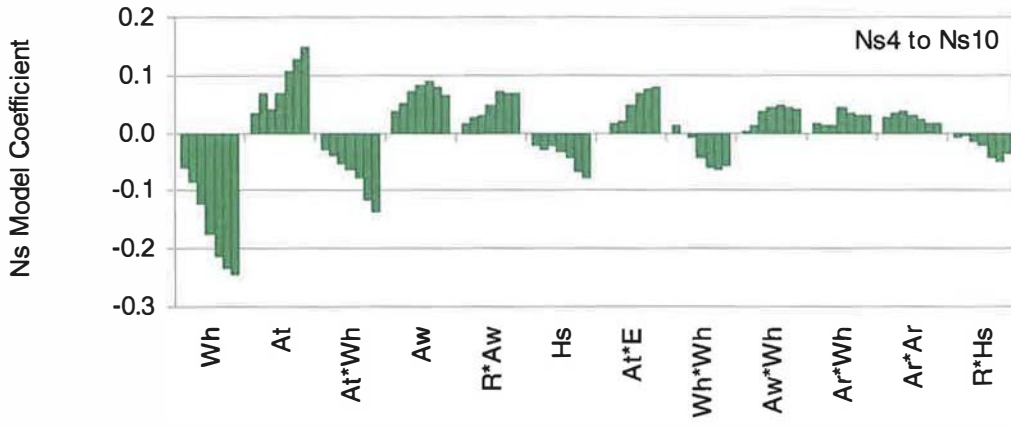
Figure 4.45: Detailed model coefficients, Ns response (helical ports)
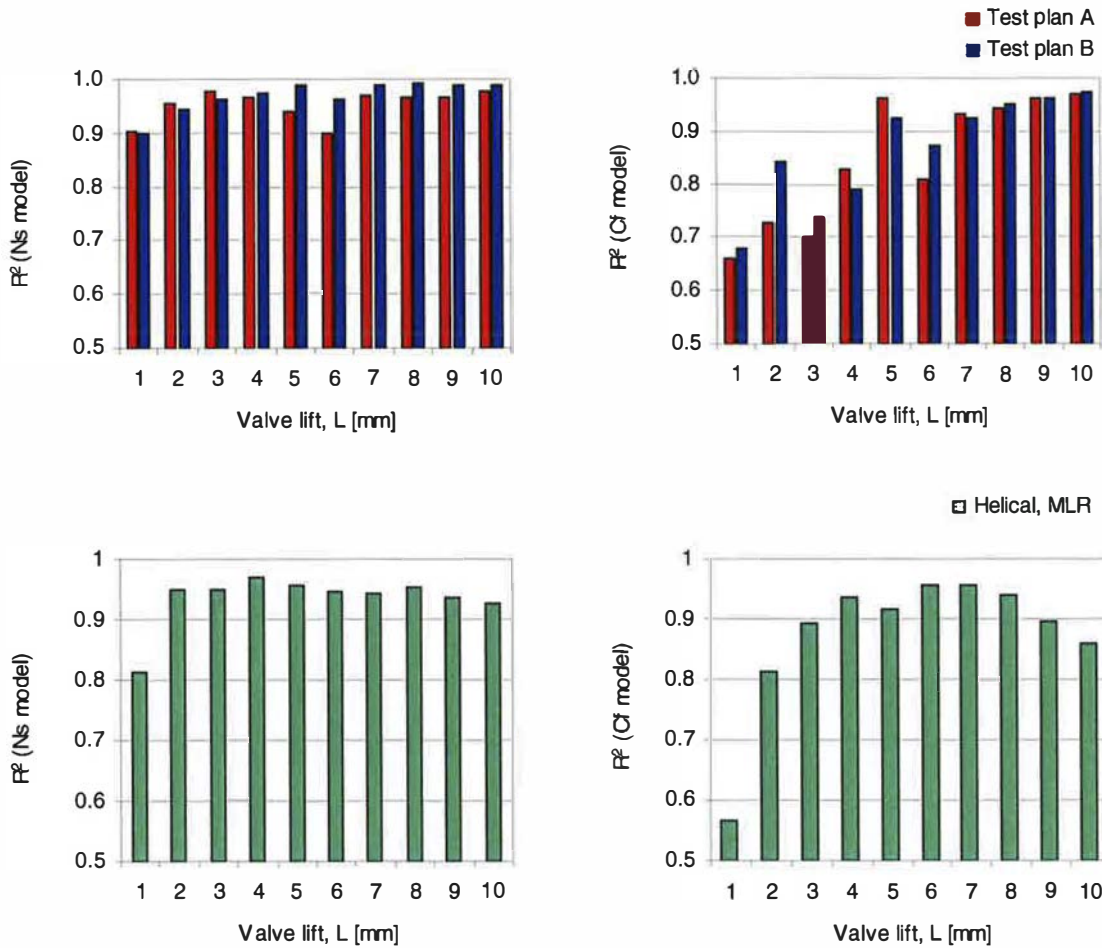
Figure 4.46: Detailed model quality

135

4.4.4 Model Predictions

Model predictions from the detailed model are more difficult to visualise than those from the simple model, as each main effect or interaction plot is only applicable to a single valve lift condition and therefore does not provide sufficient information to gain an overview of the performance response. However, the identification of significant parameters in the previous section suggests that the combined effect of the individual valve lift sub-models would result in a similar overall response to that of the simple model. In order to confirm this, MCf and Rs/Ld values were calculated using both models and these were compared. The effects of the most significant parameters were investigated and the results are shown in Figures 4.47 and 4.48. It is clearly evident from the results that the detailed models produce similar results to the simple models, including the second-order At and Wh predictions. Although this is a likely outcome given that both were derived from the same set of test data, the use of additional data in detailed model would identify any problems in the simple model.

A summary of the most important directed port Ns response surfaces is shown in Figures 4.49 to 4.51. The At*Ar, Av*At and At*E interactions at valve lift conditions between 7mm and 10mm match the general form of those in the simple Rs/Ld model. However, the effect of valve lift on the response surfaces is apparent. In particular, At and Ar are of interest. In test plan B, both parameter effects are positive and increase with valve lift. Consequently, the At*Ar interaction becomes stronger and the resulting response surface more steeply angled. The basic form of the surface remains the same. In contrast, the effect of Ar is reversed in test plan A and also increases (in a negative sense) with valve lift. Therefore, as valve lift increases, the two parameters counteract each other, resulting in a twisted response surface.

The Cf response surfaces also match those of the simple MCf model, although the effect of valve lift has a small effect on some parameter interactions. The Av*Ar interaction, shown in Figure 4.52, becomes more pronounced as valve lift increases, although this is largely due to the increased response of both parameters. The figure clearly shows a similar trend to the MCf model, in which the flow performance of the port is independent of the port curve angle at low Av values. As Av increases, changes to the port curve angle of the port have the expected effect. This characteristic is likely to be caused by flow detachment in the throat or valve seat regions, reducing the effective flow area and therefore controlling flow

performance. The Ar*R interaction, shown in Figure 4.53, indicates that the performance response becomes increasingly sensitive to valve lift. In all cases, flow performance is only dependent on R when Ar is increased. However, at high valve lift conditions, a combination of increased R and Ar causes a marked loss in flow performance.

Combined Cf and Ns plots are used to visualise the effect of each design parameter throughout the complete valve lift range, as shown in Figures 4.54 to 4.61. The effect of parameter variations at different valve lift conditions have been discussed in the previous sections, as it is possible to interpret this from the regression data and the response surfaces. However, the following figures provide a more easily understood representation of the data. There are some additional observations that may be made using this method of presentation. In particular, the level of agreement between each model for equivalent geometry cases may be assessed. The effect of Ar is shown in Figure 4.57, indicating the expected trends. When Ar=0, the port geometry is common between both models, as the port is straight and all other parameters are at their nominal settings. Inspection of the Cf and Ns curves confirms this, indicating that the models are in agreement. A difference is evident at low lift conditions on the Ns curve, as a result of the lower model quality in this region. A similar observation can be made when considering the effect of At on directed port performance (Figure 4.56). For At=0, the test plan A Ns curve is a negative of test plan B, due to identical but reversed port geometry and location. The lack of any response to Dn and the minor response to E follow the trends in the summary performance characteristics of the standard model. The influence of At on helical port performance, shown in Figure 4.60, is also primarily on swirl generation. However, the effect is exaggerated at high valve lifts. Aw also influences swirl generation, as shown in Figure 4.60. However, an increase in Aw tends to boost swirl at intermediate valve lifts. Hs has an effect on flow performance and swirl generation. A typical trade-off between the two is evident in Figure 4.61; increasing Hs results in improved Cf and reduced Ns. The effect of Wh is also shown in Figure 4.61, indicating a significant influence on swirl behaviour. Increasing Wh results in a rapid loss in swirl at high valve lift. Flow performance is also reduced, suggesting that the increase in port cross-sectional area is not utilised effectively.
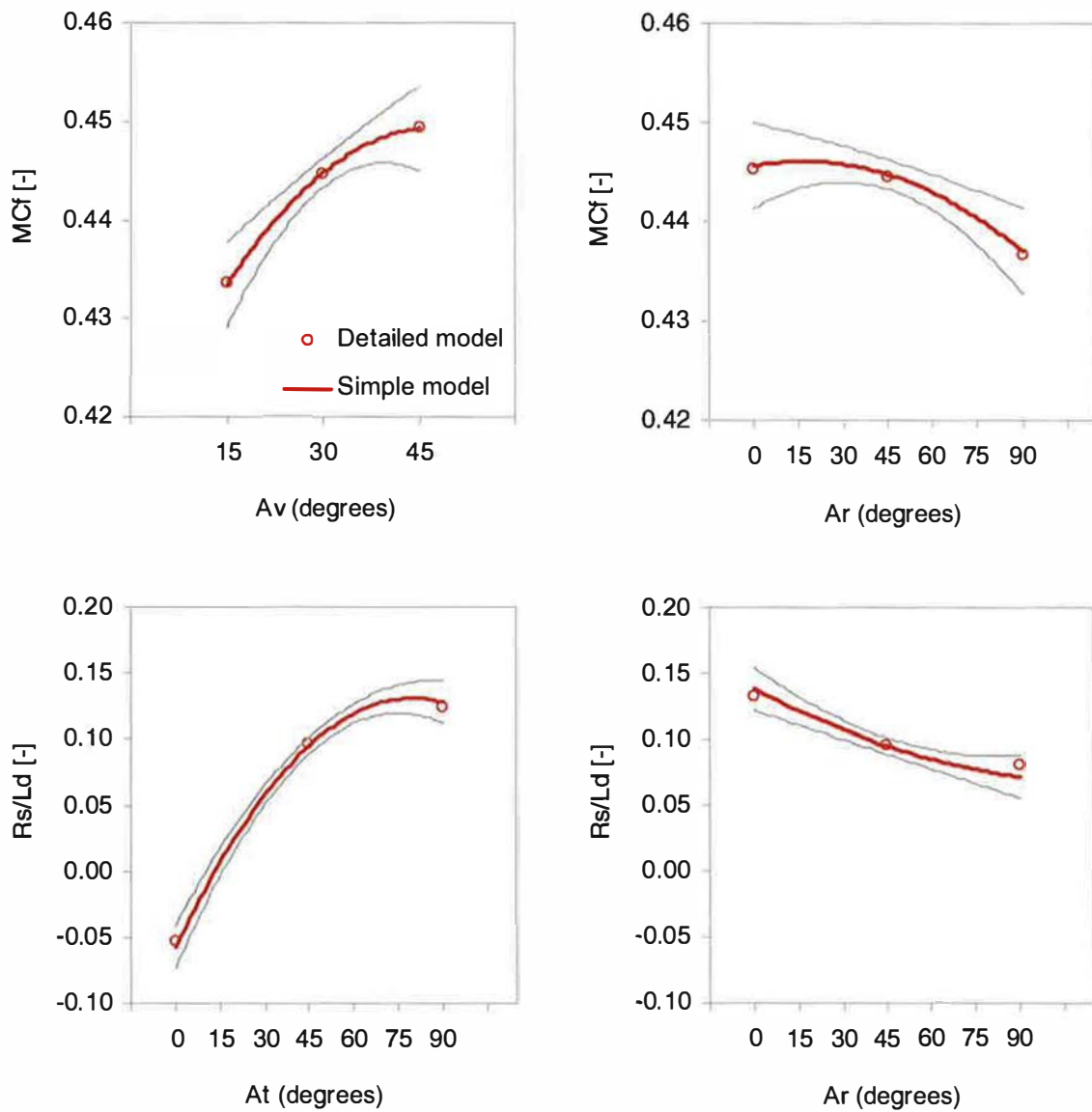
Figure 4.47: Main effects, comparison of detailed and simple models (directed ports)
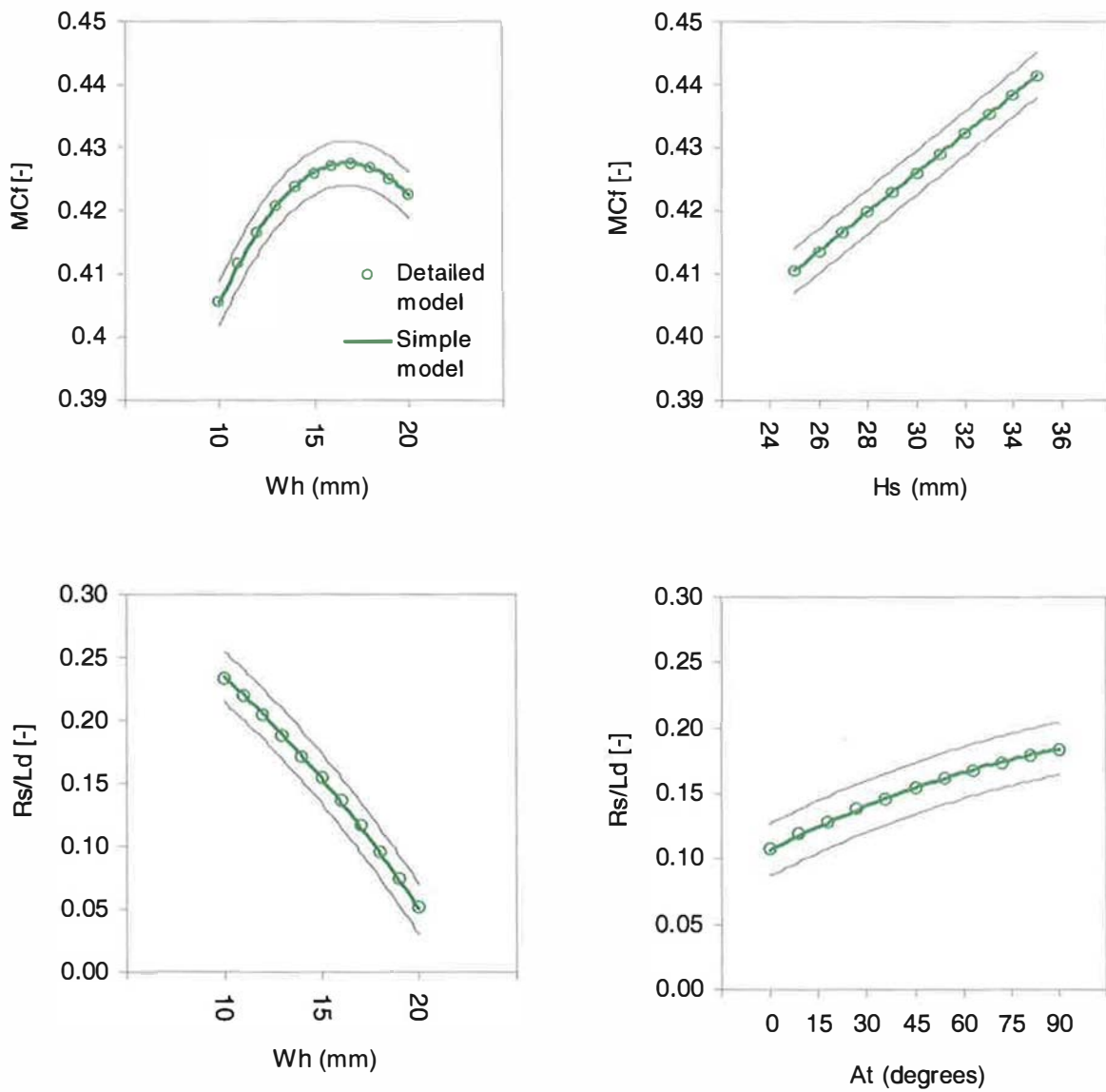
Figure 4.48, Main effects, comparison of detailed and simple models (helical ports)
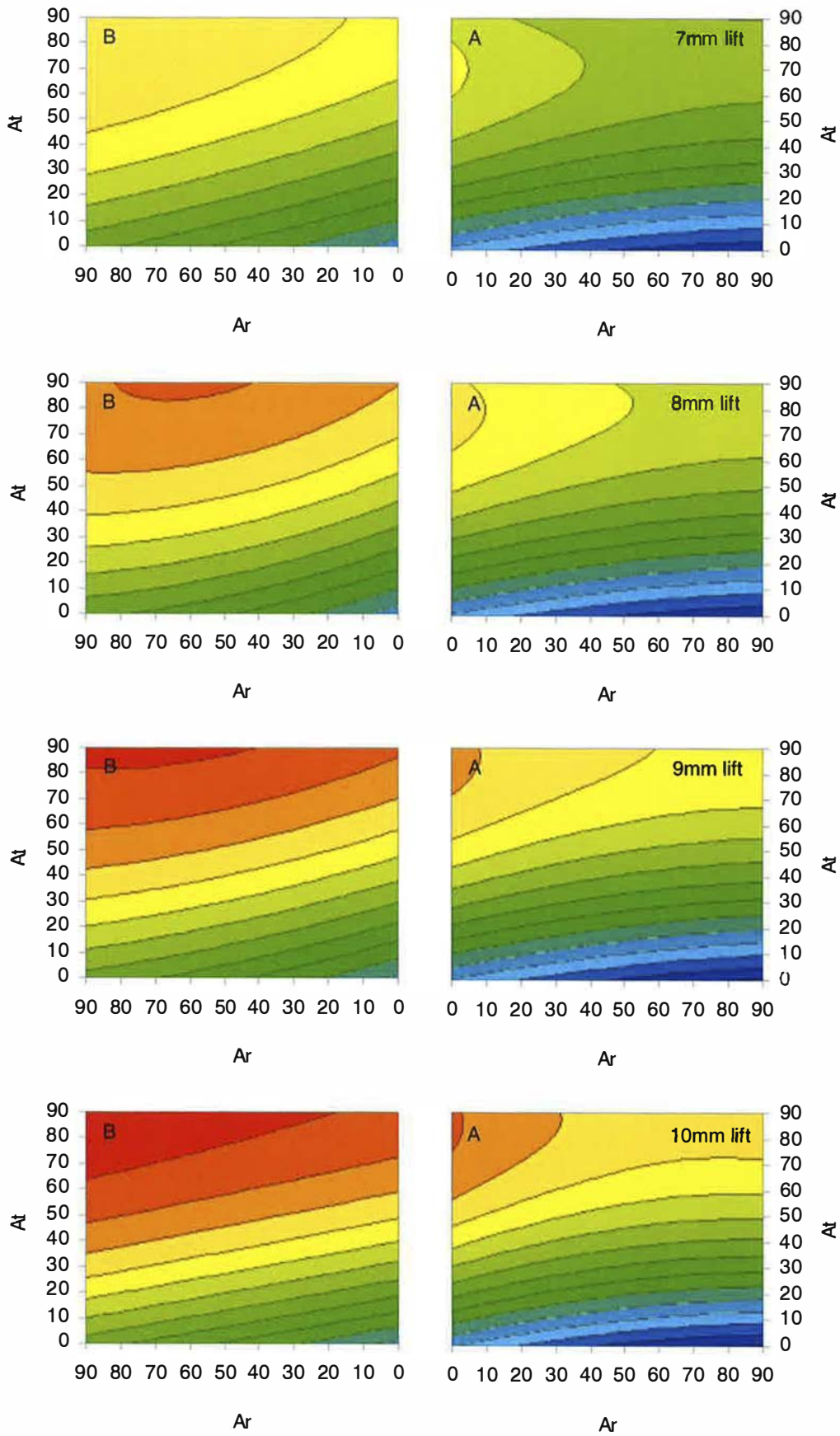
Figure 4.49: Effect of valve lift on the Ar*At interaction, Ns response (directed ports)
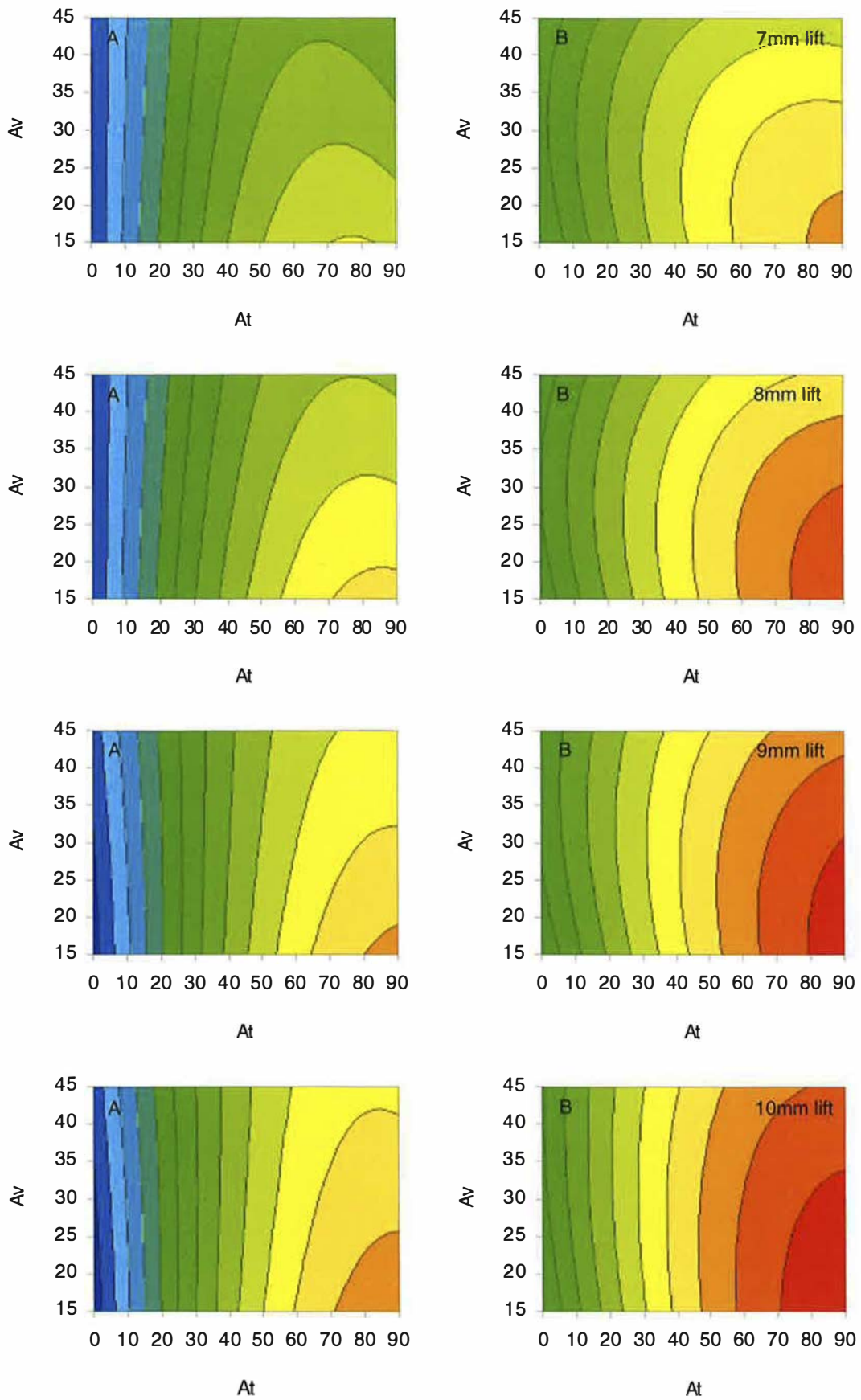
Figure 4.50: Effect of valve lift on the Av*At interaction, Ns response (directed ports)
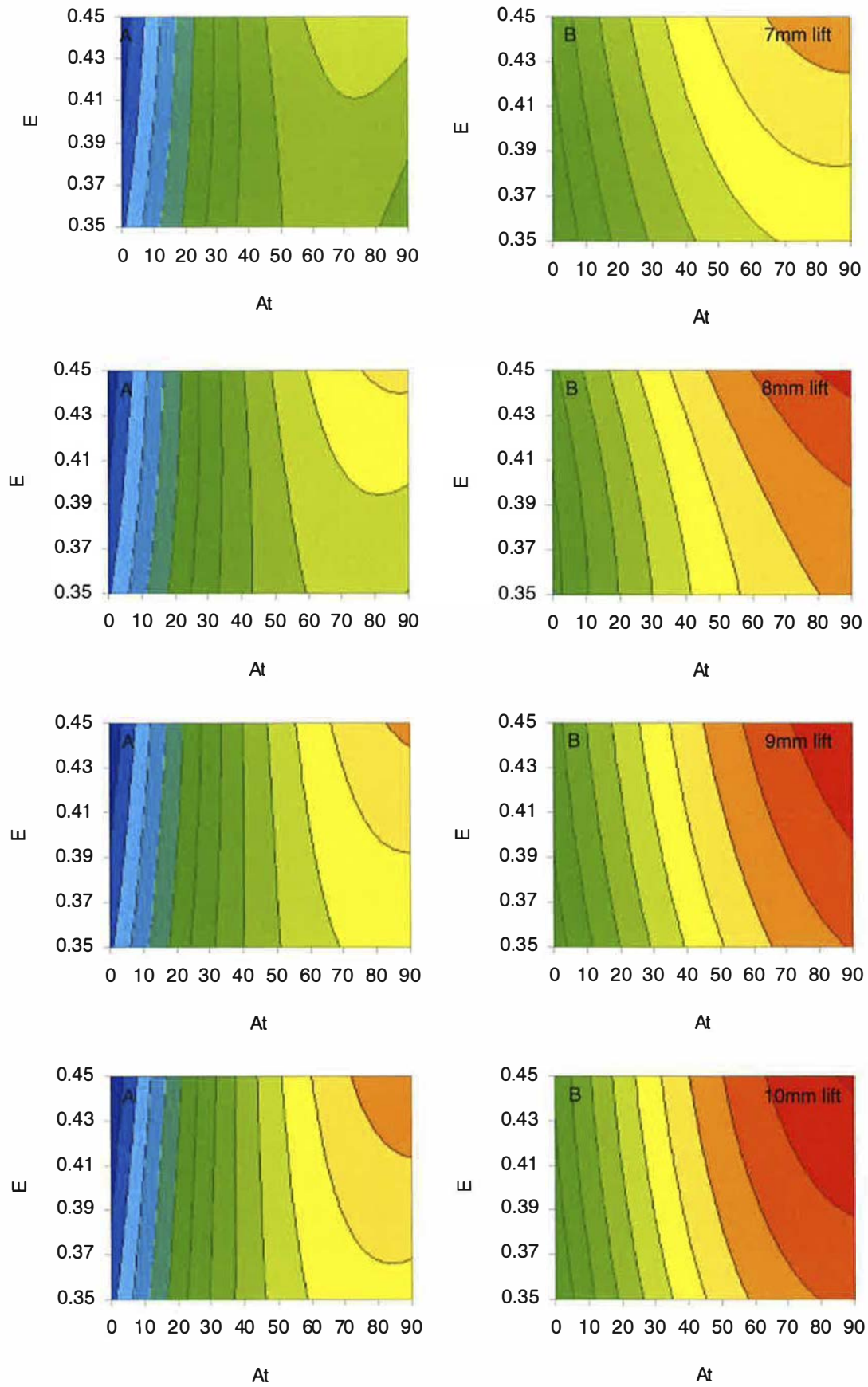
Figure 4.51: Effect of valve lift on the At*E interaction, Ns response (directed ports)
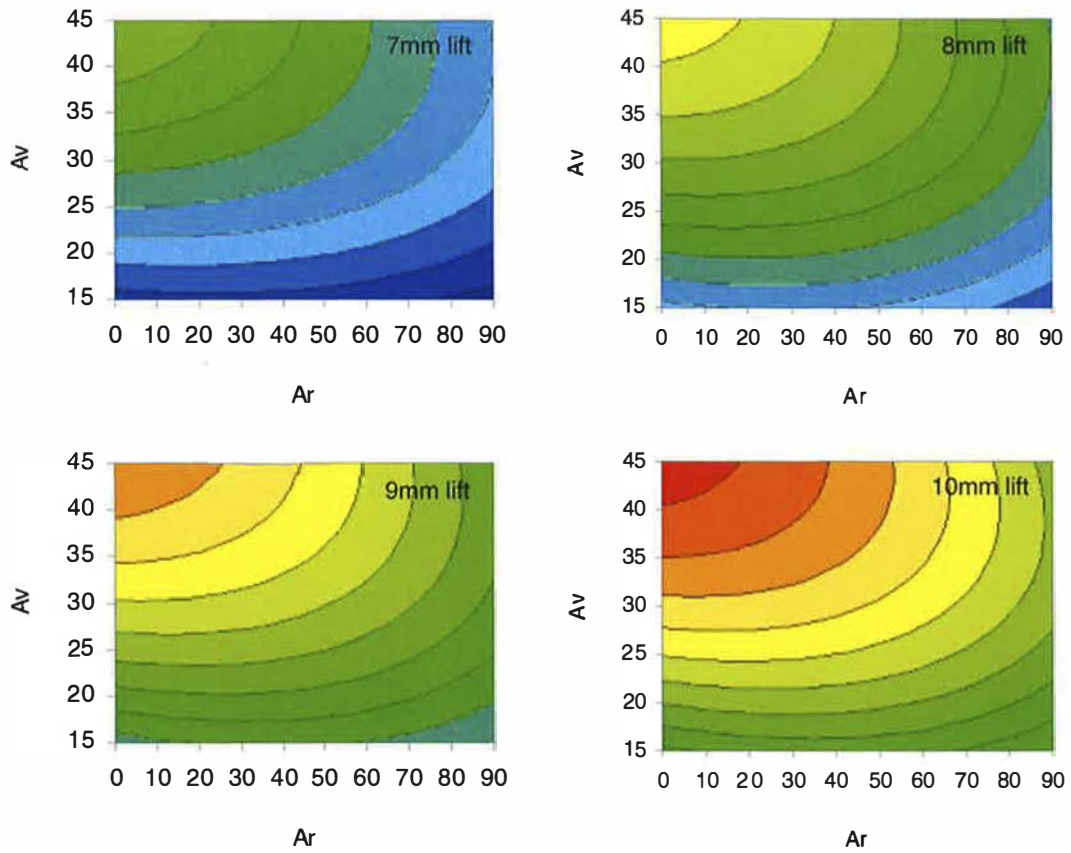
Figure 4.52: Effect of valve lift on the Av*Ar interaction, Cf response (directed ports)
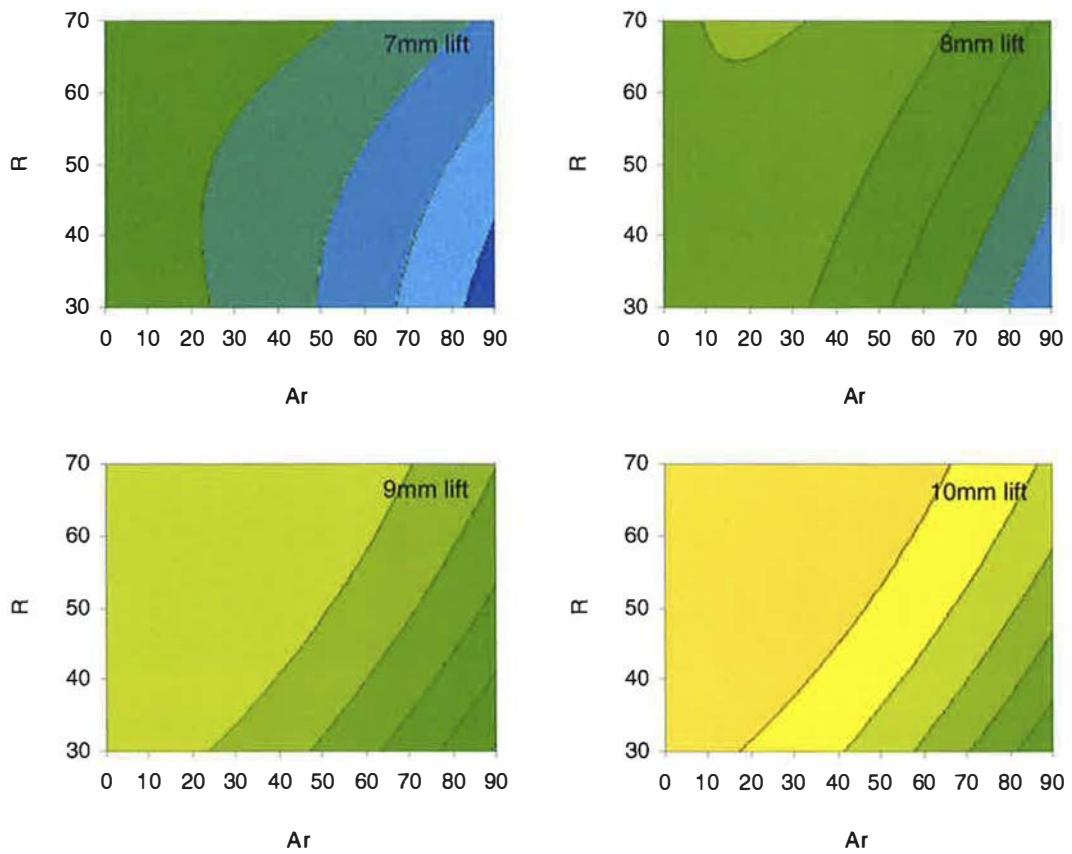
Figure 4.53: Effect of valve lift on the Ar*R interaction, Cf response (directed ports)

143
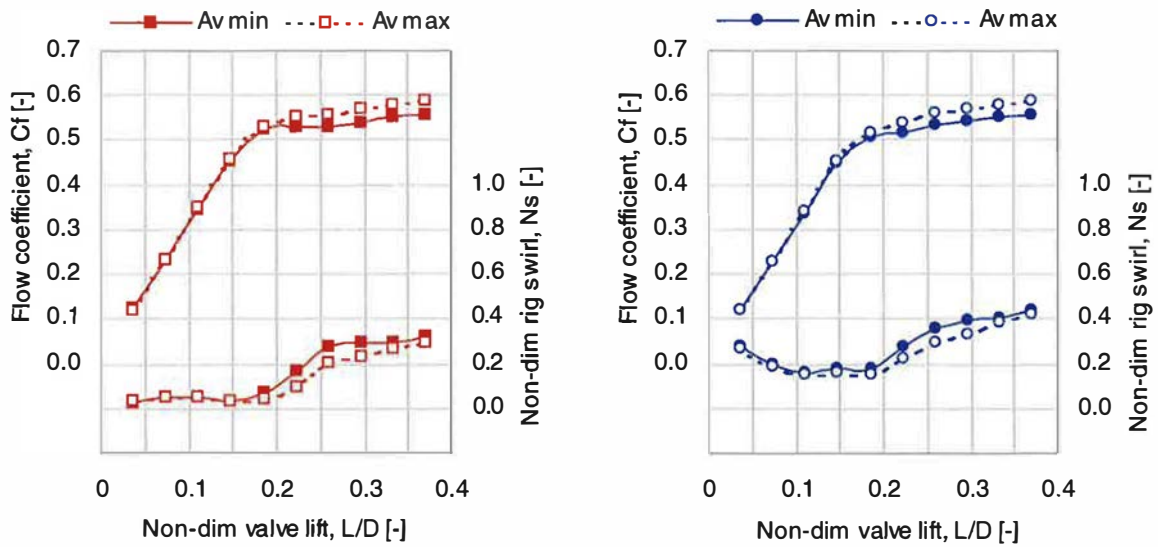
Figure 4.54: Effect of Av on Cf and Ns performance (directed ports)
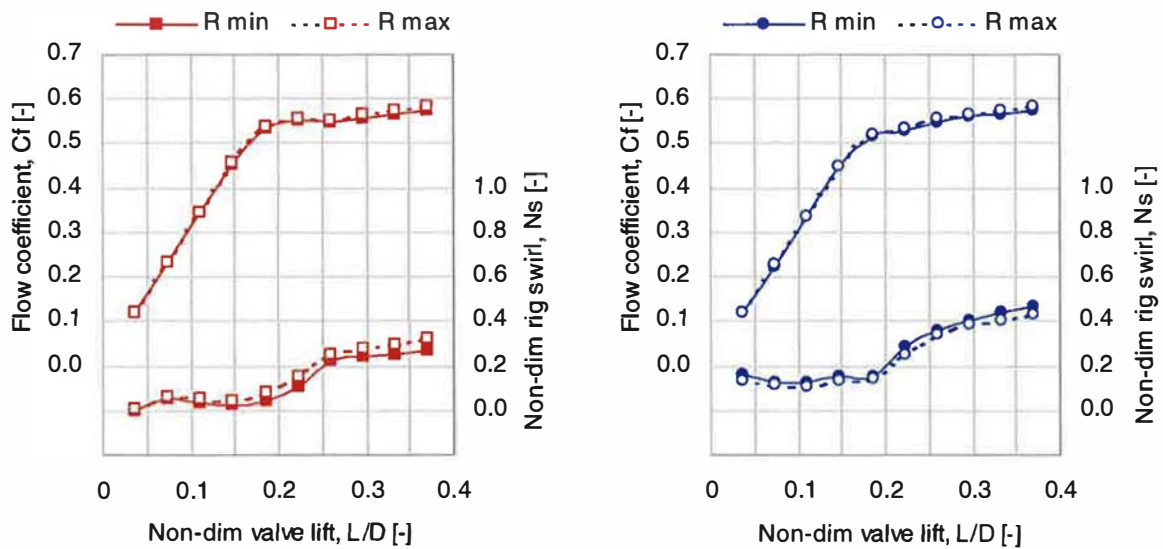
Figure 4.55: Effect of R on Cf and Ns performance (directed ports)

144
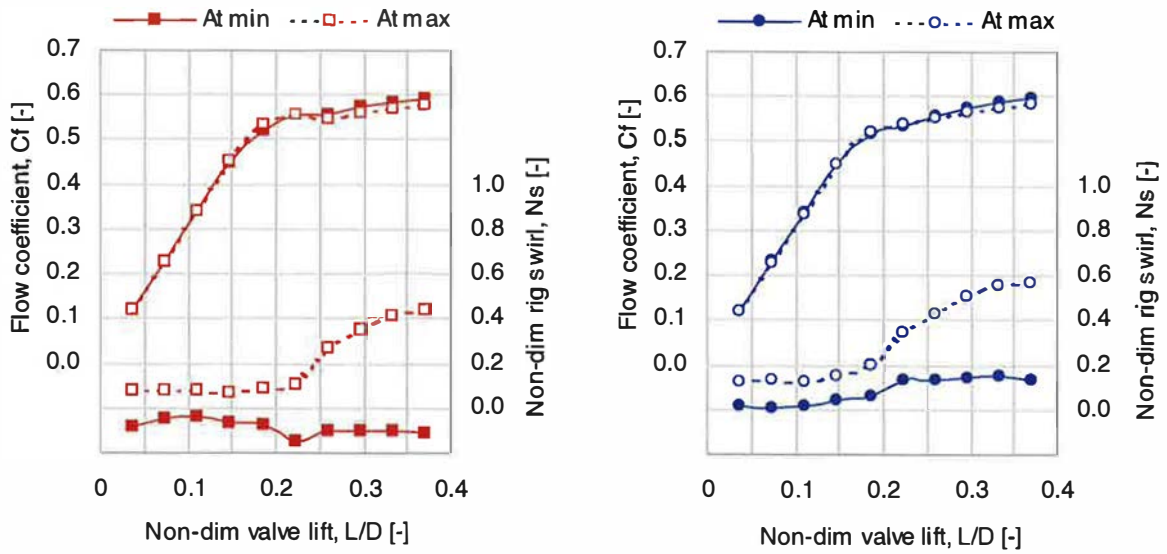
Figure 4.56: Effect of At on Cf and Ns performance (directed ports)
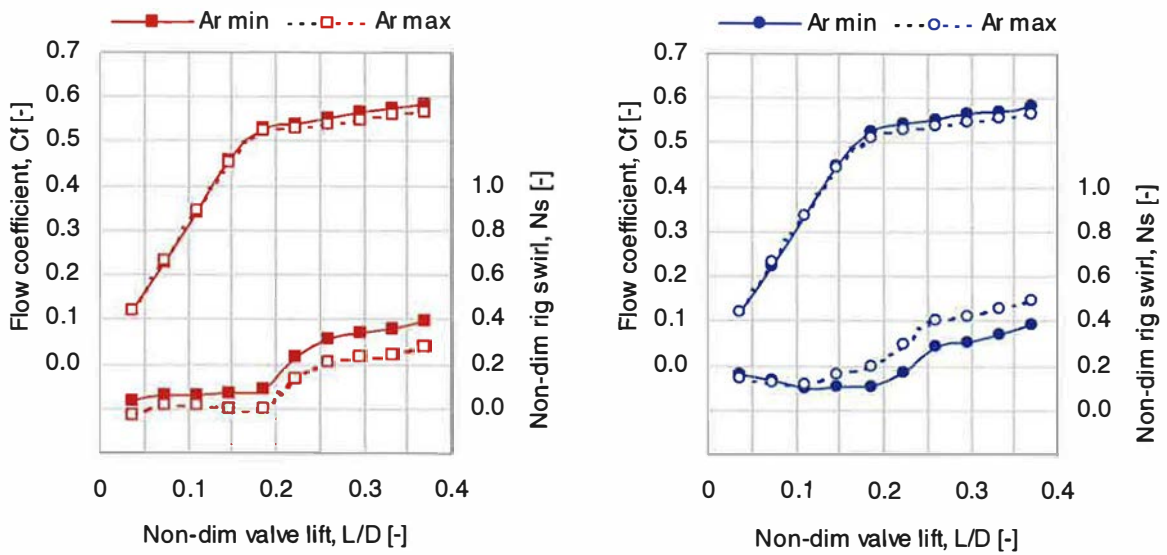
Figure 4.57: Effect of Ar on Cf and Ns performance (directed ports)

145
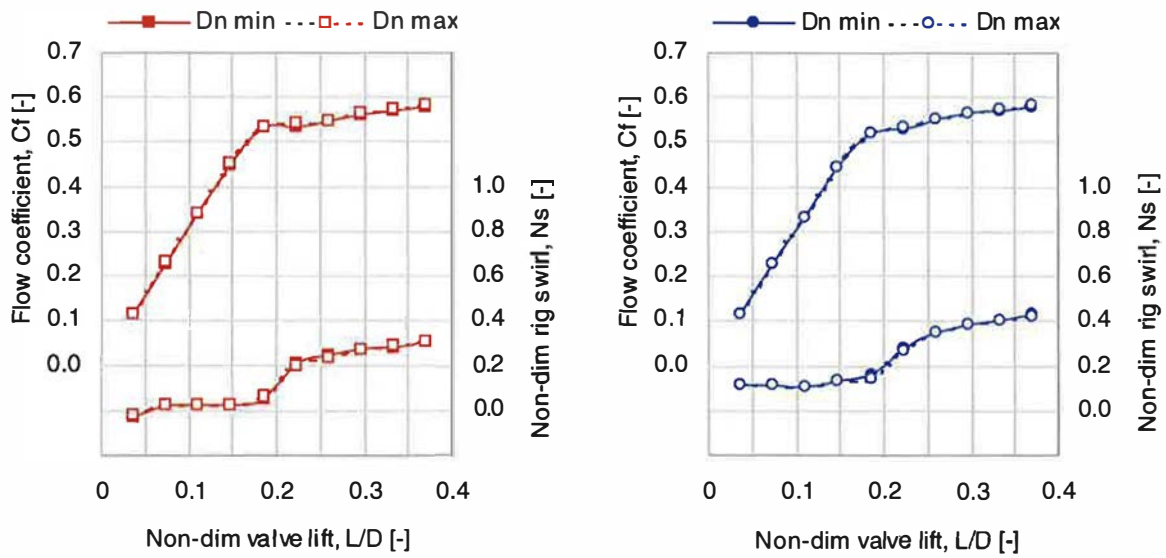
Figure 4.58: Effect of Dn on Cf and Ns performance (directed ports)
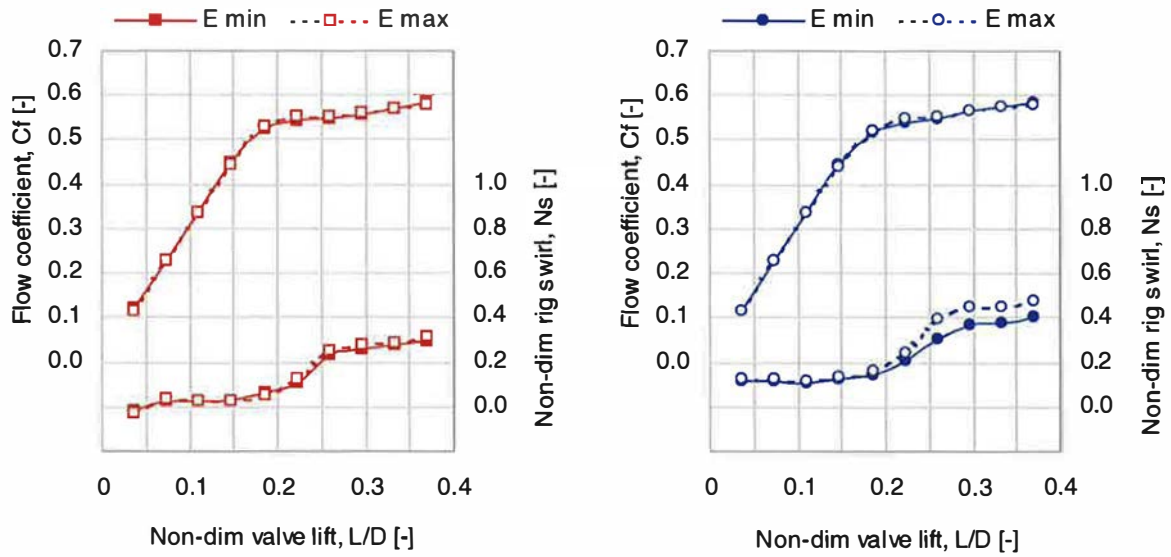
Figure 4.59: Effect of E on Cf and Ns performance (directed ports)

146
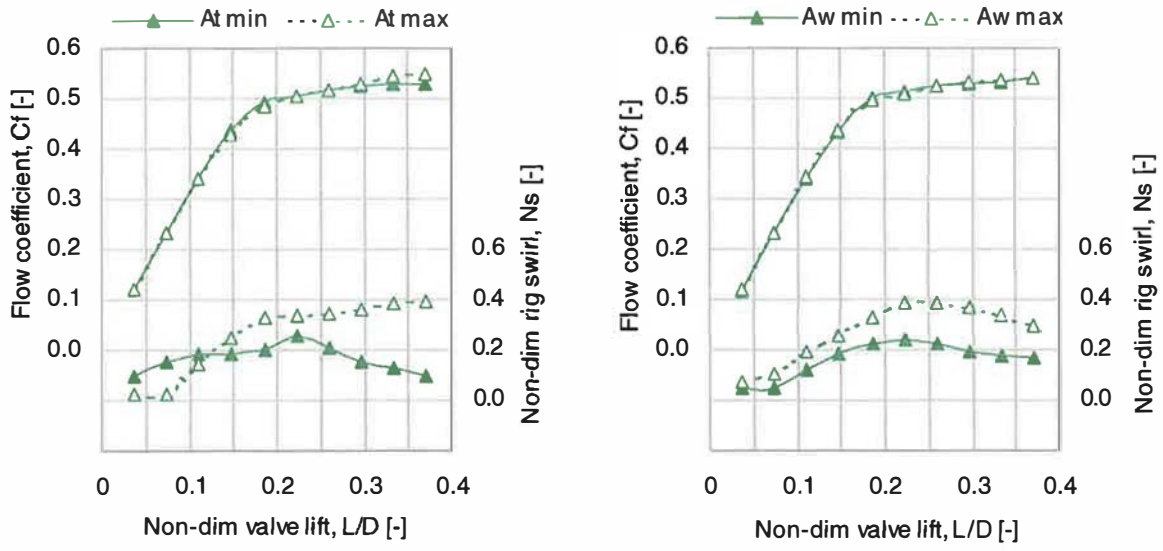
Figure 4.60: Effect of At and Aw on Cf and Ns performance (helical ports)
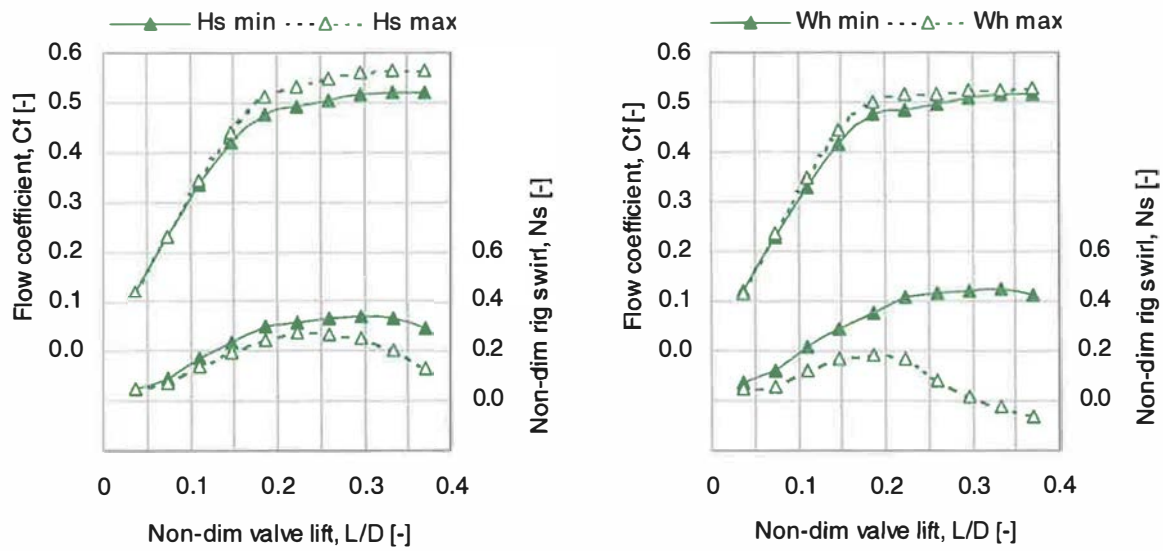
Figure 4.61: Effect of Hs and Wh on Cf and Ns performance (helical ports)

4.5 Validation and Visualisation of Inlet Port Performance Predictions

4.5.1 Introduction

In the present study, experimental data has been used to construct the DoE models; therefore validation tests are presented as a set of comparisons between model predictions and actual test data for previously untested configurations. The use of DoE in preference to traditional "one-at-a-time" methods is partly driven by the limitations imposed by scarce resources. Therefore, the test matrix used to gather the required data must use these resources efficiently. The scarce resource was the availability of physical models and it was therefore not possible to validate all model predictions by comparing them with physical test data. For this reason, CFD modelling was used to visualise performance effects associated with port geometry parameters. Where possible, additional test data was acquired by orientating existing physical models in a range of new positions in order to validate "orientation" parameter effects. The CFD results were used to visualise "shape" parameter effects in order to interpret the quantitative experimental data.

4.5.2 Validation Test Details

Individual port performance predictions were validated against new experimental data and/or visualised using CFD. Those parameters identified as being the most important, in terms of their influence on performance, were included in the validation study. In all cases, the tests were performed on the same apparatus and followed the same procedure as the tests used to build the original data set. Cf and Ns were calculated from 1mm to 10mm valve lift for comparison with the detailed models. Experimental results had shown that low lift performance was mostly independent of the chosen parameters, therefore CFD calculations were performed at 5mm and 10mm valve lift cases, in order to capture typical medium and high valve-lift flow characteristics. In-cylinder flow characteristics were captured on two lateral planes through the cylinder, using velocity vector plots and velocity magnitude plots. The validation test details for each group are shown in Table 4.4.

Parameter	Validation Test Details	CFD Visualisation
At, directed ports	0° to 90°, in 10° steps.	✓
Ar, directed ports	-	✓
Av, directed ports	-	✓
Wh, helical ports	-	✓
Aw, helical ports	-	✓
At, helical ports	0° to 90°, in 10° steps.	✓

Table 4.4: Validation test matrix (single port design parameters)

4.5.3 CFD Modelling Strategy

The Ricardo VECTIS© CFD code, version 3.5, was used for all CFD simulations, including model preparation, flow domain definition, results processing and presentation. The geometry of the experimental apparatus and steady flow test conditions were replicated in the CFD models. The flow domain was modelled from the pressure box (port entry) to the cylinder exit, including a 1-D flow element to represent the flow straightener in the impulse swirl meter (ISM). Constant pressure conditions were applied at the planar inlet and outlet boundaries. The resulting velocity profile at the inlet boundary was also constrained to be normal to the boundary, in order to simulate the effect of upstream flow straighteners fitted to the experimental apparatus.

The flow domain was defined using surface data from the original CAD model. A global Cartesian mesh structure was defined, including refinement areas in the port and valve orifice areas, where the global mesh cells were subdivided. The automatic mesh generator in VECTIS then performed additional local refinement to fit the mesh to the original model boundaries. An appropriate level of mesh refinement was necessary to ensure that the solution was independent of the mesh structure, whilst enabling calculations to be performed in a realistic time. Three different mesh densities were therefore produced for a test case, corresponding to approximately 100,000, 200,000 and 300,000 cells. The global mesh structures are shown schematically in Figure 4.61. A standard k-e turbulence model was used with wall functions to model the boundary layer. Calculations were performed until the computed mass flows and fluid velocities at selected monitoring locations had converged to within 1% of the previous iteration (in the case of mass flows, the inlet and outlet values were

also compared to ensure they were within 1% of each other). Two measurement planes perpendicular to the cylinder axis were selected to present in-cylinder velocity data. Total velocity magnitude was plotted on a plane located at the centre of the valve gap, in order to visualise the main jet flows issuing from the valves. Velocity vectors were also plotted at the ISM entry plane, in order to indicate the strength and direction of the in-cylinder flow at the point of measurement in the experimental tests. Although a 1% convergence criteria is generally not regarded as being sufficient for accurate quantitative data, a comparison of the in-cylinder topology indicated that this was sufficient for a qualitative assessment and further computational time and effort was not necessary. Each CFD run converged in approximately 36 hours on a Silicon Graphics Unix workstation. A visual comparison of the computed velocity magnitudes and vectors for each of the mesh density test cases indicated that the 300,000 and 200,000 cell variants could not be distinguished from each other. However, both contained flow features that were not captured in the 100,000 cell test case. Consequently, all validation geometry was meshed according to the 200,000 cell mesh structure.

Dimension	No. of subdivisions		
A	15	13	10
B	60	50	40
C	7	6	5
D	45	38	30
E	15	13	10
F	7	6	5
G	9	8	6
H	75	60	50

Total no. of cells	300k	200k	100k
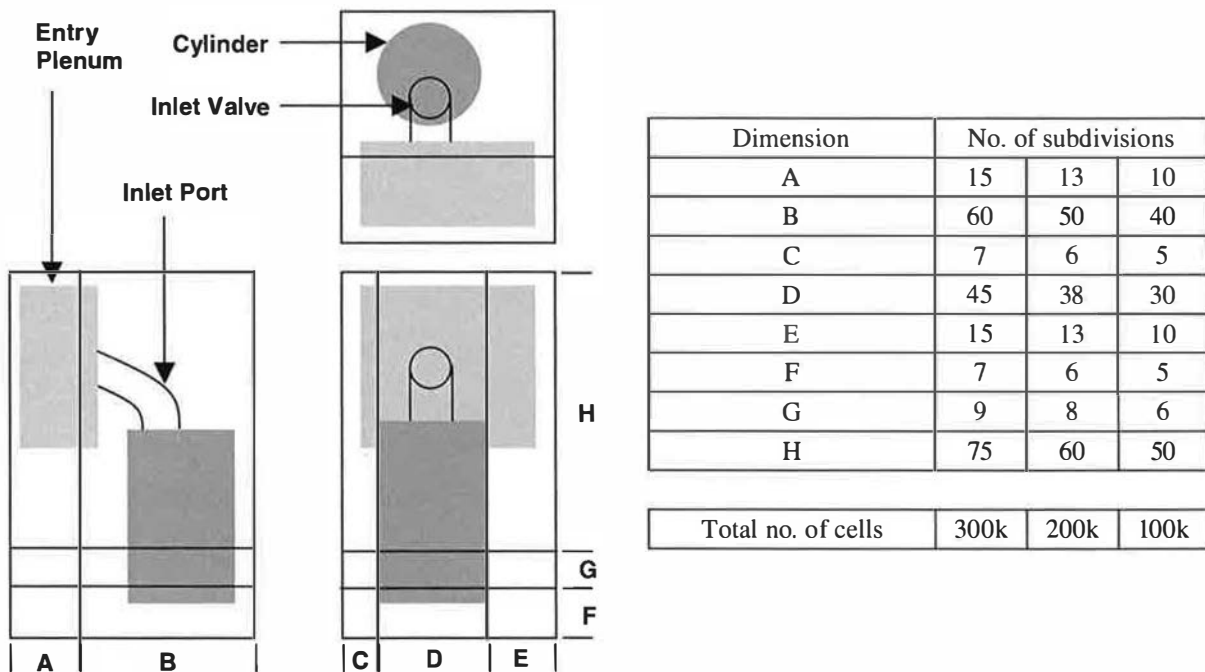
Figure 4.61: CFD Mesh Structure

150

4.5.4 Validation of Port Design Parameter Effects

4.5.4.1 At parameter – directed port

The At parameter was identified as being the most important in terms of the swirl response in directed ports. In order to validate the DoE model predictions, validation tests were performed on an existing physical port model, in which the cylinder bore was rotated about the valve axis in 10° steps from 0° (radial port orientation relative to the cylinder axis) to 90° (tangential orientation). Clockwise rotation of the cylinder represented type B directed ports and anti-clockwise rotation represented type A ports, as shown in Figure 4.62. The sign convention therefore indicates that type B ports produced negative swirl.

-90° (A)   0° (A/B)   +90° (B)
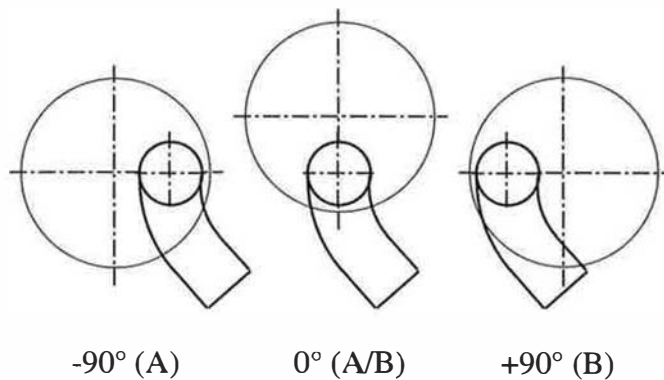
Figure 4.62: At validation – directed port location and orientation

The validation test results are compared with model predictions in Figure 4.63. The validation data follows a sinusoidal trend in the range −90° < At < +90°, matching the findings of previous researchers (Gale, 1990; Li et al, 2000). The combined use of two separate second-order models for the ranges −90<At<0 and 0<At<90 is therefore appropriate, resulting in a satisfactory agreement between predicted responses and validation data. The offset swirl response (i.e. positive swirl is generated at At=0°), caused by curvature in the port, is also captured accurately. However, the validation data indicates a maximum swirl condition at At=80°, the magnitude of which is approximately 16% greater than the model prediction. Swirl is then reduced slightly at the At=90° condition, compared to the predicted value. The lack of this characteristic at the opposite end of the At range suggests that the combined effects of swirl enhancement (due to favourable port curvature) and cylinder bore shrouding may result in a complex response that cannot be fully represented by a second-order model. A selection of predicted and measured Ns curves through the valve-lift range is shown in Figure 4.64. The effect of At, which primarily influences swirl at high valve lift, is reflected

in the validation results and the model accurately predicts the point at which swirl begins to increase rapidly. The difference between model prediction and validation data at At = +80° can be seen in detail; the low predicted Rs/Ld value is consistent with low predicted Ns values at 8 to 10mm valve lift.

Velocity magnitude and velocity vector plots, showing the effect of At on the in-cylinder flow structure, are presented in Figure 4.65. In this sequence, variations in At are shown by maintaining the orientation of the port whilst rotating the valve centre about the cylinder axis. In qualitative terms, the results provide some insight into the detailed flow features that contribute to the overall swirl trends. The velocity magnitude plots for 10mm valve lift show that at At = ±90° a well defined jet flow issues from the valve and remains attached to the cylinder wall. This forms the basis of a well-defined rotational flow structure, as shown in the corresponding vector plot immediately above the ISM measurement plane. A single vortex centre, offset from the cylinder centre, is also clearly visible and is located approximately on the valve axis. There is clear evidence of significant out-of-plane flow features, as indicated by the area of short orange/red vectors. These represent the remnants of the main jet flow, which remains attached to the cylinder wall and descends in a helical manner towards the bottom of the cylinder. At At = ±45°, the jet flow becomes more diffuse and is not attached to the cylinder wall. The resulting flow pattern at the bottom of the cylinder is, if anything, more clearly defined but with lower velocity magnitudes. At At=0°, there is little evidence of a directed jet flow from the valve, although some small areas of increased velocity magnitude are present on the side of the valve corresponding to the curved part of the inlet port. This may develop into a weak rotational flow pattern in the cylinder, although this is not clearly visible in the vector plot. The flow pattern at the base of the cylinder resembles that of a "tumbling" in-cylinder motion in which the primary axis of rotation is perpendicular to the cylinder axis. This is as expected given the orientation of the port. These results show that, despite a reversal in the direction of rotation, the type A and type B ports produce similar flow patterns. There is some evidence that the type B port forms a stronger jet flow that remains closer to the cylinder wall. However, this jet is distorted by the cylinder wall close to the valve, which may account for the small reduction in swirl generation at At = +90°. The results for 5mm valve lift clearly indicate a difference in velocity profile around the valve gap, compared to those at 10mm valve lift. Velocity magnitudes are similar in all directions; this would suggest that the strong directed flow component, caused by the orientation and shape of the directed inlet port, is not well established at the lower valve lift. However, a well-

defined rotational flow pattern is visible on the ISM plane results at At = +45°, suggesting that swirl is developed at low valve lift in type B ports.

4.5.4.2 Ar parameter – directed port

CFD simulation was used to visualise the effect of Ar on in-cylinder swirl characteristics. The DoE models indicated a weak dependence on this parameter, whereby a favourable direction of curvature (type B ports) resulted in increased swirl. The CFD results are shown in Figure 4.66; positive Ar values are used to indicate type A ports and negative Ar values represent type B ports. A straight port is representative of an extreme case of either port type. To aid interpretation of the figure, the valve location is held constant and the port entry is rotated accordingly. Note that the approach angle into the cylinder is held constant in all cases (i.e. At = 45°). The 10mm valve lift results show that a well-defined rotational flow pattern is established in all cases. However, the velocity magnitude plots in the valve gap region indicate some detailed differences. At Ar = +90°, the jet flow from the valve is approximately symmetrical about the valve stem axis and the partly tangential orientation of port causes it to adhere loosely to the cylinder wall. As Ar passes through +45° and 0°, the area of high velocity does not change substantially. At Ar = -45°, there is some indication that the jet flow becomes more closely attached to the cylinder wall. At Ar = -90°, the curvature of the port is clearly causing increased flow from the right-hand side of the valve, resulting in enhanced swirl generation. The results at 5mm valve lift indicate a similar trend, although the effect of Ar is more marked on the ISM plane plots. At Ar = +90°, there is little evidence of swirl, but a rotational flow pattern emerges as Ar is changed from positive to negative. The velocity magnitude results also indicate a developing jet flow around the cylinder wall, enhanced by favourable port curvature.

4.5.4.3 Av parameter – directed port

The Av parameter has a minor effect on swirl generation; it also has a significant influence on flow performance. Both of these effects can be seen in the CFD results, shown in Figure 4.67. At Av = 15° (representing a low approach angle into the cylinder) and 10mm valve lift, the area around the valve is characterised by a concentrated area of high velocity magnitude located opposite the port. This causes the development of an extended high-velocity region that adheres to the cylinder wall. The ISM plane results suggest an organised rotational flow, concentric with the cylinder. The pattern at 5mm valve lift is distorted but there is evidence that swirl is being established. The velocity magnitude results for Av = 45° are subtly

153

different; the in-plane velocity profile around the valve is generally weaker and is more uniform at 5mm valve lift. The extended high-velocity region, that adheres to the cylinder wall in the 15° case, is less well defined and has a diffused appearance. The ISM plane results still indicate a rotational flow pattern, as expected given the overall configuration (At = 45°, Ar = -45°), suggesting a marginal effect on measured swirl.

4.5.4.4 Wh parameter – helical port

The most significant helical port design parameter is helix width (Wh), although the detailed DoE model indicated that its effect was complex and varied with valve lift (Figure 4.27). The results of the CFD visualisation study are shown in Figure 4.68. Narrow helix designs (Wh = 10mm) result in a clearly defined rotational flow pattern at 5mm valve lift. The velocity magnitude plot at this condition indicates that a large amount of the available valve curtain area is utilised, in comparison with those directed port configurations associated with high swirl. At 10mm lift, similar conditions persist on the ISM plane, although the effects of any directed flow components are evident from the velocity magnitude results on the valve gap plane. A main jet flow appears to be directed across the cylinder, with a resulting area of high velocity, which only occupies approximately 30% of the available valve curtain area and is located opposite the port runner section. As Wh is increased to 15mm, the flow patterns at 5mm valve lift becomes more distorted and the swirl pattern is offset from the cylinder axis. However, at 10mm valve lift, the increased helix width causes the angle of the main jet to rotate around the valve axis, directing it onto the opposite side of the cylinder. The result is a clearly defined, but reversed rotational flow pattern at the bottom of the cylinder. This characteristic is amplified as Wh is increased to 20mm, resulting in a weakened swirl pattern at 5mm valve lift (but in the same direction as the orientation of the port), and a strong reverse flow pattern at the ISM plane. These findings match the quantitative results of the DoE model, and also give an insight into the underlying cause.

4.5.4.5 Aw parameter – helical port

The effect of helix wrap angle (Aw) is of secondary importance to Wh, but contributed to the overall swirl response of the DoE model. CFD results are shown in Figure 4.69, indicating some minor changes to the in-cylinder flow topology. At 5mm valve lift and Aw = 190°, the velocity magnitude pattern is equally balanced either side the cylinder. The region of maximum velocity occupies much of the valve curtain area. These two features, coupled with the organised swirl pattern on the ISM plane, indicates that the helical port design generates a

uniform tangential flow pattern from the valve. The results for 5mm valve lift and Aw = 270° are similar in form and magnitude, although the flow pattern on the valve gap plane is rotated relative to the port orientation. The DoE models indicate that increasing Aw results in increased swirl, particularly at intermediate valve lift conditions when helix features are thought to take effect. The CFD results are not conclusive in this respect, but they do indicate a strengthening of the jet flow from the side of the port where the helix is located. At 10mm valve lift, the results do not show any major differences between the two configurations. The angular location of the high velocity region is rotated by a small amount when Aw is increased to the maximum setting, although the resultant effect on the large scale flow features in the cylinder does not appear to be significant.

4.5.4.6 At parameter – helical port

The final helical port parameter to be investigated is At. In common with directed ports, it was possible to perform additional experiment to validate the response across the complete operating range from At = 0° to At = 90°. In addition, CFD simulations were performed to visualise the data. The results are shown in Figures 4.70 and 4.71 respectively. The DoE model response is essentially linear; the relatively noisy model (in comparison with the directed port model) results in a wide error band at the 95% confidence level. However, the validation data, taken in 10° intervals shows that the model predictions are sound. There is some evidence of a non-linear effect towards the higher end of the At range; in common with type B directed ports. The CFD results for At = 90°, 5mm valve lift, clearly show the effect of At; the orientation of the inlet runner section of the port to the cylinder wall maximises swirl generation and compliments the tangential flow pattern that is established in the helix. The At = 0°, 5mm valve lift plots show a complex in-cylinder flow pattern with little organised rotation; this is due to the proximity of the cylinder wall to the end of the helix section, which causes significant interference and axial flows down the cylinder wall. At the 10mm valve lift condition, the dominant directed flow component and weaker helical flow components combine, resulting in a concentrated area of high velocity at the end of the helix feature. This effectively causes a 90° rotation in the main jet flow, with respect to the direction of the inlet runner section of the port. When At = 90°, the jet is directed the centre of the cylinder and rotational flow associated with the helix is able to propagate to some extent. The result is a distorted clockwise (i.e. positive) swirling motion. The effect of reducing At under these conditions is to direct the main jet tangentially in the opposite direction. The helix is effectively redundant and strong negative rotation occurs at the ISM plane.
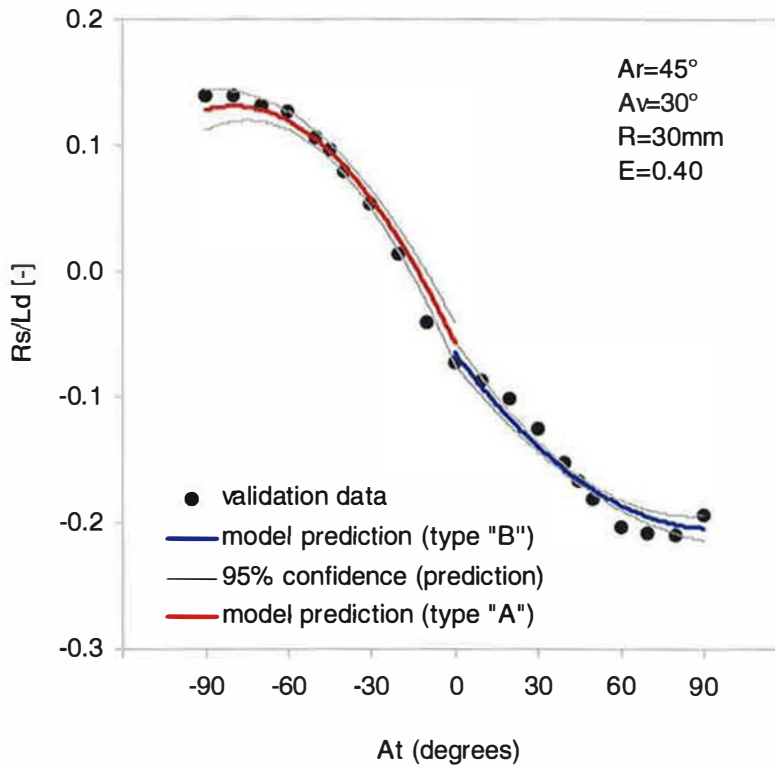
Figure 4.63: At validation (experimental), directed ports – Rs/Ld response
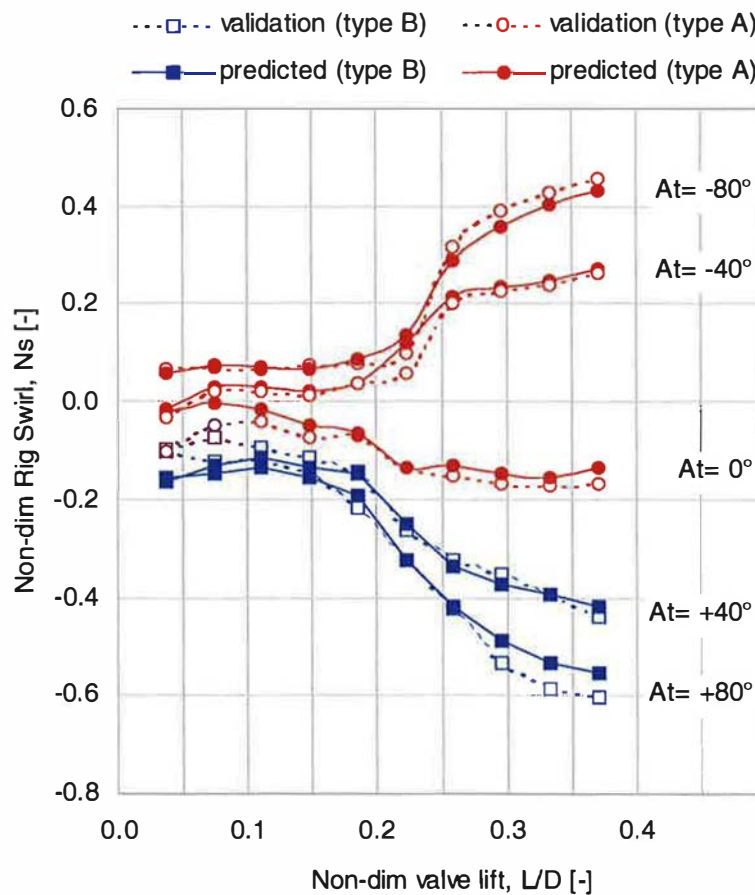
Figure 4.64: At validation (experimental), directed ports – Ns response

5mm Valve Lift   10 mm Valve Lift

-90

-45

0

+45

+90

| 0 | 40 | 0 | 100 |

velocity
(m/s)

total velocity magnitude
(m/s)

| 0 | 50 | 0 | 100 |

velocity
(m/s)

total velocity magnitude
(m/s)
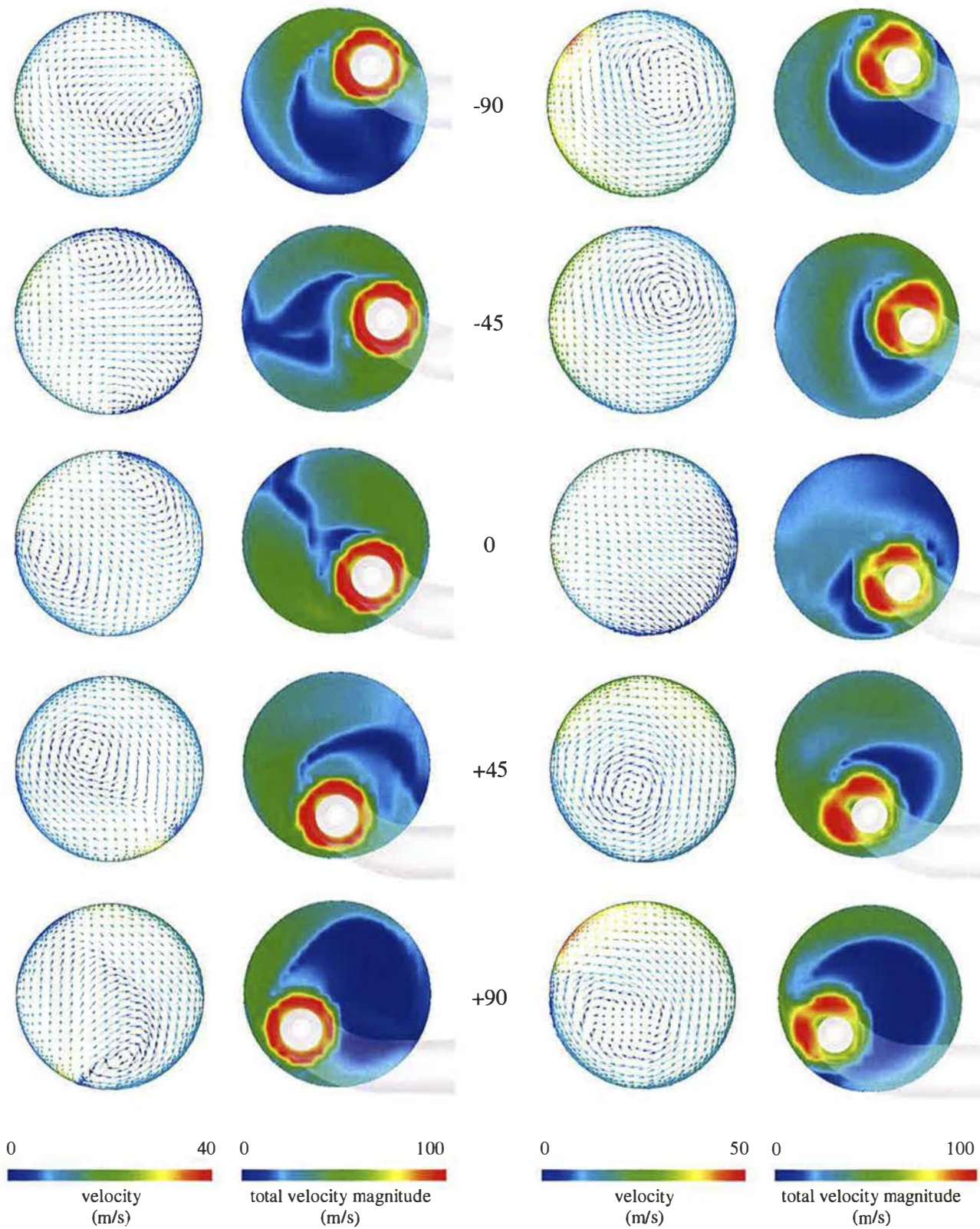
Figure 4.65: At parameter, directed ports – CFD visualisation of in-cylinder flows
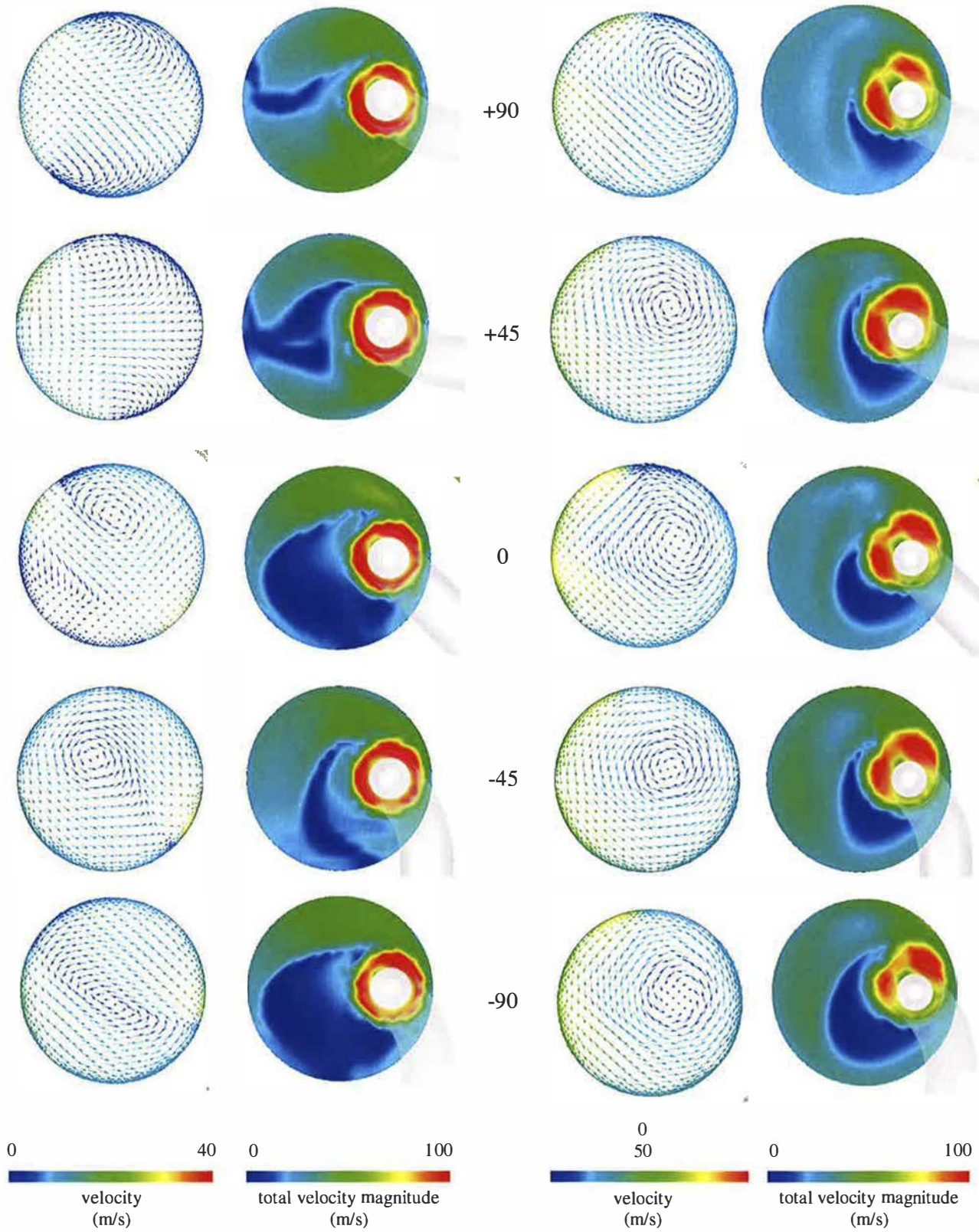
Figure 4.66: Ar parameter, directed ports – CFD visualisation of in-cylinder flows

5mm Valve Lift   10 mm Valve Lift

15

45
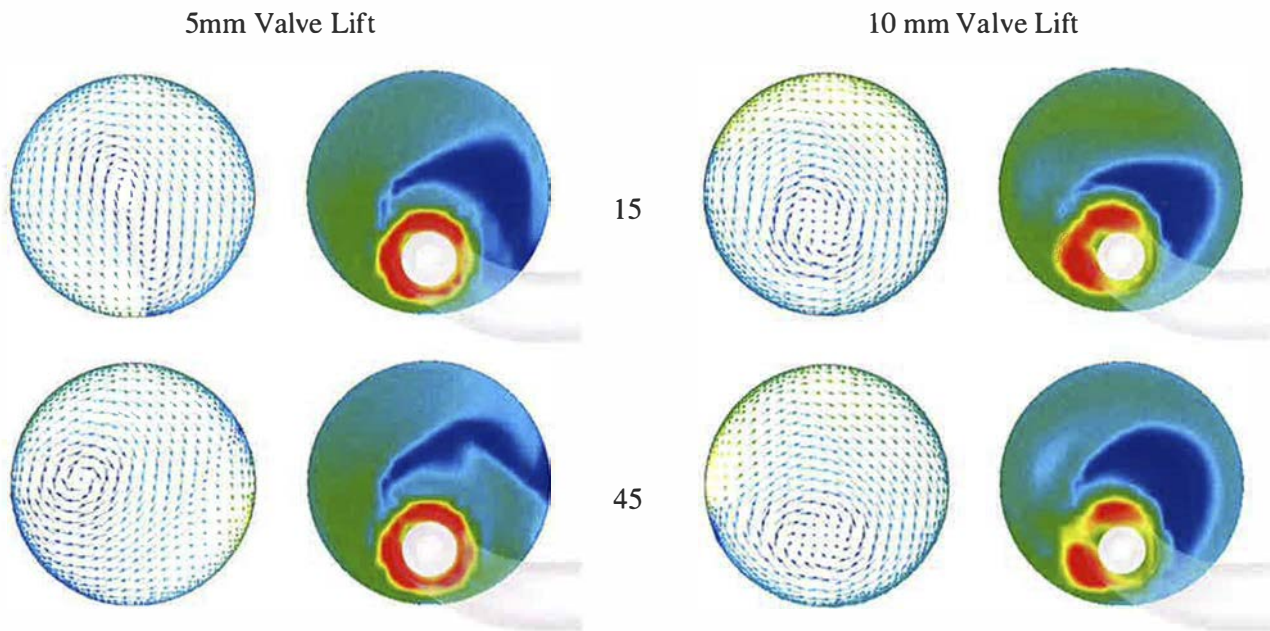
Figure 4.67: Av parameter, directed ports – visualisation of in-cylinder flows

10

15

20

| 0 | 40 | 0 | 100 |
| velocity (m/s) | | total velocity magnitude (m/s) | |

| 0 | 50 | 0 | 100 |
| velocity (m/s) | | total velocity magnitude (m/s) | |
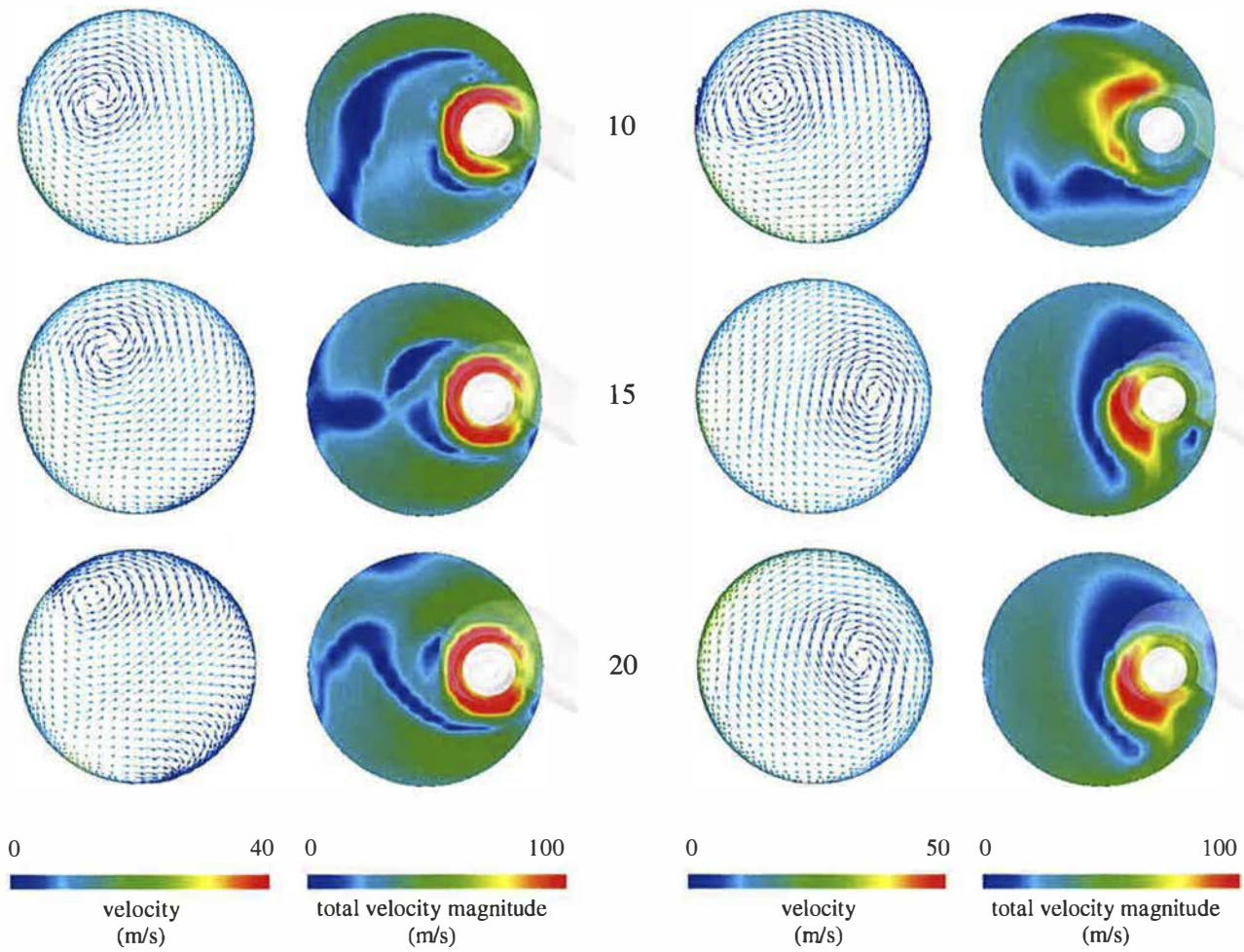
Figure 4.68: Wh parameter, helical ports – CFD visualisation of in-cylinder flows

5mm Valve Lift   10 mm Valve Lift

190

270

velocity (m/s)   total velocity magnitude (m/s)   velocity (m/s)   total velocity magnitude (m/s)
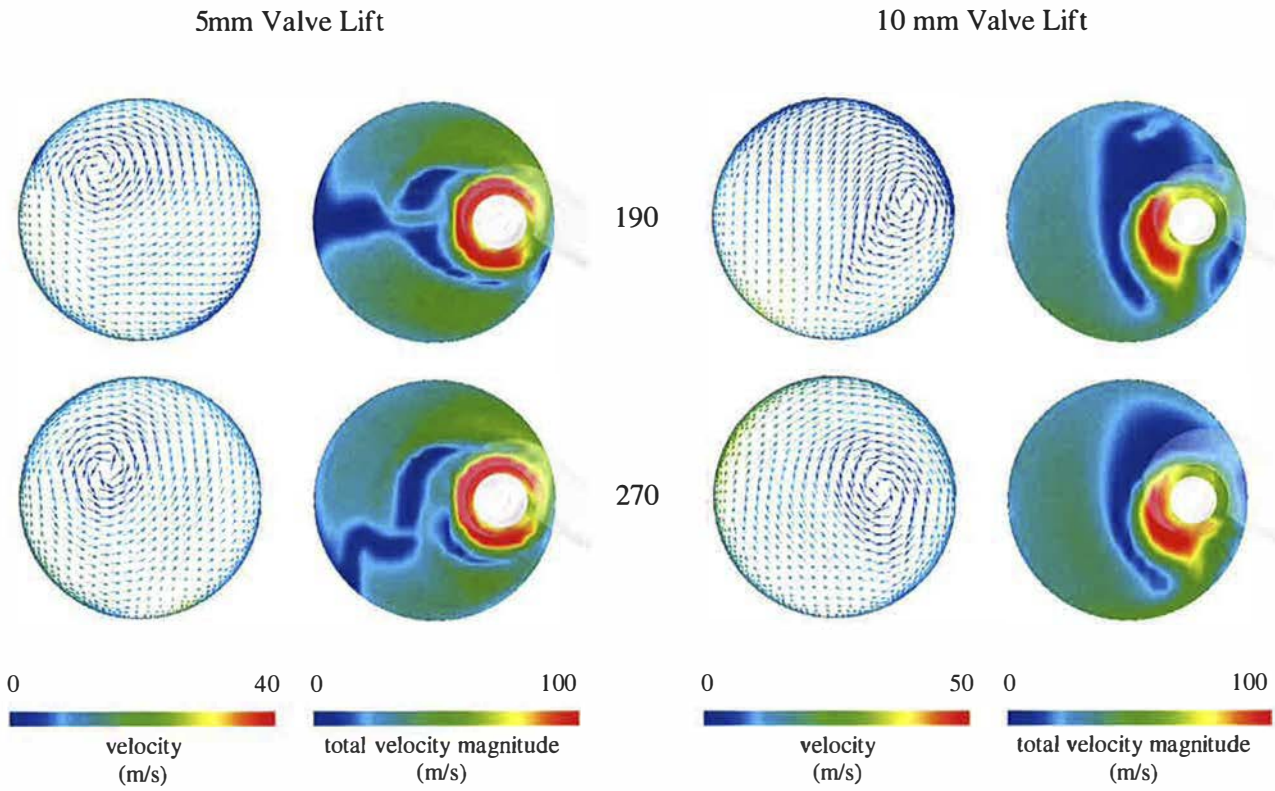
Figure 4.69: Aw parameter, helical ports – CFD visualisation of in-cylinder flows
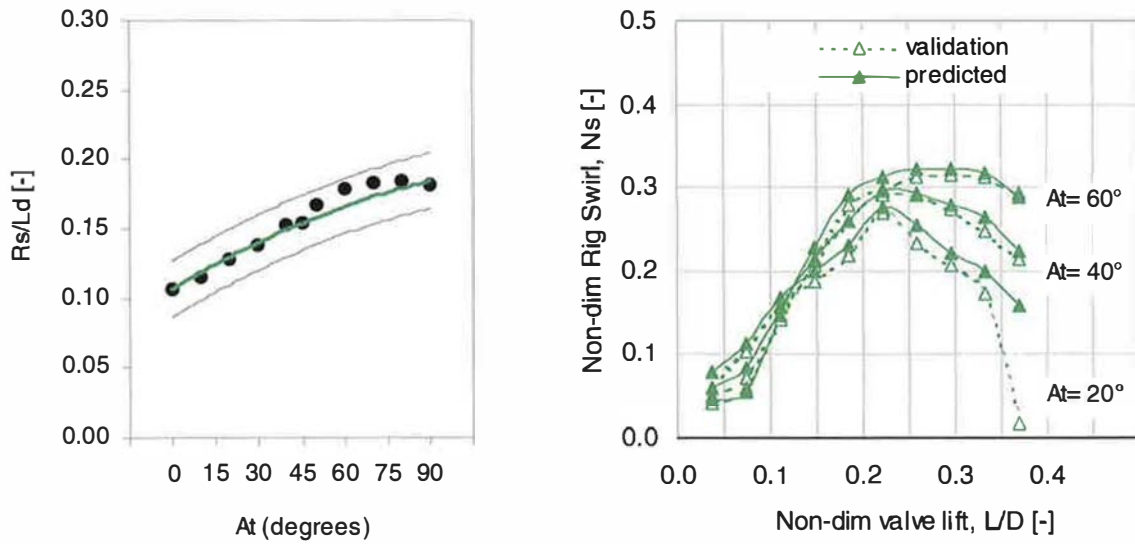
Figure 4.70: At validation (experimental), helical ports – Rs/Ld and Ns responses

5mm Valve Lift   10 mm Valve Lift

0

90

velocity (m/s)   total velocity magnitude (m/s)   velocity (m/s)   total velocity magnitude (m/s)
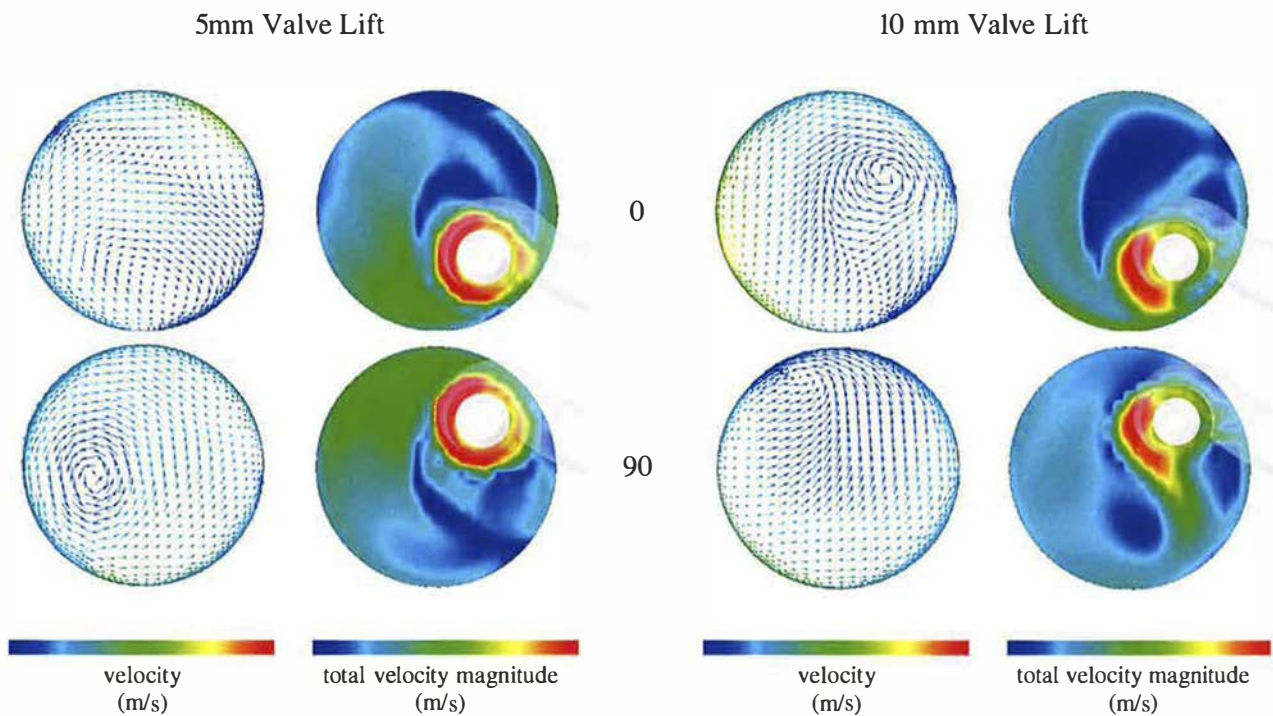
Figure 4.71: At parameter, helical ports – CFD visualisation of in-cylinder flows

4.6 Summary Of Chapter 4

In Chapter 4, the performance characteristics of selected inlet port design parameters have been established. Directed and helical port types have been investigated independently and the results of each have been analysed and compared. The use of statistical design-of-experiments has provided the basis of a knowledge-based model by defining mathematical relationships between design parameters and steady flow performance and air motion characteristics. The robustness of these relationships has been determined using statistical quality checks and validation tests. CFD simulations have also been performed to visualise the in-cylinder flows and support the qualitative data.

A series of different performance models have been developed from a single dataset. Summary performance data has been used to generate a simple model; this has been enhanced by parameterisation of the valve-lift profile and coupling this with the basic responses. A detailed model has also been derived from individual test results, enabling the prediction of flow performance and swirl characteristics throughout the valve lift range.

The flow performance of directed inlet ports is largely governed by design parameters that govern the port shape. Introducing curvature into the port increases flow resistance, as does lowering the angle of approach of the port into the cylinder, thereby restricting flow out of the valve and effectively reducing the valve curtain area. Although port swirl characteristics are strongly dependent on port location and orientation, they are also sensitive to changes in port shape parameters. Changes to port geometry that modify airflow into the cylinder and therefore enhance swirl capability often cause a flow restriction. The result is a typical trade-off between the two aspects of port performance.

Helical ports are frequently used to provide increased swirl when required by a particular combustion system. However, the test results and resulting model responses clearly show the penalty in flow performance compared to directed ports. Furthermore, the design of the helix in the port is critical to develop swirl efficiently, as indicated by the performance response to the design parameters governing helix height and width. Helical ports are less sensitive than directed ports to orientation and location effects, although swirl characteristics at high-valve lift conditions are improved by tangential flow into the cylinder.

5 Predictive Performance Modelling of Multi-Valve Inlet Port Configurations

5.1 Introduction

In practice, the majority of new HSDI diesel engines use a multi-valve cylinder head configuration. Two inlet ports and either one or two exhaust ports per cylinder are the most common options. These are frequently referred to as 3V and 4V designs respectively, denoting the total number of valve in one cylinder. In both cases, an increase in inlet valve area is possible compared to conventional single-inlet valve (2V) designs. An additional benefit of the 4V type is the ability to locate the fuel injector centrally and vertically within the cylinder, thereby generating a symmetrical spray pattern. This, combined with a central bowl in the cylinder, is thought to provide optimum fuel-air mixing and combustion. (Providing, of course, that the fuel spray and air motion characteristics have been appropriately matched)

In order to understand the influence of the port design parameters in a multi-valve context, a design scheme with two inlet ports was defined. The details of the scheme have been discussed previously, in section 3.4. In general terms, the generic design schemes used for single ports are retained but additional parameters are introduced to represent the position of both inlet valves, and the location of the fuel injector. The aim of this study is to investigate various design configurations, including combinations of different inlet port types. Optimisation of the system has also been investigated, in order to determine the most suitable design for a given performance requirement. The performance characteristics of the multi-valve configurations are predicted with an additive model; the accuracy of this approach has been determined by conducting a series of validation tests. In addition, the validation test results have been used to assess the accuracy of the DoE models.

5.2 Modelling Approach

5.2.1 Features of the Additive Model

Flow performance for both ports at a particular valve lift condition was estimated by calculating the average flow coefficient between both inlet ports (Equation 2.7) and mean

flow coefficient was determined in a similar manner using the individual mean flow coefficients from each port (Equation 2.8). Note that this method is only appropriate when inlet valves of the same size are used, and a consistent definition of flow coefficient is applied. In this case, the use of flow coefficient based on inlet valve inner seat diameter was continued. The combined swirl characteristics of both ports were estimated by summation of the individual port results, weighted according to flow coefficient, in order to account for the relative contribution of each to the total in-cylinder contents. A combined value for Ns at a particular valve lift, predicted using the detailed DoE models, was calculated using the following expression (the derivation of which closely follows those provided by Kawashima, et. al. (1988) and Li, et. al. (2000):

$$Ns = \frac{Cf_1 Ns_1 + Cf_2 Ns_2}{2Cf} \tag{5.1}$$

Where Cf is calculated using Equation 2.7 and the suffices 1 and 2 refer to each individual port. The summarised swirl characteristics, predicted using the simple DoE models, were also calculated using a summation approach, resulting in an expression that is essentially the same as that developed by Kawashima et. al. (1998).

$$Rs/Ld = \frac{1}{n} \left[\frac{(Rs/Ld)_1 MCf_1^2 + (Rs/Ld)_2 MCf_2^2}{MCf^2} \right] \tag{5.2}$$

Where MCf is calculated using Equation 2.8. This version of the expression is easily applied to the most simple DoE models. An equivalent, algebraically identical version, may be used for the enhanced simple models in which the Rs/Ld response is replaced by Rs_0 (Equation 3.2).

$$Rs/Ld = \frac{1}{2n} \left[\frac{Rs_{0.1} + Rs_{0.2}}{(MCf \cdot P)^2} \right] \tag{5.3}$$

The detailed single-port DoE models may be used to calculate combined Rs/Ld and MCf in two ways; the individual port MCf and Rs/Ld responses may be calculated using Equations 1.5a and 1.6, then Equations 1.8 and 5.2 may be used. However, it is also possible to use

Equations 1.7 and 5.1 before using equations 1.5a and 1.6. The latter approach is favoured, as the contributions of each port are combined at each valve lift condition before performing the integration. Cf and Ns curves may then be calculated for the total system, thereby allowing some interpretation throughout the valve lift event.

5.2.2   Limitations and Applications of the Additive Model

In all of the summation models, it is assumed that interactions between individual port flows are purely additive. In practice, more complex interactions are likely to occur, inducing flow interference or enhancement. The extent to which these interactions have an effect on accuracy has been investigated by Kawashima et. al. (1998), who found that errors of approximately +-3% in Cf and +-5% in swirl meter torque were typical. He concluded that this was an acceptable level of accuracy for the purposes of concept design evaluation. Li, et. al. (2000) found similar differences in Cf results. He then proposed that the difference between predicted and observed results could be used to diagnose the amount of interference between port flows and therefore assess the compatibility of two ports in a multi-valve design scheme. He found that combinations of helical and directed ports were the most susceptible to interference. In particular, when the directed port was arranged so that the main jet flow from one valve was directed towards the other, the measured swirl was up to 80% lower than predicted. HWA measurements were used to confirm his theory. In the present study, further investigations will be made into this area. A new field of study has also been initiated, considering a constrained multi-valve model to include features such as the fuel injector and cylinder bolt pattern.

5.3   Multi-Valve Design Configurations

The additive multi-valve model was used to investigate performance trends for a range of design configurations. By varying the types of ports used, four generic arrangements could be achieved. A naming convention was applied to simplify the identification of each, as shown in Table 5.1. When considering the relationships between design parameters of each port, the general layout of the cylinder head is clearly influential. The location of the inlet valve centres, described using the skew angle (As1) and valve separation angle (As2), is critical in this respect. A selection of typical design configurations are shown in Figure 5.1, illustrating the relationship between At and Ar. In this illustration, each port is orientated so that the entry

165

is perpendicular to an imaginary manifold face (horizontal in the figure). In practice, there may be some scope for angled entry conditions, although it is clear that the amount of port curvature required to achieve a tangential flow direction into the cylinder is related to the value of As1. As2 is held constant at 90°, although variations in As2 are possible and are influenced by several factors, as will be discussed in a later section. When the skew angle is small, it is not possible to achieve tangential flow from the upstream port with a realistic amount of port curvature (Ar < 90°). A helical port may be introduced to increase swirl capability, as shown in Figure 5.1(d). By increasing the skew angle, tangential flow may be achieved. In the configuration shown in Figure 5.1(b) both ports are orientated tangentially to the cylinder, although the upstream port must curve through 90°. At high skew angles, it becomes difficult to package the downstream port without intruding into space that is likely to be occupied by a neighbouring cylinder. Note that in Figure 5.1, the value of Ar for a directed port identifies it as either a type A or type B, in terms of the DoE performance model that applies. This is an important aspect of the multi-valve model because of the different performance characteristics of each type. For example, both ports in Figure 5.1(a) are type A, whereas a combination of type A and B ports are used in Figure 5.1(c). The transition between each type has been discussed in chapter 3 and a good level of agreement was achieved. Therefore, the performance of the downstream port in Figure 5.1(b) may be predicted using either DoE model.

Upstream port	Downstream port	Identification
Directed	Directed	DD
Directed	Helical	DH
Helical	Directed	HD
Helical	Helical	HH

Table 5.1: Multi-valve design configurations

(a) DD, As1=0   (b) DD, As1=45   (c) DD, As1=90

(d) HH, As1=0   (e) HH, As1=25   (f) HD, As1=90
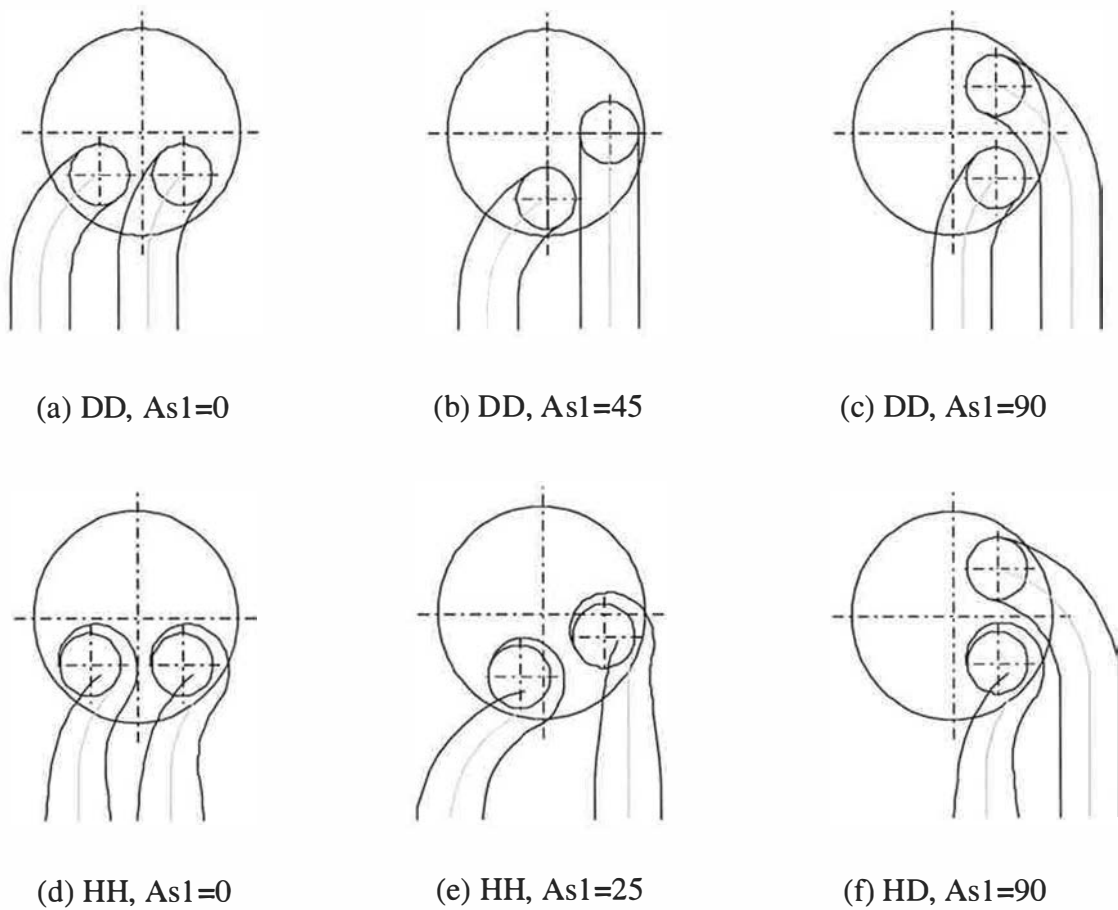
Figure 5.1: Multi-valve examples

5.4   Performance Prediction

5.4.1 Overview

The use of an additive model implies that the port performance of the complete multi-valve system is determined entirely by the performance of individual ports and therefore the design parameters of each. These relationships have been discussed in chapter four. In chapter three, a hierarchy of design features was presented and it was shown that high-level features influence port design parameters, often by constraining the space envelope in which the ports may be packaged. The multi-valve investigations presented below are focussed on the design features that govern the overall design layout and the main area of interest is how these features influence individual port design parameter values and therefore performance.

5.4.2 Effect of Skew Angle

In order to assess the effect of skew angle on each generic design configuration, a series of model predictions were performed for a range of As1 values. Port design parameters were held constant except At and Ar; At was maximised with an Ar range of +-90°. The perpendicular entry constraint was also applied. The engine design configuration is summarised in Table 5.2 and port design parameter settings are shown in Table 5.3.

Engine Configuration	
Cylinder Bore, B (mm)	84.4
Piston Stroke, S (mm)	90.0
Rated Speed, ω_E (rev/min)	4500
Inlet Valve Lift Profile	
Maximum valve lift (mm)	8.37
Duration (deg crank)	230

Table 5.2: Engine design configuration used for multi-valve model predictions

	Port 1 Configuration	Port 2 Configuration
Type	D or H	D or H
At	Maximised, max 90°	Maximised, max 90°
Ar	Variable, 0 to 90°	Variable, 0 to 90°
R	Fixed, 50mm	Fixed, 50mm
Dn	Fixed, 0.32	Fixed, 0.32
E	Fixed, 0.45	Fixed, 0.45
Av	Fixed, 30°	Fixed, 30°
Wh	Fixed, 10mm	Fixed, 10mm
Hs	Fixed, 30mm	Fixed, 30mm
Aw	Fixed, 230°	Fixed, 230°

Table 5.3: Port design parameters used for skew angle sweep

The predicted performance characteristics for each port and the complete system are shown in Figure 5.2. The geometry of the configurations dictates that all upstream directed ports are type A and the downstream port type changes from type A to type B when skew angle exceeds 45°, as indicated in the figure. The MCf response is relatively flat for downstream ports but there is a distinct improvement in the flow performance of upstream ports when skew angle exceeds 45°. For skew angles below this value, Ar must be maintained at 90° to achieve maximum tangential flow. As skew angle increases beyond 45°, tangential flow is achieved with less port curvature. Upstream ports also benefit from increased skew angle, in terms of swirl generation. A more rapid increase is apparent at low skew angles as the port becomes more tangentially orientated. A similar swirl trend is observed in downstream ports, although the absolute Rs/Ld value is higher. Note that this swirl increase is a result of varying Ar from -45° to +45° as At remains constant at 90°. As expected, helical ports generate higher levels of swirl but at the expense of flow performance, when compared to directed ports. It was not possible to package a helical port in the downstream position for skew angles beyond 45°. Consequently, HH and DH configurations were defined only up to this value. The MCf response for downstream and upstream helical ports varies to a small extent, but remains essentially constant. Swirl responds positively to increased At values as skew angle is increased from 0° to 45°. However, in contrast with the directed port results, helical ports are relatively insensitive to Ar. Consequently, decreasing Ar does not enhance swirl and the response is flat as skew angle is increased from 45° to 90°. The results also show that upstream port performance at a skew angle of 90° is identical to downstream port performance at a skew angle of 0°. This outcome is expected for a valve separation angle of 90°.

The combined characteristics of the individual port results contribute to the overall performance of multi-valve systems, as shown in Figure 5.3. DD configurations achieve the lowest swirl levels, whereas HH configurations are capable of increased swirl. The performance of HD configurations lies in between. The DD configuration at 90° skew angle and the HD configuration at 0° skew generate a similar level of swirl (0.18Rs/Ld), as do HH at 0° skew and HD at 90° (0.27Rs/Ld). This suggests that the use of helical ports could be advantageous if skew angle is constrained to a low value. However, in all cases the flow performance of directed ports is superior. Typical MCf values of 0.44, 0.42 and 0.39 were observed for DD, HD and HH configurations respectively. All multi-valve configurations respond in a similar manner to changes in skew angle. Higher levels of swirl are generated as

skew angle is increased and an influence on flow performance was observed in the DD configuration. The individual port results indicate that this is primarily due an improvement in the orientation of the upstream port.
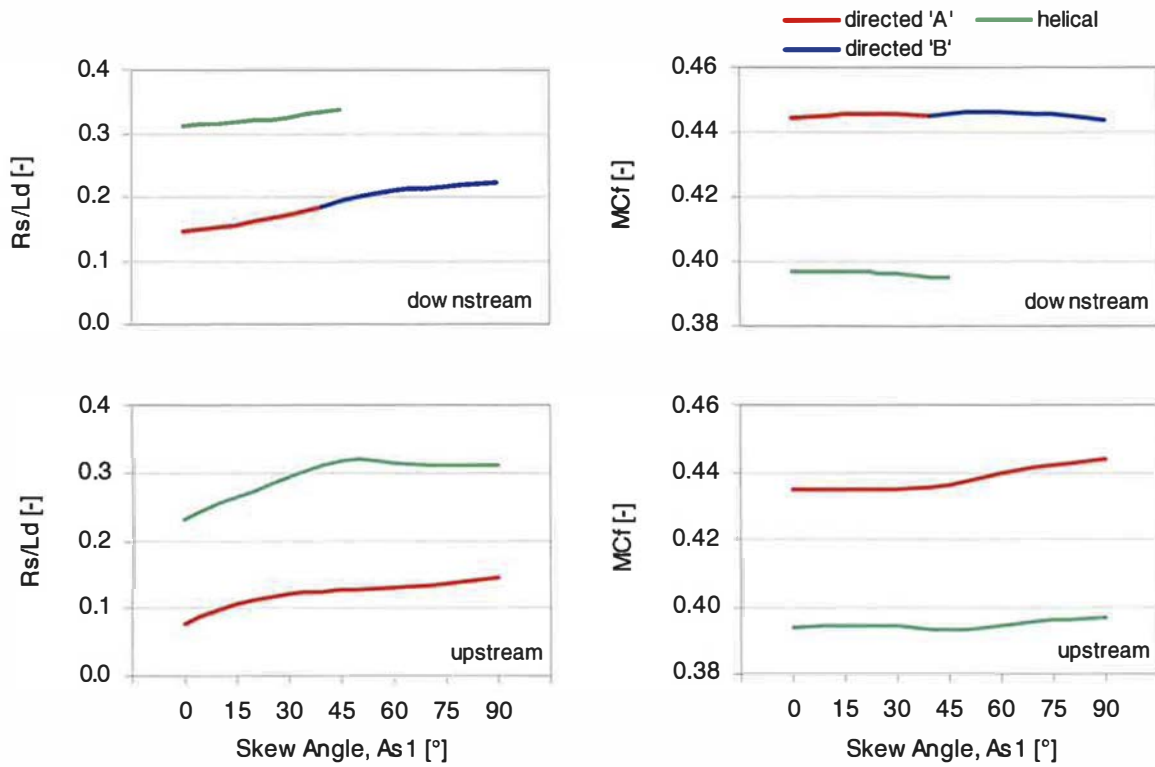
Figure 5.2: Individual port performance predictions – effect of skew angle (As1)
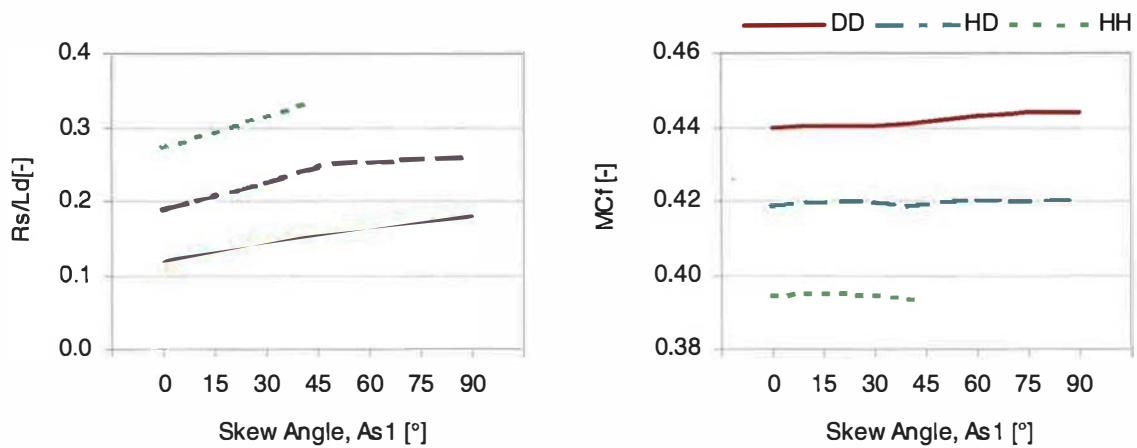
Figure 5.3: Multi-valve performance predictions – effect of skew angle (As1)

The detailed DoE models were used to investigate Ns and Cf responses. Upstream and downstream port performance curves are shown in Figures 5.4 and 5.5 respectively. In both figures, curves are shown for skew angles of 0°, 45° and where appropriate 90°. Helical and directed upstream ports exhibit a similar trend, in which increasing skew angle from 0° to 45° enhances swirl at high valve lift. A smaller increase in swirl also occurs as skew is increased further to 90°, although this is distributed throughout the valve lift range. An increase in Cf values at high valve lift can also be observed when skew angle reaches 90°, corresponding to the small improvement in MCf. Downstream port swirl characteristics also vary, increasing throughout the valve lift range as skew angle is increased. The results for DD, HD and HH multi-valve configurations are shown in Figure 5.6. The performance characteristics are a combination of the individual port results. Consequently, the effects of skew angle appear to be smoothed, resulting in a relatively linear increase in swirl with valve lift. The improved flow performance of the DD configuration is caused by the increased Cf values at high valve lift.
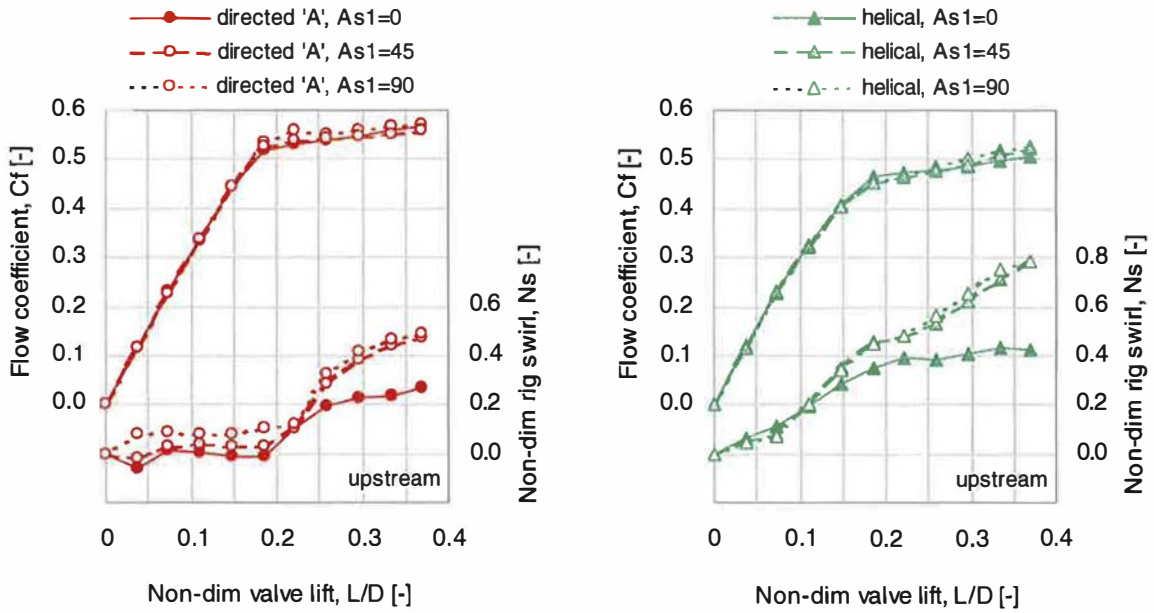
Figure 5.4: Individual port performance predictions, upstream (detailed model)
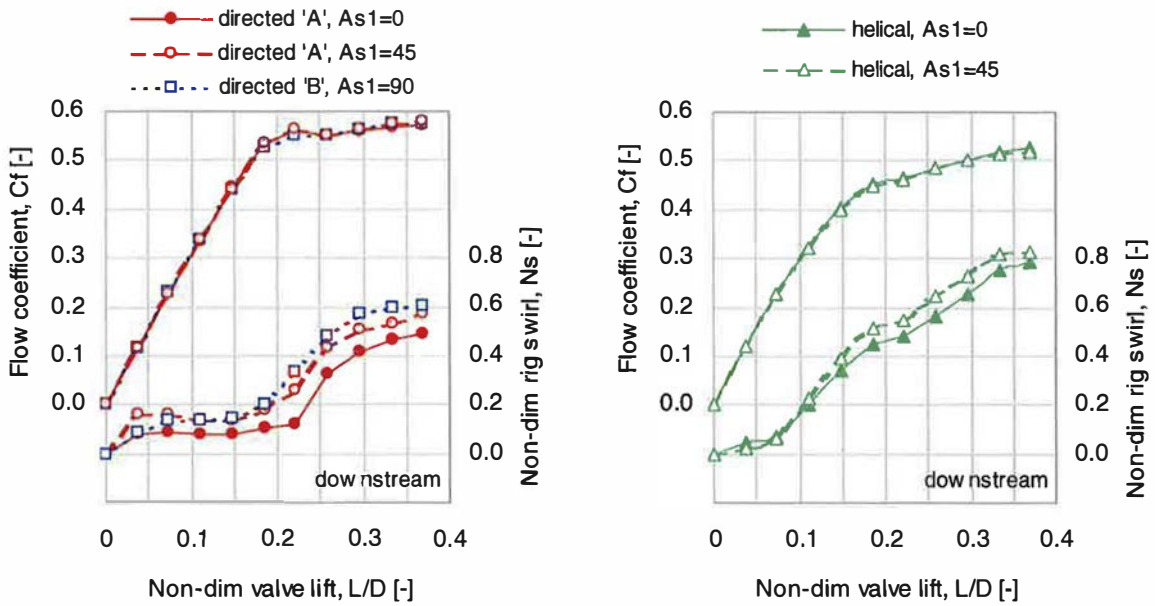
Figure 5.5: Individual port performance predictions, downstream (detailed model)
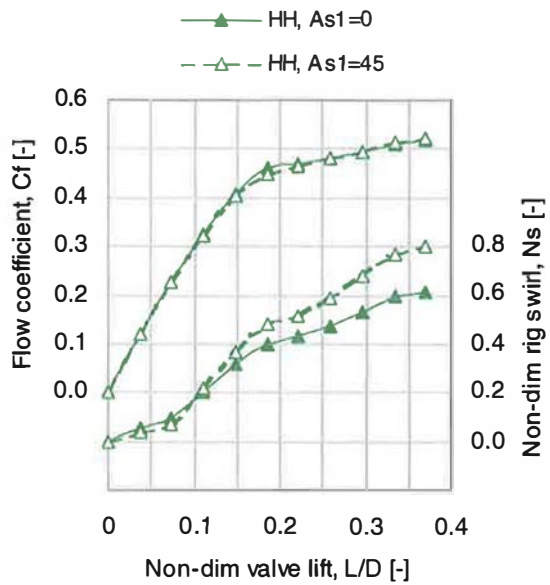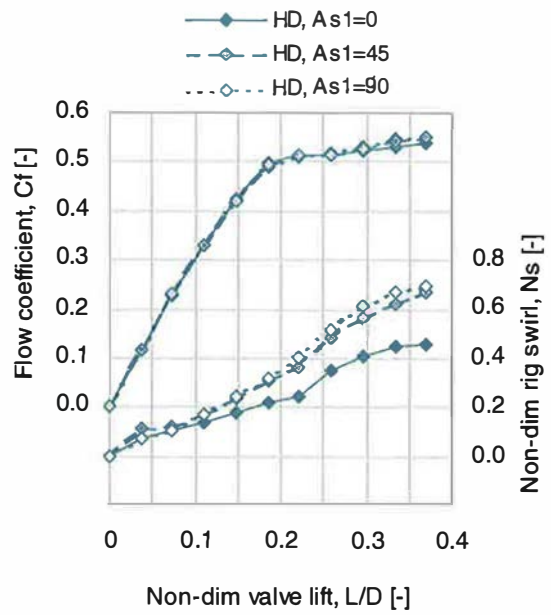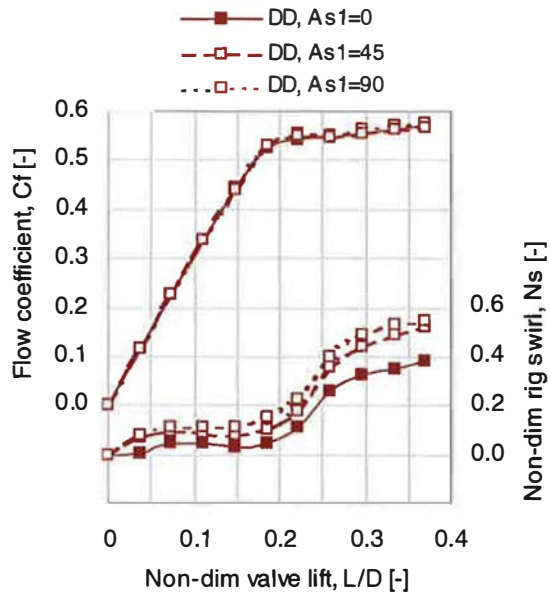
Figure 5.6: Multi-valve performance predictions (detailed model)

5.4.3 Effect of Valve Separation Angle

In order to package the inlet and exhaust valves, fuel injector and heater plug, it may be necessary to vary the valve separation angle (As2). The minimum value of As2 is determined by the minimum inlet-inlet valve bridge thickness. The maximum value of As2 is dependent on achieving sufficient inlet-exhaust and exhaust-exhaust valve bridge thickness, and therefore is also influenced by the number of exhaust valves and their diameter. The heater plug location will also influence As2; if it is to be located between the inlet valves the minimum As2 value will increase. Alternative locations are likely to limit the maximum As2 value. Increasing E will increase the distance between adjacent valves for a given As2 value. The results of an investigation into the performance effect of As2 are shown in Figure 5.7. A DD configuration was used, engine geometry from Table 5.3 was maintained and additional constraints were applied to determine the As2 range, resulting in maximum and minimum values of 130° and 86° respectively. A typical exhaust valve head diameter was used and the same value of E (0.45) as used for the inlet valves. The results do not indicate a large change in port performance as As2 is varied. However, when skew angle is set to 0°, the upstream port geometry is constrained (Ar is a maximum) and an increase in As2 forces a reduction in At. For larger skew angles, adjustments to the port geometry compensate for the change in valve separation.
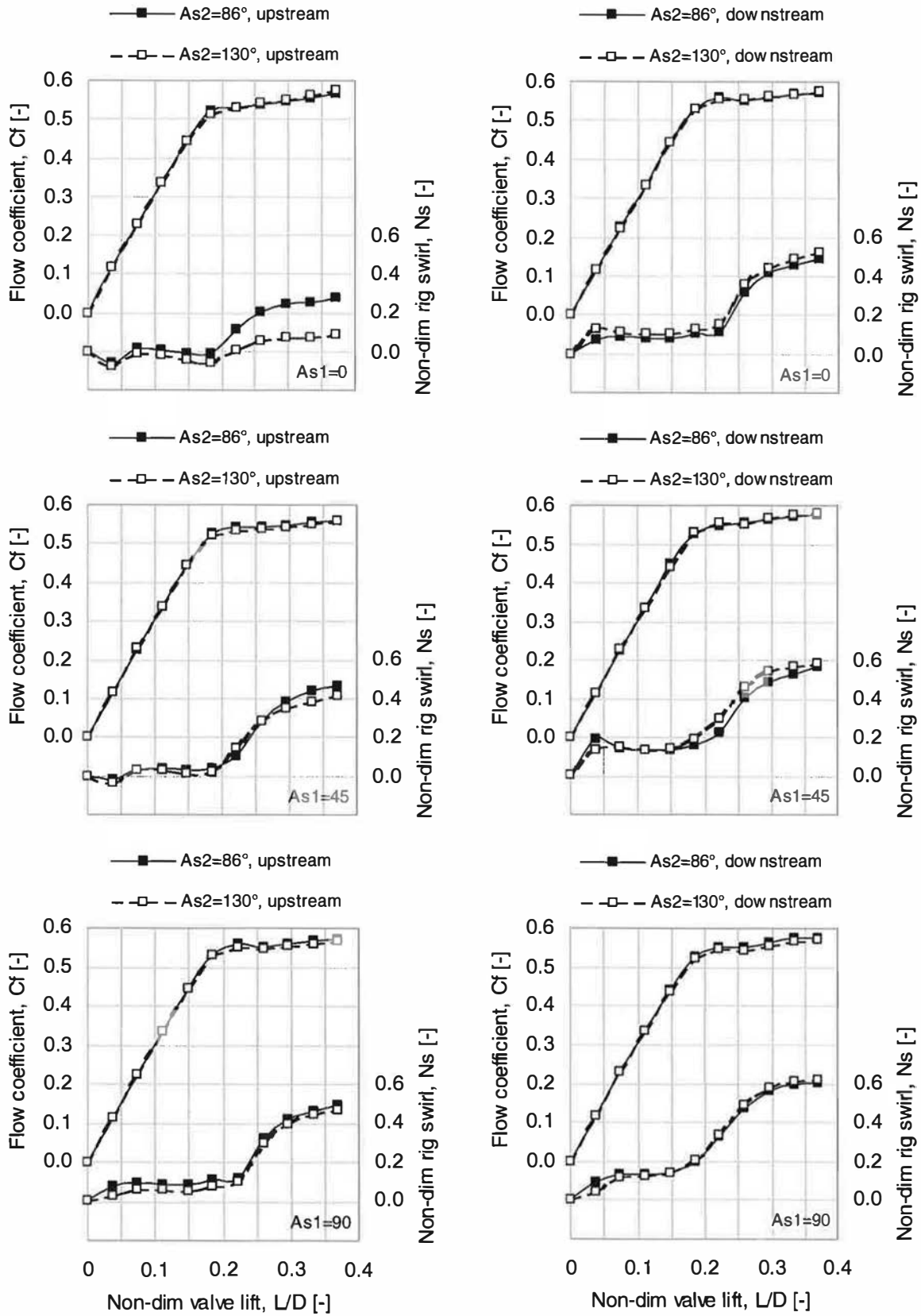
Figure 5.7: Effect of As2 (DD configuration)

Cylinder Layout	
Minimum inlet-inlet valve bridge	4mm
Minimum inlet-exhaust valve bridge	4mm
Minimum exhaust-exhaust valve bridge	6mm
Exhaust valve head diameter	26.5mm
Exhaust valve "E" parameter value	0.45

Table 5.4: design constraints used for the valve separation study

5.4.4 Effect of Valve Size

It has been shown in Chapter 3 that non-dimensional inlet valve diameter (Dn) is not significant in terms of its effect on the non-dimensional performance characteristics of a single port and valve. However, when considering real engine cylinder geometry, inlet Mach index (Z) and swirl ratio (Rs) are used to characterise port flow characteristics and both are directly influenced by valve size. The ideal relationship between valve size and performance is illustrated in Figure 5.8. Rs and Z are normalised by their respective values at Dn=0.32 in order to indicate the magnitude of the response for geometrically similar port configurations, irrespective of the actual design parameter values. Rs and Z are inversely proportional to valve area; therefore they are directly proportional to each other in terms of the response to Dn. The use of smaller inlet valves provides greater freedom in the choice of valve location and allows a larger injector to be packaged, or allows larger cooling passages around the injector. The maximum swirl level for a given configuration is increased, as is the range of swirl requirements that can be accommodated. However, port flow performance is significantly impaired. In order to maintain a constant Rs value for a typical DD configuration, increasing Dn from 0.30 to 0.34 requires a modification to the port design to promote swirl, such as decreasing the Av parameter of both ports. Although there is a loss in flow performance resulting from the lowering of the vertical port approach angle, it is outweighed by the improvement in flow performance derived from the increased valve area. Optimisation of all port parameters for different Dn values is likely to result in a different response to the simple case illustrated here. However, it is clear that valve size dominates the performance response in terms of flow capacity and therefore must be considered in the earliest stages of the design process.
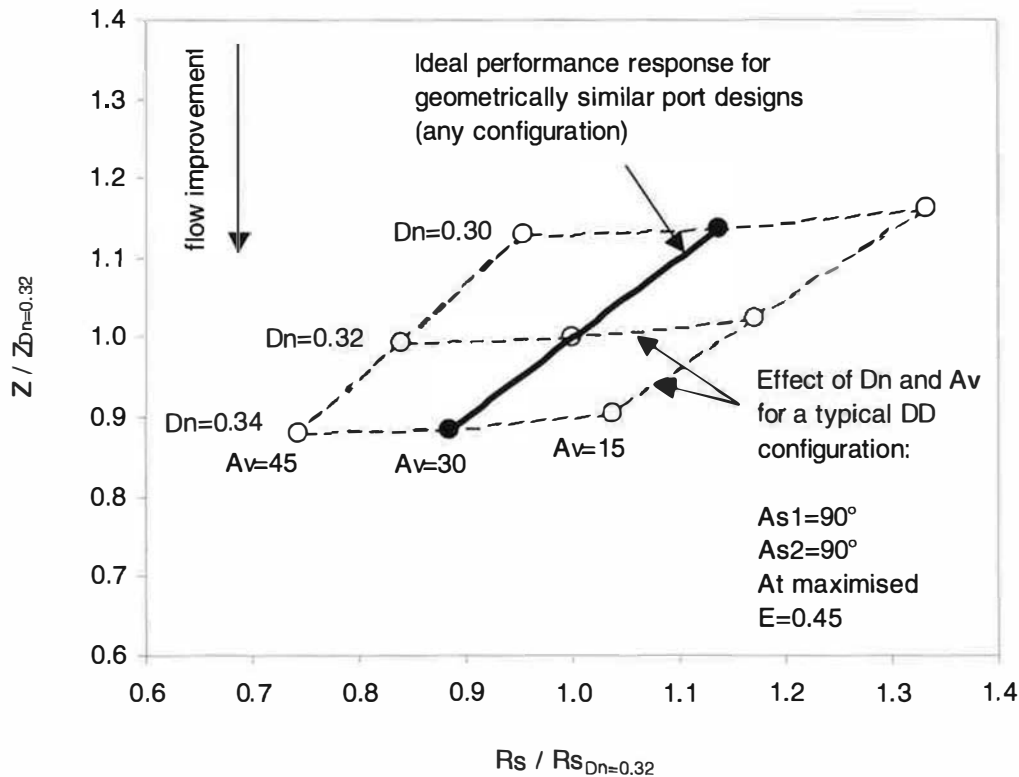
Figure 5.8: Effect of valve size

5.5   Optimisation of Multi-Valve Configurations

5.5.1 Overview

Selection of the most appropriate design configuration for a given performance target is a complex process that is often performed iteratively, using trial-and-error methods. The knowledge of individual experts is therefore important and is a scarce resource. In many cases, the ideal solution is prevented by constraints and it is almost impossible to be certain that the chosen design is optimal. The parametric models of geometry and performance response, developed in the present study, may be used to determine the influence of such constraints and optimise the design. A common optimisation problem encountered during the cylinder head design process is the maximisation of inlet port flow performance for a particular in-cylinder swirl ratio requirement. Swirl must be matched to the combustion system, which is influenced by the performance of the fuel injection equipment and combustion chamber geometry. Clearly, the established trade-off between swirl ratio and inlet port flow performance is important in this respect. Improved combustion systems, brought about by development in fuel systems technology, may tolerate decreased swirl levels and

177

therefore an improvement in flow performance would logically follow. However, it is beneficial to maximise flow performance in any case, in order to increase volumetric efficiency in naturally aspirated engines and improve fuel economy in turbocharged engines. Conversely, it is not usually necessary to investigate the maximum swirl potential of a particular configuration, although this may be of benefit during the early stages of concept design in order to eliminate unsuitable design options.

5.5.2 Optimisation Model

The generalised multi-valve performance model consists of interdependent sub-models that are used to describe inlet port flow and swirl characteristics. In the simplest case, sub-models for Rs/Ld and MCf are required for each inlet port, resulting in a total of four. Both MCf models must be optimised simultaneously in order to maximise overall flow performance, subject to a constraint on the combined value of swirl, determined by the Rs/Ld models. The MCf and Rs/Ld models for a particular inlet port are coupled, as the terms in each correspond to the geometry of that port. Likewise, the remaining two models are coupled by the geometry of the second port. These relationships are shown conceptually in Figure 5.9. The detailed DoE models, containing sub-models for Ns and Cf, for each inlet port, at each valve lift position, are clearly more complex. However, the sub-models contribute to an overall performance response in a similar way to the simple case. Individual Cf and Ns sub-models have the potential to provide more sophisticated optimisation goals, such as the shape of the Ns curve or a low valve-lift flow performance target in addition to the overall Rs and Z requirements.

An unconstrained optimisation problem, in which the geometry of each port may be considered as independent, provides an ideal solution, although it may not be feasible in practice. Optimisation of a realistic multi-valve system is rather more complex, due to key relationships involving many parameter values. In particular, a non-overlapping constraint is necessary to prevent the ports from occupying the same space in the cylinder head. Clearly, this situation cannot occur in the real world unless ports that share a common entry are represented. During the present study, these types of ports have not been considered in detail, but it is an area worthy of further investigation. The nature of this constraint is simplified compared to physical reality, which is of course three-dimensional. The constraint takes into account the silhouette of both ports in plan view and prevents them from overlapping along their full lengths between valve and entry point. An additional allowance for metal wall

thickness may also be specified. Other important practical constraints involve the inlet valve diameter and the radial distance of the valve centres, described by the Dn and E parameters respectively. In order to reduce manufacturing costs and simplify engine assembly, identical inlet valves are usually specified and are located at a common distance from the cylinder centre. There is, in fact, no fundamental reason why this should be so, although the current practice has been adopted for the purposes of investigating the models developed here. Finally, significant external constraints are provided by the size, number and location of the cylinder head bolt bosses.

An optimisation process was developed using the Microsoft Excel 2000 Solver ("the Solver"). The Solver uses the Generalized Reduced Gradient (GRG2) non-linear optimisation technique and is suitable for a range of non-linear optimisation problems (NLPs). However, the standard Solver routine is not entirely suitable for the present optimisation problem for two reasons. Firstly, the GRG2 optimisation technique is capable of finding a local optimum dependent on initial conditions and cannot reliably find a globally optimum solution if multiple local optima exist. Secondly, the Solver implementation of the GRG2 technique recommends that constraints should be constant values. In the present study, the presence of multiple local minima could not be ruled out and the construction of the models resulted in constraints being defined as functions of the design parameters. Therefore, a VBA computer program, incorporating Solver, was written to overcome these limitations. A simple global optimum search routine was created by initiating several Solver runs with randomised initial conditions. Each solution was saved to a spreadsheet and when a pre-defined number of matching solutions were found, the corresponding set of parameter values were considered to be the global optimum. The constraint limitation was overcome by reducing the Solver to a simple unconstrained problem, whilst adding external penalty values for each constraint to the objective function (i.e. maximise flow performance). The severity of each penalty could be manually adjusted to allow softer constraints, if required. This approach also allowed the solution to fall outside the boundaries of the problem, if no valid solutions existed, or if the violation of one constraint by a small amount resulted in particularly good performance. Setting up and optimising a typical design concept took approximately 5 minutes on a standard desktop PC (1GHz Pentium 3 CPU, 256Mb RAM).
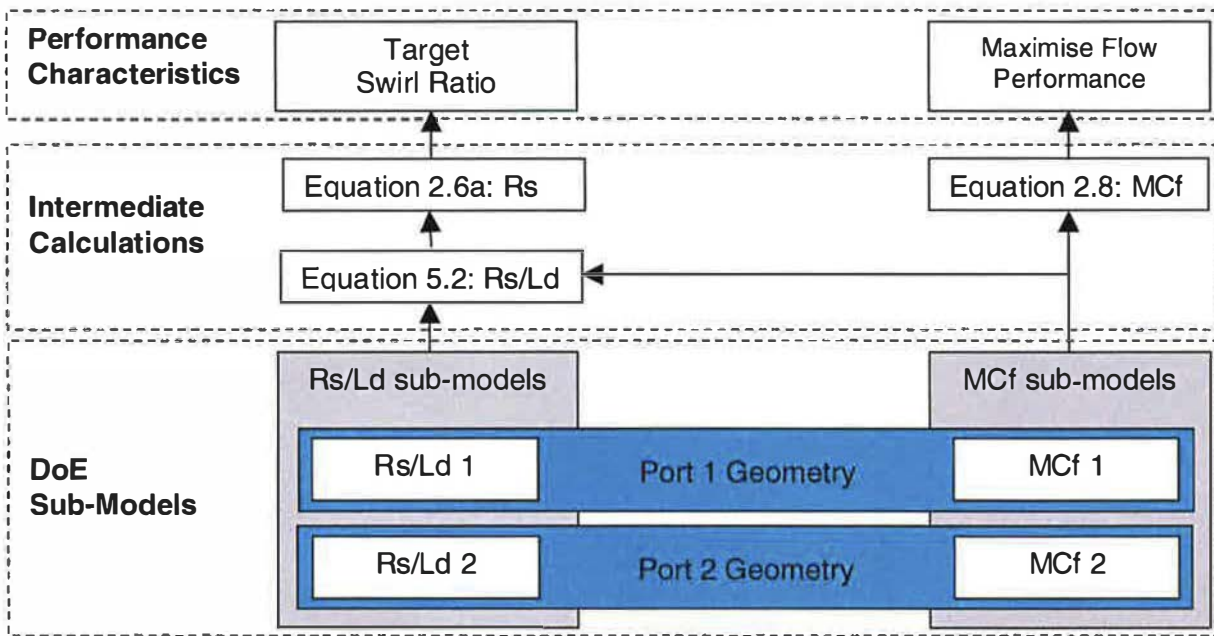
Figure 5.9: Optimisation concept

5.5.3 Unconstrained Optimisation

In order to establish the performance of the optimisation routine and to gain a basic understanding of the performance response, a series of "unconstrained" optimisation problems were performed. Note that the problems were not unconstrained in mathematical terms; the non-overlapping constraint was applied and As2 was held at 90°. In addition, the perpendicular entry constraint described previously was used to control the overall orientation of the ports towards an imaginary manifold face. Without this constraint, both ports would be free to rotate about their respective valve centres, resulting in highly efficient, but unrealistic, solutions. All other parameter values were allowed to vary through the full range and external constraints such as cylinder head bolt boss location were not applied. For each inlet port design configuration (DD/HD/HH), a range of swirl ratio targets was set and the optimisation routine performed to maximise flow performance. In all cases, the simple DoE models were used and the engine geometry settings shown in Table 5.2 were retained. The results for successive Solver runs within a single optimisation run indicated significant differences in locally optimised solutions, especially in the DD optimisation data. This was due to the discontinuity between the response surfaces of type A and B directed ports, which may have prevented the optimisation routine from crossing the boundary between the two in order to find an improved solution. In such cases, the number of Solver runs was increased and the

boundary values for the Ar parameter on both ports were artificially chosen to ensure that all possible directed port type combinations had been included in the initial conditions. The results of the unconstrained optimisation are shown in Figures 5.10, indicating the overall swirl-flow trade-off for all port design configurations. Several significant trends are immediately clear: Firstly, the expected trend of increasing inlet Mach index with increasing swirl ratio is evident, both in general terms across the complete set of configurations, but also individually for each port configuration. This characteristic has been documented extensively, and it is now possible to understand the underlying causes for this trade-off in terms of the changes in port geometry that are required to generate increased swirl. Secondly, the response curves show that DD configurations provide the best flow performance, as indicated by the low Z values, but are only capable of generating low swirl (up to 1.1Rs for the chosen set of engine design parameters). HH configurations are the least effective in terms of flow performance but are capable of generating significantly more swirl, up to 2.2Rs in this case. HD configurations fall in between in terms of flow performance and swirl generating potential. Finally, the transition points, at which each configuration becomes the most efficient compared to the others, are clearly identified. In this case, the transition point from DD to HD is at 1.0Rs. The transition from HD to HH occurs at 1.3Rs. It is also apparent that the response of DD port configurations is flat at low swirl ratios (<0.5Rs), indicating that the maximum flow potential can be maintained when low levels of swirl are generated.

Figures 5.11 to 5.13 show the changes in design parameter values as the swirl target is increased, for all port configurations. Plan view sketches of each configuration are shown, clearly indicating the increase in skew angle that is necessary as more swirl is required. The optimisation routine effectively selects the most suitable geometry changes as swirl is increased, thereby minimising any loss in flow performance. Figure 5.11 shows the results for the DD port configuration. In the range 0<Rs<0.5, flow performance is maintained by increasing skew from 0° to 45° and therefore At is increased towards 90°; it is not necessary to increase Ar by more than a small amount in both ports. As the swirl requirement increases further, it is necessary to increase skew to 90°, resulting in a greater increase in Ar and some loss in flow performance. At the highest swirl conditions, these changes must be supplemented by a reduction in port curve radius R (for port 2) and vertical port approach angle Av, both of which impair flow performance. Note that R for port 1 remains at a maximum value, as a decrease in port curve radius would counteract swirl in the required direction. Eventually all parameters are at their maximum swirl conditions. Figure 5.12 shows

the change in parameter values for the HD configuration. At low swirl conditions, the helical port parameter settings reflect the need for maximum flow performance. As the swirl requirement increases, the dominant helix feature (Wh), is progressively reduced, followed by a reduction in helix height (Hs), both of which cause a loss in flow performance. Helix wrap angle (Aw) is increased rapidly, as there is little flow penalty associated with this change in geometry. The directed port (port 2 in this example) follows a similar trend to the corresponding port in the DD configuration; Ar and At are progressively increased with skew as swirl is increased. Av and R also begin to decrease as the maximum swirl capability of the port is reached. The rate of change of these parameters appears to be slower than in the DD configuration, this is due to the increased swirl-generating capability of the helical port. Figure 5.13 shows parameter values for the HH configuration. The parameter values of port 1 closely follow those of the corresponding port in the HD configuration. The geometry of port 2 also follows a similar trend, except that Ar decreases as skew is increased.
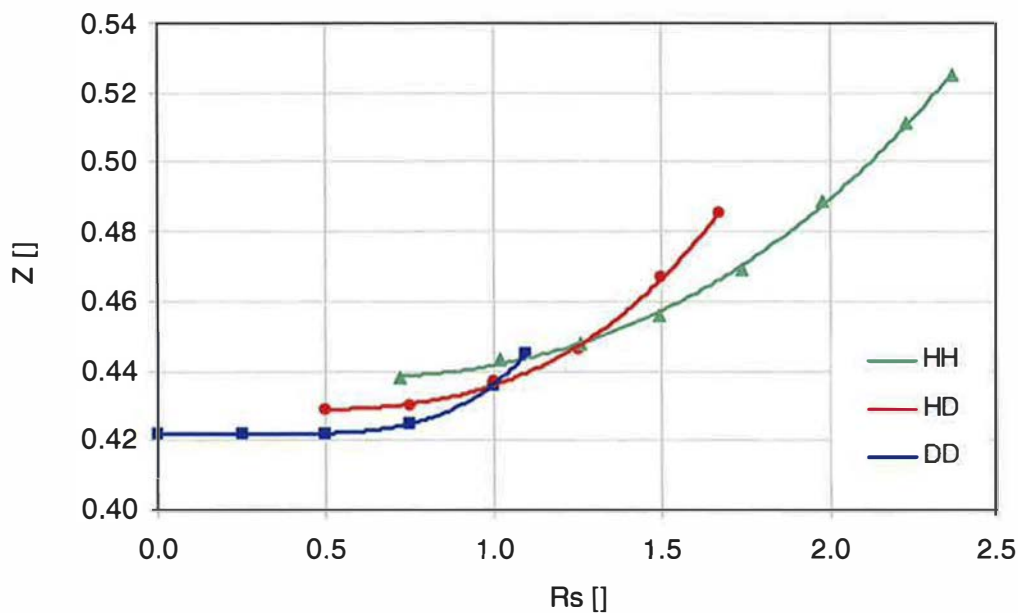
Figure 5.10: Performance trade-off (unconstrained optimisation)
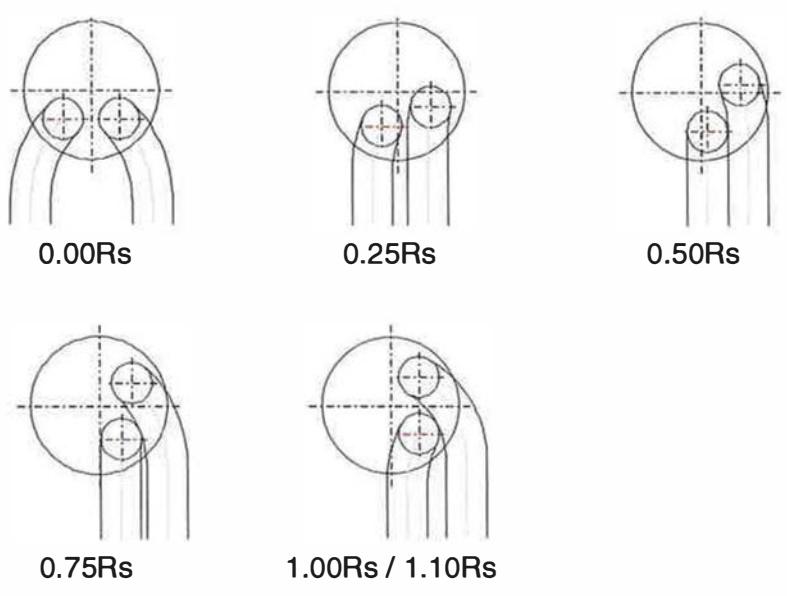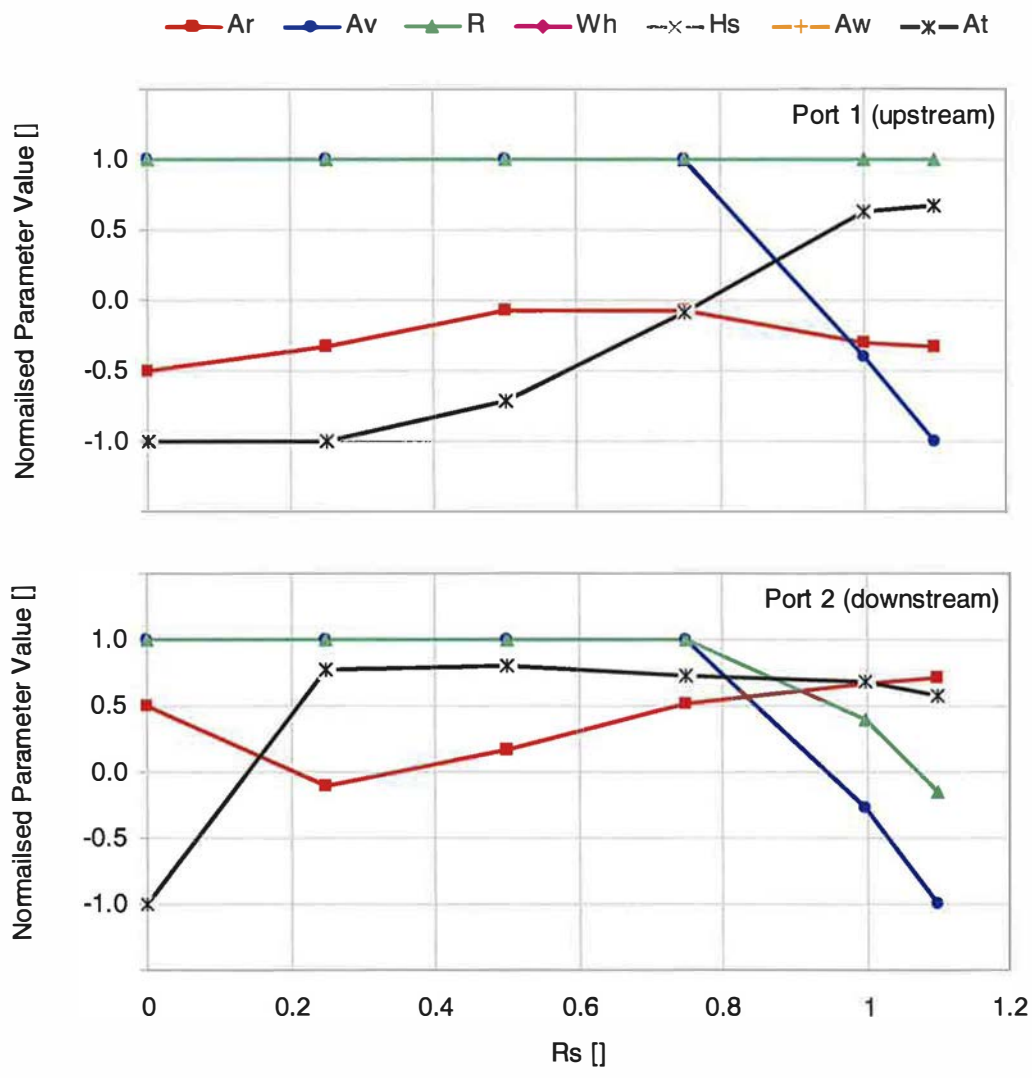
Figure 5.11: Parameter values (unconstrained optimisation, DD configuration)
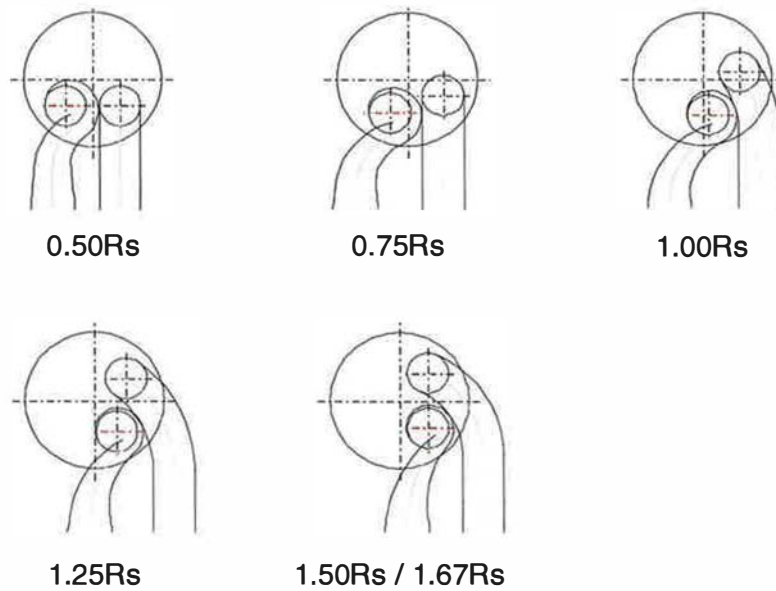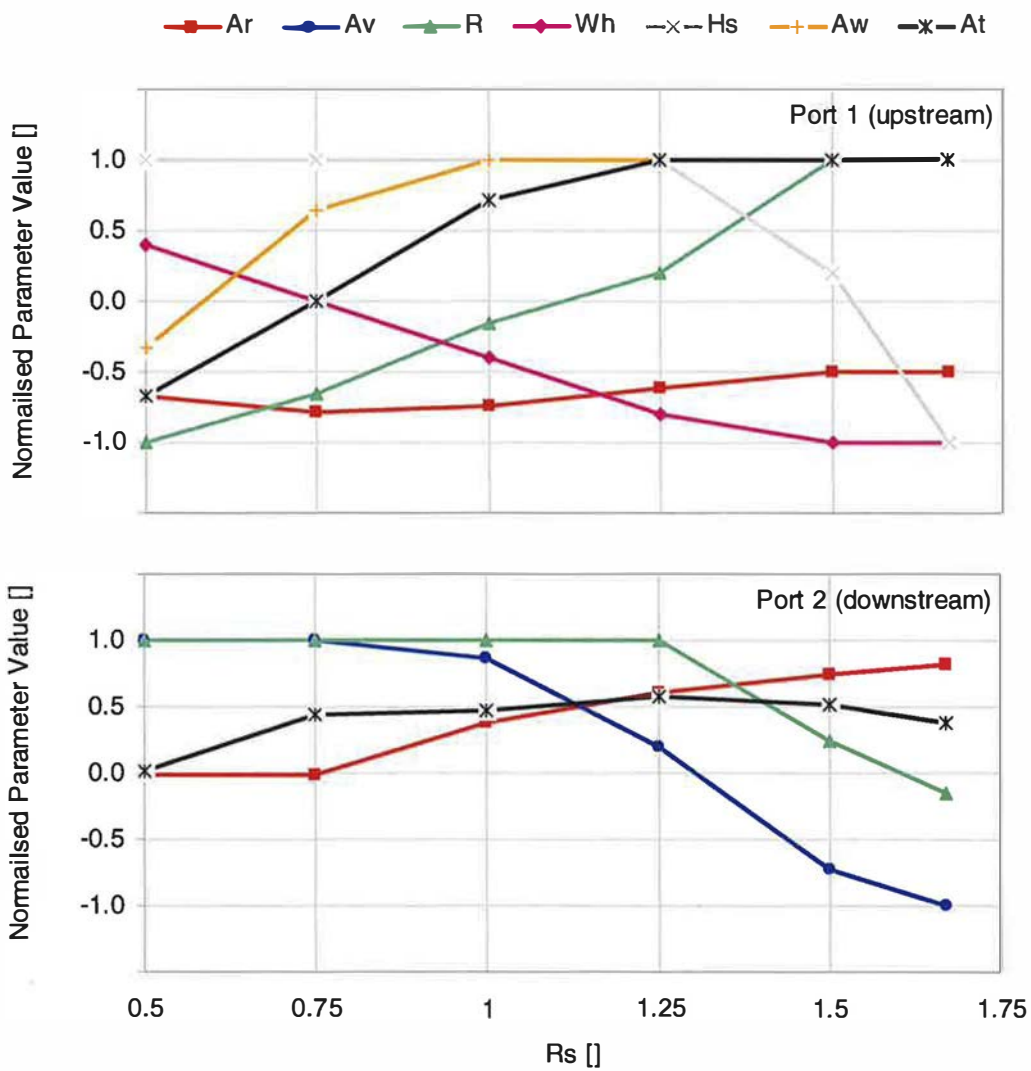
Figure 5.12: Parameter values (unconstrained optimisation, HD configuration)
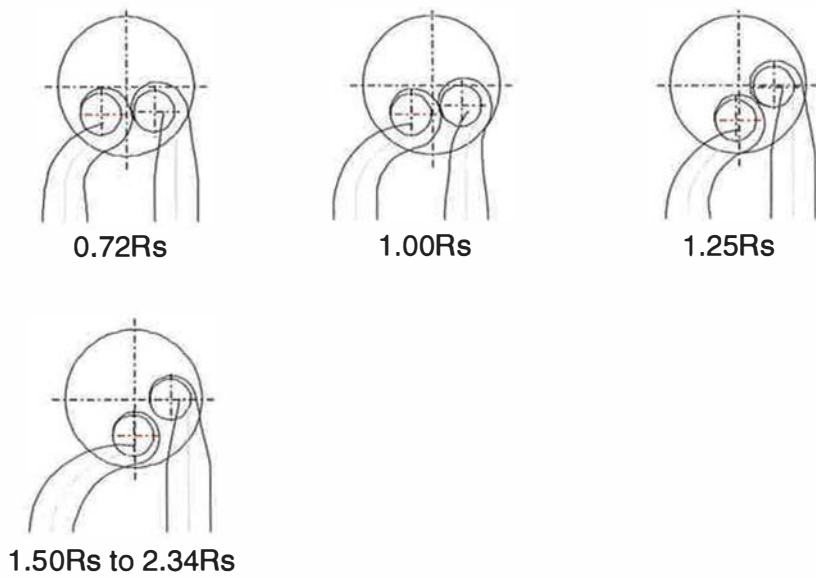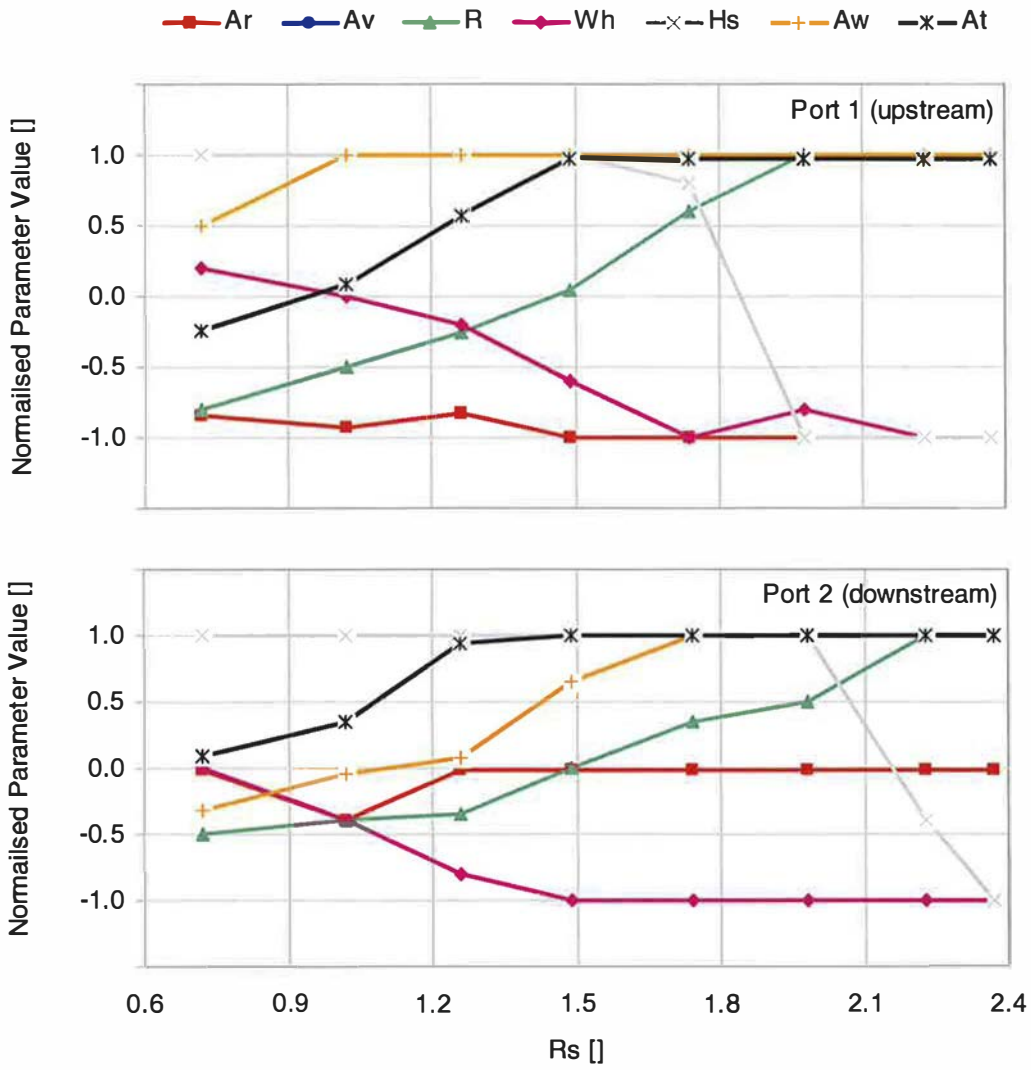
Figure 5.13: Parameter values (unconstrained optimisation, HH configuration)

5.5.4 Constrained Optimisation

In the majority of practical applications, the design is constrained. The most common constraints include a reduced skew angle range, often due to valvetrain design limitations, and reduced packaging space available, due to the cylinder head bolting pattern. These constraints may be implemented in the optimisation routine and investigated to determine their influence on port geometry and performance. Three skew angle constraint cases were investigated, based on each port configuration (DD/HD/HH). Skew angle was fixed at 0°, 45° and 90° and port geometry was optimised over a range of swirl requirements. The results were then compared with the unconstrained optimisation, as shown in Figures 5.14 (DD configuration), 5.15 (HD configuration) and 5.16 (HH configuration).

For the DD configuration, each constrained skew angle case performs most effectively at a particular swirl ratio, as might be expected given the unconstrained results. At 0° skew angle, inlet port flow performance is near optimum up to 0.25Rs, then becomes increasingly restricted as alternative geometry changes are required to generate swirl. The maximum achievable swirl is 0.75Rs; at this condition Z is approximately 5% higher than the unconstrained optimum. For a fixed skew angle of 45°, the response is relatively close to the unconstrained response throughout the swirl range. Some loss in flow performance at 0Rs is evident, although this is unlikely to be of concern in practical applications. The 90° skew angle case performs most effectively above 0.8Rs, although flow performance becomes rapidly worse at lower swirl ratios. The constrained optimisation results may be understood more clearly with the aid of the sketches, shown below the trade-off chart in Figure 5.14. Tangential orientation of both ports is not possible in the 0° skew angle configuration, resulting in poor performance at high swirl. The opposite is true for the 90° skew angle designs; in order to produce low swirl, the ports must be arranged such that they generate swirl in opposite directions. The 45° skew angle configuration can be manipulated more easily for high and low swirl requirements. At present, most combustion systems require swirl ratios in excess of 1.0Rs, therefore it is likely that a 90° skew angle would be preferred. The 45° skew angle may be an acceptable compromise if future combustion systems require lower swirl levels.

The effect of constrained skew angle on the HD configuration is shown in Figure 5.15. The unconstrained flow swirl trade-off curve is also shown for comparison. The 0° skew constraint progressively impairs flow performance beyond 0.8Rs until Z is approximately 9%

186

higher than the unconstrained optimum at 1.3Rs. This swirl ratio represents the maximum that can be achieved at 0° skew angle, a reduction in capability of 0.36Rs. The plan view sketches indicate that the compromised port orientation necessitates increased swirl from the helical port, with a resulting loss in flow performance. At a fixed skew angle of 45°, HD configurations perform close to the unconstrained optimum throughout the swirl range. Significantly, flow performance from 1.0Rs to 1.7Rs matches the unconstrained optimum curve. The 90° skew angle constraint results in poor low swirl performance and does not offer improved flow performance or increased swirl capability compared to the 45° constraint. Therefore, in contrast to the DD configuration, a 45° skew angle would be preferred if this parameter must be fixed.

The optimised results for the HH configuration with constrained skew angles of 0° and 45° are shown in Figure 5.16. Note that a 90° skew angle has not been included due to the limitations on the geometry of the helical ports. Constraining skew angle for this type of configuration has a similar effect to the HD configuration, although flow performance at 45° skew angle is even closer to the unconstrained optimum at low swirl. High swirl performance is impaired, in common with all the configurations studied. Maximum swirl capability is reduced from 2.38Rs to 2.0Rs, compared to the unconstrained design and Z at 2.0Rs is approximately 7% higher. The sketches clearly show the progressive geometry modifications that are required to reach increased swirl levels; both helical features and tangential approach angle develop simultaneously in order to minimise flow losses

In comparing the constrained results for all three configurations, it is apparent that the 0° skew angle constraint is the most limiting, both in terms of flow performance and loss in maximum swirl capability. The absolute reduction in maximum swirl capability is consistent between all three configurations, ranging from 0.35Rs to 0.38Rs. In all three configurations, the 45° skew angle has the least impact and flow-swirl trade-off curves are close to the unconstrained optima for the HD and HH configurations in particular. If skew angle must be fixed due to valvetrain limitations, 45° would be preferred in most cases to maximise the available range of swirl performance, with acceptable flow performance. The DD configuration benefits most of all from a skew angle of 90°, due to the sensitivity of the directed port type to a tangential flow direction into the cylinder. As the swirl capability of this configuration is limited in any case, it is probable that high skew angle would be required, if a reduction in valve size (and therefore a significant loss flow performance) is to be avoided.
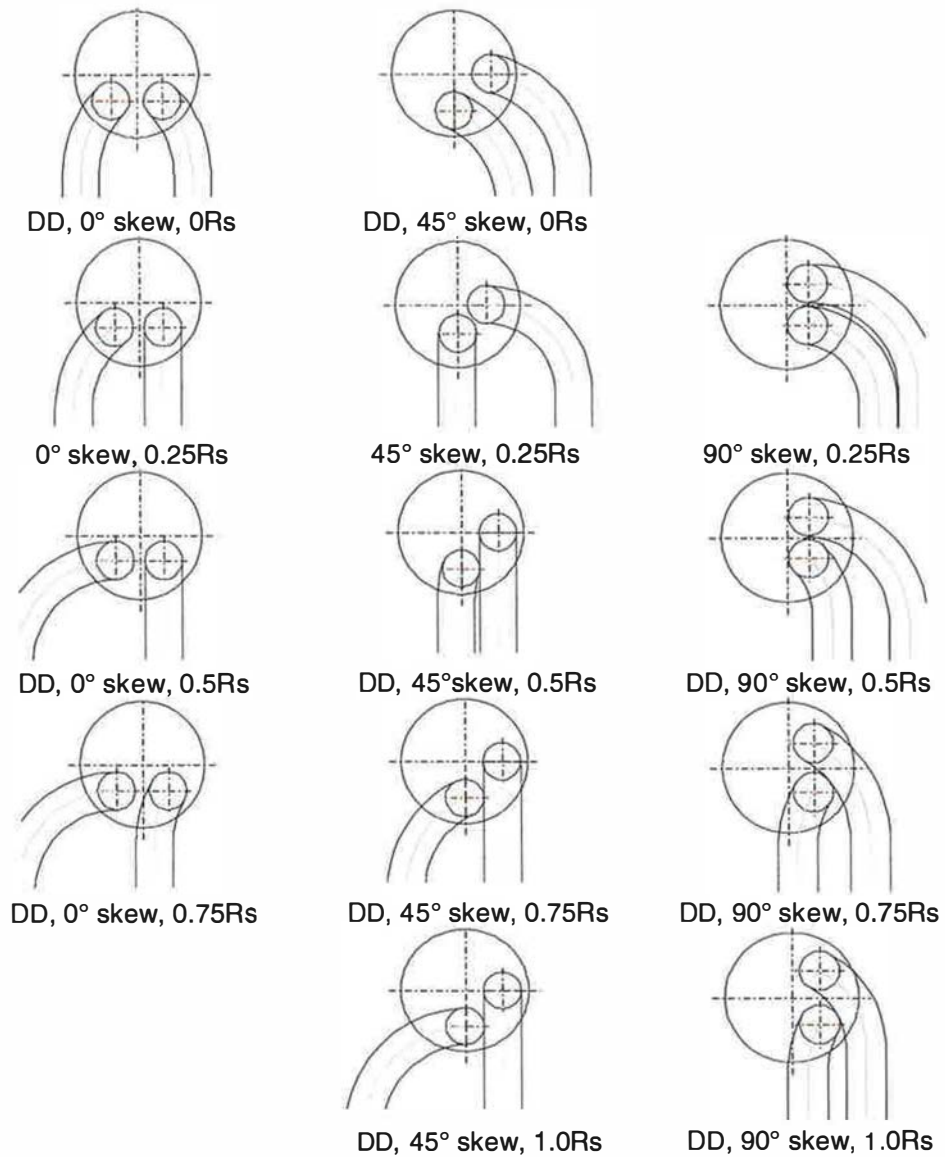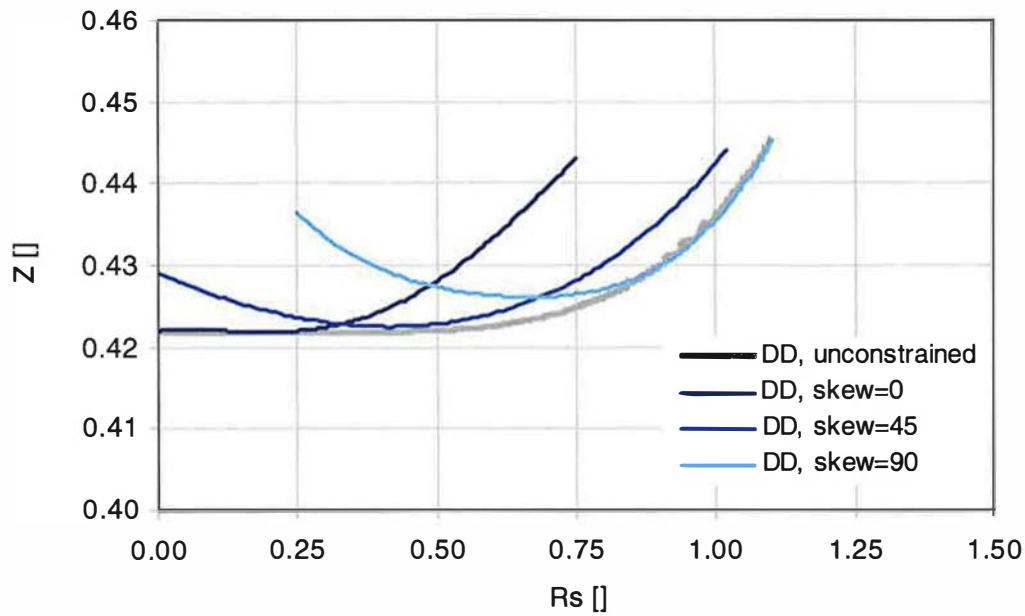
Figure 5.14: Performance trade-off and inlet port geometry

(constrained optimisation, DD configuration)
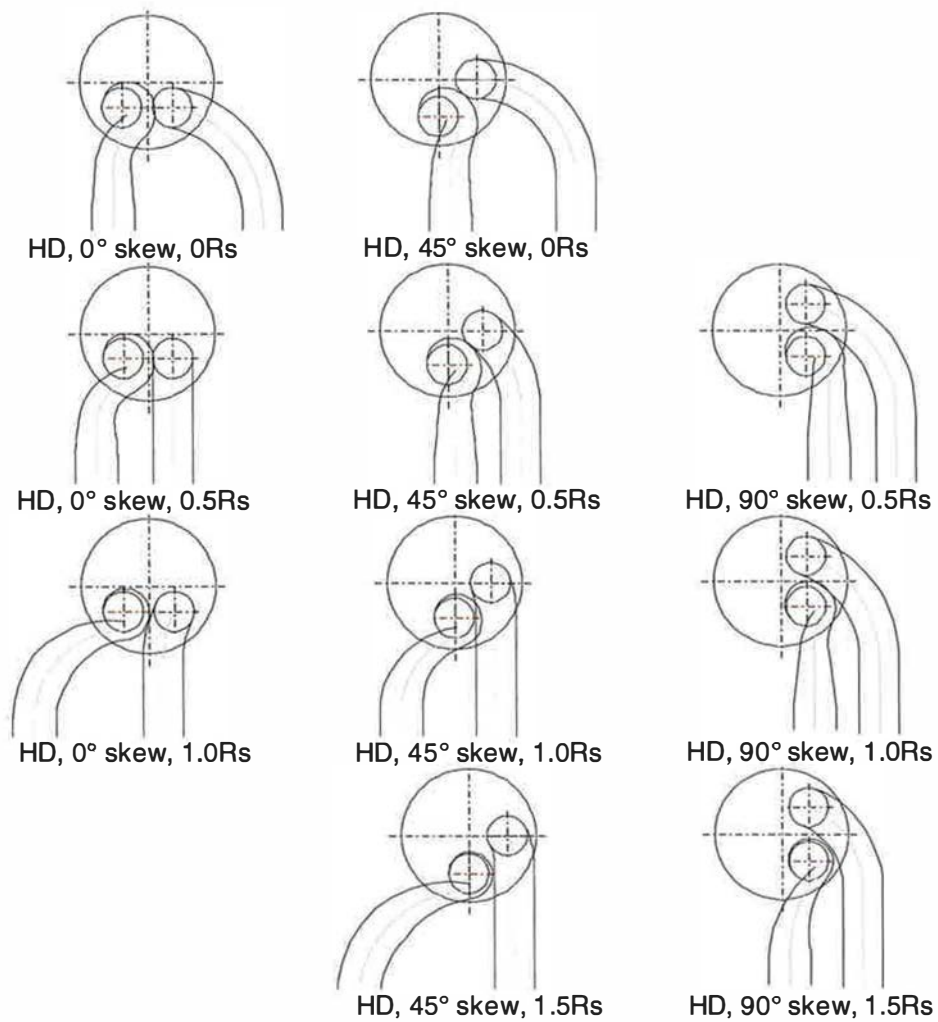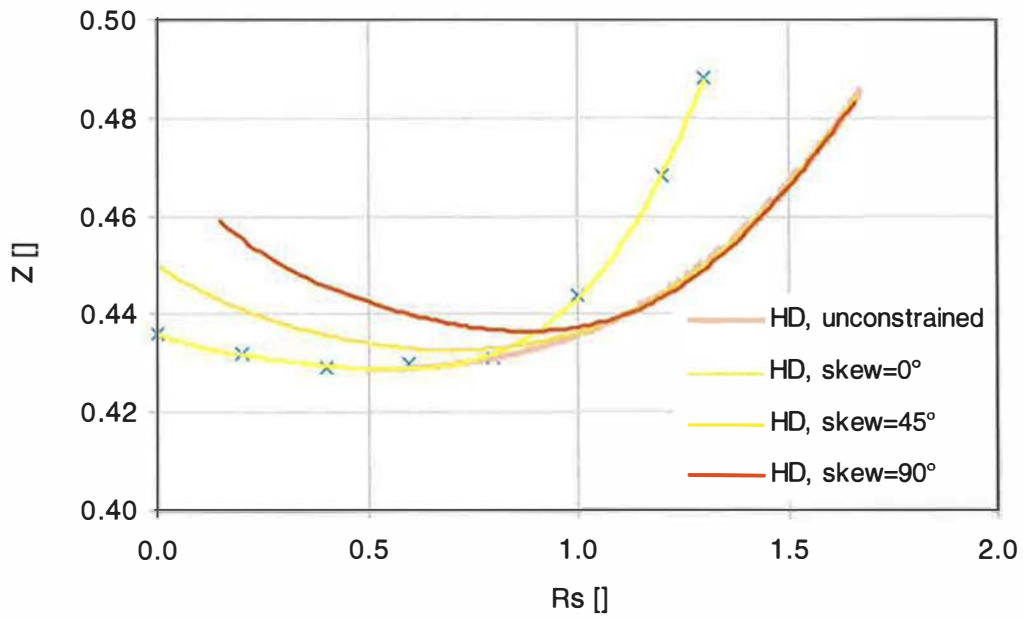
Figure 5.15: Performance trade-off and inlet port geometry
(constrained optimisation, HD configuration)
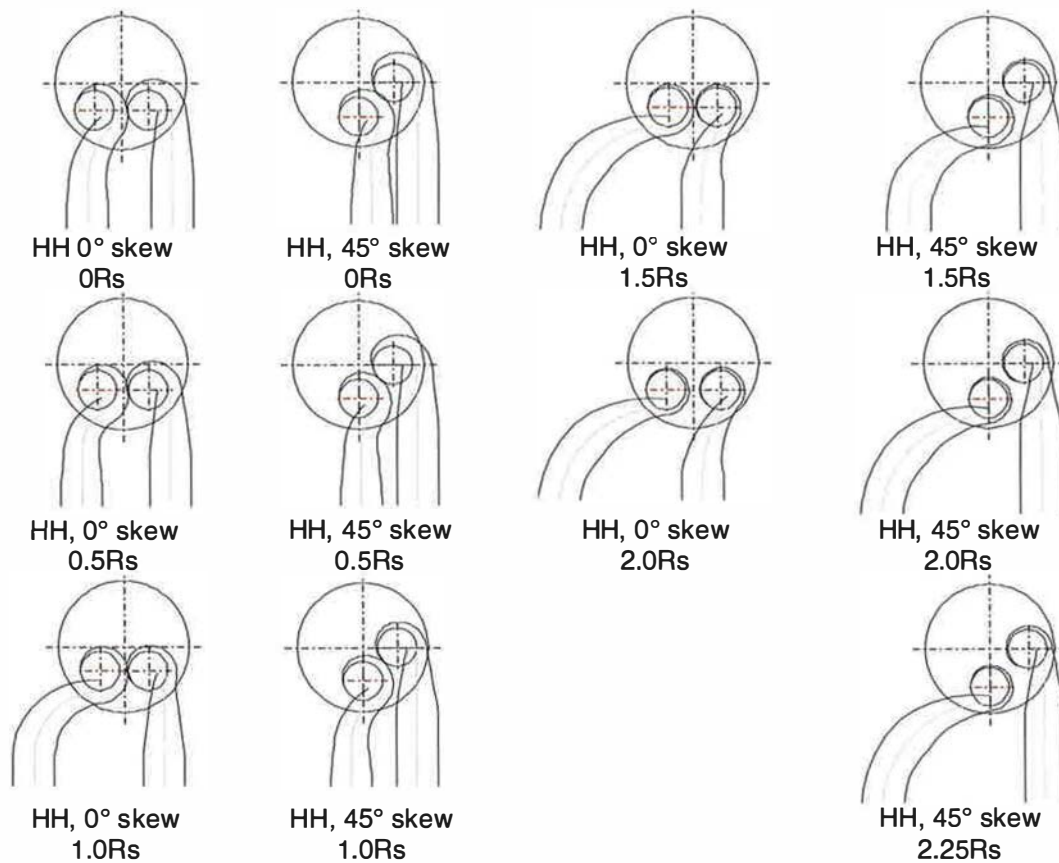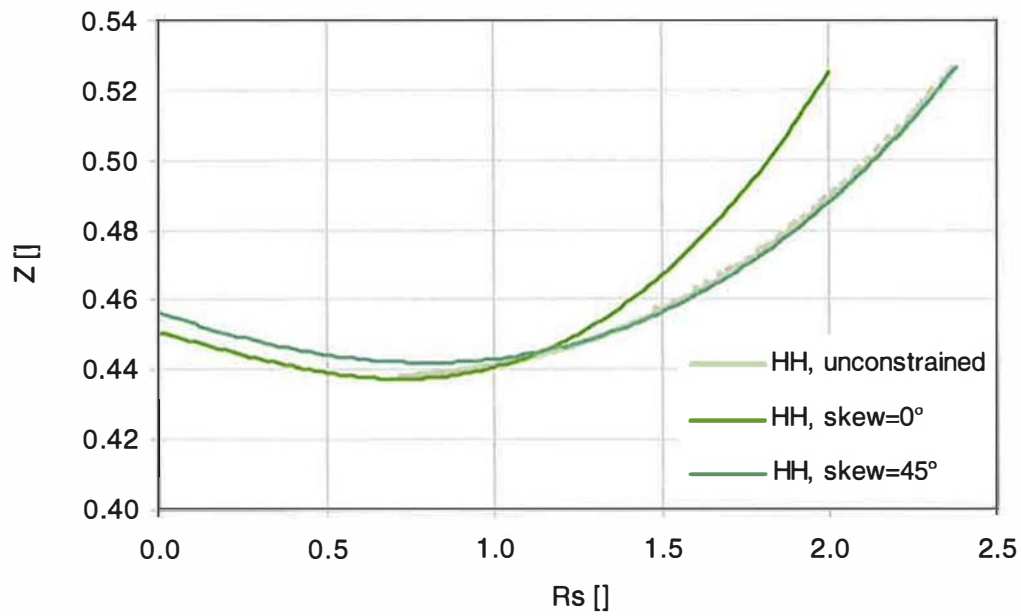
Figure 5.16: Performance trade-off and inlet port geometry

(constrained optimisation, HH configuration)

In addition to the constrained skew angle, a further constraint was applied to represent realistic cylinder head bolting patterns. Two bolting patterns were investigated, using the fixed skew angle DD port configurations as a basis for the comparison. The details of the constraints are shown in Figure 5.17. A 4-bolt pattern is the most common type encountered in light-duty applications. It is common practice to fit the ports "inside" the space provided by the cylinder head bolts, thereby preventing interference with a neighbouring cylinder. However, it is possible under certain circumstances to allow the ports to cross over into the adjoining cylinder bay. This may provide improved performance, at the expense of a longer cylinder head, as shown in Figure 5.18(a) and (b) for a fixed skew angle of 0°. The conventional method provides extremely limited swirl-generating capability (maximum 0.25Rs) whereas the second design provides a maximum swirl capability of 0.75Rs. Although either directed port (or both) could be replaced with a helical port, the second design would still provide more flexibility. At 45° skew angles, the 4-bolt pattern is not highly constrained, although the bottom-left bolt boss prevents maximum tangential orientation of the upstream port. The 4-bolt pattern necessitates routing of the downstream port into the adjoining cylinder bay. Although this configuration appears to be feasible, the location of exhaust ports and fuel injector would be extremely difficult. Orientation of the upstream port is satisfactory and there is a large amount of lateral freedom for various approach angles.

A six-bolt pattern may be required for highly rated engines with increased maximum cylinder pressure. This presents a particular problem when skew angle is fixed at 0°. The resulting port arrangement is unlikely to provide sufficient swirl capability. The six-bolt pattern is more suited to a 45° skew angle, making this configuration suitable for a range of swirl requirements. The 90° skew angle and 6-bolt pattern are not well suited and similar port routing to that required on the 4-bolt pattern is necessary. It is also difficult to orientate the upstream port tangentially, reducing the maximum swirl potential of this arrangement.

In order to quantify the effect of the two bolt patterns, an optimisation routine was performed to maximise swirl for each the three fixed skew angles. The results are shown in Figures 5.20 to 5.22. In the DD configuration (Figure 5.19), the four bolt pattern has significantly less impact than the six bolt pattern on the maximum swirl capability, causing no loss at 0° skew angle and a small reduction from 1.1Rs to 1.0Rs at 90°. The six bolt pattern causes a reduction in maximum swirl to 0.21Rs (from 0.75Rs) and 0.85Rs (from 1.1Rs) at 0° and 90° respectively. Neither pattern reduces the maximum swirl at 45° skew, as was inferred from

the plan view sketches. As a result, the 90° skew angle may not be preferred for the DD configuration as the 45° skew angle has a similar maximum swirl capability and improved low swirl performance. In the HD and HH configurations (Figures 5.21 and 5.22), the difference between four-bolt and six-bolt patterns is less marked, both constraining the design to a similar extent. Maximum swirl capability for 0° skew angle case is severely impaired once again, compounding the performance loss compared to the unconstrained designs. This is due to the highly constrained upstream port geometry, resulting from the proximity of a cylinder bolt boss in the six-bolt and four-bolt examples. Helical ports are therefore more sensitive than directed ports in this case, as it was possible to route the upstream directed port around the closest bolt on the favoured side. Of course, the precise design of the bolting pattern may well be critical in this respect. The 45° skew angle configurations are not significantly constrained by the bolting pattern, in terms of maximum swirl capability, and therefore remains as the preferred design option. Other swirl requirements may be limited, although this is unlikely given the previously discussed flexibility of the 45° skew design.
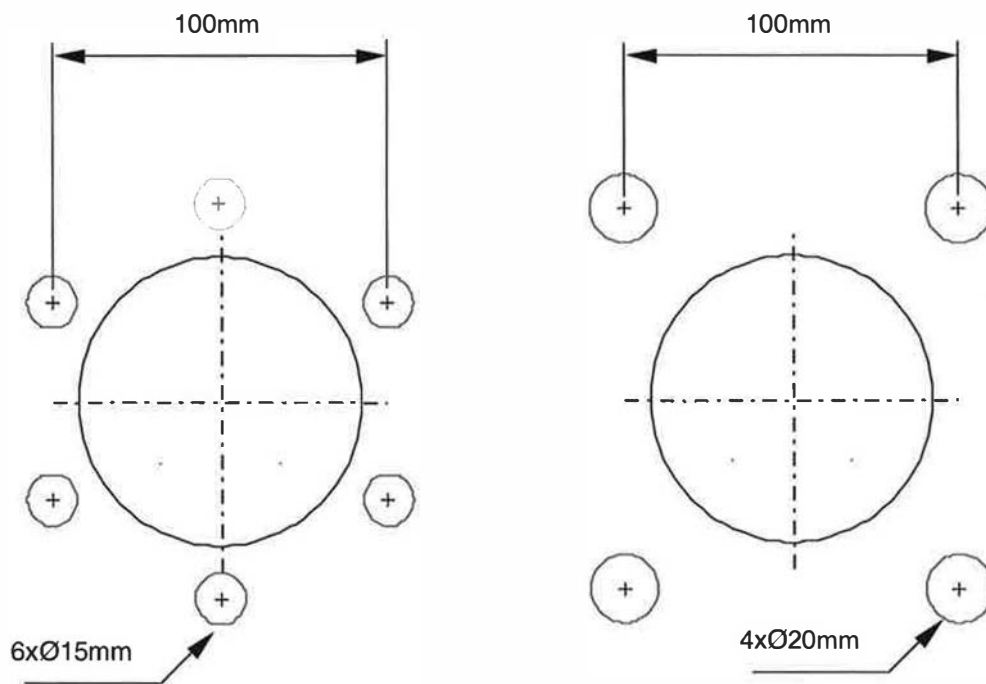
Figure 5.17: Cylinder head bolting pattern
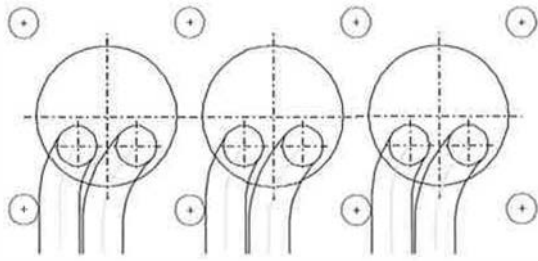
(a) 4-bolt, 0° skew I
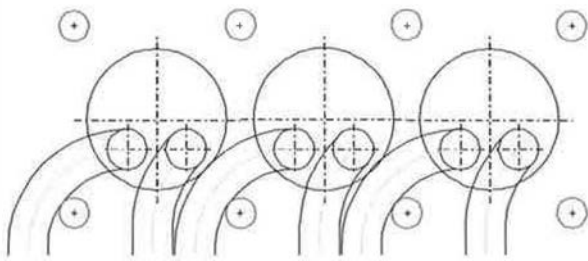
(b) 4-bolt, 0° skew II
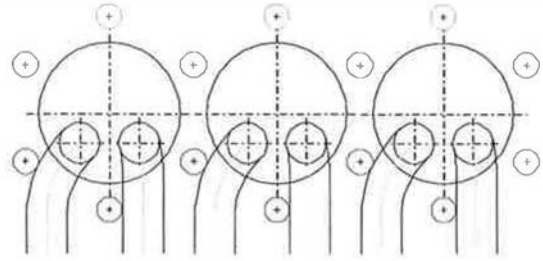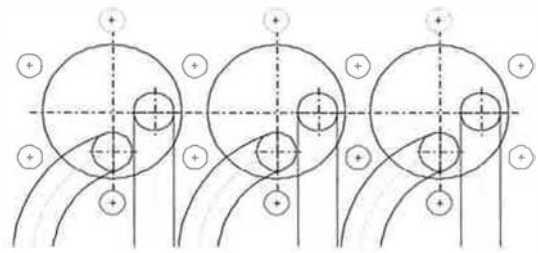
(c) 4-bolt, 45° skew

(d) 4-bolt, 90° skew

(e) 6-bolt, 0° skew
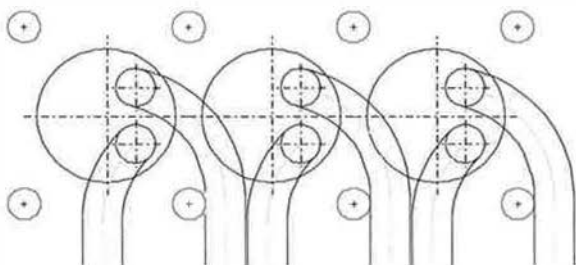
(f) 6-bolt, 45° skew
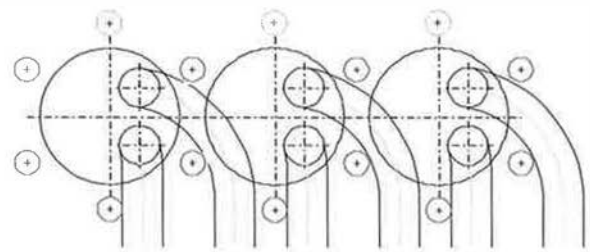
(g) 6-bolt, 90° skew

Figure 5.18: Constrained 4-bolt and 6-bolt port arrangements (DD configuration)
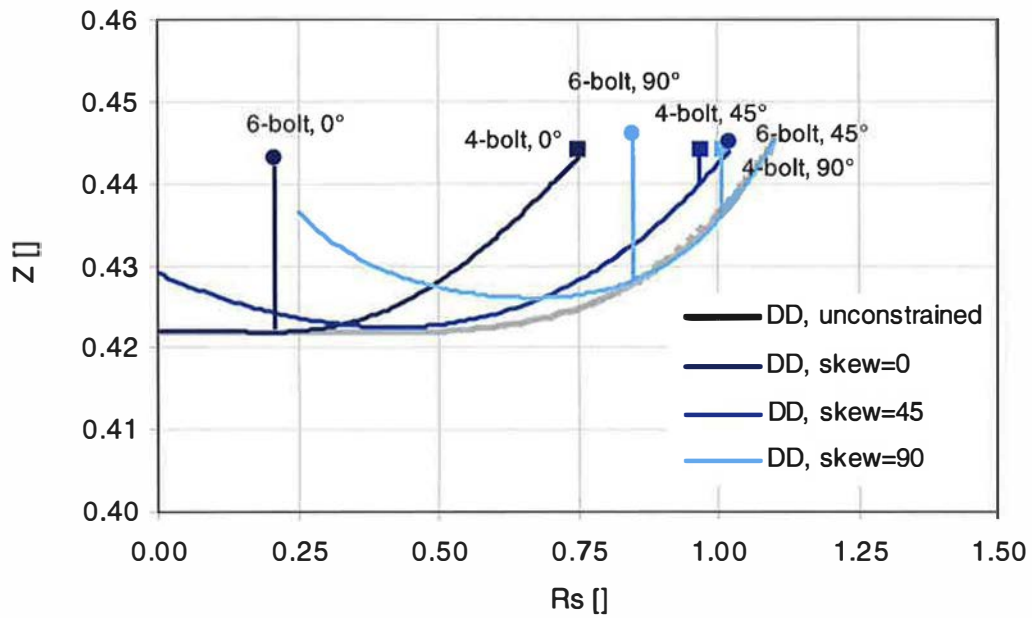
Figure 5.19: Maximum swirl capability, effect of cylinder head bolt pattern
(DD configuration)
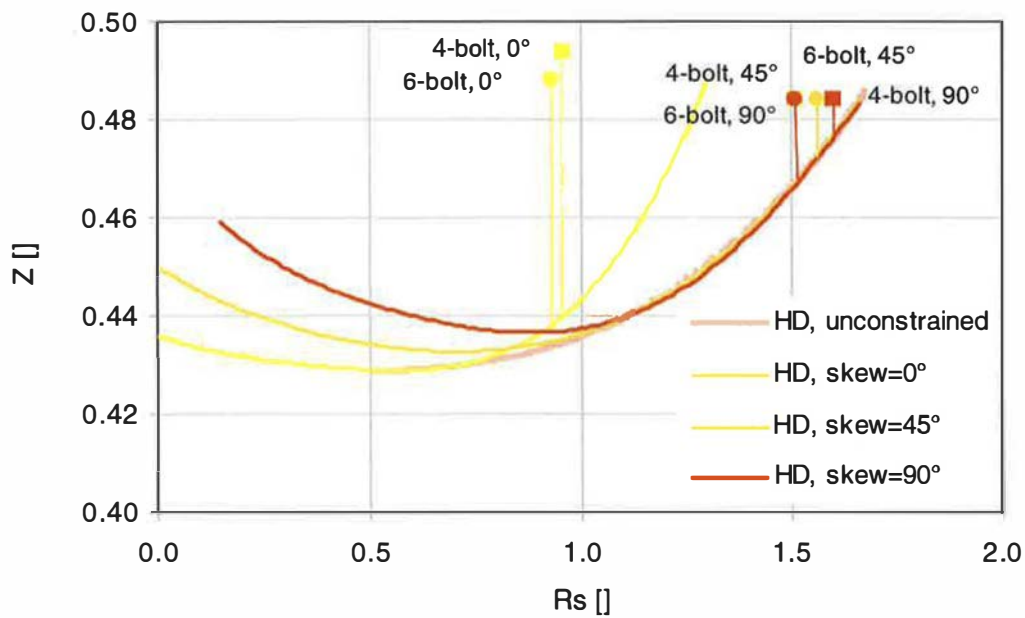
Figure 5.20: Maximum swirl capability, effect of cylinder head bolt pattern
(HD configuration)

194
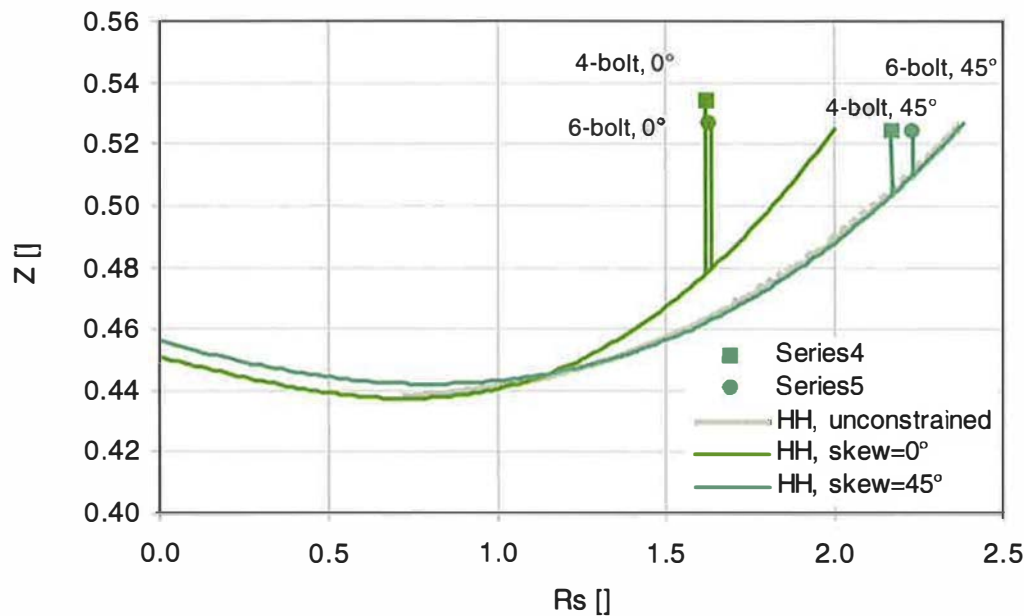
Figure 5.21: Maximum swirl capability, effect of cylinder head bolt pattern

(HH configuration)

5.5.5 Development and Further Applications of the Optimisation Technique

The optimisation routine has been used to investigate the performance response of inlet port systems to changes in geometry and other aspects of the cylinder head design. Some valuable and interesting trends have emerged, such as the optimum swirl-flow trade-off curves for each port configuration and the effect of constraints. Dominant effects are clearly evident from the optimised results; further demonstrating the influence of the key parameters identified during the construction of the basic DoE models. The accuracy, robustness and efficiency of the routine under a wide range of conditions have not yet been established and further development work in these areas is recommended. Following this, constrained optimisation of the port configurations not yet studied in detail would provide valuable information for engine designers. Finally, an investigation of optimisation methods for the detailed Cf and Ns models, with complex performance requirements and constraints, may yield further insights.

5.6 Validation of Multi-Valve Performance Predictions

5.6.1 Validation Test Details

Multi-valve performance predictions were compared with a set of test cases designed to investigate the validity of the combined DoE and additive performance models. In all cases, the tests were performed on the same apparatus and followed the same procedure as the tests used to build the original data set. Cf and Ns were calculated from 1mm to 10mm valve lift and summary results Rs, MCf and Z were calculated using the standard engine geometry used previously (Table 5.2). The validation test configurations are shown in Figure 5.22. In addition to standard configurations corresponding to DD, HD and HH layouts, a sub-experiment consisting of five DD configurations was conducted to assess the effect of upstream port orientation with respect to the downstream port.

5.6.2 Validation Test Results

A summary of the validation test results is presented in Figure 5.23. The experimental results are compared with pure model predictions and results calculated by applying the additive model to the experimental results for individual ports (using Equation 5.2). The range of swirl capability is clearly evident, as is the flow performance penalty associated with generating increased swirl. The model predictions compare well with the experimental data, indicating that the combination of DoE and additive model is sufficiently accurate to compare performance characteristics resulting from the geometry changes shown in Figure 5.22. In particular, the performance prediction of the port flow interaction study models is good enough to rank all five models correctly. There appear to be some flow interference effects in terms of the swirl prediction; the calculated results indicate that the additive model tends to under-predict swirl by up to 0.12Rs (12% of the experimental result) and over-predict flow performance by less than 1%. The combination of the detailed DoE and additive models generally results in an over prediction of swirl, compared to the additive model alone and the experimental results. This would suggest that flow interaction at each valve lift condition is significant and that interference between the flows from each port results in a reduction in overall in-cylinder swirl. These errors are broadly consistent with the findings of other researchers (Kawashima, 1998; Li, 2000) and the detailed comparisons in Figure 5.24 indicate

that some port design configurations are susceptible to flow interference, resulting in a significant over-prediction in swirl from the additive model. However, in comparison with earlier findings, the present study indicates that helical port configurations may be more susceptible at high valve lift conditions. However, as CFD visualisation of individual port flows has shown, helical ports of the type used in this validation study produce a strong jet flow at high valve lift, which may cause flow interference.
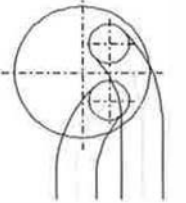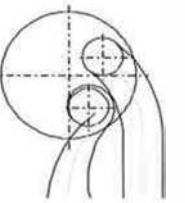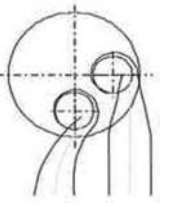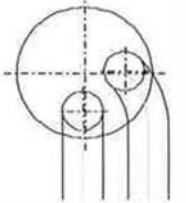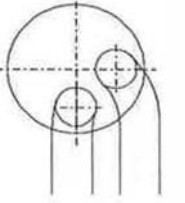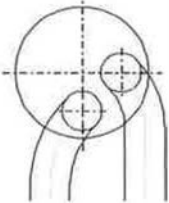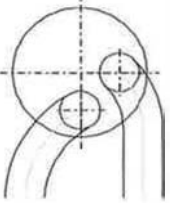
Test Case	Plan View Sketch		
Basic Configurations	DD1	HD	HH
DD Configuration: Port flow interaction study	$DD2_0$	$DD2_{15}$	$DD2_{30}$
	$DD2_{45}$	$DD2_{60}$	

Figure 5.22: Multi-valve validation configurations

■ Validation data (multi-valve test result)

▨ Calculated from validation data (additive model using single-valve test result)

□ Model data (predicted from DoE and additive models)
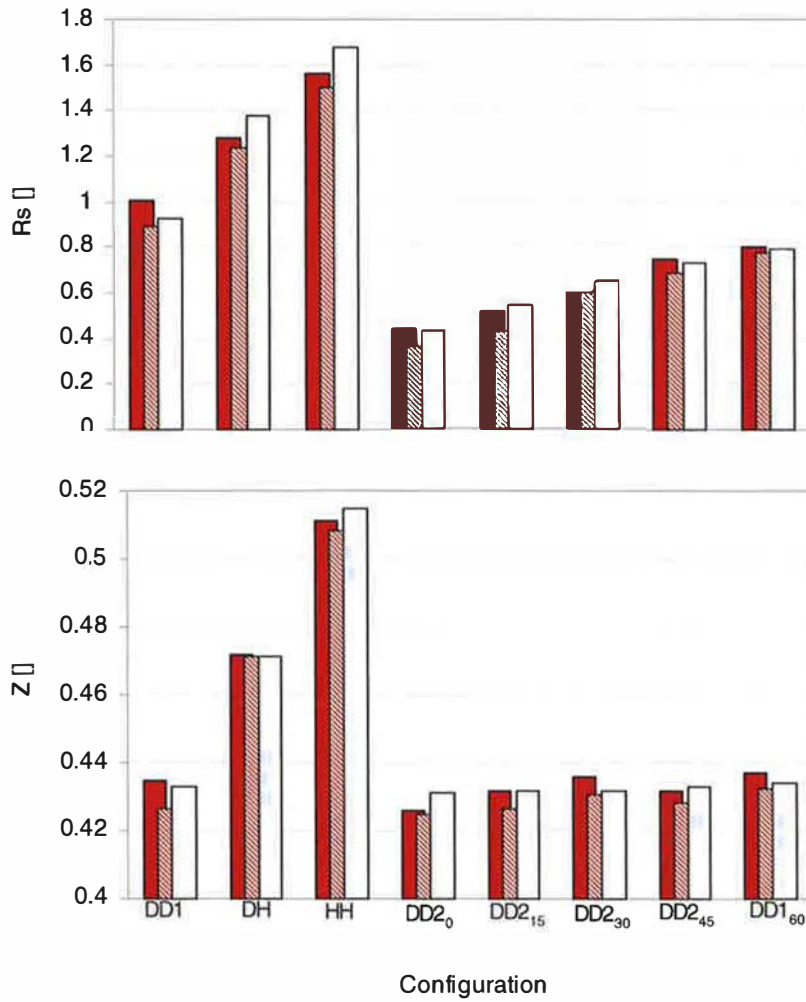
Figure 5.23: Multi-valve validation results summary (experimental data)
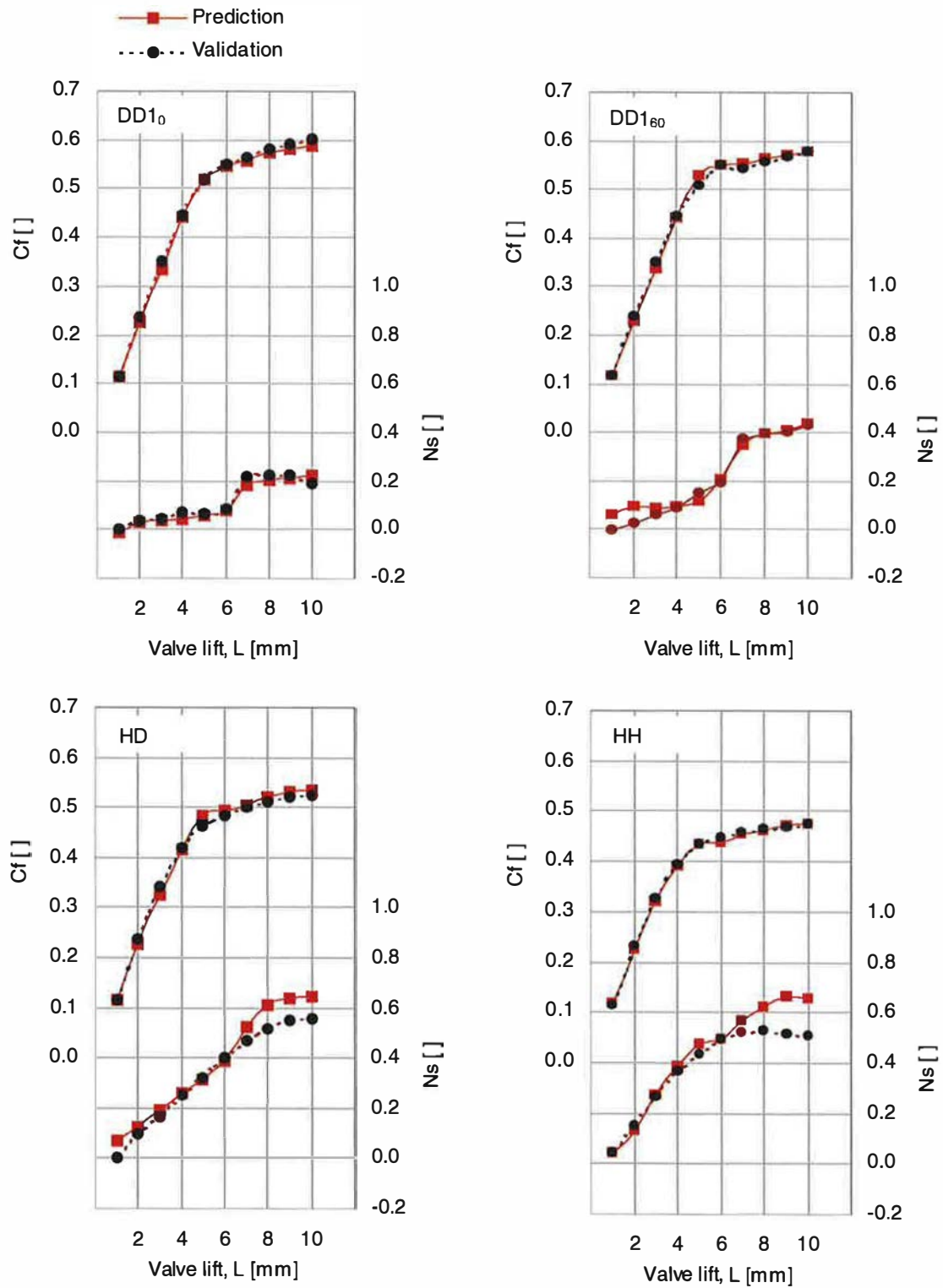
Figure 5.24: Multi-valve validation results detail (experimental data)

5.7 Summary of Chapter 5

In chapter 5, the individual elements of the parametric and knowledge-based sub-models have been combined to construct a generalised model of multi-valve inlet port geometry and performance. The model has been used to investigate the effect of the defined geometry parameters of individual port types in a realistic design context. It has been shown that the performance characteristics of various inlet port configurations are highly dependent on the overall valve layout, such as skew angle. Furthermore, the well-documented importance of valve size in determining the fundamental level of flow performance has been captured. However, the influence of valve size on swirl characteristics must also be considered, in order to achieve combustion system swirl requirements.

Optimisation of inlet port design, subject to simple constraints to represent real-life design limitations, has been demonstrated using a widely available software application (Microsoft Excel). The relative performance trade-off between helical and directed port configurations can now be understood as a function of the design parameters that control their geometry. It is therefore possible to compare the relative merits of candidate design options, including geometry modification, port type changes and valve size selection.

In order to put the multi-valve model predictions, optimisation results and validation test cases into context, they should be compared with realistic design data to ensure that the trends in the data are consistent. The results of this comparison are shown in a swirl-flow tradeoff chart in Figure 5.25. Rs/Ld and MCf are used to normalise engine geometry, valve lift profile and crankshaft speed effects. The database results represent HSDI and heavy-duty engines, representing a wide range of conventional design approaches, port configurations and constraints. The unconstrained optimised model predictions from Figure 5.10 are presented using the normalised performance expressions. Validation data (model predictions and experimental results) are also shown. Firstly, the similarity in shape of the "leading edge" of the database and the optimised curves is apparent. Secondly, there are no database results above the optimisation line but there are a small number close to it. Taken together, these observations indicate that the predictive multi-valve model is representative of port designs currently in use and that the optimised model geometry is a fair reflection of the current "state-of-the-art". The relative lack of data close to the optimised curves suggests that real-life designs are heavily compromised by constraints. This is not unexpected, as the constrained

optimisation study has provided some insight into the effect of such constraints. In practice the combined effect of many constraints is likely to result in such a loss in performance relative to the ideal. An alternative interpretation of the gap between optimised curves and the leading-edge of the database is that the model over-predicts swirl at the upper and of the swirl range. The pairs of data points representing the validation study indicate that errors in the model do not account for all of the difference and that the true optimum lies in between. In summary, the potential of the model is clear from this analysis, particularly for use as a predictive and comparative tool during concept design.
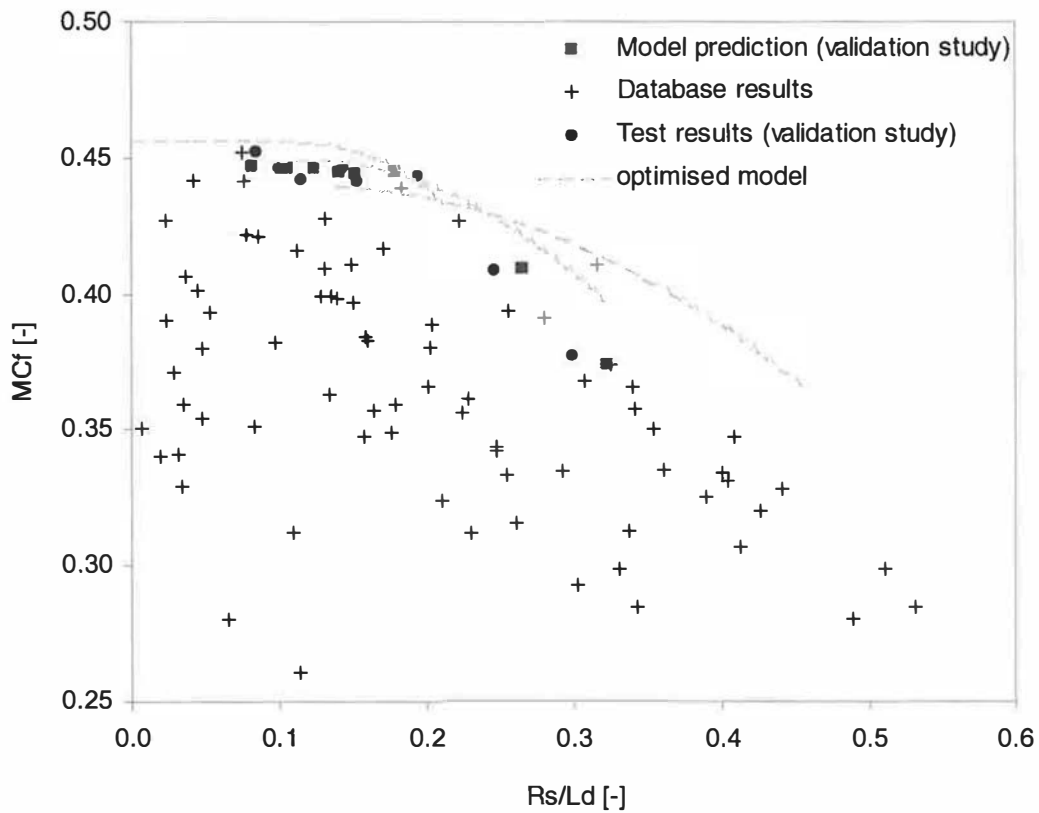
Figure 5.25: Comparison of model predictions, validation test results and HSDI database

6   Conclusions

Historically, the design and development of inlet ports has been an iterative process that relies on individual experience and skill. During the present study, an alternative approach has been considered; to select the key features of a concept design, to describe them in terms of defined parameters and to understand how they influence inlet port performance characteristics. In doing so, the interactions between those design features and external constraints have also been investigated. The result is clearly a simplified model of the fully developed and manufactured component. However, one of the most important aspects of concept design is to compare candidate solutions objectively and the parametric design scheme supports this process by imposing a structured approach to the initial stages of design.

The single inlet port results show that the performance models are robust and sufficiently well validated to provide reliable predictions. General trends such as the low swirl characteristics of directed ports and increased swirl capability (and associated reduction in flow performance) of helical ports are evident in the analysis of summary performance characteristics. Easily understood parameter responses, such as the swirl response to the At parameter in directed ports, demonstrate that the model predictions are consistent with the findings of other researchers. However, complex or non-intuitive responses, such as the swirl response to the helix width parameter, Wh, are now understood more clearly, with the aid of CFD visualisation to put the quantitative data into context. Even taking the idealised geometry into consideration, the results show that interactions between port geometry, location and orientation are significant.

The multi-valve performance model has demonstrated the importance of port configuration (including port design parameters, global engine design parameters and constraints) in relation to the requirements of the combustion system. Prior to this study, it was not possible to determine which port configurations would be optimum for a particular swirl ratio requirement, without conducting tests or performing simulations. Furthermore, the influence of constraints was not known quantitatively until now. Although the geometry cases used to investigate the effect of constraints were simplified, the results show that the performance response to these constraints varies widely from one configuration to another. These findings illustrate that the model enables an objective assessment of complex multi-valve designs

without relying on test data from physical models or the results of CFD simulations. Furthermore, the time required to optimise a concept design is considerably shorter than with other methods. It is possible to assess a range of potential design options, assess the effect of constraints and select an optimum configuration for further development within one day. In comparison, a CFD simulation will require a similar time to evaluate a single design configuration (at a limited number of valve-lift conditions) without providing any information on the effect of constraints. A conventional development process using physical port models may take two weeks, excluding procurement of the test hardware. In practice, each technique should be used at different stages of the design and development process. The predictive modelling and optimisation approach is particularly suited to the earliest stages of concept design. The results should be used as an input for the other techniques, which are more suitable for detailed design and development of a final product.

The additive multi-valve model has known limitations and the results of the validation tests confirmed some cases where flow interaction in the real world renders the predictions inaccurate. It is not immediately clear which configurations are most susceptible to this. The validation cases studied so far are sufficiently accurate in the context of the port flow database to provide input into a selection between different multi-valve port configurations. The use of steady flow characterisation is a simplification that is now giving way to dynamic flow visualisation (both experimentally, using optical techniques such as PIV, and computationally using CFD) and full engine-cycle simulation including fuel injection and combustion. However, the virtual engine is still in its infancy and there is a need for relatively simple sub-models that predict individual aspects of the system (such as in-cylinder flow characteristics – be it steady flow or dynamic). Perhaps more importantly, the benefits of knowledge-based engineering and optimisation do not diminish when the system becomes more complex ; they become stronger. As the number of design inputs grows and the interactions between them becomes less apparent, it becomes increasingly difficult to manually "optimise" the system using engineering experience alone, irrespective of the methods used to gather and present data. In the present study, particular methods were employed to meet the objectives (physical experimentation, DoE modelling, simple optimisation). The concept of knowledge-based design and optimisation is independent of the methods used; knowledge-based systems have the potential to harness the capabilities of computer simulation and experimental design and create powerful design tools in the future.

Recommendations for Further Work

The present study has successfully demonstrated the principle of a knowledge-based design tool for HSDI diesel engine inlet port design. However, further development of the models would provide enhanced predictive capabilities and a greater understanding of engine and inlet port performance characteristics. New performance models for inlet ports used with other engine types, such as direct-injection gasoline and HCCI, could be developed using similar techniques to the present study. Exhaust port models are also a natural extension of the concept. In addition, knowledge-based models of related subsystems, such as valvetrain layouts, could be developed. It is then possible to imagine an integrated system of sub-models that could be used to design cylinder heads or indeed complete engines.

The optimisation routine has been applied to a selection of geometry cases to demonstrate its potential and understand the effect of some important factors such as the cylinder head bolt boss pattern. The simple, two-dimensional approach to constrained optimisation could be enhanced to provide three-dimensional optimisation, including complex constraints such as coolant jackets and oil passages. It is likely that the implementation of such a model would be achieved by coupling the predictive model with a 3-D CAD system. As the generic port geometry used in the present study was created using such a system, this suggestion is not as ambitious as it might first appear. The benefit of this development is that a fully surfaced CAD model would be the output from the optimisation process; this could be used directly to generate physical models for testing, prototype parts, or CFD boundary models for detailed design development. Further exploitation of the detailed performance models is also possible and these could be used to optimise performance at specific valve lift conditions, or to investigate variable valve-lift strategies.

In terms of port geometry, the effects of secondary parameters should be investigated. In particular, the effect of port cross-sectional area and shape, independent of valve area, should be considered. A 3-D optimisation process would clearly benefit from such an enhancement. Further investigation of multi-valve design configurations, including alternatives such as siamesed entry inlet ports should also be undertaken to identify the boundaries and limitations of the additive model.

The effect of flow interaction between port flows and/or dynamic flow characterisation and visualisation is a longer-term goal that should be considered, particularly given the opportunity to include combustion chamber geometry such as the piston bowl. It is likely that such a model would require data from in-cylinder flow visualisation techniques and/or CFD. Even as full combustion simulation and visualisation becomes a realistic prospect, the benefits of studying in-cylinder flows and the detailed relationships with combustion may provide insights that enable engineers to develop internal combustion engines well into the future.

References

Alcock, J. F. 1934. Air Swirl in Oil Engines. *IMechE Proceedings*, pp123-193, December

Affes, H. Trigui, N., Smith, D., Griaznov, V. 1998. Shape Optimization of IC Engine Ports and Chambers. SAE Paper No. 980127

Arcoumanis, C., Bicen, A.F., Whitelaw, J.H. 1983. Squish and Swirl-Squish Interaction in Motored Model Engines. *Transactions of the ASME. Journal of Fluids Engineering.* 105: 105-112.

Arcoumanis, C., Whitelaw, J.H., Hadjiapostolou, A. 1991. Measurements of the Flow in a Hydra Direct Injection Diesel Engine. *Proceedings of the IMechE Conference on Internal Combustion Engine Research.* pp.113-121. IMechE Paper No C433/019.

Barnes-Moss, H.W. 1973. A Designer's Viewpoint. *Proceedings of the IMechE Conference on Passenger Car Engines*, pp.133-147. London, England. IMechE Paper No C343/73.

Beaumont, A.J., Frith, A.M. 1994. Adaptive Control of Transient Air-Fuel Ratio Using Neural Networks. 27th *ISATA Conference on the Motor Vehicle and the Environment*, pp217-225, Aachen, Germany, 31 October – 4 November. Paper No. 94EN001

Bensler, H.P., Oppermann, R. 1996. CFD Optimization of Powertrain Components. *IMechE Conference Transactions*, pp 249-268. Third International Conference on Computers in Reciprocating Engines and Gas Turbines. IMechE Paper No C499/057/96.

Bertrandt. 1999. Rapid Prototyping: An Important Component in the Automobile Development Process. Technology Toward the Millennium '99, MIRA

Bidanda, B., Hosni, Y.A. 1994. Reverse Engineering and Its Relevance to Industrial Engineering - A Critical Review. *Computers and Industrial Engineering.* 26(2):343-348

Bicen, A.F., Whitelaw, J.H. 1984. Steady and Unsteady Air Flow through an Intake Valve of a Reciprocating Engine. *Transactions of the ASME, Journal of Fluids Engineering.* 107:413-420

Blaxill, H., Downing, J., Seabrook, J., Fry, M 1999. A Parametric Approach to Spark-Ignition Engine Inlet-Port Design. *SAE International Congress and Exposition.* Detroit. Michigan, March 1-4. SAE Paper No 1999-01-0555.

Box, G.E.P. Draper, N.R. 1987. *Empirical Model Building and Response Surfaces.* Chichester, UK: John Wiley.

G E P Box, G.E.P., Bisgaard, S., Fung, C. 1990. *Designing Industrial Experiments.* Illinois, USA: BBBF Books,

Brace, C 1998. Prediction of Diesel Engine Exhaust Emissions Using Artificial Neural Networks. *IMechE Conference on Neural Networks in Systems Design Seminar*, Solihull, England. 10 June

Brignal, A., Jin, Z.M. 1999. Investigation of Inlet Port Design on Engine Swirl Using Orthogonal Array Experimentation and Computational Fluid Dynamics. *IMechE Conference on Fluid Mechanics and Dynamics of Multi-Valve Engines.* London, 9 June.

Calkins, D.E., Chan, W.T. 1998. "CDAero" - A Parametric Aerodynamic Drag Prediction Tool. SAE Paper No 980398

Cerny, V. 1985. Thermodynamical Approach to the Traveling Salesman Problem: An Efficient Simulation Algorithm. *Journal of Optimization Theory and Applications*, 45(1)

Chen, A., Lee, K.C., Suen, K.O., Yianneskis, M., Ganti, G. 1995. Velocity Characteristics of Steady Flow Through a Straight Generic Inlet Port. *International Journal for Numerical Methods in Fluids*, 21:571-590

Cheung, R.S.W., Nadarajah, S., Tindal, M,J., Yianneskis, M. 1990. An Experimental Study of Velocity and Reynolds Stress Distribution in a Production Engine Inlet Port Under Steady Flow Conditions. *Journal of Engines.* 99(1). SAE Paper No 900053

Choi, W.C., Guezennec, Y.G., Lee, C.W., Chun, D.C., Chi, Y.H. 1996. Effects of Intake Lift Profile and RPM on 3-D Mean and Fluctuating In-Cylinder Flows in an IC Engine. *Proceedings of the ASME,* pp.21-24. International Conference on Recent Developments on Engine Design and Systems, Youngstown, Ohio, USA, 21-24 April.

De Boer, C.D., Johns, R.J.R., Grigg, D.W., Train, B.M., Denbratt, I., Linna, J.R. 1990. Refinement With Performance and Economy for 4 Valve Automotive Engines. *Proceedings of the IMechE,* pp.147-155. International Conference on Automotive power systems - Environment and Conservation, Chester, England, 10-12 September . IMechE Paper No C394/053.

Dent, J.C., Chen, A. 1994. Investigation of Steady Flow Through a Curved Inlet Port. SAE Paper No 940522.

Dhaubhadel, M.N. 1996. Review - CFD Applications in the Automotive Industry. *Journal of Fluids Engineering.* 118:647-653

Dvorak, T.M., Hoekstra, R.L. 1996. Optimizing Internal Combustion Engine Performance Through Response Surface Methodology. SAE Paper No 962525

Edwards, S.P., Clarke, D.P., Pilley, A.D. 1997. The Role of Statistics in the Engine Development Process. *IMechE Statistics for Engine Optimisation Seminar.* London, England, 2 December.

Faure, M.A. 1996. *Particle Image Velocimetry Measurement of In-Cylinder Flows.* PhD Thesis, University of Brighton.

Faure, M.A., Sadler, M., Oversby, K.K., Stokes, J., Begg, S.M., Pommier, L.S., Heikal, M.R. 1998. Application of LDA and PIV Techniques to the Validation of a CFD Model of a Direct Injection Gasoline Engine. *SAE International Fall Fuels and Lubricants Meeting and Exposition*, San Francisco, USA, October 19-22. SAE Paper No 98705.

Fisher, W.L. 1930. Cylinder Head Design. Some Notes on a Much-discussed Controversy. Autocar. 14 March: pp494-499.

Gale, N.F. 1990. Diesel Engine Cylinder head Design – The Compromises and the Techniques. *SAE International Congress and Exposition*, Detroit, Michigan, USA, 26 February – 2 March. SAE Paper No 900133.

Gamo, S.O., Ouladsine, M., Rachid, A. 1999. Diesel Engine Exhaust Emissions Modelling Using Artificial Neural Networks. SAE Paper No 1999-10-1163

Gilbert, I.F., Heath, A.R., and Johnstone, I.D. 1992. Multivalve High Speed Direct Injection Diesel Engines – The Design Challenge. *IMechE Seminar on Recent Advances in the Mechanical Design and Development of Engines and Their Components,* pp41-51. London, England, 10 March.

Godrie, P., Zellat, M. 1994. Simulation of Flow Field Generated by Intake Port-Valve-Cylinder Configurations - Comparisons with Measurements and Applications. SAE Paper No 940521.

Gosman, A.D., Ahmed, A.M.Y. 1987. Measurement and Multidimensional Prediction of Flow in an Axisymmetric Port/Valve Assembly. SAE Paper No 870592.

Grove, D.M., Davis, T.P. 1992. *Engineering Quality and Experimental Design*. Harlow, England: Longman. ISBN 0-582-06687-5

Hadded, O., Denbratt, I 1991. Turbulence Characteristics of Tumbling Air Motion in Four-Valve SI Engines and their Correlation with Combustion Parameters. *SAE International Congress and Exposition.* Detroit, Michigan, USA, 25 February – 1 March. SAE Paper No 910478.

Hasegawa, S., Takahashi, Y. 1988. Prediction Method of Induction Swirl Parameters for Inlet Port of DI Diesel Engine and its Application to Engine Performance Improvement. SAE Paper No 885101.

Heywood, J.B. 1988. *Internal Combustion Engine Fundamentals*. New York, USA: McGraw-Hill. ISBN 0-07-81004

Holland, J.H. 1975. *Adaptation in Neural and Artificial Systems*. University of Michigan, USA.

Hundleby, G. 1989. *Internal Combustion Engines*. European Patent Application 90313093.8, Publication No. EP 0431866 BI

Jackson, N.S., Stokes, J., Heikal, M.R., Downie, J.H. 1995. A Dynamic Water Flow Visualisation Rig for Automotive Combustion System Development. *SAE International Congress and Exposition*, Detroit, USA. SAE Paper No 950728.

Jackson, N.S., Stokes, J., Sadler, M., Heikal, M.R., Faure, M.A., Pommier, L. 1997. Correlation of the Combustion Characteristics of Spark Ignition Engines with the In-Cylinder Flow Field, Characterised using PIV in a Water Analogy Rig. *SAE International Spring Fuels and Lubricants Meeting*, Dearborn, Michigan, USA, 5-8 May. SAE Paper No 971673

Kastner, L.J., Williams, T.J., White, J.B. 1963. Poppet Inlet Valve Characteristics and Their Influence on the Induction Process. *IMechE Proceedings, Internal Combustion Engines Group.* 178(1/36):955-978.

Kang, K.Y., Baek, J.H. 1995. LDV Measurement and Analysis of Tumble Formation and Decay in a Four-Valve Engine. *Experimental Thermal and Fluid Science.* 11(2):181-189

Kang, K.Y., Oh, S.M., Lee, J.W., Lee, K.H., Bae, C.S. 1997. The Effect of Tumble Flow on Lean Burn Characteristics in a Four-Valve SI Engine. SAE Paper No 970791.

Kawashima, J., Ogawa, H., Tsuru, Y. 1998. Research on a Variable Swirl Intake Port for 4-Valve High-Speed DI Diesel Engines. *SAE International Fall Fuels and Lubricants Meeting and Exposition*, San Francisco, California , USA, 19-22 October. SAE Paper No 982680.

Kent, J.C., Mikulec, A., Rimal, L., Admczyk, A.A., Mueller, S.R., Stein, R.A., Warren, C.C. 1989. Observations on the Effects of Intake-Generated Swirl and Tumble on Combustion Duration. SAE Paper No 89096.

Kent, J.C., Trigui, N., Choi, W.C., Guezennec, Y.G. 1994. Characterization of Intake Generated Fluid Flow Field in IC Engines Using 3D Particle Tracking Velocimetry (3D PTV). SAE Paper 940279

Kirkpatrick, S., Gelatt Jr, C.D., Vecchi, M.P. 1983. Optimization by Simulated Annealing. *Science*, 220(4598):671-680.

Lee, K 1999. *Principles of CAD/CAM/CAE Systems.* Addison Wesley. ISBN 0-201-38036-6

Li, Y., Li, L., Xu, J., Gong, X., Liu, S., Xu, S. 2000. Effects of Combination and Orientation of Intake Ports on Swirl Motion in Four-Valve DI Diesel Engines. SAE Paper No 2000-01-1823

Livengood, J.C., Stanitz, J.D. (1943). The Effect of Inlet Valve Design, Size and Lift on the Air Capacity and Output of a Four-Stroke Engine. NASA Technical Note. 915 (1).

Mahmood, Z., Chen, A., Yianneskis, M., Ganti, G. 1996. On the Structure of Steady Flow Through Dual-Intake Engine Ports. *International Journal for Numerical Methods in Fluids*, 23:1085-1109.

Maier, A., Sheldrake, T.H., Wilcock, D. 2000. Geometric Parameters Influencing Flow in a Axisymmetric IC Engine Inlet Port Assembly: Part 1 – Valve Flow Characteristics. *Transactions of the ASME, Journal of Fluids Engineering.* 22:650-657.

A Maier, A., Sheldrake, T.H., Wilcock, D 2000. Geometric Parameters Influencing Flow in a Axisymmetric IC Engine Inlet Port Assembly: Part II – Parametric Variation of Valve Geometry. *Transactions of the ASME, Journal of Fluids Engineering.* 22:658-665.

Monaghan, M.L., Pettifer, H.F. 1981. Air Motion and Its Effects on Diesel Engine Performance and Emissions. *SAE International Congress and Exposition,* Detroit, Michigan, USA, 23-27 February. SAE Paper No 810255.

Montgomery, D.C. 1997. *Design and Analysis of Experiments.* Chichester, England: John Wiley. ISBN 0-471-15746-5.

Myers, R.H., Montgomery, D.C. 1995. *Response Surface Methodology: Process and Product Optimization using Designed Experiments.* Chichester, England: John Wiley.

O'Conner, J.F., McKinley, N.R. 1998. CFD Simulations of Intake Port Flow using Automatic Mesh Generation: Comparison with Laser Sheet, Swirl and LDA Measurements for Steady Flow Conditions. SAE Paper No 980129.

Owen, N. 2001. The Diesel Engine: Heart of a Future Integrated Powertrain? *Well-to-Wheels 2001,* 14-16 May.

Page, V.J., Blundell, G.D. 2000. The Application of design of Experiments and CFD to the Optimisation of a Fully Parametric Helical Port Design. *IMechE Conference Transactions,* pp.69-78. Computational and Experimental Methods in Reciprocating Engines, London, England, 1-2 November, IMechE Paper No C587/014/2000.

Partington, G.D. 1982. Development and Application of a Fully Machined Helical Inlet Port for High Speed DI Engines. *Proceedings of the IMechE,* pp.277-283. Conference on Diesel Engines for Passenger Cars and Light Duty Vehicles, London, England, 5-7 October. IMechE Paper No C121/82.

Raynor, M. 1995. In Via Recta Celeriter (In The Right Way Quickly). *World Class Design to Manufacture,* 2(3):10-16.

Reeves, M., Garner, C.P., Dent, J.C., Halliwell, N.A. 1994. Particle Image Velocimetry Measurements of In-Cylinder Flow in a Multi-Valve Internal Combustion Engine. *Proceedings of the IMechE, Part D, Journal of Automotive Engineering*, 210 (1):63-70.

M Reeves, M., Garner, C.P., Dent, J.C., Halliwell, N.A. 1994. In-Cylinder Particle Image Velocimetry Measurements in a Four-Stroke, Four Valve Optical IC Engine. *Proceedings of Optical Methods and Data Processing in Heat and Fluid Flows*. IMechE Conference, London

Tabata, M., Kataoka, M., Fujimoto, M., Noh, Y. 1995. In-Cylinder Fuel Distribution, Flow Field and Combustion Characteristics of a Mixture Injected SI Engine. SAE Paper No 950104

Taguchi, G 1986. *Introduction to Quality Engineering – Designing Quality into Products and Processes*. Tokyo, Japan: Asian Productivity Organisation.

Tanaka, K. 1931. Air Flow Through Exhaust Valve of Conical Seat. *Int. Conr. Appli. Mech.* 1:287-295.

Taylor III, W., Leylek, J.A., Sommer, R.G., Jain, S.K. 1998. IC Engine Intake Region Design Modifications for Loss Reduction Based on CFD Methods. SAE Paper No 981026.

C F Taylor, C.F. 1985. *The Internal Combustion Engine in Theory and Practice, Vol 1*. Cambridge, Massachusetts, USA. MIT Press. ISBN 0-262-70026-3.

Tipplemann, G. 1977. A New Method of Investigation of Swirl Ports. *SAE International Automotive Engineering Congress and Exposition*, Detroit, USA, February 28 – March 4. SAE Paper No 770404.

Uzkan, T.B., Borgnakke, C., Morel, T. 1983. Characterization of Flow Produced by a High-Swirl Inlet Port. SAE Paper No 830266

Watts, R. 1964. Diesel Engine Port Design. *Automotive Design Engineering*, March.

Widener, S.K. 1995. Parametric Design of Helical Intake Ports. SAE Paper No 950818

Woods, W.A., Khan, S.R. 1965. An Experimental Study of Flow Through Poppet Valves. *Proceedings of the IMechE*. 180(3N):32-41.

Works Published by the Author

Bates, M.C., Heikal, M.R. 2002. A Knowledge-Based Model for Multi-Valve Diesel Engine Inlet Port Design. *SAE International Spring Fuels and Lubricants Meeting and Exhibition.* Reno, Nevada. 6-9 May SAE Paper No 2002-01-174.

Bates, M.C., Heikal, M.R. 2002. A Parametric Inlet Port Design Tool for Multi-Valve Diesel Engines. *Statistics and Analytical Methods in Automotive Engineering*, London, September IMechE Paper No C606/001/2002.

Appendices

Appendix A

Design Parameter
Brainstorming

ORIGINAL LISTING OF IDEAS	CLARIFICATION, ADDITIONAL NOTES	POSSIBLE EFFECTS
throat cutter depth	Throat cutter dimensions and shape in general. Influences floor height and radius, nose shape	Influence on flow perfomance and air motion gereration due to effect on geometry close to valve seat area.
nose shape	Determined by interaction of throat cutter and cast port shape. Generally described as flat (straight) or round (curved)	Nose shape tends to influence tumble generation (in conjunction with floor geometry). Flat nose allows flow across valve head to generate tumble. Round nose pushes air down, possibly reducing tumble. Flow area in top half of the port is important in realtion to these effects.
valve stem diameter	Determined by valve design guidelines, depends on unsupported length, valve material etc. Reduces effective area of valve at high lift conditions.	Influence on maximum flow performance
valve lift method (direct attack, rockers + roller followers etc)	Direct attack usually have more agressive lift profiles, therefore more area under lift curve for a given duration and max lift. Determined by valvetrain requirements, refinement, wear characteristics etc.	Influence on total mass of air inducted. Possible influence in connection with air motion generating characteristics (e.g. high tumble generating potential early in the lift event may not be effective if valve lift is not agressive)
valve guide protrusion	Reduces effective area of port in critical region. High port roof line in relation to valve seat may require long guide protrusion to avoid long unsupported length (see valve stem)	Influences flow area and therefore flow preformance ant high valve lift. May be critical (minimum) area. Guide boss shape probably more important
fie type	Injector type and location in both HSDI and G-DI determines space available for valves and ports. Probably a constraint. Injector pocket in PFI influences port shape and cross-sectional area close to port entry.	G-DI/HSDI: Injector is likely to compromise valve size and position, PFI injector pocket compromises port shape and therefore flow velocity profile (too large, so stangant flow and sudden changes in cross-sectional area)
bolt bosses - constraints	Bolting pattern, number of bolts etc constrains port shape, area and entry position, valve number and pattern	Determines type of port required to effectively produce level of air motion required. May comromise port shape and direction, so reduced flow peformance if optimum not possible

Table A1: Port Design Parameter Brainstorming Results

ORIGINAL LISTING OF IDEAS	CLARIFICATION, ADDITIONAL NOTES	POSSIBLE EFFECTS
cooling requirements	Need for strategic cooling close to ports (e.g. exhaust-exhaust valve bridge in diesel). May constrain available space for ports. Water jacket may also influence port design due to assembly requirements (e.g. port core fed through water jacket core)	Cooling pasages close to gas face tend to raise the height of ports, possibly reducing swirl or tumble generating potential. Possibly need to modify port shape away from ideal to match coolant core shape
shape changes / cross-section changes along port	Necessary due to constraints (see cooling, fie, bolt bosses), also required to provide desired velocity profile along port. Sudden changes in cross section generally not desired.	Loss in flow performance due to momentum loss
floor radius	Determined by interaction of throat cutter and floor angle/curvature as it meets the valve seat insert. Also influenced by manufacturing requirements - provision of undersize port core to ensure throat cutter cuts 360°. Generally sharp for 4V gasoline, but possibly smooth curve for helical	governs flow separation from floor in 4V gasoline to generate tumble, but causes loss in flow. Sharp edge often required as port shape and direction does not provide sufficient tumble air motion. Sharp edge not required in helical ports to encourage flowinto helix area.
relationship between valve head dia and inner seat diameter	Valve head diameter and inner seat diameter related by seat angle and width. Maximum valve size may be governed by proximity of valve head to cylinder wall.	valve seat geometry important at low valve lift. Large valve head in relation to inner seat may allow multiple angles and therefore improve flow.
port curvature (straight v "tap")	Note: definition of valve-to-port angle is not straighforward for curved ports but may be simpler for straight. Curvature may be in horizontal plane also.	Momentum loss in curved ports, but tradeoff between flow loss along the port and exit loss due to port-valve angle. Curved port probably necessary for low entry height, but tumble potential lower.
valve guide boss size/shape	Guide boss may be required to support valve guide if protrusion is neccessary. Guide boss feature may be "negative" if guide is recessed.	Guide boss creates a reduction in flow area, influences flow into nose area, may interact with floor (large guide boss may push flow down onto the floor, making the nose feature less sensitive). Smooth boss shapes more likely to be beneficial. "negative" bosses (negative protrusion) may cause stagnant zones and flow separation from the roof.
aspiration (na/tc)	influence on charge temperature and pressure, inlet/exhaust pressure ratio during overlap	Changes to gas exchange process (ie high inlet pressure may cause little or no backflow during overlap) may generate different flow/air motion interactions at low valve lift. Higher mass flowrate with TC may necessitate larger ports than equivalent for NA. (suggests size criteria bsed not only on migv)

Table A1: Port Design Parameter Brainstorming Results

ORIGINAL LISTING OF IDEAS	CLARIFICATION, ADDITIONAL NOTES	POSSIBLE EFFECTS
valve timing	influence on gas exchange during overlap, IVO and and tuning effects.	Effect on volumetric efficiency, unknown effect on air motion - possibly modified due to different phasing of inlet lift with gas velocity and piston position.
valve pattern	location of valves within bore. Skew angle usually defined to represent this. 0° indicates square pattern with inlet valves on inlet manifold side of head (i.e. 4V gasoline). Influenced by valvetrain design, bolting pattern, required level of air motion (for diesels)	Skew angle influences swirl generating capability for 2V and 4V engines. Limitations on skew angle imposed by valvetrain/bolting may necessitate helical ports
helix features (ramp angle, "wrap angle", width of ramp)	Helix used to generate air motion prior to entry into cylinder.	larger helix, and larger "wrap angle" (ie how far round the valve seat the helix goes) increase swirl.
port angle (to horizontal)	Determines angle of approach into critical valve seat section of port, important relative to port orientation (tangent to cylinder or straight). Possible interaction with valve head shape (backing angle)	Shallow angle (low port) generates increased tumble in 4V gasoline, reduces flow performance due to change in direction at valve
side entry v top entry	Side entry used to generate swirl and/or tumble motion. Conventional type. Top entry used to generate reverse tumble for G-DI and also swirl for 4V HSDI (note, top entry ports in HSDI tend to be more horizontal in the lower section of the port, acting more like side entry ports)	
type of air motion required	High/low swirl or tumble, reverse tumble, air motion generated at high or low valve lift?	
spark plug/injector/glow plug position	See fie, glow plug or spark plug also may constrain port shape and/or valve size/location/pattern	Likely to compromise valve position, therefore flow and air motion may be compromised. Central injector or spark plug will puch valves out towards the bore, increasing valve shrouding and possibly reducing low lift performance.

Table A1: Port Design Parameter Brainstorming Results

A4

ORIGINAL LISTING OF IDEAS	CLARIFICATION, ADDITIONAL NOTES	POSSIBLE EFFECTS
tolerances	Manufacturing tolerances influence the selection and specification of design features to provide robust design (ie peformance is relatively insensitive to variations from nominal). Identification of robust features. Definition of allowable tolerances? Tolerances usually expressed in terms of location tolerances in x,y, z directions (e.g. of port core), machining tolerance (dia & position of throat cutter)	Various possible effects. Performance characteristics that are dependent on port location may be more sensitive than those dependent on machining ops
port surface area	Contributes to flow friction. Cross-section shape, port length and curvature influence total surface area.	Larger surface area produces more friction and heat ransfer (charge heating). Aim to minimise.
steady flow v dynamic	Method of characterisation may influence the apparent response to design features. E.g effect of bore/stroke may be different in unsteady, dynamic situation	
square or round ports	suface area, effective flow area, outer dimensions/area ratio. Influenced by packaging and constraints	see surface area
valve seat shape and position (recessed?)	Additional angles on valve seat, position of seat relative to gas face, venturi seat?	increased number of seat angles and elimination of recess will improve flow, but air motion generated by partial shrouding may be impaired.
no of valves		two valves (4V) use available bore area more effectively, leading to improved flow perfomance, but increased port surface area and possibly increased shrouding may limit the benefit. Interfernce from individual valve flows may compromise air motion and flow (esp 4V hsdi)
tandem or twin (separate) port type	tandem = two ports joined together to form a single port entry. Twin/separate = two ports & two entries.	difficult to optimise both valves in tandem designs. Likely to create interfering flow patterns (see above). Port deact requires twin ports

Table A1: Port Design Parameter Brainstorming Results

ORIGINAL LISTING OF IDEAS	CLARIFICATION, ADDITIONAL NOTES	POSSIBLE EFFECTS
inlet port velocity	determined by piston speed, valve lift, port area	higher port velocity may restrict flow, but may also be required to generate air motion, esp 4V gasoline (high velocoty required to create flow separation from port floor)
port deactivation	partial or full closure of one port to modify air motion characteristics.	increased swirl when port deact is closed, unpredictable effects during partial closure.
wall/floor radius	see floor radius	see floor radius
surface finish	possible influence on flow friction, effect of suface features (machined steps etc)	very poor surface finish will degrade flow and impair the effect of air motion generating features in the port (eg helix). Good sand finish may be beneficial over smooth due to boundary layer effects?
bifurcation shape/position	point at which tandem ports separate. Usually refers to symmetrical 4V gasoline ports.	early bifurcation provides adequate section of port into valve area. Reduced disturbance close to valve. Late bifurcation may require bent port legs.
port orientation (valve positions in bore, manifold entry position, ports tangential or straight relative to cylinder)	angle of ports relative to cylinder. Related to valve pattern, entry position, port curvature etc. influenced by constraints	Tangential ports (can also be created using skew angle) create swirl. Limitations due to bolting patterns.
approach angle	see port angle, port orientation	see port angle
manufacturing constraints	limitations imposed by manufacturing process (as against packaging constraints - cooling, fie etc). Minimum wall thickness, minimum cast radius, cast surface quality, See also tolerances	minimum wall thickness condition may compromise port cross-sectional area in critical regions due to coolant jacket, valve spring pack (esp top entry). Bifurcation in cast ports cannot be sharp due to minimum rad. See also surface finish

Table A1: Port Design Parameter Brainstorming Results

ORIGINAL LISTING OF IDEAS	CLARIFICATION, ADDITIONAL NOTES	POSSIBLE EFFECTS
in-port air motion (intentional/unintentional)	Air motion created before exit into cylinder. Intentional effects include helical ports, sharp floor edges (possibly). Unintentional include port deact valve effects (may direct flow to one sdie of the port)	increased air motion = trade-off with flow performance. Should be less sensitive to valve position (ie helical v directed ports). Flow disturbance caused by unintentional features likely to reduce air motion and flow performance.
port features (ski-jump, tumble edges, directional changes)	Features generally intended to create flow separation or rapid changes in direction. Required if scope for changing the general port shape and direction is limited	Reduced effective flow area limits flow performance
manifold entry position (ie port entry)	Determined by required port shape and direction, influenced by packaging constraints and influences manifold geometry, possibly port cross-sectional shape	If packaging constraints force non-ideal position, likely loss in performance. Additional features may be required to increase air motion, possibly reducing flow performance further.
cross-section changes along port	see shape changes	
misalignment between manifold and port	not designed for, but effect should be considered re. robustness & tolerances	minor misalignment = possible reduction in flow performance. Major misalignment = possible loss in both air motion and flow peroformance.
port length	determined by width of cylinder head. Influences port direction, curvature, flow friction	increased port length increases skin friction and heat transfer to inlet air, therefore reducing flow performance. Possible trade-off between port length and curvature in terms of flow performance
bore diameter	Relative to valve size and position.	large bore allows large valves given similar constraints, therefore potentionally improved flow performance.
proximity of cylinder wall and valve	see valve head, determined by manufacturing constraints or intentional for tangential ports	valve close to cylinder wall tends to reduce flow performance due to masking effect but may be required for effective tangential ports.

Table A1: Port Design Parameter Brainstorming Results

ORIGINAL LISTING OF IDEAS	CLARIFICATION, ADDITIONAL NOTES	POSSIBLE EFFECTS
rig number!	Test repeatability - important for DOE etc	2% uncertainty in SS test results
combustion chamber volume / compression ratio	May limit available valve angles, piston crown shapes etc.	see below
combustion chamber / valve axis angles	determines angle at which air enters cylinder. Also influences valve size and position. Limited by compression ratio, possibly valve lift characteristics	shallow valve angle in 4v gasoline tends to reduce tumble; port entry must be higher to prevent excessive curvature in valve area. However, wide valve-port angles may be beneficial in encouraging flow across the valve head.
engine parameters (bore/stroke/speed/cam lift/cam profile)	see bore dia. Bore/stroke ratio influences max piston speed; related to max lift and timing. Mostly determined before port design, therefore constraints that must be considered	long stroke increases max piston speed, therefore possibly making ports more likely to be restrictive but increasing tumble generation.
valve size	Determines maximum flow area at high valve lift. Dependant on bore size, valve angle, valvetrain design	fundamental limit on maximum flow performance. Large valve close to cylinder wall may be less effective than slightly smaller valve further away.
valve head shape	Presence of multiple angles, also "backing angle". Interaction with port-valve angle (low-high lift) and seat angle (low lift).	smoother flow through valve seat area improves flow performance.
floor height	Usually defined as the height of the parallel part of the throat cutter above the seat. See also throat cutter and floor radius. For 4V gasoline, floor height and radius may interact to influence tumble generation.	higher floor on 4v gasoline tends to increase tumble as flow separates from the port floor above the valve head. Lower port floors may still allow significant flow down the port, therefore reducing tumble
production method	Sand cast, die-cast, rapid-cast or fully machined (for cylinder heads). CNC machined, SLA, SLS for flowboxes	methods capable of higher accuracy (CNC machined, higher quality sand casting) will generally improve perfomance. Poor surface finish and large location tolerance must be allowed for in some cases, possibly preventing the use of "sensitive" features.

Table A1: Port Design Parameter Brainstorming Results

Appendix B

Experimental Design Matrices

Test No.	P1 (Av) hardware	P2 (R) hardware	P3 (At) test	P4 (Ar) hardware	P5 (Dn) test	P6 (E) test	Note
45	30	50	45	45	0.32	0.40	CENTRE POINT
10	15	70	90	0	0.3	0.35	
13	15	30	90	0	0.34	0.35	
15	15	70	0	0	0.34	0.35	
16	15	30	90	0	0.3	0.45	
18	15	30	0	0	0.34	0.45	
20	15	70	0	0	0.3	0.45	
29	15	70	90	0	0.34	0.45	
32	15	30	0	0	0.3	0.35	
46	30	50	45	45	0.32	0.40	CENTRE POINT
1	45	30	0	0	0.34	0.35	
2	45	70	0	0	0.3	0.35	
3	45	70	90	0	0.3	0.45	
9	45	70	0	0	0.34	0.45	
19	45	30	0	0	0.3	0.45	
21	45	30	90	0	0.3	0.35	
23	45	30	90	0	0.34	0.45	
25	45	70	90	0	0.34	0.35	
47	30	50	45	45	0.32	0.40	CENTRE POINT
33	15	50	45	45	0.32	0.40	
34	45	50	45	45	0.32	0.40	
35	30	30	45	45	0.32	0.40	
36	30	70	45	45	0.32	0.40	
37	30	50	0	45	0.32	0.40	
38	30	50	90	45	0.32	0.40	
48	30	50	45	45	0.32	0.40	CENTRE POINT
41	30	50	45	45	0.3	0.40	
42	30	50	45	45	0.34	0.40	
43	30	50	45	45	0.32	0.35	
44	30	50	45	45	0.32	0.45	
39	30	50	45	0	0.32	0.40	
40	30	50	45	90	0.32	0.40	
49	30	50	45	45	0.32	0.40	CENTRE POINT
7	15	30	90	90	0.34	0.45	
17	15	30	0	90	0.3	0.45	
30	15	30	90	90	0.3	0.35	
31	15	30	0	90	0.34	0.35	
50	30	50	45	45	0.32	0.40	CENTRE POINT
6	15	70	90	90	0.34	0.35	
12	15	70	0	90	0.34	0.45	
22	15	70	0	90	0.3	0.35	
26	15	70	90	90	0.3	0.45	
51	30	50	45	45	0.32	0.40	CENTRE POINT
8	45	30	0	90	0.34	0.45	
11	45	30	90	90	0.3	0.45	
14	45	30	0	90	0.3	0.35	
27	45	30	90	90	0.34	0.35	
52	30	50	45	45	0.32	0.40	CENTRE POINT
4	45	70	90	90	0.3	0.35	
5	45	70	90	90	0.34	0.45	
24	45	70	0	90	0.3	0.45	
28	45	70	0	90	0.34	0.35	
53	30	50	45	45	0.32	0.40	CENTRE POINT

Table B1: Central Composite Experimental Design (6 Parameters)

Test No.	P1 (At)	P2 (R)	P3 (Ar)	P4 (E)	P6 (Aw)	P7 (Wh)	P8 (Hs)	Note
	test	hardware	hardware	test	hardware	hardware	hardware	
57	**45**	**50**	**45**	**0.4**	**230**	**15**	**30**	CENTREPOINT
41	0	50	0	0.4	190	15	30	
42	90	50	0	0.4	190	15	30	
49	45	50	0	0.4	230	10	25	
50	45	50	0	0.4	230	10	25	
33	45	50	0	0.35	230	15	30	
35	45	50	0	0.45	230	15	30	
37	45	50	0	0.35	230	15	30	
39	45	50	0	0.45	230	15	30	
53	45	50	0	0.4	230	20	35	
54	45	50	0	0.4	230	20	35	
45	0	50	0	0.4	270	15	30	
46	90	50	0	0.4	270	15	30	
58	**45**	**50**	**45**	**0.4**	**230**	**15**	**30**	**CENTREPOINT**
1	45	50	45	0.35	190	10	25	
2	45	50	45	0.45	190	10	25	
17	45	30	45	0.4	190	15	30	
21	45	30	45	0.4	190	15	30	
5	45	50	45	0.35	190	20	35	
6	45	50	45	0.45	190	20	35	
9	0	50	45	0.4	230	10	25	
10	90	50	45	0.4	230	10	25	
3	45	50	45	0.35	270	10	25	
13	0	50	45	0.4	230	10	25	
14	90	50	45	0.4	230	10	25	
59	**45**	**50**	**45**	**0.4**	**230**	**15**	**30**	**CENTREPOINT**
25	0	30	45	0.35	230	15	30	
26	90	30	45	0.35	230	15	30	
29	0	30	45	0.45	230	15	30	
30	90	30	45	0.45	230	15	30	
11	0	50	45	0.4	230	20	35	
12	90	50	45	0.4	230	20	35	
15	0	50	45	0.4	230	20	35	
16	90	50	45	0.4	230	20	35	
4	45	50	45	0.45	270	10	25	
19	45	30	45	0.4	270	15	30	
23	45	30	45	0.4	270	15	30	
7	45	50	45	0.35	270	20	35	
60	**45**	**50**	**45**	**0.4**	**230**	**15**	**30**	**CENTREPOINT**
8	45	50	45	0.45	270	20	35	
18	45	70	45	0.4	190	15	30	
22	45	70	45	0.4	190	15	30	
27	0	70	45	0.35	230	15	30	
28	90	70	45	0.35	230	15	30	
31	0	70	45	0.45	230	15	30	
32	90	70	45	0.45	230	15	30	
20	45	70	45	0.4	270	15	30	
24	45	70	45	0.4	270	15	30	
43	0	50	90	0.4	190	15	30	
44	90	50	90	0.4	190	15	30	
61	**45**	**50**	**45**	**0.4**	**230**	**15**	**30**	**CENTREPOINT**
51	45	30	90	0.4	230	10	25	
34	45	50	90	0.35	230	15	30	
36	45	50	90	0.45	230	15	30	
38	45	50	90	0.35	230	15	30	
40	45	50	90	0.45	230	15	30	
55	45	30	90	0.4	230	20	35	
47	0	50	90	0.4	270	15	30	
48	90	50	90	0.4	270	15	30	
52	45	70	90	0.4	230	10	25	
56	45	70	90	0.4	230	20	35	
62	**45**	**50**	**45**	**0.4**	**230**	**15**	**30**	**CENTREPOINT**

Table B2: Box-Behnken Experimental Design (7 Parameters)

Appendix C

Test Results: Directed Ports

Test Filename   **D53B**

Engine Details

Configuration	IL4	Inner Seat Dia, mm	27	Shape Factor, LD	10.43
Cylinder bore	84.5	Seat Angle	45	Lmax/D	0.31
Engine Stroke	90	Max Valve Lift	8.37	D/B	0.32
Inlet Valves, n	1	Valve Opens	0	MIGV	132.2
Rated Speed, rpm	4500	Valve Closes	50	MPV	13.5

Test Details

Test Date	15-Nov-00	Barometer, mmHg	756.7	VFAM Constant	77.15
Test Pressure, mmH$_2$O	900	ISM Constant	1.09E-04		

Test Summary Results

Swirl Ratio (Rs)	1.78	Gulp Factor	0.871	Cf @ 0.3 L/D	0.566
Rs/LD	0.17	MCf	0.443	Cf @ Max Lift	0.568
CCf	1.776				

Test Results

Valve Lift		Air Flow	ISM Torque	Flow	Discharge	Non-dim
Test	Non-dim	m^3/s	NmE^{-3}	Coefficient	Coefficient	Rig Swirl
mm	L/D	Q	G	Cf	Cd	Ns
0	0.000	0.0000	0.00	0.000	0.000	0.000
1	0.037	0.0078	1.95	0.116	1.085	0.158
2	0.074	0.0154	3.36	0.230	1.060	0.137
3	0.111	0.0223	4.34	0.333	1.003	0.122
4	0.148	0.0299	6.94	0.445	0.990	0.146
5	0.185	0.0348	9.11	0.520	0.908	0.164
6	0.222	0.0357	16.16	0.532	0.762	0.284
7	0.259	0.0371	21.48	0.552	0.667	0.364
8	0.296	0.0379	24.08	0.565	0.587	0.399
9	0.333	0.0385	25.82	0.573	0.521	0.422
10	0.370	0.0390	27.77	0.580	0.468	0.448

Test Filename   **D53A**

Engine Details

Configuration	IL4	Inner Seat Dia, mm	27	Shape Factor, LD	10.43
Cylinder bore	84.5	Seat Angle	45	Lmax/D	0.31
Engine Stroke	90	Max Valve Lift	8.37	D/B	0.32
Inlet Valves, n	1	Valve Opens	0	MIGV	132.2
Rated Speed, rpm	4500	Valve Closes	50	MPV	13.5

Test Details

Test Date	15-Nov-00	Barometer, mmHg	756.7	VFAM Constant	77.15
Test Pressure, mmH_2O	900	ISM Constant	1.09E-04		

Test Summary Results

Swirl Ratio (Rs)	1.1	Gulp Factor	0.865	Cf @ 0.3 L/D	0.565
Rs/LD	0.11	MCf	0.445	Cf @ Max Lift	0.568
CCf	1.788				

Test Results

Valve Lift		Air Flow	ISM Torque	Flow	Discharge	Non-dim
Test	Non-dim	m^3/s	NmE^{-3}	Coefficient	Coefficient	Rig Swirl
mm	L/D	Q	G	Cf	Cd	Ns
0	0.000	0.0000	0.00	0.000	0.000	0.000
1	0.037	0.0079	-0.33	0.118	1.107	-0.026
2	0.074	0.0154	0.43	0.230	1.058	0.018
3	0.111	0.0230	1.30	0.344	1.036	0.035
4	0.148	0.0303	1.19	0.454	1.009	0.025
5	0.185	0.0359	2.93	0.537	0.938	0.051
6	0.222	0.0357	12.58	0.535	0.766	0.220
7	0.259	0.0368	14.32	0.550	0.664	0.244
8	0.296	0.0377	16.49	0.564	0.586	0.274
9	0.333	0.0384	17.68	0.574	0.522	0.289
10	0.370	0.0391	19.53	0.583	0.470	0.314

Test Filename　　　　**D28AB**

Engine Details

Configuration	IL4	Inner Seat Dia, mm	27	Shape Factor, LD	9.88
Cylinder bore	80	Seat Angle	45	Lmax/D	0.31
Engine Stroke	90	Max Valve Lift	8.37	D/B	0.338
Inlet Valves, n	1	Valve Opens	0	MIGV	118.5
Rated Speed, rpm	4500	Valve Closes	50	MPV	13.5

Test Details

Test Date	15-Nov-00	Barometer, mmHg	757.2	VFAM Constant	77.15
Test Pressure, mmH$_2$O	900	ISM Constant	1.09E-04		

Test Summary Results

Swirl Ratio (Rs)	0.72	Gulp Factor	0.77	Cf @ 0.3 L/D	0.571
Rs/LD	0.07	MCf	0.448	Cf @ Max Lift	0.574
CCf	1.799				

Test Results

Valve Lift		Air Flow	ISM Torque	Flow	Discharge	Non-dim
Test	Non-dim	m^3/s	NmE^{-3}	Coefficient	Coefficient	Rig Swirl
mm	L/D	Q	G	Cf	Cd	Ns
0	0.000	0.0000	0.00	0.000	0.000	0.000
1	0.037	0.0079	0.98	0.119	1.111	0.081
2	0.074	0.0157	0.98	0.235	1.082	0.041
3	0.111	0.0230	1.30	0.344	1.037	0.037
4	0.148	0.0303	2.82	0.454	1.008	0.062
5	0.185	0.0341	6.62	0.511	0.893	0.128
6	0.222	0.0363	8.46	0.542	0.776	0.154
7	0.259	0.0377	8.79	0.563	0.680	0.154
8	0.296	0.0382	8.90	0.570	0.593	0.154
9	0.333	0.0389	9.11	0.580	0.528	0.155
10	0.370	0.0396	9.00	0.590	0.475	0.151

Test Filename   **D12AB**

Engine Details

Configuration	IL4	Inner Seat Dia, mm	27	Shape Factor, LD	11.11
Cylinder bore	90	Seat Angle	45	Lmax/D	0.31
Engine Stroke	90	Max Valve Lift	8.37	D/B	0.3
Inlet Valves, n	1	Valve Opens	0	MIGV	150
Rated Speed, rpm	4500	Valve Closes	50	MPV	13.5

Test Details

Test Date	15-Nov-00	Barometer, mmHg	757.2	VFAM Constant	77.15
Test Pressure, mmH$_2$O	900	ISM Constant	1.09E-04		

Test Summary Results

Swirl Ratio (Rs)	1.05	Gulp Factor	0.974	Cf @ 0.3 L/D	0.576
Rs/LD	0.09	MCf	0.449	Cf @ Max Lift	0.58
CCf	1.801				

Test Results

Valve Lift		Air Flow	ISM Torque	Flow	Discharge	Non-dim
Test	Non-dim	m^3/s	NmE^{-3}	Coefficient	Coefficient	Rig Swirl
mm	L/D	Q	G	Cf	Cd	Ns
0	0.000	0.0000	0.00	0.000	0.000	0.000
1	0.037	0.0080	1.52	0.119	1.118	0.112
2	0.074	0.0155	1.08	0.232	1.066	0.041
3	0.111	0.0227	1.19	0.340	1.024	0.031
4	0.148	0.0295	4.01	0.442	0.982	0.080
5	0.185	0.0340	8.35	0.509	0.889	0.144
6	0.222	0.0369	9.11	0.551	0.789	0.145
7	0.259	0.0376	14.64	0.561	0.677	0.230
8	0.296	0.0385	13.88	0.574	0.597	0.213
9	0.333	0.0395	13.99	0.589	0.535	0.209
10	0.370	0.0405	13.78	0.602	0.485	0.201

C5

Test Filename   **D32B**

Engine Details

Configuration	IL4	Inner Seat Dia, mm	27	Shape Factor, LD	9.88
Cylinder bore	80	Seat Angle	45	Lmax/D	0.31
Engine Stroke	90	Max Valve Lift	8.37	D/B	0.338
Inlet Valves, n	1	Valve Opens	0	MIGV	118.5
Rated Speed, rpm	4500	Valve Closes	50	MPV	13.5

Test Details

Test Date	15-Nov-00	Barometer, mmHg	757.3	VFAM Constant	77.15
Test Pressure, mmH$_2$O	900	ISM Constant	1.09E-04		

Test Summary Results

Swirl Ratio (Rs)	1.66	Gulp Factor	0.773	Cf @ 0.3 L/D	0.565
Rs/LD	0.17	MCf	0.447	Cf @ Max Lift	0.567
CCf	1.794				

Test Results

Valve Lift		Air Flow	ISM Torque	Flow	Discharge	Non-dim
Test	Non-dim	m^3/s	NmE^{-3}	Coefficient	Coefficient	Rig Swirl
mm	L/D	Q	G	Cf	Cd	Ns
0	0.000	0.0000	0.00	0.000	0.000	0.000
1	0.037	0.0080	0.43	0.119	1.120	0.036
2	0.074	0.0155	2.49	0.232	1.067	0.106
3	0.111	0.0229	4.01	0.341	1.028	0.116
4	0.148	0.0297	6.29	0.442	0.982	0.141
5	0.185	0.0347	8.57	0.516	0.902	0.164
6	0.222	0.0376	11.06	0.560	0.801	0.196
7	0.259	0.0377	20.18	0.560	0.676	0.356
8	0.296	0.0380	24.95	0.564	0.587	0.437
9	0.333	0.0385	29.07	0.572	0.520	0.503
10	0.370	0.0388	32.43	0.576	0.464	0.557

C6

Test Filename   **D32A**

Engine Details

Configuration	IL4	Inner Seat Dia, mm	27	Shape Factor, LD	9.88
Cylinder bore	80	Seat Angle	45	Lmax/D	0.31
Engine Stroke	90	Max Valve Lift	8.37	D/B	0.338
Inlet Valves, n	1	Valve Opens	0	MIGV	118.5
Rated Speed, rpm	4500	Valve Closes	50	MPV	13.5

Test Details

Test Date	15-Nov-00	Barometer, mmHg	757.2	VFAM Constant	77.15
Test Pressure, mmH$_2$O	900	ISM Constant	1.09E-04		

Test Summary Results

Swirl Ratio (Rs)	1.15	Gulp Factor	0.777	Cf @ 0.3 L/D	0.568
Rs/LD	0.12	MCf	0.445	Cf @ Max Lift	0.568
CCf	1.785				

Test Results

Valve Lift		Air Flow	ISM Torque	Flow	Discharge	Non-dim
Test	Non-dim	m^3/s	NmE^{-3}	Coefficient	Coefficient	Rig Swirl
mm	L/D	Q	G	Cf	Cd	Ns
0	0.000	0.0000	0.00	0.000	0.000	0.000
1	0.037	0.0079	0.54	0.118	1.110	0.045
2	0.074	0.0156	1.74	0.232	1.070	0.074
3	0.111	0.0227	2.17	0.340	1.024	0.063
4	0.148	0.0296	2.60	0.442	0.982	0.058
5	0.185	0.0349	3.47	0.521	0.910	0.066
6	0.222	0.0360	6.83	0.537	0.769	0.126
7	0.259	0.0372	12.04	0.555	0.669	0.215
8	0.296	0.0381	19.42	0.568	0.590	0.338
9	0.333	0.0381	23.54	0.568	0.516	0.410
10	0.370	0.0385	25.60	0.573	0.462	0.442

C7

Test Filename   **D16B**

Engine Details

Configuration	IL4	Inner Seat Dia, mm	27	Shape Factor, LD	11.11
Cylinder bore	90	Seat Angle	45	Lmax/D	0.31
Engine Stroke	90	Max Valve Lift	8.37	D/B	0.3
Inlet Valves, n	1	Valve Opens	0	MIGV	150
Rated Speed, rpm	4500	Valve Closes	50	MPV	13.5

Test Details

Test Date	15-Nov-00	Barometer, mmHg	757.4	VFAM Constant	77.15
Test Pressure, mmH$_2$O	900	ISM Constant	1.09E-04		

Test Summary Results

Swirl Ratio (Rs)	1.55	Gulp Factor	0.986	Cf @ 0.3 L/D	0.571
Rs/LD	0.14	MCf	0.443	Cf @ Max Lift	0.573
CCf	1.78				

Test Results

Valve Lift		Air Flow	ISM Torque	Flow	Discharge	Non-dim
Test	Non-dim	m^3/s	NmE^{-3}	Coefficient	Coefficient	Rig Swirl
mm	L/D	Q	G	Cf	Cd	Ns
0	0.000	0.0000	0.00	0.000	0.000	0.000
1	0.037	0.0080	0.43	0.119	1.120	0.032
2	0.074	0.0156	2.49	0.234	1.076	0.094
3	0.111	0.0226	3.80	0.338	1.020	0.099
4	0.148	0.0297	6.07	0.444	0.987	0.120
5	0.185	0.0338	10.52	0.505	0.883	0.183
6	0.222	0.0357	11.39	0.533	0.763	0.188
7	0.259	0.0369	15.95	0.551	0.665	0.254
8	0.296	0.0382	22.67	0.570	0.592	0.350
9	0.333	0.0388	28.20	0.579	0.526	0.429
10	0.370	0.0396	31.57	0.591	0.476	0.470

Test Filename   **D16A**

Engine Details

Configuration	IL4	Inner Seat Dia, mm	27	Shape Factor, LD	11.11
Cylinder bore	90	Seat Angle	45	Lmax/D	0.31
Engine Stroke	90	Max Valve Lift	8.37	D/B	0.3
Inlet Valves, n	1	Valve Opens	0	MIGV	150
Rated Speed, rpm	4500	Valve Closes	50	MPV	13.5

Test Details

Test Date	15-Nov-00	Barometer, mmHg	757.3	VFAM Constant	77.15
Test Pressure, mmH$_2$O	900	ISM Constant	1.09E-04		

Test Summary Results

Swirl Ratio (Rs)	0.88	Gulp Factor	0.982	Cf @ 0.3 L/D	0.566
Rs/LD	0.08	MCf	0.445	Cf @ Max Lift	0.57
CCf	1.786				

Test Results

Valve Lift		Air Flow	ISM Torque	Flow	Discharge	Non-dim
Test	Non-dim	m^3/s	NmE^{-3}	Coefficient	Coefficient	Rig Swirl
mm	L/D	Q	G	Cf	Cd	Ns
0	0.000	0.0000	0.00	0.000	0.000	0.000
1	0.037	0.0080	0.54	0.120	1.125	0.040
2	0.074	0.0155	1.30	0.233	1.072	0.049
3	0.111	0.0230	1.95	0.345	1.041	0.050
4	0.148	0.0305	2.60	0.457	1.016	0.050
5	0.185	0.0345	2.06	0.517	0.903	0.035
6	0.222	0.0356	4.99	0.534	0.765	0.082
7	0.259	0.0368	9.44	0.551	0.665	0.151
8	0.296	0.0377	14.32	0.565	0.587	0.223
9	0.333	0.0386	20.61	0.578	0.525	0.314
10	0.370	0.0391	23.76	0.585	0.472	0.357

Test Filename   **D52B**

Engine Details

Configuration	IL4	Inner Seat Dia, mm	27	Shape Factor, LD	10.43
Cylinder bore	84.5	Seat Angle	45	Lmax/D	0.31
Engine Stroke	90	Max Valve Lift	8.37	D/B	0.32
Inlet Valves, n	1	Valve Opens	0	MIGV	132.2
Rated Speed, rpm	4500	Valve Closes	50	MPV	13.5

Test Details

Test Date	08-Nov-00	Barometer, mmHg	742.2	VFAM Constant	77.21
Test Pressure, mmH$_2$O	900	ISM Constant	1.09E-04		

Test Summary Results

Swirl Ratio (Rs)	1.73	Gulp Factor	0.872	Cf @ 0.3 L/D	0.564
Rs/LD	0.17	MCf	0.442	Cf @ Max Lift	0.566
CCf	1.773				

Test Results

Valve Lift		Air Flow	ISM Torque	Flow	Discharge	Non-dim
Test	Non-dim	m^3/s	NmE^{-3}	Coefficient	Coefficient	Rig Swirl
mm	L/D	Q	G	Cf	Cd	Ns
0	0.000	0.0000	0.00	0.000	0.000	0.000
1	0.037	0.0080	1.19	0.118	1.106	0.095
2	0.074	0.0153	2.71	0.226	1.041	0.112
3	0.111	0.0225	3.58	0.333	1.005	0.101
4	0.148	0.0302	6.19	0.447	0.994	0.130
5	0.185	0.0351	8.47	0.520	0.908	0.153
6	0.222	0.0359	15.85	0.530	0.760	0.280
7	0.259	0.0372	20.95	0.550	0.665	0.356
8	0.296	0.0381	23.88	0.563	0.585	0.397
9	0.333	0.0388	25.62	0.572	0.520	0.420
10	0.370	0.0394	27.68	0.580	0.467	0.447

C10

Test Filename **D52A**

Engine Details

Configuration	IL4	Inner Seat Dia, mm	27	Shape Factor, LD	10.43
Cylinder bore	84.5	Seat Angle	45	Lmax/D	0.31
Engine Stroke	90	Max Valve Lift	8.37	D/B	0.32
Inlet Valves, n	1	Valve Opens	0	MIGV	132.2
Rated Speed, rpm	4500	Valve Closes	50	MPV	13.5

Test Details

Test Date	08-Nov-00	Barometer, mmHg	742.2	VFAM Constant	77.21
Test Pressure, mmH$_2$O	900	ISM Constant	1.09E-04		

Test Summary Results

Swirl Ratio (Rs)	0.99	Gulp Factor	0.868	Cf @ 0.3 L/D	0.56
Rs/LD	0.09	MCf	0.444	Cf @ Max Lift	0.562
CCf	1.783				

Test Results

Valve Lift		Air Flow	ISM Torque	Flow	Discharge	Non-dim
Test	Non-dim	m^3/s	NmE^{-3}	Coefficient	Coefficient	Rig Swirl
mm	L/D	Q	G	Cf	Cd	Ns
0	0.000	0.0000	0.00	0.000	0.000	0.000
1	0.037	0.0080	-0.65	0.119	1.111	-0.051
2	0.074	0.0156	0.54	0.232	1.068	0.022
3	0.111	0.0228	0.87	0.339	1.023	0.024
4	0.148	0.0302	1.19	0.450	0.999	0.025
5	0.185	0.0357	2.82	0.530	0.926	0.050
6	0.222	0.0374	5.64	0.554	0.793	0.095
7	0.259	0.0368	14.11	0.545	0.658	0.243
8	0.296	0.0378	16.17	0.559	0.581	0.271
9	0.333	0.0384	17.15	0.568	0.516	0.283
10	0.370	0.0391	18.99	0.577	0.465	0.308

Test Filename   **D30B**

Engine Details

Configuration	IL4	Inner Seat Dia, mm	27	Shape Factor, LD	9.88
Cylinder bore	80	Seat Angle	45	Lmax/D	0.31
Engine Stroke	90	Max Valve Lift	8.37	D/B	0.338
Inlet Valves, n	1	Valve Opens	0	MIGV	118.5
Rated Speed, rpm	4500	Valve Closes	50	MPV	13.5

Test Details

Test Date	08-Nov-00	Barometer, mmHg	742	VFAM Constant	77.21
Test Pressure, mmH$_2$O	900	ISM Constant	1.09E-04		

Test Summary Results

Swirl Ratio (Rs)	1.56	Gulp Factor	0.806	Cf @ 0.3 L/D	0.542
Rs/LD	0.16	MCf	0.428	Cf @ Max Lift	0.544
CCf	1.719				

Test Results

Valve Lift		Air Flow	ISM Torque	Flow	Discharge	Non-dim
Test	Non-dim	m^3/s	NmE^{-3}	Coefficient	Coefficient	Rig Swirl
mm	L/D	Q	G	Cf	Cd	Ns
0	0.000	0.0000	0.00	0.000	0.000	0.000
1	0.037	0.0080	0.00	0.118	1.107	0.000
2	0.074	0.0157	2.06	0.233	1.073	0.088
3	0.111	0.0226	3.04	0.336	1.014	0.089
4	0.148	0.0294	4.67	0.436	0.970	0.106
5	0.185	0.0335	9.01	0.497	0.869	0.179
6	0.222	0.0348	13.02	0.516	0.739	0.250
7	0.259	0.0358	16.93	0.531	0.641	0.315
8	0.296	0.0365	20.41	0.541	0.562	0.373
9	0.333	0.0370	23.88	0.548	0.498	0.431
10	0.370	0.0374	25.72	0.554	0.446	0.460

Test Filename   **D30A**

Engine Details

Configuration	IL4	Inner Seat Dia, mm	27	Shape Factor, LD	9.88
Cylinder bore	80	Seat Angle	45	Lmax/D	0.31
Engine Stroke	90	Max Valve Lift	8.37	D/B	0.338
Inlet Valves, n	1	Valve Opens	0	MIGV	118.5
Rated Speed, rpm	4500	Valve Closes	50	MPV	13.5

Test Details

Test Date	08-Nov-00	Barometer, mmHg	741.6	VFAM Constant	77.22
Test Pressure, mmH$_2$O	900	ISM Constant	1.09E-04		

Test Summary Results

Swirl Ratio (Rs)	0.5	Gulp Factor	0.803	Cf @ 0.3 L/D	0.539
Rs/LD	0.05	MCf	0.43	Cf @ Max Lift	0.541
CCf	1.727				

Test Results

Valve Lift		Air Flow	ISM Torque	Flow	Discharge	Non-dim
Test	Non-dim	m^3/s	NmE^{-3}	Coefficient	Coefficient	Rig Swirl
mm	L/D	Q	G	Cf	Cd	Ns
0	0.000	0.0000	0.00	0.000	0.000	0.000
1	0.037	0.0080	-0.22	0.118	1.109	-0.018
2	0.074	0.0154	0.54	0.229	1.053	0.023
3	0.111	0.0227	0.00	0.337	1.015	0.000
4	0.148	0.0297	-0.11	0.440	0.979	-0.002
5	0.185	0.0345	-0.87	0.511	0.893	-0.017
6	0.222	0.0360	-1.09	0.533	0.764	-0.020
7	0.259	0.0358	6.95	0.529	0.638	0.130
8	0.296	0.0364	9.66	0.538	0.559	0.178
9	0.333	0.0370	12.27	0.547	0.497	0.222
10	0.370	0.0375	14.11	0.553	0.446	0.252

C13

Test Filename   **D10AB**

Engine Details

Configuration	IL4	Inner Seat Dia, mm	27	Shape Factor, LD	11.11
Cylinder bore	90	Seat Angle	45	Lmax/D	0.31
Engine Stroke	90	Max Valve Lift	8.37	D/B	0.3
Inlet Valves, n	1	Valve Opens	0	MIGV	150
Rated Speed, rpm	4500	Valve Closes	50	MPV	13.5

Test Details

Test Date	08-Nov-00	Barometer, mmHg	741.2	VFAM Constant	77.22
Test Pressure, mmH_2O	900	ISM Constant	1.09E-04		

Test Summary Results

Swirl Ratio (Rs)	0.88	Gulp Factor	1.009	Cf @ 0.3 L/D	0.549
Rs/LD	0.08	MCf	0.433	Cf @ Max Lift	0.551
CCf	1.739				

Test Results

Valve Lift		Air Flow	ISM Torque	Flow	Discharge	Non-dim
Test	Non-dim	m^3/s	NmE^{-3}	Coefficient	Coefficient	Rig Swirl
mm	L/D	Q	G	Cf	Cd	Ns
0	0.000	0.0000	0.00	0.000	0.000	0.000
1	0.037	0.0079	-0.54	0.117	1.097	-0.041
2	0.074	0.0156	-0.33	0.232	1.066	-0.012
3	0.111	0.0229	0.54	0.340	1.024	0.014
4	0.148	0.0298	3.80	0.442	0.983	0.076
5	0.185	0.0336	7.38	0.499	0.872	0.130
6	0.222	0.0354	9.33	0.525	0.751	0.156
7	0.259	0.0362	9.99	0.538	0.649	0.163
8	0.296	0.0369	11.07	0.548	0.569	0.178
9	0.333	0.0376	12.48	0.557	0.507	0.197
10	0.370	0.0380	13.13	0.563	0.453	0.205

Test Filename   **D14B**

Engine Details

Configuration	IL4	Inner Seat Dia, mm	27	Shape Factor, LD	11.11
Cylinder bore	90	Seat Angle	45	Lmax/D	0.31
Engine Stroke	90	Max Valve Lift	8.37	D/B	0.3
Inlet Valves, n	1	Valve Opens	0	MIGV	150
Rated Speed, rpm	4500	Valve Closes	50	MPV	13.5

Test Details

Test Date	07-Nov-00	Barometer, mmHg	734.6	VFAM Constant	77.25
Test Pressure, mmH$_2$O	900	ISM Constant	1.09E-04		

Test Summary Results

Swirl Ratio (Rs)	2.29	Gulp Factor	1.023	Cf @ 0.3 L/D	0.537
Rs/LD	0.21	MCf	0.427	Cf @ Max Lift	0.538
CCf	1.715				

Test Results

Valve Lift		Air Flow	ISM Torque	Flow	Discharge	Non-dim
Test	Non-dim	m^3/s	NmE^{-3}	Coefficient	Coefficient	Rig Swirl
mm	L/D	Q	G	Cf	Cd	Ns
0	0.000	0.0000	0.00	0.000	0.000	0.000
1	0.037	0.0079	0.00	0.117	1.097	0.000
2	0.074	0.0155	2.61	0.229	1.053	0.100
3	0.111	0.0229	3.80	0.337	1.015	0.099
4	0.148	0.0298	5.75	0.439	0.975	0.115
5	0.185	0.0336	12.16	0.495	0.865	0.216
6	0.222	0.0355	19.43	0.522	0.748	0.327
7	0.259	0.0362	25.84	0.532	0.643	0.427
8	0.296	0.0365	30.07	0.536	0.558	0.493
9	0.333	0.0369	35.07	0.541	0.492	0.570
10	0.370	0.0372	36.15	0.545	0.439	0.583

Test Filename   **D14A**

Engine Details

Configuration	IL4	Inner Seat Dia, mm	27	Shape Factor, LD	11.11
Cylinder bore	90	Seat Angle	45	Lmax/D	0.31
Engine Stroke	90	Max Valve Lift	8.37	D/B	0.3
Inlet Valves, n	1	Valve Opens	0	MIGV	150
Rated Speed, rpm	4500	Valve Closes	50	MPV	13.5

Test Details

Test Date	07-Nov-00	Barometer, mmHg	734.4	VFAM Constant	77.25
Test Pressure, mmH$_2$O	900	ISM Constant	1.09E-04		

Test Summary Results

Swirl Ratio (Rs)	1.2	Gulp Factor	1.017	Cf @ 0.3 L/D	0.541
Rs/LD	0.11	MCf	0.43	Cf @ Max Lift	0.54
CCf	1.726				

Test Results

Valve Lift		Air Flow	ISM Torque	Flow	Discharge	Non-dim
Test	Non-dim	m^3/s	NmE^{-3}	Coefficient	Coefficient	Rig Swirl
mm	L/D	Q	G	Cf	Cd	Ns
0	0.000	0.0000	0.00	0.000	0.000	0.000
1	0.037	0.0079	0.43	0.117	1.096	0.033
2	0.074	0.0155	1.63	0.229	1.052	0.063
3	0.111	0.0227	1.41	0.335	1.010	0.037
4	0.148	0.0295	0.76	0.435	0.966	0.015
5	0.185	0.0347	0.33	0.512	0.895	0.006
6	0.222	0.0356	7.49	0.524	0.750	0.126
7	0.259	0.0363	13.03	0.534	0.645	0.215
8	0.296	0.0368	19.43	0.541	0.563	0.316
9	0.333	0.0367	24.32	0.539	0.490	0.397
10	0.370	0.0370	26.82	0.543	0.437	0.434

Test Filename   **D26AB**

Engine Details

Configuration	IL4	Inner Seat Dia, mm	27	Shape Factor, LD	9.88
Cylinder bore	80	Seat Angle	45	Lmax/D	0.31
Engine Stroke	90	Max Valve Lift	8.37	D/B	0.338
Inlet Valves, n	1	Valve Opens	0	MIGV	118.5
Rated Speed, rpm	4500	Valve Closes	50	MPV	13.5

Test Details

Test Date	07-Nov-00	Barometer, mmHg	734.2	VFAM Constant	77.25
Test Pressure, mmH$_2$O	900	ISM Constant	1.09E-04		

Test Summary Results

Swirl Ratio (Rs)	1.26	Gulp Factor	0.797	Cf @ 0.3 L/D	0.551
Rs/LD	0.13	MCf	0.433	Cf @ Max Lift	0.554
CCf	1.739				

Test Results

Valve Lift		Air Flow	ISM Torque	Flow	Discharge	Non-dim
Test	Non-dim	m^3/s	NmE^{-3}	Coefficient	Coefficient	Rig Swirl
mm	L/D	Q	G	Cf	Cd	Ns
0	0.000	0.0000	0.00	0.000	0.000	0.000
1	0.037	0.0079	0.33	0.117	1.094	0.028
2	0.074	0.0159	-0.22	0.235	1.082	-0.009
3	0.111	0.0234	1.09	0.346	1.043	0.031
4	0.148	0.0296	4.13	0.438	0.972	0.093
5	0.185	0.0338	8.36	0.500	0.874	0.165
6	0.222	0.0353	12.92	0.522	0.747	0.245
7	0.259	0.0362	14.87	0.534	0.644	0.276
8	0.296	0.0373	16.29	0.550	0.571	0.293
9	0.333	0.0381	17.15	0.562	0.511	0.302
10	0.370	0.0388	17.37	0.572	0.461	0.300

Test Filename   **D51B**

Engine Details

Configuration	IL4	Inner Seat Dia, mm	27	Shape Factor, LD	10.43
Cylinder bore	84.5	Seat Angle	45	Lmax/D	0.31
Engine Stroke	90	Max Valve Lift	8.37	D/B	0.32
Inlet Valves, n	1	Valve Opens	0	MIGV	132.2
Rated Speed, rpm	4500	Valve Closes	50	MPV	13.5

Test Details

Test Date	09-Nov-00	Barometer, mmHg	754.8	VFAM Constant	77.16
Test Pressure, mmH$_2$O	900	ISM Constant	1.09E-04		

Test Summary Results

Swirl Ratio (Rs)	1.76	Gulp Factor	0.871	Cf @ 0.3 L/D	0.566
Rs/LD	0.17	MCf	0.442	Cf @ Max Lift	0.568
CCf	1.775				

Test Results

Valve Lift		Air Flow	ISM Torque	Flow	Discharge	Non-dim
Test	Non-dim	m^3/s	NmE^{-3}	Coefficient	Coefficient	Rig Swirl
mm	L/D	Q	G	Cf	Cd	Ns
0	0.000	0.0000	0.00	0.000	0.000	0.000
1	0.037	0.0079	1.84	0.118	1.104	0.147
2	0.074	0.0153	3.25	0.229	1.052	0.133
3	0.111	0.0224	4.12	0.335	1.010	0.115
4	0.148	0.0300	6.73	0.448	0.996	0.141
5	0.185	0.0348	8.68	0.520	0.908	0.156
6	0.222	0.0355	15.73	0.529	0.757	0.279
7	0.259	0.0369	21.37	0.550	0.664	0.364
8	0.296	0.0379	23.98	0.565	0.587	0.398
9	0.333	0.0386	25.49	0.574	0.522	0.416
10	0.370	0.0393	27.45	0.584	0.470	0.440

Test Filename   **D51A**

Engine Details

Configuration	IL4	Inner Seat Dia, mm	27	Shape Factor, LD	10.43
Cylinder bore	84.5	Seat Angle	45	Lmax/D	0.31
Engine Stroke	90	Max Valve Lift	8.37	D/B	0.32
Inlet Valves, n	1	Valve Opens	0	MIGV	132.2
Rated Speed, rpm	4500	Valve Closes	50	MPV	13.5

Test Details

Test Date	09-Nov-00	Barometer, mmHg	754.5	VFAM Constant	77.16
Test Pressure, mmH$_2$O	900	ISM Constant	1.09E-04		

Test Summary Results

Swirl Ratio (Rs)	1	Gulp Factor	0.861	Cf @ 0.3 L/D	0.564
Rs/LD	0.1	MCf	0.447	Cf @ Max Lift	0.566
CCf	1.795				

Test Results

Valve Lift		Air Flow	ISM Torque	Flow	Discharge	Non-dim
Test	Non-dim	m^3/s	NmE^{-3}	Coefficient	Coefficient	Rig Swirl
mm	L/D	Q	G	Cf	Cd	Ns
0	0.000	0.0000	0.00	0.000	0.000	0.000
1	0.037	0.0079	-0.43	0.118	1.110	-0.034
2	0.074	0.0154	0.65	0.231	1.063	0.026
3	0.111	0.0229	1.08	0.343	1.034	0.030
4	0.148	0.0304	1.19	0.455	1.011	0.025
5	0.185	0.0356	2.82	0.533	0.931	0.050
6	0.222	0.0373	6.18	0.558	0.799	0.104
7	0.259	0.0368	14.32	0.549	0.663	0.244
8	0.296	0.0377	16.38	0.563	0.585	0.273
9	0.333	0.0384	17.57	0.573	0.521	0.287
10	0.370	0.0392	19.53	0.583	0.470	0.314

Test Filename   **D15B**

Engine Details

Configuration	IL4	Inner Seat Dia, mm	27	Shape Factor, LD	11.11
Cylinder bore	90	Seat Angle	45	Lmax/D	0.31
Engine Stroke	90	Max Valve Lift	8.37	D/B	0.3
Inlet Valves, n	1	Valve Opens	0	MIGV	150
Rated Speed, rpm	4500	Valve Closes	50	MPV	13.5

Test Details

Test Date	09-Nov-00	Barometer, mmHg	753.6	VFAM Constant	77.16
Test Pressure, mmH$_2$O	900	ISM Constant	1.09E-04		

Test Summary Results

Swirl Ratio (Rs)	2.6	Gulp Factor	1.022	Cf @ 0.3 L/D	0.535
Rs/LD	0.23	MCf	0.428	Cf @ Max Lift	0.537
CCf	1.717				

Test Results

Valve Lift		Air Flow	ISM Torque	Flow	Discharge	Non-dim
Test	Non-dim	m^3/s	NmE^{-3}	Coefficient	Coefficient	Rig Swirl
mm	L/D	Q	G	Cf	Cd	Ns
0	0.000	0.0000	0.00	0.000	0.000	0.000
1	0.037	0.0079	-1.74	0.118	1.108	-0.129
2	0.074	0.0155	1.19	0.232	1.066	0.045
3	0.111	0.0227	3.69	0.340	1.024	0.096
4	0.148	0.0295	6.62	0.441	0.981	0.132
5	0.185	0.0346	12.37	0.518	0.905	0.210
6	0.222	0.0345	22.02	0.515	0.737	0.376
7	0.259	0.0352	30.27	0.526	0.635	0.506
8	0.296	0.0359	35.80	0.534	0.555	0.589
9	0.333	0.0364	37.65	0.542	0.492	0.611
10	0.370	0.0368	39.17	0.547	0.441	0.630

Test Filename   **D15A**

Engine Details

Configuration	IL4	Inner Seat Dia, mm	27	Shape Factor, LD	11.11
Cylinder bore	90	Seat Angle	45	Lmax/D	0.31
Engine Stroke	90	Max Valve Lift	8.37	D/B	0.3
Inlet Valves, n	1	Valve Opens	0	MIGV	150
Rated Speed, rpm	4500	Valve Closes	50	MPV	13.5

Test Details

Test Date	09-Nov-00	Barometer, mmHg	753.2	VFAM Constant	77.16
Test Pressure, mmH_2O	900	ISM Constant	1.09E-04		

Test Summary Results

Swirl Ratio (Rs)	2.1	Gulp Factor	1.017	Cf @ 0.3 L/D	0.534
Rs/LD	0.19	MCf	0.43	Cf @ Max Lift	0.536
CCf	1.725				

Test Results

Valve Lift		Air Flow	ISM Torque	Flow	Discharge	Non-dim
Test	Non-dim	m^3/s	NmE^{-3}	Coefficient	Coefficient	Rig Swirl
mm	L/D	Q	G	Cf	Cd	Ns
0	0.000	0.0000	0.00	0.000	0.000	0.000
1	0.037	0.0079	-1.52	0.118	1.104	-0.113
2	0.074	0.0153	0.54	0.229	1.054	0.021
3	0.111	0.0227	1.52	0.338	1.020	0.039
4	0.148	0.0298	2.82	0.445	0.988	0.056
5	0.185	0.0353	5.42	0.525	0.918	0.091
6	0.222	0.0350	18.01	0.520	0.745	0.304
7	0.259	0.0358	25.60	0.532	0.643	0.423
8	0.296	0.0358	31.14	0.533	0.554	0.514
9	0.333	0.0364	34.28	0.541	0.491	0.558
10	0.370	0.0368	36.24	0.546	0.440	0.583

Test Filename   **D11AB**

Engine Details

Configuration	IL4	Inner Seat Dia, mm	27	Shape Factor, LD	11.11
Cylinder bore	90	Seat Angle	45	Lmax/D	0.31
Engine Stroke	90	Max Valve Lift	8.37	D/B	0.3
Inlet Valves, n	1	Valve Opens	0	MIGV	150
Rated Speed, rpm	4500	Valve Closes	50	MPV	13.5

Test Details

Test Date	09-Nov-00	Barometer, mmHg	753.3	VFAM Constant	77.16
Test Pressure, mmH$_2$O	900	ISM Constant	1.09E-04		

Test Summary Results

Swirl Ratio (Rs)	0.54	Gulp Factor	1.018	Cf @ 0.3 L/D	0.544
Rs/LD	0.05	MCf	0.429	Cf @ Max Lift	0.547
CCf	1.724				

Test Results

Valve Lift		Air Flow	ISM Torque	Flow	Discharge	Non-dim
Test	Non-dim	m^3/s	NmE^{-3}	Coefficient	Coefficient	Rig Swirl
mm	L/D	Q	G	Cf	Cd	Ns
0	0.000	0.0000	0.00	0.000	0.000	0.000
1	0.037	0.0079	-0.33	0.119	1.111	-0.024
2	0.074	0.0156	-0.43	0.233	1.073	-0.016
3	0.111	0.0228	0.76	0.340	1.025	0.020
4	0.148	0.0297	3.04	0.443	0.984	0.060
5	0.185	0.0336	4.67	0.502	0.876	0.082
6	0.222	0.0345	7.38	0.514	0.736	0.126
7	0.259	0.0354	6.29	0.528	0.637	0.105
8	0.296	0.0365	5.75	0.543	0.564	0.093
9	0.333	0.0372	5.64	0.553	0.503	0.090
10	0.370	0.0379	5.42	0.562	0.453	0.085

Test Filename   **D27AB**

Engine Details

Configuration	IL4	Inner Seat Dia, mm	27	Shape Factor, LD	9.88
Cylinder bore	80	Seat Angle	45	Lmax/D	0.31
Engine Stroke	90	Max Valve Lift	8.37	D/B	0.338
Inlet Valves, n	1	Valve Opens	0	MIGV	118.5
Rated Speed, rpm	4500	Valve Closes	50	MPV	13.5

Test Details

Test Date	09-Nov-00	Barometer, mmHg	753.3	VFAM Constant	77.16
Test Pressure, mmH$_2$O	900	ISM Constant	1.09E-04		

Test Summary Results

Swirl Ratio (Rs)	0.75	Gulp Factor	0.799	Cf @ 0.3 L/D	0.551
Rs/LD	0.08	MCf	0.432	Cf @ Max Lift	0.555
CCf	1.734				

Test Results

Valve Lift		Air Flow	ISM Torque	Flow	Discharge	Non-dim
Test	Non-dim	m^3/s	NmE^{-3}	Coefficient	Coefficient	Rig Swirl
mm	L/D	Q	G	Cf	Cd	Ns
0	0.000	0.0000	0.00	0.000	0.000	0.000
1	0.037	0.0079	-0.65	0.119	1.116	-0.054
2	0.074	0.0156	-0.33	0.234	1.075	-0.014
3	0.111	0.0227	0.43	0.340	1.024	0.013
4	0.148	0.0292	2.06	0.437	0.970	0.047
5	0.185	0.0335	2.93	0.501	0.875	0.058
6	0.222	0.0349	3.58	0.521	0.746	0.068
7	0.259	0.0355	10.85	0.529	0.639	0.203
8	0.296	0.0369	11.17	0.549	0.571	0.201
9	0.333	0.0379	11.07	0.565	0.513	0.194
10	0.370	0.0383	9.44	0.571	0.460	0.164

Test Filename   **D31B**

Engine Details

Configuration	IL4	Inner Seat Dia, mm	27	Shape Factor, LD	9.88
Cylinder bore	80	Seat Angle	45	Lmax/D	0.31
Engine Stroke	90	Max Valve Lift	8.37	D/B	0.338
Inlet Valves, n	1	Valve Opens	0	MIGV	118.5
Rated Speed, rpm	4500	Valve Closes	50	MPV	13.5

Test Details

Test Date	09-Nov-00	Barometer, mmHg	753.1	VFAM Constant	77.16
Test Pressure, mmH_2O	900	ISM Constant	1.09E-04		

Test Summary Results

Swirl Ratio (Rs)	1.75	Gulp Factor	0.801	Cf @ 0.3 L/D	0.542
Rs/LD	0.18	MCf	0.431	Cf @ Max Lift	0.545
CCf	1.731				

Test Results

Valve Lift		Air Flow	ISM Torque	Flow	Discharge	Non-dim
Test	Non-dim	m^3/s	NmE^{-3}	Coefficient	Coefficient	Rig Swirl
mm	L/D	Q	G	Cf	Cd	Ns
0	0.000	0.0000	0.00	0.000	0.000	0.000
1	0.037	0.0080	-1.19	0.119	1.120	-0.099
2	0.074	0.0157	0.98	0.236	1.088	0.041
3	0.111	0.0229	2.28	0.344	1.036	0.066
4	0.148	0.0300	4.67	0.450	1.000	0.103
5	0.185	0.0336	11.07	0.504	0.880	0.217
6	0.222	0.0345	15.41	0.517	0.741	0.295
7	0.259	0.0354	19.31	0.530	0.640	0.360
8	0.296	0.0361	24.09	0.541	0.562	0.440
9	0.333	0.0369	27.56	0.552	0.502	0.494
10	0.370	0.0375	29.73	0.561	0.452	0.525

Test Filename   **D31A**

Engine Details

Configuration	IL4	Inner Seat Dia, mm	27	Shape Factor, LD	9.88
Cylinder bore	80	Seat Angle	45	Lmax/D	0.31
Engine Stroke	90	Max Valve Lift	8.37	D/B	0.338
Inlet Valves, n	1	Valve Opens	0	MIGV	118.5
Rated Speed, rpm	4500	Valve Closes	50	MPV	13.5

Test Details

Test Date	09-Nov-00	Barometer, mmHg	752.9	VFAM Constant	77.17
Test Pressure, mmH$_2$O	900	ISM Constant	1.09E-04		

Test Summary Results

Swirl Ratio (Rs)	1.08	Gulp Factor	0.802	Cf @ 0.3 L/D	0.538
Rs/LD	0.11	MCf	0.431	Cf @ Max Lift	0.541
CCf	1.728				

Test Results

Valve Lift		Air Flow	ISM Torque	Flow	Discharge	Non-dim
Test	Non-dim	m^3/s	NmE^{-3}	Coefficient	Coefficient	Rig Swirl
mm	L/D	Q	G	Cf	Cd	Ns
0	0.000	0.0000	0.00	0.000	0.000	0.000
1	0.037	0.0078	-1.08	0.118	1.108	-0.091
2	0.074	0.0156	0.00	0.235	1.081	0.000
3	0.111	0.0229	0.76	0.344	1.037	0.022
4	0.148	0.0300	1.52	0.451	1.002	0.033
5	0.185	0.0343	4.01	0.516	0.902	0.077
6	0.222	0.0346	8.79	0.519	0.744	0.167
7	0.259	0.0351	12.48	0.527	0.636	0.234
8	0.296	0.0358	16.17	0.537	0.558	0.298
9	0.333	0.0366	20.51	0.548	0.499	0.370
10	0.370	0.0373	23.22	0.559	0.450	0.411

Test Filename　　　**D50B**

Engine Details

Configuration	IL4	Inner Seat Dia, mm	27	Shape Factor, LD	10.43
Cylinder bore	84.5	Seat Angle	45	Lmax/D	0.31
Engine Stroke	90	Max Valve Lift	8.37	D/B	0.32
Inlet Valves, n	1	Valve Opens	0	MIGV	132.2
Rated Speed, rpm	4500	Valve Closes	50	MPV	13.5

Test Details

Test Date	08-Nov-00	Barometer, mmHg	744.4	VFAM Constant	77.2
Test Pressure, mmH_2O	900	ISM Constant	1.09E-04		

Test Summary Results

Swirl Ratio (Rs)	1.74	Gulp Factor	0.873	Cf @ 0.3 L/D	0.566
Rs/LD	0.17	MCf	0.441	Cf @ Max Lift	0.568
CCf	1.771				

Test Results

Valve Lift		Air Flow	ISM Torque	Flow	Discharge	Non-dim
Test	Non-dim	m^3/s	NmE^{-3}	Coefficient	Coefficient	Rig Swirl
mm	L/D	Q	G	Cf	Cd	Ns
0	0.000	0.0000	0.00	0.000	0.000	0.000
1	0.037	0.0079	1.74	0.117	1.097	0.139
2	0.074	0.0154	3.04	0.227	1.044	0.126
3	0.111	0.0226	4.12	0.334	1.006	0.116
4	0.148	0.0301	6.51	0.443	0.985	0.138
5	0.185	0.0350	8.47	0.516	0.901	0.154
6	0.222	0.0359	15.41	0.529	0.757	0.273
7	0.259	0.0373	21.05	0.549	0.663	0.359
8	0.296	0.0384	23.77	0.565	0.587	0.394
9	0.333	0.0389	25.29	0.572	0.520	0.414
10	0.370	0.0396	27.35	0.582	0.468	0.440

Test Filename   **D50A**

Engine Details

Configuration	IL4	Inner Seat Dia, mm	27	Shape Factor, LD	10.43
Cylinder bore	84.5	Seat Angle	45	Lmax/D	0.31
Engine Stroke	90	Max Valve Lift	8.37	D/B	0.32
Inlet Valves, n	1	Valve Opens	0	MIGV	132.2
Rated Speed, rpm	4500	Valve Closes	50	MPV	13.5

Test Details

Test Date	08-Nov-00	Barometer, mmHg	744.3	VFAM Constant	77.2
Test Pressure, mmH$_2$O	900	ISM Constant	1.09E-04		

Test Summary Results

Swirl Ratio (Rs)	0.99	Gulp Factor	0.868	Cf @ 0.3 L/D	0.56
Rs/LD	0.09	MCf	0.444	Cf @ Max Lift	0.562
CCf	1.781				

Test Results

Valve Lift		Air Flow	ISM Torque	Flow	Discharge	Non-dim
Test	Non-dim	m^3/s	NmE^{-3}	Coefficient	Coefficient	Rig Swirl
mm	L/D	Q	G	Cf	Cd	Ns
0	0.000	0.0000	0.00	0.000	0.000	0.000
1	0.037	0.0080	-0.33	0.118	1.106	-0.026
2	0.074	0.0153	0.98	0.227	1.046	0.040
3	0.111	0.0228	1.09	0.339	1.022	0.030
4	0.148	0.0302	1.19	0.448	0.996	0.025
5	0.185	0.0360	2.82	0.534	0.932	0.050
6	0.222	0.0375	5.64	0.554	0.793	0.095
7	0.259	0.0369	14.11	0.544	0.656	0.243
8	0.296	0.0379	15.95	0.559	0.581	0.267
9	0.333	0.0385	17.36	0.568	0.516	0.287
10	0.370	0.0392	19.10	0.578	0.465	0.310

Test Filename　　　　**D25AB**

Engine Details

Configuration	IL4	Inner Seat Dia, mm	27	Shape Factor, LD	11.11
Cylinder bore	90	Seat Angle	45	Lmax/D	0.31
Engine Stroke	90	Max Valve Lift	8.37	D/B	0.3
Inlet Valves, n	1	Valve Opens	0	MIGV	150
Rated Speed, rpm	4500	Valve Closes	50	MPV	13.5

Test Details

Test Date	08-Nov-00	Barometer, mmHg	744	VFAM Constant	77.21
Test Pressure, mmH$_2$O	900	ISM Constant	1.09E-04		

Test Summary Results

Swirl Ratio (Rs)	0.77	Gulp Factor	1.022	Cf @ 0.3 L/D	0.542
Rs/LD	0.07	MCf	0.428	Cf @ Max Lift	0.545
CCf	1.717				

Test Results

Valve Lift		Air Flow	ISM Torque	Flow	Discharge	Non-dim
Test	Non-dim	m^3/s	NmE^{-3}	Coefficient	Coefficient	Rig Swirl
mm	L/D	Q	G	Cf	Cd	Ns
0	0.000	0.0000	0.00	0.000	0.000	0.000
1	0.037	0.0080	1.41	0.119	1.112	0.105
2	0.074	0.0156	1.63	0.232	1.066	0.062
3	0.111	0.0228	2.17	0.338	1.020	0.056
4	0.148	0.0296	5.54	0.439	0.975	0.111
5	0.185	0.0338	8.03	0.500	0.875	0.141
6	0.222	0.0349	6.62	0.516	0.738	0.113
7	0.259	0.0355	6.84	0.524	0.633	0.115
8	0.296	0.0366	8.14	0.540	0.561	0.133
9	0.333	0.0376	9.01	0.555	0.504	0.143
10	0.370	0.0382	9.66	0.563	0.453	0.151

Test Filename   **D13B**

Engine Details

Configuration	IL4	Inner Seat Dia, mm	27	Shape Factor, LD	11.11
Cylinder bore	90	Seat Angle	45	Lmax/D	0.31
Engine Stroke	90	Max Valve Lift	8.37	D/B	0.3
Inlet Valves, n	1	Valve Opens	0	MIGV	150
Rated Speed, rpm	4500	Valve Closes	50	MPV	13.5

Test Details

Test Date	08-Nov-00	Barometer, mmHg	743.9	VFAM Constant	77.21
Test Pressure, mmH$_2$O	900	ISM Constant	1.09E-04		

Test Summary Results

Swirl Ratio (Rs)	2.35	Gulp Factor	1.029	Cf @ 0.3 L/D	0.533
Rs/LD	0.21	MCf	0.425	Cf @ Max Lift	0.535
CCf	1.705				

Test Results

Valve Lift		Air Flow	ISM Torque	Flow	Discharge	Non-dim
Test	Non-dim	m^3/s	NmE^{-3}	Coefficient	Coefficient	Rig Swirl
mm	L/D	Q	G	Cf	Cd	Ns
0	0.000	0.0000	0.00	0.000	0.000	0.000
1	0.037	0.0080	0.65	0.119	1.114	0.048
2	0.074	0.0157	3.15	0.234	1.077	0.118
3	0.111	0.0228	4.34	0.340	1.023	0.112
4	0.148	0.0297	7.60	0.441	0.979	0.152
5	0.185	0.0337	14.33	0.500	0.874	0.252
6	0.222	0.0345	20.08	0.512	0.733	0.345
7	0.259	0.0352	24.75	0.521	0.629	0.418
8	0.296	0.0359	29.85	0.532	0.553	0.493
9	0.333	0.0364	32.67	0.539	0.490	0.533
10	0.370	0.0368	34.40	0.544	0.439	0.556

Test Filename **D13A**

Engine Details

Configuration	IL4	Inner Seat Dia, mm	27	Shape Factor, LD	11.11
Cylinder bore	90	Seat Angle	45	Lmax/D	0.31
Engine Stroke	90	Max Valve Lift	8.37	D/B	0.3
Inlet Valves, n	1	Valve Opens	0	MIGV	150
Rated Speed, rpm	4500	Valve Closes	50	MPV	13.5

Test Details

Test Date	08-Nov-00	Barometer, mmHg	743.4	VFAM Constant	77.21
Test Pressure, mmH$_2$O	900	ISM Constant	1.09E-04		

Test Summary Results

Swirl Ratio (Rs)	1.48	Gulp Factor	1.026	Cf @ 0.3 L/D	0.531
Rs/LD	0.13	MCf	0.426	Cf @ Max Lift	0.533
CCf	1.71				

Test Results

Valve Lift		Air Flow	ISM Torque	Flow	Discharge	Non-dim
Test	Non-dim	m^3/s	NmE^{-3}	Coefficient	Coefficient	Rig Swirl
mm	L/D	Q	G	Cf	Cd	Ns
0	0.000	0.0000	0.00	0.000	0.000	0.000
1	0.037	0.0082	0.43	0.121	1.133	0.032
2	0.074	0.0156	1.41	0.231	1.062	0.054
3	0.111	0.0229	1.52	0.338	1.019	0.040
4	0.148	0.0298	2.28	0.441	0.980	0.045
5	0.185	0.0352	5.10	0.519	0.907	0.086
6	0.222	0.0348	12.37	0.514	0.736	0.212
7	0.259	0.0354	17.04	0.522	0.630	0.287
8	0.296	0.0359	20.62	0.530	0.550	0.342
9	0.333	0.0366	23.44	0.538	0.490	0.383
10	0.370	0.0369	24.64	0.543	0.437	0.399

Test Filename   **D9AB**

Engine Details

Configuration	IL4	Inner Seat Dia, mm	27	Shape Factor, LD	11.11
Cylinder bore	90	Seat Angle	45	Lmax/D	0.31
Engine Stroke	90	Max Valve Lift	8.37	D/B	0.3
Inlet Valves, n	1	Valve Opens	0	MIGV	150
Rated Speed, rpm	4500	Valve Closes	50	MPV	13.5

Test Details

Test Date	08-Nov-00	Barometer, mmHg	743.4	VFAM Constant	77.21
Test Pressure, mmH$_2$O	900	ISM Constant	1.09E-04		

Test Summary Results

Swirl Ratio (Rs)	1.21	Gulp Factor	1.018	Cf @ 0.3 L/D	0.547
Rs/LD	0.11	MCf	0.429	Cf @ Max Lift	0.551
CCf	1.723				

Test Results

Valve Lift		Air Flow	ISM Torque	Flow	Discharge	Non-dim
Test	Non-dim	m^3/s	NmE^{-3}	Coefficient	Coefficient	Rig Swirl
mm	L/D	Q	G	Cf	Cd	Ns
0	0.000	0.0000	0.00	0.000	0.000	0.000
1	0.037	0.0080	2.17	0.118	1.107	0.162
2	0.074	0.0156	1.85	0.230	1.060	0.070
3	0.111	0.0227	3.26	0.337	1.016	0.085
4	0.148	0.0292	6.51	0.433	0.961	0.132
5	0.185	0.0331	8.90	0.490	0.855	0.160
6	0.222	0.0347	9.77	0.513	0.735	0.167
7	0.259	0.0362	12.05	0.535	0.646	0.198
8	0.296	0.0370	14.33	0.546	0.568	0.231
9	0.333	0.0378	18.23	0.558	0.507	0.287
10	0.370	0.0381	20.51	0.562	0.453	0.321

Test Filename   **D29B**

Engine Details

Configuration	IL4	Inner Seat Dia, mm	27	Shape Factor, LD	9.88
Cylinder bore	80	Seat Angle	45	Lmax/D	0.31
Engine Stroke	90	Max Valve Lift	8.37	D/B	0.338
Inlet Valves, n	1	Valve Opens	0	MIGV	118.5
Rated Speed, rpm	4500	Valve Closes	50	MPV	13.5

Test Details

Test Date	08-Nov-00	Barometer, mmHg	743.3	VFAM Constant	77.21
Test Pressure, mmH$_2$O	900	ISM Constant	1.09E-04		

Test Summary Results

Swirl Ratio (Rs)	2.55	Gulp Factor	0.81	Cf @ 0.3 L/D	0.531
Rs/LD	0.26	MCf	0.426	Cf @ Max Lift	0.532
CCf	1.712				

Test Results

Valve Lift		Air Flow	ISM Torque	Flow	Discharge	Non-dim
Test	Non-dim	m^3/s	NmE^{-3}	Coefficient	Coefficient	Rig Swirl
mm	L/D	Q	G	Cf	Cd	Ns
0	0.000	0.0000	0.00	0.000	0.000	0.000
1	0.037	0.0080	0.65	0.118	1.110	0.054
2	0.074	0.0156	3.15	0.231	1.065	0.135
3	0.111	0.0227	5.21	0.337	1.016	0.153
4	0.148	0.0293	7.71	0.435	0.966	0.175
5	0.185	0.0342	12.26	0.507	0.885	0.239
6	0.222	0.0356	24.09	0.527	0.754	0.453
7	0.259	0.0356	29.30	0.527	0.636	0.550
8	0.296	0.0359	32.13	0.531	0.552	0.599
9	0.333	0.0362	34.19	0.536	0.487	0.632
10	0.370	0.0364	34.73	0.539	0.434	0.638

Test Filename   **D29A**

Engine Details

Configuration	IL4	Inner Seat Dia, mm	27	Shape Factor, LD	9.88
Cylinder bore	80	Seat Angle	45	Lmax/D	0.31
Engine Stroke	90	Max Valve Lift	8.37	D/B	0.338
Inlet Valves, n	1	Valve Opens	0	MIGV	118.5
Rated Speed, rpm	4500	Valve Closes	50	MPV	13.5

Test Details

Test Date	08-Nov-00	Barometer, mmHg	743.2	VFAM Constant	77.21
Test Pressure, mmH$_2$O	900	ISM Constant	1.09E-04		

Test Summary Results

Swirl Ratio (Rs)	1.49	Gulp Factor	0.797	Cf @ 0.3 L/D	0.533
Rs/LD	0.15	MCf	0.433	Cf @ Max Lift	0.534
CCf	1.738				

Test Results

Valve Lift		Air Flow	ISM Torque	Flow	Discharge	Non-dim
Test	Non-dim	m^3/s	NmE^{-3}	Coefficient	Coefficient	Rig Swirl
mm	L/D	Q	G	Cf	Cd	Ns
0	0.000	0.0000	0.00	0.000	0.000	0.000
1	0.037	0.0080	0.54	0.119	1.118	0.045
2	0.074	0.0158	1.85	0.235	1.081	0.078
3	0.111	0.0234	2.06	0.348	1.048	0.059
4	0.148	0.0303	2.82	0.450	1.000	0.062
5	0.185	0.0350	5.75	0.521	0.910	0.109
6	0.222	0.0362	8.90	0.538	0.770	0.164
7	0.259	0.0360	16.82	0.535	0.646	0.311
8	0.296	0.0359	22.90	0.533	0.554	0.425
9	0.333	0.0361	25.61	0.535	0.486	0.474
10	0.370	0.0363	27.03	0.539	0.434	0.496

C33

Test Filename   **D49B**

Engine Details

Configuration	IL4	Inner Seat Dia, mm	27	Shape Factor, LD	10.43
Cylinder bore	84.5	Seat Angle	45	Lmax/D	0.31
Engine Stroke	90	Max Valve Lift	8.37	D/B	0.32
Inlet Valves, n	1	Valve Opens	0	MIGV	132.2
Rated Speed, rpm	4500	Valve Closes	50	MPV	13.5

Test Details

Test Date	03-Nov-00	Barometer, mmHg	747.2	VFAM Constant	77.19
Test Pressure, mmH$_2$O	900	ISM Constant	1.09E-04		

Test Summary Results

Swirl Ratio (Rs)	1.76	Gulp Factor	0.871	Cf @ 0.3 L/D	0.566
Rs/LD	0.17	MCf	0.443	Cf @ Max Lift	0.568
CCf	1.777				

Test Results

Valve Lift		Air Flow	ISM Torque	Flow	Discharge	Non-dim
Test	Non-dim	m^3/s	NmE^{-3}	Coefficient	Coefficient	Rig Swirl
mm	L/D	Q	G	Cf	Cd	Ns
0	0.000	0.0000	0.00	0.000	0.000	0.000
1	0.037	0.0079	2.28	0.118	1.106	0.181
2	0.074	0.0152	3.26	0.226	1.039	0.135
3	0.111	0.0223	4.34	0.332	1.001	0.123
4	0.148	0.0301	7.05	0.447	0.992	0.148
5	0.185	0.0349	8.90	0.518	0.905	0.161
6	0.222	0.0358	15.63	0.532	0.761	0.275
7	0.259	0.0374	21.16	0.555	0.670	0.357
8	0.296	0.0381	23.87	0.565	0.587	0.396
9	0.333	0.0387	25.39	0.574	0.521	0.415
10	0.370	0.0392	27.46	0.581	0.468	0.443

Test Filename   **D49A**

Engine Details

Configuration	IL4	Inner Seat Dia, mm	27	Shape Factor, LD	10.43
Cylinder bore	84.5	Seat Angle	45	Lmax/D	0.31
Engine Stroke	90	Max Valve Lift	8.37	D/B	0.32
Inlet Valves, n	1	Valve Opens	0	MIGV	132.2
Rated Speed, rpm	4500	Valve Closes	50	MPV	13.5

Test Details

Test Date	03-Nov-00	Barometer, mmHg	747.2	VFAM Constant	77.19
Test Pressure, mmH$_2$O	900	ISM Constant	1.09E-04		

Test Summary Results

Swirl Ratio (Rs)	0.97	Gulp Factor	0.862	Cf @ 0.3 L/D	0.563
Rs/LD	0.09	MCf	0.447	Cf @ Max Lift	0.566
CCf	1.795				

Test Results

Valve Lift		Air Flow	ISM Torque	Flow	Discharge	Non-dim
Test	Non-dim	m^3/s	NmE^{-3}	Coefficient	Coefficient	Rig Swirl
mm	L/D	Q	G	Cf	Cd	Ns
0	0.000	0.0000	0.00	0.000	0.000	0.000
1	0.037	0.0080	-0.22	0.119	1.113	-0.017
2	0.074	0.0155	0.87	0.230	1.060	0.035
3	0.111	0.0230	1.41	0.343	1.035	0.039
4	0.148	0.0305	1.41	0.455	1.010	0.029
5	0.185	0.0359	3.04	0.535	0.935	0.053
6	0.222	0.0375	4.56	0.558	0.799	0.077
7	0.259	0.0369	13.89	0.548	0.662	0.237
8	0.296	0.0378	16.06	0.562	0.584	0.268
9	0.333	0.0385	17.36	0.572	0.520	0.284
10	0.370	0.0392	19.21	0.582	0.469	0.309

Test Filename   **D40B**

Engine Details

Configuration	IL4	Inner Seat Dia, mm	27	Shape Factor, LD	10.43
Cylinder bore	84.5	Seat Angle	45	Lmax/D	0.31
Engine Stroke	90	Max Valve Lift	8.37	D/B	0.32
Inlet Valves, n	1	Valve Opens	0	MIGV	132.2
Rated Speed, rpm	4500	Valve Closes	50	MPV	13.5

Test Details

Test Date	03-Nov-00	Barometer, mmHg	745.1	VFAM Constant	77.2
Test Pressure, mmH$_2$O	900	ISM Constant	1.09E-04		

Test Summary Results

Swirl Ratio (Rs)	1.83	Gulp Factor	0.883	Cf @ 0.3 L/D	0.551
Rs/LD	0.18	MCf	0.436	Cf @ Max Lift	0.553
CCf	1.752				

Test Results

Valve Lift		Air Flow	ISM Torque	Flow	Discharge	Non-dim
Test	Non-dim	m^3/s	NmE^{-3}	Coefficient	Coefficient	Rig Swirl
mm	L/D	Q	G	Cf	Cd	Ns
0	0.000	0.0000	0.00	0.000	0.000	0.000
1	0.037	0.0079	1.84	0.118	1.105	0.147
2	0.074	0.0154	3.04	0.229	1.056	0.124
3	0.111	0.0228	3.91	0.339	1.022	0.108
4	0.148	0.0302	7.92	0.448	0.996	0.165
5	0.185	0.0345	10.85	0.512	0.895	0.198
6	0.222	0.0359	18.34	0.533	0.763	0.323
7	0.259	0.0365	21.49	0.541	0.653	0.372
8	0.296	0.0371	22.57	0.550	0.571	0.385
9	0.333	0.0377	25.61	0.558	0.507	0.430
10	0.370	0.0383	28.43	0.566	0.456	0.470

Test Filename   **D40A**

Engine Details

Configuration	IL4	Inner Seat Dia, mm	27	Shape Factor, LD	10.43
Cylinder bore	84.5	Seat Angle	45	Lmax/D	0.31
Engine Stroke	90	Max Valve Lift	8.37	D/B	0.32
Inlet Valves, n	1	Valve Opens	0	MIGV	132.2
Rated Speed, rpm	4500	Valve Closes	50	MPV	13.5

Test Details

Test Date	03-Nov-00	Barometer, mmHg	745	VFAM Constant	77.2
Test Pressure, mmH$_2$O	900	ISM Constant	1.09E-04		

Test Summary Results

Swirl Ratio (Rs)	0.83	Gulp Factor	0.88	Cf @ 0.3 L/D	0.55
Rs/LD	0.08	MCf	0.438	Cf @ Max Lift	0.551
CCf	1.757				

Test Results

Valve Lift		Air Flow	ISM Torque	Flow	Discharge	Non-dim
Test	Non-dim	m^3/s	NmE^{-3}	Coefficient	Coefficient	Rig Swirl
mm	L/D	Q	G	Cf	Cd	Ns
0	0.000	0.0000	0.00	0.000	0.000	0.000
1	0.037	0.0081	-0.54	0.120	1.124	-0.042
2	0.074	0.0157	0.65	0.234	1.077	0.026
3	0.111	0.0234	0.54	0.348	1.049	0.015
4	0.148	0.0306	-0.54	0.456	1.013	-0.011
5	0.185	0.0352	-0.54	0.524	0.915	-0.010
6	0.222	0.0354	7.05	0.526	0.754	0.126
7	0.259	0.0361	11.94	0.537	0.648	0.208
8	0.296	0.0369	13.46	0.549	0.570	0.230
9	0.333	0.0374	14.33	0.556	0.505	0.241
10	0.370	0.0381	16.06	0.566	0.456	0.266

Test Filename **D39B**

Engine Details

Configuration	IL4	Inner Seat Dia, mm	27	Shape Factor, LD	10.43
Cylinder bore	84.5	Seat Angle	45	Lmax/D	0.31
Engine Stroke	90	Max Valve Lift	8.37	D/B	0.32
Inlet Valves, n	1	Valve Opens	0	MIGV	132.2
Rated Speed, rpm	4500	Valve Closes	50	MPV	13.5

Test Details

Test Date	02-Nov-00	Barometer, mmHg	739.5	VFAM Constant	77.23
Test Pressure, mmH_2O	900	ISM Constant	1.09E-04		

Test Summary Results

Swirl Ratio (Rs)	1.39	Gulp Factor	0.869	Cf @ 0.3 L/D	0.563
Rs/LD	0.13	MCf	0.443	Cf @ Max Lift	0.565
CCf	1.78				

Test Results

Valve Lift		Air Flow	ISM Torque	Flow	Discharge	Non-dim
Test	Non-dim	m^3/s	NmE^{-3}	Coefficient	Coefficient	Rig Swirl
mm	L/D	Q	G	Cf	Cd	Ns
0	0.000	0.0000	0.00	0.000	0.000	0.000
1	0.037	0.0080	2.39	0.118	1.107	0.189
2	0.074	0.0153	3.58	0.226	1.040	0.148
3	0.111	0.0224	4.02	0.332	1.000	0.113
4	0.148	0.0300	4.88	0.444	0.986	0.103
5	0.185	0.0353	5.43	0.523	0.914	0.097
6	0.222	0.0371	6.73	0.549	0.786	0.115
7	0.259	0.0373	18.02	0.551	0.665	0.306
8	0.296	0.0381	20.52	0.562	0.584	0.342
9	0.333	0.0386	22.58	0.570	0.519	0.371
10	0.370	0.0393	25.18	0.580	0.467	0.407

Test Filename   **D38A**

Engine Details

Configuration	IL4	Inner Seat Dia, mm	27	Shape Factor, LD	10.43
Cylinder bore	84.5	Seat Angle	45	Lmax/D	0.31
Engine Stroke	90	Max Valve Lift	8.37	D/B	0.32
Inlet Valves, n	1	Valve Opens	0	MIGV	132.2
Rated Speed, rpm	4500	Valve Closes	50	MPV	13.5

Test Details

Test Date	02-Nov-00	Barometer, mmHg	739.6	VFAM Constant	77.23
Test Pressure, mmH$_2$O	900	ISM Constant	1.09E-04		

Test Summary Results

Swirl Ratio (Rs)	1.37	Gulp Factor	0.866	Cf @ 0.3 L/D	0.564
Rs/LD	0.13	MCf	0.445	Cf @ Max Lift	0.568
CCf	1.786				

Test Results

Valve Lift		Air Flow	ISM Torque	Flow	Discharge	Non-dim
Test	Non-dim	m^3/s	NmE^{-3}	Coefficient	Coefficient	Rig Swirl
mm	L/D	Q	G	Cf	Cd	Ns
0	0.000	0.0000	0.00	0.000	0.000	0.000
1	0.037	0.0079	0.76	0.118	1.105	0.060
2	0.074	0.0154	1.41	0.229	1.052	0.058
3	0.111	0.0228	2.28	0.339	1.021	0.063
4	0.148	0.0306	3.47	0.455	1.011	0.072
5	0.185	0.0357	4.88	0.530	0.926	0.086
6	0.222	0.0362	13.79	0.537	0.769	0.241
7	0.259	0.0373	17.91	0.553	0.667	0.303
8	0.296	0.0380	19.54	0.562	0.585	0.325
9	0.333	0.0391	21.49	0.579	0.526	0.348
10	0.370	0.0395	24.32	0.584	0.471	0.390

Test Filename **D44B**

Engine Details

Configuration	IL4	Inner Seat Dia, mm	27	Shape Factor, LD	10.43
Cylinder bore	84.5	Seat Angle	45	Lmax/D	0.31
Engine Stroke	90	Max Valve Lift	8.37	D/B	0.32
Inlet Valves, n	1	Valve Opens	0	MIGV	132.2
Rated Speed, rpm	4500	Valve Closes	50	MPV	13.5

Test Details

Test Date	01-Nov-00	Barometer, mmHg	747.3	VFAM Constant	77.19
Test Pressure, mmH$_2$O	900	ISM Constant	1.09E-04		

Test Summary Results

Swirl Ratio (Rs)	1.95	Gulp Factor	0.876	Cf @ 0.3 L/D	0.56
Rs/LD	0.19	MCf	0.44	Cf @ Max Lift	0.563
CCf	1.766				

Test Results

Valve Lift		Air Flow	ISM Torque	Flow	Discharge	Non-dim
Test	Non-dim	m^3/s	NmE^{-3}	Coefficient	Coefficient	Rig Swirl
mm	L/D	Q	G	Cf	Cd	Ns
0	0.000	0.0000	0.00	0.000	0.000	0.000
1	0.037	0.0077	1.84	0.114	1.068	0.152
2	0.074	0.0152	3.47	0.226	1.041	0.144
3	0.111	0.0224	4.67	0.333	1.003	0.131
4	0.148	0.0293	6.51	0.434	0.964	0.141
5	0.185	0.0351	9.22	0.520	0.908	0.166
6	0.222	0.0372	13.56	0.550	0.788	0.231
7	0.259	0.0367	23.44	0.542	0.655	0.405
8	0.296	0.0379	28.11	0.559	0.581	0.471
9	0.333	0.0386	29.41	0.569	0.517	0.484
10	0.370	0.0390	30.82	0.575	0.463	0.502

Test Filename   **D44A**

Engine Details

Configuration	IL4	Inner Seat Dia, mm	27	Shape Factor, LD	10.43
Cylinder bore	84.5	Seat Angle	45	Lmax/D	0.31
Engine Stroke	90	Max Valve Lift	8.37	D/B	0.32
Inlet Valves, n	1	Valve Opens	0	MIGV	132.2
Rated Speed, rpm	4500	Valve Closes	50	MPV	13.5

Test Details

Test Date	01-Nov-00	Barometer, mmHg	747.2	VFAM Constant	77.19
Test Pressure, mmH$_2$O	900	ISM Constant	1.09E-04		

Test Summary Results

Swirl Ratio (Rs)	1.11	Gulp Factor	0.87	Cf @ 0.3 L/D	0.555
Rs/LD	0.11	MCf	0.443	Cf @ Max Lift	0.559
CCf	1.777				

Test Results

Valve Lift		Air Flow	ISM Torque	Flow	Discharge	Non-dim
Test	Non-dim	m^3/s	NmE^{-3}	Coefficient	Coefficient	Rig Swirl
mm	L/D	Q	G	Cf	Cd	Ns
0	0.000	0.0000	0.00	0.000	0.000	0.000
1	0.037	0.0078	-0.33	0.116	1.087	-0.026
2	0.074	0.0152	0.76	0.227	1.043	0.031
3	0.111	0.0226	1.41	0.337	1.016	0.039
4	0.148	0.0298	0.98	0.444	0.986	0.021
5	0.185	0.0355	2.06	0.528	0.923	0.037
6	0.222	0.0375	3.36	0.557	0.797	0.057
7	0.259	0.0371	16.82	0.551	0.665	0.286
8	0.296	0.0374	18.88	0.554	0.576	0.319
9	0.333	0.0383	19.97	0.567	0.516	0.330
10	0.370	0.0390	21.38	0.577	0.465	0.347

Test Filename   **D43B**

Engine Details

Configuration	IL4	Inner Seat Dia, mm	27	Shape Factor, LD	10.43
Cylinder bore	84.5	Seat Angle	45	Lmax/D	0.31
Engine Stroke	90	Max Valve Lift	8.37	D/B	0.32
Inlet Valves, n	1	Valve Opens	0	MIGV	132.2
Rated Speed, rpm	4500	Valve Closes	50	MPV	13.5

Test Details

Test Date	01-Nov-00	Barometer, mmHg	746.9	VFAM Constant	77.19
Test Pressure, mmH$_2$O	900	ISM Constant	1.09E-04		

Test Summary Results

Swirl Ratio (Rs)	1.42	Gulp Factor	0.863	Cf @ 0.3 L/D	0.573
Rs/LD	0.14	MCf	0.447	Cf @ Max Lift	0.575
CCf	1.793				

Test Results

Valve Lift		Air Flow	ISM Torque	Flow	Discharge	Non-dim
Test	Non-dim	m^3/s	NmE^{-3}	Coefficient	Coefficient	Rig Swirl
mm	L/D	Q	G	Cf	Cd	Ns
0	0.000	0.0000	0.00	0.000	0.000	0.000
1	0.037	0.0079	1.52	0.117	1.096	0.122
2	0.074	0.0154	2.82	0.229	1.052	0.116
3	0.111	0.0226	3.47	0.337	1.015	0.097
4	0.148	0.0302	5.75	0.449	0.999	0.120
5	0.185	0.0348	7.49	0.518	0.905	0.135
6	0.222	0.0362	11.18	0.539	0.771	0.194
7	0.259	0.0375	17.15	0.558	0.673	0.288
8	0.296	0.0385	20.51	0.572	0.595	0.336
9	0.333	0.0392	21.49	0.581	0.528	0.346
10	0.370	0.0396	23.44	0.588	0.473	0.374

Test Filename **D43AB**

Engine Details

Configuration	IL4	Inner Seat Dia, mm	27	Shape Factor, LD	10.43
Cylinder bore	84.5	Seat Angle	45	Lmax/D	0.31
Engine Stroke	90	Max Valve Lift	8.37	D/B	0.32
Inlet Valves, n	1	Valve Opens	0	MIGV	132.2
Rated Speed, rpm	4500	Valve Closes	50	MPV	13.5

Test Details

Test Date	01-Nov-00	Barometer, mmHg	746.6	VFAM Constant	77.19
Test Pressure, mmH$_2$O	900	ISM Constant	1.09E-04		

Test Summary Results

Swirl Ratio (Rs)	0.87	Gulp Factor	0.869	Cf @ 0.3 L/D	0.566
Rs/LD	0.08	MCf	0.443	Cf @ Max Lift	0.569
CCf	1.78				

Test Results

Valve Lift		Air Flow	ISM Torque	Flow	Discharge	Non-dim
Test	Non-dim	m^3/s	NmE^{-3}	Coefficient	Coefficient	Rig Swirl
mm	L/D	Q	G	Cf	Cd	Ns
0	0.000	0.0000	0.00	0.000	0.000	0.000
1	0.037	0.0080	-0.11	0.119	1.111	-0.009
2	0.074	0.0152	0.76	0.226	1.039	0.032
3	0.111	0.0226	0.65	0.336	1.012	0.018
4	0.148	0.0304	1.30	0.451	1.002	0.027
5	0.185	0.0356	3.80	0.528	0.922	0.067
6	0.222	0.0362	9.77	0.535	0.767	0.171
7	0.259	0.0369	11.18	0.546	0.660	0.192
8	0.296	0.0383	12.37	0.565	0.588	0.205
9	0.333	0.0389	13.57	0.574	0.522	0.221
10	0.370	0.0397	15.30	0.586	0.472	0.245

C43

Test Filename   **D42B**

Engine Details

Configuration	IL4	Inner Seat Dia, mm	27	Shape Factor, LD	9.88
Cylinder bore	80	Seat Angle	45	Lmax/D	0.31
Engine Stroke	90	Max Valve Lift	8.37	D/B	0.338
Inlet Valves, n	1	Valve Opens	0	MIGV	118.5
Rated Speed, rpm	4500	Valve Closes	50	MPV	13.5

Test Details

Test Date	01-Nov-00	Barometer, mmHg	746.6	VFAM Constant	77.19
Test Pressure, mmH$_2$O	900	ISM Constant	1.09E-04		

Test Summary Results

Swirl Ratio (Rs)	1.61	Gulp Factor	0.78	Cf @ 0.3 L/D	0.566
Rs/LD	0.16	MCf	0.443	Cf @ Max Lift	0.568
CCf	1.776				

Test Results

Valve Lift		Air Flow	ISM Torque	Flow	Discharge	Non-dim
Test	Non-dim	m^3/s	NmE^{-3}	Coefficient	Coefficient	Rig Swirl
mm	L/D	Q	G	Cf	Cd	Ns
0	0.000	0.0000	0.00	0.000	0.000	0.000
1	0.037	0.0079	1.74	0.116	1.092	0.147
2	0.074	0.0153	2.82	0.227	1.044	0.123
3	0.111	0.0224	3.58	0.333	1.003	0.106
4	0.148	0.0299	5.64	0.444	0.986	0.126
5	0.185	0.0349	7.38	0.518	0.904	0.141
6	0.222	0.0361	14.11	0.535	0.765	0.261
7	0.259	0.0373	19.64	0.552	0.667	0.352
8	0.296	0.0382	22.46	0.566	0.588	0.393
9	0.333	0.0388	23.44	0.573	0.521	0.405
10	0.370	0.0393	24.85	0.581	0.468	0.423

Test Filename   **D42A**

Engine Details

Configuration	IL4	Inner Seat Dia, mm	27	Shape Factor, LD	9.88
Cylinder bore	80	Seat Angle	45	Lmax/D	0.31
Engine Stroke	90	Max Valve Lift	8.37	D/B	0.338
Inlet Valves, n	1	Valve Opens	0	MIGV	118.5
Rated Speed, rpm	4500	Valve Closes	50	MPV	13.5

Test Details

Test Date	01-Nov-00	Barometer, mmHg	746.6	VFAM Constant	77.19
Test Pressure, mmH$_2$O	900	ISM Constant	1.09E-04		

Test Summary Results

Swirl Ratio (Rs)	0.95	Gulp Factor	0.777	Cf @ 0.3 L/D	0.562
Rs/LD	0.1	MCf	0.445	Cf @ Max Lift	0.565
CCf	1.785				

Test Results

Valve Lift		Air Flow	ISM Torque	Flow	Discharge	Non-dim
Test	Non-dim	m^3/s	NmE^{-3}	Coefficient	Coefficient	Rig Swirl
mm	L/D	Q	G	Cf	Cd	Ns
0	0.000	0.0000	0.00	0.000	0.000	0.000
1	0.037	0.0078	-0.22	0.116	1.090	-0.018
2	0.074	0.0153	0.65	0.229	1.052	0.028
3	0.111	0.0229	0.87	0.342	1.030	0.025
4	0.148	0.0303	0.98	0.452	1.004	0.021
5	0.185	0.0360	2.60	0.536	0.936	0.048
6	0.222	0.0367	11.18	0.546	0.782	0.203
7	0.259	0.0369	12.59	0.547	0.660	0.228
8	0.296	0.0378	14.11	0.561	0.583	0.249
9	0.333	0.0387	14.98	0.573	0.521	0.259
10	0.370	0.0392	16.39	0.581	0.468	0.279

Test Filename   **D41B**

Engine Details

Configuration	IL4	Inner Seat Dia, mm	27	Shape Factor, LD	11.11
Cylinder bore	90	Seat Angle	45	Lmax/D	0.31
Engine Stroke	90	Max Valve Lift	8.37	D/B	0.3
Inlet Valves, n	1	Valve Opens	0	MIGV	150
Rated Speed, rpm	4500	Valve Closes	50	MPV	13.5

Test Details

Test Date	01-Nov-00	Barometer, mmHg	746.5	VFAM Constant	77.19
Test Pressure, mmH$_2$O	900	ISM Constant	1.09E-04		

Test Summary Results

Swirl Ratio (Rs)	1.78	Gulp Factor	0.991	Cf @ 0.3 L/D	0.564
Rs/LD	0.16	MCf	0.441	Cf @ Max Lift	0.566
CCf	1.771				

Test Results

Valve Lift		Air Flow	ISM Torque	Flow	Discharge	Non-dim
Test	Non-dim	m^3/s	NmE^{-3}	Coefficient	Coefficient	Rig Swirl
mm	L/D	Q	G	Cf	Cd	Ns
0	0.000	0.0000	0.00	0.000	0.000	0.000
1	0.037	0.0078	1.52	0.116	1.088	0.115
2	0.074	0.0152	3.36	0.226	1.040	0.131
3	0.111	0.0224	4.45	0.333	1.004	0.117
4	0.148	0.0299	7.16	0.445	0.988	0.142
5	0.185	0.0350	9.22	0.520	0.908	0.156
6	0.222	0.0359	15.84	0.533	0.764	0.261
7	0.259	0.0369	21.16	0.548	0.662	0.339
8	0.296	0.0379	24.09	0.563	0.585	0.376
9	0.333	0.0385	26.26	0.572	0.520	0.404
10	0.370	0.0391	28.54	0.579	0.466	0.433

C46

Test Filename   **D41A**

Engine Details

Configuration	IL4	Inner Seat Dia, mm	27	Shape Factor, LD	11.11
Cylinder bore	90	Seat Angle	45	Lmax/D	0.31
Engine Stroke	90	Max Valve Lift	8.37	D/B	0.3
Inlet Valves, n	1	Valve Opens	0	MIGV	150
Rated Speed, rpm	4500	Valve Closes	50	MPV	13.5

Test Details

Test Date	01-Nov-00	Barometer, mmHg	746.2	VFAM Constant	77.2
Test Pressure, mmH$_2$O	900	ISM Constant	1.09E-04		

Test Summary Results

Swirl Ratio (Rs)	1.15	Gulp Factor	0.986	Cf @ 0.3 L/D	0.565
Rs/LD	0.1	MCf	0.443	Cf @ Max Lift	0.567
CCf	1.779				

Test Results

Valve Lift		Air Flow	ISM Torque	Flow	Discharge	Non-dim
Test	Non-dim	m^3/s	NmE^{-3}	Coefficient	Coefficient	Rig Swirl
mm	L/D	Q	G	Cf	Cd	Ns
0	0.000	0.0000	0.00	0.000	0.000	0.000
1	0.037	0.0079	-0.33	0.118	1.106	-0.024
2	0.074	0.0155	0.87	0.230	1.060	0.033
3	0.111	0.0228	1.19	0.339	1.023	0.031
4	0.148	0.0302	1.41	0.450	1.000	0.028
5	0.185	0.0357	3.47	0.531	0.929	0.057
6	0.222	0.0355	12.26	0.528	0.756	0.204
7	0.259	0.0369	14.65	0.548	0.661	0.235
8	0.296	0.0380	17.15	0.564	0.586	0.267
9	0.333	0.0386	18.99	0.573	0.521	0.292
10	0.370	0.0393	20.94	0.582	0.469	0.316

Test Filename   **D48B**

Engine Details

Configuration	IL4	Inner Seat Dia, mm	27	Shape Factor, LD	10.43
Cylinder bore	84.5	Seat Angle	45	Lmax/D	0.31
Engine Stroke	90	Max Valve Lift	8.37	D/B	0.32
Inlet Valves, n	1	Valve Opens	0	MIGV	132.2
Rated Speed, rpm	4500	Valve Closes	50	MPV	13.5

Test Details

Test Date	31-Oct-00	Barometer, mmHg	747.3	VFAM Constant	77.19
Test Pressure, mmH$_2$O	900	ISM Constant	1.09E-04		

Test Summary Results

Swirl Ratio (Rs)	1.7	Gulp Factor	0.875	Cf @ 0.3 L/D	0.563
Rs/LD	0.16	MCf	0.44	Cf @ Max Lift	0.566
CCf	1.767				

Test Results

Valve Lift		Air Flow	ISM Torque	Flow	Discharge	Non-dim
Test	Non-dim	m^3/s	NmE^{-3}	Coefficient	Coefficient	Rig Swirl
mm	L/D	Q	G	Cf	Cd	Ns
0	0.000	0.0000	0.00	0.000	0.000	0.000
1	0.037	0.0079	1.84	0.117	1.097	0.148
2	0.074	0.0151	3.04	0.223	1.026	0.128
3	0.111	0.0224	4.02	0.331	0.999	0.113
4	0.148	0.0300	6.62	0.443	0.985	0.140
5	0.185	0.0350	8.46	0.516	0.902	0.154
6	0.222	0.0360	14.65	0.531	0.760	0.258
7	0.259	0.0372	20.29	0.549	0.663	0.346
8	0.296	0.0382	23.11	0.562	0.584	0.385
9	0.333	0.0388	24.85	0.572	0.520	0.407
10	0.370	0.0394	26.59	0.580	0.467	0.430

Test Filename   **D48A**

Engine Details

Configuration	IL4	Inner Seat Dia, mm	27	Shape Factor, LD	10.43
Cylinder bore	84.5	Seat Angle	45	Lmax/D	0.31
Engine Stroke	90	Max Valve Lift	8.37	D/B	0.32
Inlet Valves, n	1	Valve Opens	0	MIGV	132.2
Rated Speed, rpm	4500	Valve Closes	50	MPV	13.5

Test Details

Test Date	31-Oct-00	Barometer, mmHg	747.3	VFAM Constant	77.19
Test Pressure, mmH$_2$O	900	ISM Constant	1.09E-04		

Test Summary Results

Swirl Ratio (Rs)	1	Gulp Factor	0.87	Cf @ 0.3 L/D	0.559
Rs/LD	0.1	MCf	0.443	Cf @ Max Lift	0.562
CCf	1.778				

Test Results

Valve Lift		Air Flow	ISM Torque	Flow	Discharge	Non-dim
Test	Non-dim	m^3/s	NmE^{-3}	Coefficient	Coefficient	Rig Swirl
mm	L/D	Q	G	Cf	Cd	Ns
0	0.000	0.0000	0.00	0.000	0.000	0.000
1	0.037	0.0079	0.00	0.117	1.100	0.000
2	0.074	0.0152	0.76	0.225	1.037	0.032
3	0.111	0.0228	1.19	0.337	1.017	0.033
4	0.148	0.0301	1.30	0.446	0.990	0.027
5	0.185	0.0357	3.04	0.529	0.924	0.054
6	0.222	0.0376	5.43	0.557	0.797	0.091
7	0.259	0.0369	14.11	0.544	0.657	0.243
8	0.296	0.0378	16.06	0.557	0.579	0.270
9	0.333	0.0386	17.04	0.569	0.518	0.280
10	0.370	0.0393	18.99	0.579	0.466	0.307

Test Filename   **D38B**

Engine Details

Configuration	IL4	Inner Seat Dia, mm	27	Shape Factor, LD	10.43
Cylinder bore	84.5	Seat Angle	45	Lmax/D	0.31
Engine Stroke	90	Max Valve Lift	8.37	D/B	0.32
Inlet Valves, n	1	Valve Opens	0	MIGV	132.2
Rated Speed, rpm	4500	Valve Closes	50	MPV	13.5

Test Details

Test Date	31-Oct-00	Barometer, mmHg	747.3	VFAM Constant	77.19
Test Pressure, mmH_2O	900	ISM Constant	1.09E-04		

Test Summary Results

Swirl Ratio (Rs)	2.02	Gulp Factor	0.871	Cf @ 0.3 L/D	0.565
Rs/LD	0.19	MCf	0.442	Cf @ Max Lift	0.567
CCf	1.775				

Test Results

Valve Lift		Air Flow	ISM Torque	Flow	Discharge	Non-dim
Test	Non-dim	m^3/s	NmE^{-3}	Coefficient	Coefficient	Rig Swirl
mm	L/D	Q	G	Cf	Cd	Ns
0	0.000	0.0000	0.00	0.000	0.000	0.000
1	0.037	0.0080	0.98	0.119	1.116	0.077
2	0.074	0.0155	2.71	0.230	1.060	0.110
3	0.111	0.0225	3.80	0.333	1.005	0.107
4	0.148	0.0300	6.08	0.446	0.990	0.128
5	0.185	0.0350	10.42	0.519	0.907	0.188
6	0.222	0.0362	18.12	0.536	0.767	0.317
7	0.259	0.0370	23.11	0.548	0.661	0.395
8	0.296	0.0381	28.97	0.564	0.586	0.481
9	0.333	0.0388	33.10	0.574	0.522	0.540
10	0.370	0.0393	33.10	0.581	0.468	0.534

C50

Test Filename   **D38A**

Engine Details

Configuration	IL4	Inner Seat Dia, mm	27	Shape Factor, LD	10.43
Cylinder bore	84.5	Seat Angle	45	Lmax/D	0.31
Engine Stroke	90	Max Valve Lift	8.37	D/B	0.32
Inlet Valves, n	1	Valve Opens	0	MIGV	132.2
Rated Speed, rpm	4500	Valve Closes	50	MPV	13.5

Test Details

Test Date	31-Oct-00	Barometer, mmHg	746.8	VFAM Constant	77.19
Test Pressure, mmH$_2$O	900	ISM Constant	1.09E-04		

Test Summary Results

Swirl Ratio (Rs)	1.45	Gulp Factor	0.865	Cf @ 0.3 L/D	0.561
Rs/LD	0.14	MCf	0.446	Cf @ Max Lift	0.563
CCf	1.789				

Test Results

Valve Lift		Air Flow	ISM Torque	Flow	Discharge	Non-dim
Test	Non-dim	m^3/s	NmE^{-3}	Coefficient	Coefficient	Rig Swirl
mm	L/D	Q	G	Cf	Cd	Ns
0	0.000	0.0000	0.00	0.000	0.000	0.000
1	0.037	0.0079	1.41	0.118	1.105	0.112
2	0.074	0.0152	2.17	0.226	1.038	0.090
3	0.111	0.0227	3.04	0.337	1.017	0.084
4	0.148	0.0302	3.91	0.448	0.995	0.082
5	0.185	0.0361	4.23	0.535	0.935	0.074
6	0.222	0.0381	5.43	0.564	0.807	0.090
7	0.259	0.0371	18.01	0.548	0.662	0.308
8	0.296	0.0378	24.20	0.560	0.582	0.405
9	0.333	0.0385	28.22	0.569	0.517	0.465
10	0.370	0.0389	29.41	0.575	0.463	0.479

Test Filename   **D37AB**

Engine Details

Configuration	IL4	Inner Seat Dia, mm	27	Shape Factor, LD	10.43
Cylinder bore	84.5	Seat Angle	45	Lmax/D	0.31
Engine Stroke	90	Max Valve Lift	8.37	D/B	0.32
Inlet Valves, n	1	Valve Opens	0	MIGV	132.2
Rated Speed, rpm	4500	Valve Closes	50	MPV	13.5

Test Details

Test Date	31-Oct-00	Barometer, mmHg	746.6	VFAM Constant	77.19
Test Pressure, mmH$_2$O	900	ISM Constant	1.09E-04		

Test Summary Results

Swirl Ratio (Rs)	0.75	Gulp Factor	0.858	Cf @ 0.3 L/D	0.577
Rs/LD	0.07	MCf	0.449	Cf @ Max Lift	0.58
CCf	1.803				

Test Results

Valve Lift		Air Flow	ISM Torque	Flow	Discharge	Non-dim
Test	Non-dim	m^3/s	NmE^{-3}	Coefficient	Coefficient	Rig Swirl
mm	L/D	Q	G	Cf	Cd	Ns
0	0.000	0.0000	0.00	0.000	0.000	0.000
1	0.037	0.0079	1.30	0.118	1.107	0.103
2	0.074	0.0155	1.19	0.230	1.059	0.049
3	0.111	0.0230	1.52	0.343	1.033	0.042
4	0.148	0.0304	3.47	0.453	1.006	0.072
5	0.185	0.0350	3.91	0.520	0.909	0.070
6	0.222	0.0365	7.81	0.542	0.776	0.135
7	0.259	0.0375	8.90	0.557	0.672	0.150
8	0.296	0.0388	10.20	0.575	0.598	0.166
9	0.333	0.0396	10.74	0.588	0.534	0.171
10	0.370	0.0402	10.53	0.595	0.480	0.166

Test Filename   **D36B**

Engine Details

Configuration	IL4	Inner Seat Dia, mm	27	Shape Factor, LD	10.43
Cylinder bore	84.5	Seat Angle	45	Lmax/D	0.31
Engine Stroke	90	Max Valve Lift	8.37	D/B	0.32
Inlet Valves, n	1	Valve Opens	0	MIGV	132.2
Rated Speed, rpm	4500	Valve Closes	50	MPV	13.5

Test Details

Test Date	31-Oct-00	Barometer, mmHg	745.6	VFAM Constant	77.2
Test Pressure, mmH$_2$O	900	ISM Constant	1.09E-04		

Test Summary Results

Swirl Ratio (Rs)	1.65	Gulp Factor	0.875	Cf @ 0.3 L/D	0.56
Rs/LD	0.16	MCf	0.44	Cf @ Max Lift	0.563
CCf	1.768				

Test Results

Valve Lift		Air Flow	ISM Torque	Flow	Discharge	Non-dim
Test	Non-dim	m^3/s	NmE^{-3}	Coefficient	Coefficient	Rig Swirl
mm	L/D	Q	G	Cf	Cd	Ns
0	0.000	0.0000	0.00	0.000	0.000	0.000
1	0.037	0.0080	1.09	0.119	1.113	0.086
2	0.074	0.0151	2.17	0.224	1.030	0.091
3	0.111	0.0225	3.15	0.333	1.005	0.088
4	0.148	0.0304	6.08	0.451	1.002	0.126
5	0.185	0.0351	7.60	0.519	0.907	0.137
6	0.222	0.0359	15.30	0.531	0.760	0.270
7	0.259	0.0372	20.08	0.550	0.663	0.342
8	0.296	0.0378	22.68	0.559	0.581	0.380
9	0.333	0.0386	24.64	0.570	0.518	0.405
10	0.370	0.0393	26.70	0.580	0.467	0.431

Test Filename　　　　**D36A**

Engine Details

Configuration	IL4	Inner Seat Dia, mm	27	Shape Factor, LD	10.43
Cylinder bore	84.5	Seat Angle	45	Lmax/D	0.31
Engine Stroke	90	Max Valve Lift	8.37	D/B	0.32
Inlet Valves, n	1	Valve Opens	0	MIGV	132.2
Rated Speed, rpm	4500	Valve Closes	50	MPV	13.5

Test Details

Test Date	31-Oct-00	Barometer, mmHg	745.4	VFAM Constant	77.2
Test Pressure, mmH$_2$O	900	ISM Constant	1.09E-04		

Test Summary Results

Swirl Ratio (Rs)	1.11	Gulp Factor	0.865	Cf @ 0.3 L/D	0.562
Rs/LD	0.11	MCf	0.445	Cf @ Max Lift	0.564
CCf	1.787				

Test Results

Valve Lift		Air Flow	ISM Torque	Flow	Discharge	Non-dim
Test	Non-dim	m^3/s	NmE^{-3}	Coefficient	Coefficient	Rig Swirl
mm	L/D	Q	G	Cf	Cd	Ns
0	0.000	0.0000	0.00	0.000	0.000	0.000
1	0.037	0.0080	-0.22	0.120	1.120	-0.017
2	0.074	0.0156	1.41	0.232	1.066	0.057
3	0.111	0.0232	1.30	0.345	1.039	0.035
4	0.148	0.0306	1.30	0.454	1.009	0.027
5	0.185	0.0360	3.36	0.535	0.935	0.059
6	0.222	0.0367	11.72	0.545	0.780	0.202
7	0.259	0.0370	14.65	0.547	0.660	0.251
8	0.296	0.0380	16.50	0.561	0.583	0.276
9	0.333	0.0386	17.58	0.571	0.519	0.289
10	0.370	0.0393	19.75	0.579	0.467	0.319

Test Filename   **D35B**

Engine Details

Configuration	IL4	Inner Seat Dia, mm	27	Shape Factor, LD	10.43
Cylinder bore	84.5	Seat Angle	45	Lmax/D	0.31
Engine Stroke	90	Max Valve Lift	8.37	D/B	0.32
Inlet Valves, n	1	Valve Opens	0	MIGV	132.2
Rated Speed, rpm	4500	Valve Closes	50	MPV	13.5

Test Details

Test Date	31-Oct-00	Barometer, mmHg	744.4	VFAM Constant	77.2
Test Pressure, mmH$_2$O	900	ISM Constant	1.09E-04		

Test Summary Results

Swirl Ratio (Rs)	1.78	Gulp Factor	0.869	Cf @ 0.3 L/D	0.566
Rs/LD	0.17	MCf	0.444	Cf @ Max Lift	0.567
CCf	1.781				

Test Results

Valve Lift		Air Flow	ISM Torque	Flow	Discharge	Non-dim
Test	Non-dim	m^3/s	NmE^{-3}	Coefficient	Coefficient	Rig Swirl
mm	L/D	Q	G	Cf	Cd	Ns
0	0.000	0.0000	0.00	0.000	0.000	0.000
1	0.037	0.0082	3.15	0.122	1.146	0.241
2	0.074	0.0153	4.02	0.227	1.045	0.166
3	0.111	0.0227	5.43	0.336	1.014	0.151
4	0.148	0.0301	7.81	0.446	0.991	0.164
5	0.185	0.0351	8.57	0.520	0.909	0.154
6	0.222	0.0363	14.00	0.537	0.769	0.244
7	0.259	0.0373	20.95	0.552	0.666	0.356
8	0.296	0.0382	24.42	0.565	0.587	0.405
9	0.333	0.0386	26.92	0.570	0.518	0.442
10	0.370	0.0390	28.76	0.576	0.464	0.468

Test Filename   **D35A**

Engine Details

Configuration	IL4	Inner Seat Dia, mm	27	Shape Factor, LD	10.43
Cylinder bore	84.5	Seat Angle	45	Lmax/D	0.31
Engine Stroke	90	Max Valve Lift	8.37	D/B	0.32
Inlet Valves, n	1	Valve Opens	0	MIGV	132.2
Rated Speed, rpm	4500	Valve Closes	50	MPV	13.5

Test Details

Test Date	31-Oct-00	Barometer, mmHg	744.2	VFAM Constant	77.2
Test Pressure, mmH$_2$O	900	ISM Constant	1.09E-04		

Test Summary Results

Swirl Ratio (Rs)	0.84	Gulp Factor	0.861	Cf @ 0.3 L/D	0.561
Rs/LD	0.08	MCf	0.447	Cf @ Max Lift	0.563
CCf	1.796				

Test Results

Valve Lift		Air Flow	ISM Torque	Flow	Discharge	Non-dim
Test	Non-dim	m^3/s	NmE^{-3}	Coefficient	Coefficient	Rig Swirl
mm	L/D	Q	G	Cf	Cd	Ns
0	0.000	0.0000	0.00	0.000	0.000	0.000
1	0.037	0.0083	0.43	0.123	1.149	0.033
2	0.074	0.0157	1.52	0.234	1.075	0.061
3	0.111	0.0232	1.95	0.345	1.041	0.053
4	0.148	0.0306	1.74	0.454	1.008	0.036
5	0.185	0.0359	3.04	0.534	0.932	0.053
6	0.222	0.0376	3.15	0.558	0.799	0.053
7	0.259	0.0371	12.26	0.551	0.665	0.208
8	0.296	0.0377	13.46	0.560	0.582	0.225
9	0.333	0.0384	14.76	0.570	0.518	0.243
10	0.370	0.0390	15.85	0.578	0.465	0.257

Test Filename   **D34B**

Engine Details

Configuration	IL4	Inner Seat Dia, mm	27	Shape Factor, LD	10.43
Cylinder bore	84.5	Seat Angle	45	Lmax/D	0.31
Engine Stroke	90	Max Valve Lift	8.37	D/B	0.32
Inlet Valves, n	1	Valve Opens	0	MIGV	132.2
Rated Speed, rpm	4500	Valve Closes	50	MPV	13.5

Test Details

Test Date	30-Oct-00	Barometer, mmHg	739.2	VFAM Constant	77.23
Test Pressure, mmH$_2$O	900	ISM Constant	1.09E-04		

Test Summary Results

Swirl Ratio (Rs)	1.52	Gulp Factor	0.866	Cf @ 0.3 L/D	0.572
Rs/LD	0.15	MCf	0.445	Cf @ Max Lift	0.575
CCf	1.786				

Test Results

Valve Lift		Air Flow	ISM Torque	Flow	Discharge	Non-dim
Test	Non-dim	m^3/s	NmE^{-3}	Coefficient	Coefficient	Rig Swirl
mm	L/D	Q	G	Cf	Cd	Ns
0	0.000	0.0000	0.00	0.000	0.000	0.000
1	0.037	0.0081	3.58	0.119	1.115	0.282
2	0.074	0.0154	4.56	0.228	1.049	0.187
3	0.111	0.0228	4.99	0.337	1.015	0.139
4	0.148	0.0303	6.95	0.447	0.993	0.146
5	0.185	0.0343	8.03	0.505	0.883	0.149
6	0.222	0.0365	11.07	0.538	0.770	0.193
7	0.259	0.0378	17.26	0.557	0.673	0.290
8	0.296	0.0388	20.84	0.571	0.594	0.342
9	0.333	0.0395	23.56	0.580	0.528	0.380
10	0.370	0.0400	25.29	0.587	0.473	0.404

C57

Test Filename   **D34A**

Engine Details

Configuration	IL4	Inner Seat Dia, mm	27	Shape Factor, LD	10.43
Cylinder bore	84.5	Seat Angle	45	Lmax/D	0.31
Engine Stroke	90	Max Valve Lift	8.37	D/B	0.32
Inlet Valves, n	1	Valve Opens	0	MIGV	132.2
Rated Speed, rpm	4500	Valve Closes	50	MPV	13.5

Test Details

Test Date	30-Oct-00	Barometer, mmHg	739.2	VFAM Constant	77.23
Test Pressure, mmH$_2$O	900	ISM Constant	1.09E-04		

Test Summary Results

Swirl Ratio (Rs)	0.68	Gulp Factor	0.853	Cf @ 0.3 L/D	0.572
Rs/LD	0.07	MCf	0.452	Cf @ Max Lift	0.576
CCf	1.814				

Test Results

Valve Lift		Air Flow	ISM Torque	Flow	Discharge	Non-dim
Test	Non-dim	m^3/s	NmE^{-3}	Coefficient	Coefficient	Rig Swirl
mm	L/D	Q	G	Cf	Cd	Ns
0	0.000	0.0000	0.00	0.000	0.000	0.000
1	0.037	0.0082	0.11	0.122	1.140	0.008
2	0.074	0.0156	1.30	0.231	1.064	0.053
3	0.111	0.0235	1.74	0.348	1.050	0.047
4	0.148	0.0308	1.41	0.456	1.012	0.029
5	0.185	0.0359	1.19	0.531	0.928	0.021
6	0.222	0.0379	0.22	0.561	0.803	0.004
7	0.259	0.0377	10.53	0.557	0.672	0.177
8	0.296	0.0387	12.05	0.571	0.593	0.198
9	0.333	0.0396	13.57	0.585	0.532	0.217
10	0.370	0.0401	15.52	0.592	0.477	0.246

Test Filename   **D33B**

Engine Details

Configuration	IL4	Inner Seat Dia, mm	27	Shape Factor, LD	10.43
Cylinder bore	84.5	Seat Angle	45	Lmax/D	0.31
Engine Stroke	90	Max Valve Lift	8.37	D/B	0.32
Inlet Valves, n	1	Valve Opens	0	MIGV	132.2
Rated Speed, rpm	4500	Valve Closes	50	MPV	13.5

Test Details

Test Date	30-Oct-00	Barometer, mmHg	738.8	VFAM Constant	77.23
Test Pressure, mmH$_2$O	900	ISM Constant	1.09E-04		

Test Summary Results

Swirl Ratio (Rs)	1.84	Gulp Factor	0.888	Cf @ 0.3 L/D	0.545
Rs/LD	0.18	MCf	0.434	Cf @ Max Lift	0.546
CCf	1.742				

Test Results

Valve Lift		Air Flow	ISM Torque	Flow	Discharge	Non-dim
Test	Non-dim	m^3/s	NmE^{-3}	Coefficient	Coefficient	Rig Swirl
mm	L/D	Q	G	Cf	Cd	Ns
0	0.000	0.0000	0.00	0.000	0.000	0.000
1	0.037	0.0082	3.80	0.122	1.142	0.292
2	0.074	0.0154	5.32	0.228	1.047	0.219
3	0.111	0.0229	6.51	0.338	1.018	0.181
4	0.148	0.0307	9.34	0.454	1.008	0.193
5	0.185	0.0351	9.88	0.518	0.906	0.179
6	0.222	0.0355	16.50	0.523	0.749	0.295
7	0.259	0.0364	19.97	0.536	0.647	0.349
8	0.296	0.0369	22.04	0.544	0.565	0.380
9	0.333	0.0374	24.32	0.551	0.501	0.414
10	0.370	0.0378	27.03	0.556	0.448	0.455

Test Filename **D33A**

Engine Details

Configuration	IL4	Inner Seat Dia, mm	27	Shape Factor, LD	10.43
Cylinder bore	84.5	Seat Angle	45	Lmax/D	0.31
Engine Stroke	90	Max Valve Lift	8.37	D/B	0.32
Inlet Valves, n	1	Valve Opens	0	MIGV	132.2
Rated Speed, rpm	4500	Valve Closes	50	MPV	13.5

Test Details

Test Date	30-Oct-00	Barometer, mmHg	738.8	VFAM Constant	77.23
Test Pressure, mmH$_2$O	900	ISM Constant	1.09E-04		

Test Summary Results

Swirl Ratio (Rs)	1.37	Gulp Factor	0.893	Cf @ 0.3 L/D	0.538
Rs/LD	0.13	MCf	0.431	Cf @ Max Lift	0.54
CCf	1.732				

Test Results

Valve Lift		Air Flow	ISM Torque	Flow	Discharge	Non-dim
Test	Non-dim	m^3/s	NmE^{-3}	Coefficient	Coefficient	Rig Swirl
mm	L/D	Q	G	Cf	Cd	Ns
0	0.000	0.0000	0.00	0.000	0.000	0.000
1	0.037	0.0083	0.76	0.123	1.157	0.058
2	0.074	0.0155	1.63	0.231	1.061	0.066
3	0.111	0.0234	1.95	0.347	1.046	0.053
4	0.148	0.0305	2.28	0.452	1.004	0.047
5	0.185	0.0355	4.88	0.525	0.917	0.087
6	0.222	0.0350	14.44	0.518	0.741	0.261
7	0.259	0.0356	16.50	0.527	0.636	0.294
8	0.296	0.0363	18.24	0.537	0.558	0.318
9	0.333	0.0371	19.54	0.547	0.497	0.335
10	0.370	0.0375	20.84	0.553	0.446	0.353

Test Filename   **D47B**

Engine Details

Configuration	IL4	Inner Seat Dia, mm	27	Shape Factor, LD	10.43
Cylinder bore	84.5	Seat Angle	45	Lmax/D	0.31
Engine Stroke	90	Max Valve Lift	8.37	D/B	0.32
Inlet Valves, n	1	Valve Opens	0	MIGV	132.2
Rated Speed, rpm	4500	Valve Closes	50	MPV	13.5

Test Details

Test Date	30-Oct-00	Barometer, mmHg	737.6	VFAM Constant	77.23
Test Pressure, mmH$_2$O	900	ISM Constant	1.09E-04		

Test Summary Results

Swirl Ratio (Rs)	1.74	Gulp Factor	0.873	Cf @ 0.3 L/D	0.564
Rs/LD	0.17	MCf	0.441	Cf @ Max Lift	0.566
CCf	1.771				

Test Results

Valve Lift		Air Flow	ISM Torque	Flow	Discharge	Non-dim
Test	Non-dim	m^3/s	NmE^{-3}	Coefficient	Coefficient	Rig Swirl
mm	L/D	Q	G	Cf	Cd	Ns
0	0.000	0.0000	0.00	0.000	0.000	0.000
1	0.037	0.0080	1.95	0.118	1.107	0.155
2	0.074	0.0153	3.04	0.225	1.035	0.127
3	0.111	0.0228	4.23	0.335	1.011	0.118
4	0.148	0.0305	6.62	0.449	0.997	0.138
5	0.185	0.0352	8.36	0.518	0.905	0.151
6	0.222	0.0361	15.20	0.531	0.760	0.268
7	0.259	0.0374	20.95	0.548	0.662	0.358
8	0.296	0.0384	23.77	0.563	0.585	0.396
9	0.333	0.0389	25.19	0.571	0.519	0.413
10	0.370	0.0396	26.92	0.580	0.467	0.435

Test Filename   **D47A**

Engine Details

Configuration	IL4	Inner Seat Dia, mm	27	Shape Factor, LD	10.43
Cylinder bore	84.5	Seat Angle	45	Lmax/D	0.31
Engine Stroke	90	Max Valve Lift	8.37	D/B	0.32
Inlet Valves, n	1	Valve Opens	0	MIGV	132.2
Rated Speed, rpm	4500	Valve Closes	50	MPV	13.5

Test Details

Test Date	30-Oct-00	Barometer, mmHg	737.1	VFAM Constant	77.24
Test Pressure, mmH_2O	900	ISM Constant	1.09E-04		

Test Summary Results

Swirl Ratio (Rs)	1.08	Gulp Factor	0.869	Cf @ 0.3 L/D	0.563
Rs/LD	0.1	MCf	0.443	Cf @ Max Lift	0.565
CCf	1.779				

Test Results

Valve Lift		Air Flow	ISM Torque	Flow	Discharge	Non-dim
Test	Non-dim	m^3/s	NmE^{-3}	Coefficient	Coefficient	Rig Swirl
mm	L/D	Q	G	Cf	Cd	Ns
0	0.000	0.0000	0.00	0.000	0.000	0.000
1	0.037	0.0081	0.11	0.119	1.117	0.009
2	0.074	0.0154	0.98	0.228	1.049	0.040
3	0.111	0.0231	1.30	0.341	1.028	0.036
4	0.148	0.0305	1.41	0.451	1.002	0.029
5	0.185	0.0360	3.15	0.532	0.929	0.055
6	0.222	0.0359	11.72	0.530	0.758	0.207
7	0.259	0.0373	14.00	0.549	0.663	0.239
8	0.296	0.0382	15.85	0.562	0.584	0.264
9	0.333	0.0388	17.15	0.570	0.518	0.282
10	0.370	0.0395	18.89	0.580	0.468	0.305

Test Filename   **D24B**

Engine Details

Configuration	IL4	Inner Seat Dia, mm	27	Shape Factor, LD	9.88
Cylinder bore	80	Seat Angle	45	Lmax/D	0.31
Engine Stroke	90	Max Valve Lift	8.37	D/B	0.338
Inlet Valves, n	1	Valve Opens	0	MIGV	118.5
Rated Speed, rpm	4500	Valve Closes	50	MPV	13.5

Test Details

Test Date	30-Oct-00	Barometer, mmHg	736	VFAM Constant	77.24
Test Pressure, mmH$_2$O	900	ISM Constant	1.09E-04		

Test Summary Results

Swirl Ratio (Rs)	1.17	Gulp Factor	0.768	Cf @ 0.3 L/D	0.58
Rs/LD	0.12	MCf	0.45	Cf @ Max Lift	0.583
CCf	1.805				

Test Results

Valve Lift		Air Flow	ISM Torque	Flow	Discharge	Non-dim
Test	Non-dim	m^3/s	NmE^{-3}	Coefficient	Coefficient	Rig Swirl
mm	L/D	Q	G	Cf	Cd	Ns
0	0.000	0.0000	0.00	0.000	0.000	0.000
1	0.037	0.0081	1.95	0.118	1.110	0.163
2	0.074	0.0153	2.82	0.225	1.034	0.124
3	0.111	0.0228	3.58	0.335	1.009	0.106
4	0.148	0.0304	4.78	0.445	0.989	0.106
5	0.185	0.0349	6.08	0.512	0.894	0.118
6	0.222	0.0373	7.49	0.546	0.782	0.136
7	0.259	0.0386	12.49	0.565	0.682	0.219
8	0.296	0.0396	17.81	0.579	0.602	0.304
9	0.333	0.0404	22.47	0.590	0.536	0.377
10	0.370	0.0413	25.62	0.604	0.486	0.420

Test Filename　　　　**D24A**

Engine Details

Configuration	IL4	Inner Seat Dia, mm	27	Shape Factor, LD	9.88
Cylinder bore	80	Seat Angle	45	Lmax/D	0.31
Engine Stroke	90	Max Valve Lift	8.37	D/B	0.338
Inlet Valves, n	1	Valve Opens	0	MIGV	118.5
Rated Speed, rpm	4500	Valve Closes	50	MPV	13.5

Test Details

Test Date	30-Oct-00	Barometer, mmHg	737	VFAM Constant	77.24
Test Pressure, mmH$_2$O	900	ISM Constant	1.09E-04		

Test Summary Results

Swirl Ratio (Rs)	1.2	Gulp Factor	0.766	Cf @ 0.3 L/D	0.584
Rs/LD	0.12	MCf	0.451	Cf @ Max Lift	0.587
CCf	1.809				

Test Results

Valve Lift		Air Flow	ISM Torque	Flow	Discharge	Non-dim
Test	Non-dim	m^3/s	NmE^{-3}	Coefficient	Coefficient	Rig Swirl
mm	L/D	Q	G	Cf	Cd	Ns
0	0.000	0.0000	0.00	0.000	0.000	0.000
1	0.037	0.0081	1.95	0.120	1.121	0.162
2	0.074	0.0153	3.04	0.225	1.035	0.134
3	0.111	0.0227	3.69	0.334	1.006	0.109
4	0.148	0.0303	5.21	0.445	0.989	0.116
5	0.185	0.0345	6.73	0.506	0.884	0.132
6	0.222	0.0374	8.14	0.549	0.786	0.147
7	0.259	0.0387	12.70	0.567	0.685	0.222
8	0.296	0.0398	17.91	0.583	0.606	0.304
9	0.333	0.0406	22.69	0.594	0.540	0.378
10	0.370	0.0416	25.51	0.608	0.490	0.415

Test Filename　　　　**D22B**

Engine Details

Configuration	IL4	Inner Seat Dia, mm	27	Shape Factor, LD	9.88
Cylinder bore	80	Seat Angle	45	Lmax/D	0.31
Engine Stroke	90	Max Valve Lift	8.37	D/B	0.338
Inlet Valves, n	1	Valve Opens	0	MIGV	118.5
Rated Speed, rpm	4500	Valve Closes	50	MPV	13.5

Test Details

Test Date	30-Oct-00	Barometer, mmHg	736.7	VFAM Constant	77.24
Test Pressure, mmH_2O	900	ISM Constant	1.09E-04		

Test Summary Results

Swirl Ratio (Rs)	1.55	Gulp Factor	0.766	Cf @ 0.3 L/D	0.578
Rs/LD	0.16	MCf	0.451	Cf @ Max Lift	0.579
CCf	1.81				

Test Results

Valve Lift		Air Flow	ISM Torque	Flow	Discharge	Non-dim
Test	Non-dim	m^3/s	NmE^{-3}	Coefficient	Coefficient	Rig Swirl
mm	L/D	Q	G	Cf	Cd	Ns
0	0.000	0.0000	0.00	0.000	0.000	0.000
1	0.037	0.0080	2.28	0.117	1.101	0.192
2	0.074	0.0154	3.91	0.227	1.045	0.170
3	0.111	0.0229	4.89	0.337	1.017	0.143
4	0.148	0.0298	5.75	0.439	0.976	0.130
5	0.185	0.0358	7.49	0.527	0.921	0.141
6	0.222	0.0374	11.40	0.550	0.788	0.205
7	0.259	0.0388	17.80	0.570	0.688	0.309
8	0.296	0.0393	23.34	0.577	0.600	0.400
9	0.333	0.0397	25.84	0.583	0.530	0.438
10	0.370	0.0402	28.88	0.589	0.474	0.485

C65

Test Filename　　　　**D22A**

Engine Details

Configuration	IL4	Inner Seat Dia, mm	27	Shape Factor, LD	9.88
Cylinder bore	80	Seat Angle	45	Lmax/D	0.31
Engine Stroke	90	Max Valve Lift	8.37	D/B	0.338
Inlet Valves, n	1	Valve Opens	0	MIGV	118.5
Rated Speed, rpm	4500	Valve Closes	50	MPV	13.5

Test Details

Test Date	30-Oct-00	Barometer, mmHg	736.7	VFAM Constant	77.24
Test Pressure, mmH$_2$O	900	ISM Constant	1.09E-04		

Test Summary Results

Swirl Ratio (Rs)	1.42	Gulp Factor	0.766	Cf @ 0.3 L/D	0.579
Rs/LD	0.14	MCf	0.451	Cf @ Max Lift	0.581
CCf	1.81				

Test Results

Valve Lift		Air Flow	ISM Torque	Flow	Discharge	Non-dim
Test	Non-dim	m^3/s	NmE^{-3}	Coefficient	Coefficient	Rig Swirl
mm	L/D	Q	G	Cf	Cd	Ns
0	0.000	0.0000	0.00	0.000	0.000	0.000
1	0.037	0.0079	2.17	0.117	1.092	0.184
2	0.074	0.0153	3.26	0.226	1.038	0.143
3	0.111	0.0230	4.34	0.339	1.022	0.127
4	0.148	0.0305	5.65	0.449	0.998	0.124
5	0.185	0.0347	7.49	0.510	0.892	0.145
6	0.222	0.0375	10.64	0.551	0.789	0.191
7	0.259	0.0387	15.96	0.570	0.688	0.277
8	0.296	0.0394	21.28	0.579	0.601	0.364
9	0.333	0.0398	24.64	0.585	0.532	0.417
10	0.370	0.0401	27.90	0.589	0.474	0.469

Test Filename   **D6B**

Engine Details

Configuration	IL4	Inner Seat Dia, mm	27	Shape Factor, LD	11.11
Cylinder bore	90	Seat Angle	45	Lmax/D	0.31
Engine Stroke	90	Max Valve Lift	8.37	D/B	0.3
Inlet Valves, n	1	Valve Opens	0	MIGV	150
Rated Speed, rpm	4500	Valve Closes	50	MPV	13.5

Test Details

Test Date	30-Oct-00	Barometer, mmHg	736.7	VFAM Constant	77.24
Test Pressure, mmH$_2$O	900	ISM Constant	1.09E-04		

Test Summary Results

Swirl Ratio (Rs)	1.35	Gulp Factor	0.974	Cf @ 0.3 L/D	0.581
Rs/LD	0.12	MCf	0.449	Cf @ Max Lift	0.584
CCf	1.802				

Test Results

Valve Lift		Air Flow	ISM Torque	Flow	Discharge	Non-dim
Test	Non-dim	m^3/s	NmE^{-3}	Coefficient	Coefficient	Rig Swirl
mm	L/D	Q	G	Cf	Cd	Ns
0	0.000	0.0000	0.00	0.000	0.000	0.000
1	0.037	0.0080	2.28	0.117	1.099	0.171
2	0.074	0.0153	3.26	0.226	1.040	0.127
3	0.111	0.0225	4.13	0.331	0.999	0.110
4	0.148	0.0300	5.75	0.442	0.981	0.115
5	0.185	0.0349	7.06	0.513	0.897	0.121
6	0.222	0.0370	7.38	0.544	0.779	0.119
7	0.259	0.0384	13.57	0.564	0.680	0.212
8	0.296	0.0395	21.28	0.580	0.602	0.323
9	0.333	0.0402	26.71	0.590	0.537	0.398
10	0.370	0.0412	29.86	0.604	0.486	0.435

Test Filename   **D6A**

Engine Details

Configuration	IL4	Inner Seat Dia, mm	27	Shape Factor, LD	11.11
Cylinder bore	90	Seat Angle	45	Lmax/D	0.31
Engine Stroke	90	Max Valve Lift	8.37	D/B	0.3
Inlet Valves, n	1	Valve Opens	0	MIGV	150
Rated Speed, rpm	4500	Valve Closes	50	MPV	13.5

Test Details

Test Date	30-Oct-00	Barometer, mmHg	736.4	VFAM Constant	77.24
Test Pressure, mmH$_2$O	900	ISM Constant	1.09E-04		

Test Summary Results

Swirl Ratio (Rs)	1.37	Gulp Factor	0.974	Cf @ 0.3 L/D	0.581
Rs/LD	0.12	MCf	0.449	Cf @ Max Lift	0.585
CCf	1.802				

Test Results

Valve Lift		Air Flow	ISM Torque	Flow	Discharge	Non-dim
Test	Non-dim	m^3/s	NmE^{-3}	Coefficient	Coefficient	Rig Swirl
mm	L/D	Q	G	Cf	Cd	Ns
0	0.000	0.0000	0.00	0.000	0.000	0.000
1	0.037	0.0078	2.06	0.116	1.085	0.157
2	0.074	0.0151	3.37	0.223	1.027	0.133
3	0.111	0.0227	4.34	0.335	1.010	0.114
4	0.148	0.0301	5.97	0.445	0.988	0.118
5	0.185	0.0341	6.62	0.504	0.881	0.116
6	0.222	0.0369	7.71	0.545	0.780	0.124
7	0.259	0.0384	14.00	0.566	0.683	0.218
8	0.296	0.0393	21.50	0.580	0.603	0.326
9	0.333	0.0402	27.03	0.592	0.538	0.401
10	0.370	0.0410	29.96	0.604	0.487	0.436

Test Filename   **D2AB**

Engine Details

Configuration	IL4	Inner Seat Dia, mm	27	Shape Factor, LD	11.11
Cylinder bore	90	Seat Angle	45	Lmax/D	0.31
Engine Stroke	90	Max Valve Lift	8.37	D/B	0.3
Inlet Valves, n	1	Valve Opens	0	MIGV	150
Rated Speed, rpm	4500	Valve Closes	50	MPV	13.5

Test Details

Test Date	30-Oct-00	Barometer, mmHg	735.9	VFAM Constant	77.24
Test Pressure, mmH$_2$O	900	ISM Constant	1.09E-04		

Test Summary Results

Swirl Ratio (Rs)	-0.03	Gulp Factor	0.95	Cf @ 0.3 L/D	0.6
Rs/LD	0	MCf	0.46	Cf @ Max Lift	0.599
CCf	1.848				

Test Results

Valve Lift		Air Flow	ISM Torque	Flow	Discharge	Non-dim
Test	Non-dim	m^3/s	NmE^{-3}	Coefficient	Coefficient	Rig Swirl
mm	L/D	Q	G	Cf	Cd	Ns
0	0.000	0.0000	0.00	0.000	0.000	0.000
1	0.037	0.0079	-2.17	0.116	1.091	-0.164
2	0.074	0.0155	-1.74	0.229	1.055	-0.067
3	0.111	0.0230	-1.63	0.341	1.027	-0.042
4	0.148	0.0300	-1.41	0.444	0.986	-0.028
5	0.185	0.0352	-0.43	0.520	0.909	-0.007
6	0.222	0.0376	0.43	0.556	0.796	0.007
7	0.259	0.0394	-0.11	0.582	0.703	-0.002
8	0.296	0.0407	0.00	0.601	0.624	0.000
9	0.333	0.0404	6.41	0.596	0.542	0.094
10	0.370	0.0413	4.67	0.609	0.491	0.067

Test Filename   **D20AB**

Engine Details

Configuration	IL4	Inner Seat Dia, mm	27	Shape Factor, LD	9.88
Cylinder bore	80	Seat Angle	45	Lmax/D	0.31
Engine Stroke	90	Max Valve Lift	8.37	D/B	0.338
Inlet Valves, n	1	Valve Opens	0	MIGV	118.5
Rated Speed, rpm	4500	Valve Closes	50	MPV	13.5

Test Details

Test Date	25-Oct-00	Barometer, mmHg	756.8	VFAM Constant	77.15
Test Pressure, mmH$_2$O	900	ISM Constant	1.09E-04		

Test Summary Results

Swirl Ratio (Rs)	-0.03	Gulp Factor	0.748	Cf @ 0.3 L/D	0.6
Rs/LD	0	MCf	0.461	Cf @ Max Lift	0.6
CCf	1.852				

Test Results

Valve Lift		Air Flow	ISM Torque	Flow	Discharge	Non-dim
Test	Non-dim	m^3/s	NmE^{-3}	Coefficient	Coefficient	Rig Swirl
mm	L/D	Q	G	Cf	Cd	Ns
0	0.000	0.0000	0.00	0.000	0.000	0.000
1	0.037	0.0078	-1.74	0.117	1.097	-0.147
2	0.074	0.0153	-1.30	0.228	1.051	-0.056
3	0.111	0.0228	-1.19	0.341	1.029	-0.035
4	0.148	0.0300	-1.08	0.448	0.995	-0.024
5	0.185	0.0351	-0.54	0.524	0.915	-0.010
6	0.222	0.0377	0.00	0.562	0.805	0.000
7	0.259	0.0390	0.00	0.581	0.702	0.000
8	0.296	0.0403	-0.22	0.600	0.624	-0.004
9	0.333	0.0404	5.97	0.601	0.546	0.098
10	0.370	0.0413	4.99	0.613	0.494	0.081

C70

Test Filename　　　　　**D8B**

Engine Details

Configuration	IL4	Inner Seat Dia, mm	27	Shape Factor, LD	11.11
Cylinder bore	90	Seat Angle	45	Lmax/D	0.31
Engine Stroke	90	Max Valve Lift	8.37	D/B	0.3
Inlet Valves, n	1	Valve Opens	0	MIGV	150
Rated Speed, rpm	4500	Valve Closes	50	MPV	13.5

Test Details

Test Date	25-Oct-00	Barometer, mmHg	756.4	VFAM Constant	77.15
Test Pressure, mmH$_2$O	900	ISM Constant	1.09E-04		

Test Summary Results

Swirl Ratio (Rs)	1.81	Gulp Factor	0.965	Cf @ 0.3 L/D	0.577
Rs/LD	0.16	MCf	0.453	Cf @ Max Lift	0.579
CCf	1.817				

Test Results

Valve Lift		Air Flow	ISM Torque	Flow	Discharge	Non-dim
Test	Non-dim	m^3/s	NmE^{-3}	Coefficient	Coefficient	Rig Swirl
mm	L/D	Q	G	Cf	Cd	Ns
0	0.000	0.0000	0.00	0.000	0.000	0.000
1	0.037	0.0080	2.93	0.119	1.118	0.216
2	0.074	0.0155	4.66	0.231	1.063	0.178
3	0.111	0.0228	6.18	0.341	1.029	0.159
4	0.148	0.0299	7.38	0.446	0.991	0.145
5	0.185	0.0358	10.09	0.535	0.935	0.166
6	0.222	0.0370	14.54	0.552	0.790	0.232
7	0.259	0.0380	21.05	0.566	0.684	0.327
8	0.296	0.0387	26.25	0.577	0.599	0.400
9	0.333	0.0392	29.61	0.584	0.531	0.446
10	0.370	0.0396	33.30	0.589	0.475	0.497

Test Filename   **D8A**

Engine Details

Configuration	IL4	Inner Seat Dia, mm	27	Shape Factor, LD	11.11
Cylinder bore	90	Seat Angle	45	Lmax/D	0.31
Engine Stroke	90	Max Valve Lift	8.37	D/B	0.3
Inlet Valves, n	1	Valve Opens	0	MIGV	150
Rated Speed, rpm	4500	Valve Closes	50	MPV	13.5

Test Details

Test Date	25-Oct-00	Barometer, mmHg	756.2	VFAM Constant	77.15
Test Pressure, mmH$_2$O	900	ISM Constant	1.09E-04		

Test Summary Results

Swirl Ratio (Rs)	1.73	Gulp Factor	0.965	Cf @ 0.3 L/D	0.576
Rs/LD	0.16	MCf	0.453	Cf @ Max Lift	0.578
CCf	1.818				

Test Results

Valve Lift		Air Flow	ISM Torque	Flow	Discharge	Non-dim
Test	Non-dim	m^3/s	NmE^{-3}	Coefficient	Coefficient	Rig Swirl
mm	L/D	Q	G	Cf	Cd	Ns
0	0.000	0.0000	0.00	0.000	0.000	0.000
1	0.037	0.0079	3.47	0.118	1.107	0.259
2	0.074	0.0155	4.99	0.231	1.064	0.190
3	0.111	0.0229	6.07	0.343	1.033	0.156
4	0.148	0.0302	8.14	0.451	1.003	0.158
5	0.185	0.0360	10.63	0.538	0.940	0.174
6	0.222	0.0370	13.99	0.551	0.790	0.223
7	0.259	0.0379	19.09	0.565	0.683	0.297
8	0.296	0.0386	24.73	0.576	0.598	0.378
9	0.333	0.0391	29.07	0.582	0.530	0.439
10	0.370	0.0395	33.52	0.588	0.474	0.501

Test Filename   **D4AB**

Engine Details

Configuration	IL4	Inner Seat Dia, mm	27	Shape Factor, LD	11.11
Cylinder bore	90	Seat Angle	45	Lmax/D	0.31
Engine Stroke	90	Max Valve Lift	8.37	D/B	0.3
Inlet Valves, n	1	Valve Opens	0	MIGV	150
Rated Speed, rpm	4500	Valve Closes	50	MPV	13.5

Test Details

Test Date	25-Oct-00	Barometer, mmHg	756.2	VFAM Constant	77.15
Test Pressure, mmH$_2$O	900	ISM Constant	1.09E-04		

Test Summary Results

Swirl Ratio (Rs)	-0.27	Gulp Factor	0.968	Cf @ 0.3 L/D	0.581
Rs/LD	-0.02	MCf	0.451	Cf @ Max Lift	0.585
CCf	1.812				

Test Results

Valve Lift		Air Flow	ISM Torque	Flow	Discharge	Non-dim
Test	Non-dim	m^3/s	NmE^{-3}	Coefficient	Coefficient	Rig Swirl
mm	L/D	Q	G	Cf	Cd	Ns
0	0.000	0.0000	0.00	0.000	0.000	0.000
1	0.037	0.0082	-1.52	0.122	1.146	-0.109
2	0.074	0.0152	-1.41	0.227	1.045	-0.055
3	0.111	0.0227	-1.19	0.340	1.024	-0.031
4	0.148	0.0303	-1.19	0.452	1.004	-0.023
5	0.185	0.0348	0.00	0.519	0.906	0.000
6	0.222	0.0369	-3.58	0.548	0.784	-0.057
7	0.259	0.0379	-3.04	0.563	0.679	-0.047
8	0.296	0.0390	-3.36	0.579	0.602	-0.051
9	0.333	0.0401	-3.25	0.595	0.541	-0.048
10	0.370	0.0406	0.54	0.602	0.485	0.008

C73

Test Filename   **D18AB**

Engine Details

Configuration	IL4	Inner Seat Dia, mm	27	Shape Factor, LD	9.88
Cylinder bore	80	Seat Angle	45	Lmax/D	0.31
Engine Stroke	90	Max Valve Lift	8.37	D/B	0.338
Inlet Valves, n	1	Valve Opens	0	MIGV	118.5
Rated Speed, rpm	4500	Valve Closes	50	MPV	13.5

Test Details

Test Date	25-Oct-00	Barometer, mmHg	756.3	VFAM Constant	77.15
Test Pressure, mmH$_2$O	900	ISM Constant	1.09E-04		

Test Summary Results

Swirl Ratio (Rs)	-0.23	Gulp Factor	0.757	Cf @ 0.3 L/D	0.586
Rs/LD	-0.02	MCf	0.456	Cf @ Max Lift	0.59
CCf	1.832				

Test Results

Valve Lift		Air Flow	ISM Torque	Flow	Discharge	Non-dim
Test	Non-dim	m^3/s	NmE^{-3}	Coefficient	Coefficient	Rig Swirl
mm	L/D	Q	G	Cf	Cd	Ns
0	0.000	0.0000	0.00	0.000	0.000	0.000
1	0.037	0.0081	-1.08	0.121	1.131	-0.089
2	0.074	0.0155	-0.76	0.232	1.066	-0.032
3	0.111	0.0231	-0.87	0.345	1.039	-0.025
4	0.148	0.0307	-0.87	0.459	1.020	-0.019
5	0.185	0.0348	-3.58	0.520	0.908	-0.068
6	0.222	0.0373	-3.04	0.557	0.797	-0.054
7	0.259	0.0382	-2.50	0.569	0.687	-0.043
8	0.296	0.0392	-2.60	0.585	0.608	-0.044
9	0.333	0.0402	-0.33	0.599	0.544	-0.005
10	0.370	0.0409	-0.22	0.609	0.490	-0.004

C74

Test Filename   **D46B**

Engine Details

Configuration	IL4	Inner Seat Dia, mm	27	Shape Factor, LD	10.43
Cylinder bore	84.5	Seat Angle	45	Lmax/D	0.31
Engine Stroke	90	Max Valve Lift	8.37	D/B	0.32
Inlet Valves, n	1	Valve Opens	0	MIGV	132.2
Rated Speed, rpm	4500	Valve Closes	50	MPV	13.5

Test Details

Test Date	25-Oct-00	Barometer, mmHg	756.1	VFAM Constant	77.15
Test Pressure, mmH$_2$O	900	ISM Constant	1.09E-04		

Test Summary Results

Swirl Ratio (Rs)	1.72	Gulp Factor	0.873	Cf @ 0.3 L/D	0.564
Rs/LD	0.16	MCf	0.441	Cf @ Max Lift	0.566
CCf	1.772				

Test Results

Valve Lift		Air Flow	ISM Torque	Flow	Discharge	Non-dim
Test	Non-dim	m^3/s	NmE^{-3}	Coefficient	Coefficient	Rig Swirl
mm	L/D	Q	G	Cf	Cd	Ns
0	0.000	0.0000	0.00	0.000	0.000	0.000
1	0.037	0.0080	2.17	0.120	1.123	0.170
2	0.074	0.0151	3.36	0.226	1.039	0.140
3	0.111	0.0226	4.34	0.337	1.017	0.121
4	0.148	0.0299	6.51	0.446	0.991	0.137
5	0.185	0.0347	7.81	0.517	0.903	0.142
6	0.222	0.0356	15.08	0.530	0.759	0.266
7	0.259	0.0369	20.61	0.549	0.662	0.352
8	0.296	0.0378	23.43	0.563	0.585	0.390
9	0.333	0.0385	25.06	0.572	0.520	0.410
10	0.370	0.0390	26.69	0.579	0.467	0.432

Test Filename   **D46A**

Engine Details

Configuration	IL4	Inner Seat Dia, mm	27	Shape Factor, LD	10.43
Cylinder bore	84.5	Seat Angle	45	Lmax/D	0.31
Engine Stroke	90	Max Valve Lift	8.37	D/B	0.32
Inlet Valves, n	1	Valve Opens	0	MIGV	132.2
Rated Speed, rpm	4500	Valve Closes	50	MPV	13.5

Test Details

Test Date	25-Oct-00	Barometer, mmHg	756.1	VFAM Constant	77.15
Test Pressure, mmH$_2$O	900	ISM Constant	1.09E-04		

Test Summary Results

Swirl Ratio (Rs)	1.15	Gulp Factor	0.869	Cf @ 0.3 L/D	0.562
Rs/LD	0.11	MCf	0.444	Cf @ Max Lift	0.564
CCf	1.781				

Test Results

Valve Lift		Air Flow	ISM Torque	Flow	Discharge	Non-dim
Test	Non-dim	m^3/s	NmE^{-3}	Coefficient	Coefficient	Rig Swirl
mm	L/D	Q	G	Cf	Cd	Ns
0	0.000	0.0000	0.00	0.000	0.000	0.000
1	0.037	0.0081	0.22	0.121	1.133	0.017
2	0.074	0.0155	1.19	0.232	1.068	0.048
3	0.111	0.0232	1.30	0.347	1.046	0.035
4	0.148	0.0305	1.84	0.456	1.014	0.038
5	0.185	0.0355	3.47	0.531	0.928	0.061
6	0.222	0.0354	12.48	0.528	0.756	0.221
7	0.259	0.0367	14.86	0.547	0.660	0.255
8	0.296	0.0376	16.92	0.561	0.583	0.283
9	0.333	0.0383	18.12	0.570	0.519	0.298
10	0.370	0.0390	20.07	0.581	0.468	0.323

Test Filename   **D1AB**

Engine Details

Configuration	IL4	Inner Seat Dia, mm	27	Shape Factor, LD	11.11
Cylinder bore	90	Seat Angle	45	Lmax/D	0.31
Engine Stroke	90	Max Valve Lift	8.37	D/B	0.3
Inlet Valves, n	1	Valve Opens	0	MIGV	150
Rated Speed, rpm	4500	Valve Closes	50	MPV	13.5

Test Details

Test Date	23-Oct-00	Barometer, mmHg	761.8	VFAM Constant	77.13
Test Pressure, mmH$_2$O	900	ISM Constant	1.09E-04		

Test Summary Results

Swirl Ratio (Rs)	0.16	Gulp Factor	1.021	Cf @ 0.3 L/D	0.542
Rs/LD	0.01	MCf	0.428	Cf @ Max Lift	0.545
CCf	1.719				

Test Results

Valve Lift		Air Flow	ISM Torque	Flow	Discharge	Non-dim
Test	Non-dim	m^3/s	NmE^{-3}	Coefficient	Coefficient	Rig Swirl
mm	L/D	Q	G	Cf	Cd	Ns
0	0.000	0.0000	0.00	0.000	0.000	0.000
1	0.037	0.0080	-0.76	0.119	1.113	-0.056
2	0.074	0.0150	-0.87	0.224	1.031	-0.034
3	0.111	0.0223	-0.43	0.333	1.003	-0.011
4	0.148	0.0296	-1.19	0.441	0.980	-0.024
5	0.185	0.0337	-0.43	0.503	0.878	-0.008
6	0.222	0.0346	3.15	0.514	0.737	0.054
7	0.259	0.0357	2.60	0.531	0.641	0.043
8	0.296	0.0364	2.71	0.541	0.562	0.044
9	0.333	0.0371	2.28	0.551	0.501	0.036
10	0.370	0.0378	0.43	0.561	0.452	0.007

Test Filename   **D23B**

Engine Details

Configuration	IL4	Inner Seat Dia, mm	27	Shape Factor, LD	9.88
Cylinder bore	80	Seat Angle	45	Lmax/D	0.31
Engine Stroke	90	Max Valve Lift	8.37	D/B	0.338
Inlet Valves, n	1	Valve Opens	0	MIGV	118.5
Rated Speed, rpm	4500	Valve Closes	50	MPV	13.5

Test Details

Test Date	23-Oct-00	Barometer, mmHg	761.7	VFAM Constant	77.13
Test Pressure, mmH_2O	900	ISM Constant	1.09E-04		

Test Summary Results

Swirl Ratio (Rs)	2.23	Gulp Factor	0.8	Cf @ 0.3 L/D	0.538
Rs/LD	0.23	MCf	0.431	Cf @ Max Lift	0.542
CCf	1.732				

Test Results

Valve Lift		Air Flow	ISM Torque	Flow	Discharge	Non-dim
Test	Non-dim	m^3/s	NmE^{-3}	Coefficient	Coefficient	Rig Swirl
mm	L/D	Q	G	Cf	Cd	Ns
0	0.000	0.0000	0.00	0.000	0.000	0.000
1	0.037	0.0080	2.39	0.119	1.115	0.198
2	0.074	0.0152	4.12	0.227	1.045	0.180
3	0.111	0.0225	5.31	0.335	1.009	0.157
4	0.148	0.0294	6.72	0.438	0.973	0.152
5	0.185	0.0349	10.41	0.520	0.908	0.198
6	0.222	0.0366	16.16	0.544	0.779	0.294
7	0.259	0.0355	26.68	0.528	0.638	0.500
8	0.296	0.0361	29.93	0.536	0.557	0.552
9	0.333	0.0371	31.13	0.552	0.501	0.558
10	0.370	0.0370	33.84	0.549	0.442	0.610

Test Filename   **D23A**

Engine Details

Configuration	IL4	Inner Seat Dia, mm	27	Shape Factor, LD	9.88
Cylinder bore	80	Seat Angle	45	Lmax/D	0.31
Engine Stroke	90	Max Valve Lift	8.37	D/B	0.338
Inlet Valves, n	1	Valve Opens	0	MIGV	118.5
Rated Speed, rpm	4500	Valve Closes	50	MPV	13.5

Test Details

Test Date	23-Oct-00	Barometer, mmHg	761.8	VFAM Constant	77.13
Test Pressure, mmH$_2$O	900	ISM Constant	1.09E-04		

Test Summary Results

Swirl Ratio (Rs)	2.16	Gulp Factor	0.798	Cf @ 0.3 L/D	0.54
Rs/LD	0.22	MCf	0.433	Cf @ Max Lift	0.542
CCf	1.738				

Test Results

Valve Lift		Air Flow	ISM Torque	Flow	Discharge	Non-dim
Test	Non-dim	m^3/s	NmE^{-3}	Coefficient	Coefficient	Rig Swirl
mm	L/D	Q	G	Cf	Cd	Ns
0	0.000	0.0000	0.00	0.000	0.000	0.000
1	0.037	0.0082	2.60	0.122	1.144	0.211
2	0.074	0.0155	4.12	0.232	1.066	0.176
3	0.111	0.0228	5.10	0.340	1.026	0.148
4	0.148	0.0298	6.72	0.445	0.988	0.150
5	0.185	0.0350	9.54	0.523	0.913	0.181
6	0.222	0.0353	18.33	0.526	0.754	0.345
7	0.259	0.0358	24.19	0.534	0.645	0.448
8	0.296	0.0362	29.17	0.539	0.561	0.535
9	0.333	0.0367	30.26	0.546	0.497	0.548
10	0.370	0.0370	32.32	0.551	0.444	0.580

Test Filename   **D3AB**

Engine Details

Configuration	IL4	Inner Seat Dia, mm	27	Shape Factor, LD	11.11
Cylinder bore	90	Seat Angle	45	Lmax/D	0.31
Engine Stroke	90	Max Valve Lift	8.37	D/B	0.3
Inlet Valves, n	1	Valve Opens	0	MIGV	150
Rated Speed, rpm	4500	Valve Closes	50	MPV	13.5

Test Details

Test Date	23-Oct-00	Barometer, mmHg	761.8	VFAM Constant	77.13
Test Pressure, mmH$_2$O	900	ISM Constant	1.09E-04		

Test Summary Results

Swirl Ratio (Rs)	-0.12	Gulp Factor	0.992	Cf @ 0.3 L/D	0.566
Rs/LD	-0.01	MCf	0.44	Cf @ Max Lift	0.564
CCf	1.768				

Test Results

Valve Lift		Air Flow	ISM Torque	Flow	Discharge	Non-dim
Test	Non-dim	m^3/s	NmE^{-3}	Coefficient	Coefficient	Rig Swirl
mm	L/D	Q	G	Cf	Cd	Ns
0	0.000	0.0000	0.00	0.000	0.000	0.000
1	0.037	0.0080	-1.30	0.120	1.121	-0.096
2	0.074	0.0153	-1.08	0.229	1.055	-0.042
3	0.111	0.0228	-1.19	0.342	1.030	-0.031
4	0.148	0.0297	-1.08	0.444	0.987	-0.021
5	0.185	0.0338	-1.19	0.506	0.885	-0.021
6	0.222	0.0351	-0.33	0.526	0.753	-0.005
7	0.259	0.0364	-0.65	0.545	0.658	-0.011
8	0.296	0.0379	-0.43	0.567	0.589	-0.007
9	0.333	0.0375	-5.97	0.560	0.509	-0.094
10	0.370	0.0380	-4.66	0.567	0.457	-0.072

Test Filename   **D17AB**

Engine Details

Configuration	IL4	Inner Seat Dia, mm	27	Shape Factor, LD	9.88
Cylinder bore	80	Seat Angle	45	Lmax/D	0.31
Engine Stroke	90	Max Valve Lift	8.37	D/B	0.338
Inlet Valves, n	1	Valve Opens	0	MIGV	118.5
Rated Speed, rpm	4500	Valve Closes	50	MPV	13.5

Test Details

Test Date	23-Oct-00	Barometer, mmHg	761.9	VFAM Constant	77.13
Test Pressure, mmH$_2$O	900	ISM Constant	1.09E-04		

Test Summary Results

Swirl Ratio (Rs)	-0.09	Gulp Factor	0.79	Cf @ 0.3 L/D	0.562
Rs/LD	-0.01	MCf	0.437	Cf @ Max Lift	0.561
CCf	1.755				

Test Results

Valve Lift		Air Flow	ISM Torque	Flow	Discharge	Non-dim
Test	Non-dim	m^3/s	NmE^{-3}	Coefficient	Coefficient	Rig Swirl
mm	L/D	Q	G	Cf	Cd	Ns
0	0.000	0.0000	0.00	0.000	0.000	0.000
1	0.037	0.0080	-1.08	0.119	1.112	-0.090
2	0.074	0.0153	-0.43	0.228	1.051	-0.019
3	0.111	0.0228	-0.76	0.339	1.023	-0.022
4	0.148	0.0295	-0.43	0.439	0.975	-0.010
5	0.185	0.0337	-0.87	0.503	0.878	-0.017
6	0.222	0.0351	-1.08	0.522	0.748	-0.021
7	0.259	0.0364	-0.43	0.541	0.653	-0.008
8	0.296	0.0379	-0.11	0.563	0.585	-0.002
9	0.333	0.0377	-4.99	0.559	0.508	-0.088
10	0.370	0.0382	-3.47	0.567	0.456	-0.061

Test Filename   **D5B**

Engine Details

Configuration	IL4	Inner Seat Dia, mm	27	Shape Factor, LD	11.11
Cylinder bore	90	Seat Angle	45	Lmax/D	0.31
Engine Stroke	90	Max Valve Lift	8.37	D/B	0.3
Inlet Valves, n	1	Valve Opens	0	MIGV	150
Rated Speed, rpm	4500	Valve Closes	50	MPV	13.5

Test Details

Test Date	23-Oct-00	Barometer, mmHg	762.1	VFAM Constant	77.12
Test Pressure, mmH$_2$O	900	ISM Constant	1.09E-04		

Test Summary Results

Swirl Ratio (Rs)	2.56	Gulp Factor	1.013	Cf @ 0.3 L/D	0.535
Rs/LD	0.23	MCf	0.431	Cf @ Max Lift	0.537
CCf	1.732				

Test Results

Valve Lift		Air Flow	ISM Torque	Flow	Discharge	Non-dim
Test	Non-dim	m^3/s	NmE^{-3}	Coefficient	Coefficient	Rig Swirl
mm	L/D	Q	G	Cf	Cd	Ns
0	0.000	0.0000	0.00	0.000	0.000	0.000
1	0.037	0.0081	2.82	0.120	1.128	0.206
2	0.074	0.0153	4.99	0.229	1.053	0.192
3	0.111	0.0226	6.51	0.337	1.015	0.170
4	0.148	0.0294	8.57	0.439	0.975	0.172
5	0.185	0.0349	13.45	0.520	0.908	0.228
6	0.222	0.0368	20.06	0.547	0.784	0.322
7	0.259	0.0355	30.26	0.528	0.637	0.504
8	0.296	0.0360	32.75	0.535	0.556	0.538
9	0.333	0.0364	35.68	0.540	0.491	0.581
10	0.370	0.0369	39.59	0.548	0.441	0.636

Test Filename   **D5A**

Engine Details

Configuration	IL4	Inner Seat Dia, mm	27	Shape Factor, LD	11.11
Cylinder bore	90	Seat Angle	45	Lmax/D	0.31
Engine Stroke	90	Max Valve Lift	8.37	D/B	0.3
Inlet Valves, n	1	Valve Opens	0	MIGV	150
Rated Speed, rpm	4500	Valve Closes	50	MPV	13.5

Test Details

Test Date	23-Oct-00	Barometer, mmHg	762.6	VFAM Constant	77.12
Test Pressure, mmH$_2$O	900	ISM Constant	1.09E-04		

Test Summary Results

Swirl Ratio (Rs)	2.47	Gulp Factor	1.014	Cf @ 0.3 L/D	0.536
Rs/LD	0.22	MCf	0.431	Cf @ Max Lift	0.538
CCf	1.73				

Test Results

Valve Lift		Air Flow	ISM Torque	Flow	Discharge	Non-dim
Test	Non-dim	m^3/s	NmE^{-3}	Coefficient	Coefficient	Rig Swirl
mm	L/D	Q	G	Cf	Cd	Ns
0	0.000	0.0000	0.00	0.000	0.000	0.000
1	0.037	0.0080	2.82	0.119	1.117	0.208
2	0.074	0.0154	4.99	0.230	1.060	0.191
3	0.111	0.0229	6.29	0.342	1.032	0.162
4	0.148	0.0300	8.46	0.449	0.998	0.166
5	0.185	0.0354	12.36	0.529	0.924	0.206
6	0.222	0.0346	21.37	0.516	0.739	0.364
7	0.259	0.0356	29.28	0.531	0.641	0.485
8	0.296	0.0359	30.80	0.536	0.557	0.506
9	0.333	0.0363	33.73	0.541	0.492	0.548
10	0.370	0.0367	37.53	0.547	0.441	0.603

Test Filename   **D21B**

Engine Details

Configuration	IL4	Inner Seat Dia, mm	27	Shape Factor, LD	9.88
Cylinder bore	80	Seat Angle	45	Lmax/D	0.31
Engine Stroke	90	Max Valve Lift	8.37	D/B	0.338
Inlet Valves, n	1	Valve Opens	0	MIGV	118.5
Rated Speed, rpm	4500	Valve Closes	50	MPV	13.5

Test Details

Test Date	23-Oct-00	Barometer, mmHg	762.6	VFAM Constant	77.12
Test Pressure, mmH_2O	900	ISM Constant	1.09E-04		

Test Summary Results

Swirl Ratio (Rs)	1.78	Gulp Factor	0.804	Cf @ 0.3 L/D	0.545
Rs/LD	0.18	MCf	0.429	Cf @ Max Lift	0.548
CCf	1.723				

Test Results

Valve Lift		Air Flow	ISM Torque	Flow	Discharge	Non-dim
Test	Non-dim	m^3/s	NmE^{-3}	Coefficient	Coefficient	Rig Swirl
mm	L/D	Q	G	Cf	Cd	Ns
0	0.000	0.0000	0.00	0.000	0.000	0.000
1	0.037	0.0079	1.95	0.118	1.107	0.164
2	0.074	0.0151	2.93	0.226	1.039	0.128
3	0.111	0.0223	4.01	0.332	1.002	0.119
4	0.148	0.0297	5.64	0.443	0.984	0.126
5	0.185	0.0337	9.65	0.502	0.877	0.190
6	0.222	0.0347	13.77	0.517	0.740	0.264
7	0.259	0.0356	18.87	0.530	0.640	0.352
8	0.296	0.0365	23.64	0.543	0.565	0.431
9	0.333	0.0374	27.11	0.556	0.505	0.483
10	0.370	0.0379	29.17	0.563	0.454	0.512

C84

Test Filename   **D19AB**

Engine Details

Configuration	IL4	Inner Seat Dia, mm	27	Shape Factor, LD	9.88
Cylinder bore	80	Seat Angle	45	Lmax/D	0.31
Engine Stroke	90	Max Valve Lift	8.37	D/B	0.338
Inlet Valves, n	1	Valve Opens	0	MIGV	118.5
Rated Speed, rpm	4500	Valve Closes	50	MPV	13.5

Test Details

Test Date	23-Oct-00	Barometer, mmHg	762.7	VFAM Constant	77.12
Test Pressure, mmH$_2$O	900	ISM Constant	1.09E-04		

Test Summary Results

Swirl Ratio (Rs)	-0.09	Gulp Factor	0.801	Cf @ 0.3 L/D	0.545
Rs/LD	-0.01	MCf	0.431	Cf @ Max Lift	0.548
CCf	1.73				

Test Results

Valve Lift		Air Flow	ISM Torque	Flow	Discharge	Non-dim
Test	Non-dim	m^3/s	NmE^{-3}	Coefficient	Coefficient	Rig Swirl
mm	L/D	Q	G	Cf	Cd	Ns
0	0.000	0.0000	0.00	0.000	0.000	0.000
1	0.037	0.0081	-0.65	0.121	1.131	-0.053
2	0.074	0.0152	-0.54	0.226	1.042	-0.024
3	0.111	0.0224	-0.43	0.334	1.008	-0.013
4	0.148	0.0298	-0.76	0.445	0.988	-0.017
5	0.185	0.0339	-0.22	0.505	0.883	-0.004
6	0.222	0.0349	-2.82	0.520	0.745	-0.054
7	0.259	0.0358	-2.06	0.532	0.643	-0.038
8	0.296	0.0366	0.43	0.544	0.565	0.008
9	0.333	0.0374	0.43	0.556	0.505	0.008
10	0.370	0.0378	0.33	0.562	0.453	0.006

Test Filename **D21A**

Engine Details

Configuration	IL4	Inner Seat Dia, mm	27	Shape Factor, LD	9.88
Cylinder bore	80	Seat Angle	45	Lmax/D	0.31
Engine Stroke	90	Max Valve Lift	8.37	D/B	0.338
Inlet Valves, n	1	Valve Opens	0	MIGV	118.5
Rated Speed, rpm	4500	Valve Closes	50	MPV	13.5

Test Details

Test Date	23-Oct-00	Barometer, mmHg	762.8	VFAM Constant	77.12
Test Pressure, mmH_2O	900	ISM Constant	1.09E-04		

Test Summary Results

Swirl Ratio (Rs)	1.64	Gulp Factor	0.805	Cf @ 0.3 L/D	0.542
Rs/LD	0.17	MCf	0.429	Cf @ Max Lift	0.545
CCf	1.723				

Test Results

Valve Lift		Air Flow	ISM Torque	Flow	Discharge	Non-dim
Test	Non-dim	m^3/s	NmE^{-3}	Coefficient	Coefficient	Rig Swirl
mm	L/D	Q	G	Cf	Cd	Ns
0	0.000	0.0000	0.00	0.000	0.000	0.000
1	0.037	0.0080	2.17	0.120	1.124	0.179
2	0.074	0.0152	3.15	0.227	1.045	0.137
3	0.111	0.0224	3.90	0.336	1.012	0.115
4	0.148	0.0297	5.31	0.443	0.985	0.119
5	0.185	0.0339	8.68	0.506	0.885	0.170
6	0.222	0.0346	12.58	0.517	0.740	0.241
7	0.259	0.0354	17.14	0.528	0.638	0.321
8	0.296	0.0363	21.58	0.541	0.563	0.394
9	0.333	0.0369	25.38	0.551	0.501	0.456
10	0.370	0.0376	27.76	0.560	0.451	0.490

Test Filename   **D7B**

Engine Details

Configuration	IL4	Inner Seat Dia, mm	27	Shape Factor, LD	11.11
Cylinder bore	90	Seat Angle	45	Lmax/D	0.31
Engine Stroke	90	Max Valve Lift	8.37	D/B	0.3
Inlet Valves, n	1	Valve Opens	0	MIGV	150
Rated Speed, rpm	4500	Valve Closes	50	MPV	13.5

Test Details

Test Date	23-Oct-00	Barometer, mmHg	762.5	VFAM Constant	77.12
Test Pressure, mmH$_2$O	900	ISM Constant	1.09E-04		

Test Summary Results

Swirl Ratio (Rs)	2.11	Gulp Factor	1.016	Cf @ 0.3 L/D	0.542
Rs/LD	0.19	MCf	0.43	Cf @ Max Lift	0.545
CCf	1.726				

Test Results

Valve Lift		Air Flow	ISM Torque	Flow	Discharge	Non-dim
Test	Non-dim	m^3/s	NmE^{-3}	Coefficient	Coefficient	Rig Swirl
mm	L/D	Q	G	Cf	Cd	Ns
0	0.000	0.0000	0.00	0.000	0.000	0.000
1	0.037	0.0078	2.71	0.118	1.102	0.203
2	0.074	0.0150	4.01	0.225	1.037	0.157
3	0.111	0.0224	5.10	0.336	1.014	0.133
4	0.148	0.0298	7.27	0.447	0.993	0.143
5	0.185	0.0341	10.41	0.511	0.894	0.179
6	0.222	0.0344	16.49	0.516	0.739	0.281
7	0.259	0.0355	22.88	0.531	0.641	0.379
8	0.296	0.0362	27.76	0.541	0.562	0.451
9	0.333	0.0369	31.45	0.552	0.502	0.501
10	0.370	0.0372	32.32	0.555	0.447	0.512

C87

Test Filename   **D7A**

Engine Details

Configuration	IL4	Inner Seat Dia, mm	27	Shape Factor, LD	11.11
Cylinder bore	90	Seat Angle	45	Lmax/D	0.31
Engine Stroke	90	Max Valve Lift	8.37	D/B	0.3
Inlet Valves, n	1	Valve Opens	0	MIGV	150
Rated Speed, rpm	4500	Valve Closes	50	MPV	13.5

Test Details

Test Date	23-Oct-00	Barometer, mmHg	762.7	VFAM Constant	77.12
Test Pressure, mmH$_2$O	900	ISM Constant	1.09E-04		

Test Summary Results

Swirl Ratio (Rs)	1.98	Gulp Factor	1.019	Cf @ 0.3 L/D	0.54
Rs/LD	0.18	MCf	0.429	Cf @ Max Lift	0.543
CCf	1.722				

Test Results

Valve Lift		Air Flow	ISM Torque	Flow	Discharge	Non-dim
Test	Non-dim	m^3/s	NmE^{-3}	Coefficient	Coefficient	Rig Swirl
mm	L/D	Q	G	Cf	Cd	Ns
0	0.000	0.0000	0.00	0.000	0.000	0.000
1	0.037	0.0078	2.49	0.118	1.101	0.187
2	0.074	0.0149	3.80	0.223	1.028	0.149
3	0.111	0.0223	4.88	0.334	1.007	0.129
4	0.148	0.0298	6.51	0.446	0.991	0.128
5	0.185	0.0345	9.76	0.515	0.900	0.167
6	0.222	0.0345	14.97	0.515	0.738	0.255
7	0.259	0.0354	20.50	0.528	0.638	0.341
8	0.296	0.0361	26.35	0.539	0.560	0.430
9	0.333	0.0369	30.26	0.550	0.500	0.483
10	0.370	0.0374	31.89	0.558	0.449	0.503

Test Filename   **D45B**

Engine Details

Configuration	IL4	Inner Seat Dia, mm	27	Shape Factor, LD	10.43
Cylinder bore	84.5	Seat Angle	45	Lmax/D	0.31
Engine Stroke	90	Max Valve Lift	8.37	D/B	0.32
Inlet Valves, n	1	Valve Opens	0	MIGV	132.2
Rated Speed, rpm	4500	Valve Closes	50	MPV	13.5

Test Details

Test Date	20-Oct-00	Barometer, mmHg	759.2	VFAM Constant	77.14
Test Pressure, mmH$_2$O	900	ISM Constant	1.09E-04		

Test Summary Results

Swirl Ratio (Rs)	1.71	Gulp Factor	0.87	Cf @ 0.3 L/D	0.564
Rs/LD	0.16	MCf	0.443	Cf @ Max Lift	0.567
CCf	1.778				

Test Results

Valve Lift		Air Flow	ISM Torque	Flow	Discharge	Non-dim
Test	Non-dim	m^3/s	NmE^{-3}	Coefficient	Coefficient	Rig Swirl
mm	L/D	Q	G	Cf	Cd	Ns
0	0.000	0.0000	0.00	0.000	0.000	0.000
1	0.037	0.0079	2.06	0.118	1.110	0.163
2	0.074	0.0151	2.93	0.226	1.042	0.121
3	0.111	0.0227	4.23	0.340	1.026	0.116
4	0.148	0.0301	6.51	0.451	1.003	0.135
5	0.185	0.0348	9.00	0.521	0.911	0.162
6	0.222	0.0356	16.16	0.532	0.762	0.284
7	0.259	0.0367	20.61	0.550	0.664	0.351
8	0.296	0.0376	22.78	0.563	0.585	0.379
9	0.333	0.0383	25.16	0.572	0.520	0.412
10	0.370	0.0389	27.55	0.581	0.468	0.444

Test Filename   **D45A**

Engine Details

Configuration	IL4	Inner Seat Dia, mm	27	Shape Factor, LD	10.43
Cylinder bore	84.5	Seat Angle	45	Lmax/D	0.31
Engine Stroke	90	Max Valve Lift	8.37	D/B	0.32
Inlet Valves, n	1	Valve Opens	0	MIGV	132.2
Rated Speed, rpm	4500	Valve Closes	50	MPV	13.5

Test Details

Test Date	23-Oct-00	Barometer, mmHg	761.9	VFAM Constant	77.13
Test Pressure, mmH$_2$O	900	ISM Constant	1.09E-04		

Test Summary Results

Swirl Ratio (Rs)	0.95	Gulp Factor	0.868	Cf @ 0.3 L/D	0.56
Rs/LD	0.09	MCf	0.444	Cf @ Max Lift	0.563
CCf	1.783				

Test Results

Valve Lift		Air Flow	ISM Torque	Flow	Discharge	Non-dim
Test	Non-dim	m^3/s	NmE^{-3}	Coefficient	Coefficient	Rig Swirl
mm	L/D	Q	G	Cf	Cd	Ns
0	0.000	0.0000	0.00	0.000	0.000	0.000
1	0.037	0.0079	-0.11	0.119	1.111	-0.009
2	0.074	0.0151	0.65	0.226	1.039	0.027
3	0.111	0.0228	1.08	0.342	1.030	0.030
4	0.148	0.0302	1.08	0.451	1.003	0.023
5	0.185	0.0356	2.82	0.532	0.930	0.050
6	0.222	0.0372	4.88	0.555	0.795	0.082
7	0.259	0.0364	13.67	0.543	0.655	0.236
8	0.296	0.0375	15.62	0.559	0.581	0.262
9	0.333	0.0382	16.70	0.569	0.518	0.275
10	0.370	0.0389	18.55	0.579	0.467	0.300

Appendix D

Test Results: Helical Ports

Test Filename   **H62**

Engine Details

Configuration	IL4	Inner Seat Dia, mm	27	Shape Factor, LD	10.43
Cylinder bore	84.5	Seat Angle	45	Lmax/D	0.31
Engine Stroke	90	Max Valve Lift	8.37	D/B	0.32
Inlet Valves, n	1	Valve Opens	0	MIGV	132.2
Rated Speed, rpm	4500	Valve Closes	50	MPV	13.5

Test Details

Test Date	07-Mar-01	Barometer, mmHg	754.8	VFAM Constant	77.16
Test Pressure, mmH$_2$O	900	ISM Constant	1.09E-04		

Test Summary Results

Swirl Ratio (Rs)	1.64	Gulp Factor	0.902	Cf @ 0.3 L/D	0.541
Rs/LD	0.16	MCf	0.427	Cf @ Max Lift	0.542
CCf	1.715				

Test Results

Valve Lift		Air Flow	ISM Torque	Flow	Discharge	Non-dim
Test	Non-dim	m^3/s	NmE^{-3}	Coefficient	Coefficient	Rig Swirl
mm	L/D	Q	G	Cf	Cd	Ns
0	0.000	0.0000	0.00	0.000	0.000	0.000
1	0.037	0.0079	0.54	0.117	1.101	0.043
2	0.074	0.0156	1.63	0.233	1.071	0.066
3	0.111	0.0228	5.32	0.340	1.024	0.147
4	0.148	0.0292	9.87	0.436	0.969	0.212
5	0.185	0.0333	14.54	0.496	0.867	0.274
6	0.222	0.0345	16.60	0.514	0.736	0.302
7	0.259	0.0354	17.68	0.528	0.637	0.314
8	0.296	0.0363	17.36	0.540	0.561	0.301
9	0.333	0.0368	16.82	0.546	0.497	0.288
10	0.370	0.0370	14.32	0.549	0.442	0.244

Test Filename **H56**

Engine Details

Configuration	IL4	Inner Seat Dia, mm	27	Shape Factor, LD	10.43
Cylinder bore	84.5	Seat Angle	45	Lmax/D	0.31
Engine Stroke	90	Max Valve Lift	8.37	D/B	0.32
Inlet Valves, n	1	Valve Opens	0	MIGV	132.2
Rated Speed, rpm	4500	Valve Closes	50	MPV	13.5

Test Details

Test Date	07-Mar-01	Barometer, mmHg	755.1	VFAM Constant	77.16
Test Pressure, mmH$_2$O	900	ISM Constant	1.09E-04		

Test Summary Results

Swirl Ratio (Rs)	0.8	Gulp Factor	0.944	Cf @ 0.3 L/D	0.501
Rs/LD	0.08	MCf	0.408	Cf @ Max Lift	0.5
CCf	1.638				

Test Results

Valve Lift		Air Flow	ISM Torque	Flow	Discharge	Non-dim
Test	Non-dim	m^3/s	NmE^{-3}	Coefficient	Coefficient	Rig Swirl
mm	L/D	Q	G	Cf	Cd	Ns
0	0.000	0.0000	0.00	0.000	0.000	0.000
1	0.037	0.0079	0.87	0.116	1.091	0.070
2	0.074	0.0161	2.39	0.238	1.093	0.094
3	0.111	0.0232	5.86	0.342	1.032	0.160
4	0.148	0.0292	10.63	0.431	0.959	0.231
5	0.185	0.0319	12.04	0.471	0.823	0.240
6	0.222	0.0332	9.76	0.490	0.702	0.187
7	0.259	0.0346	8.46	0.511	0.617	0.155
8	0.296	0.0341	2.17	0.502	0.521	0.041
9	0.333	0.0338	-1.52	0.497	0.452	-0.029
10	0.370	0.0339	-2.50	0.499	0.402	-0.047

Test Filename   **H52**

Engine Details

Configuration	IL4	Inner Seat Dia, mm	27	Shape Factor, LD	10.43
Cylinder bore	84.5	Seat Angle	45	Lmax/D	0.31
Engine Stroke	90	Max Valve Lift	8.37	D/B	0.32
Inlet Valves, n	1	Valve Opens	0	MIGV	132.2
Rated Speed, rpm	4500	Valve Closes	50	MPV	13.5

Test Details

Test Date	07-Mar-01	Barometer, mmHg	755.2	VFAM Constant	77.15
Test Pressure, mmH$_2$O	900	ISM Constant	1.09E-04		

Test Summary Results

Swirl Ratio (Rs)	2.69	Gulp Factor	0.971	Cf @ 0.3 L/D	0.497
Rs/LD	0.26	MCf	0.397	Cf @ Max Lift	0.499
CCf	1.592				

Test Results

Valve Lift		Air Flow	ISM Torque	Flow	Discharge	Non-dim
Test	Non-dim	m^3/s	NmE^{-3}	Coefficient	Coefficient	Rig Swirl
mm	L/D	Q	G	Cf	Cd	Ns
0	0.000	0.0000	0.00	0.000	0.000	0.000
1	0.037	0.0078	0.98	0.116	1.091	0.079
2	0.074	0.0152	2.82	0.225	1.037	0.117
3	0.111	0.0218	7.27	0.324	0.977	0.210
4	0.148	0.0276	13.56	0.409	0.909	0.311
5	0.185	0.0314	18.98	0.465	0.812	0.383
6	0.222	0.0320	23.22	0.474	0.679	0.459
7	0.259	0.0328	24.30	0.485	0.585	0.469
8	0.296	0.0335	25.49	0.496	0.515	0.482
9	0.333	0.0341	25.39	0.503	0.457	0.473
10	0.370	0.0343	24.84	0.506	0.408	0.459

D4

Test Filename   **H48**

Engine Details

Configuration	IL4	Inner Seat Dia, mm	27	Shape Factor, LD	10.43
Cylinder bore	84.5	Seat Angle	45	Lmax/D	0.31
Engine Stroke	90	Max Valve Lift	8.37	D/B	0.32
Inlet Valves, n	1	Valve Opens	0	MIGV	132.2
Rated Speed, rpm	4500	Valve Closes	50	MPV	13.5

Test Details

Test Date	07-Mar-01	Barometer, mmHg	755.1	VFAM Constant	77.16
Test Pressure, mmH$_2$O	900	ISM Constant	1.09E-04		

Test Summary Results

Swirl Ratio (Rs)	2.67	Gulp Factor	0.91	Cf @ 0.3 L/D	0.535
Rs/LD	0.26	MCf	0.423	Cf @ Max Lift	0.54
CCf	1.699				

Test Results

Valve Lift		Air Flow	ISM Torque	Flow	Discharge	Non-dim
Test	Non-dim	m^3/s	NmE^{-3}	Coefficient	Coefficient	Rig Swirl
mm	L/D	Q	G	Cf	Cd	Ns
0	0.000	0.0000	0.00	0.000	0.000	0.000
1	0.037	0.0078	0.54	0.116	1.087	0.044
2	0.074	0.0159	1.84	0.237	1.090	0.073
3	0.111	0.0232	6.73	0.344	1.037	0.183
4	0.148	0.0287	13.67	0.426	0.948	0.300
5	0.185	0.0328	20.83	0.487	0.850	0.401
6	0.222	0.0345	24.08	0.511	0.732	0.441
7	0.259	0.0351	27.12	0.520	0.628	0.488
8	0.296	0.0360	30.59	0.534	0.555	0.537
9	0.333	0.0371	34.72	0.550	0.500	0.592
10	0.370	0.0378	36.34	0.559	0.451	0.609

Test Filename   **H47**

Engine Details

Configuration	IL4	Inner Seat Dia, mm	27	Shape Factor, LD	10.43
Cylinder bore	84.5	Seat Angle	45	Lmax/D	0.31
Engine Stroke	90	Max Valve Lift	8.37	D/B	0.32
Inlet Valves, n	1	Valve Opens	0	MIGV	132.2
Rated Speed, rpm	4500	Valve Closes	50	MPV	13.5

Test Details

Test Date	07-Mar-01	Barometer, mmHg	755.1	VFAM Constant	77.16
Test Pressure, mmH$_2$O	900	ISM Constant	1.09E-04		

Test Summary Results

Swirl Ratio (Rs)	1.75	Gulp Factor	0.923	Cf @ 0.3 L/D	0.519
Rs/LD	0.17	MCf	0.417	Cf @ Max Lift	0.519
CCf	1.676				

Test Results

Valve Lift		Air Flow	ISM Torque	Flow	Discharge	Non-dim
Test	Non-dim	m^3/s	NmE^{-3}	Coefficient	Coefficient	Rig Swirl
mm	L/D	Q	G	Cf	Cd	Ns
0	0.000	0.0000	0.00	0.000	0.000	0.000
1	0.037	0.0079	1.19	0.118	1.105	0.095
2	0.074	0.0159	3.58	0.237	1.090	0.142
3	0.111	0.0230	7.49	0.343	1.034	0.204
4	0.148	0.0291	10.85	0.435	0.966	0.234
5	0.185	0.0325	16.82	0.485	0.848	0.325
6	0.222	0.0337	20.50	0.502	0.719	0.383
7	0.259	0.0348	18.44	0.518	0.625	0.334
8	0.296	0.0349	14.32	0.519	0.539	0.259
9	0.333	0.0350	12.48	0.520	0.473	0.225
10	0.370	0.0349	9.22	0.517	0.417	0.167

Test Filename **H55**

Engine Details

Configuration	IL4	Inner Seat Dia, mm	27	Shape Factor, LD	10.43
Cylinder bore	84.5	Seat Angle	45	Lmax/D	0.31
Engine Stroke	90	Max Valve Lift	8.37	D/B	0.32
Inlet Valves, n	1	Valve Opens	0	MIGV	132.2
Rated Speed, rpm	4500	Valve Closes	50	MPV	13.5

Test Details

Test Date	07-Mar-01	Barometer, mmHg	754.6	VFAM Constant	77.16
Test Pressure, mmH$_2$O	900	ISM Constant	1.09E-04		

Test Summary Results

Swirl Ratio (Rs)	0.7	Gulp Factor	0.913	Cf @ 0.3 L/D	0.525
Rs/LD	0.07	MCf	0.422	Cf @ Max Lift	0.525
CCf	1.694				

Test Results

Valve Lift		Air Flow	ISM Torque	Flow	Discharge	Non-dim
Test	Non-dim	m^3/s	NmE^{-3}	Coefficient	Coefficient	Rig Swirl
mm	L/D	Q	G	Cf	Cd	Ns
0	0.000	0.0000	0.00	0.000	0.000	0.000
1	0.037	0.0079	0.76	0.118	1.104	0.060
2	0.074	0.0160	2.28	0.239	1.099	0.089
3	0.111	0.0233	5.42	0.346	1.044	0.147
4	0.148	0.0292	8.79	0.434	0.964	0.190
5	0.185	0.0327	10.09	0.487	0.851	0.194
6	0.222	0.0345	9.44	0.513	0.734	0.172
7	0.259	0.0354	7.16	0.525	0.633	0.128
8	0.296	0.0354	2.71	0.525	0.546	0.048
9	0.333	0.0354	1.08	0.523	0.476	0.019
10	0.370	0.0350	-1.08	0.519	0.418	-0.020

Test Filename   **H40**

Engine Details

Configuration	IL4	Inner Seat Dia, mm	27	Shape Factor, LD	10.43
Cylinder bore	84.5	Seat Angle	45	Lmax/D	0.31
Engine Stroke	90	Max Valve Lift	8.37	D/B	0.32
Inlet Valves, n	1	Valve Opens	0	MIGV	132.2
Rated Speed, rpm	4500	Valve Closes	50	MPV	13.5

Test Details

Test Date	06-Mar-01	Barometer, mmHg	755.4	VFAM Constant	77.15
Test Pressure, mmH$_2$O	900	ISM Constant	1.09E-04		

Test Summary Results

Swirl Ratio (Rs)	1.15	Gulp Factor	0.904	Cf @ 0.3 L/D	0.536
Rs/LD	0.11	MCf	0.426	Cf @ Max Lift	0.537
CCf	1.711				

Test Results

Valve Lift		Air Flow	ISM Torque	Flow	Discharge	Non-dim
Test	Non-dim	m^3/s	NmE^{-3}	Coefficient	Coefficient	Rig Swirl
mm	L/D	Q	G	Cf	Cd	Ns
0	0.000	0.0000	0.00	0.000	0.000	0.000
1	0.037	0.0080	0.76	0.118	1.107	0.060
2	0.074	0.0158	2.06	0.234	1.076	0.083
3	0.111	0.0228	5.21	0.338	1.018	0.144
4	0.148	0.0290	9.44	0.429	0.954	0.206
5	0.185	0.0339	13.45	0.502	0.876	0.251
6	0.222	0.0349	14.32	0.515	0.738	0.260
7	0.259	0.0359	11.50	0.529	0.639	0.203
8	0.296	0.0363	9.66	0.536	0.557	0.169
9	0.333	0.0365	5.64	0.539	0.490	0.098
10	0.370	0.0370	1.63	0.545	0.439	0.028

Test Filename   **H38**

Engine Details

Configuration	IL4	Inner Seat Dia, mm	27	Shape Factor, LD	10.43
Cylinder bore	84.5	Seat Angle	45	Lmax/D	0.31
Engine Stroke	90	Max Valve Lift	8.37	D/B	0.32
Inlet Valves, n	1	Valve Opens	0	MIGV	132.2
Rated Speed, rpm	4500	Valve Closes	50	MPV	13.5

Test Details

Test Date	06-Mar-01	Barometer, mmHg	755.8	VFAM Constant	77.15
Test Pressure, mmH$_2$O	900	ISM Constant	1.09E-04		

Test Summary Results

Swirl Ratio (Rs)	1.29	Gulp Factor	0.895	Cf @ 0.3 L/D	0.542
Rs/LD	0.12	MCf	0.431	Cf @ Max Lift	0.539
CCf	1.729				

Test Results

Valve Lift		Air Flow	ISM Torque	Flow	Discharge	Non-dim
Test	Non-dim	m^3/s	NmE^{-3}	Coefficient	Coefficient	Rig Swirl
mm	L/D	Q	G	Cf	Cd	Ns
0	0.000	0.0000	0.00	0.000	0.000	0.000
1	0.037	0.0079	0.54	0.118	1.102	0.043
2	0.074	0.0160	2.06	0.238	1.097	0.081
3	0.111	0.0235	5.42	0.350	1.054	0.145
4	0.148	0.0298	9.55	0.442	0.982	0.202
5	0.185	0.0336	14.75	0.498	0.870	0.278
6	0.222	0.0348	14.75	0.516	0.739	0.268
7	0.259	0.0361	13.78	0.534	0.645	0.242
8	0.296	0.0368	12.58	0.543	0.565	0.217
9	0.333	0.0360	4.23	0.532	0.484	0.074
10	0.370	0.0359	2.71	0.530	0.427	0.048

Test Filename   **H36**

Engine Details

Configuration	IL4	Inner Seat Dia, mm	27	Shape Factor, LD	10.43
Cylinder bore	84.5	Seat Angle	45	Lmax/D	0.31
Engine Stroke	90	Max Valve Lift	8.37	D/B	0.32
Inlet Valves, n	1	Valve Opens	0	MIGV	132.2
Rated Speed, rpm	4500	Valve Closes	50	MPV	13.5

Test Details

Test Date	06-Mar-01	Barometer, mmHg	756.9	VFAM Constant	77.15
Test Pressure, mmH$_2$O	900	ISM Constant	1.09E-04		

Test Summary Results

Swirl Ratio (Rs)	1.96	Gulp Factor	0.959	Cf @ 0.3 L/D	0.503
Rs/LD	0.19	MCf	0.402	Cf @ Max Lift	0.505
CCf	1.613				

Test Results

Valve Lift		Air Flow	ISM Torque	Flow	Discharge	Non-dim
Test	Non-dim	m^3/s	NmE^{-3}	Coefficient	Coefficient	Rig Swirl
mm	L/D	Q	G	Cf	Cd	Ns
0	0.000	0.0000	0.00	0.000	0.000	0.000
1	0.037	0.0079	0.65	0.117	1.095	0.052
2	0.074	0.0159	2.49	0.236	1.088	0.099
3	0.111	0.0224	6.18	0.333	1.002	0.174
4	0.148	0.0275	11.06	0.408	0.906	0.254
5	0.185	0.0314	15.19	0.466	0.814	0.305
6	0.222	0.0324	14.97	0.481	0.688	0.292
7	0.259	0.0333	17.36	0.493	0.595	0.330
8	0.296	0.0339	19.42	0.502	0.522	0.362
9	0.333	0.0344	19.74	0.509	0.463	0.363
10	0.370	0.0344	16.71	0.509	0.410	0.307

Test Filename   **H34**

Engine Details

Configuration	IL4	Inner Seat Dia, mm	27	Shape Factor, LD	10.43
Cylinder bore	84.5	Seat Angle	45	Lmax/D	0.31
Engine Stroke	90	Max Valve Lift	8.37	D/B	0.32
Inlet Valves, n	1	Valve Opens	0	MIGV	132.2
Rated Speed, rpm	4500	Valve Closes	50	MPV	13.5

Test Details

Test Date	06-Mar-01	Barometer, mmHg	757.2	VFAM Constant	77.15
Test Pressure, mmH$_2$O	900	ISM Constant	1.09E-04		

Test Summary Results

Swirl Ratio (Rs)	1.68	Gulp Factor	0.956	Cf @ 0.3 L/D	0.503
Rs/LD	0.16	MCf	0.403	Cf @ Max Lift	0.506
CCf	1.618				

Test Results

Valve Lift		Air Flow	ISM Torque	Flow	Discharge	Non-dim
Test	Non-dim	m^3/s	NmE^{-3}	Coefficient	Coefficient	Rig Swirl
mm	L/D	Q	G	Cf	Cd	Ns
0	0.000	0.0000	0.00	0.000	0.000	0.000
1	0.037	0.0079	0.54	0.118	1.107	0.043
2	0.074	0.0160	2.60	0.239	1.099	0.102
3	0.111	0.0229	6.73	0.341	1.027	0.185
4	0.148	0.0282	11.28	0.420	0.933	0.252
5	0.185	0.0313	13.67	0.467	0.816	0.274
6	0.222	0.0320	14.43	0.477	0.683	0.283
7	0.259	0.0330	14.86	0.491	0.593	0.283
8	0.296	0.0338	15.19	0.502	0.522	0.283
9	0.333	0.0345	16.38	0.513	0.467	0.299
10	0.370	0.0350	17.57	0.520	0.419	0.316

Test Filename   **H51**

Engine Details

Configuration	IL4	Inner Seat Dia, mm	27	Shape Factor, LD	10.43
Cylinder bore	84.5	Seat Angle	45	Lmax/D	0.31
Engine Stroke	90	Max Valve Lift	8.37	D/B	0.32
Inlet Valves, n	1	Valve Opens	0	MIGV	132.2
Rated Speed, rpm	4500	Valve Closes	50	MPV	13.5

Test Details

Test Date	06-Mar-01	Barometer, mmHg	759.5	VFAM Constant	77.14
Test Pressure, mmH$_2$O	900	ISM Constant	1.09E-04		

Test Summary Results

Swirl Ratio (Rs)	2.44	Gulp Factor	0.968	Cf @ 0.3 L/D	0.495
Rs/LD	0.23	MCf	0.398	Cf @ Max Lift	0.496
CCf	1.598				

Test Results

Valve Lift		Air Flow	ISM Torque	Flow	Discharge	Non-dim
Test	Non-dim	m^3/s	NmE^{-3}	Coefficient	Coefficient	Rig Swirl
mm	L/D	Q	G	Cf	Cd	Ns
0	0.000	0.0000	0.00	0.000	0.000	0.000
1	0.037	0.0079	0.87	0.118	1.109	0.069
2	0.074	0.0156	3.36	0.233	1.071	0.135
3	0.111	0.0221	7.38	0.330	0.993	0.210
4	0.148	0.0279	12.58	0.416	0.923	0.284
5	0.185	0.0312	17.03	0.464	0.811	0.344
6	0.222	0.0319	21.04	0.475	0.681	0.415
7	0.259	0.0327	21.69	0.486	0.587	0.418
8	0.296	0.0333	23.21	0.494	0.514	0.440
9	0.333	0.0335	23.86	0.497	0.452	0.449
10	0.370	0.0339	23.86	0.503	0.405	0.445

D12

Test Filename   **H61**

Engine Details

Configuration	IL4	Inner Seat Dia, mm	27	Shape Factor, LD	10.43
Cylinder bore	84.5	Seat Angle	45	Lmax/D	0.31
Engine Stroke	90	Max Valve Lift	8.37	D/B	0.32
Inlet Valves, n	1	Valve Opens	0	MIGV	132.2
Rated Speed, rpm	4500	Valve Closes	50	MPV	13.5

Test Details

Test Date	06-Mar-01	Barometer, mmHg	760.2	VFAM Constant	77.13
Test Pressure, mmH_2O	900	ISM Constant	1.09E-04		

Test Summary Results

Swirl Ratio (Rs)	1.59	Gulp Factor	0.904	Cf @ 0.3 L/D	0.54
Rs/LD	0.15	MCf	0.426	Cf @ Max Lift	0.542
CCf	1.712				

Test Results

Valve Lift		Air Flow	ISM Torque	Flow	Discharge	Non-dim
Test	Non-dim	m^3/s	NmE^{-3}	Coefficient	Coefficient	Rig Swirl
mm	L/D	Q	G	Cf	Cd	Ns
0	0.000	0.0000	0.00	0.000	0.000	0.000
1	0.037	0.0080	0.43	0.120	1.120	0.034
2	0.074	0.0155	1.52	0.232	1.070	0.061
3	0.111	0.0228	5.31	0.342	1.030	0.146
4	0.148	0.0289	9.87	0.434	0.964	0.213
5	0.185	0.0331	14.32	0.496	0.866	0.271
6	0.222	0.0341	16.05	0.511	0.731	0.295
7	0.259	0.0351	16.27	0.525	0.634	0.290
8	0.296	0.0361	17.03	0.539	0.561	0.296
9	0.333	0.0365	16.59	0.546	0.496	0.285
10	0.370	0.0365	13.67	0.545	0.439	0.235

Test Filename   **H31**

Engine Details

Configuration	IL4	Inner Seat Dia, mm	27	Shape Factor, LD	10.43
Cylinder bore	84.5	Seat Angle	45	Lmax/D	0.31
Engine Stroke	90	Max Valve Lift	8.37	D/B	0.32
Inlet Valves, n	1	Valve Opens	0	MIGV	132.2
Rated Speed, rpm	4500	Valve Closes	50	MPV	13.5

Test Details

Test Date	06-Mar-01	Barometer, mmHg	760.8	VFAM Constant	77.13
Test Pressure, mmH$_2$O	900	ISM Constant	1.09E-04		

Test Summary Results

Swirl Ratio (Rs)	0.49	Gulp Factor	0.95	Cf @ 0.3 L/D	0.503
Rs/LD	0.05	MCf	0.406	Cf @ Max Lift	0.505
CCf	1.629				

Test Results

Valve Lift		Air Flow	ISM Torque	Flow	Discharge	Non-dim
Test	Non-dim	m^3/s	NmE^{-3}	Coefficient	Coefficient	Rig Swirl
mm	L/D	Q	G	Cf	Cd	Ns
0	0.000	0.0000	0.00	0.000	0.000	0.000
1	0.037	0.0079	0.76	0.119	1.117	0.060
2	0.074	0.0155	3.58	0.233	1.074	0.144
3	0.111	0.0225	6.51	0.339	1.022	0.180
4	0.148	0.0288	8.13	0.433	0.962	0.176
5	0.185	0.0315	5.97	0.473	0.827	0.118
6	0.222	0.0323	8.13	0.484	0.693	0.157
7	0.259	0.0330	3.47	0.495	0.597	0.066
8	0.296	0.0335	0.00	0.502	0.522	0.000
9	0.333	0.0339	-1.63	0.508	0.462	-0.030
10	0.370	0.0344	-2.17	0.516	0.415	-0.039

Test Filename　　　　**H44**

Engine Details

Configuration	IL4	Inner Seat Dia, mm	27	Shape Factor, LD	10.43
Cylinder bore	84.5	Seat Angle	45	Lmax/D	0.31
Engine Stroke	90	Max Valve Lift	8.37	D/B	0.32
Inlet Valves, n	1	Valve Opens	0	MIGV	132.2
Rated Speed, rpm	4500	Valve Closes	50	MPV	13.5

Test Details

Test Date	05-Mar-01	Barometer, mmHg	763.2	VFAM Constant	77.12
Test Pressure, mmH$_2$O	900	ISM Constant	1.09E-04		

Test Summary Results

Swirl Ratio (Rs)	1.38	Gulp Factor	0.939	Cf @ 0.3 L/D	0.51
Rs/LD	0.13	MCf	0.41	Cf @ Max Lift	0.512
CCf	1.646				

Test Results

Valve Lift		Air Flow	ISM Torque	Flow	Discharge	Non-dim
Test	Non-dim	m^3/s	NmE^{-3}	Coefficient	Coefficient	Rig Swirl
mm	L/D	Q	G	Cf	Cd	Ns
0	0.000	0.0000	0.00	0.000	0.000	0.000
1	0.037	0.0079	0.33	0.118	1.107	0.026
2	0.074	0.0157	0.33	0.235	1.081	0.013
3	0.111	0.0228	4.55	0.341	1.029	0.125
4	0.148	0.0287	10.95	0.431	0.957	0.238
5	0.185	0.0321	14.21	0.481	0.840	0.277
6	0.222	0.0326	13.12	0.488	0.699	0.252
7	0.259	0.0336	12.58	0.503	0.607	0.234
8	0.296	0.0340	12.26	0.509	0.529	0.225
9	0.333	0.0346	12.91	0.517	0.470	0.234
10	0.370	0.0353	15.18	0.526	0.424	0.270

Test Filename   **H43**

Engine Details

Configuration	IL4	Inner Seat Dia, mm	27	Shape Factor, LD	10.43
Cylinder bore	84.5	Seat Angle	45	Lmax/D	0.31
Engine Stroke	90	Max Valve Lift	8.37	D/B	0.32
Inlet Valves, n	1	Valve Opens	0	MIGV	132.2
Rated Speed, rpm	4500	Valve Closes	50	MPV	13.5

Test Details

Test Date	05-Mar-01	Barometer, mmHg	763.2	VFAM Constant	77.12
Test Pressure, mmH$_2$O	900	ISM Constant	1.09E-04		

Test Summary Results

Swirl Ratio (Rs)	0.6	Gulp Factor	0.942	Cf @ 0.3 L/D	0.499
Rs/LD	0.06	MCf	0.409	Cf @ Max Lift	0.498
CCf	1.642				

Test Results

Valve Lift		Air Flow	ISM Torque	Flow	Discharge	Non-dim
Test	Non-dim	m^3/s	NmE^{-3}	Coefficient	Coefficient	Rig Swirl
mm	L/D	Q	G	Cf	Cd	Ns
0	0.000	0.0000	0.00	0.000	0.000	0.000
1	0.037	0.0079	0.76	0.118	1.108	0.060
2	0.074	0.0158	2.93	0.238	1.094	0.115
3	0.111	0.0228	5.21	0.342	1.031	0.143
4	0.148	0.0289	6.83	0.433	0.963	0.148
5	0.185	0.0326	9.11	0.488	0.853	0.175
6	0.222	0.0331	10.41	0.496	0.710	0.197
7	0.259	0.0337	5.75	0.505	0.610	0.107
8	0.296	0.0333	0.43	0.499	0.518	0.008
9	0.333	0.0333	-0.87	0.498	0.452	-0.016
10	0.370	0.0336	-1.84	0.503	0.405	-0.034

Test Filename   **H24**

Engine Details

Configuration	IL4	Inner Seat Dia, mm	27	Shape Factor, LD	10.43
Cylinder bore	84.5	Seat Angle	45	Lmax/D	0.31
Engine Stroke	90	Max Valve Lift	8.37	D/B	0.32
Inlet Valves, n	1	Valve Opens	0	MIGV	132.2
Rated Speed, rpm	4500	Valve Closes	50	MPV	13.5

Test Details

Test Date	05-Mar-01	Barometer, mmHg	763.3	VFAM Constant	77.12
Test Pressure, mmH$_2$O	900	ISM Constant	1.09E-04		

Test Summary Results

Swirl Ratio (Rs)	2.19	Gulp Factor	0.887	Cf @ 0.3 L/D	0.553
Rs/LD	0.21	MCf	0.434	Cf @ Max Lift	0.547
CCf	1.744				

Test Results

Valve Lift		Air Flow	ISM Torque	Flow	Discharge	Non-dim
Test	Non-dim	m^3/s	NmE^{-3}	Coefficient	Coefficient	Rig Swirl
mm	L/D	Q	G	Cf	Cd	Ns
0	0.000	0.0000	0.00	0.000	0.000	0.000
1	0.037	0.0078	0.98	0.118	1.101	0.078
2	0.074	0.0158	3.04	0.236	1.087	0.120
3	0.111	0.0231	7.70	0.347	1.045	0.208
4	0.148	0.0295	13.12	0.442	0.981	0.278
5	0.185	0.0331	20.06	0.495	0.866	0.379
6	0.222	0.0346	23.32	0.518	0.741	0.422
7	0.259	0.0363	24.84	0.542	0.654	0.429
8	0.296	0.0372	24.94	0.556	0.577	0.421
9	0.333	0.0357	12.80	0.533	0.484	0.225
10	0.370	0.0361	11.06	0.539	0.434	0.192

Test Filename   **H20**

Engine Details

Configuration	IL4	Inner Seat Dia, mm	27	Shape Factor, LD	10.43
Cylinder bore	84.5	Seat Angle	45	Lmax/D	0.31
Engine Stroke	90	Max Valve Lift	8.37	D/B	0.32
Inlet Valves, n	1	Valve Opens	0	MIGV	132.2
Rated Speed, rpm	4500	Valve Closes	50	MPV	13.5

Test Details

Test Date	05-Mar-01	Barometer, mmHg	763.3	VFAM Constant	77.12
Test Pressure, mmH$_2$O	900	ISM Constant	1.09E-04		

Test Summary Results

Swirl Ratio (Rs)	2.47	Gulp Factor	0.956	Cf @ 0.3 L/D	0.5
Rs/LD	0.24	MCf	0.403	Cf @ Max Lift	0.503
CCf	1.618				

Test Results

Valve Lift		Air Flow	ISM Torque	Flow	Discharge	Non-dim
Test	Non-dim	m^3/s	NmE^{-3}	Coefficient	Coefficient	Rig Swirl
mm	L/D	Q	G	Cf	Cd	Ns
0	0.000	0.0000	0.00	0.000	0.000	0.000
1	0.037	0.0077	0.87	0.115	1.080	0.071
2	0.074	0.0153	3.25	0.229	1.053	0.133
3	0.111	0.0223	8.35	0.334	1.006	0.234
4	0.148	0.0282	14.10	0.421	0.935	0.314
5	0.185	0.0319	19.09	0.476	0.831	0.376
6	0.222	0.0323	21.69	0.481	0.689	0.422
7	0.259	0.0333	22.56	0.496	0.598	0.426
8	0.296	0.0336	23.32	0.500	0.519	0.437
9	0.333	0.0341	22.99	0.508	0.462	0.424
10	0.370	0.0339	16.48	0.505	0.407	0.306

Test Filename   **H32**

Engine Details

Configuration	IL4	Inner Seat Dia, mm	27	Shape Factor, LD	10.43
Cylinder bore	84.5	Seat Angle	45	Lmax/D	0.31
Engine Stroke	90	Max Valve Lift	8.37	D/B	0.32
Inlet Valves, n	1	Valve Opens	0	MIGV	132.2
Rated Speed, rpm	4500	Valve Closes	50	MPV	13.5

Test Details

Test Date	05-Mar-01	Barometer, mmHg	762.8	VFAM Constant	77.12
Test Pressure, mmH$_2$O	900	ISM Constant	1.09E-04		

Test Summary Results

Swirl Ratio (Rs)	1.81	Gulp Factor	0.935	Cf @ 0.3 L/D	0.529
Rs/LD	0.17	MCf	0.412	Cf @ Max Lift	0.533
CCf	1.653				

Test Results

Valve Lift		Air Flow	ISM Torque	Flow	Discharge	Non-dim
Test	Non-dim	m^3/s	NmE^{-3}	Coefficient	Coefficient	Rig Swirl
mm	L/D	Q	G	Cf	Cd	Ns
0	0.000	0.0000	0.00	0.000	0.000	0.000
1	0.037	0.0078	0.43	0.117	1.093	0.035
2	0.074	0.0153	0.43	0.228	1.051	0.018
3	0.111	0.0219	4.56	0.327	0.985	0.131
4	0.148	0.0280	10.85	0.417	0.926	0.244
5	0.185	0.0310	15.18	0.462	0.807	0.308
6	0.222	0.0327	15.18	0.487	0.697	0.292
7	0.259	0.0342	16.92	0.508	0.613	0.312
8	0.296	0.0355	18.98	0.527	0.548	0.337
9	0.333	0.0365	22.23	0.541	0.492	0.385
10	0.370	0.0369	24.19	0.548	0.441	0.414

Test Filename   **H28**

Engine Details

Configuration	IL4	Inner Seat Dia, mm	27	Shape Factor, LD	10.43
Cylinder bore	84.5	Seat Angle	45	Lmax/D	0.31
Engine Stroke	90	Max Valve Lift	8.37	D/B	0.32
Inlet Valves, n	1	Valve Opens	0	MIGV	132.2
Rated Speed, rpm	4500	Valve Closes	50	MPV	13.5

Test Details

Test Date	05-Mar-01	Barometer, mmHg	762.7	VFAM Constant	77.12
Test Pressure, mmH$_2$O	900	ISM Constant	1.09E-04		

Test Summary Results

Swirl Ratio (Rs)	1.52	Gulp Factor	0.935	Cf @ 0.3 L/D	0.514
Rs/LD	0.15	MCf	0.412	Cf @ Max Lift	0.516
CCf	1.655				

Test Results

Valve Lift		Air Flow	ISM Torque	Flow	Discharge	Non-dim
Test	Non-dim	m^3/s	NmE^{-3}	Coefficient	Coefficient	Rig Swirl
mm	L/D	Q	G	Cf	Cd	Ns
0	0.000	0.0000	0.00	0.000	0.000	0.000
1	0.037	0.0078	0.54	0.118	1.102	0.043
2	0.074	0.0154	0.76	0.231	1.065	0.031
3	0.111	0.0226	5.21	0.339	1.022	0.144
4	0.148	0.0286	11.60	0.429	0.954	0.253
5	0.185	0.0319	16.27	0.479	0.837	0.318
6	0.222	0.0328	15.18	0.493	0.706	0.289
7	0.259	0.0341	13.56	0.511	0.616	0.249
8	0.296	0.0342	13.34	0.513	0.533	0.244
9	0.333	0.0349	14.10	0.523	0.475	0.253
10	0.370	0.0354	14.10	0.531	0.427	0.249

Test Filename   **H27**

Engine Details

Configuration	IL4	Inner Seat Dia, mm	27	Shape Factor, LD	10.43
Cylinder bore	84.5	Seat Angle	45	Lmax/D	0.31
Engine Stroke	90	Max Valve Lift	8.37	D/B	0.32
Inlet Valves, n	1	Valve Opens	0	MIGV	132.2
Rated Speed, rpm	4500	Valve Closes	50	MPV	13.5

Test Details

Test Date	05-Mar-01	Barometer, mmHg	762.7	VFAM Constant	77.12
Test Pressure, mmH$_2$O	900	ISM Constant	1.09E-04		

Test Summary Results

Swirl Ratio (Rs)	1.15	Gulp Factor	0.921	Cf @ 0.3 L/D	0.52
Rs/LD	0.11	MCf	0.418	Cf @ Max Lift	0.52
CCf	1.679				

Test Results

Valve Lift		Air Flow	ISM Torque	Flow	Discharge	Non-dim
Test	Non-dim	m^3/s	NmE^{-3}	Coefficient	Coefficient	Rig Swirl
mm	L/D	Q	G	Cf	Cd	Ns
0	0.000	0.0000	0.00	0.000	0.000	0.000
1	0.037	0.0081	0.76	0.122	1.144	0.058
2	0.074	0.0157	3.36	0.236	1.086	0.133
3	0.111	0.0229	6.40	0.345	1.040	0.174
4	0.148	0.0292	8.24	0.440	0.978	0.175
5	0.185	0.0322	10.85	0.485	0.847	0.210
6	0.222	0.0333	12.80	0.501	0.718	0.239
7	0.259	0.0342	10.95	0.515	0.622	0.199
8	0.296	0.0346	9.76	0.520	0.541	0.176
9	0.333	0.0346	7.59	0.520	0.473	0.137
10	0.370	0.0347	5.64	0.521	0.419	0.101

Test Filename   **H22**

Engine Details

Configuration	IL4	Inner Seat Dia, mm	27	Shape Factor, LD	10.43
Cylinder bore	84.5	Seat Angle	45	Lmax/D	0.31
Engine Stroke	90	Max Valve Lift	8.37	D/B	0.32
Inlet Valves, n	1	Valve Opens	0	MIGV	132.2
Rated Speed, rpm	4500	Valve Closes	50	MPV	13.5

Test Details

Test Date	27-Feb-01	Barometer, mmHg	742.2	VFAM Constant	77.21
Test Pressure, mmH$_2$O	900	ISM Constant	1.09E-04		

Test Summary Results

Swirl Ratio (Rs)	0.3	Gulp Factor	0.907	Cf @ 0.3 L/D	0.524
Rs/LD	0.03	MCf	0.425	Cf @ Max Lift	0.525
CCf	1.704				

Test Results

Valve Lift		Air Flow	ISM Torque	Flow	Discharge	Non-dim
Test	Non-dim	m^3/s	NmE^{-3}	Coefficient	Coefficient	Rig Swirl
mm	L/D	Q	G	Cf	Cd	Ns
0	0.000	0.0000	0.00	0.000	0.000	0.000
1	0.037	0.0078	0.43	0.115	1.079	0.035
2	0.074	0.0155	0.98	0.229	1.055	0.040
3	0.111	0.0228	3.47	0.337	1.017	0.096
4	0.148	0.0294	6.73	0.435	0.967	0.145
5	0.185	0.0341	9.01	0.504	0.882	0.167
6	0.222	0.0353	8.68	0.521	0.746	0.156
7	0.259	0.0363	4.78	0.536	0.648	0.083
8	0.296	0.0355	-3.80	0.524	0.544	-0.068
9	0.333	0.0358	-5.86	0.528	0.480	-0.104
10	0.370	0.0361	-7.27	0.532	0.429	-0.128

Test Filename   **H18**

Engine Details

Configuration	IL4	Inner Seat Dia, mm	27	Shape Factor, LD	10.43
Cylinder bore	84.5	Seat Angle	45	Lmax/D	0.31
Engine Stroke	90	Max Valve Lift	8.37	D/B	0.32
Inlet Valves, n	1	Valve Opens	0	MIGV	132.2
Rated Speed, rpm	4500	Valve Closes	50	MPV	13.5

Test Details

Test Date	27-Feb-01	Barometer, mmHg	741.6	VFAM Constant	77.22
Test Pressure, mmH$_2$O	900	ISM Constant	1.09E-04		

Test Summary Results

Swirl Ratio (Rs)	1.34	Gulp Factor	0.952	Cf @ 0.3 L/D	0.505
Rs/LD	0.13	MCf	0.405	Cf @ Max Lift	0.507
CCf	1.625				

Test Results

Valve Lift		Air Flow	ISM Torque	Flow	Discharge	Non-dim
Test	Non-dim	m^3/s	NmE^{-3}	Coefficient	Coefficient	Rig Swirl
mm	L/D	Q	G	Cf	Cd	Ns
0	0.000	0.0000	0.00	0.000	0.000	0.000
1	0.037	0.0080	0.87	0.118	1.110	0.069
2	0.074	0.0156	1.63	0.232	1.069	0.066
3	0.111	0.0224	4.88	0.333	1.004	0.137
4	0.148	0.0284	9.66	0.422	0.938	0.214
5	0.185	0.0319	12.81	0.473	0.827	0.254
6	0.222	0.0325	12.05	0.482	0.691	0.234
7	0.259	0.0334	11.29	0.496	0.599	0.213
8	0.296	0.0340	11.61	0.504	0.524	0.216
9	0.333	0.0345	13.35	0.512	0.465	0.244
10	0.370	0.0351	14.44	0.519	0.418	0.260

Test Filename   **H8**

Engine Details

Configuration	IL4	Inner Seat Dia, mm	27	Shape Factor, LD	10.43
Cylinder bore	84.5	Seat Angle	45	Lmax/D	0.31
Engine Stroke	90	Max Valve Lift	8.37	D/B	0.32
Inlet Valves, n	1	Valve Opens	0	MIGV	132.2
Rated Speed, rpm	4500	Valve Closes	50	MPV	13.5

Test Details

Test Date	27-Feb-01	Barometer, mmHg	742.1	VFAM Constant	77.21
Test Pressure, mmH$_2$O	900	ISM Constant	1.09E-04		

Test Summary Results

Swirl Ratio (Rs)	0.66	Gulp Factor	0.923	Cf @ 0.3 L/D	0.523
Rs/LD	0.06	MCf	0.417	Cf @ Max Lift	0.521
CCf	1.676				

Test Results

Valve Lift		Air Flow	ISM Torque	Flow	Discharge	Non-dim
Test	Non-dim	m^3/s	NmE^{-3}	Coefficient	Coefficient	Rig Swirl
mm	L/D	Q	G	Cf	Cd	Ns
0	0.000	0.0000	0.00	0.000	0.000	0.000
1	0.037	0.0080	0.33	0.118	1.105	0.026
2	0.074	0.0160	1.63	0.237	1.093	0.064
3	0.111	0.0235	4.88	0.349	1.052	0.131
4	0.148	0.0296	8.47	0.439	0.975	0.181
5	0.185	0.0333	9.66	0.493	0.862	0.183
6	0.222	0.0333	10.09	0.493	0.707	0.192
7	0.259	0.0342	6.08	0.507	0.612	0.112
8	0.296	0.0354	2.60	0.523	0.544	0.047
9	0.333	0.0349	-1.63	0.517	0.470	-0.030
10	0.370	0.0350	-3.15	0.517	0.417	-0.057

Test Filename   **H60**

Engine Details

Configuration	IL4	Inner Seat Dia, mm	27	Shape Factor, LD	10.43
Cylinder bore	84.5	Seat Angle	45	Lmax/D	0.31
Engine Stroke	90	Max Valve Lift	8.37	D/B	0.32
Inlet Valves, n	1	Valve Opens	0	MIGV	132.2
Rated Speed, rpm	4500	Valve Closes	50	MPV	13.5

Test Details

Test Date	26-Feb-01	Barometer, mmHg	746	VFAM Constant	77.2
Test Pressure, mmH$_2$O	900	ISM Constant	1.09E-04		

Test Summary Results

Swirl Ratio (Rs)	1.57	Gulp Factor	0.905	Cf @ 0.3 L/D	0.537
Rs/LD	0.15	MCf	0.426	Cf @ Max Lift	0.54
CCf	1.709				

Test Results

Valve Lift		Air Flow	ISM Torque	Flow	Discharge	Non-dim
Test	Non-dim	m^3/s	NmE^{-3}	Coefficient	Coefficient	Rig Swirl
mm	L/D	Q	G	Cf	Cd	Ns
0	0.000	0.0000	0.00	0.000	0.000	0.000
1	0.037	0.0080	0.87	0.118	1.107	0.069
2	0.074	0.0155	2.06	0.230	1.060	0.084
3	0.111	0.0227	5.64	0.337	1.016	0.157
4	0.148	0.0291	10.20	0.433	0.961	0.221
5	0.185	0.0336	14.11	0.499	0.871	0.265
6	0.222	0.0347	16.39	0.515	0.737	0.298
7	0.259	0.0356	16.39	0.526	0.635	0.292
8	0.296	0.0363	15.74	0.536	0.557	0.275
9	0.333	0.0370	15.63	0.546	0.496	0.268
10	0.370	0.0370	13.24	0.546	0.440	0.227

Test Filename   **H7**

Engine Details

Configuration	IL4	Inner Seat Dia, mm	27	Shape Factor, LD	10.43
Cylinder bore	84.5	Seat Angle	45	Lmax/D	0.31
Engine Stroke	90	Max Valve Lift	8.37	D/B	0.32
Inlet Valves, n	1	Valve Opens	0	MIGV	132.2
Rated Speed, rpm	4500	Valve Closes	50	MPV	13.5

Test Details

Test Date	26-Feb-01	Barometer, mmHg	747.2	VFAM Constant	77.19
Test Pressure, mmH$_2$O	900	ISM Constant	1.09E-04		

Test Summary Results

Swirl Ratio (Rs)	0.89	Gulp Factor	0.921	Cf @ 0.3 L/D	0.513
Rs/LD	0.08	MCf	0.418	Cf @ Max Lift	0.514
CCf	1.68				

Test Results

Valve Lift		Air Flow	ISM Torque	Flow	Discharge	Non-dim
Test	Non-dim	m^3/s	NmE^{-3}	Coefficient	Coefficient	Rig Swirl
mm	L/D	Q	G	Cf	Cd	Ns
0	0.000	0.0000	0.00	0.000	0.000	0.000
1	0.037	0.0081	0.87	0.120	1.127	0.068
2	0.074	0.0159	2.39	0.237	1.091	0.094
3	0.111	0.0236	5.64	0.352	1.060	0.150
4	0.148	0.0302	9.01	0.451	1.001	0.187
5	0.185	0.0334	13.02	0.498	0.870	0.245
6	0.222	0.0343	13.78	0.510	0.730	0.253
7	0.259	0.0343	8.14	0.509	0.614	0.150
8	0.296	0.0346	3.80	0.513	0.533	0.069
9	0.333	0.0348	2.39	0.515	0.468	0.043
10	0.370	0.0351	0.87	0.520	0.419	0.016

Test Filename   **H23**

Engine Details

Configuration	IL4	Inner Seat Dia, mm	27	Shape Factor, LD	10.43
Cylinder bore	84.5	Seat Angle	45	Lmax/D	0.31
Engine Stroke	90	Max Valve Lift	8.37	D/B	0.32
Inlet Valves, n	1	Valve Opens	0	MIGV	132.2
Rated Speed, rpm	4500	Valve Closes	50	MPV	13.5

Test Details

Test Date	26-Feb-01	Barometer, mmHg	748.7	VFAM Constant	77.18
Test Pressure, mmH$_2$O	900	ISM Constant	1.09E-04		

Test Summary Results

Swirl Ratio (Rs)	1.68	Gulp Factor	0.873	Cf @ 0.3 L/D	0.566
Rs/LD	0.16	MCf	0.441	Cf @ Max Lift	0.562
CCf	1.771				

Test Results

Valve Lift		Air Flow	ISM Torque	Flow	Discharge	Non-dim
Test	Non-dim	m^3/s	NmE^{-3}	Coefficient	Coefficient	Rig Swirl
mm	L/D	Q	G	Cf	Cd	Ns
0	0.000	0.0000	0.00	0.000	0.000	0.000
1	0.037	0.0081	0.76	0.122	1.142	0.058
2	0.074	0.0157	2.50	0.235	1.081	0.100
3	0.111	0.0232	6.19	0.348	1.048	0.167
4	0.148	0.0295	10.31	0.441	0.980	0.219
5	0.185	0.0336	14.97	0.503	0.879	0.279
6	0.222	0.0352	19.97	0.525	0.752	0.356
7	0.259	0.0368	20.18	0.549	0.663	0.344
8	0.296	0.0381	19.32	0.568	0.590	0.319
9	0.333	0.0370	8.68	0.551	0.501	0.147
10	0.370	0.0372	3.04	0.554	0.447	0.051

Test Filename   H19

Engine Details

Configuration	IL4	Inner Seat Dia, mm	27	Shape Factor, LD	10.43
Cylinder bore	84.5	Seat Angle	45	Lmax/D	0.31
Engine Stroke	90	Max Valve Lift	8.37	D/B	0.32
Inlet Valves, n	1	Valve Opens	0	MIGV	132.2
Rated Speed, rpm	4500	Valve Closes	50	MPV	13.5

Test Details

Test Date	22-Feb-01	Barometer, mmHg	762.9	VFAM Constant	77.12
Test Pressure, mmH$_2$O	900	ISM Constant	1.09E-04		

Test Summary Results

Swirl Ratio (Rs)	1.61	Gulp Factor	0.952	Cf @ 0.3 L/D	0.505
Rs/LD	0.15	MCf	0.405	Cf @ Max Lift	0.506
CCf	1.625				

Test Results

Valve Lift		Air Flow	ISM Torque	Flow	Discharge	Non-dim
Test	Non-dim	m^3/s	NmE^{-3}	Coefficient	Coefficient	Rig Swirl
mm	L/D	Q	G	Cf	Cd	Ns
0	0.000	0.0000	0.00	0.000	0.000	0.000
1	0.037	0.0080	0.87	0.121	1.133	0.067
2	0.074	0.0156	2.39	0.234	1.078	0.095
3	0.111	0.0222	6.29	0.334	1.007	0.176
4	0.148	0.0281	10.52	0.423	0.939	0.233
5	0.185	0.0314	14.10	0.472	0.824	0.280
6	0.222	0.0320	14.64	0.480	0.687	0.286
7	0.259	0.0330	14.21	0.495	0.597	0.269
8	0.296	0.0337	14.32	0.504	0.524	0.266
9	0.333	0.0340	14.53	0.509	0.463	0.267
10	0.370	0.0338	11.71	0.505	0.407	0.217

Test Filename   H4

Engine Details

Configuration	IL4	Inner Seat Dia, mm	27	Shape Factor, LD	10.43
Cylinder bore	84.5	Seat Angle	45	Lmax/D	0.31
Engine Stroke	90	Max Valve Lift	8.37	D/B	0.32
Inlet Valves, n	1	Valve Opens	0	MIGV	132.2
Rated Speed, rpm	4500	Valve Closes	50	MPV	13.5

Test Details

Test Date	22-Feb-01	Barometer, mmHg	763.4	VFAM Constant	77.12
Test Pressure, mmH$_2$O	900	ISM Constant	1.09E-04		

Test Summary Results

Swirl Ratio (Rs)	2.65	Gulp Factor	0.987	Cf @ 0.3 L/D	0.485
Rs/LD	0.25	MCf	0.39	Cf @ Max Lift	0.487
CCf	1.568				

Test Results

Valve Lift		Air Flow	ISM Torque	Flow	Discharge	Non-dim
Test	Non-dim	m^3/s	NmE^{-3}	Coefficient	Coefficient	Rig Swirl
mm	L/D	Q	G	Cf	Cd	Ns
0	0.000	0.0000	0.00	0.000	0.000	0.000
1	0.037	0.0079	0.87	0.119	1.112	0.068
2	0.074	0.0152	3.69	0.230	1.057	0.150
3	0.111	0.0216	8.68	0.326	0.981	0.250
4	0.148	0.0272	14.21	0.409	0.910	0.325
5	0.185	0.0307	19.09	0.461	0.806	0.387
6	0.222	0.0307	20.82	0.461	0.660	0.423
7	0.259	0.0316	22.77	0.475	0.574	0.449
8	0.296	0.0322	23.75	0.484	0.503	0.460
9	0.333	0.0328	23.64	0.492	0.447	0.450
10	0.370	0.0331	23.21	0.496	0.399	0.438

Test Filename   **H16**

Engine Details

Configuration	IL4	Inner Seat Dia, mm	27	Shape Factor, LD	10.43
Cylinder bore	84.5	Seat Angle	45	Lmax/D	0.31
Engine Stroke	90	Max Valve Lift	8.37	D/B	0.32
Inlet Valves, n	1	Valve Opens	0	MIGV	132.2
Rated Speed, rpm	4500	Valve Closes	50	MPV	13.5

Test Details

Test Date	22-Feb-01	Barometer, mmHg	764.7	VFAM Constant	77.11
Test Pressure, mmH$_2$O	900	ISM Constant	1.08E-04		

Test Summary Results

Swirl Ratio (Rs)	0.23	Gulp Factor	0.927	Cf @ 0.3 L/D	0.508
Rs/LD	0.02	MCf	0.416	Cf @ Max Lift	0.51
CCf	1.669				

Test Results

Valve Lift		Air Flow	ISM Torque	Flow	Discharge	Non-dim
Test	Non-dim	m^3/s	NmE^{-3}	Coefficient	Coefficient	Rig Swirl
mm	L/D	Q	G	Cf	Cd	Ns
0	0.000	0.0000	0.00	0.000	0.000	0.000
1	0.037	0.0078	-0.33	0.117	1.099	-0.026
2	0.074	0.0157	-0.22	0.236	1.087	-0.009
3	0.111	0.0232	2.82	0.349	1.052	0.076
4	0.148	0.0298	7.16	0.447	0.993	0.150
5	0.185	0.0328	9.98	0.492	0.859	0.190
6	0.222	0.0344	6.18	0.516	0.739	0.112
7	0.259	0.0337	0.00	0.504	0.609	0.000
8	0.296	0.0339	-2.17	0.507	0.527	-0.040
9	0.333	0.0345	-4.23	0.515	0.468	-0.077
10	0.370	0.0352	-6.18	0.525	0.423	-0.110

Test Filename   **H15**

Engine Details

Configuration	IL4	Inner Seat Dia, mm	27	Shape Factor, LD	10.43
Cylinder bore	84.5	Seat Angle	45	Lmax/D	0.31
Engine Stroke	90	Max Valve Lift	8.37	D/B	0.32
Inlet Valves, n	1	Valve Opens	0	MIGV	132.2
Rated Speed, rpm	4500	Valve Closes	50	MPV	13.5

Test Details

Test Date	22-Feb-01	Barometer, mmHg	764.7	VFAM Constant	77.11
Test Pressure, mmH$_2$O	900	ISM Constant	1.08E-04		

Test Summary Results

Swirl Ratio (Rs)	0.44	Gulp Factor	0.891	Cf @ 0.3 L/D	0.542
Rs/LD	0.04	MCf	0.433	Cf @ Max Lift	0.542
CCf	1.737				

Test Results

Valve Lift		Air Flow	ISM Torque	Flow	Discharge	Non-dim
Test	Non-dim	m^3/s	NmE^{-3}	Coefficient	Coefficient	Rig Swirl
mm	L/D	Q	G	Cf	Cd	Ns
0	0.000	0.0000	0.00	0.000	0.000	0.000
1	0.037	0.0078	1.41	0.118	1.107	0.112
2	0.074	0.0159	4.12	0.240	1.106	0.161
3	0.111	0.0234	6.18	0.352	1.062	0.164
4	0.148	0.0299	7.92	0.450	1.001	0.165
5	0.185	0.0339	7.37	0.509	0.890	0.136
6	0.222	0.0342	9.87	0.515	0.737	0.180
7	0.259	0.0356	3.25	0.535	0.646	0.057
8	0.296	0.0361	-1.30	0.542	0.563	-0.023
9	0.333	0.0362	-0.43	0.543	0.494	-0.007
10	0.370	0.0364	-1.30	0.545	0.439	-0.022

Test Filename   **H12**

Engine Details

Configuration	IL4	Inner Seat Dia, mm	27	Shape Factor, LD	10.43
Cylinder bore	84.5	Seat Angle	45	Lmax/D	0.31
Engine Stroke	90	Max Valve Lift	8.37	D/B	0.32
Inlet Valves, n	1	Valve Opens	0	MIGV	132.2
Rated Speed, rpm	4500	Valve Closes	50	MPV	13.5

Test Details

Test Date	22-Feb-01	Barometer, mmHg	766.4	VFAM Constant	77.11
Test Pressure, mmH_2O	900	ISM Constant	1.08E-04		

Test Summary Results

Swirl Ratio (Rs)	1.08	Gulp Factor	0.944	Cf @ 0.3 L/D	0.508
Rs/LD	0.1	MCf	0.408	Cf @ Max Lift	0.505
CCf	1.638				

Test Results

Valve Lift		Air Flow	ISM Torque	Flow	Discharge	Non-dim
Test	Non-dim	m^3/s	NmE^{-3}	Coefficient	Coefficient	Rig Swirl
mm	L/D	Q	G	Cf	Cd	Ns
0	0.000	0.0000	0.00	0.000	0.000	0.000
1	0.037	0.0077	0.00	0.116	1.087	0.000
2	0.074	0.0156	0.22	0.235	1.083	0.009
3	0.111	0.0229	4.12	0.344	1.036	0.112
4	0.148	0.0287	9.22	0.430	0.956	0.201
5	0.185	0.0311	13.55	0.467	0.816	0.272
6	0.222	0.0328	12.58	0.492	0.704	0.240
7	0.259	0.0334	10.30	0.500	0.603	0.193
8	0.296	0.0340	8.24	0.509	0.529	0.152
9	0.333	0.0333	0.54	0.497	0.452	0.010
10	0.370	0.0329	-2.71	0.492	0.396	-0.052

Test Filename   **H11**

Engine Details

Configuration	IL4	Inner Seat Dia, mm	27	Shape Factor, LD	10.43
Cylinder bore	84.5	Seat Angle	45	Lmax/D	0.31
Engine Stroke	90	Max Valve Lift	8.37	D/B	0.32
Inlet Valves, n	1	Valve Opens	0	MIGV	132.2
Rated Speed, rpm	4500	Valve Closes	50	MPV	13.5

Test Details

Test Date	22-Feb-01	Barometer, mmHg	766.2	VFAM Constant	77.11
Test Pressure, mmH$_2$O	900	ISM Constant	1.08E-04		

Test Summary Results

Swirl Ratio (Rs)	0.97	Gulp Factor	0.959	Cf @ 0.3 L/D	0.493
Rs/LD	0.09	MCf	0.402	Cf @ Max Lift	0.494
CCf	1.613				

Test Results

Valve Lift		Air Flow	ISM Torque	Flow	Discharge	Non-dim
Test	Non-dim	m^3/s	NmE^{-3}	Coefficient	Coefficient	Rig Swirl
mm	L/D	Q	G	Cf	Cd	Ns
0	0.000	0.0000	0.00	0.000	0.000	0.000
1	0.037	0.0078	1.41	0.119	1.111	0.111
2	0.074	0.0157	4.01	0.238	1.096	0.158
3	0.111	0.0228	6.61	0.345	1.038	0.180
4	0.148	0.0287	8.35	0.434	0.965	0.180
5	0.185	0.0313	10.08	0.473	0.826	0.200
6	0.222	0.0320	12.58	0.482	0.690	0.245
7	0.259	0.0322	8.13	0.486	0.586	0.157
8	0.296	0.0327	4.55	0.492	0.512	0.087
9	0.333	0.0331	4.12	0.498	0.452	0.078
10	0.370	0.0334	3.36	0.501	0.404	0.063

Test Filename   **H30**

Engine Details

Configuration	IL4	Inner Seat Dia, mm	27	Shape Factor, LD	10.43
Cylinder bore	84.5	Seat Angle	45	Lmax/D	0.31
Engine Stroke	90	Max Valve Lift	8.37	D/B	0.32
Inlet Valves, n	1	Valve Opens	0	MIGV	132.2
Rated Speed, rpm	4500	Valve Closes	50	MPV	13.5

Test Details

Test Date	21-Feb-01	Barometer, mmHg	771.1	VFAM Constant	77.09
Test Pressure, mmH$_2$O	900	ISM Constant	1.08E-04		

Test Summary Results

Swirl Ratio (Rs)	1.89	Gulp Factor	0.94	Cf @ 0.3 L/D	0.523
Rs/LD	0.18	MCf	0.41	Cf @ Max Lift	0.527
CCf	1.644				

Test Results

Valve Lift		Air Flow	ISM Torque	Flow	Discharge	Non-dim
Test	Non-dim	m^3/s	NmE^{-3}	Coefficient	Coefficient	Rig Swirl
mm	L/D	Q	G	Cf	Cd	Ns
0	0.000	0.0000	0.00	0.000	0.000	0.000
1	0.037	0.0078	0.33	0.116	1.091	0.026
2	0.074	0.0154	0.43	0.229	1.054	0.018
3	0.111	0.0220	4.66	0.327	0.987	0.133
4	0.148	0.0277	10.63	0.413	0.917	0.241
5	0.185	0.0307	15.18	0.457	0.798	0.311
6	0.222	0.0326	15.40	0.486	0.696	0.297
7	0.259	0.0343	17.56	0.510	0.616	0.322
8	0.296	0.0351	20.06	0.521	0.542	0.360
9	0.333	0.0361	23.64	0.537	0.488	0.413
10	0.370	0.0371	27.43	0.551	0.444	0.467

Test Filename   **H29**

Engine Details

Configuration	IL4	Inner Seat Dia, mm	27	Shape Factor, LD	10.43
Cylinder bore	84.5	Seat Angle	45	Lmax/D	0.31
Engine Stroke	90	Max Valve Lift	8.37	D/B	0.32
Inlet Valves, n	1	Valve Opens	0	MIGV	132.2
Rated Speed, rpm	4500	Valve Closes	50	MPV	13.5

Test Details

Test Date	21-Feb-01	Barometer, mmHg	771.1	VFAM Constant	77.09
Test Pressure, mmH_2O	900	ISM Constant	1.08E-04		

Test Summary Results

Swirl Ratio (Rs)	0.61	Gulp Factor	0.948	Cf @ 0.3 L/D	0.503
Rs/LD	0.06	MCf	0.406	Cf @ Max Lift	0.505
CCf	1.631				

Test Results

Valve Lift		Air Flow	ISM Torque	Flow	Discharge	Non-dim
Test	Non-dim	m^3/s	NmE^{-3}	Coefficient	Coefficient	Rig Swirl
mm	L/D	Q	G	Cf	Cd	Ns
0	0.000	0.0000	0.00	0.000	0.000	0.000
1	0.037	0.0078	1.19	0.117	1.095	0.096
2	0.074	0.0153	3.69	0.229	1.055	0.151
3	0.111	0.0223	6.61	0.334	1.005	0.186
4	0.148	0.0284	8.13	0.425	0.944	0.179
5	0.185	0.0326	7.59	0.487	0.851	0.146
6	0.222	0.0330	8.67	0.492	0.704	0.165
7	0.259	0.0332	4.88	0.495	0.597	0.092
8	0.296	0.0338	1.08	0.503	0.522	0.020
9	0.333	0.0342	-0.54	0.509	0.462	-0.010
10	0.370	0.0345	-1.95	0.513	0.414	-0.036

Test Filename   **H26**

Engine Details

Configuration	IL4	Inner Seat Dia, mm	27	Shape Factor, LD	10.43
Cylinder bore	84.5	Seat Angle	45	Lmax/D	0.31
Engine Stroke	90	Max Valve Lift	8.37	D/B	0.32
Inlet Valves, n	1	Valve Opens	0	MIGV	132.2
Rated Speed, rpm	4500	Valve Closes	50	MPV	13.5

Test Details

Test Date	21-Feb-01	Barometer, mmHg	771.5	VFAM Constant	77.08
Test Pressure, mmH$_2$O	900	ISM Constant	1.08E-04		

Test Summary Results

Swirl Ratio (Rs)	1.61	Gulp Factor	0.936	Cf @ 0.3 L/D	0.517
Rs/LD	0.15	MCf	0.412	Cf @ Max Lift	0.521
CCf	1.652				

Test Results

Valve Lift		Air Flow	ISM Torque	Flow	Discharge	Non-dim
Test	Non-dim	m^3/s	NmE^{-3}	Coefficient	Coefficient	Rig Swirl
mm	L/D	Q	G	Cf	Cd	Ns
0	0.000	0.0000	0.00	0.000	0.000	0.000
1	0.037	0.0079	0.43	0.118	1.107	0.034
2	0.074	0.0155	0.43	0.231	1.064	0.018
3	0.111	0.0224	4.66	0.334	1.008	0.131
4	0.148	0.0286	11.28	0.427	0.949	0.247
5	0.185	0.0318	16.70	0.475	0.830	0.329
6	0.222	0.0329	15.94	0.491	0.703	0.304
7	0.259	0.0340	15.07	0.507	0.612	0.278
8	0.296	0.0346	14.31	0.515	0.535	0.260
9	0.333	0.0356	16.26	0.530	0.482	0.287
10	0.370	0.0362	16.91	0.539	0.434	0.294

Test Filename   **H25**

Engine Details

Configuration	IL4	Inner Seat Dia, mm	27	Shape Factor, LD	10.43
Cylinder bore	84.5	Seat Angle	45	Lmax/D	0.31
Engine Stroke	90	Max Valve Lift	8.37	D/B	0.32
Inlet Valves, n	1	Valve Opens	0	MIGV	132.2
Rated Speed, rpm	4500	Valve Closes	50	MPV	13.5

Test Details

Test Date	21-Feb-01	Barometer, mmHg	771.4	VFAM Constant	77.08
Test Pressure, mmH$_2$O	900	ISM Constant	1.08E-04		

Test Summary Results

Swirl Ratio (Rs)	1.25	Gulp Factor	0.93	Cf @ 0.3 L/D	0.52
Rs/LD	0.12	MCf	0.414	Cf @ Max Lift	0.521
CCf	1.664				

Test Results

Valve Lift		Air Flow	ISM Torque	Flow	Discharge	Non-dim
Test	Non-dim	m^3/s	NmE^{-3}	Coefficient	Coefficient	Rig Swirl
mm	L/D	Q	G	Cf	Cd	Ns
0	0.000	0.0000	0.00	0.000	0.000	0.000
1	0.037	0.0079	1.30	0.118	1.106	0.103
2	0.074	0.0153	3.90	0.229	1.055	0.160
3	0.111	0.0223	6.61	0.333	1.005	0.186
4	0.148	0.0288	8.56	0.431	0.957	0.186
5	0.185	0.0321	10.84	0.479	0.838	0.212
6	0.222	0.0332	12.68	0.496	0.711	0.239
7	0.259	0.0343	11.93	0.513	0.619	0.218
8	0.296	0.0348	10.73	0.520	0.540	0.193
9	0.333	0.0350	9.00	0.523	0.475	0.161
10	0.370	0.0349	6.18	0.520	0.419	0.111

D37

Test Filename   **H59**

Engine Details

Configuration	IL4	Inner Seat Dia, mm	27	Shape Factor, LD	10.43
Cylinder bore	84.5	Seat Angle	45	Lmax/D	0.31
Engine Stroke	90	Max Valve Lift	8.37	D/B	0.32
Inlet Valves, n	1	Valve Opens	0	MIGV	132.2
Rated Speed, rpm	4500	Valve Closes	50	MPV	13.5

Test Details

Test Date	21-Feb-01	Barometer, mmHg	771.6	VFAM Constant	77.08
Test Pressure, mmH$_2$O	900	ISM Constant	1.08E-04		

Test Summary Results

Swirl Ratio (Rs)	1.64	Gulp Factor	0.904	Cf @ 0.3 L/D	0.537
Rs/LD	0.16	MCf	0.426	Cf @ Max Lift	0.539
CCf	1.712				

Test Results

Valve Lift		Air Flow	ISM Torque	Flow	Discharge	Non-dim
Test	Non-dim	m^3/s	NmE^{-3}	Coefficient	Coefficient	Rig Swirl
mm	L/D	Q	G	Cf	Cd	Ns
0	0.000	0.0000	0.00	0.000	0.000	0.000
1	0.037	0.0079	1.19	0.119	1.112	0.094
2	0.074	0.0156	2.49	0.234	1.077	0.100
3	0.111	0.0226	6.07	0.340	1.025	0.167
4	0.148	0.0288	10.30	0.433	0.962	0.223
5	0.185	0.0333	14.42	0.500	0.874	0.270
6	0.222	0.0343	16.91	0.516	0.739	0.307
7	0.259	0.0350	17.35	0.526	0.635	0.309
8	0.296	0.0357	16.80	0.536	0.557	0.294
9	0.333	0.0363	15.94	0.544	0.495	0.274
10	0.370	0.0362	13.77	0.543	0.437	0.237

D38

Test Filename   **H14**

Engine Details

Configuration	IL4	Inner Seat Dia, mm	27	Shape Factor, LD	10.43
Cylinder bore	84.5	Seat Angle	45	Lmax/D	0.31
Engine Stroke	90	Max Valve Lift	8.37	D/B	0.32
Inlet Valves, n	1	Valve Opens	0	MIGV	132.2
Rated Speed, rpm	4500	Valve Closes	50	MPV	13.5

Test Details

Test Date	21-Feb-01	Barometer, mmHg	772.9	VFAM Constant	77.08
Test Pressure, mmH_2O	900	ISM Constant	1.08E-04		

Test Summary Results

Swirl Ratio (Rs)	2.27	Gulp Factor	0.899	Cf @ 0.3 L/D	0.547
Rs/LD	0.22	MCf	0.428	Cf @ Max Lift	0.551
CCf	1.72				

Test Results

Valve Lift		Air Flow	ISM Torque	Flow	Discharge	Non-dim
Test	Non-dim	m^3/s	NmE^{-3}	Coefficient	Coefficient	Rig Swirl
mm	L/D	Q	G	Cf	Cd	Ns
0	0.000	0.0000	0.00	0.000	0.000	0.000
1	0.037	0.0080	0.22	0.119	1.117	0.017
2	0.074	0.0154	0.65	0.230	1.060	0.026
3	0.111	0.0224	5.20	0.335	1.008	0.146
4	0.148	0.0287	12.58	0.430	0.955	0.274
5	0.185	0.0332	19.51	0.496	0.867	0.368
6	0.222	0.0342	19.95	0.510	0.730	0.366
7	0.259	0.0355	22.44	0.530	0.640	0.396
8	0.296	0.0366	27.64	0.546	0.568	0.474
9	0.333	0.0375	31.44	0.559	0.508	0.527
10	0.370	0.0380	34.26	0.566	0.456	0.567

Test Filename H13

Engine Details

Configuration	IL4	Inner Seat Dia, mm	27	Shape Factor, LD	10.43
Cylinder bore	84.5	Seat Angle	45	Lmax/D	0.31
Engine Stroke	90	Max Valve Lift	8.37	D/B	0.32
Inlet Valves, n	1	Valve Opens	0	MIGV	132.2
Rated Speed, rpm	4500	Valve Closes	50	MPV	13.5

Test Details

Test Date	21-Feb-01	Barometer, mmHg	773.1	VFAM Constant	77.08
Test Pressure, mmH$_2$O	900	ISM Constant	1.08E-04		

Test Summary Results

Swirl Ratio (Rs)	1.2	Gulp Factor	0.905	Cf @ 0.3 L/D	0.538
Rs/LD	0.11	MCf	0.426	Cf @ Max Lift	0.537
CCf	1.709				

Test Results

Valve Lift		Air Flow	ISM Torque	Flow	Discharge	Non-dim
Test	Non-dim	m^3/s	NmE^{-3}	Coefficient	Coefficient	Rig Swirl
mm	L/D	Q	G	Cf	Cd	Ns
0	0.000	0.0000	0.00	0.000	0.000	0.000
1	0.037	0.0079	1.08	0.120	1.121	0.085
2	0.074	0.0150	4.01	0.227	1.044	0.166
3	0.111	0.0224	7.26	0.338	1.019	0.201
4	0.148	0.0290	9.65	0.437	0.972	0.207
5	0.185	0.0328	9.21	0.494	0.864	0.175
6	0.222	0.0340	15.18	0.511	0.732	0.278
7	0.259	0.0352	12.68	0.529	0.638	0.225
8	0.296	0.0359	9.76	0.538	0.559	0.170
9	0.333	0.0358	8.02	0.537	0.488	0.140
10	0.370	0.0356	5.64	0.533	0.430	0.099

Test Filename   **H3**

Engine Details

Configuration	IL4	Inner Seat Dia, mm	27	Shape Factor, LD	10.43
Cylinder bore	84.5	Seat Angle	45	Lmax/D	0.31
Engine Stroke	90	Max Valve Lift	8.37	D/B	0.32
Inlet Valves, n	1	Valve Opens	0	MIGV	132.2
Rated Speed, rpm	4500	Valve Closes	50	MPV	13.5

Test Details

Test Date	21-Feb-01	Barometer, mmHg	773.3	VFAM Constant	77.08
Test Pressure, mmH$_2$O	900	ISM Constant	1.08E-04		

Test Summary Results

Swirl Ratio (Rs)	2.64	Gulp Factor	0.985	Cf @ 0.3 L/D	0.489
Rs/LD	0.25	MCf	0.391	Cf @ Max Lift	0.491
CCf	1.571				

Test Results

Valve Lift		Air Flow	ISM Torque	Flow	Discharge	Non-dim
Test	Non-dim	m^3/s	NmE^{-3}	Coefficient	Coefficient	Rig Swirl
mm	L/D	Q	G	Cf	Cd	Ns
0	0.000	0.0000	0.00	0.000	0.000	0.000
1	0.037	0.0077	0.87	0.116	1.086	0.070
2	0.074	0.0150	3.79	0.226	1.042	0.157
3	0.111	0.0216	8.46	0.326	0.982	0.243
4	0.148	0.0271	14.09	0.410	0.910	0.322
5	0.185	0.0304	18.97	0.458	0.800	0.388
6	0.222	0.0306	21.79	0.462	0.661	0.442
7	0.259	0.0317	22.66	0.477	0.576	0.445
8	0.296	0.0324	23.42	0.488	0.507	0.450
9	0.333	0.0330	23.85	0.496	0.450	0.451
10	0.370	0.0331	23.63	0.498	0.401	0.445

Test Filename　　　　**H10**

Engine Details

Configuration	IL4	Inner Seat Dia, mm	27	Shape Factor, LD	10.43
Cylinder bore	84.5	Seat Angle	45	Lmax/D	0.31
Engine Stroke	90	Max Valve Lift	8.37	D/B	0.32
Inlet Valves, n	1	Valve Opens	0	MIGV	132.2
Rated Speed, rpm	4500	Valve Closes	50	MPV	13.5

Test Details

Test Date	21-Feb-01	Barometer, mmHg	773.6	VFAM Constant	77.08
Test Pressure, mmH$_2$O	900	ISM Constant	1.08E-04		

Test Summary Results

Swirl Ratio (Rs)	3.39	Gulp Factor	1.023	Cf @ 0.3 L/D	0.462
Rs/LD	0.32	MCf	0.377	Cf @ Max Lift	0.463
CCf	1.512				

Test Results

Valve Lift		Air Flow	ISM Torque	Flow	Discharge	Non-dim
Test	Non-dim	m^3/s	NmE^{-3}	Coefficient	Coefficient	Rig Swirl
mm	L/D	Q	G	Cf	Cd	Ns
0	0.000	0.0000	0.00	0.000	0.000	0.000
1	0.037	0.0079	0.43	0.119	1.118	0.034
2	0.074	0.0152	2.28	0.229	1.056	0.093
3	0.111	0.0214	8.78	0.324	0.977	0.254
4	0.148	0.0264	17.02	0.399	0.886	0.400
5	0.185	0.0292	24.18	0.442	0.772	0.513
6	0.222	0.0296	25.37	0.448	0.641	0.530
7	0.259	0.0301	27.32	0.455	0.549	0.563
8	0.296	0.0306	28.40	0.462	0.480	0.576
9	0.333	0.0308	28.73	0.466	0.423	0.578
10	0.370	0.0310	28.40	0.467	0.376	0.570

Test Filename   **H9**

Engine Details

Configuration	IL4	Inner Seat Dia, mm	27	Shape Factor, LD	10.43
Cylinder bore	84.5	Seat Angle	45	Lmax/D	0.31
Engine Stroke	90	Max Valve Lift	8.37	D/B	0.32
Inlet Valves, n	1	Valve Opens	0	MIGV	132.2
Rated Speed, rpm	4500	Valve Closes	50	MPV	13.5

Test Details

Test Date	21-Feb-01	Barometer, mmHg	773.8	VFAM Constant	77.07
Test Pressure, mmH$_2$O	900	ISM Constant	1.08E-04		

Test Summary Results

Swirl Ratio (Rs)	1.57	Gulp Factor	1.033	Cf @ 0.3 L/D	0.459
Rs/LD	0.15	MCf	0.373	Cf @ Max Lift	0.46
CCf	1.498				

Test Results

Valve Lift		Air Flow	ISM Torque	Flow	Discharge	Non-dim
Test	Non-dim	m^3/s	NmE^{-3}	Coefficient	Coefficient	Rig Swirl
mm	L/D	Q	G	Cf	Cd	Ns
0	0.000	0.0000	0.00	0.000	0.000	0.000
1	0.037	0.0079	1.52	0.120	1.128	0.118
2	0.074	0.0150	5.31	0.228	1.051	0.218
3	0.111	0.0212	8.56	0.322	0.970	0.249
4	0.148	0.0261	9.11	0.397	0.881	0.215
5	0.185	0.0284	12.58	0.431	0.753	0.273
6	0.222	0.0290	12.90	0.440	0.630	0.275
7	0.259	0.0298	11.27	0.453	0.546	0.233
8	0.296	0.0303	9.76	0.459	0.477	0.199
9	0.333	0.0304	8.56	0.461	0.419	0.174
10	0.370	0.0307	7.81	0.465	0.375	0.157

Test Filename   **H6**

Engine Details

Configuration	IL4	Inner Seat Dia, mm	27	Shape Factor, LD	10.43
Cylinder bore	84.5	Seat Angle	45	Lmax/D	0.31
Engine Stroke	90	Max Valve Lift	8.37	D/B	0.32
Inlet Valves, n	1	Valve Opens	0	MIGV	132.2
Rated Speed, rpm	4500	Valve Closes	50	MPV	13.5

Test Details

Test Date	20-Feb-01	Barometer, mmHg	775.6	VFAM Constant	77.07
Test Pressure, mmH$_2$O	900	ISM Constant	1.08E-04		

Test Summary Results

Swirl Ratio (Rs)	-0.28	Gulp Factor	0.929	Cf @ 0.3 L/D	0.513
Rs/LD	-0.03	MCf	0.415	Cf @ Max Lift	0.514
CCf	1.664				

Test Results

Valve Lift		Air Flow	ISM Torque	Flow	Discharge	Non-dim
Test	Non-dim	m^3/s	NmE^{-3}	Coefficient	Coefficient	Rig Swirl
mm	L/D	Q	G	Cf	Cd	Ns
0	0.000	0.0000	0.00	0.000	0.000	0.000
1	0.037	0.0078	0.33	0.117	1.099	0.026
2	0.074	0.0154	0.54	0.232	1.070	0.022
3	0.111	0.0223	2.82	0.337	1.015	0.078
4	0.148	0.0284	5.53	0.430	0.954	0.121
5	0.185	0.0329	5.64	0.498	0.870	0.106
6	0.222	0.0333	2.82	0.503	0.720	0.053
7	0.259	0.0338	-4.01	0.511	0.617	-0.074
8	0.296	0.0340	-9.54	0.513	0.533	-0.174
9	0.333	0.0342	-12.47	0.516	0.469	-0.226
10	0.370	0.0344	-13.98	0.518	0.418	-0.253

Test Filename   **H5**

Engine Details

Configuration	IL4	Inner Seat Dia, mm	27	Shape Factor, LD	10.43
Cylinder bore	84.5	Seat Angle	45	Lmax/D	0.31
Engine Stroke	90	Max Valve Lift	8.37	D/B	0.32
Inlet Valves, n	1	Valve Opens	0	MIGV	132.2
Rated Speed, rpm	4500	Valve Closes	50	MPV	13.5

Test Details

Test Date	20-Feb-01	Barometer, mmHg	775.9	VFAM Constant	77.07
Test Pressure, mmH$_2$O	900	ISM Constant	1.08E-04		

Test Summary Results

Swirl Ratio (Rs)	-0.22	Gulp Factor	0.942	Cf @ 0.3 L/D	0.499
Rs/LD	-0.02	MCf	0.409	Cf @ Max Lift	0.5
CCf	1.642				

Test Results

Valve Lift		Air Flow	ISM Torque	Flow	Discharge	Non-dim
Test	Non-dim	m^3/s	NmE^{-3}	Coefficient	Coefficient	Rig Swirl
mm	L/D	Q	G	Cf	Cd	Ns
0	0.000	0.0000	0.00	0.000	0.000	0.000
1	0.037	0.0076	0.76	0.114	1.073	0.062
2	0.074	0.0154	0.76	0.233	1.073	0.031
3	0.111	0.0227	3.04	0.344	1.036	0.083
4	0.148	0.0289	5.53	0.437	0.970	0.119
5	0.185	0.0327	4.99	0.495	0.865	0.094
6	0.222	0.0332	1.30	0.502	0.719	0.024
7	0.259	0.0329	-4.12	0.497	0.600	-0.078
8	0.296	0.0330	-7.37	0.499	0.518	-0.138
9	0.333	0.0333	-8.67	0.501	0.456	-0.162
10	0.370	0.0338	-9.32	0.509	0.410	-0.172

Test Filename   **H21**

Engine Details

Configuration	IL4	Inner Seat Dia, mm	27	Shape Factor, LD	10.43
Cylinder bore	84.5	Seat Angle	45	Lmax/D	0.31
Engine Stroke	90	Max Valve Lift	8.37	D/B	0.32
Inlet Valves, n	1	Valve Opens	0	MIGV	132.2
Rated Speed, rpm	4500	Valve Closes	50	MPV	13.5

Test Details

Test Date	20-Feb-01	Barometer, mmHg	776.5	VFAM Constant	77.06
Test Pressure, mmH$_2$O	900	ISM Constant	1.08E-04		

Test Summary Results

Swirl Ratio (Rs)	1.1	Gulp Factor	0.871	Cf @ 0.3 L/D	0.562
Rs/LD	0.11	MCf	0.442	Cf @ Max Lift	0.565
CCf	1.775				

Test Results

Valve Lift		Air Flow	ISM Torque	Flow	Discharge	Non-dim
Test	Non-dim	m^3/s	NmE^{-3}	Coefficient	Coefficient	Rig Swirl
mm	L/D	Q	G	Cf	Cd	Ns
0	0.000	0.0000	0.00	0.000	0.000	0.000
1	0.037	0.0079	0.87	0.119	1.119	0.068
2	0.074	0.0155	1.41	0.235	1.081	0.056
3	0.111	0.0226	3.58	0.343	1.035	0.098
4	0.148	0.0291	7.59	0.441	0.980	0.161
5	0.185	0.0341	10.95	0.517	0.903	0.198
6	0.222	0.0352	11.60	0.534	0.764	0.204
7	0.259	0.0364	11.92	0.551	0.665	0.203
8	0.296	0.0371	12.57	0.561	0.583	0.210
9	0.333	0.0377	12.25	0.571	0.519	0.201
10	0.370	0.0381	11.71	0.575	0.463	0.191

Test Filename   **H17**

Engine Details

Configuration	IL4	Inner Seat Dia, mm	27	Shape Factor, LD	10.43
Cylinder bore	84.5	Seat Angle	45	Lmax/D	0.31
Engine Stroke	90	Max Valve Lift	8.37	D/B	0.32
Inlet Valves, n	1	Valve Opens	0	MIGV	132.2
Rated Speed, rpm	4500	Valve Closes	50	MPV	13.5

Test Details

Test Date	20-Feb-01	Barometer, mmHg	777.9	VFAM Constant	77.06
Test Pressure, mmH$_2$O	900	ISM Constant	1.08E-04		

Test Summary Results

Swirl Ratio (Rs)	1.34	Gulp Factor	0.947	Cf @ 0.3 L/D	0.508
Rs/LD	0.13	MCf	0.407	Cf @ Max Lift	0.51
CCf	1.632				

Test Results

Valve Lift		Air Flow	ISM Torque	Flow	Discharge	Non-dim
Test	Non-dim	m^3/s	NmE^{-3}	Coefficient	Coefficient	Rig Swirl
mm	L/D	Q	G	Cf	Cd	Ns
0	0.000	0.0000	0.00	0.000	0.000	0.000
1	0.037	0.0076	0.22	0.115	1.079	0.018
2	0.074	0.0153	1.41	0.232	1.069	0.057
3	0.111	0.0220	4.34	0.334	1.006	0.122
4	0.148	0.0277	8.78	0.420	0.933	0.196
5	0.185	0.0316	12.57	0.479	0.837	0.246
6	0.222	0.0321	11.71	0.487	0.697	0.225
7	0.259	0.0329	12.14	0.498	0.601	0.228
8	0.296	0.0335	12.36	0.508	0.528	0.228
9	0.333	0.0339	13.22	0.514	0.467	0.241
10	0.370	0.0344	13.77	0.521	0.419	0.248

Test Filename   H2

Engine Details

Configuration	IL4	Inner Seat Dia, mm	27	Shape Factor, LD	10.43
Cylinder bore	84.5	Seat Angle	45	Lmax/D	0.31
Engine Stroke	90	Max Valve Lift	8.37	D/B	0.32
Inlet Valves, n	1	Valve Opens	0	MIGV	132.2
Rated Speed, rpm	4500	Valve Closes	50	MPV	13.5

Test Details

Test Date	19-Feb-01	Barometer, mmHg	778.4	VFAM Constant	77.06
Test Pressure, mmH$_2$O	900	ISM Constant	1.08E-04		

Test Summary Results

Swirl Ratio (Rs)	2.44	Gulp Factor	0.968	Cf @ 0.3 L/D	0.497
Rs/LD	0.23	MCf	0.398	Cf @ Max Lift	0.498
CCf	1.598				

Test Results

Valve Lift		Air Flow	ISM Torque	Flow	Discharge	Non-dim
Test	Non-dim	m^3/s	NmE^{-3}	Coefficient	Coefficient	Rig Swirl
mm	L/D	Q	G	Cf	Cd	Ns
0	0.000	0.0000	0.00	0.000	0.000	0.000
1	0.037	0.0080	0.87	0.121	1.137	0.067
2	0.074	0.0150	2.38	0.228	1.050	0.098
3	0.111	0.0215	6.18	0.326	0.983	0.177
4	0.148	0.0269	11.60	0.409	0.908	0.266
5	0.185	0.0306	16.37	0.464	0.811	0.330
6	0.222	0.0313	19.73	0.475	0.680	0.389
7	0.259	0.0324	22.76	0.489	0.591	0.436
8	0.296	0.0328	24.28	0.497	0.516	0.458
9	0.333	0.0331	23.85	0.501	0.455	0.446
10	0.370	0.0334	22.55	0.504	0.406	0.419

Test Filename   H1

Engine Details

Configuration	IL4	Inner Seat Dia, mm	27	Shape Factor, LD	10.43
Cylinder bore	84.5	Seat Angle	45	Lmax/D	0.31
Engine Stroke	90	Max Valve Lift	8.37	D/B	0.32
Inlet Valves, n	1	Valve Opens	0	MIGV	132.2
Rated Speed, rpm	4500	Valve Closes	50	MPV	13.5

Test Details

Test Date	19-Feb-01	Barometer, mmHg	778.9	VFAM Constant	77.05
Test Pressure, mmH$_2$O	900	ISM Constant	1.08E-04		

Test Summary Results

Swirl Ratio (Rs)	2.25	Gulp Factor	0.964	Cf @ 0.3 L/D	0.497
Rs/LD	0.22	MCf	0.399	Cf @ Max Lift	0.498
CCf	1.604				

Test Results

Valve Lift		Air Flow	ISM Torque	Flow	Discharge	Non-dim
Test	Non-dim	m^3/s	NmE^{-3}	Coefficient	Coefficient	Rig Swirl
mm	L/D	Q	G	Cf	Cd	Ns
0	0.000	0.0000	0.00	0.000	0.000	0.000
1	0.037	0.0078	0.76	0.119	1.112	0.060
2	0.074	0.0150	2.60	0.227	1.046	0.107
3	0.111	0.0215	6.61	0.326	0.982	0.190
4	0.148	0.0272	11.71	0.412	0.915	0.266
5	0.185	0.0310	15.72	0.470	0.821	0.313
6	0.222	0.0317	20.38	0.480	0.688	0.398
7	0.259	0.0325	20.81	0.492	0.593	0.397
8	0.296	0.0328	21.14	0.496	0.516	0.399
9	0.333	0.0333	21.57	0.503	0.457	0.402
10	0.370	0.0337	21.14	0.508	0.409	0.389

Test Filename   **H58**

Engine Details

Configuration	IL4	Inner Seat Dia, mm	27	Shape Factor, LD	10.43
Cylinder bore	84.5	Seat Angle	45	Lmax/D	0.31
Engine Stroke	90	Max Valve Lift	8.37	D/B	0.32
Inlet Valves, n	1	Valve Opens	0	MIGV	132.2
Rated Speed, rpm	4500	Valve Closes	50	MPV	13.5

Test Details

Test Date	19-Feb-01	Barometer, mmHg	779.1	VFAM Constant	77.05
Test Pressure, mmH$_2$O	900	ISM Constant	1.08E-04		

Test Summary Results

Swirl Ratio (Rs)	1.55	Gulp Factor	0.912	Cf @ 0.3 L/D	0.533
Rs/LD	0.15	MCf	0.423	Cf @ Max Lift	0.535
CCf	1.696				

Test Results

Valve Lift		Air Flow	ISM Torque	Flow	Discharge	Non-dim
Test	Non-dim	m^3/s	NmE^{-3}	Coefficient	Coefficient	Rig Swirl
mm	L/D	Q	G	Cf	Cd	Ns
0	0.000	0.0000	0.00	0.000	0.000	0.000
1	0.037	0.0077	0.43	0.117	1.098	0.035
2	0.074	0.0150	1.52	0.228	1.049	0.062
3	0.111	0.0221	5.31	0.336	1.012	0.148
4	0.148	0.0282	9.86	0.429	0.953	0.215
5	0.185	0.0324	13.66	0.493	0.861	0.260
6	0.222	0.0337	16.04	0.511	0.732	0.294
7	0.259	0.0345	16.15	0.523	0.631	0.289
8	0.296	0.0351	15.72	0.532	0.553	0.276
9	0.333	0.0357	15.17	0.540	0.491	0.263
10	0.370	0.0360	14.09	0.544	0.439	0.242

Test Filename   **H46**

Engine Details

Configuration	IL4	Inner Seat Dia, mm	27	Shape Factor, LD	10.43
Cylinder bore	84.5	Seat Angle	45	Lmax/D	0.31
Engine Stroke	90	Max Valve Lift	8.37	D/B	0.32
Inlet Valves, n	1	Valve Opens	0	MIGV	132.2
Rated Speed, rpm	4500	Valve Closes	50	MPV	13.5

Test Details

Test Date	16-Feb-01	Barometer, mmHg	775.7	VFAM Constant	77.07
Test Pressure, mmH_2O	900	ISM Constant	1.08E-04		

Test Summary Results

Swirl Ratio (Rs)	2.64	Gulp Factor	0.928	Cf @ 0.3 L/D	0.524
Rs/LD	0.25	MCf	0.415	Cf @ Max Lift	0.527
CCf	1.666				

Test Results

Valve Lift		Air Flow	ISM Torque	Flow	Discharge	Non-dim
Test	Non-dim	m^3/s	NmE^{-3}	Coefficient	Coefficient	Rig Swirl
mm	L/D	Q	G	Cf	Cd	Ns
0	0.000	0.0000	0.00	0.000	0.000	0.000
1	0.037	0.0079	0.11	0.120	1.126	0.008
2	0.074	0.0152	1.41	0.229	1.056	0.058
3	0.111	0.0222	6.94	0.335	1.010	0.194
4	0.148	0.0280	13.77	0.422	0.938	0.305
5	0.185	0.0318	20.27	0.480	0.839	0.396
6	0.222	0.0329	24.61	0.497	0.711	0.464
7	0.259	0.0338	26.56	0.510	0.616	0.488
8	0.296	0.0348	28.29	0.523	0.544	0.506
9	0.333	0.0354	29.27	0.533	0.484	0.515
10	0.370	0.0363	31.98	0.546	0.440	0.548

Test Filename   **H45**

Engine Details

Configuration	IL4	Inner Seat Dia, mm	27	Shape Factor, LD	10.43
Cylinder bore	84.5	Seat Angle	45	Lmax/D	0.31
Engine Stroke	90	Max Valve Lift	8.37	D/B	0.32
Inlet Valves, n	1	Valve Opens	0	MIGV	132.2
Rated Speed, rpm	4500	Valve Closes	50	MPV	13.5

Test Details

Test Date	16-Feb-01	Barometer, mmHg	775.7	VFAM Constant	77.07
Test Pressure, mmH$_2$O	900	ISM Constant	1.08E-04		

Test Summary Results

Swirl Ratio (Rs)	1.55	Gulp Factor	0.95	Cf @ 0.3 L/D	0.491
Rs/LD	0.15	MCf	0.406	Cf @ Max Lift	0.494
CCf	1.628				

Test Results

Valve Lift		Air Flow	ISM Torque	Flow	Discharge	Non-dim
Test	Non-dim	m^3/s	NmE^{-3}	Coefficient	Coefficient	Rig Swirl
mm	L/D	Q	G	Cf	Cd	Ns
0	0.000	0.0000	0.00	0.000	0.000	0.000
1	0.037	0.0079	1.63	0.120	1.125	0.127
2	0.074	0.0156	5.31	0.236	1.087	0.211
3	0.111	0.0224	9.97	0.340	1.026	0.274
4	0.148	0.0285	13.01	0.433	0.962	0.281
5	0.185	0.0316	15.18	0.479	0.838	0.297
6	0.222	0.0326	18.54	0.493	0.707	0.352
7	0.259	0.0333	14.85	0.504	0.608	0.276
8	0.296	0.0324	8.67	0.490	0.510	0.166
9	0.333	0.0331	8.13	0.501	0.455	0.152
10	0.370	0.0338	7.48	0.511	0.412	0.137

Test Filename   **H53**

Engine Details

Configuration	IL4	Inner Seat Dia, mm	27	Shape Factor, LD	10.43
Cylinder bore	84.5	Seat Angle	45	Lmax/D	0.31
Engine Stroke	90	Max Valve Lift	8.37	D/B	0.32
Inlet Valves, n	1	Valve Opens	0	MIGV	132.2
Rated Speed, rpm	4500	Valve Closes	50	MPV	13.5

Test Details

Test Date	16-Feb-01	Barometer, mmHg	774.9	VFAM Constant	77.07
Test Pressure, mmH$_2$O	900	ISM Constant	1.08E-04		

Test Summary Results

Swirl Ratio (Rs)	0.2	Gulp Factor	0.922	Cf @ 0.3 L/D	0.515
Rs/LD	0.02	MCf	0.418	Cf @ Max Lift	0.516
CCf	1.678				

Test Results

Valve Lift		Air Flow	ISM Torque	Flow	Discharge	Non-dim
Test	Non-dim	m^3/s	NmE^{-3}	Coefficient	Coefficient	Rig Swirl
mm	L/D	Q	G	Cf	Cd	Ns
0	0.000	0.0000	0.00	0.000	0.000	0.000
1	0.037	0.0078	0.22	0.118	1.106	0.017
2	0.074	0.0153	0.76	0.232	1.067	0.031
3	0.111	0.0225	4.01	0.341	1.029	0.110
4	0.148	0.0290	8.78	0.440	0.977	0.187
5	0.185	0.0333	11.38	0.505	0.882	0.211
6	0.222	0.0341	8.78	0.515	0.738	0.160
7	0.259	0.0336	-0.54	0.508	0.613	-0.010
8	0.296	0.0341	-4.77	0.515	0.535	-0.087
9	0.333	0.0344	-7.70	0.519	0.472	-0.139
10	0.370	0.0350	-9.76	0.527	0.424	-0.173

Test Filename   **H39**

Engine Details

Configuration	IL4	Inner Seat Dia, mm	27	Shape Factor, LD	10.43
Cylinder bore	84.5	Seat Angle	45	Lmax/D	0.31
Engine Stroke	90	Max Valve Lift	8.37	D/B	0.32
Inlet Valves, n	1	Valve Opens	0	MIGV	132.2
Rated Speed, rpm	4500	Valve Closes	50	MPV	13.5

Test Details

Test Date	15-Feb-01	Barometer, mmHg	773.1	VFAM Constant	77.08
Test Pressure, mmH$_2$O	900	ISM Constant	1.08E-04		

Test Summary Results

Swirl Ratio (Rs)	1.69	Gulp Factor	0.891	Cf @ 0.3 L/D	0.556
Rs/LD	0.16	MCf	0.432	Cf @ Max Lift	0.559
CCf	1.735				

Test Results

Valve Lift		Air Flow	ISM Torque	Flow	Discharge	Non-dim
Test	Non-dim	m^3/s	NmE^{-3}	Coefficient	Coefficient	Rig Swirl
mm	L/D	Q	G	Cf	Cd	Ns
0	0.000	0.0000	0.00	0.000	0.000	0.000
1	0.037	0.0078	0.43	0.117	1.095	0.035
2	0.074	0.0151	1.30	0.226	1.040	0.054
3	0.111	0.0218	4.88	0.327	0.985	0.140
4	0.148	0.0282	9.97	0.422	0.937	0.221
5	0.185	0.0334	14.42	0.501	0.875	0.270
6	0.222	0.0349	16.26	0.522	0.748	0.292
7	0.259	0.0361	18.32	0.540	0.652	0.318
8	0.296	0.0371	19.84	0.555	0.576	0.335
9	0.333	0.0379	18.54	0.565	0.514	0.307
10	0.370	0.0363	1.52	0.541	0.436	0.026

Test Filename   **H37**

Engine Details

Configuration	IL4	Inner Seat Dia, mm	27	Shape Factor, LD	10.43
Cylinder bore	84.5	Seat Angle	45	Lmax/D	0.31
Engine Stroke	90	Max Valve Lift	8.37	D/B	0.32
Inlet Valves, n	1	Valve Opens	0	MIGV	132.2
Rated Speed, rpm	4500	Valve Closes	50	MPV	13.5

Test Details

Test Date	15-Feb-01	Barometer, mmHg	773.6	VFAM Constant	77.08
Test Pressure, mmH$_2$O	900	ISM Constant	1.08E-04		

Test Summary Results

Swirl Ratio (Rs)	1.52	Gulp Factor	0.895	Cf @ 0.3 L/D	0.548
Rs/LD	0.15	MCf	0.43	Cf @ Max Lift	0.55
CCf	1.727				

Test Results

Valve Lift		Air Flow	ISM Torque	Flow	Discharge	Non-dim
Test	Non-dim	m^3/s	NmE^{-3}	Coefficient	Coefficient	Rig Swirl
mm	L/D	Q	G	Cf	Cd	Ns
0	0.000	0.0000	0.00	0.000	0.000	0.000
1	0.037	0.0077	0.22	0.116	1.090	0.017
2	0.074	0.0150	1.52	0.225	1.037	0.063
3	0.111	0.0222	5.20	0.333	1.004	0.146
4	0.148	0.0287	10.30	0.432	0.959	0.223
5	0.185	0.0334	14.31	0.501	0.876	0.267
6	0.222	0.0348	18.10	0.521	0.747	0.325
7	0.259	0.0357	16.59	0.535	0.646	0.290
8	0.296	0.0365	15.07	0.547	0.568	0.258
9	0.333	0.0373	13.88	0.557	0.506	0.233
10	0.370	0.0379	13.12	0.566	0.456	0.217

Test Filename   **H35**

Engine Details

Configuration	IL4	Inner Seat Dia, mm	27	Shape Factor, LD	10.43
Cylinder bore	84.5	Seat Angle	45	Lmax/D	0.31
Engine Stroke	90	Max Valve Lift	8.37	D/B	0.32
Inlet Valves, n	1	Valve Opens	0	MIGV	132.2
Rated Speed, rpm	4500	Valve Closes	50	MPV	13.5

Test Details

Test Date	15-Feb-01	Barometer, mmHg	773.7	VFAM Constant	77.07
Test Pressure, mmH$_2$O	900	ISM Constant	1.08E-04		

Test Summary Results

Swirl Ratio (Rs)	2.06	Gulp Factor	0.955	Cf @ 0.3 L/D	0.508
Rs/LD	0.2	MCf	0.403	Cf @ Max Lift	0.51
CCf	1.62				

Test Results

Valve Lift		Air Flow	ISM Torque	Flow	Discharge	Non-dim
Test	Non-dim	m^3/s	NmE^{-3}	Coefficient	Coefficient	Rig Swirl
mm	L/D	Q	G	Cf	Cd	Ns
0	0.000	0.0000	0.00	0.000	0.000	0.000
1	0.037	0.0078	-0.22	0.117	1.100	-0.017
2	0.074	0.0150	1.08	0.226	1.038	0.045
3	0.111	0.0216	5.31	0.325	0.979	0.153
4	0.148	0.0273	10.73	0.409	0.910	0.246
5	0.185	0.0313	15.72	0.470	0.820	0.314
6	0.222	0.0323	17.35	0.484	0.693	0.336
7	0.259	0.0332	19.73	0.497	0.600	0.372
8	0.296	0.0339	20.81	0.507	0.527	0.385
9	0.333	0.0344	20.81	0.515	0.468	0.379
10	0.370	0.0348	19.51	0.520	0.419	0.351

Test Filename   **H33**

Engine Details

Configuration	IL4	Inner Seat Dia, mm	27	Shape Factor, LD	10.43
Cylinder bore	84.5	Seat Angle	45	Lmax/D	0.31
Engine Stroke	90	Max Valve Lift	8.37	D/B	0.32
Inlet Valves, n	1	Valve Opens	0	MIGV	132.2
Rated Speed, rpm	4500	Valve Closes	50	MPV	13.5

Test Details

Test Date	15-Feb-01	Barometer, mmHg	773.8	VFAM Constant	77.07
Test Pressure, mmH$_2$O	900	ISM Constant	1.08E-04		

Test Summary Results

Swirl Ratio (Rs)	1.9	Gulp Factor	0.953	Cf @ 0.3 L/D	0.508
Rs/LD	0.18	MCf	0.404	Cf @ Max Lift	0.51
CCf	1.623				

Test Results

Valve Lift		Air Flow	ISM Torque	Flow	Discharge	Non-dim
Test	Non-dim	m^3/s	NmE^{-3}	Coefficient	Coefficient	Rig Swirl
mm	L/D	Q	G	Cf	Cd	Ns
0	0.000	0.0000	0.00	0.000	0.000	0.000
1	0.037	0.0079	0.00	0.119	1.120	0.000
2	0.074	0.0152	1.63	0.230	1.059	0.066
3	0.111	0.0218	5.96	0.330	0.996	0.169
4	0.148	0.0278	11.27	0.420	0.932	0.252
5	0.185	0.0311	16.80	0.469	0.820	0.335
6	0.222	0.0319	17.89	0.482	0.690	0.348
7	0.259	0.0327	17.45	0.493	0.595	0.332
8	0.296	0.0337	17.56	0.507	0.527	0.325
9	0.333	0.0343	17.24	0.516	0.469	0.313
10	0.370	0.0349	18.00	0.525	0.423	0.321

Test Filename   **H49**

Engine Details

Configuration	IL4	Inner Seat Dia, mm	27	Shape Factor, LD	10.43
Cylinder bore	84.5	Seat Angle	45	Lmax/D	0.31
Engine Stroke	90	Max Valve Lift	8.37	D/B	0.32
Inlet Valves, n	1	Valve Opens	0	MIGV	132.2
Rated Speed, rpm	4500	Valve Closes	50	MPV	13.5

Test Details

Test Date	15-Feb-01	Barometer, mmHg	773.6	VFAM Constant	77.08
Test Pressure, mmH$_2$O	900	ISM Constant	1.08E-04		

Test Summary Results

Swirl Ratio (Rs)	2.64	Gulp Factor	0.96	Cf @ 0.3 L/D	0.501
Rs/LD	0.25	MCf	0.401	Cf @ Max Lift	0.504
CCf	1.61				

Test Results

Valve Lift		Air Flow	ISM Torque	Flow	Discharge	Non-dim
Test	Non-dim	m^3/s	NmE^{-3}	Coefficient	Coefficient	Rig Swirl
mm	L/D	Q	G	Cf	Cd	Ns
0	0.000	0.0000	0.00	0.000	0.000	0.000
1	0.037	0.0078	0.98	0.119	1.112	0.077
2	0.074	0.0149	3.25	0.226	1.042	0.135
3	0.111	0.0216	8.56	0.329	0.990	0.244
4	0.148	0.0274	15.18	0.417	0.926	0.341
5	0.185	0.0311	20.27	0.473	0.826	0.402
6	0.222	0.0315	23.74	0.477	0.683	0.466
7	0.259	0.0323	24.18	0.490	0.592	0.462
8	0.296	0.0331	24.39	0.501	0.520	0.456
9	0.333	0.0336	24.39	0.508	0.462	0.450
10	0.370	0.0337	23.63	0.511	0.411	0.434

Test Filename   **H42**

Engine Details

Configuration	IL4	Inner Seat Dia, mm	27	Shape Factor, LD	10.43
Cylinder bore	84.5	Seat Angle	45	Lmax/D	0.31
Engine Stroke	90	Max Valve Lift	8.37	D/B	0.32
Inlet Valves, n	1	Valve Opens	0	MIGV	132.2
Rated Speed, rpm	4500	Valve Closes	50	MPV	13.5

Test Details

Test Date	14-Feb-01	Barometer, mmHg	773.8	VFAM Constant	77.07
Test Pressure, mmH$_2$O	900	ISM Constant	1.08E-04		

Test Summary Results

Swirl Ratio (Rs)	1.86	Gulp Factor	0.936	Cf @ 0.3 L/D	0.518
Rs/LD	0.18	MCf	0.412	Cf @ Max Lift	0.521
CCf	1.653				

Test Results

Valve Lift		Air Flow	ISM Torque	Flow	Discharge	Non-dim
Test	Non-dim	m^3/s	NmE^{-3}	Coefficient	Coefficient	Rig Swirl
mm	L/D	Q	G	Cf	Cd	Ns
0	0.000	0.0000	0.00	0.000	0.000	0.000
1	0.037	0.0077	-0.22	0.117	1.096	-0.017
2	0.074	0.0154	0.00	0.233	1.070	0.000
3	0.111	0.0223	4.88	0.336	1.013	0.136
4	0.148	0.0283	12.68	0.426	0.947	0.279
5	0.185	0.0314	18.32	0.474	0.828	0.362
6	0.222	0.0326	18.54	0.491	0.704	0.353
7	0.259	0.0336	17.24	0.506	0.611	0.319
8	0.296	0.0343	17.89	0.517	0.537	0.324
9	0.333	0.0351	18.43	0.527	0.479	0.327
10	0.370	0.0362	22.22	0.543	0.438	0.383

Test Filename H41

Engine Details

Configuration	IL4	Inner Seat Dia, mm	27	Shape Factor, LD	10.43
Cylinder bore	84.5	Seat Angle	45	Lmax/D	0.31
Engine Stroke	90	Max Valve Lift	8.37	D/B	0.32
Inlet Valves, n	1	Valve Opens	0	MIGV	132.2
Rated Speed, rpm	4500	Valve Closes	50	MPV	13.5

Test Details

Test Date	14-Feb-01	Barometer, mmHg	773.7	VFAM Constant	77.07
Test Pressure, mmH$_2$O	900	ISM Constant	1.08E-04		

Test Summary Results

Swirl Ratio (Rs)	1.08	Gulp Factor	0.928	Cf @ 0.3 L/D	0.518
Rs/LD	0.1	MCf	0.415	Cf @ Max Lift	0.515
CCf	1.667				

Test Results

Valve Lift		Air Flow	ISM Torque	Flow	Discharge	Non-dim
Test	Non-dim	m^3/s	NmE^{-3}	Coefficient	Coefficient	Rig Swirl
mm	L/D	Q	G	Cf	Cd	Ns
0	0.000	0.0000	0.00	0.000	0.000	0.000
1	0.037	0.0078	0.98	0.118	1.105	0.078
2	0.074	0.0150	2.71	0.228	1.047	0.112
3	0.111	0.0221	5.75	0.335	1.010	0.161
4	0.148	0.0282	8.24	0.427	0.949	0.181
5	0.185	0.0323	9.65	0.489	0.854	0.185
6	0.222	0.0332	13.88	0.502	0.719	0.259
7	0.259	0.0340	11.71	0.514	0.621	0.213
8	0.296	0.0344	8.35	0.520	0.540	0.150
9	0.333	0.0336	-1.19	0.508	0.462	-0.022
10	0.370	0.0337	-2.49	0.508	0.409	-0.046

Test Filename   **H57**

Engine Details

Configuration	IL4	Inner Seat Dia, mm	27	Shape Factor, LD	10.43
Cylinder bore	84.5	Seat Angle	45	Lmax/D	0.31
Engine Stroke	90	Max Valve Lift	8.37	D/B	0.32
Inlet Valves, n	1	Valve Opens	0	MIGV	132.2
Rated Speed, rpm	4500	Valve Closes	50	MPV	13.5

Test Details

Test Date	14-Feb-01	Barometer, mmHg	774	VFAM Constant	77.07
Test Pressure, mmH_2O	900	ISM Constant	1.08E-04		

Test Summary Results

Swirl Ratio (Rs)	1.65	Gulp Factor	0.901	Cf @ 0.3 L/D	0.538
Rs/LD	0.16	MCf	0.428	Cf @ Max Lift	0.54
CCf	1.717				

Test Results

Valve Lift		Air Flow	ISM Torque	Flow	Discharge	Non-dim
Test	Non-dim	m^3/s	NmE^{-3}	Coefficient	Coefficient	Rig Swirl
mm	L/D	Q	G	Cf	Cd	Ns
0	0.000	0.0000	0.00	0.000	0.000	0.000
1	0.037	0.0079	0.87	0.120	1.121	0.068
2	0.074	0.0155	2.06	0.234	1.079	0.082
3	0.111	0.0226	5.85	0.342	1.031	0.160
4	0.148	0.0287	10.52	0.434	0.965	0.227
5	0.185	0.0332	14.42	0.502	0.877	0.269
6	0.222	0.0341	16.80	0.516	0.739	0.305
7	0.259	0.0350	17.67	0.529	0.638	0.313
8	0.296	0.0356	17.13	0.537	0.558	0.299
9	0.333	0.0361	16.80	0.545	0.495	0.289
10	0.370	0.0363	14.64	0.548	0.442	0.250

Appendix E

Related Published Works
by the Author

E

Rs

parameters.

nBV_o

A Parametric Inlet Port Design Tool for Multi-Valve Diesel Engines

M. C. Bates, M. R. Heikal
Ricardo Consulting Engineers Ltd, University of Brighton Engineering Research Centre

ABSTRACT

A fully-parametric, multi-valve inlet port design tool has been developed using statistical design-of-experiments (DoE) techniques. A modular approach was adopted so that a complete port layout could be constructed using flexible, interchangeable, generic models. Additional cylinder head features and external packaging requirements were considered throughout, as were production requirements. Reliable experimental methods were used to quantify the influence of key design parameters. A predictive, knowledge-based model was developed from the DoE results and was used to predict optimum configurations for a range of scenarios. The models were successfully validated by comparing predicted results with new test data.

An overview of the tasks undertaken in developing the model is presented, including a discussion of the major findings and conclusions. An investigation using the knowledge-based model is also presented to demonstrate the practical use of the system.

1   INTRODUCTION

Inlet port flow characteristics are a critical factor in the performance of diesel combustion systems. In-cylinder flows created during the intake stroke influence bulk charge motion, turbulence generation and therefore fuel-air mixing and combustion rates. The flow capacity of the inlet ports and valves is also a key factor in determining volumetric efficiency. Increasingly stringent emissions legislation, higher customer expectations and pressure to reduce engineering costs has driven the development of new approaches to engine design. In particular, the fundamental advantages of multi-valve technology, coupled with rapidly improving fuel delivery systems has placed new requirements on inlet port performance characteristics, including low-swirl systems and small capacity hybrid engines for maximised fuel economy.

The influence of inlet ports on cylinder head design has been investigated by several authors during design studies (1,2). Inlet valve positions and port layout are major aspects of the overall design scheme and should therefore be considered at the concept stage of the design process. During this phase, care must be taken in order to meet the conflicting requirements of the various functions of the cylinder head. The development of a successful inlet port configuration remains an iterative process and the final design is often a compromise between performance and packaging. Numerous researchers have sought to identify key design parameters and their relationship with performance characteristics. The fundamental differences between directed (tangential) and helical ports have been widely studied in order

to select the most appropriate type for different engine applications (3,4,5). In more recent studies, a limited number of key design features have been used to describe realistic geometry parametrically (6) and this development has been exploited to a certain extent by researchers who have used statistical methods to develop simple predictive models (7,8,9). Parametric modelling, statistical techniques and knowledge-based design are therefore emerging as potentially powerful design tools in this field of research, supported by rapid developments in computing power.

The present study was instigated to develop a predictive parametric model for multi-valve diesel engine inlet ports. The activities undertaken in meeting this objective are discussed in the next section. The most important aspects of the development process are briefly described and the experimental methods and results are presented in more detail. This paper builds on the findings of a study previously published by the authors (10) by discussing a new approach to the construction of the predictive model. Validation test results are also presented and significant trends in the model are investigated.

2   MODEL DEVELOPMENT

2.1   Parameter Selection and Definition

2.1.1 Initial Selection

Two basic port types were defined using the generic terms "directed" and "helical" to describe the overall port geometry. Because of the different swirl generation mechanisms present in each type, it was considered likely that the governing geometry parameters would be different. Therefore, it was deemed more appropriate to use two different port types in preference to a single, highly complex model. Port design parameters were selected by referring to the literature and by conducting a "brainstorming" session to develop new ideas. Features were then ranked in order of importance using a paired-comparison approach. In some cases, complex design features were investigated further in order to simplify them whilst maintaining their overall function and likely effect on flow characteristics. This was necessary to avoid the need for large numbers of parameters to describe a single feature.

2.1.2 Final design scheme – directed port

The design scheme for the directed port consisted of six parameters. Two parameters, E and At, describe the location of the inlet valve in the cylinder bore and the approach angle of the port relative to the cylinder respectively, as shown in the plan view in Figure 1(a). At may also be interpreted as the angular location of the inlet valve if the port orientation is fixed. E is a dimensionless parameter indicating the distance of the valve centre from the cylinder centre. A third parameter, Dn, was defined as the inlet valve inner seat diameter, divided by the bore diameter. The remaining parameters, Av, Ar and R, were used to describe the vertical approach angle of the port, the angle through which the port curved from entry face to inlet valve, and the radius of the curve respectively.

2.1.3 Final design scheme – helical port

The design scheme for the helical port consisted of seven parameters, four of which were common with the directed port (E, At, R and Ar). The remaining parameters were used to describe the dimensions of the helix. Wh represented the initial width of the helix, Aw represented the angle through which the helix wrapped around the central axis of the port and

Hs was used to define the maximum height of the helix roof above the port throat. The scheme is shown diagrammatically in Figure 1(b).
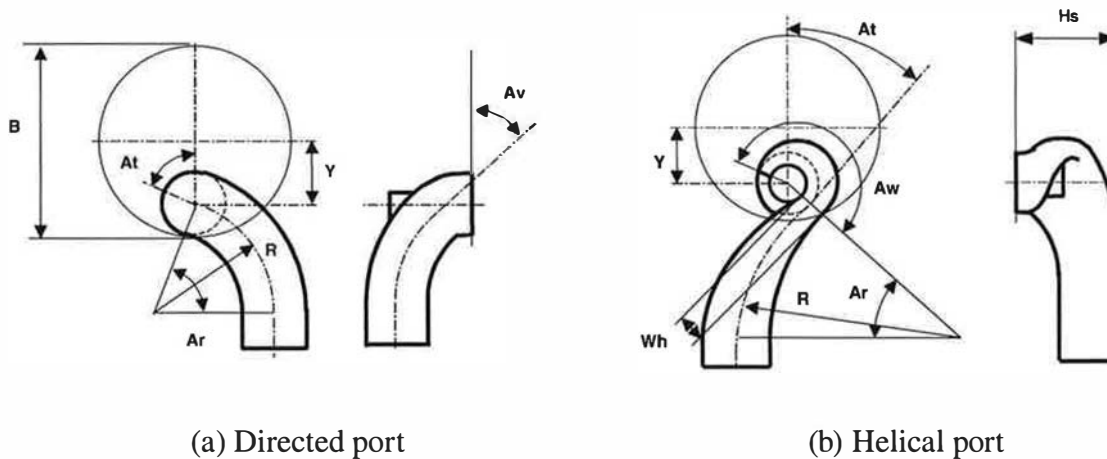

(a) Directed port   (b) Helical port

Figure 1: Port Design Schemes

2.1.4 Final design scheme – parameter ranges

Design guidelines, databases and consideration of the relevant geometry were used to define ranges for each of the parameters. For example, the minimum value of *E* was determined by considering the likely position of a centrally-mounted fuel injector and surrounding boss. The maximum value was governed by a design guideline recommending the minimum clearance between valve head and cylinder bore. The range for *Dn* was determined by analysing a database of 4V HSDI engines. Over a range of cylinder bore sizes from 70mm to 100mm, approximately 90% of the engines surveyed had a *Dn* value between 0.30 and 0.34. Changes in *Dn* were applied by varying the size of the cylinder bore rather than the valve and port. This made it possible to investigate the relative size of inlet valves whilst maintaining an acceptable number of physical models for the test programme. A 27mm valve inner-seat diameter was chosen and used with cylinder bore sizes between 80mm and 90mm to provide the required *Dn* range. As non-dimensional flow characteristics were used in the experimental phase of the project, this approach was considered to be valid.

2.2   Experimental Design

A Design-of-Experiments (DoE) approach was adopted to investigate the relationships between design parameters and port performance in a systematic and efficient manner. This approach has been successfully demonstrated in previous studies (8,10), using simplified port geometry and has also been used extensively in other fields of engine research (13,14). Classical experimental plans were chosen to provide robust models suitable for visualisation and optimisation using Response Surface Methods (RSM). The likelihood of non-linear effects and possible interactions between input parameters necessitated the use of these plans in preference to simpler screening experiments. A three-level central composite (CC) plan for six factors was selected for the directed port scheme, requiring 53 test runs. This type of plan was chosen to provide second-order main effects and linear two-way interactions. A three-level Box-Behnken (BB) plan for seven factors was chosen for the helical port scheme; 62 experiments were required, compared to 84 for the equivalent CC plan. The standard run order of both plans was randomised in order to provide a final test matrix. Within each test plan, several repeat tests ("centrepoints") were performed to provide a measure of repeatability.

2.3 CAD model construction and hardware manufacture

The generic design scheme was used to develop parametric 3-D CAD models. Throughout the design process, realistic manufacturing features were added, including a machined throat and a pocket to accept the valve guide. In the helical port design, a valve guide boss was added and all radii were compatible with typical casting requirements. Particular attention was paid to the robustness of the models to ensure that the geometry could be modified using the main driving parameters. The CAD process also involved generating the required number of model variants to populate the DoE test matrix. For the directed port, 13 unique models were necessary. 33 helical port models were required due to the increased number of hardware variables. Variations in the At and E parameters were achieved by changing the position of the port in the cylinder. Therefore, extra models were not required to investigate them.

Physical port models were manufactured using rapid prototyping (RP) techniques. After trials involving several methods, selective laser sintering (SLS) was chosen as the most suitable. The physical properties of the SLS models were found to be acceptable and an accuracy check was performed by comparing the original CAD surface with a set of curves constructed from a 3-D scan of the physical model. Although some distortion of the part occurred during the production process, this was small compared to the intentional variation in geometry resulting from the parameter changes. A skeletal frame consisting of the essential mating surfaces and location points was constructed to house the port models. The throat and entry ends of each model were fitted into recesses machined into the frame to provide positive location. A poppet valve, valve seat insert and valve guide were designed using typical geometry for a modern HSDI diesel engine. The valve guide was mounted concentrically to the valve seat by means of an adjustable location device. A fixture was also made for manually lifting the inlet valve to a known height above the valve seat using a 1mm pitch screw thread.

2.4 Test apparatus and experimental procedure

A conventional steady flow experimental procedure was followed, details of which may be found in previous studies (3, 11). A brief overview of the procedure is provided in the Appendix. A systematic method of preparing each test was developed to ensure that the experimental plan was followed accurately. This involved the use of unique identification labels for each RP model and a pre-test checklist to confirm parameter settings.

2.5 Data analysis

The raw test data was processed using a standard software routine (10) to calculate flow parameters. Non-dimensional rig swirl (Ns) and flow coefficient based on constant inner-seat area (Cf) were calculated at each valve lift point. Mean flow coefficient (MCf), gulp factor (inlet mach index, Z) and swirl ratio (Rs) were also calculated using all test points plus additional engine data and valve lift profile. Raw and processed data for all models were then recorded in a database for further analysis. Definitions for these flow parameters are provided in the Appendix.

The processed test data was analysed using MODDE, a commercial software package from Umetrics AB, to identify significant design parameters and construct polynomial response surface models. These were used to interpret the results and visualise the relationships between the parameters and responses. Alternative models, using either the individual Ns and Cf values at each valve lift, or summary parameters Rs and Z, were developed. The Ns and Cf models were used to investigate the detailed effect of parameters throughout the valve lift range. The Rs and Z models were then used to develop a software program based on

Microsoft Excel and Visual Basic to optimise port geometry for a range of realistic performance targets. The port design parameters were used as input variables and the Z response was minimised, subject to various Rs targets and external constraints, to provide trade-off curves and other significant trends.

3   TEST RESULTS AND DISCUSSION

3.1   Directed ports

A summary of the test results for the directed port study is shown in Figure 2. Cf values were highly dependent on valve lift as expected, exhibiting a typical rising trend before flattening off as maximum valve lift was reached. The variation in Cf values was much greater at high lift, indicating that the valve seat geometry governed low lift characteristics. A greater range of Ns values was observed at all valve lifts, although the greatest variation was at high lifts. Ns values at 10mm varied from approximately −0.1 to 0.6, indicating that the design parameters strongly influenced swirl direction and magnitude.

Multiple linear regression was used to determine the most significant parameters and interactions. Av (vertical port angle) was the most important parameter in terms of the Cf response throughout the valve lift range. At (tangential approach angle), Ar (port curve angle) and R (port curve radius) were also influential, as were the $Av*Ar$ and $Ar*R$ interactions. The Ns responses varied with lift but At, Ar, E (eccentricity) and the $At*Ar$ and $At*E$ interactions were important throughout. Dn (non-dimensional valve diameter) did not significantly influence swirl generation or flow performance, although this was partly due to the setting of engine parameters to ensure constant mean inlet gas velocity. Therefore, this result only showed the effect of Dn in terms of its impact on the position of the valve in the cylinder. The real effect of Dn in engines is likely to be significant due to gas velocity effects; these may be investigated by post-processing of the raw steady-flow results using alternative bore/stroke ratios or engine speeds.

The quality of fit for the DoE models was examined using the squared correlation coefficient R^2. A comparison of observed responses with those predicted from the model was also used as an indication of model quality, as shown in Figure 3. R^2 values tended to increase with valve lift as the parameter effects became more significant and the flow regime became more stable. The regression analysis results were used to investigate the relationships between input parameters and performance responses. The most significant Ns and Cf responses are shown in Figure 4. The predicted Ns response, shown in Figure 4(a) indicated that high valve-lift Ns values increased with At. This response is logical when the geometry is considered. High At values were associated with increased tangential flow into the cylinder and therefore increased swirl. Low valve-lift Ns values were also increased but to a lesser extent. The effect of At on the Cf response is also apparent, as was observed from the regression analysis. Low valve-lift Cf values were not sensitive to port geometry changes, but the high-lift response to Av was significant, as shown in Figure 4(b). An increase in Av caused an improvement in flow performance at high valve-lifts. This was likely to be due to reduced losses in the transition area where the port blended into the throat. Figure 4 also shows experimental Cf and Ns curves for comparison. The agreement with predicted values was excellent, although this was expected as these test results were used to build the DoE model. The At parameter effect was investigated further by performing an additional set of experiments. At was varied from minimum to maximum in several steps to characterise the true response and this was

compared with the predicted values. The results are shown as a surface plot in Figure 5, indicating a good level of agreement between experimental and predicted values. Note that the predicted *At* effect each 1mm valve lift increment is represented by an independent second-order model and the continuous surface was produced by hermite interpolation. The same treatment was also applied for the observed data, although the *At* parameter effect does not follow a smooth trend throughout the range of valve lifts and therefore the surface has a "crumpled" appearance.
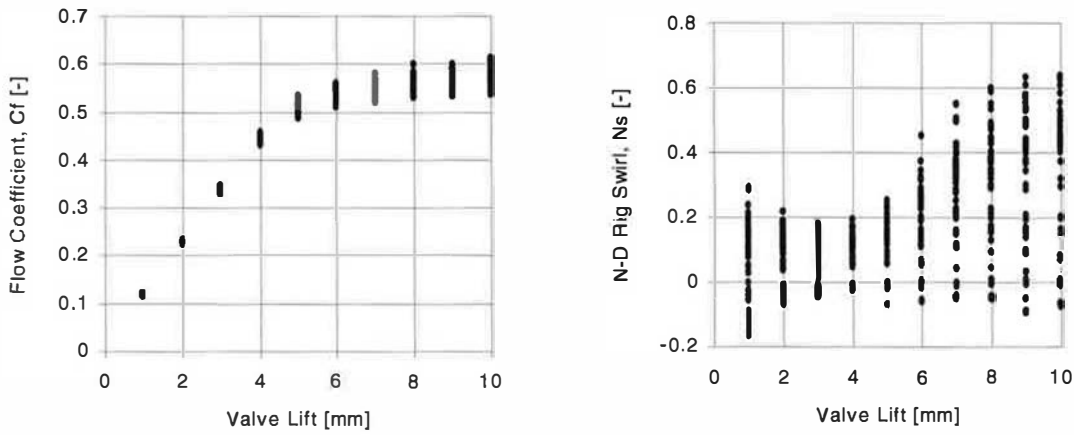
Figure 2: Results summary (directed ports)
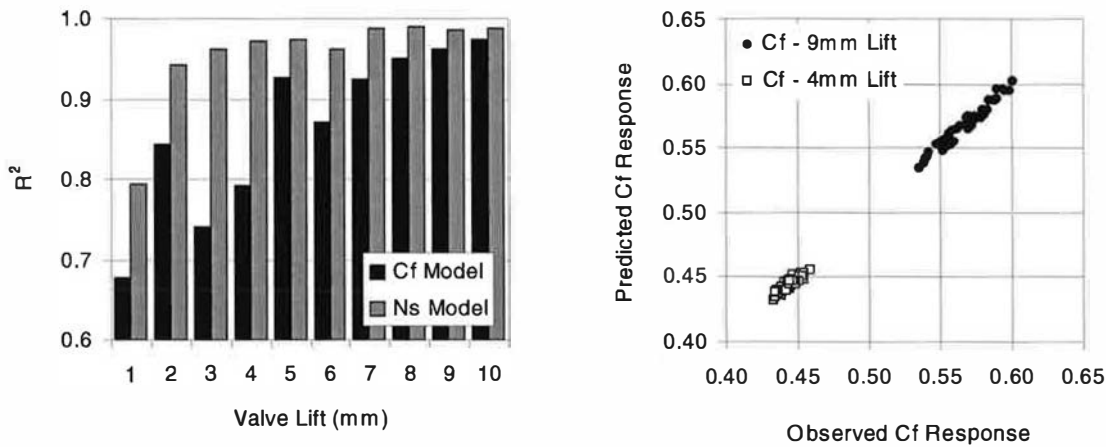
Figure 3: DoE model quality (directed ports)
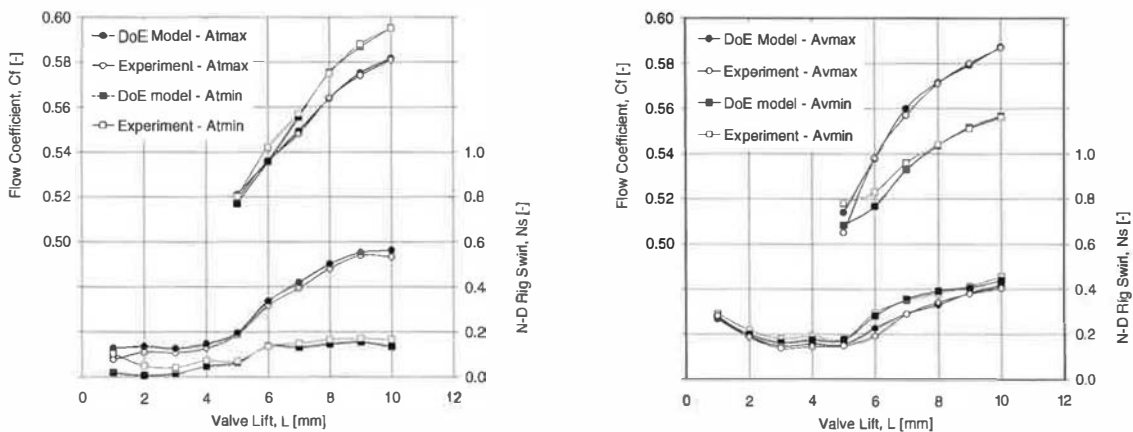
Figure 4: Performance responses (directed ports)

Predicted response   Observed response
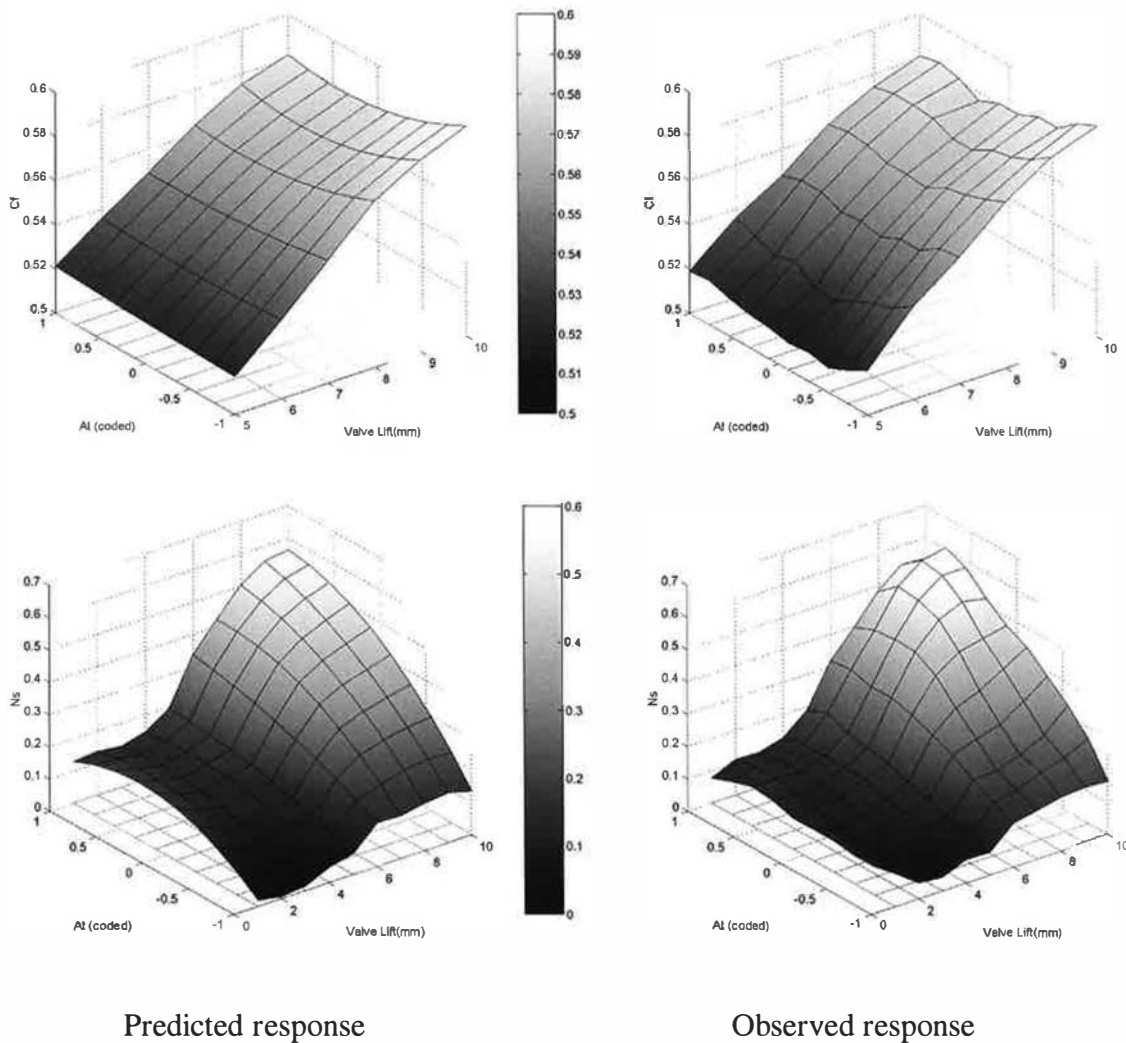
Figure 5: *At* validation (directed ports)

3.2 Helical ports

In comparison with the directed port results, swirl levels for the helical ports were generally higher, particularly at lower valve lifts. Flow performance suffered as a result, with generally lower maximum Cf values. The rate of increase of Cf at low-lift remained similar, as expected given the common valve seat geometry. The data was analysed using the same method described for the directed ports. The model fits were comparable to those of the directed port, with approximate R^2 values of 0.94 for the Ns responses and 0.92 for the Cf responses. It was noticeable, however, that the low-lift Ns models were more robust than the equivalent directed port models. This was attributed to the likely presence of a well-defined flow structure, due to the helical port features. Regression analysis showed that the most significant parameters were *At*, *Aw* (helix wrap angle), *Wh* (helix width) and *Hs* (helix start height). The importance of the *At* parameter, shown in Figure 6(a), indicated that the helical ports relied to

a certain extent on a tangential flow component to generate swirl. At low *At* settings, maximum Ns was achieved at approximately 6mm lift. As *At* increased, the maximum Ns value occurred at 10mm lift. Large *Wh* values (i.e. a wide helix) resulted in a rapid decrease in swirl as valve lift increased, as shown in Figure 6(b). The loss in high-lift swirl was possibly due to the inlet air travelling further around the helix before exiting into the cylinder. This could result in the main jet flow from the port striking the cylinder wall or creating swirl in a reverse direction with respect to swirl created in the helix. Further analysis is required to fully understand this effect. *Wh* and *Hs* influenced the Cf response significantly (Figures 6(c) and (d)), this was attributed to their effect on the flow area of the critical helix entry section of the port.
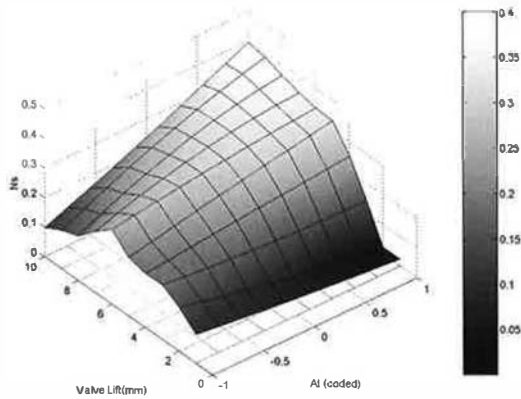
(a) *At* parameter, Ns response
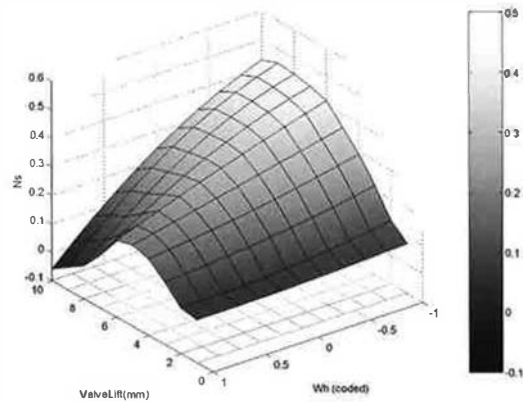
(b) *Wh* parameter, Ns response
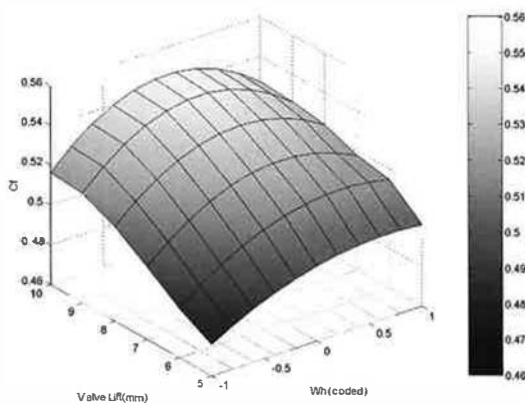
(c) *Wh* parameter, Cf response
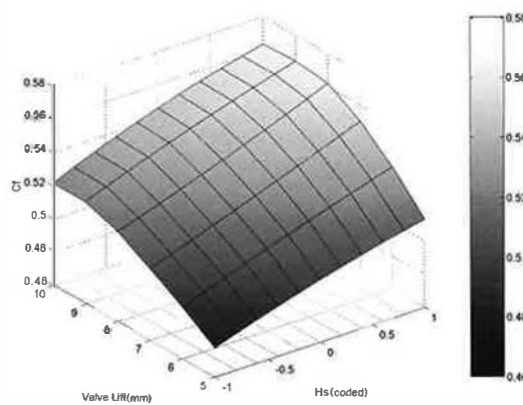
(d) *Hs* parameter, Cf response

Figure 6: Performance responses (helical ports)

5   KNOWLEDGE-BASED MODEL

The single-port DoE models were used to create a predictive multi-valve model. The Rs and Z response models were used for this purpose. An additive method used by previous workers (4,5) was adopted to estimate the performance of a multi-valve configuration from the individual port flow predictions. A range of configurations could be simulated by combining any two ports and the resulting performance trends investigated. It is important to note that,

although this approach was limited as flow interactions between ports could not be characterised, its use has been demonstrated successfully. During the concept stage of the design process, the primary requirement is to evaluate candidate solutions rapidly and compare them objectively. An optimisation routine was developed in Microsoft Excel to maximise the flow performance of a particular port configuration for a given swirl ratio target. Predicted performance for three typical port configurations is shown in Figure 7. Combinations using either two directed ports, two helical ports or one of each type were optimised to assess their operating ranges. Twin directed configurations were most efficient at low swirl ratios. Twin helical configuration were capable of higher swirl ratios but generated low swirl less efficiently. Mixed configurations performed well over an intermediate swirl range, but were also less efficient than the directed ports at low swirl ratios. The results showed that it is important to consider the likely swirl requirements of the combustion system during the concept design phase in order to select the most appropriate port configuration. Experimental results for these configurations are also shown in Figure 7. The experimental results were obtained using new, multi-valve RP models. The accuracy of predictions was encouraging, indicating that the multi-valve model performed well. However, further tests are required to fully validate the model and identify conditions under which the additive assumption is sufficient.
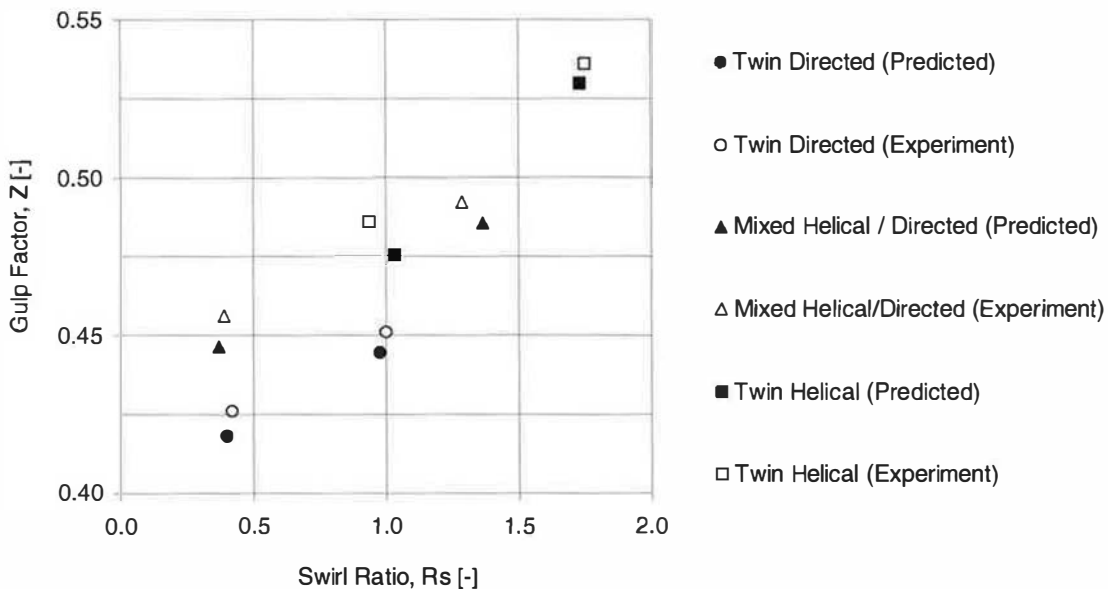

Figure 7: Optimum performance curves (multi-valve model)

6   CONCLUSIONS

- A knowledge-based model of inlet port performance for HSDI diesel engines has been successfully developed
- Robust generic port models have been constructed to capture the major design parameters of helical and directed inlet ports and a design-of-experiments approach has been employed to quantitatively assess their influence on port performance characteristics
- A range of typical multi-valve design concepts have been investigated and port performance optimised whilst meeting realistic external constraints

ACKNOWLEDGEMENTS

REFERENCES

1. I P Gilbert, A R Heath and ID Johnstone. Multivalve High Speed Direct Injection Diesel Engines – The Design Challenge. ImechE Seminar on Recent Advances in the Mechanical Design and Development of Engines and their Components. London, 1992
2. N F Gale. Diesel Engine Cylinder Head Design – The Compromises and the Techniques. SAE900133
3. M L Monaghan, H F Pettifer. Air Motion and its Effects on Diesel Engine Performance and Emissions. SAE810255
4. J Kawashima, H Ogawa, Y Tsuru. Research on a Variable Swirl Intake Port for 4-Valve High-Speed DI Diesel Engines. SAE982680
5. Y Li, L Li, J Xu, X Gong, S Liu, S Xu. Effects of Combination and Orientation of Intake Ports on Swirl Motion in Four-Valve DI Diesel Engines. SAE2000-01-1823
6. S K Widener. Parametric Design of Helical Intake Ports. SAE950818
7. H Blaxill, J Downing, J Seabrook, M Fry. A Parametric Approach to Spark-Ignition Engine Inlet-Port Design. SAE1999-01-0555
8. A Brignall, Z M Jin. Investigation of Inlet Port Design on Engine Swirl using Orthoganol Array Experimentation and Computational Fluid Dynamics. ImechE Conference on Fluid Mechanics and Dynamics of Multi-Valve Engines. London, 9 June 1999
9. V J Page, G D Blundell. The Application of Design of Experiments and CFD to the Optimisation of a Fully Parametric Helical Port Design. Computational and Experimental Methods in Reciprocating Engines, London, Nov 2000. ImechE Paper C587/014/2000
10. M C Bates, M R Heikal. A Knowledge-Based Model for Multi-Valve Diesel Engine Inlet Port Design. SAE 2002-01-1747
11. P Lambert. Computer Applications User Note: Blowrig. DP 94/2148 (Confidential)
12. C D De Boer, R J R Johns, D W Grigg, B M Train, I Denbratt, J R Linna. Refinement with Performance and Economy for 4 Valve Automotive Engines. Automotive Power Systems - Environment and Conservation. ImechE Paper C394/053, 1990
13. S P Edwards, D P Clarke, A D Pilley. The Role of Statistics in the Engine Development Process. Statistics for Engine Optimisation Seminar, IMechE, London, 2 Dec 1998
14. R A Bates, R Gilliver, A Hughes, T Shahin, S Sivaloganathan, H P Wynn. Fast Emulation of Mechanical Designs Using Computer Aided Design/Computer Aided Engineering Emulation: A Case Study. Journal of Automobile Engineering, IMechE, Vol 213, no D1, Part D, pp27-35

APPENDIX

EXPERIMENTAL PROCEDURE

Prior to each test, the impulse swirl meter (ISM) was checked, zeroed and spanned to ensure a linear response over the operating range. The pressure at the port inlet was set according to the valve size to ensure turbulent flow in the port. The model assembly was visually checked, then tested for air leaks by closing the valve and running the fan to a pressure above the required test pressure. A measured flow through the laminar flow meter (LFM) would signify a leak between it and the port model. Any small leaks were sealed before commencing the first test. The inlet valve was opened 1mm above the valve seat using the lifting screw, with the fan running. Gauge pressure at the port entry was then set by adjustment of the fan speed. Following a short period to allow the instruments to settle, the test results were recorded. A series of test points were recorded with the inlet valve lift increased incrementally by 1mm to a maximum beyond that expected in an operating engine. A maximum lift of 10mm was deemed sufficient in this study. At each test point, the fan speed was adjusted to maintain a constant gauge pressure at the port entry.

Equations used in steady flow analysis:

$$Cf = \frac{Q}{AV_o}$$

Q = volumetric flow rate (m³/s)

A = reference area (inlet valve inner seat area)

$$V_o = \sqrt{2\delta P / \rho}$$

(velocity head)

ΔP = differential pressure across port and valve (Pa)

ρ = inlet air density (kg/m³)

$$Ns = \frac{8G}{\dot{m} B V_o}$$

G = swirl meter torque (Nm)

m = air mass flow rate through port (kg/s)

B = cylinder bore (m)

$$Z = \left(\frac{B}{D}\right)^2 \frac{2S\omega_E}{na\ MCf}$$

D = inlet valve inner seat diameter (mm)

ω_E = engine crankshaft speed (rad/s)

a = sonic velocity at port inlet conditions

$$MCf = \frac{\int_{\alpha 1}^{\alpha 2} Cf\ d\alpha}{\alpha 2 - \alpha 1}$$

$\alpha 1, \alpha 2$ = crank angle, inlet valve opening and closing

$$Rs = \frac{\dfrac{BS}{nD^2} \displaystyle\int_{\alpha 1}^{\alpha 2} Cf\, Ns\, d\alpha}{\left[\displaystyle\int_{\alpha 1}^{\alpha 2} Cf\, d\alpha\right]^2}$$